SUPERCRITICAL FLUID EXTRACTION OF TURMERIC ROOT AND CARROT SEED AND ITS ANALYSIS

Ph.D. THESIS

by

PRIYANKA

DEPARTMENT OF CHEMICAL ENGINEERING
INDIAN INSTITUTE OF TECHNOLOGY ROORKEE
ROORKEE-247667 (INDIA)
JUNE, 2018

SUPERCRITICAL FLUID EXTRACTION OF TURMERIC ROOT AND CARROT SEED AND ITS ANALYSIS

A THESIS

*Submitted in partial fulfilment of the
requirements for the award of the degree*

of

DOCTOR OF PHILOSOPHY

in

CHEMICAL ENGINEERING

by

PRIYANKA

**DEPARTMENT OF CHEMICAL ENGINEERING
INDIAN INSTITUTE OF TECHNOLOGY ROORKEE
ROORKEE – 247 667 (INDIA)
JUNE, 2018**

INDIAN INSTITUTE OF TECHNOLOGY ROORKEE
ROORKEE

CANDIDATE'S DECLARATION

I hereby certify that the work which is being presented in the thesis entitled "**SUPERCRITICAL FLUID EXTRACTION OF TURMERIC ROOT AND CARROT SEED AND ITS ANALYSIS**" in partial fulfilment of the requirements for the award of the degree of Doctor of Philosophy and submitted in the Department of Chemical Engineering of the Indian Institute of Technology Roorkee, Roorkee, is an authentic record of my own work carried out during a period from July, 2013 to June, 2018 under the supervision of Dr. Shabina Khanam, Associate Professor, Department of Chemical Engineering, Indian Institute of Technology Roorkee, Roorkee.

The matter presented in this thesis has not been submitted by me for the award of any other degree of this or any other institution.

(PRIYANKA)

This is to certify that the above statement made by the candidate is correct to the best of my knowledge.

Dated: June, 2018

(Shabina Khanam)
Supervisor

ABSTRACT

Supercritical fluid extraction (SFE) technology for the extraction of different type of species is gaining interest in food, pharmaceutical and chemical industries from last decades. Utilization of natural products, which are safe for humans and environment, is increasing day by day. Therefore, investigation of new natural products including plant extracts seems to be important. Further, due to increased public awareness for health, environmental and safety hazards associated with the use of organic solvents in extraction, SFE using supercritical CO_2 provides necessary impetus to substitute petroleum based solvent such as hexane, ethers and chloroform, etc.

In the present study, oils are extracted from Turmeric root and Carrot seed using SFE process where CO_2 is utilized as supercritical solvent. These are used in pharmaceutical, cosmetics and food industry due to several medicinal effects. To extract oil experimental study is carried out using setup (SFE 1000F), procured from Thar Technologies Inc., Pittsburgh. Effects of five input parameters such as pressure, temperature, particle size, solvent flow rate and addition of co-solvent on the extraction yield (g oil/ g solid) are identified. Characterization of solid materials and their oils are performed through scanning electron microscopy (SEM), Thermo-gravimetric analysis (TGA), Differential thermal analysis (DTA), Differential scanning calorimetry (DSC) and Fourier-transform infrared (FTIR) spectroscopy. Physico-chemical properties such as refractive index, peroxide value, acid value, iodine value, saponification value, un-saponifiable matter, and specific gravity of oil samples are determined using standard methods of analysis. Essential oil and fatty acid composition of extracted oils are obtained using gas chromatography (GC), gas chromatography mass-spectroscopy (GC-MS) and ultra-violet (UV) spectroscopy.

Full-face central composite design (CCD) is employed to optimize operating parameters of SFE of turmeric root oil. These parameters are pressure, temperature, solvent flow rate, particle size and addition of co-solvent (ethanol), which vary as 20-40 MPa, 40-60 °C, 5-15 g/min, 0.2-0.8mm and 0-15% of solvent rate, respectively. Turmeric oil yield found through Soxhlet extraction is 5.954 wt% of turmeric powder whereas through SFE, it varies from 2 to 5.3 wt%. Turmerone and Curcumin are identified as principle compounds of turmeric essential oil, which are analyzed using GC-MS and UV spectroscopy, respectively. Fatty acid analysis shows that oleic acid (cis and trans) is major monounsaturated fatty acid (MUFA) found in turmeric oil, which contributes 2.9 to 61.5% of turmeric oil followed by Linoleic acid (22.56%) and Linolenic acid (21.3%). Experimental data of oil yield, Curcumin content and Turmerone content are fitted well in the

Quadratic model. Optimized values of operating parameters for maximizing these responses are also predicted.

In the case of carrot seed, screening design is applied on pressure, temperature, solvent to feed ratio, particle size and co-solvent to study the contribution of each parameter on responses i.e. extraction oil yield (EOY) and Carotol content (CC). CCD is employed on reduced operating parameters where ranges are 20-40 MPa (pressure), 50-70 °C (temperature), 5-15 g/min (flow rate) and 0-10% of solvent to feed ratio(co-solvent). Extraction oil yield varies from 2.8 to 12.9 wt% of carrot seed using SFE process while it is 13.5 wt% for Soxhlet extraction. Operating parameters are optimized for maximizing both responses for SFE of carrot seed oil. Characterization of carrot seed and oil are also carried out using FTIR, SEM, TGA and DSC. Carotol and Daucol are found as primary compounds of carrot seed essential oil through GC-MS analyses, which contribute 82.19 to 94.09% and 0.53 to 5.85%, respectively, of carrot seed oil. Carrot seed oil comprises of 28 to 78% Oleic acid, which is the major MUFA of carrot seed oil. In addition, Pentadecylic acid, Margaric acid, γ-Linolenic acid, cis-Arachidic acid and cis-eicosatetraenoic acid are the USFA found in carrot seed oil.

Further, effects of solute matrices such as leaves, flower concrete, flower bud, herb plant, shrub seed and vegetable matter are studied on extraction yield through different models. The models are solved using COMSOL Multiphysics 5.2 solver and results are validated with that of literature. Experimental data of each type of solute matrices are fitted in various models and best-suited model is predicted. Model proposed by Reverchon (1996) and Sovova (1994) are found suitable for leaves whereas Reverchon and Poletto (1996) and Reverchon et al. (2000) are suitable for flower and flowerhip seed, respectively. Reverchon (1996), Reverchon and Marrone (1997) and Sovova (1994) models are found suitable for flower bud. Further, Reverchon (1996) is well suited model for herb plant also. Model proposed by Reverchon (1996), Sovova (1994) and Nobre et al. (2006) are suitable models for shrub seed while, for vegetable matter, Sovova (1994) and Goto et al. (1996) are well suited model. Therefore, Sovova (1994) model is found suitable for most of the matrices.

Experimental data of SFE of turmeric root and carrot seed oil are fitted in the model proposed by Sovova (1994) to validate experimental results. Oil yield of turmeric root is increasing with pressure from 200 to 300 bar and then decreasing for 400 bar. However, oil yield is increasing with temperature from 40 to 50 °C and then no significant effect is visible up to 60 °C. It is increasing with solvent flow rate whereas it is first increasing and then decreasing with increase in particle

size and co-solvent. Models proposed by Sovova (1994) and Goto et al. (1996) are investigated as most suitable models for SFE of turmeric root oil while fitting experimental data of optimum points (300 bar, 60 °C, 15 g/min, 0.45 mm and 7.5%) into different models. On the other hand, oil yield of carrot seed is increased with pressure (400 bar) and temperature (70 °C) whereas, highest yield is observed at solvent flow rate of 10 g/min, and addition of co-solvent of 5% of solvent flow rate. Thus, these values of parameters are considered as optimum points and its experimental data is fitted into different models. Consequently, models proposed by Sovova (1994) and Reverchon and Marrone (1997) are found most suitable for SFE of carrot seed oil.

Industrial-scale economic assessment of SFE process is carried out considering 60 t/y and 120 t/y production capacities for turmeric root and carrot seed oil respectively whereas SFE is found economically feasible and profitable extraction process.

iv

ACKNOWLEDGEMENT

The **journey** of a thousand miles **begins** with **one step**. This thesis is the culmination of my journey of Ph.D which was just like climbing a high peak step by step accompanied with encouragement, hardship, trust, and frustration. When I found myself at top experiencing the feeling of fulfillment, I realized though only my name appears on the cover of this dissertation but I owe great many thanks to great many people who mentored, helped and supported me during the completion of my Ph.D. Though I have taken effort in my Ph.D work but it would not been possible without kind support of many individuals and organizations. I would like to extend my sincere thanks to all of them.

First, I feel myself fortunate to get an opportunity to work under the supervision of **Dr. Shabina Khanam**, Associate Professor, Department of Chemical Engineering. I would like to express my sincere gratitude to her for showing confidence in me and encouraged me to purse my research goals. She has been guiding me and helping me to achieve my goals. Due to her constant motivation, support and advice it became possible to achieve new heights. Her immense enthusiasm and unlimited zeal have been major driving force during my Ph.D work which helped me a lot to develop myself professionally. Apart from Ph.D work, she had given me opportunities to learn new technologies and process which helped me to become an expert in this domain.

I would like to express my sincere gratitude to **Prof. Bikash Mohanty**, Department of Chemical Engineering for their priceless advice and support during this work.

I would like to express my sincere gratitude to **Prof. Shishir Sinha**, Head Department of Chemical Engineering, **Prof. C. B. Majumdar** former Head, Department of Chemical Engineering, **Prof. I D Mall**, **Prof. Basheshwer Prasad**, **Dr. V. C. Srivastava,** and **Prof. V. K. Agarwal** for their kind help in departmental affairs.

I owe thanks to a very special person, my husband, **Mr. Pushpraj Katiyar** for his continued and unfailing love, support and understanding during my pursuit of Ph.D work that made the completion of thesis possible. You were always around at times I thought that it is impossible to continue, you helped me to keep things in perspective. I greatly value his contribution and deeply appreciate his belief in me.

CONTENTS

LIST OF FIGURES

g/min, 0.45 mm and 7.5%.

LIST OF TABLES

NOMENCLATURE

$\rho/\rho f$	Solvent density (kg/ m^3)
ρ_s	Seed density (kg/ m^3)
y	Solute mass fraction in solvent phase (kg/kg)
x	Solute mass fraction in solid phase (kg/kg)
c	Concentration of solute in solvent phase (kg/ m^3)
q	Concentration of solute in solid phase (kg/ m^3)
$k_f a_0$	Solvent phase mass transfer coefficient (m^3/s)
$k_s a_0$	Solid phase mass transfer coefficient (m^3/s)
x_0	Initial fraction of solute in solid phase (kg/kg)
x_k	Easily accessible fraction of solute (kg/kg)
y_r	Solubility (kg/kg solvent)
ε	Porosity
U/u	superficial velocity (m/s)
L	Height of extractor (m)
V	Volume of extractor (m^3)
A_p	Total surface of particle (m^2)
K	Internal mass transfer coefficient (m/s)
q*	Concentration at solid phase interface (kg/ m^3)
k_p	Partition coefficient
t_i	Internal diffusion time (s)
P_e	Peclet number
B_i	Biot number
dp	Particle diameter (m)
R	Particle radius (m)
D_e	Effective diffusivity (m^2/s)
C_{sat}	saturation concentration (kg/ m^3)
Θ	Dimensionless time
Z	Axial coordinate of extractor
ζ_c	Dimensionless radius of unleached core
ε_c	Concrete volume fraction

y^*	Solute fraction in the solvent in equilibrium with the concrete (kg/kg)
h_0	Proportionality constant
x_t	Solute fraction in the concrete at the transition extraction regime at solid phase interface (kg/kg)
δ	Thickness of concrete film (m)
δ_0	Thickness of the fictitious external layer in the film (m)
K	Equilibrium constant in model
ke	External mass transfer coefficient (m/s)
a	Particle surface (m^2)
c^*	Solvent phase interface concentration (kg/ m^3)
K_{eq}	Equilibrium constant
K_{i0}	Initial mass transfer coefficient (m/s)
yf	Asymptotic value of yield
A_pK_s	Overall internal mass transfer coefficient (m^3/s)
R_1	Reading at T_1 °C in equation 5.1
K	constant (0.000385 for oils) in equation 5.1
T_1	temperature at which the reading R_1 is taken in equation 5.1
T	specified temperature (generally 30 °C.) in equation 5.1
A	weight of pycnometer with oil at 30 °C in equation 5.2, gm
B	weight of pycnometer without oil at 30 °C in equation 5.2, gm
C	weight of pycnometer with water at 30 °C in equation 5.2, gm
S	ml of sodium thio-sulphate, in equation 5.3 and 5.4
N	normality of sodium thio-sulphate solution, in equation 5.3 and 5.4
B	ml of sodium thio-sulphate solution for the blank in equation 5.4,
V	ml of standard potassium hydroxide used in equation 5.5
N	Normality of the potassium hydroxide solution in equation 5.5
w	gm of sample in equation 5.4, 5.5, 5.7 and 5.9
B	ml of standard hydrochloric acid for the blank solution in equation 5.7
S	ml of standard hydrochloric acid for the oil sample in equation 5.7
N	Normality of the standard hydrochloric acid in equation 5.7
V	ml of standard sodium hydroxide solution in equation 5.8

N	Normality of standard sodium hydroxide solution in equation 5.8
A	gm of the residue in equation 5.9
B	gm of the free fatty acid in the extract in equation 5.9

INTRODUCTION

In the present study, supercritical fluid extraction (SFE) technique is adopted to extract oil from natural products using CO_2 as supercritical solvent. SFE is a replacement of conventional extraction processes, which use organic solvents (Phelps et al., 1996). This interest is fueled by increasingly stringent environmental regulations together with new requirements of medical and food industries for ultra-pure and high value-added products (Mohamed and Mansoori, 2002; Pitchaiah et al., 2018). SFE with supercritical carbon dioxide (SC-CO_2) reduces the threat imposed by organic solvents in the environment as it is gentle, clean and green extraction process (Baldino et al., 2017). It is the best combination found so far because of its non-toxic, non-flammable, non-corrosive and non-explosive properties (Kueh et al., 2018). SFE is employed on various species such as Seeds, Roots, Flowers, Leaves, Fruits, and Herbs etc.

In recent years, nutraceuticals sector, which deals with the use of dietary substances for prevention of diseases, is gaining attention of researchers and food industries (de Melo et al., 2014). Various researchers are discovering and documenting the effectiveness of plants and its different parts (Chaudhury and Rafei, 2001). Although many species are still to be recognized for their health/nutrition benefits by health authorities such as World Health Organization (de Melo et al., 2014). A few amongst these species are turmeric root and carrot seed, which are considered to be extracted using SFE in the present study.

In India, turmeric root is grown in all states of country majorly Uttarakhand, Maharashtra, Tamilnadu and West Bengal (Raina et al., 2002). Turmeric root oil consists of different sesquiterpenes (ar-turmerone,α- turmerone, β- turmerone, turmerol) and α-atlantone along with Curcuminoids and some fatty acids such as Myristic, Palmitic acid, Oleic acid, Linoleic acid, Linolenic acid and Ecosenoic acid (Paul et al., 2011). Curcuminoids (Curcumin) is a yellow-orange crystalline powder insoluble in water, poorly soluble in hydrocarbon solvents, and soluble in alcohols (Chassagnez-mendez et al., 2000). It is beneficial to human health due to its anti-inflammatory, antioxidant, antifungal, anticarcinogenic, antiviral, antimutagenic, anticoagulant, antidiabetic, antibacterial, antiprotozoal, antifibrotic, antifertility, hypotensive and hypocholesteremic properties (Bagchi, 2012; Prasad et al., 2017). Carrot seed is cultivated worldwide including India and its oil is widely used in pharmaceutical and cosmetic industry as it fights cancer cells, acts as powerful antioxidants, supports skin and hair health and acts as natural

sunscreen. Carrot seed contains about 0.5-1.6% (v/w) essential oil, which is used for medicinal purposes such as diuretic, stomachic. It is also used in the formulation of certain alcoholic liguors as well as aromatic and fragrance compositions (Ozcan and Chalchat, 2007). Carotol and Daucol are the major essential oil compounds of carrot seed oil whereas Oleic acid, Linoleic acid, Linolenic acid, and Stearic acid are fatty acid compounds. It is recommended to replace saturated fatty acid (SFA) by USFA due to health concerns such as lower cardiovascular risk, low-density lipoprotein cholesterol level and risk of coronary heart disease (Gao et al., 2016; Paul et al., 2011; Rai et al., 2016a).

To extract oil from turmeric root, various conventional extraction methods were used such as hydro-distillation, solvent extraction, Soxhlet extraction, microwave assisted extraction (MAE) and steam distillation (Garg et al., 2002; Laokuldilok et al., 2015; Negi et al., 1999; Paul et al., 2011; Raina et al., 2002; Revathy et al., 2011). Solvent extraction method was employed by Negi et al. (1999) and Jayaprakasha et al. (2001) to extract essential oil from mother liquor/curcumin removed turmeric oleoresin considering hexane as a solvent. Raina et al. (2002) and Garg et al. (2002) extracted essential oil from leaf and rhizome of turmeric through hydro-distillation method and analyzed oil using GC-MS. Paul et al. (2011) used Soxhlet extraction method to extract oil from turmeric root, collected from three different places of Bangladesh. Further, its fatty acid composition and physico-chemical properties were compared. Screening of solvents for extraction of curcuminoids from turmeric root using Soxhlet extraction process was performed where Hexane, Chloroform, Ethyl acetate, Methanol and Acetone were considered as solvents. Isolation and purification of curcuminoids by column chromatography followed by purity analysis through high performance liquid chromatography revealed that acetone showed maximum yield of each curcuminoids.

Began et al. (2000) and Gopalan et al. (2000) extracted turmeric root using SFE and studied effects of operating parameters such as pressure, temperature, flow rate and particle size. Chang et al. (2006) extracted turmeric oil using SFE process, which was further analyzed through liquid chromatography to isolate turmerones. Effects of pressure and temperature were also studied considering two responses i.e. oil yield and concentration of turmerones. Chassagnez-mendez et al. (2000) studied the influence of drying temperature on the SFE of turmeric root oil and its curcuminoid profile. Kao et al. (2007) studied the enrichment of turmeric α-β-Ar turmerone using SFE followed by solid–liquid column partition fractionation.

Carrot seed oil was extracted through hydro-distillation and soxhlet extraction methods using different types of solvents (1,1,2-trichloro-l,2,2-trifluoroethane, methylfuran, ethanol and dichloromethane) and found that extraction yield of essential oil from hydro-distillation method was minimum (Cu et al., 1989). Carrot seed oil extracted through SFE was collected from an industry and physicochemical characteristics, oxidative ability, thermal properties, phenolic acids, flavonoids, tocopherol and fatty acid content of oil were studied (Gao et al., 2016; Gao and Birch, 2016).

It appears that effects of five operating parameters such pressure, temperature, solvent flow rate, particle size and the addition of co-solvent are not studied on the SFE of turmeric oil. However, neither SFE of carrot seed oil is carried out so far nor effects of operating parameters on extracted oil are studied. Further, it is observed that screening design is not applied on any type of solid materials to be extracted using SFE. Moreover, it also appears that no research work is published to study the effect of solute matrix on the extraction yield. In addition, modeling of SFE of turmeric root and carrot seed oil is also not carried out using different mathematical models. Based on these gaps in the literature, following objectives are formulated for the present study:

1. To select raw materials for the SFE process, which include significant medicinal benefits such as turmeric root and carrot seed are considered in present study.

2. To utilize screening design and central composite design for investigating most influential parameter and optimum operating parameters, respectively.

3. To maximize responses of SFE of turmeric root and carrot seed oils while optimizing the input parameters.

4. To characterize raw materials and extracted oils using SEM, FTIR, TGA/DTA and DSC analyses and to investigate the physico-chemical properties of extracted oils.

5. To solve various mathematical models using COMSOL Multyphysics 5.3 and to predict the most suitable model/s for different types of solute matrices while fitting experimental data into various models.

6. To compare experimental results with that found through the model proposed by Sovova (1994) and to optimize model parameters. To investigate the suitable model/s for the SFE of turmeric root and carrot seed oil through fitting of experimental data into various models, at optimum points.

7. To study the feasibility and profitability of SFE process for extraction of turmeric root and carrot seed oils based on economic analyses for industrial-scale productions.

LITERATURE REVIEW

In this chapter, a literature review based on past, present and future scope of supercritical fluid extraction (SFE) method is presented. History, properties, type and application of supercritical fluid (SCF) along with advantages, disadvantage and different aspects of SFE are reported. Literature survey based on the type of raw materials, solvents, optimization techniques and co-solvents used in SFE process is presented. Further, effects of various operating parameters affecting the SFE process are discussed. Finally, composition of extracted oils and analysis techniques are presented.

2.1 History

The phenomena and behavior of SCF has been the subject of research right from 1800's. SCF fluid phase was first identified by Charles Cagniard de La Tour in 1822 as he noticed that the distinction between liquid and gas phase disappeared above the critical point (McNally, 2006). Originally, he was studying the equilibrium of both phases for carbon dioxide and observed that the meniscus between the two phases disappeared above critical point. However, the phenomena of SFE was discovered by Hannay and Hogarth at a meeting of the Royal society of London in 1879, after more than 50 years from the discovery of SCF (Stahl et al., 1980). The precise meaning of this point was established by the Irish Physicist Thomas Andrews in 1885 (Taleb, 1885).

The ability of SCF to dissolve organic compounds was utilized in industrial operations in the middle of the twentieth century (Wilson et al., 1936). However, SFE was not considered for the industrial application till 1950. First time it was used in industry at the Max Planck Institute for Kohlenforschung and filed for the patent in 1977 (Phelps et al., 1996). They studied the feasibility of SFE in different sectors such as foods, petroleum, and chemical industries. They also identified the use of supercritical CO_2 as an alternative solvent for caffeine because the use of organic solvent (methylene chloride) was prohibited by the Ministry of Commerce.

The business division of the Max Planck Institute had licensed rights for the decaffeination of coffee using SFE. In 1976, Hag AG Corporation started to build the first industrial scale decaffeination plant where, the production started in 1978. Then, the constructions of hops extraction plant in Manchester and tea decaffeination plant were started from 1982. Further, Maxwell House and John Haas, Inc., installed a decaffeination plant and hops extraction plant in

Houston, Texas and Yakima, Washington, in 1988 and 1990, respectively. Due to changes in government regulations by U.S. Environmental Protection Agency (EPA), the use of organic solvents needed to be replaced by a "cleaner process", which did not impose any environmental threat by leaving residual toxic chemicals (Phelps et al., 1996). Official regulations motivated producers to manufacture products, which were less harmful to the people and environment, and to initiate new environment friendly technologies (Hong and Pyun, 2001).

2.2 Supercritical Fluids (SCF)

For every substance, there is a critical temperature (Tc) and pressure (Pc) above which no applied pressure can convert the substance into its liquid phase. If the temperature and pressure of a substance are both higher than respective Tc and Pc, the substance is defined as SCF and region is called supercritical fluid region as shown in Fig. 2.1 (Srivastava et al., 2018). At the critical point, densities of gas and liquid phases are same i.e. there is no distinction between the phases (Mukhopadhyay, 2000; Mukhopadhyay, 2009).
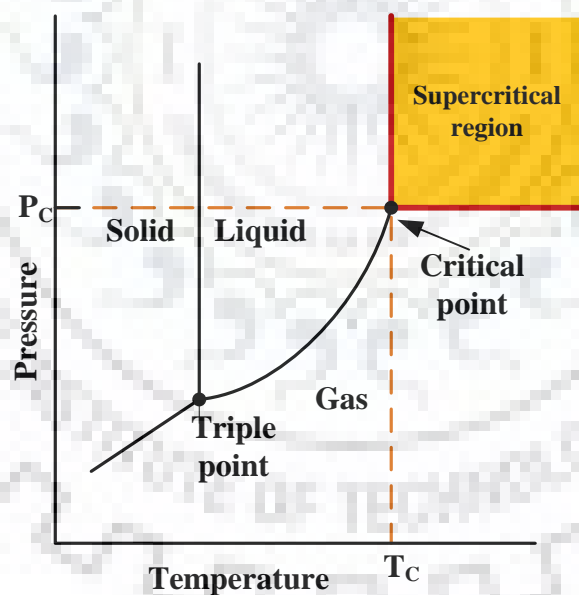
Fig. 2.1 Phase diagram showing supercritical region for a pure component.

2.2.1 Physical properties of SCFs

A SCF has physical and thermal properties between those of the pure liquid and gas (Mukhopadhyay, 2000). Density and diffusivity of SCF strongly depend upon its temperature and

pressure. However, diffusivity of SCF is much higher than that of liquid and therefore, it readily penetrates porous and fibrous solids and can offer good catalytic activity.

It generates no liquid (condensed) phase under pressure change or on solid surfaces and no gas forms while increasing temperature (Mohamed and Mansoori, 2002). It is highly compressible as it possesses liquid-like density and gas-like viscosity as the range of densities of the most common SCFs vary from 0.1-0.9 g/ml under normal working pressures (75-450 bar). Table 2.1 shows a comparison between values of density, viscosity and diffusivity for gas, liquid and supercritical fluid. Liquid-like density of SCF provides a high solvation power, whereas intermediate diffusivity and low viscosity values allow desired penetration power in the solid(Machado et al., 2013).

Table 2.1 Density, viscosity and diffusivity of gases, liquids and supercritical fluids.

Physical state	Density (g/ml)	Viscosity (g/cm * s)	Diffusivity (cm^2/s)
Gas	10^{-3}	10^{-4}	10^{-1}
Liquid	1	10^{-2}	10^{-6}
Supercritical fluid	0.2-0.9	10^{-4}	10^{-3}

Physical properties of SCF are varied sharply with minor change in pressure, particularly in the vicinity of the critical temperature and pressure (Hampson and Ashby, 1999). The solvation power or solubility of solute in SCF is directly proportional to density of SCF, which can be enhanced while increasing pressure and temperature. Generally, the solubility of SCF increases with increasing temperature in isobaric condition. However, two complex factors are noticed in the SCF with increasing temperature on pressurized systems: (1) increase in vapor pressure and solubility with increasing temperature, (2) decrease in the density and solubility with increasing temperature (Machado et al., 2013). This behavior of SCF is referred as retrograde phenomena. Solubility of solute in SCF is also affected by several factors such as mass molecular and polarity of the solute, the position of a functional group in the molecule, solid matrix interactions, and type of SCF used (Pereira and Meireles, 2010).

2.2.2 Types of SCF

At present, several solvents are used as SCF as provided in Table 2.2 with respective critical constants. However, it is observed that some of these require special handling e.g. ammonia, benzene, and cyclohexane and are not feasible as SCF (Machado et al., 2013). The selection of appropriate SCF for SFE depends on several factors such as desired solubility of solute in SCF,

should be inert to the matrix, easy separation from the product, low cost, and not too high critical pressure (Machado et al., 2013).

Carbon dioxide is found to be the most desirable SCF for SFE of natural products due to its a low critical temperature of 304 K and a moderate critical pressure of 73 bar. It is an inert, inexpensive, easily available, non-flammable, non-polar, non-toxic and environmentally friendly and often used to replace toxic freons and certain organic solvents (Dalvi and Mukhopadhyay, 2009; Naik et al., 2010). Ethane and ethylene also have easily achievable critical points however, are not economically feasible due to high cost (Machado et al., 2013). Carbon dioxide is referred as natural solvent, which is easily miscible with a variety of organic solvents and is readily recovered after processing. Its "greener" nature makes it a desirable option when compared with traditional organic solvent extractions.

Table 2.2 Critical constants of some common solvents used as SCF (Machado et al., 2013; Mukhopadhyay, 2000).

SCF	Critical Constants	
	Pressure (bar)	Temperature (°C)
Carbon dioxide	73.8	31.1
Ethane	48.8	32.2
Ethylene	50.4	9.3
Propane	42.5	96.7
Propylene	46.2	91.9
Benzene	48.9	289.0
Toluene	41.1	318.6
Chlorotrifluoromethane	39.2	28.9
Trichlorofluoromethane	44.1	196.6
Nitrous oxide	71.0	36.5
Ammonia	112.8	132.5
Water	220.5	374.2
Cyclohexane	40.73	280.3

In addition, carbon dioxide is present abundantly in environment, which does not impose any extra load to environment. Due to non-polar behavior of carbon dioxide, polar solvent can be added as modifier or co-solvent to extract polar compounds, which enhances the polarity of carbon dioxide (Rout et al., 2007).

2.2.3 Application of SCFs

The extraction process using SCFs is being used extensively in industries in fractionation of products, dyeing of fibers, treatment of contaminated soils, food and drug areas, fat and oil extraction, obtaining bioactive functional compounds, removal of heavy metals, polymer processing, fuel production, production of powders in micron and submicron range and reactions in or with SCFs (Machado et al., 2013; Marr and Gamse, 2000; Reddy and Madras, 2012). Several applications are found in pharmacological field such as extraction of fennel, rosemary, and anise essential oils (Pereira and Meireles, 2007), valerian (Safaralie et al., 2010), and bioactive substances of propolis (Zordi et al., 2014).

Table 2.3 Utilization of extracted solute by means of SFE process (Mukhopadhyay, 2000)**.**

Extracted solute/ oil	Industrial application
Ginger root oil	Asian food, energy drinks
Pimento berry oil	Savory sauces, oral hygiene products
Nutmeg oil	Soups, sauces, vegetable juices
Celery seed oil	Soups ,vegetable juice
Coriander oil	Curry, fruit flavor , chocolate
Cumin oil	Mexican and Asian food, medicines
Clove bud oil	Oral hygiene products, pickles
Pepper oil	Spices, salad dressing, meat
Vanilla absolute	Dairy products, ice-cream
Marjoram oil	Soups, savory sauces
Juniper berry oil	Alcoholic drinks
Aniseed oil	Oral hygiene products, Alcoholic drinks
Cinnamon bark oil	Sweet products, spices, baked products
Cardamom oil	Spices, meat, pickles
Savory oil	Savory sauces, soups
Sage oil	Savory sauces, soups
Paprika oil	Savory sauces, soups,sweets
Rosemary oil	Soaps, perfumes,antioxidant
Thyme oil	Medicines, meat

In polymer processing, SC-CO_2 is utilized as a solvent in the modification, composite formation, production of micro cellular foam particles, and polymerization (Tomasko et al., 2003). It is also used in the pollution abatement area to remove heavy metal ions from water, soil, tissues, wood (Wang et al., 2009).

SC-CO$_2$ is used in bio-fuel production area (Gui et al., 2009; Wen et al., 2009), fatty acids extraction from natural products such as sunflower, hemp seed and watermelon (Porto et al., 2012; Rai et al., 2016a, 2015), and in the production of bio-ethanol through treatment of sugar cane bagasse from the cellulose matrix (Machado et al., 2013). Some industrial applications of extracted solutes using SFE process are reported in Table 2.3.

2.3 Supercritical Fluid Extraction (SFE)

There are many reasons found in literature for the development of SFE technology in extraction field such as high cost of organic solvents, the strict environmental regulations, increasing demand of ultra-pure and value added product (Mohamed and Mansoori, 2002; Mukhopadhyay, 2009). SFE is the process of separating one component (solute) from another (the matrix) using SCFs as an extracting solvent. Extraction usually happens from a solid matrix, though it also can be from liquids and takes place at temperature and pressure exceeding critical values of the solvent (Reverchon and De Marco, 2006). The separation process is possible because of differences in the specific molecular interactions between various mixture components (solute) and supercritical fluid (solvent). The extraction of selected compounds can be controlled by density of solvent, which can be recovered by simply depressurizing solvent. Depressurized solvent returns to gas phase, which gets evaporated leaving no residue of solvent in extract(Abbas et al., 2008). SFE is used in larger scale to separate essential oils and its derivatives for use in food, cosmetics, pharmaceutical and other related industries (Mohamed and Mansoori, 2002; Salgin et al., 2004). As discussed in section 2.2.2, SC-CO$_2$ is the most suitable SCFs due to its relatively low temperature condition, which allows the extraction of thermally labile compounds (Rout et al., 2008). Sometimes, modifiers or co-solvents such as ethanol, methanol, water and Acetone etc. are added with SC-CO$_2$ when it is unable to extract more polar compounds (Machado et al., 2013).

2.4 Advantages of SFE

SFE technology has several advantages while comparing with other extraction processes as (Micic et al., 2011):

- ➢ Operating pressure and temperature control the dissolving power of SCFs.
- ➢ SCFs can be easily recovered from the extract due to its volatility.
- ➢ Utilization of non-toxic solvents leaves no harmful residue.
- ➢ High boiling components can be extracted at relatively low temperatures
- ➢ Thermally labile components can be extracted at low temperatures with minimal damage.
- ➢ SCF such as Carbon dioxide acts as an inert to the product.

2.5 Disadvantages of SFE

Besides several advantages, SFE has some disadvantages also as (Micic et al., 2011; Rosa and Meireles, 2005):

➢ Requirement of High pressure to perform the process.

➢ Solvent must be compressed at elevated pressure.

➢ High capital investment.

➢ Relatively high manufacturing cost.

2.6 Different aspects of SFE

SFE is an unique extraction process, which embodies several features of conventional solvent extraction while, at the same time, having important features of its own such as use of non-toxic solvent, no residual solvent in extract. Different aspects of SFE are identified as:

- Extraction of different species
- Pretreatment of seed
- Mathematical modelling of SFE process
- Utilization of Design of experiment
- Selection of solvent
- Selection of co-solvent (modifier)
- Kinetics of SFE process
- Computational fluid dynamics of SFE process
- Effect of operating parameters
- Effect of seed matrix
- Economics of SFE
- Pollution abatement of Contaminated soil
- Artificial neural network modeling of SFE process
- Application of process integation on the SFE

Amongst all these aspects, detailed literature on few important aspects is presented in this chapter as discussed further:

2.6.1 Extraction of different raw materials

Different species for which SFE process is used are categorized as Seeds, Roots, Flowers, Leaves, Fruits, Herbs, Meat, Algae, Stem, and Fractionation of Oil components.

To show the literature available from the year 1980 to present on these solute categories, a pie chart of total number of papers available against type of solute is drawn in Fig. 2.2. It shows that maximum research has been done on seed category i.e. 41% of total published article. Further, it is followed by Leaves, Fruits, Root, Flowers, Plant/Stem, Herbs, Algae, Meat and Oil, which contribute 16%, 13%, 7%, 7%, 6%, 5%, 2%, 2% and 1% of total research work done, respectively. As already discussed, most of the research is done on seed category where soybean, Coffee beans, Sunflower seed, Black pepper, Coriander seed and Clove bud etc. are considered for SFE as shown in Fig. 2.3. To study the chronological progress of the SFE of particular category of solute, bar charts are drawn as shown from Fig. 2.3 to 2.12. Abbreviations of these solutes are shown in Appendix A. These stacked bar charts show percentage of research work done in a particular year under a particular type of solute category. Fig. 2.3 shows year-wise plotting of various types of seeds (more than 70) as research has been started from year 1980 to 2018 and can be arranged for total number of papers available as:

[SBF=CFE>SF=BLP>COR=CB=GS=CS>BO>MO=SBT=CAS=NS>SB=BCS=HPS>SES=CG=Rape=FS=BS=TES>SFF>OH=CRS>Cel=TFP=HS=NUS=PPS=RS=CTS=CTR=FXS=PFS=WG=SCB=GuS>SCG=JOJ=SC=PS=SHI=YH=AS=MC=EYP=PES=AKP=TOS=POS=MS=LOS=CpS=RoS=RB=HyP=WM=PVL=KU=ChS=JCL=JOS=DSBF=FG=BEP=Pea=MM=CMS=CBL=AMS=BTS=CPH=OTS] (de Melo et al., 2014).

As can be seen from Fig. 2.3, the study on Coffee (CFE) and Soybean (SBF) is started in year 1990 and 1995 respectively which is continuously going on until present year. It indicates that maximum research is carried out on CFE and SBF as each contributes 5.6% of total research work done in seed category in 28 and 23 years, respectively. Further, Sunflower seed and Black pepper are subjected to SFE where each contributes 4.3% of total research done in seed category as shown in Fig. 2.3. Then, other seeds i.e. Coriander seed (COR), Clove bud (CB), Grape seed, Canola seed (CS) and *Bixa orellana* (BO) seed are considered as raw materials for SFE as shown in Fig. 2.3. Watermelon seed (WM), Jatropha seed (JS), Fenugreek seed (FG), Camelina seed (CMS), Capsicum seed (CSS), Muskmelon seed (MM) etc. show some scope of research as given in Fig. 2.3 as very limited papers i.e. 5 approx. are available in the literature on SFE of these seeds. In last five years, Coriander (Pavlić et al., 2015; Zekovic et al., 2017, 2016, 2015), Moringa oleifera (Lee et al., 2017; Martins et al., 2016; Porto et al., 2016; Rai et al., 2017; Rodriguez-Perez et al., 2016; Ruttarattanamongkol et al., 2014; Wang et al., 2017; Zhao and Zhang, 2014, 2013a, 2013b), Sunflower (Rai et al., 2016b), Seabuckthorn (Jawad et al., 2013; Mihalcea et al., 2017; Pavlovic et

al., 2016; Zheng et al., 2017), Canola (Honarvar et al., 2013), Bixa orellana (Alcázar-Alay et al., 2017; Rodrigues et al., 2014; Vardanega et al., 2017), Coffee (Barbosa et al., 2014; Manna et al., 2015; Melo et al., 2014), Hemp (K. Aladic et al., 2015; Krunoslav Aladic et al., 2015; Hong et al., 2015; Kitryte et al., 2017)seeds etc are considered for extraction using SFE method. However, no study is reported on the SFE of carrot seed oil which shows a future scope as carrot seed oil has several medicinal properties (Gao et al., 2016).
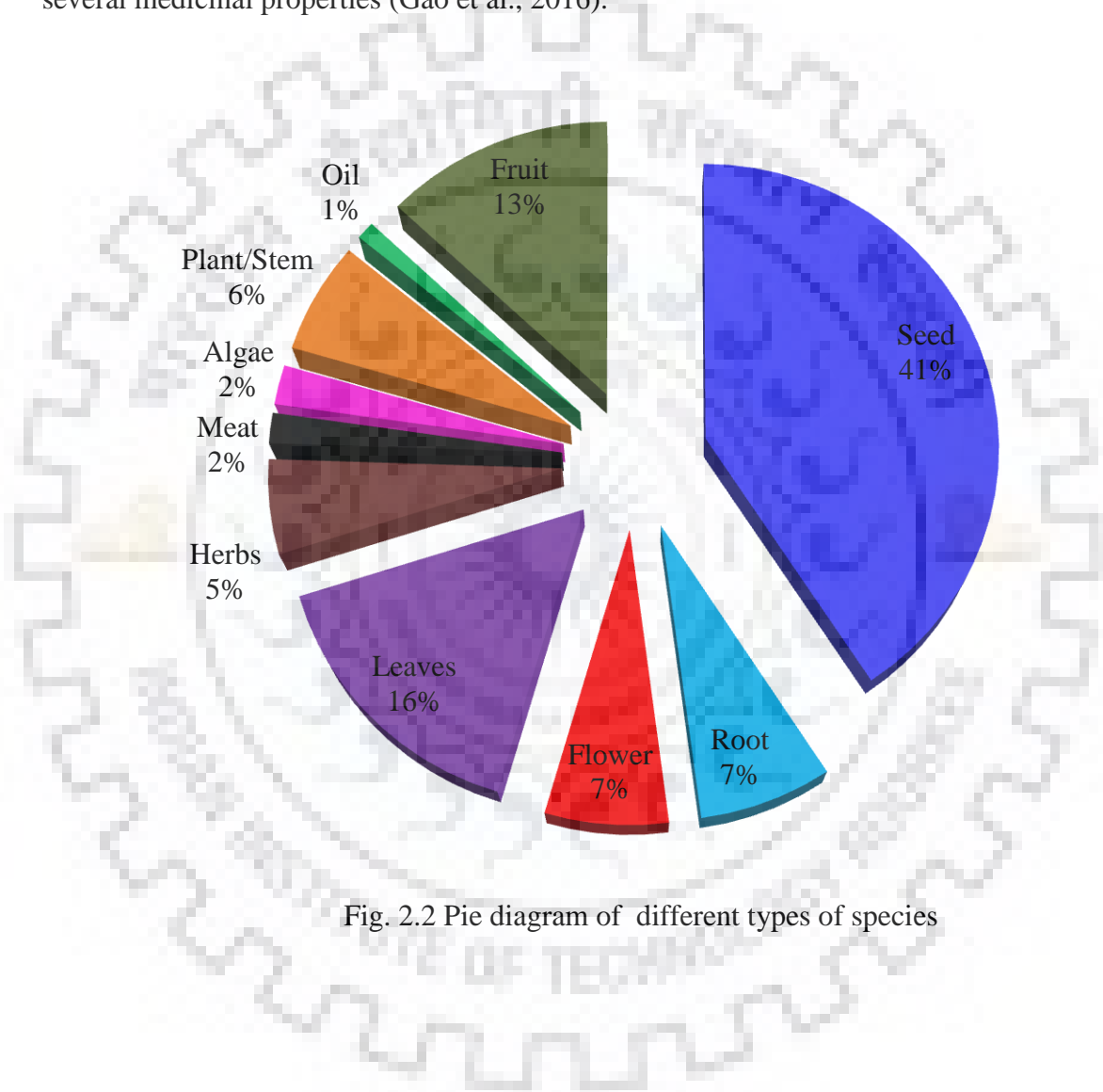
Fig. 2.2 Pie diagram of different types of species
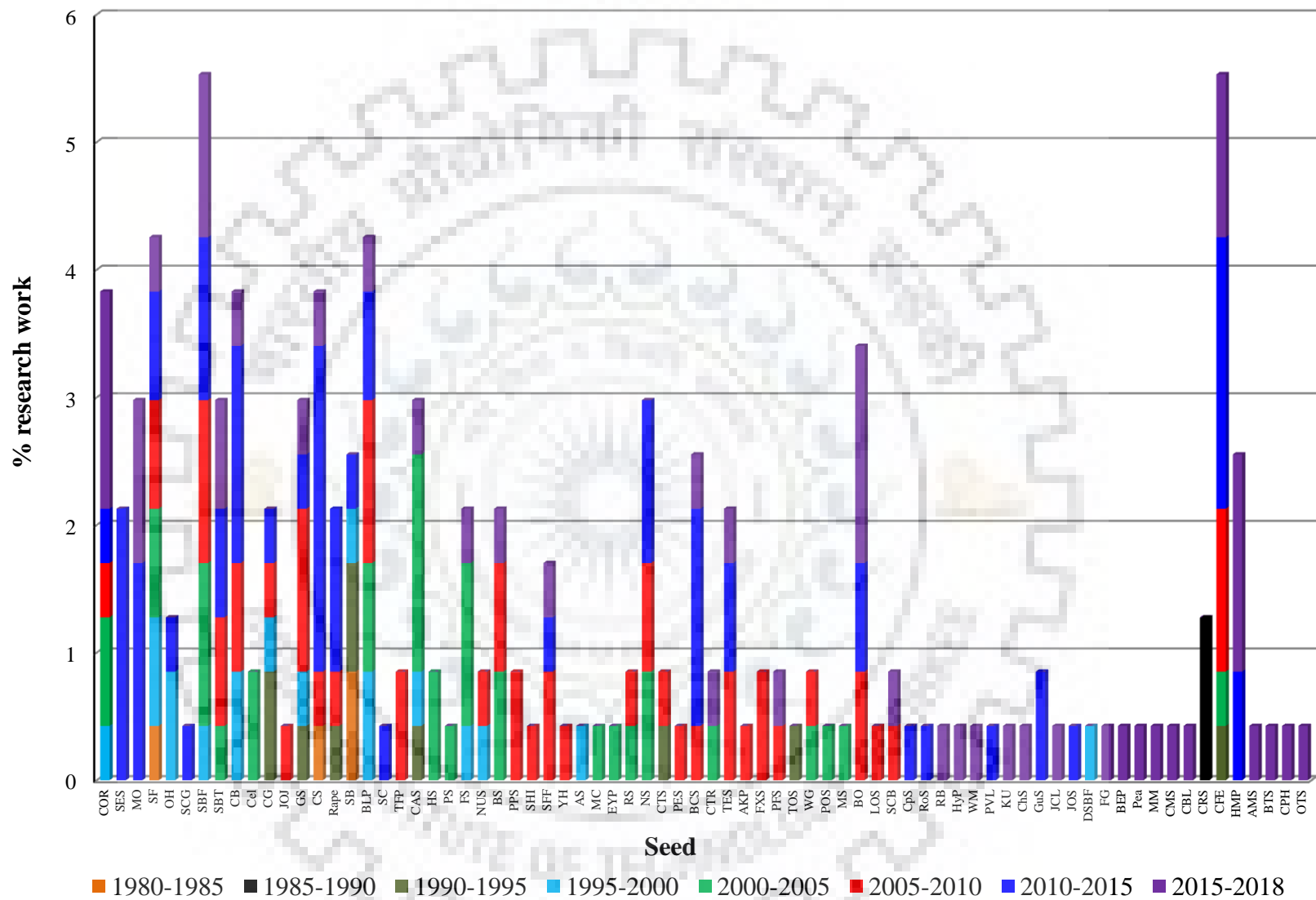
Fig. 2.3 Research work done in seed category.

Similarly, total research work available in the literature for root, flower, leaf, herb, meat, algae, and stem category are shown in Fig. 2.4 to 2.12, respectively. Fig. 2.4 shows the percentage of research work done in leaves category and can be arranged for different type of leaves as:

[GT>EGL>OL>BD>MO=SFL=RoseL>SL=OB=AP=WW>BL=ML=PL=PPL>PGL=FLG=PO=MAL=SA=SML=CL=MCL=HL=PB=BrL=PV=IE=Ditt=PP=CV=ES=EC=PM=SBT] (de Melo et al., 2014).

It shows that research on leaves category was started in 1985 where Peppermint leaves (PL) was considered for SFE as shown in Fig. 2.4. However, maximum research is carried out on Green tea leaves (GT), which contributes approximate 11% of total research done in leaves category followed by Eucalyptus globules (EG), Olive leaves (OL) and Baccharis dracunculifolia (BD). It can be seen from Fig. 2.4 that research on the SFE of leaves is going on till present year, which shows that various type of leaves can be considered as raw material for SFE.

After leaves, fruit category is also explored through SFE to extract oil from various kinds of fruit and its parts as shown in Fig. 2.2. Research work done on different kind of fruits is shown in Fig. 2.5. It shows that fruit category came into existence for the SFE in 1995 until today. Whole Red pepper (RP) is considered for SFE in 2005, which continues up to present year i.e. 2018. It contributes around 14% research work done in fruit category, which is followed by Seabuckthorn (SBT), Paprika (PAP) and Cashew nut shell (CNS).

Flower and root category are less explored in comparison to seed and fruit category as shown in Fig. 2.2. Percentage research work carried out on these categories is given in Fig. 2.6 and 2.7, which show that research was started in year 1990 and 1995 respectively. These figures depict that maximum research is carried out on Marigold flower (MGF) and Ginger root (Gin), which contribute 27% and 30% of total research work done in respective category. SFE of root and flower is less explored because of availability of raw material and oil availability in solute. The research is started on flower category from 1990 and still going on in 2018 though, a few types of flowers are explored for less time of period and then stopped. Jasmine flower (JF) was explored from 1990 to 1995, Lavender flower (LF) and *Spilanthes americana* (SA) were explored in from 1995 to 2000, *Silybum marianum* in from 2000 to 2005, *Gardenia jasminoides Ells* (GJE), *Magnolia officinalis* (MLO) and Chamomile flower (CMH) in from 2005 to 2010 and Hawthorn flower (HF) and Dittany (Ditt) from 2010 to 2015. It can be seen from Fig. 2.7 that turmeric root (TR) is being explored as raw material for SFE from 2000 to present however; precise information on the effects of operating parameters are still not available in literature. Modeling and simulation

15

study for SFE of turmeric root is also not reported in literature which shows a future scope for turmeric root.

Similarly, research in Plant/stem, Herb and Algae categories were started early i.e. in periods of 1985-1990, 1980-1985 and 1990-1995, respectively, as shown in Fig. 2.8 to 2.10. However, number of different types of Algae to be studied using SFE process is less. Research in meat category was started in 1985 as given in Fig. 2.11 although no research can be found in this field after 2010 and reason could be the non-availability of meat and difficulty in the handling as raw material. Fig. 2.12 presents the research work carried out on the fractionation of oil compounds from oil itself. It shows that this category is also less explored where research has been started in a period of 1985-1990. However, not much research was carried out thereafter as this category contributes only 1% of total work done on SFE field as shown in Fig. 2.2. Thus, it can be concluded from Fig. 2.2 to 2.12 that SFE area still has a scope of further research as many natural species are untouched, which posses many health and nutrition benefits.
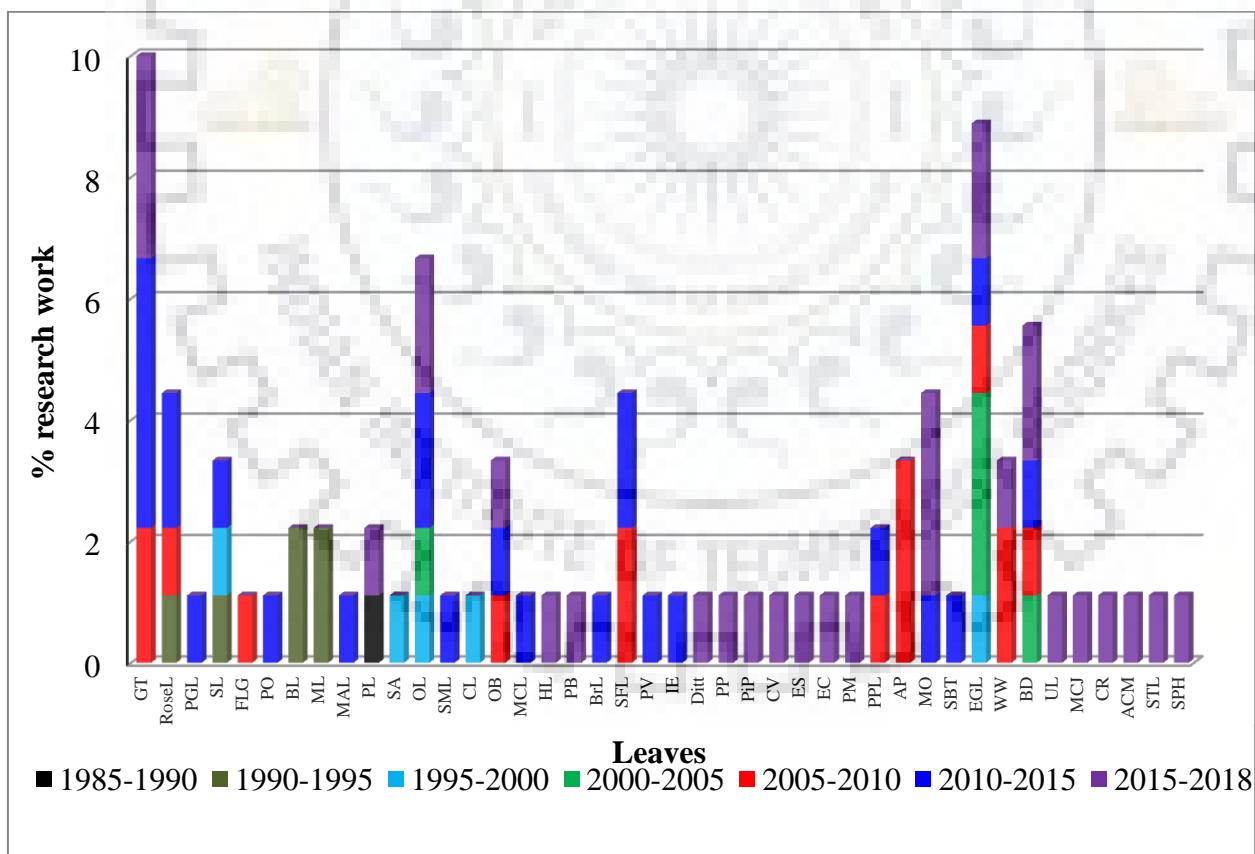
Fig. 2.4 Research work done in Leaves category.

16
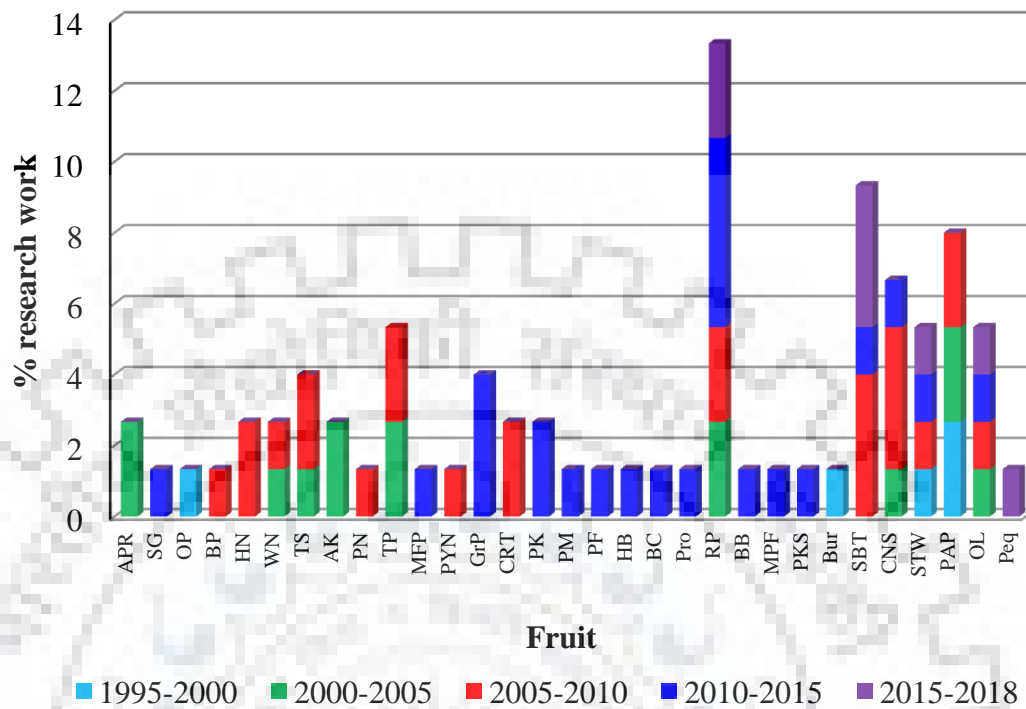
Fig. 2.5 Research work done in Fruit category.
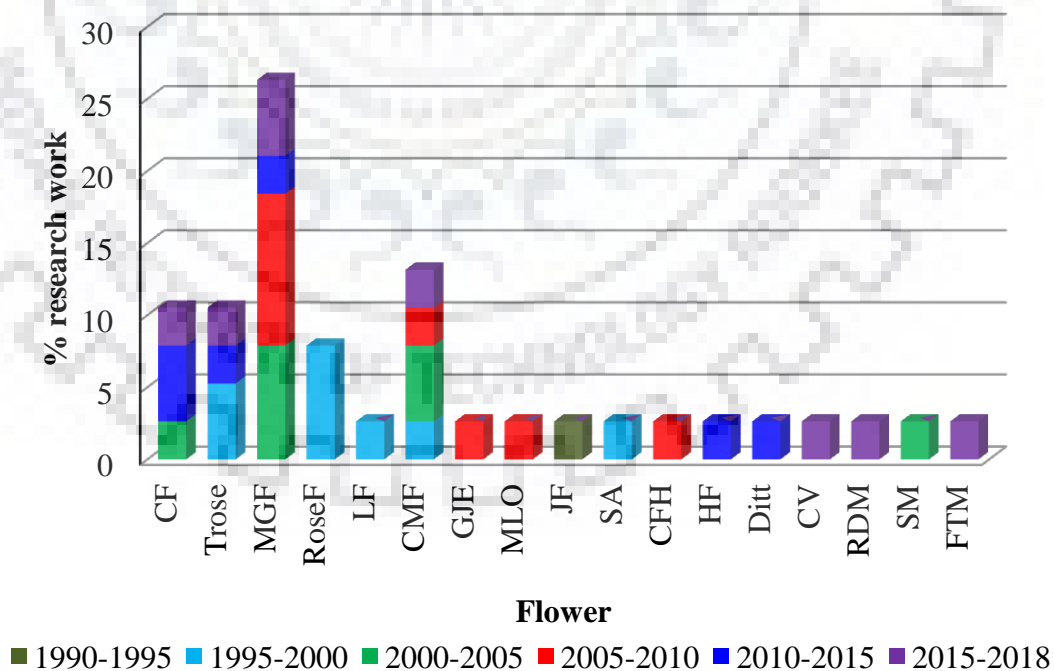
Fig. 2.6 Research work done in Flower category.
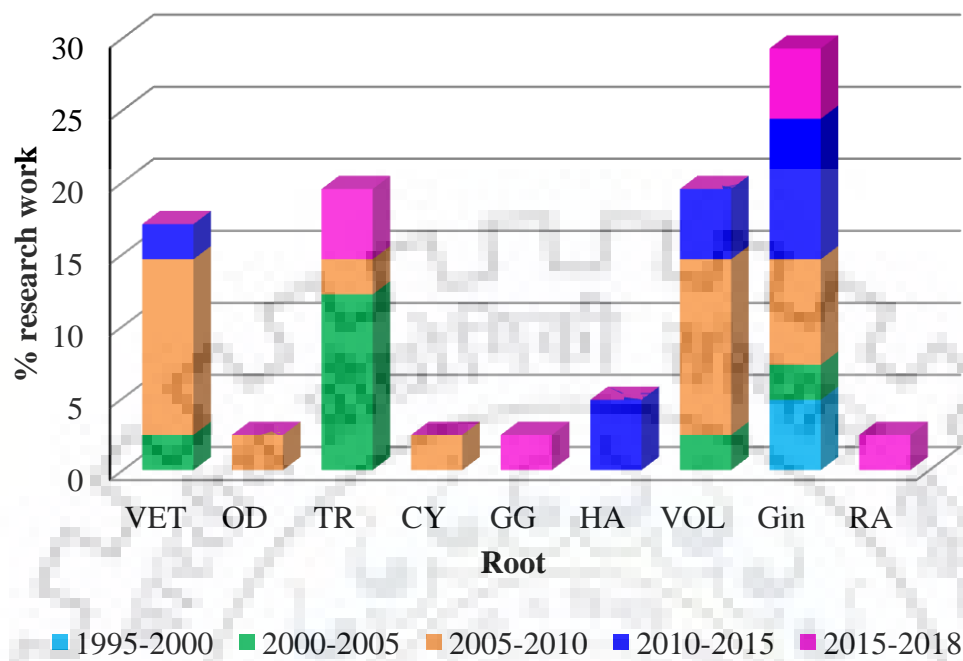
Fig. 2.7 Research work done in Root category.
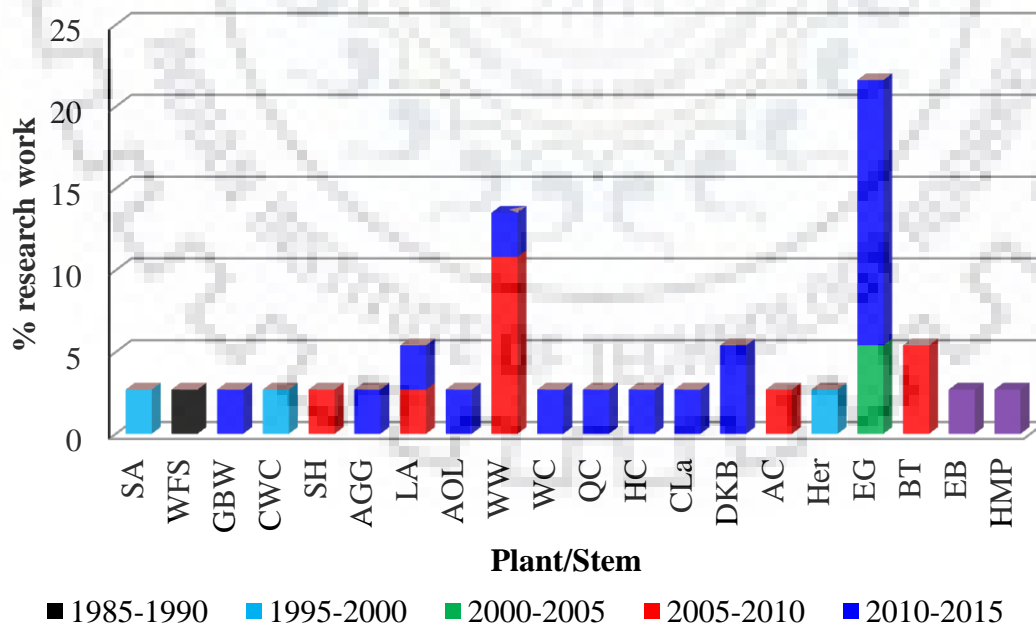
Fig. 2.8 Research work done in Plant/Stem category.
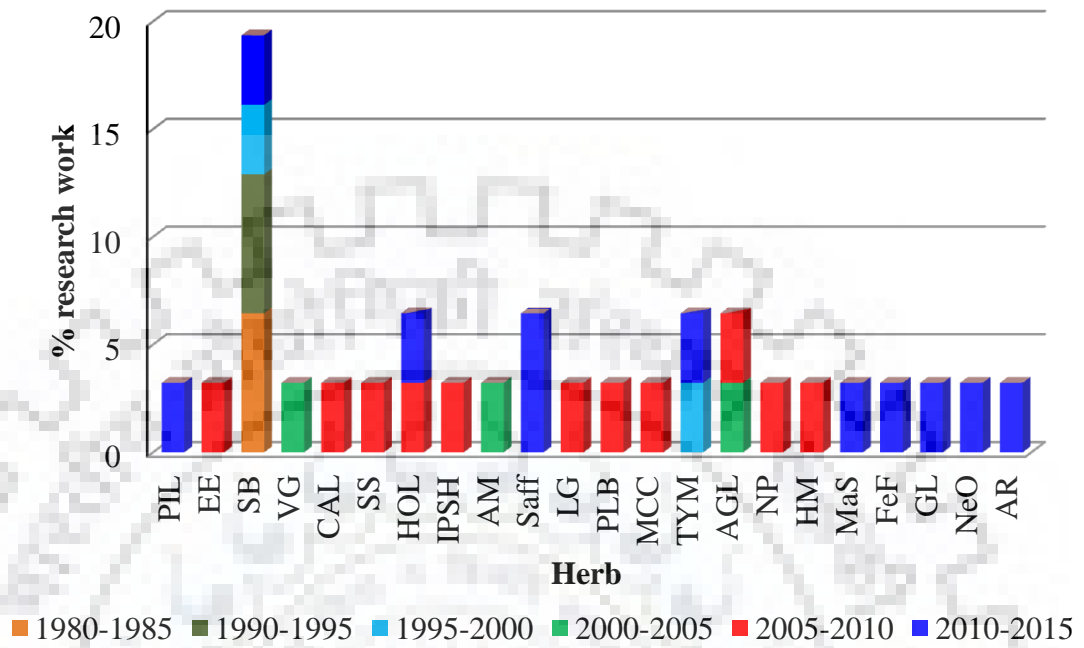
Fig. 2.9 Research work done in Herb category.
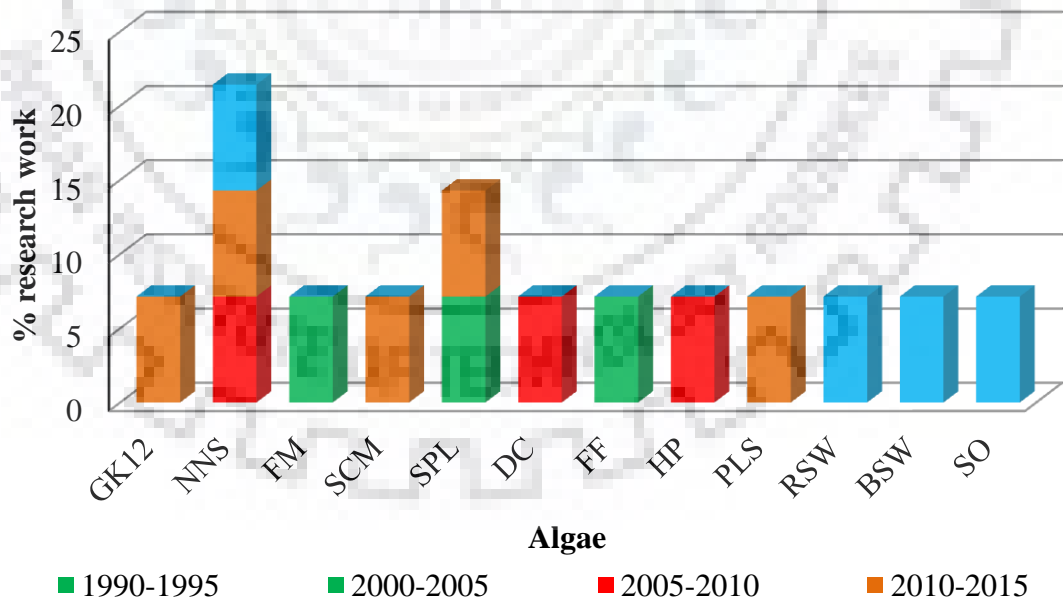
Fig. 2.10 Research work done in Algae category.
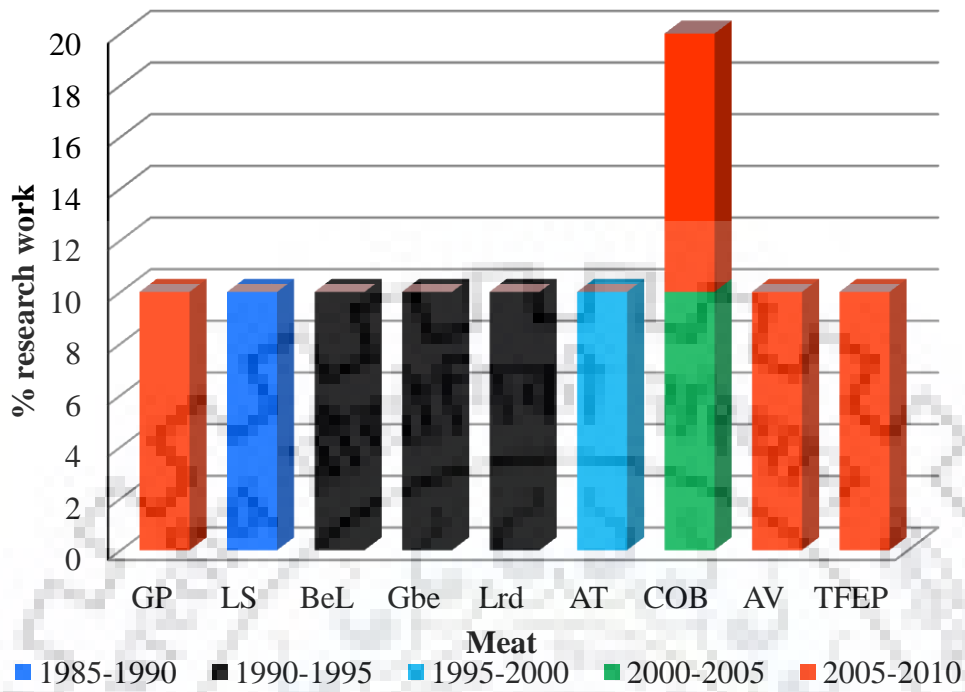
Fig. 2.11 Research work done in Meat category.
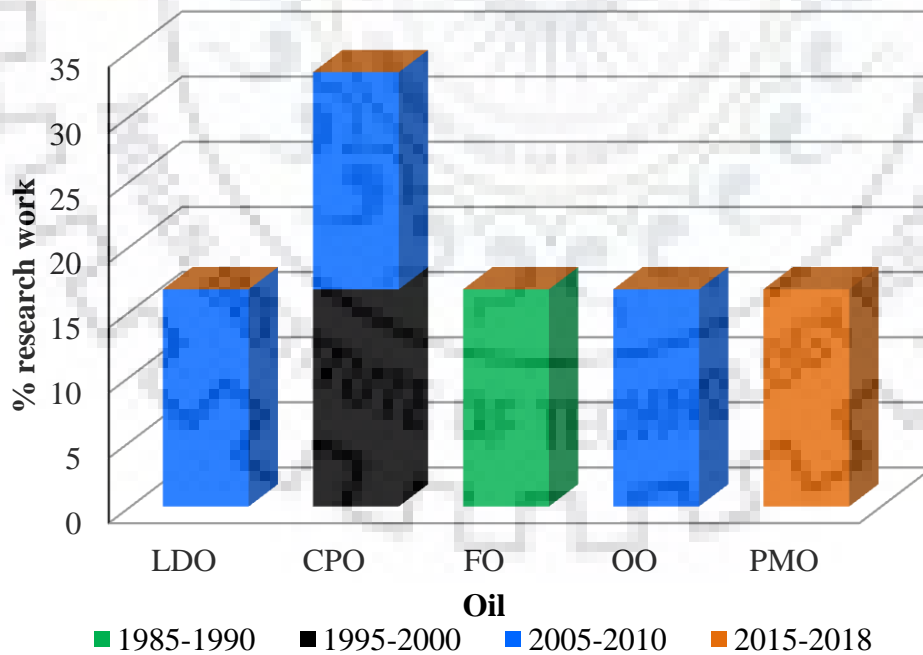
Fig. 2.12 Research work done in oil category.

2.6.2 Selection of SCF

The selection of SCF depends on the specific application and additional factors such as safety, flammability, phase behavior and solubility at operating conditions and of course cost of fluid (Mark McHugh, 1994). A SCF or solvent should posses physical and thermal properties between that of pure liquid and gas (Mukhopadhyay, 2009). It has liquid-like density, gas-like viscosity and diffusivity at least an order of magnitude higher than that of normal liquid, which may result in superior mass transfer characteristics. Further, solvent density as well as solvent effectiveness can be controlled by small changes in temperature and pressure (Ghoreishi and Shahrestani, 2009a). Selection of solvent for the SFE also depends on the fact that it would be able to diffuse up to the centre of the particle of seed (Louli et al., 2004). Various types of supercritical solvent are available as reported in Table 2.2 with respective supercritical properties but very few of these are found useful for the SFE i.e., Carbon dioxide (Asep et al., 2013; Cheah et al., 2010; Zarena et al., 2010), Water (Ghoreishi and Shahrestani, 2009b; Goodarznia and Abdollahi Govar, 2009; Martinez-Correa et al., 2017), Propane (Corso et al., 2010; Pederssetti et al., 2011; Skerget and Knez, 2001), Methanol (Demirbas, 2000), Ethanol (Demirbas, 2000; Martinez-Correa et al., 2017; Sheibani and Ghaziaskar, 2008) and Acetone (Demirbas, 2000). Fig. 2.13 represents a pie diagram of various solvents used in SFE process, which depicts that 95% of total research work is carried out using carbon dioxide as a solvent. Most of researchers used carbon dioxide whereas, a few of these compared CO_2 with other solvent as well. Corso et al. (2010), Pederssetti et al. (2011) and Nimet et al. (2011) used CO_2 and propane as a solvent for the extraction of Sesame oil, Canola oil and Sunflower oil, respectively, and found that the extraction with propane was much faster than that of carbon dioxide. It is due to the fact that propane is a better solvent for vegetable oil due to shorter times and lower pressures required for the extraction compared to carbon dioxide (Pederssetti et al., 2011). Propane has other favorable properties i.e. high solvation power, relatively cheap, does not leave toxic residues and requires lower pressures in comparison to extraction performed with supercritical carbon dioxide (Nimet et al., 2011).

Ghoreishi and Shahrestani (2009)b, Goodarznia and Abdollahi Govar (2009) and Martinez-Correa et al. (2017) used water as solvent for the supercritical extraction in order to avoid organic solvents in the extraction of active or marker compounds from medicinal plants. Subcritical water extraction was investigated as a novel and alternative technology in the food and pharmaceutical

industry (Ghoreishi and Shahrestani, 2009a).

Carbon dioxide is the most desirable supercritical fluid solvent for the extraction of natural products from foods as its critical pressure (73 bars) and temperature (304 K) can be achieved easily. Further, it is an inert, inexpensive, easily available, non-flammable, non-toxic and environmental friendly and often used to replace toxic freons and certain organic solvents (Mohamed and Mansoori, 2002; Mukhopadhyay, 2009). Carbon dioxide is miscible with a variety of organic solvents and is readily recovered after processing.
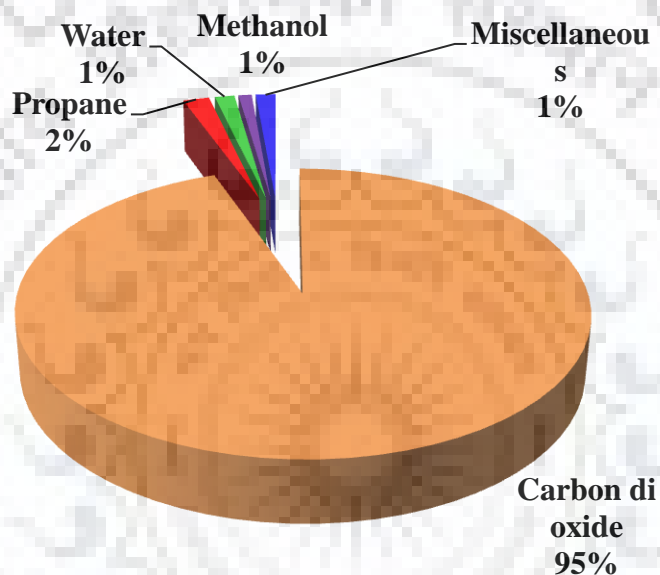
Fig. 2.13 Pie diagram of publications on Solvent used in SFE process.

2.6.3 Selection of co-solvent or modifiers

Supercritical CO_2 is widely used as a non-polar solvent for the extraction of non-polar compounds, such as hydrocarbons (Mukhopadhyay, 2009). In addition, its quadrupole moment also helps for dissolution of some moderately polar compounds such as alcohols, esters, aldehydes and ketones (Beckman, 2004; Lang and Wai, 2001; Mark McHugh, 1994). However, extraction of polar compounds may also be possible or increased by addition of small amount of supercritical polar solvents such as methanol, ethanol, and 2-propanol. The addition of polar co-solvent, increases the polarity of supercritical CO_2 due to dipole-dipole movement and hydrogen bonding (Mukhopadhyay, 2009; Shi et al., 2009).

22

In addition, use of a co-solvent along with supercritical solvent generally increases bulk density of supercritical mixture causing solubility enhancement and thus, increases the extraction yield. Moreover, large variation in density occurs due to large isothermal compressibility in the vicinity of critical points.

Several modifiers such as methanol (Brachet et al., 2000; Nam and King, 1994; Rao et al., 1992; Xiao et al., 2007), ethanol (Danh et al., 2010; Montanari et al., 1999; Rai et al., 2015, 2016a; Sanal et al., 2005), 2-propanol (Kuk and Hron, 1994), acetone (Asep et al., 2013; Demirbas, 2000) etc. are used by different researchers. Table 2.4 contains detailed literature survey (1989-2018) on the use of co-solvents/modifiers in SFE process and it can be observed from Table 2.4 that co-solvents are being used to enhance the extraction yield and reduce the extraction time. Generally, amount of co-solvent used in SFE process is 0 to 30% though some authors considered it upto 90 and 100% of solvent flow rate as can be seen from Table 2.4 (Mendes et al., 2005; Shortle et al., 2013). It is expected that extraction yield should be increased by 10 to 50% after the addition of co-solvents. However, sometimes no significant effect of co-solvent is also observed on extraction yield even if amount added is high enough as observed by Shortle et al. (2013) in the case of SFE of Hawthorn leaf/fruit and berries. Another advantage of adding co-solvent is that extraction time reduces for same value of extraction yield. The extent of utilization of co-solvents/modifiers is given in Fig. 2.14, which shows that Ethanol (64% usage) is used extensively as a modifier for SFE process followed by Methanol (14% usage). Methanol is a very effective polar modifier and is miscible with CO_2 up to 20% (Lang and Wai, 2001). Use of methanol in high percentages with supercritical fluid CO_2 may break the bonding between solutes and plant matrices and enhances yield (Lang and Wai, 2001). Although ethanol is not polar as methanol; however, it is also a convenient choice in SFE of natural products because of its lower toxicity to the human body and high miscibility with supercritical CO_2. Co-solvents (modifiers) are used as operational parameter by varying their amounts in supercritical fluids. A literature review is carried out to find out that which modifier is most used for any type of solute and shown in Fig. 2.15. It depicts that ethanol is widely used modifier for all types of solutes.

Co-solvents may be mixed with the supercritical CO_2 through one of the three different modes; firstly, the modifier can be added directly into the flowing supercritical CO_2 with the help of second pump (Taguchi et al., 1991). Secondly, the known quantity of modifier may be added directly in to CO_2 cylinder while maintaining specific temperature and pressure of the system during extraction process to avoid phase separation (Lang and Wai, 2001; Wheeler and McNally,

1989). Another way of adding co-solvent is to add directly into the sample before extraction. However, third one is a very simple and economic method but it also include major drawbacks such as most of the added modifiers flushed out in the beginning of the extraction, which lead to inconsistent extraction (Fernandez et al., 1996; Marsili and Callahan, 1993).
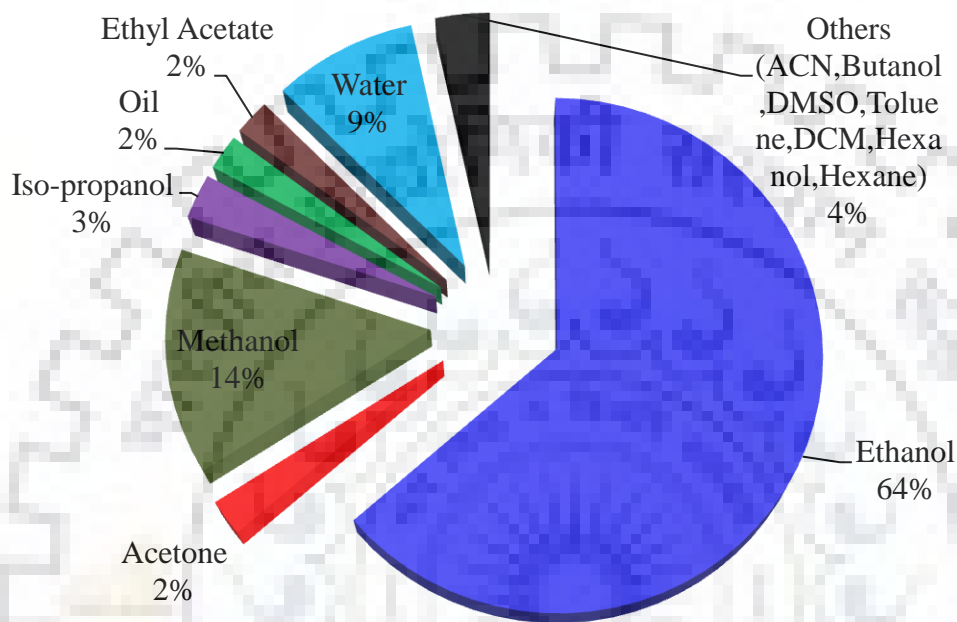
Fig. 2.14 Pie diagram of different co-solvents used in SFE process.
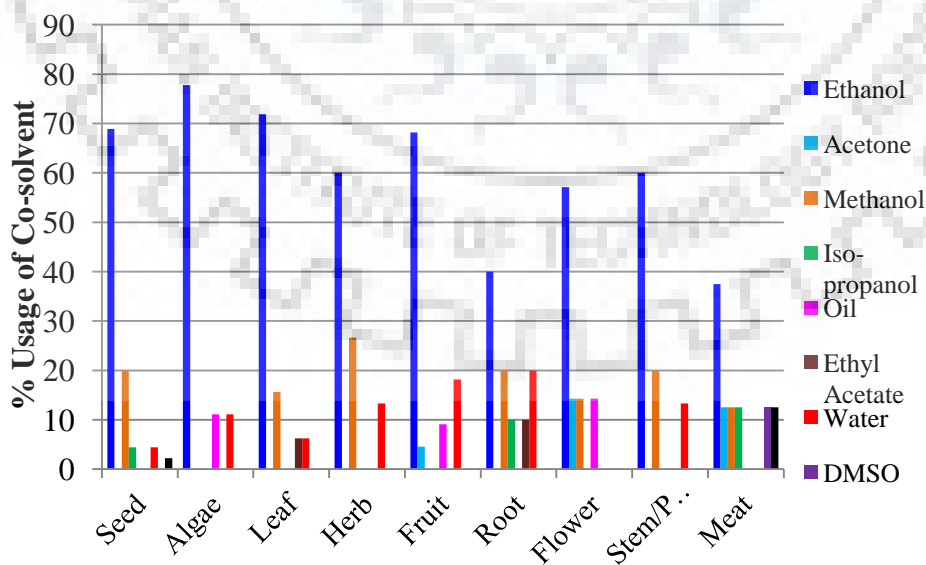
Fig. 2.15 Co-solvents used in SFE of different type of solute matrix.

24

Table 2.4 Type and amount of Co-solvent used in SFE process.

S. No.	Reference	Solute Type	Co-solvent Name	Co-solvent Amount	Yield Pure CO_2	Yield CO_2+Co-solvent
1	Schaeffer et al. (1989)	CrS (seed)	Ethanol	5%		
2	Cygnarowicz-Provost et al. (1992)	*FF (fungi)*	Ethanol	10%	48%	89%
3	Rao et al. (1992)	JF (flower)	Acetone, Methanol, DMSO	3.5%		For Methanol and DMSO-200-600% enhancment For Acetone-solubility of cis-jasmone by 266%
4	Goto et al. (1993)	PL (leaf)	Ethanol	2-6%		-Only extraction rate was increased by adding co-solvent.
5	Taylor et al. (1993)	CG	ACN/methanol (2:1)	(5-20%)	69%	95%
6	Kuk and Hron (1994)	CTS	Ethanol, 2-Propanol	0-5%	30%	33%
7	Nam and King (1994)	Bel, Gbe, Lrd	Methanol	5%	-	20% enhancement
8	(Tong and Imagawa (1995)	PCB	DCM	5-20%	-	90% (15% DCM)
9	Cygnarowicz-Provost et al. (1995)	*FM*	Ethanol	10%	6.71 kg	9.98 kg
10	Cocero and Calvo (1996)	SF	Ethanol	5-20%	-	99%
11	Fernandez et al. (1996)	SDMT	Methanol	2,10%	7%	23%
12	Rónyai et al. (1998)	CG	Ethanol	0-10%	51%	51% (improves functionality of protein material)
13	Montanari et al. (1999)	DSBF	Ethanol	10%	-	100%
14	Lin et al. (1999)	*SB*	Methanol	5-15%	negligble	69%
15	Abaroudi et al. (1999)	α-naph	Toluene	6,10%	21.5%	26.9%
16	Chassagnez-Mendez et al. (2000)	*TR*	Ethanol		6.51%	22.58%
17	Brachet et al. (2000)	CL	Methanol	5-30%	negligble	0.6%
18	King et al. (2001)	VG	Ethanol	5-15%	35%	47%
19	Cocero and García (2001)	SF	Methanol, Ethanol,Butanol, Hexanol	2.5-12.5%	-	49.5%(Methanol) 49.4%(Ethanol) 49.4%(Butanol) 49.5%(Hexanol)
20	Tonthubthimthong et al. (2004)	NS	Methanol	8,10%	85%	99%
21	Yang et al. (2004)	TP	Ethanol	1-20%		
22	Sanal et al. (2005)	APR	Water, Ethanol	2–28%	50%	68% (water) 95% (Ethanol)
23	Mendes et al. (2005)	*AM*	Ethanol	20,100%	0.6%	2%
24	Turner et al. (2005)	CTR	Methanol	1-5%		91.6%
25	Ozkal et al. (2005b)	AK	Ethanol	0-3%	35% (55 min)	35% (extraction time is less,35 min)
26	Rajaei et al. (2005)	TES	Ethanol	7.5,15%	23.7%	31.6%
27	Nobre et al. (2006)	*BO*	Ethanol	5%	1%	45%
28	Sun and Temelli (2006)	CRT	Canola oil	2.5% and 5%	2.7%	9.69%
29	Lin et al. (2006)	*WW*	N-Hexane	0-22.56 %		1.59%
30	Salgin (2007)	JOJ	Ethanol	2-8%	----	-----
31	Xiao et al. (2007)	*MCC*	Methanol	10-40ml		4.69%
32	Lucas et al. (2007)	WG	Ethanol	10%	-	100%
33	Talansier et al. (2008)	VET	Ethanol	0-10%	2.9%	4.7%
34	Salimi et al. (2008)	*VOL*	Ethanol	46.9 μL/g		46.36%

35	Wang et al. (2008)	*PLB*	Ethanol	100-200ml	0.82%	1.7%
36	Liu et al. (2008)	CY	Ethanol,Methanol, 1,2-Propanediol	0.4 mL/min		0.12% (Ethanol) 0.12% (Methanol) 0.13% (1,2-Propanediol)
37	Huang et al. (2008)	TP	Ethanol	16%		93% recovery
38	Vedaraman et al. (2008)	COB	Acetone, 2-propanol, Ethanol	2-6%	48%	52% (2-propanol, Ethanol) 48% (Acetone)
39	Shen et al. (2008)	TFEP	Ethanol	1:1 (TFEP:E)	47.7%	70.1%
40	Sánchez-Vicente et al. (2009)	*DC*	Ethanol	5%		0.6%
41	Bensebia et al. (2009)	Rose	Ethanol	3%	1.8%	3%
42	Kitzberger et al. (2009)	SHI	Ethanol	5-15%	1.2%	4%
43	Ghoreishi et al. (2009)	OL	Ethanol	0-20%	-	1.1%
44	Shi et al. (2009)	TS	Ethanol, water, Olive oil Ethanol + water Water + olive oil Ethanol + olive oil Ethanol +Water+ olive oil	(5-15%) (5 or 10% each) (5%) + water(5%) + olive oil (5%)	25.5%	51.7% (Ethanol) 48.8% (Water) 58.2% (Olive oil) 62.5%(E+W) 73.3%(E+O) 56.8% (W+O) 57.9%(E+W+O)
45	Sánchez-Vicente et al. (2009)	PES	Ethanol	2.5,5%	30%	38%
46	Zhou and Li (2009)	AV	Ethanol	25-100%	-	8.64%
47	Kong et al. (2009)	PPL	Ethanol	70-90%		1.2% [CSA] 0.4% [PI]
48	Khajeh et al. (2010)	*NP*	Methanol	15%	6.2%	8.9%
49	Danh et al. (2010)	VET	Ethanol	15%	3.2%	5.77%
50	Ghafoor et al. (2010)	GrP	Ethanol	5-8%	-	13.22%
51	Comim et al. (2010)	BP	Ethanol	(3.82:1)solvent:co-solvent		6.9%
52	Liau et al. (2010)	*NO*	Ethanol	16.7%	4.7%	15.5%
53	Nyam et al. (2010)	RoS	Ethanol	2 ml/min		112.85% (Recovery)
54	Zahedi et al. (2010)	NS	Methanol	8% and 10%	80%	90%
55	Gao et al. (2010)	MGF	Medium-chain triglycerides (MCTs), sunflower seed oil, soybean oil, rapeseed oil, n-hexane	0.74%-2.26%		1.06% (MCT) 0.96%(SFO) 0.72%(SBO) 0.67%(RSO) 1.03% (Hex)
56	Khajeh (2011)	*SH*	Methanol	0-2.5%	4.7%	5.51%
57	Nguyen et al. (2011)	MO	Ethanol	0-15%	28.71%	31.74%
58	Liu et al. (2011)	MaS	Ethanol/Water	2.0 mL/g	0.3%	0.4%
59	Gracia et al. (2011)	OH	Ethanol	1-5%	12.5%	16%
60	Kagliwal et al. (2011)	SBT	Methanol , Ethanol and Isopropanol	10-30%	Tocopherols 85.45 Carotenes 56.76	Tocopherols 85.47%(Me) 87.36% (Et) 91.14% (IP) Carotenes 59.27%(Me) 62.77% (Et) 70.11% (IP)
61	Martín et al. (2011)	PIL	Ethanol	50 ml	1.2%	2%
62	Yilmaz et al. (2011)	GS	Ethanol	5-20%	-	32.9 (CA)
63	Hegel et al. (2011)	*SC*	Ethanol	9%		90% Lipids
64	Ghasemi et al. (2011)	MCL	Methanol	0-150 µL	5%	6.3%
65	Martín et al. (2011b)	WW	Ethanol	50 mL	2.65%	3.73%
66	Veggi et al. (2011)	*HA,PV,IE, HCS,PVL*	Ethanol	10%	1.55%	2.8%
67	Castro-Vargas et al.	GuS	Ethanol	10%	1.4%	17.3%

	(2010)					
68	Allawzi et al. (2011)	*JOS*	Hexane			88.92%
69	Fujii (2012)	GK12	Ethanol	0-20 ml	0.2% (AXA) 2.9% (Chlorophyll)	0.25% (AXA) 3.1% (Chlorophyll)
70	Domingues et al. (2012)	*EG*	Ethanol	0-5%	0.6%	1.33%
71	Arnaiz et al. (2012)	BrL	Methanol	20-35%		4.5
72	Felfoldi-Gava et al. (2012)	*AGG*	Ethanol	0/5/10%	2.56%	3.81%
73	Santos et al. (2012)	*EG*	Ethanol,Ethyl Acetate,Water	15%(E), 15%(EA), 2% (W)	0.05%	0.32%(E) 0.08%(EA) 0.04% (W)
74	Moura et al. (2012)	PGL	Ethanol,Isopropyl alcohol	5%	-	2.9%
75	Ghoreishi and Heidari (2013a)	GT	Ethanol	1ml	-	7.33%
76	Shortle et al. (2013)	HL,HF,HB	Ethanol	0-90%	2.765%	2.781%
77	Domingues et al. (2013)	*EG*	Ethanol	0-5%	0.77%	1.23%
78	Pilavtepe and Yesil-Celiktas (2013)	*PO*	Ethanol	10 and 20%		80%
79	Honarvar et al. (2013)	CS, SES	Ethanol	10%		63% (SES) 50%(CS)
80	Asep et al. (2013)	COL	Ethanol, Isopropanol, Acetone	5-25%		100% (Et) 95%(IP) 82% (Ace)
81	Scopel et al. (2013)	*SML*	Water, Ethanol	5g/min	2.7%	0.4% (w) 1%(Et)
82	Marsni et al. (2013)	SFL	Ethanol	9%	2.5%	13%
83	Salgin and Salgin (2013)	PK	Ethanol	2.5 and 5%	58%	85%
84	Lemonis et al. (2013)	Ditt	Ethyl Acetate	2% and 5%	5%	7.2%
85	Pimentel et al. (2013)	*PiP*	Ethanol, Methanol	10%	Fresh leaves 0.86% Dry leaves 1.78%	Fresh leaves 3.07% (E) 1.64% (M) Dry leaves 2.54% (E) 2.36%(M)
86	Lim and Lee (2013)	*JCL*	Methanol	1-5 mL/g	-	100%
87	Almeida et al. (2013)	*HC*	Ethanol:Water	0:100-100:0	2.9%	3.6%
88	Guan et al. (2014)	SG	Ethanol	70-90%		2584.9 (ORAC*)
89	Ara et al. (2014)	CpS	Methanol	0-100 μL	16.82%	23.78%
90	Sodeifian et al. (2014)	SmC	Ethanol	1mL		0.7990%
91	Bhattacharya et al. (2014)	PLS	Ethanol	100-200 mL		0.135% (Ergothioneine)
92	Rodriguez-Solana et al. (2014)	FS	Methanol	0-6%	0.45%	1.26%
93	Solana et al. (2014)	*ES*	Water, Etahnol, Methanol	8%	1.5%	29.20% (W) 5054% (E) 5.56% (M)
94	Barbosa et al. (2014)	SCG	Ethanol	0-5%	8.98%	11.97%
95	Végh et al. (2014)	*FeF*	Ethanol	0-10%	2.497%	3.075%
96	García-Abarrio et al. (2014)	*LA*	Ethanol	0-10%	1.87%	3.03%
97	Kazan et al. (2014)	*PP*	Ethanol	6-20%	-	7.99%
98	Patil et al. (2014)	*WC*	Methanol	5-15%	-	$5.9*10^{-3}$%
99	Da Porto et al. (2014)	GrP	Water, Etahnol	15%		10.2% (W) 6.9%(E)

100	Da Porto et al. (2014a)	GrP	Etahnol:Water (15%:57%)	7.5% and 10%		14.6%
101	Hedayati and Ghoreishi (2015)	GG	Water, Methanol (binary)	0-100%	45.42%	71.76%
102	Sharif et al. (2015)	*PB*	Ethanol	0-90%	4.34%	5.60%
103	Rai et al. (2015)	WM	Ethanol	0-10%	51.83%	51.81%
104	Solana et al. (2015)	*AOL*	Water, Etahnol, Methanol, Water:Ethanol (1:1,7:3,3:7)	8%		42.6% (W) 9.5% (E) 5% (M) 37% (W:E::7:3)
105	Şen et al. (2015)	*QC*	Ethanol	10%	2%	3%
106	Garcia-Risco et al. (2015)	*CV*	Ethanol	0-15%	3.35%	7.31%
107	Lin et al. (2015)	*SCB*	Ethanol	0-10.8%	18%	25%
108	Costa et al. (2015)	CLa	Ethanol	0-50%	1.06%	14.5%
109	Fathordoobady et al. (2016)	HyP	Ethanol/Water	0E/100W-100E/0W	Peel 3.91% Flesh 10.36%	Peel 4.12% Flesh 11.76%
110	Li et al. (2016)	*GL*	Ethanol	20%	29.5%	37.2%
111	Nerome et al. (2016)	Saff	Water, Methanol	0.2 mL/min	3.8	3.2 (Water) 3.4 (Methanol)
112	Bermejo et al. (2016)	GT	Ethyl lactate, Ethyl acetate, Ethanol	2% (mass)	3.7%	9.1% (EL) 10.9% (ETOH) 8.1% (EAC)
113	Rai et al. (2016a)	SF	Ethanol	0-10%	54.37%	54.66%
114	Duval et al. (2016)	*KU*	Ethanol Ethanol:Water	5% and 30% 4:1 and 24:6	22.5%	30.4% (E) 44.1% (E:W)
115	Guindani et al. (2016)	ChS	Ethanol, Ethyl acetate	2.5-7.5%	10.6%	11.5% (E) 11%(EA)
116	Ghoreishi et al. (2016a)	PK	Ethanol	1/20 of solvent flow rate	-	31.9%
117	Ghoreishi et al. (2016b)	*RDM*	Ethanol		-	30.4%
118	Reyes et al. (2016)	NeO	Ethanol	10%	-	58%
119	Melo et al. (2016)	*EC*	Ethanol	0 and 5%	0.8%	1.3%
120	Pereira et al. (2016)	PM-L,Be	Ethanol	0.09 kg/h	-	14% (Leaves) 10%(Berries)
121	Zaghdoudi et al. (2016)	PF	Ethanol	5-25%	-	76.07% (Four carotenoids)
122	Rai et al. (2017)	MO	Ethanol	0-10%	0.1784 kg oil/kg CO_2	0.33 kg oil/kg CO_2
123	Ruan et al. (2017a)	*FTM*	Ethanol: Water	80-100%	-	2.8 mg/g (Total Alkaloids)
124	Ospina et al. (2017)	RSW	Ethanol	2,5 and 8%		0.1-3.03%
125	Porto and Natolino (2017)	GS	Ethanol	10,15 and 20%		481-5446 (mg GAE/100 g DM)
126	Santos et al. (2017)	RA	Ethanol	15%		0.78%
127	Sato et al. (2017)	STW	Ethanol, Acetone, Water	0.1 (molar ratio)	0.26%	0.24, 0.24 and 0.26%
128	Cruz et al. (2017)	BTS	Ethanol	2, 5 and 7.5%	13%	16%
129	Falcao et al. (2017)	CR	Ethanol	2-10%	-	1.-5%
130	Ortega et al. (2017)	SP	Ethanol	10%	13%	15%
131	Villanueva-Bermejo et al. (2017)	ACM	Ethanol	0-10%	3.42%	5.15%
132	Ameer et al. (2017)	STL	Ethanol	0-40%	12.81%	15.85%
133	Saravana et al. (2017)	BSW	Sunflower oil, soybean oil, canola oil, ethanol, and water	0.5-2%	1 mg/g	2.2, 2.1, 2.2, 1.8 and 0.2 mg/g

134	Rovetto and Aieta (2017)	HMP	Ethanol	0-10%	95 g	350 g
135	Sokmen et al. (2018)	GT	Ethanol	0.2-0.5 ml/min	-	0.2-3% (Catechin yield)
136	Valadez-Carmona et al. (2018)	CPH	Ethanol	5- 15%		0.15-0.47%
137	Rodrigues et al. (2018)	EG	Ethanol	0-5%	1.52%	3.95%
138	Escobedo-Flores et al. (2018)	OTS	Ethanol	15 ml		1.250 mg GAE/g
139	Derrien et al. (2018)	SPH	Ethanol	0-10%	31.5% (Lutin) 5.3% (Chlorophyll)	78.2% (Lutin) 71.0% (Chlorophyll)

*-Oxygen radical absorbance capacity

2.6.4 Use of design of experiment for optimization of SFE

Quantitative SC-CO$_2$ extraction of extractable materials involves three steps: (i) partitioning of solute from sample to extraction fluid (ii) removal from the extraction vessel and (iii) collection of the extracted solute (Fernandez et al., 1996). All of these must be optimized to obtain the highest extraction efficiency. Experimental designs are being used extensively for optimization of different operating conditions of various processes for achieving high extraction efficiency (Sharif et al., 2014). Therefore, the experimental design is an approach to solve the problem systematically and it is applied to get optimum and valid results with minimum effort, time and resources (Gooding, 2004). The choice of experimental design for SFE depends on objectives of the study, investigators intention, and feasibility of experiment, cost-effectiveness, time consumption and many other important factors (Sharif et al., 2014). Once, these parameters are decided then design of experiment (DOE) can be performed using software like Minitab, MATLAB, Design Expert, and Quantum XL, etc.

Building a design through DOE helps to select a small number of experiments which need to be performed under controlled conditions. This design is obtained in such a way that its analysis will lead to valid statistical inferences. There are a few interrelated steps in building a design as:

1. To define objectives for the research e.g. sort out important input and output variables for a process.

2. To define important input variables, which need to be controlled during the experiment and its maximum and minimum levels.

3. To define the response variables this will describe results of experimental runs.

4. To select the design from all the available standard designs that suits to the objective e.g. number of input design variables that can be performed at a reasonable cost.

29

There are various well-known classes of standard designs available for DOE. Once, the objective, number and nature of input variables, nature of responses and number of experimental runs are decided, the experimental design can be generated using various software like Minitab, Matlab, Design Expert, and Quantum XL etc.

Quantum XL uses Ordinary Least Squares Regression as a primary method of analysis for quantitative outputs. It also supports Binary Logistic Regression for Binary output and Nominal Logistic Regression for Nominal Outputs. Quantum XL automatically selects correct type of regression for any type of model.

2.6.4.1 Screening experimental design (SED)

The key objective of SED is to find most influential input parameter related to desired output amongst all potential parameters (Sharif et al., 2014). Several screening designs were used such as two-level full factorial, two level fractional factorial and Plackett-Burman design (Sharif et al., 2014). These kinds of designs can examine qualitative, quantitative and mixer-related factors simultaneously. Several advantages and disadvantages are reported by Sharif et al. (2014) for above mentioned screening designs. Design expert version 10.0 has a new user friendly feature of "Design wizard" which actually guides to user interface. Design wizard contains three stages of designing: screening, characterization and optimization. While choosing screening stage, it asks for no of operating parameters need to be screened and based on these, it suggests minimum number of experimental runs.

2.6.4.2 Response surface methodology (RSM)

DOE is mainly classified into four categories such as: Factorial design, full or fractional, (FFD), Mixture design, Response surface method (RSM) and Taguchi orthogonal array design (OAD) method.

Amongst all categories of DOE, RSM is essentially a set of mathematical and statistical methods for experimental design. RSM is capable of evaluating effects of variables and searching optimum conditions, required to predict targeted responses. It is also used extensively in industrial research where large number of variables affects the process. It is a well suited approach to study the primary and interactive effects of distinct variables and also for optimization of the process. Many authors adopted the RSM to optimize the extraction of vegetable oil from the various seed materials with SC-CO$_2$ (Jiao et al., 2008; Liu et al., 2009; Mitra et al., 2009; Rai et al., 2016a). Various design techniques, which fall under RSM, are

- Three-level factorial design (FD)
- Central composite design (CCD) and
- Box-Behnken design (BBD)

The three-level design is denoted as 3^k factorial design and used by several authors to optimize the SFE process (Corso et al., 2010; Danh et al., 2010; Ferreira et al., 1999). It means that 'k' factors are considered, each at three levels. Usually, these are referred to as low, intermediate and high levels as -1, 0 and +1, respectively.

CCD is another design of the RSM, which consists of factorial or cube points, axial or star points and center points(Sharif et al., 2014). There are 2k cube points, where k is the number of factors/input parameters. The cube portion and its center points may serve as a preliminary stage where first-order linear model can be fitted. However, these points can also be used for the fitting of a second-order (quadratic) model.

The most commonly used design of RSM is the central composite design (CCD), which has been suggested by Box and Wilson in the 1957 (Sharif et al., 2014). It is used to estimate a model that has at least as many different combinations as terms in the models and has at least three levels for each variable. CCD is the most popular of many classes of RSM designs as it can be run sequentially, and is very efficient and flexible. Amongst different classes of CCDs such as rotatable, spherical, face centered, etc., face centered design ($\alpha=1$) is simpler one as it requires operating the process at only three levels of each variable in contrast to other five level designs. The increased number of reconfigurations in rotatable or spherical design may introduce greater chances for sources of experimental error associated with setup and operational procedures. However, benefits of rotatable or spherical designs do not offset the added complexity and associated risk in most cases. Therefore, face-centered CCD is found more than adequate for most experiments (Montgomery, 2004).

BBD is one of the classes of rotatable or nearly rotatable second-order designs, which is based on three-level incomplete factorial designs (Demirbas, 2000; Ozkal et al., 2005a). The number of experiments (N) required for the development of BBD is defined as $N=2k$ $(k-1)$ $+C_o$, (where, k is number of factors and C_o is the number of central points). For comparison, the number of experiments for a CCD is $N=2k$ $+2k$ $+C_0$ (Ferreira et al., 2007). Several researchers used optimization design techniques from more than 20 years as shown in Table 2.5 where number of parameters considered for optimization is from 2 to 5. These parameters are pressure (P),

temperature (T), flow rate (FR), co-solvent (CS), particle size (PS), dynamic time (DT), extraction time (ET), crushed glass (CG), solvent volume (SV), density (ρ) and static time (ST). Number of operating parameters/ input parameters shows total required number of experimental runs to perform so the selection of operating parameters should be done wisely. If number of operating parameters to be optimized is five or greater than five then, screening design should be used to reduce the number of operating parameter. It gives a measure of contribution of individual parameter on response and helps in finding the less contributing factor, which can be neglected for optimization design process (Sharif et al., 2014). Several parameters affect SFE process, which need to be optimized for maximizing the oil yield, which is very cumbersome and time consuming. Therefore,. Most of the researchers have considered two main parameters for optimization i.e. Temperature and Pressure. Other than these parameters, flow rate of solvent, extraction time, particle size, addition of co-solvent and density of solvent are also considered as input parameters as shown in Table 2.5. It can be concluded from Table 2.5 that optimization techniques are being used extensively from the year 1993-2018 where CCD is adopted majorly.
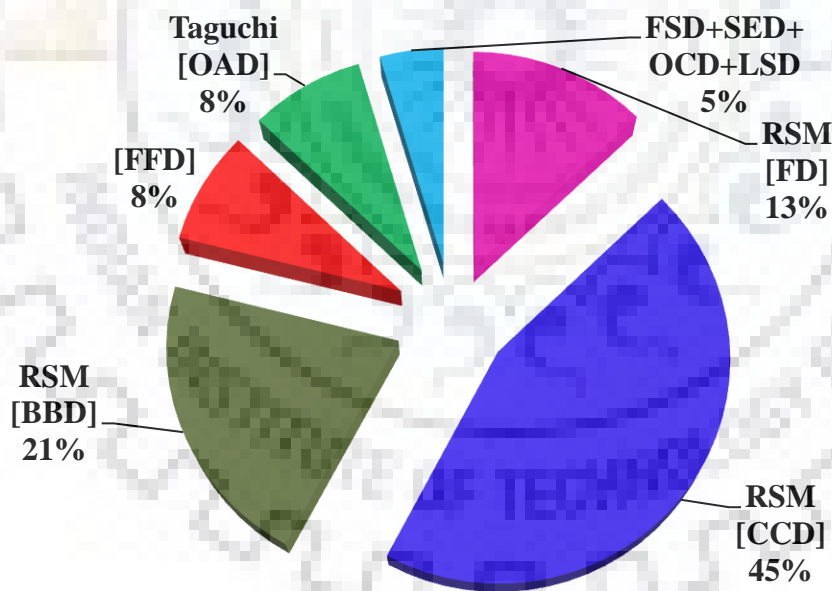
Fig. 2.16 Pie diagram of publications on design of experiment techniques.

A pie diagram is shown in Fig. 2.16, which depicts the number of research article published on different design techniques. It shows that CCD contributes 45% of total research work followed by

32

BBD (21%) and FD (13%) under RSM. Other techniques such as Taguchi-OAD, FFD, least significant difference (LSD), orthogonal composite design (OCD), factorial spherical design (FSD) and screening experimental design (SED) are also applied for optimization of SFE process.

CCD is adopted mostly because both linear and quadric models can be determined by this design, which provides less number of experiments for given factors and central point. CCD could be a good alternative of a three level full factorial design as it provides comparable results with smaller number of experiments. A further refining of literature on optimization design techniques is done to find out the best optimization designs for different type of solutes as shown in Fig. 2.17. It shows that CCD is the mostly adopted design technique for all types of solute matrices followed by BBD. Other than CCD and BBD, Taguchi and FFD design are also used for optimization of SFE of leaves and roots.
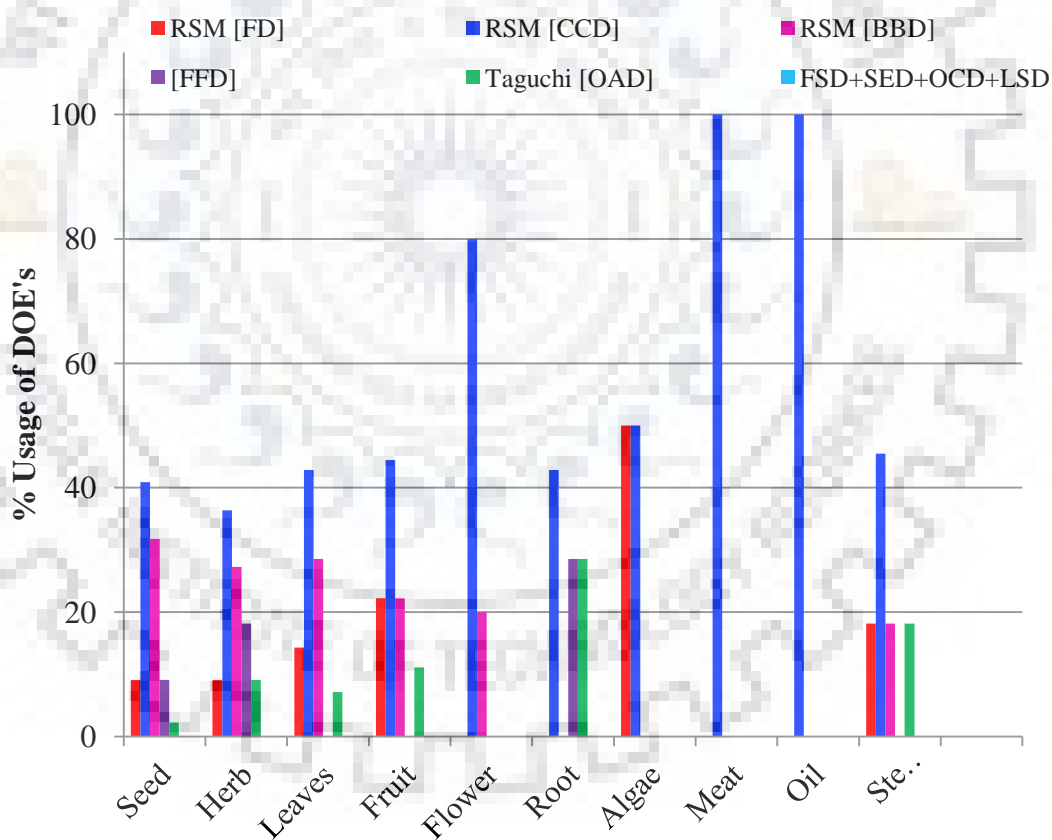
Fig. 2.17 Solvents used in SFE of different type of solute matrix.

Table 2.5 Optimization designs used for the SFE of different type of solute.

S. No.	References	Design	Solute type	Solute	Levels	Operating parameters
1	Kane et al. (1993)	RSM [FD]	Mixture of steroid	Steroidal compounds	Four	T, ρ , FR, ET
2	Lanças et al. (1995)	[FFD]	Herb	SB	Four	T,P,PS,DT
3	Fernandez et al. (1996)	RSM [CCD]	Sediment	SDMT	Two	T,P
4	Barrado et al. (1997)	[SOD]	Black residue	black residue	Three	T,P,DT
5	Notar et al. (1997)	[FSD]	PAH	Spiked soil	Four	P, T, FR, CS
6	Zhou et al. (1997)	[SED]	Pesticide residues	soil sample	Three	T,P, CS
7	Ferreira et al. (1999)	RSM [FD]	Seed	BLP	Four	T,P,PS,FR
8	Fullana et al. (2000)	[FFD]	Seed	BCS	Three	T,P,DT
9	Brachet et al. (2000)	RSM [FD]	Leaves	CL	Three	T,P,PS
10	Moldao-Martins et al. (2000)	RSM [CCD]	Herb	TYM	Three	T,P,DT
11	Oliveira et al. (2002)	RSM[CCD]	Seed	WN	Four	T,P,PS,DT
12	Bozan and Temelli (2003)	LSD	Seed	POS	Two	T,P
13	Sanal et al. (2005)	RSM [FD]	Pomace	APR	Four	T,P,PS,FR
14	Turner et al. (2005)	RSM [BBD]	Seed	CTR	Three	T,P,DT
15	Ozkal et al. (2005b	RSM [BBD]	Seed	AK	Three	T,P,FR
16	Lin et al. (2006)	RSM [CCD]	Stem/Plant	*WW*	Two	T,P
17	Huynh et al. (2007)	RSM [FD]	Herb	LG	Four	T,P,PS,DT
18	Xiao et al. (2007)	TM [OAD]	Herb	MCC	Four	T,P,PS,DT
19	Bhattacharjee et al. (2007)	RSM [CCD]	Seed	CTS	Three	T,P,DT
20	Wang et al. (2008)	RSM [BBD]	Herb	PLB	Two	T,P
21	Yothipitak et al. (2008)	RSM [CCD]	Algee	HP	Three	T,P,DT
22	Yothipitak et al. (2008)	RSM [CCD]	Seed	AKP	Three	T,P,DT
23	Saikaew and Kajorncheappunngam (2008)	RSM [FD]	Seed	GS	Two	T,P
24	Tan et al. (2008)	RSM [CCD]	Cocoa liquor	COL	Four	T,P,PS,DT
25	Huang et al. (2008)	RSM [CCD]	Seed	TP	Three	T,P,DT
26	Jiao et al. (2008)	[OCD]	Seed	FXS	Four	T,P,PS,DT
27	Davarnejad et al, (2008)	RSM [CCD]	Oil	CPO	Three	T,P,DT

28	Liu et al. (2008)	OAD	Root	CY	Four	P, T, ET, CS
29	Sheibani and Ghaziaskar (2008)	FD	Fruit	PN	Three	T,CG,SV
30	Shen et al. (2008)	RSM	Meat	TFEP	Two	P,CS
31	Liu et al. (2009)	RSM [FFD]	Root	OD	Four	T,P,FR,DT
32	Mitra et al. (2009)	RSM [CCD]	Seed	PPS	Three	T,P,DT
33	Liu et al.(2009)	RSM[CCD]	Seed	PFS	Four	T,P,PS,DT
34	Ozkal (2009)	RSM [BBD]	Seed	FXS	Three	T,P,FR
35	Danh et al. (2009)	RSM [CCD]	Root	VET	Three	T,P,DT
36	Kong et al. (2009)	RSM [CCD]	Leaves	PPL	Three	T,P,ET
37	Corso et al. (2010)	RSM [FD]	Seed	SES	Three , Four	For CO_2, T,P,FR For propane, T,P,FR,PS
38	Danh et al. (2010)	RSM [CCD]	Root	VET	Three	T,P,FR
39	Zhang et al. (2010)	RSM [CCD]	Seed	YH	Four	T,P,PS,FR
40	He et al. (2010)	RSM [CCD]	Flower	GJE	Three	T,P,FR
41	Zarena et al. (2010)	RSM [BBD]	Seed	MFP	Three	T,P,FR
42	Hou et al. (2010)	RSM [CCD]	Meat	GP	Three	T,P,DT
43	Cheah et al. (2010)	TM [OAD]	Flower	MLO	Four	T,P,PS,DT
44	Nie et al. (2010)	RSM [BBD]	Herb	HM	Three	T,P,DT
45	Li et al. (2010)	RSM [BBD]	Seed	SCB	Two	T,P
46	Ghafoor et al. (2010)	OAD	Fruit	GrP	Three	P, T, CS
47	Nyam et al. (2010)	RSM [CCD]	Seed	RoS	Three	T,P,FR
48	Gao et al. (2010)	RSM [CCD]	Flower	MGF	Three	P,T,CS
49	Mhemdi et al. (2011)	LSD	Seed	COR	Four	T, P, PS,FR
50	Nguyen et al. (2011)	RSM [CCD]	Seed	MO	Four	T,P,PS,FR
51	Nimet et al. (2011)	RSM [FD]	Seed	SF	Three , Four	For CO_2, T,P,FR For propane, T,P,FR,PS
52	Gracia et al. (2011)	RSM [FD]	Husk	OH	Four	T,P,FR,PS
53	Kagliwal et al. (2011)	RSM [BBD]	Seed	SBT	Four	T,P,FR,DT
54	Pederssetti et al. (2011)	[FFD]	Seed	CS	Four, Five	For CO_2, T,P,FR,DT For propane,

					T,P,FR,DT,PS
55	Liu et al. (2011)	RSM [BBD]	Herb	MaS	Three	P, T,CS
56	Khajeh (2011)	RSM [BBD]	Stem/Plant	SH	Three	P, T, CS
57	Ghasemi et al. (2011)	RSM [CCD]	Leaves	MCL	Five	P,T,ST,DT,CS
58	Santos et al. (2012)	FFD	Root	*EG*	Three	T,CS,FR
59	Moura et al. (2012)	FD	Leaves	*PGL*	Two	P,T
60	Ghoreishi and Heidari (2013a)	RSM [CCD]	Leaves	GT	Five	T,P,FR,PS,DT
61	Domingues et al. (2013)	RSM [FD]	Bark	EG	Three	T,P,CS
62	Guan et al. (2014)	RSM [CCD]	Molasses	SG	Five	T,P,FR,PS,DT
63	Akalin et al. (2013)	RSM [CCD]	Stem	GBW	Two	T,DT
64	Santos et al. (2013)	RSM [CCD]	Leaves	MAL	Four	T,P,FR,PS
65	Shortle et al. (2013)	RSM [BBD]	Leaves,Flower,Fruit	HL,HF,HB	Three	P,T,CS
66	Zhao and Zhang (2013a)	[OAD]	Leaves	MOL	Three	P,T,ET
67	Barbosa et al. (2014b)	RSM [BBD]	Seed	SCG	Three	T,P,FR
68	Ara et al. (2014)	FFD/CCD	Seed	CpS	Four	P, T, ET, CS
69	Shao et al. (2014)	RSM [CCD]	Herb	*AR*	Four	T,P,FR,ET
70	Sodeifian et al. (2014)	RSM [CCD]	Stem/Plant	SmC	Four	T,P,FR,ET
71	Bhattacharya et al. (2014)	RSM	Algae	PLS	Three	P,T,CS
72	Rodriguez-Solana et al. (2014)	RSM [BBD]	Seed	FS	Three	P,T,ET
73	Zordi et al. (2014)	RSM [CCD]	Fruit	Pro	Three	P,T,ET
74	Végh et al. (2014)	RSM [FFD]	Herb	FeF	Three	P,T,CS
75	Anggrianto et al. (2014)	Taguchi [OAD]	Seed	BEP, Pea	Three	P,T,FR
76	Kazan et al. (2014)	RSM [BBD]	Leaves	*PP*	Three	P,T,CS
77	Patil et al. (2014)	Taguchi [OAD]	Stem/Plant	*WC*	Four	P,T,CS,ET
78	Hedayati and Ghoreishi (2015)	RSM [CCD]	Root	GG	Five	T,P,FR,DT, CS
79	Mackela et al. (2015)	RSM [CCD]	Fruit	BC	Three	P,T,ET
80	Przygoda and Zyna Wejnerowska (2015)	RSM [CCD]	Seed	QS	Three	P,T,ET
81	Sharif et al. (2015)	PBD,BBD	Leaves	*PB*	PBD-Five BBD-Three	PBD-T,P,FR,ET, CS BBD-T,P,CS
82	Rai et al. (2015)	RSM [CCD]	Seed	WM	Five	T,P,FR,PS, CS

83	Danlami et al. (2015)	RSM [BBD]	Seed	CTR	Three	T,P,FR
84	Povilaitis and Venskutonis (2015)	RSM [CCD]	Seed	RB	Three	P,T,ET
85	Nejad-Sadeghi et al. (2015)	Taguchi [OAD]	Stem/Plant	DKB	Five	P,T,PS,FR,ET
86	Maran and Priya (2015)	[BBD]	Seed	MM	Four	P,T,FR,ET
87	Costa et al. (2015)	RSM [BBD]	Stem/Plant	CLa	Three	P,T,CS
88	Belayneh et al. (2015)	RSM [CCD]	Seed	CMS	Three	P,T,ET
89	Ghoreishi et al. (2016a)	RSM [CCD]	Bark	PK	Four	T,P,FR,ET
90	Goleroudbary and Ghoreishi (2016)	[CCD]	Herb	Saff	Four	T,P,FR,ET
91	Sodeifian et al. (2016b)	RSM [CCD]	Stem/Plant	*DKB*	Four	T,P,FR,DT
92	Bogdanovic et al. (2016)	RSM [CCD]	Seed	FG	Three	T,P,FR
93	Li et al. (2016)	RSM [CCD]	Herb	*GL*	Three	P,T,ET
94	Ahmed et al. (2012)	RSM	Leaves	RoseL	Two	P,T
95	Ghoreishi et al. (2016b)	RSM [CCD]	Flower	*RDM*	Four	P,T,ET,FR
96	Zaghdoudi et al. (2016)	RSM [CCD]	Fruit	PF	Five	P,T,CS,ET,FR
97	Sodeifian et al. (2016a)	RSM [CCD]	Fruit	PKS	Four	P,T,FR,ET
98	Wang et al. (2016)	RSM [BBD]	Seed	GPS	Three	P,T,ET
99	Rai et al. (2016a)	RSM [CCD]	Seed	SF	Five	P,T,CS,PS,FR
100	Ruan et al. (2017)	RSM [CCD]	Flower	*FTM*	Four	P,T,ET,CS
101	Salea et al. (2017)	Taguchi [OAD]	Root	Gin	Three	P,T,FR
102	Gilbert-Lopez et al. (2017)	RSM [FD]	Algae	*SO*	Two	P,T
103	Sodeifian et al. (2017)	RSM [CCD]	Stem/Plant	*EB*	Four	P,T,PS,ET
104	Ospina et al.,2017	RSM [CCD]	Algae	RSW	Three	P,T,CS
105	Wang et al. (2017)	RSM [BBD]	Leaves	MO	Three	ET,T,CS
106	Da Porto and Natolino (2017)	RSM [BBD]	Seed	*GS*	Three	P,FR,CS
107	Belbaki et al. (2017)	RSM [BBD]	Fruit	OL	Three	P,T,ET
108	Sodeifian et al. (2017b)	RSM [CCD]	Seed	*DKB*	Four	P,T,PS,DT
109	Rodrigues et al. (2018)	RSM [FD]	Leaves	*EG*	Four	P,T,FR,CS
110	Kueh et al. (2018)	RSM [CCD]	Leaves	*MCJ*	Three	P,T,FR
111	Patil et al. (2018)	RSM [FD]	Algae	*NNS*	Three	P,T,CS
112	Sodeifian et al. (2018)	RSM [CCD]	Seed	*POA*	Four	P,T,PS,DT
113	Valadez-Carmona et al. (2018)	RSM [BBD]	Seed	*CPH*	Three	P,T,CS

2.6.5 Effect of various operating parameters on SFE

The selection and optimization of various operating parameters, provided in Table 2.5, plays an important role in SFE process. Several researchers studied the effect of various parameters such as pressure, temperature, solvent flow rate, particle size, extraction time, bed void fraction, pretreatment of raw material, moisture content and initial oil content on the extraction yield using SFE process (Döker et al., 2010; Papamichail et al., 2000; Pederssetti et al., 2011; Rai et al., 2016a; Shilpi et al., 2013).

2.6.5.1 Effect of pressure

SFE is referred as a high pressure technology where pressure has supreme importance due to many technical and economic aspects of this process (de Melo et al., 2014). Pressure directly affects the density of supercritical solvent and consequentially, solvent power is affected (Mukhopadhyay, 2000; Zaghdoudi et al., 2016; Zarena et al., 2010).

The density of CO_2 shows non-linear behavior with temperature and pressure and therefore, CO_2 properties such as density, viscosity, acentric factor etc. must be selected or calculated carefully at desired pressure and temperature (Span and Wagner, 1996). In addition, pressure can be considered an important factor to tune the selectivity of the SCF. The solubility of solutes in SCF is also a main concern to determine the extraction efficiency (Lang and Wai, 2001). An isothermal increase in pressure increases density of the solvent as well as solubility of solute in solvent whereas vapor pressure decreases (Shilpi et al., 2013). However, high pressure is not always recommended because elevated pressure also has negative effect on extraction yield as solute-solvent repulsion occurs from the highly compressed solvent (CO_2) (Liu et al., 2009; Sodeifian et al., 2016a). On other hand, an isothermal increase in pressure reduces the extraction of selective compounds from solutes (Pourmortazavi and Hajimirsadeghi, 2007; Reverchon and De Marco, 2006). Therefore, SFE at high pressure is not favorable for selective extraction. In addition, the extraction of undesired compounds of solute can change the solubility level of the solute of interest (Pourmortazavi and Hajimirsadeghi, 2007).

Various researchers studied the effect of pressure on the extraction yield of different type of solute matrices. In leaves category, coca leaves, pigeonpea leaves, *Myrtus communis* leaves, green tea leaves, mango leaves and Eucalyptus globules are considered for SFE considering pressure as variable parameter (Brachet et al., 2000; Ghasemi et al., 2011; Ghoreishi and Heidari, 2013; Kong et al., 2009; Rodrigues et al., 2018; Santos et al., 2013). Similarly, the effect of pressure on roots

such as *Corydalis yanhusuo*, Vetiver root, Ginger root, etc. (Danh et al., 2010; Liu et al., 2008) and flowers such as *Fritillaria thunbergii Miq, Rosa damascena Mill*, Marigol flower (Gao et al., 2010; Ghoreishi et al., 2016b; Ruan et al., 2017) is also studied. For seed category, large number of research articles is published, which study the effect of pressure on extraction yield as provided in Table 2.5. It can be noticed from literature review on the effect of pressure that extraction yield increases with pressure whereas sometimes it decreases also. It may be due to the enhancement of solubility and occurrence of repulsion between solute and solvent, respectively. Therefore, it can be concluded that pressure plays a vital role in maximizing the extraction yield of any solute matrix and its effect must be studied.

2.6.5.2 Effect of temperature

Extraction temperature is also an important parameter in SFE process as solvent properties vary with temperature. An isobaric increase in temperature reduces the density of solvent, which results a decrease in the solubility of compound. This effect is termed as density effect while varying temperature. On other hand, vapor pressure is increased with temperature, which increases volatility of compounds to be extracted. This effect is referred as vapor pressure effect (Reverchon and De Marco, 2006; Shilpi et al., 2013). The effect of temperature on the extraction yield can be explained considering these two opposite effects as these two phenomena show counter effects on solubility of solutes in solvent. Solubility of solvent is a key factor in SFE process because of high dependency of solvent capacity on it as higher solubility of solvent in solute gives higher dissolution of solute in solvent. Hence, prediction of temperature effect on extraction yield is difficult and depends on the nature of solute.

In addition, these opposite effects of temperature on extraction yield are also responsible for the inversion of the extraction curves of different temperature. It is called retrograde phenomena, which is referred as a decrease in solubility with an isobaric increase in temperature and conversion of isotherms at a point (Mukhopadhyay, 2000). Therefore, it is reported that the density effect becomes dominant at pressures below the crossover pressure whereas vapor pressure effect becomes more pronounced above this condition (Shilpi et al., 2013).

Mass transfer coefficients (solvent and solid phase) as well as mass transfer rate of solute to bulk liquid phase are also increased with increasing temperature due to high diffusivity of oil in solvent (Rai et al., 2015). Hence, increase in temperature results an enhancement in mass transfer rate as well as extraction yield (Shilpi et al., 2013).

In addition to pressure, various researchers as provided in Table 2.5 also study effect of temperature on extraction yield.

Began et al. (2000) considered temperature as variable parameter to be varied with pressure and solvent flow rate to study its effect on the oil yield of turmeric root. They varied temperature, pressure and solvent flow rate as 313 to 333 K, 10 to 30 MPa and 3 to 9 ml/min, respectively. They investigated that oil yield of turmeric root was decreased with increasing temperature due to the decrease in density of solvent(Began et al., 2000). Gopalan et al. (2000) also studied the effect of temperature, pressure, particle size and solvent flow rate on the extraction yield of turmeric root. They found that oil yield of turmeric root was decreased with increasing temperature from 313 to 333K.

2.6.5.3 Effect of solvent flow rate

Solvent flow rate is also a critical parameter for SFE, which extracted solute from solid matrix through following steps: (i) Diffusion of solvent (SCF) inside the solid matrix, (ii) Formation of thin liquid film surrounding the solid particle due to transport of solute into outer layer, (iii) Dissolution of solute in solvent and transport of solute to the bulk liquid phase by means of convection (Mukhopadhyay, 2000).

Solvent flow rate controls the mass transfer rate, especially when extraction process is controlled by external mass transfer resistance (Reverchon and De Marco, 2006). The extraction of easily accessible solute from solid matrix is affected by solvent flow rate. Therefore, extraction yield increases linearly with solvent flow rate at the starting of extraction process (Diaz-Reinoso et al., 2006; Sovova et al., 1994a). This behavior can be explained by the mechanism that if solvent flow rate is increased sufficiently, number of molecules per unit volume of solvent entering to the extractor is increased. It enhances the surface renewable of solid particles, which results increase in inter-molecular interaction between solvent and solute as well as extraction yield.

Another reason could be that thickness of the film layer and mass transfer resistance surrounding the solid particle reduces with increasing solvent flow rate. Therefore, extraction yield increases when solvent flow rate is increased (Doker et al., 2004; Sodeifian et al., 2016b; Yin et al., 2005). However, high solvent flow rate is not always recommended because it decreases extraction yield sometimes. Due to high solvent flow rate, residence time considered by solute to get soluble into the solvent reduces, which decreases the extraction yield (Zaghdoudi et al., 2016).

Several researchers indicated that higher solvent flow rate may cause negligible, little or weak positive effects on the extraction process (Bhupesh C Roy et al., 1996; Rozzi et al., 2002). It is due

to the fact that the process may be in equilibrium or intra particle diffusion resistance may control the extraction process. Apart from it, lower flow rate provides an opportunity for deeper penetration into the matrix, which increases extraction (Pourmortazavi and Hajimirsadeghi, 2007). As reported in section 2.6.5.2 , solvent flow rate was also considered as variable parameter for SFE of turmeric root oil while varying other parameters such as pressure, temperature and particle size (Began et al., 2000; Gopalan et al., 2000). They observed that extraction yield of turmeric oil was increasing with increasing flow rate.

2.6.5.4 Effect of particle size

The size of solid matrix (raw material) has a critical impact on the efficiency of SFE process to extract solute. Generally, smaller particle size offers the greater effective solvent-solid contact area, which results higher extraction rate. Several researchers investigated that large particles of solid matrix can be broken into smaller one through milling, which reduces diffusion path as well as intra-particle diffusion resistance (Gopalan et al., 2000). Intact cells are ruptured by means of milling and ratio of broken to intact cells is increased resulting to an increase in easily accessible oil molecules (Ozkal et al., 2005b). The effect of intra-particle diffusion on the large particle seems to be very crucial as it can cause considerable decrease in the extraction yield. In addition, the slope of initial part of extraction curve is lower for large particles than that of small particles. It indicates that quantity or surface area of easily accessible oil is not sufficient and oil is not saturated with solvent (Xu et al., 2011). Moreover, mean particle size determines whether the solvent is able to diffuse up to the centre of the particle or not (Louli et al., 2004).

Therefore, it can be concluded that particle size of solid matrix should be taken small enough so that the oil can be rapidly transported from solid matrix to the bulk solvent phase (Goto et al., 1996; Mukhopadhyay, 2000). However, a reverse effect can also exist if particle size is too small, fluid channeling may occur inside the fixed bed resulting in inhomogeneous extraction (Liu et al., 2011). It may reduce the extraction yield because solute re-adsorbs on solid surface (Pourmortazavi and Hajimirsadeghi, 2007). Fluid channeling can cause a lower or no contact of solvent with the solid material to be extracted and thus, causing lesser extraction yield (Reverchon and De Marco, 2006). However, glass beads can be mixed with solid material while preparing the bed for extraction to avoid this problem. In addition, some volatile compounds might be lost while preparing the solid material of very small particle size.

Xu et al. (2011) reported that particle size does not show any influence on the extraction yield in two outermost cases: Fine milled material and coarsely ground plant material. Therefore, the

knowledge of inside structure of solid matrix helps to predict the behavior of herbaceous material during SFE of essential oils (Xu et al., 2011). Hence, a specific investigation should be carried out to determine whether sample particle size can influence extraction yield or not and then, a suitable particle size can be suggested.

The shape of solid particle is also found a key factor as experimental results are fitted well with model when the conventional spherical geometry is replaced by realistic slab geometry (Reverchon, 1996).

Gopalan et al. (2000b) studied the effect of particle size on the yield of turmeric oil using SFE process. They varied the particle size from 0.208 to 1.158 mm and found that oil yield was decreased with increasing particle size.

2.6.5.5 Effect of co-solvent

Carbon dioxide, in its supercritical phase, is a non-polar solvent suitable for extraction of non-polar compounds, such as hydrocarbons due to the limited solubility of polar organic compounds in it (Xu et al., 2011). However, its quadruple moment helps for the dissolution of some moderately polar compounds such as, alcohols, esters, aldehydes and ketones (Beckman, 2004; Lang and Wai, 2001; Mark McHugh, 1994). The extraction of polar compounds can be carried out or increased while adding a small amount of polar co-solvents such as methanol, ethanol, 2-propanol. A co-solvent is an organic solvent, which has volatility intermediate to solvent and the solute to be extracted. It only changes the solvent characteristics such as polarity and specific interactions without changing the sensitivity of solubility with respect to pressure and temperature (Mukhopadhyay, 2000).

A mixture of co-solvent and solvent is said to be in supercritical phase when its pressure and temperature are above critical pressure and temperature of the mixture. It is given that mixture critical pressure is always higher than that of pure solvent. However, mixture critical pressure and temperature are not very different from the critical values of pure solvent (Mukhopadhyay, 2000). The properties of supercritical solvent can be readily manipulated while changing the molar ratio of co-solvent. Large variation in density occurs due to large isothermal compressibility near critical points and vice-versa (Li et al., 2003). In addition, co-solvent mixed with supercritical solvent generally increases the bulk density of the mixture causing solubility enhancement, which increases the extraction yield. However, excessive polarity of solvent due to addition of excess amount of co-solvent may affect the extraction yield negatively (Liu et al., 2011). Co-solvent is

soluble in solvent up to an extent and this limitation may increase the mass transfer resistance and hence, extraction yield is decreased (Liu et al., 2011).

Various organic solvents such as methanol, ethanol, water, Iso-propanol, acetone etc. were used as co-solvents in SFE process as discussed in section 2.6.3. The nature of co-solvent depends on the nature of solute to be extracted (Pourmortazavi and Hajimirsadeghi, 2007). Ethanol and methanol are the most commonly used modifiers where ethanol is adopted majorly as a co-solvent, shown in Fig. 2.14. Ethanol is used in different concentrations to study its effect on the extraction yield of sunflower seed, green tea, *Catharanthus roseus*, Saw palmetto, *Prunus persica* leaves, *Kniphofia uvaria* etc (Duval et al., 2016; Falcao et al., 2017; Kazan et al., 2014; Ortega et al., 2017; Rai et al., 2016a; Sokmen et al., 2018).

2.6.5.6 Effect of extraction time

Extraction time is also considered as an important factor, which influences the SFE process in various ways. It is inter-connected with solvent flow rate and particle size and has to be properly selected to maximize the extraction yield (Reverchon and De Marco, 2006). SFE process is analyzed through the overall extraction curves (yield vs extraction time), which gives information regarding time required for extraction process to obtain an economical advantageous process (Shilpi et al., 2013). The extraction process can be divided into three stages: Rapid extraction of free solute, transitional stage of surface and internal diffusion and slow extraction mainly based on the internal diffusion (Xu et al., 2011). These three stages are named as fast extraction rate period (FER), transition extraction rate period (TER) and constant extraction rate period (CER) respectively by Sovová (1994). The time consumed in FER period is responsible for the extraction of solute due to solubility of solute in solvent and easily accessible solute during milling of solid material (Xu et al., 2011).

Contact of solvent with solid material can be enhanced with increasing extraction time, which increases extraction yield (Pourmortazavi and Hajimirsadeghi, 2007). Extraction time increases the amount of fresh solvent available on a fixed bed, which provides suitable driving force between solvent and solute to increase extraction yield (Sodeifian et al., 2018). In addition, increase in extraction time enhances the extraction of heavy compounds with large retention indices from the solid material (Pourmortazavi et al., 2004).

Various researchers optimized the extraction time with other operating parameters for SFE process as reported in Table 2.5. The effect of extraction time was studied for olive fruits, Portulaca oleracea seed, *Eryngium billardieri, Dracocephalum kotschyi* seed, *Fritillaria thunbergii Miq*

flower etc. and found that extraction yield was increasing with extraction time (Belbaki et al., 2017; Ruan et al., 2017; Sodeifian et al., 2017a, 2017b, 2018).

2.6.5.7 Effect of properties of bed

Various properties of packed bed, consisting of extractable solid material, such as bed void fraction, bed length and packed amount also have considerable impact on extraction yield using SFE process. Bed void fraction depends upon the particle size and nature of solid material. Extraction yield increases with bed void fraction as greater void bed may provide enlarged contact area between solvent and solid (Nei et al., 2008). Another reason may be that channeling occurs in the packed bed due to compact particle arrangement.

Similarly, extraction yield increases with the length of packed bed because it provides greater residence time for solvent inside the bed (Lu et al., 2007). However, amount of packed bed (amount of raw material) affects the extraction yield negatively. It is increased with decreasing the amount of packed bed as lesser amount can enlarge the contact area between the solvent and the solid hence, mass transfer enhances (Yin et al., 2005). From the economic point of view, the loaded fraction of 75–80 wt% is recommended (Yin et al., 2005).

2.6.5.8 Effect of moisture and initial oil content

Moisture content of solid material plays an important role during SFE process. It creates hindrance for solvent to diffuse into pores and makes the solid material sticky, which reduces contact of solvent with solid material (Shilpi et al., 2013). Thus, different techniques such as oven-drying, freeze-drying or using adsorbent can be used to reduce moisture content where extraction yield of freeze- dried samples was higher than that of oven-dried sample (Shilpi et al., 2013).

In case of initial oil content, Nagy and Andi (2008) reported that initial oil content of 5 to10% showed a self-entraining effect for the SFE of paprika. Therefore, an increase in extraction yield was observed when initial oil content was increased. This may be because oil may act as co-solvent for compounds, which have slight solubility in carbon dioxide. However, no significant effect was visible when oil content was increased from 10 to 27% (Nagy and Andi, 2008).

2.6.5.9 Effect of matrix of raw material

Supercritical extraction of any seed strongly depends upon the type of seed matrix or geometry of seed and availability of oil in the seed. Researchers reported that oil particles are bound by channels, which can be broken through milling. Consequently, a few channels can be broken and oil can be easily accessible. However, extraction of oil available inside the intact channels is difficult because of intermolecular resistance. Each type of raw material involves different type of

matrix and it shows different type of inside mechanism for the extraction of oil. Type of raw material matrix or type of oil availability helps to decide the size of solid particle for the SFE. In addition, inside mechanism of solid matrix helps to predict resistances working on extraction and based on these assumptions a model can be proposed. Several types of raw material matrices are identified by different authors i.e. oil availability at broken and intact channels (Louli et al., 2004; Ozkal et al., 2005b; Reverchon et al., 2000), in secretory ducts (Misic et al., 2008; Zizovic et al., 2007b), in cavities or spherical and hexagonal cells (Bensebia et al., 2009; Della Porta et al., 1999; Zarena et al., 2010), in plate type geometry (Campos et al., 2005; Gaspar et al., 2003) and in glandular trichomes (Martin et al., 2011) etc. These different types of solute matrices can be predicted through respective SEM images as morphological structure are reported in Table 2.6. It shows that a particular type of solute matrix shows same type of morphological structure. Reverchon et al. (2000) studied the extraction of hiprose seed and from the SEM images, they found that broken and intact cells model could not be used as seeds included broken and intact channels but only the oil contained near the opening of the channel was readily available. They reported that solvent faced an increasing resistance due to the diffusion in the channels at an increasing depth, as long as the extraction lasts. To extract the hiprose oil, they proposed a new model by inserting an internal mass transfer resistance that increases linearly till the oil contained in channels was extracted. del Valle and Uquiche (2002) also extracted hiprose seed and they reported that oil was enclosed in a form of cells by a thick and highly lignified testa as shown by microscopic analysis of seed. They used microscopic images of seed to segregate the seed part having different oil content. According to Campos et al. (2005), SEM image of marigold flowers were used to predict the geometry of particle so that the model based on the same type of geometry could be applied. To evaluate the solid geometry, authors calculated the ratio between particle diameter and particle thickness (dp/δ) and value was in better agreement to use simple single plate model. Ozkal et al. (2005b) considered SEM images of apricot kernel (pre and post-extraction) and found that grinding of apricot kernel before extraction not only increased the interfacial area but also released oil from the broken cells which led to presence of two extraction period (fast and slow). Zizovic et al. (2005) used SEM images for the modeling of Mentha piperita leaves and reported that peltate gland disruption occurred during the SC-CO$_2$ pretreatment. They considered the fraction of peltate glands disrupted by the grinding pretreatment and fraction of peltate glands, which were disrupted later during the extraction process as two main fitting parameters.

Table 2.6 Type of seed matrix and oil availability.

S. No.	References	Seed	Solute type	Oil available at	Size (mm)	Remarks
1	Marrone et al. (1998)	AS	seed	In cavities or spherical cells	0.3-1.9 cell dia=0.02	The starch is not extractable and can be seen agglomerated after the extraction. The mass transfer resistance to extract the oil available at the surface is considerably lower than that to extract the remaining part of it.
2	Reverchon et al. (1999)	FS	seed	In cavities or hexagonal cells	0.37 cell dia=0.01	In the inner portion of the particles, the remaining part of the vegetable oil is contained inside closed cells even after the extraction.
3	Reverchon et al. (2000b)	HS	seed	Broken and intact channels	0.42,0.79, 1.03	Oil contained in the unbroken channels was not accessible. Only the oil contained near the opening of the channel was readily available for extraction.
4	Del Valle et al. (2006)	HS	seed	Oil is enclosed in a form of cells by a thick and highly lignified testa	0.15-0.425 0.85-2.36	
5	Lu et al. (2007b)	BS	Seed	Closed structure of the seeds	0.3	
6	Zizovic et al. (2007b)	MGF, CMF, FS	Seed	Secretory duct		The values of secretory duct diameters were 2.3 μm for marigold, 2 μm for chamomile and 70 μm for fennel. The cross-section of fennel fruit showed six oil channels and the longitudinal section showed only one secretory duct is visible.
7	Grosso et al. (2008)	COR	Seed	The oil is secreted in ducts located in the pericarp of the fruit	0.4,0.6, 0.8 mm	The schizocarpic coriander fruits (seeds) show two dry segments (mericarps) attached to a more or less deeply forked central stalk. The ducts are damaged during grinding, leading to the release of the oil which produces an external film around the endosperm particles. The highest yield was obtained for the smallest particle size, indicating that more ducts were damaged and, therefore, the oil was more accessible to carbon dioxide.
8	Fiori et al. (2009)	GS	Seed	In layer of cells	cell dia=0.02	By milling, some cells are broken (lower right side, higher left side) and showed free oil,

						while other cells are intact and contained tied oil.
9	Mhemdi et al. (2011)	COR	Seed	Random	0.5-0.9	Scanning electron microscope images of ground coriander seeds before and after supercritical extraction show holes on the particle surface after extraction that are not present before extraction.
10	Romo-Hualde et al. (2012)	RP	Seed	Entrapped in spherical shaped microcapsules	0.2-0.5 mm	The microcapsules were of spherical shape with characteristic dents on their surface. The average size of the microcapsules was 5.46 µm.
11	Ayas and Yilmaz (2014)	SFF	Seed	Uniformly distributed inside pores	0.5 mm	The porosity of the treated seeds easily shows that oil has been extracted.
12	Barrales et al. (2015)	PFS	Seed	Inside the tissue that covers the seed particles after milling,		Superficial tissue that covers the seed particles and of the broken material that is deposed on the surface. In the greater portion of the tissue that covers the seed particles,the surfaces remain smooth and without striations or pores after the extraction.
13	Rai et al. (2015)	WM	Seed	In a sequence of layers of oil and uniformly distributed in every layer	0.75 mm	SEM images clearly show that oil and non-extracted solid phase are closely interpenetrating. High pressure is required to rupture the layer of the seed material for better oil extraction.
14	Rai et al. (2016a)	SF	Seed	In a sequence of layers of oil and uniformly distributed in every layer	0.75 mm	SEM images clearly show that oil and non-extracted solid phase are closely interpenetrating. High pressure is required to rupture the layer of the seed material for better oil extraction.
15	Dias et al. (2016)	CSS	Seed	Inside the disrupted cell walls	0.177-1.19 mm	
16	Koubaa et al. (2016)	CS	Seed	Inside the vesicles	<0.63 mm	The oil bodies can be seen on the surface, due to grinding.
17	Wang et al. (2016)	GPS	Seed	A sequence of layers and a large amount of oil is distributed in the lamellar structure	0.42 mm	High pressure in the SC-CO_2 procedure could disrupt tissues and cell walls of seed powder on some level to improve the extraction yield effectively
1	Gaspar et al. (2003)	OB	Leaf	In plate type geometry	1.55 mm	
2	Zizovic et al. (2005b)	MP	Leaf	Peltate glands in matrix of leaf samples.		peltate gland disruption occurred during the SC CO_2 pretreatment.

3	Bensebia et al. (2009)	RoseL	Leaf	In cells	0.15-0.43	Analysis of SEM images showed the intact cells (a), the broken cells (b) and the existence of peltate gland (c,d)
4	Kong et al. (2009)	PPL	Leaf	In palisade parenchyma and spongy parenchyma	0.25-0.4 mm	SFE influences the structure of mesophyll cells.
5	Herzi et al. (2013)	*TA*	Leaf	In secretory ducts	1.5 mm	SFE had almost no effect on the structure of the plant, at least on a visual point of view. SEM images tend to confirm thehypothesis of secretory ducts, since the plant is actually made of acore of interconnected channels surrounded by a dense bark.
6	Stamenić and Zizovic (2013)	*HOL, PL,TYM, OB*	Leaf	In peltate glandular trichome	0.4 mm	Peltate glands are made of stalk cell attached to the leaf, four to eight secretory cells attached to the stalk cell, and the oil sac above the secretory cells. As the gland develops, the secretory disc cells expand and become full of essential oil covered with a loose-fitting, overlying oil sac membrane.
7	Akalın et al. (2015)	SL	Leaf	Linear string of cells with hairy-like structures.		After extraction, the surface of the solid residues deteriorated and cavities were formed.
1	Campos et al. (2005)	MGF	Flower	MGF particles have a plate type geometry	0.62 mm	The ratio between particle diameter and particle thickness (dp/δ) was 258
2	Lin et al. (2006)	*WW*	Flower	In glandular T-trichomes	<0.42 mm	
3	Zizovic et al. (2007b)	MGF, CMF, FS	Flower	Secretory duct		The values of secretory duct diameters were 2.3 μm for marigold, 2 μm for chamomile and 70 μm for fennel. The cross-section of fennel fruit showed six oil channels and the longitudinal section showed only one secretory duct is visible.
4	Yang et al. (2007)	*WW ,AC*	Flower	In T-grandular trichomes (WW)	<0.420 mm	Magnified pictures revealed that the floral parts of A. capillaris had smoother surfaces than those of A. annua.
1	Ozkal et al. (2005b)	AK	Fruit	Broken and intact channels	0.425-1.5 mm	Grinding of apricot kernel before extraction not only increases the interfacial area but also releases oil from the broken cells.
2	Glisic et al. (2007)	CRT	Fruit	The oil is in channels (vittae)	700μm	

3	Zarena et al. (2010)	MFP	Fruit	In cells		Pretreating results the swelling of the pericarp matrix. Swelling aids cell rupture resulting in increased surface area for exposing the active constituents in intact form and facilitating easy mass transfer into the carbon dioxide.
4	Romo-Hualde et al. (2012)	RP	fruit	Entrapped in spherical shaped microcapsules	0.2-0.5 mm	The microcapsules were of spherical shape with characteristic dents on their surface. The average size of the microcapsules was 5.46 μm.
5	Reategui et al. (2014)	BB	Fruit	Inside the cells	0.34 mm	
6	Santos et al. (2015)	MPF	Fruit	Inside the disrupted cell walls	0.17-1.68 mm	The flux of the supercritical fluid and mainly the ultrasound waves disturbed the cell walls, leading to the displacement of microparticles from the internal part of the vegetable matrix to its surface.
7	Sodeifian et al. (2016a)	PKS	Fruit	An uneven and rough surface covered uniformly with a layer of oil	0.6 mm	The structure of the treated samples seems more porous and the surface is clearly deflated and depleted of oil signifying high extraction efficiency by supercritical CO_2.
1	Westerman et al. (2006)	AMC	Herb	Oil glands in layers	0.1-0.2	The whole grain was lenticular in shape with a diameter of 1.0–1.5 mm. Oil predominates in the germinating end while the glycerides, starches and other sugars occupy the perisperm seed bulk.
2	Misic et al. (2008)	AGL	Herb	secretory duct	secretory duct dia=0.07	The secretory ducts are marked with the arrows. Three of the six ducts (each mericarp has six oil channels) are visible on the image.
3	Langa et al. (2009a)	HOL	Herb	Located in trichomes	0.3-0.8	
4	Langa et al. (2009b)	SS	Herb	In peltate trichomes	0.3-0.8	
5	Martín et al, (2011a)	PIL	Herb	In glandular trichomes	0.8-1.44	PIL have both non-glandular trichomes or hairs and glandular trichomes. Hairs help to reduce leaf evaporation while glandular trichomes accumulate oil.
1	Yang et al. (2007)	WW ,AC	Flower, Plant	In T-grandular trichomes (WW)	<0.420 mm	Magnified pictures revealed that the floral parts of A. capillaris had smoother surfaces than those of A. annua.

2	Martín et al. (2011b)	WW	Plant	Essential oil is stored in glandular trichomes	0.56 mm	The essential oil is located in the plant is quite a difficult issue.
3	(Romo-Hualde et al., 2012)	RP	stem	Entrapped in spherical shaped microcapsules	0.2-0.5 mm	The microcapsules were of spherical shape with characteristic dents on their surface. The average size of the microcapsules was 5.46 µm.
4	Akalın et al. (2015)	GBW	Plant	In the fiber like structure		The fiber-like structure started tobreak down and the formation of an amorf structure was observedin the bio-chars. It is believed that the removal of volatiles in the char matrix. Char formation is strongly affected by temperatures.
5	García-Abarrio et al. (2014)	*LA*	Plant	Inside the secretory structures	0.56 mm	FSEM images shows a glandular and group of a glandular trichome of *Lippia alba.*
1	Braga et al. (2006)	TR, Gin	Root	In cellular structure	-	Ginger granules are spherical (10–28 mm along the major axis). Turmeric granules are elliptical (10–33 mm along the major axis)
2	Zizovic et al. (2007a)	*VOL*	Root	In sectretory cell	70µm	Sectretory cell diameter is estimated to be 8 µm
3	Danh et al. (2009)	VET	Root	In pitch region in the centre of vetiver roots	0.6	Large sizes of root particles correspond to high mass transfer resistance as the CO_2 and the oil droplets must diffuse through thick layers of cells before freely mixing with the flowing solvent. The reduction of particle size increases the contact surface area between oil cells and solvent.

Similarly, other researchers also used SEM images for the modeling purpose or for the selection of particle size of seed as can be seen in Table 2.6. It shows that all types of seeds and fruit (pulp, peel) contain oil inside different shape and size of cells and channels. Leaves, flowers, roots and stem are parts of a plant and generally show similar type of morphology such as inside the glandular T-trichomes, Linear string of cells with hairy-like structures and secretory duct/cells. Herbs are also a kind of plants so morphological structure of herbs is similar to that of plant and contains oil inside the Peltate trichomes/ Secretory duct as shown in Table 2.6. Particle size of raw material is also mentioned in Table 2.6 for different type of raw materials considered for the SFE process and plays an important role in the extraction of raw material. Morphological structure of

raw material gives information about oil presence inside the structure and based on this, particle size of raw material can be decided to maximize the extraction yield.

2.6.6   Mathematical modeling of SFE

A reliable and simple mass transfer model is necessary to design extraction plant and determine the optimum operating conditions (Reverchon, 1996). Modeling of SFE of essential oils is difficult due to the complexity of the vegetable structure and lack of reliable experimental data on the yield of the process (Reverchon, 1996). It is evident that various models differ not only from a mathematical point of view, but also due to mass transfer mechanisms, which control the SFE process of different matrices. Thus, a single model cannot describe all experimental results (Sovova et al., 1994a).

Main goal of modeling is to predict the large scale extraction curves as a function of the experimental parameters such as temperature, pressure, solvent flow rate, particle size, co-solvent % and other new introduced parameters such as bed height, matrix of seed particles and solubility parameters as real experiments at large scale are extremely expensive. The literature shows that more than 70 models have been proposed by various authors to simulate the SFE process for seeds, roots, flowers, stems, meat, etc. A modeling tree showing connection between different models is presented in Fig. 2.18. Details of these models available in the literature are shown in Table 2.7 with assumptions made, solution techniques, tuning parameter, fitting error and findings of the study. Several assumptions were considered by researchers to develop the models for the SFE of different solute matrix and a list of assumptions available in literature is given in Table 2.8. Generally, tuning parameters in the models are considered to study the effect of that parameter on the SFE process and are based on the mass transfer operation. Table 2.7 consists of details of tuning parameters accounted by different authors to model the SFE process and can be seen that tuning parameters taken are Overall mass transfer coefficient, Diffusion coefficient, Solvent phase (external) mass transfer coefficient, Solid phase (Internal) mass transfer coefficient, Axial dispersion, Shock wave velocity, Equilibrium constant and Desorption rate constant. Most of the authors considered solid phase and solvent phase mass transfer coefficients as tuning parameters while assuming that mass transfer between both phases are primary parameters that affect the SFE process. Some authors also coined diffusivity and axial dispersion as tuning parameters only when they assumed that diffusion and axial dispersion process were showing considerable effect on SFE process (Bartle et al., 1990; Goto et al., 1996; Hong et al., 1990; Reverchon et al., 1993a, 1994; Roy et al., 1994). An Error value between experimental data and model data shows a measure of

model fitting with experimental data of SFE process and are reported in Table 2.7. Based on the literature review, it can be noticed that the model proposed by Sovova (1994) is extensively used model for all types of solute matrices except flower category. Lee et al. (1986) proposed a one-dimensional, unsteady state mathematical model to obtain the oil concentration profiles in solvent and solid phases and to determine overall volumetric mass transfer coefficients, K. The model proposed by Lee et al. (1986) has been taken as a base model by Lack with one extra assumption that solvent was free from solute concentration at the entrance of the extractor. Further, Sovova (1994) extended the Lack (1985) model considering three zones of extraction. Many researchers used the model proposed by Sovova (1994) as a base model (Beckman, 2004; Louli et al., 2004; Sovova et al., 1994a; Sovova, 2005; Sovova et al., 1995; Stastova et al., 1996; Xavier et al., 2011)and made several needful modifications for SFE of different solute matrices as can be seen from Fig. 2.18.

Tan and Liou, 1988 → Tan and Liou, 1989

Bartley et al.,1990 → Gasper et al.,2003

King et al.,1997 → Bartley et al.,1991 → Gasper et al.,2003 (SSP Model)

Wong,1997 → Gasper et al.,2003 (SP Model)

Roy et al.,1996 → Steffani et al.,2006

Esquivel's model (1999) → Silva et al., 2011

Provost et al.,1992 ← Lee et al.,1986 → Lack model, 1985

Schaeffer et al.,1989, Tan et al.,1988 → Reverchon et al,1993 → Reverchon and Osseo,1994

Lack model, 1985 → Sovova, 1994, Mendes et al.,2005

Marrone et al.,1998, Reverchon and Marrone, 2001 → Fiori, 2007

Sovova, 1994 → Sovova et al., 1994, Louli et al.,2004

Goto et al. 1993 → Hatami et al.,2010, Goto et al.1994

Reverchon and Osseo,1994 → Papamichail et al.,2000, Reverchon ,1996

Sovova et al., 1994 → Sovova et al.,1995, Stastova et al., 1996, Sovova, 2005

Reverchon ,1996 → Reverchon and Poletto, 1996, Reverchon and Marrone, 1997

Goto et al.1994 → Mongkholkhajornsilp et al.,2005

Sovova, 2005 → Xavier et al.,2011

Reverchon and Poletto, 1996 → Sovova, 2005

Reverchon and Poletto, 1996 → Perrut et al.,1997

Goto et al.,1996, Perrut et al.,1997 → Machmudah et al.,2006

Fig. 2.18 Sequential developmnt of different model

53

Table 2.7 Model variations based on different assumptions

S.No.	Reference	Solute	Tuning parameter	% error	Solution techniques	Findings	Validation	Assumptions
1	Lee et al. (1986)	CS (Seed)		0.09	- Method of characteristics - Computer program to solve partial differential equations.	-Oil concentration profiles in both solvent and solid phases. -The overall volumetric mass transfer Coefficients.	-The overall volumetric mass transfer coefficient gave the best agreement with the experimental in the constant rate period.	[1], [2], [3], [4], [5], [6], [7]
2	Schaeffer et al. (1989)	CrS (Flower)	-Overall mass transfer coefficient.	4- 5.8%	-Method of characteristics. -Computer program to solve partial differential equations.	-Explained the dependence of the concentration.		[2],[4],[5],[8],[9],[10]
3	Hong et al. (1990)	SB (Seed)	-Diffusivity in the solid phase.	0.47%	-Solved analytically	-External mass transfer coefficient	-Combined mass transfer models for CER & FER but Best agreement in constant rate period.	[7],[11], [12]
4	Bartle et al. (1990)	Railroad bed soil	-Diffusivity in the solid phase.		-Adaption of the published solutions equations	-Concentration profile with respect to extraction time was predicted.	-It gives little information about the early stage of extraction (CER) in which the majority of the material is extracted.	[4], [13], [15], [16],
5	Cygnarowicz-Provost et al. (1992)	*FM* (Algae)	Overall mass transfer coefficient.	15%	-Method of characteristics. - Modified Euler's method to integrate the equations - Computer program to solve partial differential	Lipids concentration profiles in both solvent and solid phases. - The overall volumetric mass transfer coefficients.	Overall volumetric mass transfer coefficient gave the best agreement with the experimental in the constant rate period.	[1], [2], [3], [4], [5], [6], [7]

					equations			
6	Reverchon et al. (1993a)	Her (plant)	-External mass transfer coefficients -Solid diffusivity (D_{mi})	8.77 - 11.75	-Fourier transforms and the heat-mass transfer analogy	-Oils yield prediction. -The overall volumetric mass transfer coefficients.	-The extraction process from a single (spherical particle) is described by five steps. -Further refinements of the model are possible in order to take into account particle shape and size distribution.	[17], [13], [18], [19], [20], [21], [22], [7]
7	Sovova (1994)	GS (Seed)	-Parameters of slow and fast extraction periods		Method of characteristics.	-Mass transfer coefficient in the solid phase. - Oil yield prediction. -Concentration profiles in solid and solvent phases.	Model shows the best suitability for fast extraction period and slow extraction period. Transition Period (TR) is also considered between both fast and slow extraction period.	[3], [5],[6] [7], [24],
8	Roy et al. (1994)	TOS (Seed)		0.66-3.17	Runge-kutta method of solution	-Mass transfer coefficient in the solid phase. - Oil yield prediction.	Model has the best suitability for FER period.	[2], [3], [5], [6],[21], [28]
9	Sovova et al. (1994)	GS (Seed)	-Parameters of mass transfer in solvent and solid phases.		Method of characteristics.	-The effects of milling, amount of solid material, solvent velocity and flow direction on the extraction curves. - Mass transfer coefficients in SCF and solid phases	-Best suitability for fast extraction period and slow extraction period. Also considered Transition Period (TR)	[3],[5], [6], [7] [26], [29],
10	Reverchon et al. (1994)	BL (Leaf)	-Internal diffusion coefficient. -Internal mass transfer coefficient	10.3-19.08	The Fourier transform was used to obtain the analytical solution.	-External mass transfer coefficient. - Oil yield prediction. - Concentration profile.	-The model describes the mass transfer between a single spherical particle and the supercritical solvent. -Extraction mainly	[13], [17], [27], [24]

							depends on the internal mass transfer process.	
11	Roy et al. (1996)	Gin (Root)	-Effective diffusivity -Solubility	0.83-2.10	-Numerical solution by Crank Nicholson's method.	-External mass transfer coefficient. -Binary diffusivity.		[3],[6], [13], [28], [29], [30],
12	Reverchon and Poletto (1996)	RoseF, Trose	Constant mass transfer coefficient between the phases. -Shock wave velocity.	2.24-3.65	Numerical solution by Fourth order Runge-Kutta method.	-Oil yield prediction. -External mass Transfer coefficient. -Resistance behavior during the mass transfer from the oily phase to solvent. -Concentration profile between the regions.	Two stages of the extraction process were modeled in a best way.	[1], [2],[6], [21], [23], [31], [32], [33],
13	Goto et al. (1996)	solid matrix	-Intra-particle effective diffusivity.		-Numerical solution by Crank Nicholson's method	-Oil yield prediction. -Effect of dimensionless numbers (Peclet and Biot no.) on extracted concentration.		[3], [6] [28], [30], [39]
14	Perrut et al. (1997b)	SF (Seed)	-Mass transfer Coefficients -Parameter of equilibrium function	1.12-6.89	-Method of characteristics. -Fourth order Runge-Kutta method.	-Oil yield prediction. -Effect of solid matrix.	-Best description/ suitable for the linear parts of the extraction curve.	[2], [4] ,[21], [32], [35], [36], [37],
15	Goodarznia and Eikani (1998)	Her (plant)	-Mass transfer, axial dispersion and intra-particle diffusion coefficients		-Numerical solution by Crank Nicholson's implicit method	-Mass transfer coefficient. -Axial dispersion coefficient in the SC phase. -Diffusion coefficient in the solid phase. -Oil yield prediction.	-Two stages of the extraction process were modeled in a best way. -The model indicates dependability of extraction to the particle size.	[4], [6], [13], [21], [22], [30], [38], [40],

16	de Franca et al. (1999)	Bur (Fruit)	-Parameters of slow and fast extraction periods.	4.50	-Method of characteristics.	-Mass transfer coefficient in the solid phase. -Oil yield prediction	-Constant extraction rate and diffusion controlled rate periods were considered.	[3], [6], [7], [24]
17	Abaroudi et al. (1999b)	Impregnated porous pellets			-The numerical solution of the model equations was Performed using a MOLCH a computer Program based on the method of lines.	-External and internal mass transfer coefficients. -Axial dispersion coefficient. -Intra-particle diffusivity.		[4],[6],[28], [34],[40]
18	Reis-Vasco et al. (2000)	PEL (Leaf)	-Internal mass transfer coefficient[axial dispersion neglected]. -Internal mass transfer coefficient and the axial dispersion [axial dispersion accounted]	3.90-7.89	-Integrated using an implicit method based on the Crank-Nicholson numerical cell, when axial dispersion is taken into account. -When axial dispersion was neglected, the corresponding model equations were numerically integrated using an explicit method based on the Wendroff numerical cell.	-Internal mass transfer coefficient -Oil yield prediction		[4],[6],[21], [30],[41]
19	Reverchon et al. (2000)	HS (Seed)	-Internal mass Transfer coefficient	7.40%	-Finite difference method (Explicit numerical cell)	-Internal mass transfer coefficient. -Oil yield prediction.	-Suitable for linear part of the curve. - Improvement is possible in the fitting between model curves and data for different particle sizes.	[2],[21],[32], [35], [37],[48]
20	Cocero and García (2001)	SF (Seed)	-Equilibrium coefficient. -Mass transfer parameter.	5.94	-(Numerical & Analytical solution) -Fourth order Runge-Kutta method. -Laplace transform.	-External mass transfer coefficient		[6],[7],[21], [32], [40], [41],[46]

21	Skerget and Knez (2001)	SM, BLP, PAP,COL, (Flower, seed)	-Adsorption equilibrium constant	3.8 - 13%	-Laplace transformations	-External mass transfer coefficient. -Adsorption equilibrium constant		[42], [43], [44]
22	Ruetsch et al. (2003)	CB (Seed)	-Equilibrium coefficient. -Mass transfer parameter.	6.67	-Fourth order Runge-Kutta method.	-External mass transfer coefficient		[4],[6], [21], [24], [30], [43], [45], [46]
23	Mongkholk hajornsilp et al. (2005)	NS (Seed)	-Axial dispersion coefficient -External mass transfer coefficient	0.87-24.52%	ODE method	-External mass transfer coefficient. - Effective intra-particle diffusion coefficient.	The model indicates the dependability of extraction yield on the particle size and temperature.	[1],[2], [4],[6],[7],[40] ,[47]
24	Kumoro and Hasan (2006)	AP (Leaf)	-Desorption rate constant.	1.89%, 2.05%	MATLAB	-Fluid - solid phase mass transfer coefficient. -Effective diffusivity of solute in SC-CO_2.		[2], [6], [7], [21], [40] [46],
25	Nei et al. (2008)	TFP (Seed)	-Mass transfer coefficient - Axial dispersion coefficient in the Bulk phase -Effective diffusivity into the pores -Henry coefficient		-Implicit finite difference method.	-Mass transfer coefficients. -Axial dispersion coefficient in the bulk phase. -Effective diffusivity.		[4] ,[6], [21],[41],[48],
26	Ghoreishi et al. (2009)	OL (Leaf)	-Adsorption equilibrium constant. -Transfer parameter. -Fraction of internal sites.	0.06%	-Modified 4th-order Runge Kutta finite Difference method.	-Distribution Coefficient and extraction yield.		[4], [13], [49], [50]

27	Patel et al. (2011)	CNS, BLP (Seed)		0.74 - 2.97%	-Analytical solution	-Yield prediction at different operating parameters for the CNS and black pepper.	-Best description of CER and FER period.	[3],[5],[6],[7], [21], [24], [41],
28	Kumhom et al. (2011)	SBF (Seed)		6.54%	Solved by method of lines using Mathcad software	-Solubility. -Film mass transfer coefficient. -Effective diffusivity. -Axial dispersion coefficient.		[6], [21], [30], [40],[46],
30	Maksimovic et al. (2012)	MP (Leaf)		6.21	-Simulation of SCFE of Mentha was done by using Polymath Educational, Matlab and origin Pro Software	-External mass transfer coefficient. -Apparent internal mass transfer coefficient	-Described SCFE process in two steps as **Fast** & **Slow** extraction periods. (best suitable)	[14],[23],[25] [53]
31	Honarvar et al. (2013)	CS, SES (Seed)	-Effective diffusivity. -Mass transfer coefficient. -Axial dispersion coefficient	4.58 - 9.84%	-Solved numerically by the Method of Lines available in MATLAB 7.1	-Yield prediction at Different operating parameters for the canola and Sesame seeds oil.	Described SCFE process in two steps as **Fast** & **Slow** extraction periods. (best suitable)	[6],[7],[21], [30],[40],[41]
32	Scopel et al. (2013)	*SML* (Leaf)	-Effective diffusivity. -The convective Mass transfer coefficient.			-Effective diffusivity. -The convective mass transfer coefficient.	Described SCFE process in two periods as CER & FER extraction periods. (best suitable)	[4],[6],[21]

Table 2.8 Assumptions used in Table 2.7.

[1]	One dimensional steady state.	[28]	Solvent flows axially.
[2]	Axial dispersion is negligible inside the bed.	[29]	Three extraction periods were considered.
[3]	Solvent is oil-free at the entrance of the bed.	[30]	Axial dispersion is considered.
[4]	The solute concentration is radially uniform throughout the seed material.	[31]	Volume fraction of the glass beads (packing) is constant.
[5]	Plug flow exists in the bed.	[32]	Uniformly distribution of solvent flow rate.
[6]	Physical properties and Temperature, pressure and fluid flow rate are constant.	[33]	Uniformly distribution of concretes on the surface of the glass beads (packing
[7]	Fixed bed.	[34]	Isotropic system with regards to diffusion.
[8]	The surface solute concentration in the fluid phase is in equilibrium with the solute concentration in the solid phase.	[35]	Implicit hypothesis has been adopted (relevant conc. gradients in the fluid phase develop at larger scales than the particle size).
[9]	Solubility of the solute in the fluid phase is low.	[36]	The value of solute concentration in solid is an average value within the particle and depends on time and height. Means concentration gradients within the particles were not resolved.
[10]	Intra-particle diffusion is neglected.	[37]	Volume fraction of the fluid is not affected by the reduction of the solid mass during the extraction.
[11]	Constant rate extraction region controlled by a film controlling mass transfer and falling rate region by a diffusional mass transfer.	[38]	Two- phase unsteady-state mass balance.
[12]	Un-steady state mass transfer.	[39]	Intra-particle diffusion consideration
[13]	particles of uniform size.	[40]	Radial conc. gradients neglected/ Radial dispersion neglected
[14]	The rate of extraction from intact cells depends mainly on resistance to diffusion through the cells membrane and it is time dependent process.	[41]	Superficial velocity of SCF is constant along the extractor.
[15]	The rate of flow of SCF past the particles is fast enough that the concentration of the extracted material in the fluid is always close to zero.	[42]	Adsorption –desorption equilibrium of extractable component from solid tissue.
[16]	Extractable compounds are moving through the matrix by a process of diffusion.	[43]	Mass transfer through the external film into the bulk.
[17]	Single particle approach and an internal diffusivity consideration.	[44]	Semi-batch extraction.

[18]	The particle diameter is the weight mean diameter of the measured size distribution.	[45]	Extraction bed is made of spherical, isotropic micro porous particles arranged in a cylindrical geometry
[19]	Extraction of essential oils and of cuticular waxes are parallel and Non-interacting processes.	[46]	Particle porosity, particle size, Void fraction in the bed, solute diffusivity inside solid particles and dispersion coefficient are constant and uniform along the bed.
[20]	Particle radius does not affect the diffusivity of both oils in the matrix.	[47]	No interaction among solutes in the fluid and solid phase.
[21]	Essential oil is treated as a single component (solute) means extraction can be described as a single pseudo-compound.	[48]	Solute conc. in the particle pores was a function of radius and time as well as the bed length.
[22]	Solute concentration does not depend on spherical coordinates.	[49]	System is assimilated into a batch extraction column (the possible extraction During discharge period may be the cause of small deviations between the modeling predictions compared to experimental measurements).
[23]	The rate of extraction from disrupted cells of plant material depends on resistance to the external mass transfer which is governed mainly by hydrodynamic conditions inside extractor and particle size.	[50]	There is no mass transfer resistance for the exterior sites on the particle surface.
[24]	Solid Bed is homogeneous w.r.t. to particle size and initial distribution of solute.	[51]	The mass transfer rate is controlled by the phase equilibrium and the oil diffusion in the solid.
[25]	They assumed that supercritical extraction consists of two main steps as Fast (disrupted cells) & Slow (intact cells) extraction periods.	[52]	Accumulation of the solute in the fluid phase ($\partial y/\partial t /\ =0$) and the extraction is not uniform along the bed ($\partial y/\partial h$ =constant).
[26]	Down flow of CO_2 through the bed.	[53]	Supercritical extraction was considered as chemical reaction, although it is a physical Phenomenon.

2.7 Composition of Extracted Oil

In recent years, oils and fats are in great demand due to their importance in human nutrition such as vitamins and essential unsaturated fatty acids (USFA)(Piras et al., 2013). It is said that overall health and quality of life directly depends upon dietary factors (Parker et al., 2003). Therefore, it is recommended to replace saturated fatty acid (SFA) by USFA due to health concerns such as lower the cardiovascular (CVD) risk, low-density lipoprotein (LDL) cholesterol level and risk of coronary heart disease (CHD)(Gao et al., 2016; Paul et al., 2011; Rai et al., 2016a). USFA found in many vegetables and edible oils is main source of dietary for human consumption. USFA such as linoleic acid (C18:2) and α-linolenic acid (C18:3) are necessary to maintain cell membranes, brain function, hemoglobin synthesis, cell division and nerve impulse transmission under normal conditions (Sodeifian et al., 2017b). However, USFA are more likely to oxidize and leads to decrease in quality, stability and safety of oils (Gao et al., 2016). Apart from it, many oils are also used to make perfumes, cosmetics, soaps candles, insulators, biodiesel etc. (Gao et al., 2016). Identification and characterization of health beneficial factors of various food products and food ingredients can help in selection and consumption of food with these beneficial factors (Parker et al., 2003). Edible oils are common food ingredients and may contain significant levels of α-linolenic acid. It is recommended to have daily intake of n-3 unsaturated fatty acids from 0.1–0.2 g to 0.6 g to increase the potential of disease prevention (Parker et al., 2003). In addition, dietary sources of n-3 polyunsaturated fatty acids (PUFAs) are advisable for those who do not consume adequate account of fish and/or fish-based products rich in n-3 PUFAs (Parker et al., 2003).

Various oils have several health benefits where turmeric root and carrot seed oils are considered in the present study. The literature available on qualitative and quantitative analysis on these oils is reviewed hereunder.

2.7.1 Turmeric root Oil

Turmeric root (*Curcuma longa)* is a typical root/ perennial herb of Zingiberaceae family which is used as spice, natural dye, preservative, pharmaceuticals, confectionery and cosmetics (Laokuldilok et al., 2015; Singh et al., 2010). Turmeric root oil consists of essential oil as well as oil rich in fatty acids. It is used as scenting agents in detergents, soaps, air fresheners and insect repellents, intermediate in the synthesis of perfume chemicals and as a pharmaceutical aid (Paul et al., 2011). Its USFA and SFA contents were found as 22.25 - 23.44% and 76.11 - 77.59%, respectively. The fatty acid composition of Turmeric oil is reported in Table 2.9. It shows that oleic acid contributes the highest proportion (56.24 - 58.88%), followed by myristic acid (16.25 -

17.71%), palmitic (5.59 - 6.00%), linoleic (10.90 - 12.82%), linolenic (4.15- 5.46%) and ecosenoic acid (2.72 - 3.25%) (Paul et al., 2011). Hence, it can be utilized successfully as a source of edible oil for human consumption.

Essential oil of turmeric consists of different sesquiterpenes (*ar*-turmerone, *α*- turmerone, *β*-turmerone, turmerol) and *α*-atlantone along with Curcuminoids(Chang et al., 2006). Turmerone protect cells from damage, enhance wound healing capacities, controls type 2 diabetes symptoms, inhibit replication of HIV (human immunodeficiency virus), conceal formation of tumors and protect liver damage. ar-turmerone plays an important role in self-repair and recovery of brain function in neurodegenerative diseases (Park et al., 2012). Curcuminoids (Curcumin) is a yellow-orange crystalline powder insoluble in water, poorly soluble in hydrocarbon solvents, and soluble in alcohols (Chassagnez-mendez et al., 2000). It is beneficial to human health due to its anti-inflammatory, antioxidant, antifungal, anticarcinogenic, antiviral, antimutagenic, anticoagulant, antidiabetic, antibacterial, antiprotozoal, antifibrotic, antifertility, hypotensive and hypocholesteremic properties (Bagchi, 2012; Chang et al., 2006). Other than turmerone and curcumin, various bioactive compounds were found in turmeric root oil as reported in Table 2.9.

To extract oil from turmeric root, various conventional extraction methods are used such as hydro-distillation, Soxhlet extraction, microwave-assisted extraction and steam distillation (Garg et al., 2002; Laokuldilok et al., 2015; Negi et al., 1999). SFE can be used to extract oils from natural products as it does not produce substantial thermal degradation or organic solvent contamination (Banchero et al., 2013; Gilbert-Lopez et al., 2017; Todd and Baroutian, 2017). Antibacterial activity of turmeric oil and composition of essential oil from turmeric root as well as leaves were investigated by many researchers (Awasthi and Dixit, 2009; Negi et al., 1999; Raina et al., 2005). Solvent extraction method was employed by Negi et al. (1999) and Jayaprakasha et al. (2001) to extract essential oil from mother liquor/curcumin removed turmeric oleoresin considering hexane as a solvent. Further, essential oil was separated into three fractions using silica gel column chromatography to perform the antibacterial activity test and Gas chromatography–mass spectrometry (GC-MS) analysis of these fractions. Raina et al. (2002) and Garg et al. (2002) extracted essential oil from leaf and rhizome of turmeric through hydro-distillation method and analyzed oil using GC-MS. Began et al. (2000) and Gopalan et al. (2000) extracted turmeric root using SFE and studied effects of operating parameters such as pressure, temperature, flow rate and particle size. Chang et al., (2006) extracted turmeric oil using SFE process, which was further analyzed through liquid chromatography to isolate turmerones. Effects of pressure and temperature

were also studied considering two responses i.e. oil yield and concentration of turmerones. Authors observed that SFE below 47 °C and above 26 MPa is a suitable condition to extract oil where it consists of 71 wt% purity of three turmerones.

Table 2.9 Fatty Acid and Essential oil composition of the Turmeric root oil.

Fatty acids						
References	Oleic acid (%)	Myristic acid (%)	Linoleic acid (%)	Palmitic acid (%)	Linolenic acid (%)	Eicosenoic acid (%)
Paul et al. (2011)	56.24 - 58.88	16.25 - 17.71	10.90 - 12.82	5.59 - 6.00	4.15- 5.46	2.72 - 3.25
Essential oil						
References	Turmerone (%)	Curlone (%)	ar-turmerone (%)	Curcumene (%)	β-bisabolene (%)	α-zingiberene (%)	Curcumin
Negi et al. (1999)	5.09	3.88	62.00	3.49	2.1	2.48	-
Began et al. (2000)	-	-	55	-	-	-	-
Gopalan et al. (2000a)	16.12	-	42	4.23	-	-	-
Chassagnez-mendez et al. (2000)	-	-	15.5	3.6	1.7	-	-
Jayaprakasha et al. (2001)	6.2	5.1	21.4	2.31	3.55	15.03	-
Raina et al. (2002)	11.1	-	7.3	8.6	2.8	5.6	-
Braga et al. (2003)	-	-	15.4	1.0	1.3	2.4	-
Asghari et al. (2009)	20.9	-	68.9	0.8	0.4	1.5	-
Singh et al. (2010)	4.3	-	21.4	6.6	4.1	0.8	-
Tsai et al. (2011)	-	-	49.04	-	-	-	-
Laokuldilok et al. (2015)	-	4.7	26.82	-	2.25	-	-
Singh and Jain (2011)	-	-	-	-	-	-	7.57%

2.7.2 Carrot seed Oil

Oils are derived from plant seeds and used extensively in food beverage, pharmaceutical, bio fuel production and also used as a natural solvent (Keshav et al., 2009a). Carrot seed oil is widely used

in pharmaceutical and cosmetic industry because it may fight cancer cells, acts as powerful antioxidants, supports skin and hair health and acts as natural sunscreen. It also consists of fatty acid as well as essential oil, which are provided in Table 2.10 as reported by various researchers. Fatty acids support the brain development of the newborn and children and mostly extracted by reactive extraction (Keshav et al., 2009b). It shows that Oleic acid, monounsaturated omega-9 fatty acid, is the principle compound, which contributes more than 80% of carrot seed oil. It consists of other fatty acid, USFA and SFA both, in different concentration as reported in Table 2.10.

In case of essential oil composition of carrot seed oil, Carotol is found as dominant compound, which comprises of 13.97 to 52.73% of carrot seed oil as investigated by various researchers (Acimovic et al., 2016; Cu et al., 1989; Jasicka-Misiak et al., 2004). Carrot seed oil also consists of Daucol, Farnesene, Daucene and Caryophyllene in significant amount with other bioactive compounds as reported in Table 2.10.

Table 2.10 Fatty Acid and Essential oil composition of the Carrot seed oil.

Fatty acids						
References	Oleic acid (%)	Stearic acid (%)	Linoleic acid (%)	Palmitic acid (%)	Petroselinic acid (%)	Arachidic acid (%)	Linolenic acid (%)
Parker et al. (2003)	82.08	0.42	13.19	3.71	-	0.33	0.28
Ozcan and Chalchat (2007)	0.17	2.41	11.82	10.01	59.35	0.81	-
Gao et al. (2016)	81.5	0.87	13.3	3.75	-	0.13	0.48
Gao and Birch (2016)	81.45	0.87	13.32	3.75	-	0.14	0.48
Essential oil						
References	Daucol (%)	Carotol (%)	Farnesene (%)	Caryophyllene (%)	β-bisabolene (%)	β-Cubebene (%)	Daucene (%)
Cu et al. (1989)	0.96	13.97	2.33	1.61	0.27		1.68
Jasicka-Misiak et al. (2004)	2.00	38.85	4.03	10.66	-	0.53	-
Acimovic et al. (2016)	0.3	22.0	8.2	5.7	2.4	-	1.0
Chahal et al. (2016)	5.1	52.73	5.40	1.22	2.95	3.19	5.68
Sieniawska et al. (2016)	2.54-6.22	19.62-33.37	0.12-1.01	0.06-5.59	0.87-4.71	-	0.24-1.13

Carrot seed oil was extracted through hydro-distillation and soxhlet extraction methods using different types of solvents (1,1,2-trichloro-l,2,2-trifluoroethane, methylfuran, ethanol and dichloromethane) and found that extraction yield of essential oil from hydro-distillation method was minimum (Cu et al., 1989). Authors observed that ethanol is sufficient polar to extract terpenoid oxides of carrot seed and quantified carrot seed oil with GC-MS. Isolation of major Sesquiterpenes of oil i.e. Carotol and Daucol were performed using extracted carrot seed oil (Jasicka-Misiak et al., 2004). Petroleum ether was used to extract carrot seed oil by Soxhlet extraction method and investigated fatty acid, essential oil, mineral content of oil (Ozcan and Chalchat, 2007). Carrot seed oil extracted through SFE was collected from an industry and physicochemical characteristics, oxidative ability, thermal properties, phenolic acids, flavonoids, tocopherol and fatty acid content of oil were studied (Gao et al., 2016; Gao and Birch, 2016). Carrot seed oil was extracted using hydro-distillation method and analyzed through GC-MS to identify the composition of compounds present in oil (Chahal et al., 2016). Carrot seed oil majorly contains unsaturaed fatty acids (USFA).

CHAPTER 3

MATERIALS, METHODS AND EXPERIMENTATION

In this Chapter, materials, methods and experimental techniques used in the present study are discussed. Based on the literature review, carried out in Chapter 2, turmeric root and carrot seed are considered for the study. Preparation of raw materials and chemicals used in the process are discussed in this Chapter. Operating parameters involved in supercritical fluid extraction (SFE) of turmeric root and carrot seed are described. Design of experiment technique is used for optimization of operating parameters and to study the effect of operating parameters. Experimental setup and procedure for extraction of turmeric root oil and carrot seed oil is discussed. Methods and techniques used for the characterization of raw materials are presented.

3.1 Raw Materials and Chemicals

In this section, selection of raw materials and its preparation prior to extraction is explained. Chemicals used in the extraction processes, characterization techniques and analysis techniques are also discussed.

3.1.1 Raw material and its preparation

Based on literature review, presented in chapter 2, turmeric root and carrot seed were selected as raw materials to study the SFE process.

Fresh turmeric root was purchased from local market in Roorkee, Uttarakhand, which was washed with water to remove dust and dried in oven at 60 °C for 24 hours to remove moisture. Further, it was grounded in domestic mixer grinder (Bajaj, India). The milled turmeric powder was separated and graded according to their particle size using certified test sieves (Endecotts Ltd., London, England) with a vibratory sieve shaker (octagon 200, Endecotts Ltd., London, England). The turmeric powder was separated into three ranges: 0.73 mm, 0.45 mm and 0.2 mm and these were found through sizes of two successive sieves such as -0.850+0.600, -0.600+0.300, -0.300+0.100.

For carrot seed, dried and clean carrot seed was purchased from local market which was then milled in domestic mixer grinder (Bajaj, India). Further, carrot seed of different sizes were found through vibratory sieve shaker (octagon 200, Endecotts Ltd., London, England). In the present work, Carrot seed of three different sizes are considered i.e. 0.9 mm, 0.6 mm and 0.3 mm.

3.1.2 Chemicals

CO_2 with purity of 99.9% was used as a supercritical fluid in the SFE experiments, which was available in pressurized deep tube cylinders supplied by Sigma gases, India. The ethanol used as a

co-solvent for experiments was purchased from Merck Ltd. (Darmstadt, Germany). Standard chemicals of Turmerone, Curcumin and fatty acid methyl esters (FAMEs) were obtained from Sigma Chemicals (St. Louis, MO, USA). Other chemicals such as Hexane, Acetone, Methanol, Toluene, Anhydrous sodium sulfate, Sulfuric acid (98.5%), Potassium bicarbonate and Sodium chloride of analytical grades were procured from Merck Ltd. (Mumbai, India).

3.2 Selection of Operating Parameters

Supercritical fluid extraction of any species depends on several operating parameters such as temperature, pressure, solvent flow rate, particle size, addition of co-solvent, extraction time, properties of bed, initial content of oil, type of matrix of raw material and pretreatment of raw materials (Doker et al., 2004; Koga et al., 1996; Mitra et al., 2009; Rai et al., 2015; Taher et al., 2014). Generally, the extent of recovery of solute/oil from the raw materials is represented by the extraction yield of oil, which must be at its maximum value. Effect of different operating parameters on the extraction yield is discussed in section 2.6.3. Values of operating parameters are considered as optimum conditions, at which, extraction yield is highest. To investigate optimum operating conditions, experimental study is required however; large number of parameters increases the number of experimental runs. Therefore, selection of significant operating parameters for the SFE is required. Based on literature review, temperature, pressure, particle size, solvent flow rate and addition of co-solvent were found to be important parameters for the SFE process and thus, used in the present work also (de Melo et al., 2014).

3.2.1 Raw material-I (turmeric root)

To study the SFE of turmeric root, five operating parameters such as temperature, pressure, solvent flow rate, particle size and addition of co-solvent were varied into different ranges. Other parameters such as extraction time and amount of feed material were kept constant for all experiments. Extraction time and amount of seed (properties of bed) was constant at 260 min and 100 g for all experimental runs. Ranges of operating parameters were decided based on literature review. For turmeric root, Began (2000) varied temperature, pressure and solvent flow rate as; 10-30 MPa, 40-60 ° C and 3-9 ml/min, respectively. However, Gopalan et al. (2000) considered ranges of temperature, pressure, solvent flow rate and particle size as: 10-30 MPa, 40-60 °C, 0.035-0.085 g/s and 0.208-1.158 mm, respectively. Chassagnez-mendez et al. (2000) also extracted the turmeric root with the SFE process at pressures of 25 and 30 MPa and temperatures of 40 and 45 °C. Chassagnez-mendez et al. (2000) used ethanol as a co-solvent with the pure CO_2 and reported that extraction yield was increased with addition of co-solvent. In the present study,

68

pressure, temperature, solvent flow rate, particle size and addition of co-solvent were considered to vary as: 200-400 bar, 40-60 °C, 5-15 g/min, 0.2-0.73 mm and 0-15 % of solvent flow rate. Gopalan et al. (2000) reported that increasing pressure and solvent flow rate led to an increase in extraction yield of turmeric oil, hence, pressure and solvent flow rate were increased up to 40 MPa (= 400 bar) and 15 g/min, respectively, in the present study. Ranges for temperature and particle size were selected as same as proposed by Gopalan et al. (2000). To study the effect of co-solvent, ethanol was added as co-solvent, which varied from 0 to 15% of solvent flow rate.

3.2.2 Raw material-II (carrot seed)

For carrot seed, it appears that no study has been performed on the SFE of carrot seed oil and hence, selection of parameters and its ranges were difficult to predict. Fennel seed, cumin seed and celery seed, which are look-alike of carrot seed and have somewhat similar properties, were studied for the selection of operating parameters of carrot seed. Reverchon et al. (1999) performed the SFE of fennel seed at temperature of 40 and 50 °C, pressure of 90 and 200 bar, particle size of 0.3 mm and flow rate of 0.5,1 and 1.5 kg/h. Rodríguez-Solana et al. (2014) selected four operating parameters for the optimization of SFE of fennel seed as: temperature of 40-60 °C, pressure of 10-25 MPa, extraction time of 1-4 h and co-solvent (methanol) of 0-6%. Similarly, Papamichail et al. (2000) identified four operating parameters for the optimization of SFE of celery seed such as pressure (100-200 bar), temperature (45-55 °C), particle size (210-490 μm) and solvent flow rate (1.1-3.0 kg/h). In the present study, pressure, temperature, solvent flow rate, particle size and addition of co-solvent were varied from 100-400 bar, 40-70 °C, 5-20 g/min, 0.3-0.9 mm and 0-10% of solvent flow rate for the SFE of carrot seed.

3.3 Experimental Setup

The SFE setup (1000F) was purchased from Thar Technologies Inc., Pittsburgh and was used for extraction of turmeric root and carrot seed oil using CO_2 at above its critical conditions as shown in Fig. 3.1. A schematic representation of the SFE system is also shown in Fig. 3.2.

Fig. 3.1 Experimental setup of SFE used in present study.
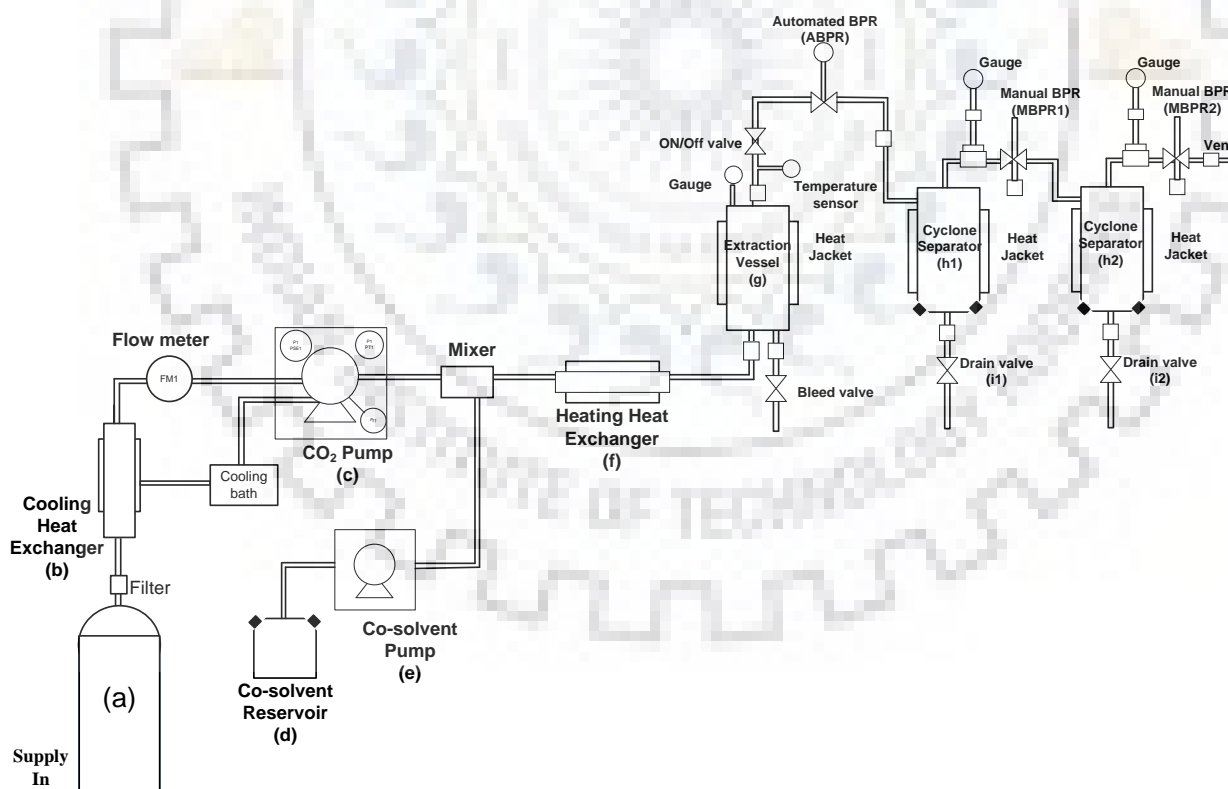
Fig. 3.2 Schematic diagram of SFE setup.

Fig. 3.2 shows the operating procedure to perform SFE of any solute. The liquid CO_2 is supplied from cylinder (a) and passed through a 0.22 µm sintered stainless steel metal filter. Supplied CO_2 must be at less than 5 °C, therefore it passes through a cooling Heat exchanger (b) where, water is flowing at 2.5 °C in counter current direction. The head of high pressure CO_2 pump is also cooled by circulating chilled water. Further, cooled CO_2 is pressurized by high pressure piston pump then it gets mixed with co-solvent supplied by co-solvent reservoir (d) through co-solvent pump (e). The mixer of CO_2 and co-solvent is heated up to a desired temperature through the heat exchanger (f) to attain supercritical conditions. Further, it enters into the extraction vessel (g) where transport of oil from solid material to the supercritical CO_2 occurs. The feed material is charged into a stainless steel basket placed inside the extraction vessel for easy and fast charging and discharging of the extraction cell. Desired flow rate of CO_2 is maintained for the duration of 260 minutes. Automated Back Pressure Regulator (ABPR) maintains desired supercritical pressure inside the extraction vessel. Then extract rich supercritical-CO_2 flows through a flash vessel called cyclone separator (h1) where pressure of the mixture is throttled from operating pressure to 65 bar using Manual Back Pressure Regulator (MBPR1). Hence, supercritical CO_2 converts into gas and oil is separated which is collected from the bottom of the flash vessel (i1) at every five minutes in a separate collection vials. Further, CO_2 gas enters in another separator (h2) maintained at 40 bar using manual back pressure regulator (MBPR2). Remaining oil is collected in this separator from the bottom and CO_2 is vent off to the atmosphere from the top of it. The setup is then shut down to unload the oil free seed material from the extractor and a new batch of seed material is then charged into the extractor.

Various parts of SFE setup are explained as:

3.3.1 CO_2 pump

In SFE experiment, CO_2 must be pumped in liquid form, below 5°C and at a pressure of minimum 70 bar. In the present study, a duel piston high pressure pump (P-200A, P-series, Thar Technologies Inc.) is used, which provides a low dead volume head and pulse free supply of the CO_2. The front view of high pressure CO_2 pump is shown in Fig. 3.3. To refill the piston chamber, piston moves back and inlet check valves open up hence, CO_2 flows into the chamber. As refilling is completed, piston starts to move forward and inlet check valves are closed. If pressure inside the piston chamber exceeds the system pressure, outlet check valves open up and CO_2 starts flowing into the system. Since, the CO_2 is being compressed inside the piston chamber, cooling of pump

head is carried out using cold water. The CO_2 pump is designed to operate between 5 to -45 ºC and up to 600 bar with a flow rate of 3 to 200 g/min of CO_2.
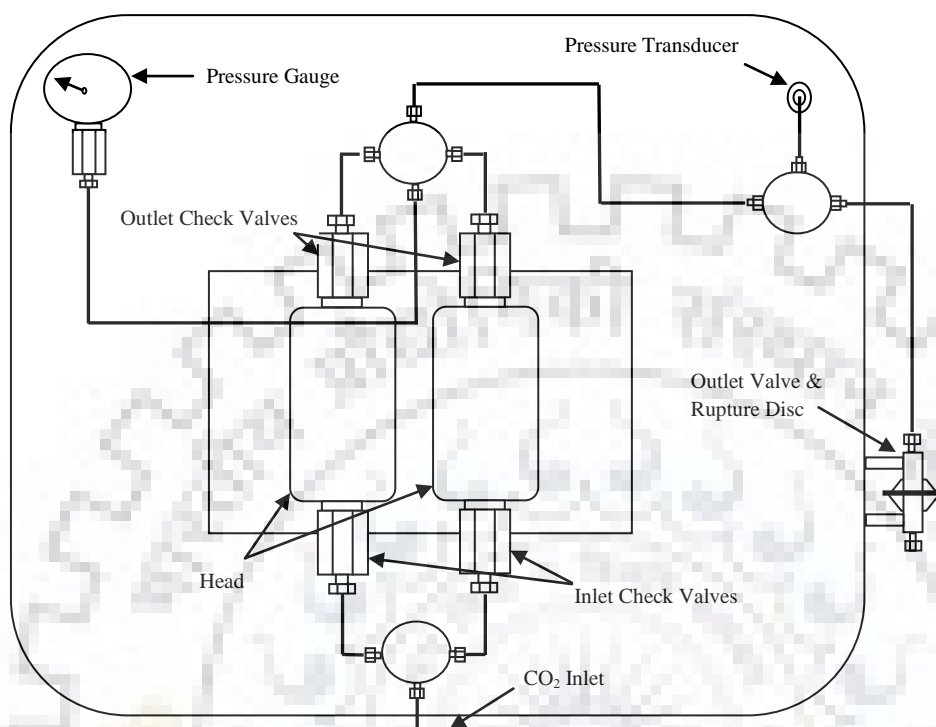
Fig. 3.3 Front view of high pressure CO_2 pump.

3.3.2 Co-solvent pump

Various co-solvents are used to enhance the polarity of CO_2 such as ethanol, methanol, 2-propanol, dichloromethane and acetic acid for supercritical extraction process. A highly accurate High pressure liquid chromatography (HPLC) grade modifier pump (A21635, Scientific System, Inc., PA, USA) is used to supply desired amount of co-solvent into the system. Pump includes a diaphragm-type pulse damper, which reduces pulsation in the system by 90%. It also consists of separate pressure transducers, which automatically turn off if pressure exceeds the maximum design pressure. Co-solvent pump is designed to operate up to 410 bar and in a flow rate range of 0.01-10 ml/min.

3.3.3 Extraction vessel

In the SFE setup, extraction vessel is used to hold seed material where, supercritical CO_2 extracts the solute from seed material. Extraction vessel is available in different sizes according to requirement such as 100ml, 500ml, 1000ml, 2000ml, or 5000ml. Multiple extraction vessels can

also be installed in a single setup to extract different sample sizes or to increase output of the system. However, in the present setup, an extraction vessel of 1000 ml, made of stainless steel is installed. Pressure requirement for SFE is at least 74 bar, which goes up to 350 bar for most of the extraction process. However, for vegetable oil extraction, higher pressure (up to 600 bar) may be required for complete miscibility of two phases. The extraction vessel used in the present study is designed to handle high pressure up to 680 bar. It is also equipped with electrically heated jacket, where two thermocouples are placed to maintain uniform temperature throughout the vessel. To prevent chocking of tube through entrainment of large solid particles, a stainless steel frit filter is placed under the vessel head.

3.3.4 Automatic back pressure regulator (ABPR)

In the SFE setup, ABPR is employed to maintain the pressure between CO_2 pump outlet and extraction vessel. In the present system, ABPR maintains upstream pressure of the regulator by means of an electronically driven valve. It is designed to maintain the pressure up to 680 bar. Adiabatic expansion of CO_2 takes place inside the system, which leads to ice formation in the restrictor or valve and causes blockages. To prevent ice formation, a low voltage and low wattage heater is also equipped in ABPR assembly to supply heat.

3.3.5 Cyclone separators

Cyclone separators are used to separate oil from oil-laden supercritical CO_2. Separators are operated at lower pressure than that of extraction vessel as dissolving power of supercritical fluid varies with pressure and temperature. At lower pressure, solubility of oil gets reduced in less dense CO_2 and therefore, oil separates for collection. In the present setup, two separators are installed in series to separate dissolved material at reduced pressures. Lower pressure inside the separators is maintained by MBPR1 and MBPR2 mounted at the top of each separator as shown in Fig. 3.2. Supercritical CO_2 gets depressurized to atmospheric pressure and vents off into atmosphere. Extracted oil is collected from bottom of each separator during regular interval of time, which is stored at 4°C in dark for further analysis.

3.3.6 Heat exchangers

Heat exchangers are essential parts of the SFE setup since CO_2 must be cooled prior to pumping inside the CO_2 pump and then heated after pressurization. As fluid expansion takes place inside the separator, heat must be provided to prevent excessive cooling. A low pressure shell and tube type heat exchanger (b) is installed to cool the supplied CO_2 and exit water from heat exchanger is

connected to pump head to cool chamber of the pump. Similarly, an electric high pressure heat exchanger (f) is installed to heat CO_2 up to required supercritical temperature. A thermocouple is also installed with electric high pressure heat exchanger to read temperature where, thermocouple sensors are capable to measure temperature in a range of 100 to 1000ºC. A temperature controller is also installed to control temperature of various parts of the SFE unit, which can handle up to six independent PID control zones with its own thermocouple and control relay. It is designed to operate at normal power supply (85-240 VAC, 50/60 Hz).

3.3.7 Tubing and lining

In the present SFE setup, tubes with 1/8" outer diameter and 0.035" wall thickness are used in high pressure sections. However, 1/8" outer diameter and 0.020" wall thickness tubes are used for low pressure section (tubing between CO_2 cylinders to pump inlet through a stainless steel Swagelok fitting). A computer is required to operate the setup where setting of parameters is carried out through computer via keyboard.

3.4 Experimental Procedure

In this section, experimental procedure to perform SFE of turmeric root and carrot seed using supercritical CO_2 is explained.

3.4.1 Loading of feed material

To extract oil from solid material, it is fed into the extraction vessel with the help of extraction basket. SFE of turmeric root and carrot seed is operated in batch mode and consists of one extraction vessel with the capacity of 1 l each. A cylindrical stainless steel basket of 19 cm height and 7.5 cm diameter is used as packed bed for extraction, which contains desired solid material and glass beads of 5 mm diameter. To prepare the bed for experiment, initially 100 g glass beads (2.0 cm height) were placed at the bottom of basket and then glass wool with a thickness of 0.5 cm is placed over it followed by 100 g of glass beads over the glass wool. This arrangement was made for uniform distribution of supercritical CO_2 inside the bed and better contact with solid material. Finally, a layer of 100 g (x cm) of solid material is placed followed by glass beads, glass wool and again glass beads of heights 2.0, 0.5 and 2.0 cm, respectively. This arrangement was used to stop the carryover of solid particles with supercritical CO_2. Height of solid material in packed bed varies according to different particle sizes of solid material as it is longer for smaller particle and vice-versa. Upper layer of glass beads is then covered using thin steel sheet to prevent the

carryover of glass beads inside the line. Schematic representation of extraction basket is shown in Fig. 3.4.
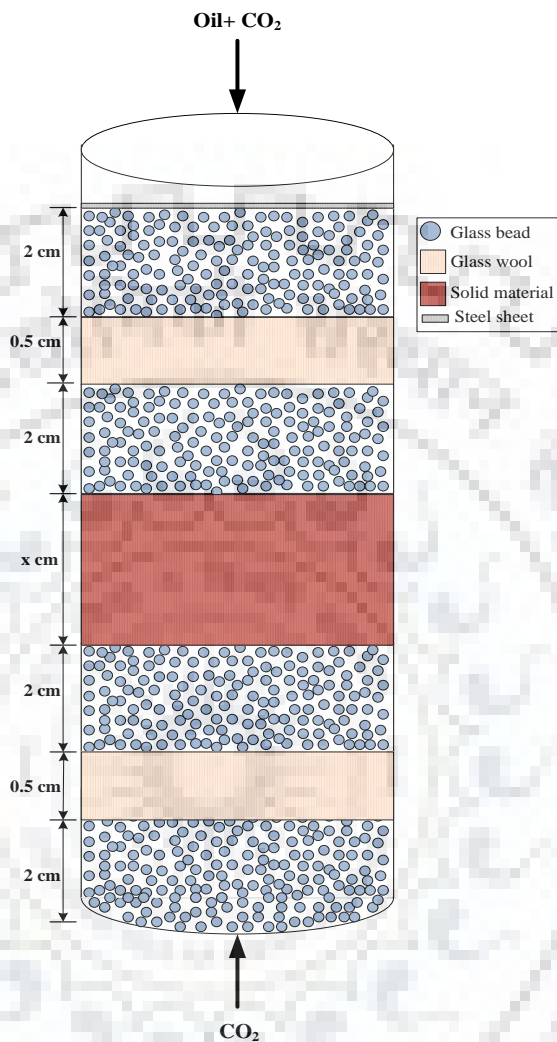
Fig. 3.4 Schematic representation of packed bed for SFE process.

3.4.2 Startup of SFE setup

To perform experimental run, chiller must be turned on for 1-2 h prior to start the setup. Extraction vessel and separators should be cleaned with Acetone before starting the experiment to wash off the traces of previous experiment. Then, extraction basket, prepared according to procedure explained in section 3.4.1, is inserted into the extraction vessel where lid is hand-tightly closed. Further, tubing coming through ABPR is connected to extraction vessel and closed tightly to avoid leakage of CO_2.

As chiller temperature reaches below 5°C, power for the SFE setup and computer is switched on. Values of parameters are filled using pre-loaded software, called Process Suite as shown in Fig. 3.5. It shows whole SFE setup, its parts, its connections and values of parameters. Values of parameters can be inserted by clicking on the "View" option in the device appearing on the suite window. Extraction pressure, temperature, solvent flow rate and co-solvent flow rate can be inserted in "Device setting" option of "Pressure Regulator", "Heater", " CO_2 pump" and "Co-solvent pump wizard, respectively, as shown in Fig. 3.6 to 3.9.

In Fig. 3.6, back pressure is initially set at 70 bar through ABPR, which can be further increased slowly up to the required operating pressure that is inserted at the "pressure set point" column in as shown in Fig. 3.6. However, maximum allowable pressure is set by default in the "pressure alarm" column as at high pressure than allowable pressure, an alarm starts beeping and the system shuts off automatically. The "valve heater set point" is set to near critical temperature of the solvent as less heat is required to melt ice formation at the restrictor to prevent blockage inside the valve during adiabatic expansion of supercritical CO_2. The "current profile settings" is opted to tune the system as "attenuation factor" is inserted to control fluctuation of valve in ABPR caused by change in pressure. This value should normally be set to 1 as given in Fig. 3.6. A larger value of "proportional constant" is responsible for further opening of valve from set point. Similarly, "integral constant" is also set to move pressure slowly towards the set point if it is too close for proportional constant to have any effect. The value of "output max" represents the valve opening limit while the "derivative constant" influences rate of change in pressure as larger value causes slower changes in pressure.

Parameters of heaters and heat exchangers are set through "Heater controller" window, which displays all heating zones as shown in Fig. 3.7. "Heater Controller Settings" wizard appears while clicking the "Device Settings" button at the bottom of "Heater controller" window. Temperature of "Electrical heat exchanger", "Vessel 1 heater", "Vessel 1 internal temperature", "Collection vessel 1 heater" and "Collection vessel 2 heater" are inserted by selecting zone 1 to 5 from drop down list of "select zone". In the present setup, Zone 6 is not available for setting. Parameters of configuration setting are set as recommended by Thar technologies Inc.

After heater controller setting, parameters for CO_2 pump settings need to be inserted through "Device setting" option. As can be seen from Fig. 3.8, pump can be operated using two different modes such that flow and pressure, which maintain constant flow and constant pressure,

respectively. In the present study, flow mode is selected to maintain constant flow of CO_2 during the experiment and operating flow rate is inserted in "set point" column. The maximum allowable pressure is also set in the "pressure alarm" column to prevent any hazard. Parameters in the "current profile setting" are set as per the recommendation of system manufacturer. CO_2 pump flow and pressure trends with respect to time are also visible to insure the smooth running of pump.

Co-solvent flow rate is inserted in the "Co-solvent pump" setting, which should not be more than 30% of solvent flow rate. Co-solvent flow and pressure trend along with pump setting are shown in Fig. 3.9.

After setting parameters of all parts, the valve of CO_2 cylinder is opened manually to allow flow of CO_2 into the setup. Simultaneously, the CO_2 pump is started by clicking on the "Start Pump" option in "CO_2 pump" wizard. Then, ABPR and co-solvent pumps are turned on using "Start ABPR" and "Start pump" buttons in "Pressure regulator" and "Co-solvent pump" windows. ABPR takes little longer to reach at desired pressure therefore, sampling of oil can be started once ABPR has acquired the set pressure. A block diagram is also given in Fig. 3.10, which shows the experimental procedure of SFE process.
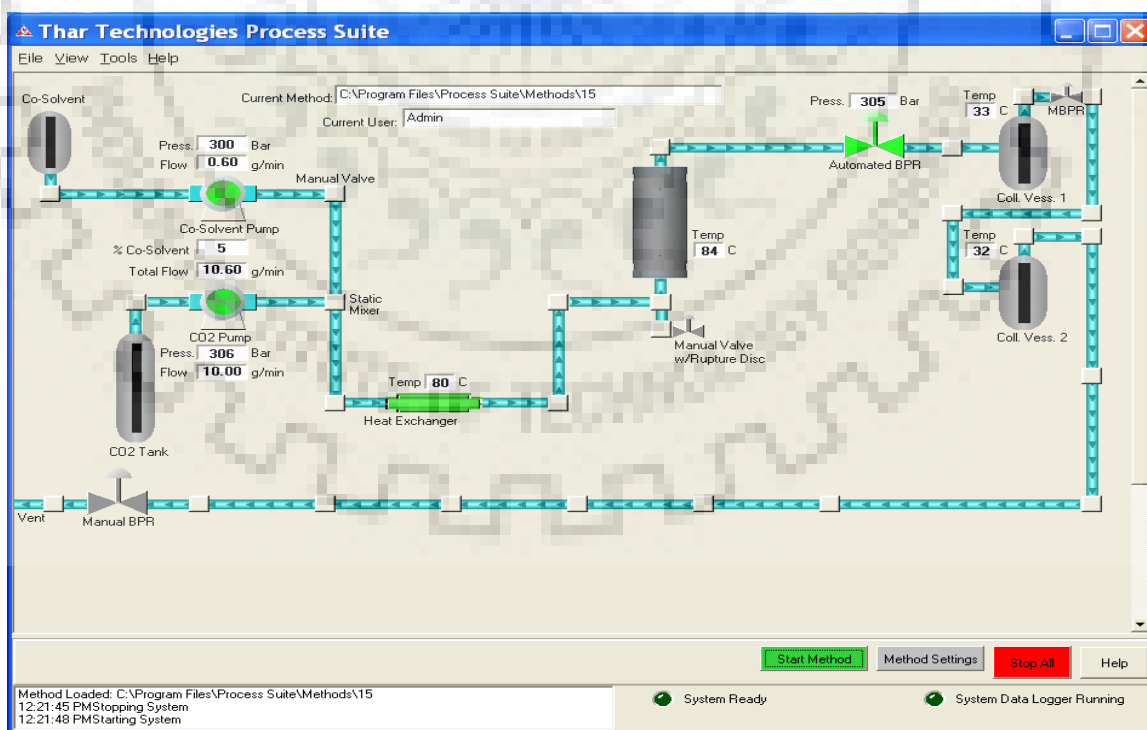

Fig. 3.5 Home wizard of Process Suite software.
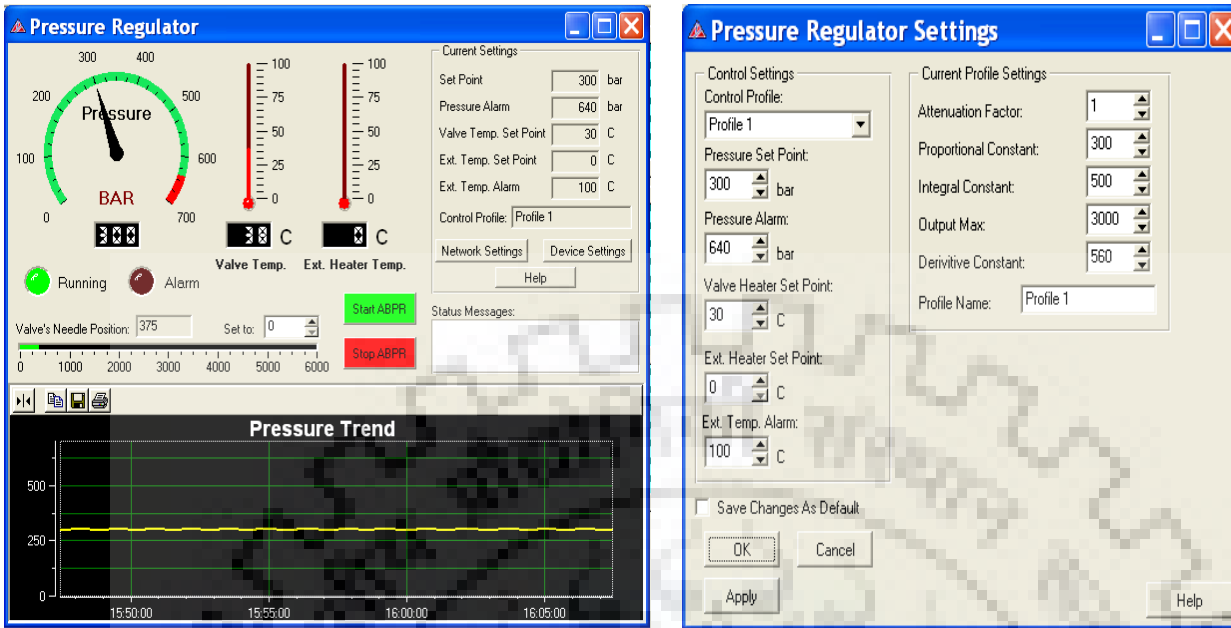
Fig. 3.6 Automatic Back Process Regulator setting in Process Suite software.
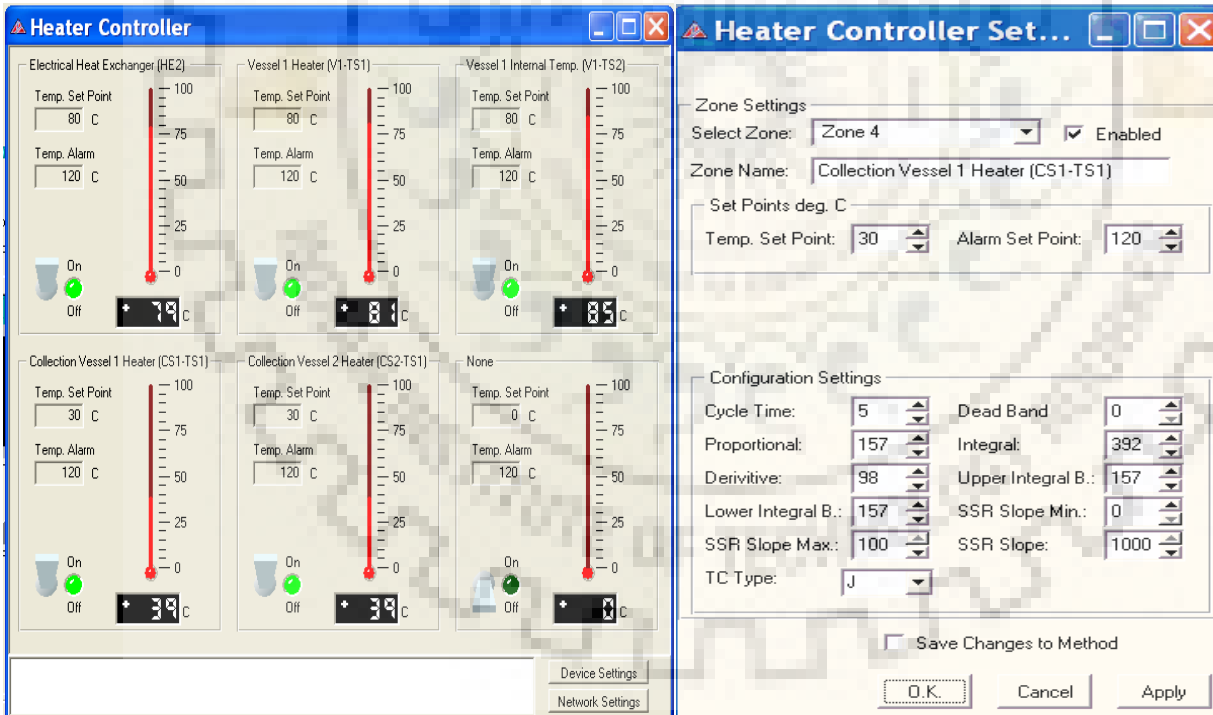
Fig. 3.7 Heater setting in Process Suite software.
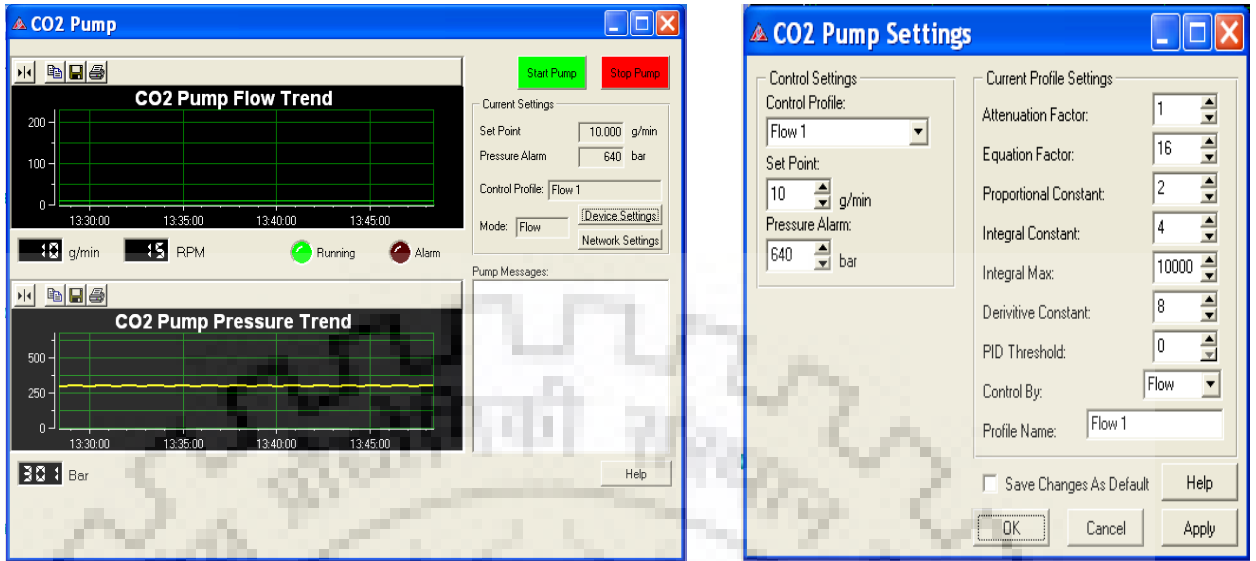
Fig. 3.8 CO$_2$ pump setting in Process Suite software.

Fig. 3.9 Co-solvent pump setting in Process Suite software.
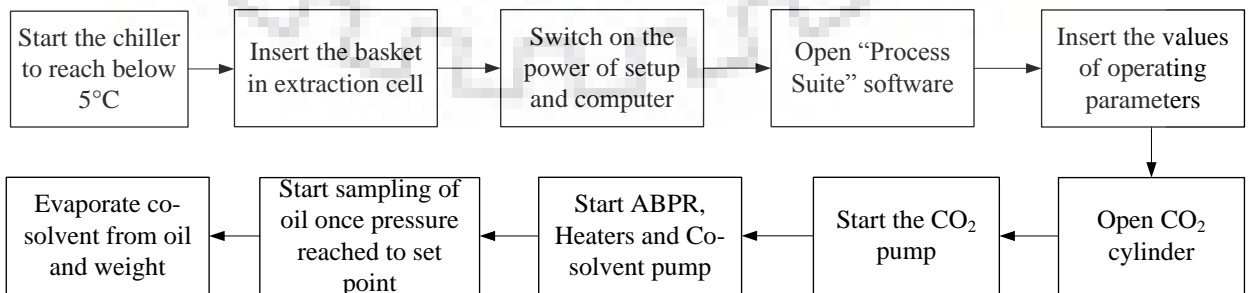
Fig. 3.10 Block diagram to represent the experimental procedure of SFE process.

3.4.3 Collection and sampling of oil

Extracted oil can be collected in a regular interval (5 or 10 min) from the bottom of each separator once ABPR pressure is reached at set point and all parts are working properly. Oil is collected in sampling vials and most of the oil is collected from the first separator. Co-solvent is removed from extracted oil using rotary vacuum evaporator and then remaining oil samples are weighed. Total cumulative extraction yield is determined as the sum of oil extracted in given extraction time.

3.4.4 Shutdown procedure of setup

The SFE setup needs to be shut down properly to avoid damage as it operates at very high pressure and temperature. After completion of extraction run, the electrical heat exchanger is turned off then flow rate of CO_2 and co-solvent pump is reduced to zero and finally pumps are stopped. All heaters are switched off after ensuring that both pumps are stopped. Green light in each window turns off and indicates that all pumps and heaters are stopped. After that, CO_2 cylinder is closed manually and pressure of ABPR is released gradually below 30 bar. For safety point of view, pressure on each gauge must be showing zero before opening the extraction vessel. In the end, the extraction vessel is opened and the basket is removed and cleaned using acetone for loading of the next run.

3.5 Determination of Initial Oil Content of Raw Material

Soxhlet extraction method is primarily used for the extraction of organic compounds from solid samples. In the present work, this method is adopted to determine the total extractable oil content of turmeric root and carrot seed as shown in schematic diagram of setup i.e. Fig. 3.11. A dried and milled solid sample of approximately 100 ± 0.2 g is loaded in the glass thimble separately, which is connected to a 500 ml round bottom flask shown in Fig. 3.11. Extraction is carried out using 250 ml n-hexane for 24 h and hexane is removed by rotary vacuum evaporator at 50°C. This procedure is repeated three times for single type of raw material and all oil samples are stored in dark for further analysis. Initial oil content, computed using equation 3.1, is found to be approximately 5.954 and 13.5 wt% for turmeric root and carrot seed, respectively.

$$\text{Oil content}(\%) = \frac{\text{Total Oil extracted (g)}}{\text{Solid sample (g)}} \times 100 \qquad (3.1)$$
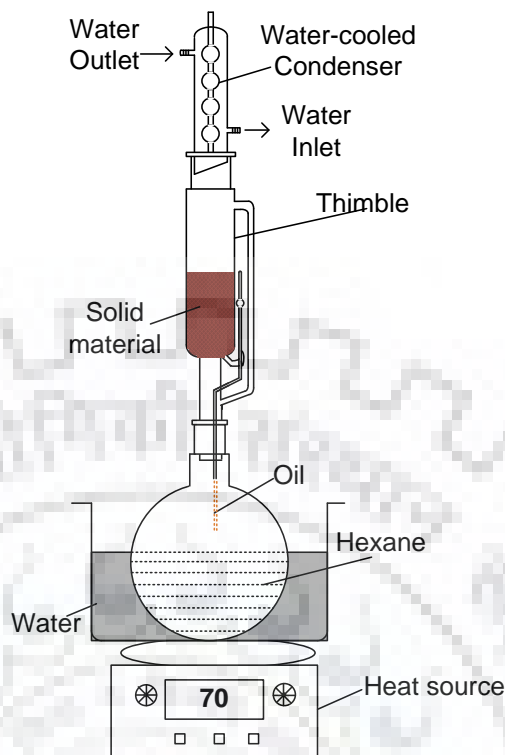
Fig. 3.11 Schematic diagram of Soxhlet extraction setup.

3.6 Moisture and Ash Content of Raw Materials

Moisture and Ash contents of turmeric root and carrot seed are determined using standard method 926.12 recommended by Association of analytical communities (AOAC). Turmeric root and carrot seed samples of 5 ± 0.2 g are taken into the dry petridish and kept in oven at $105 \pm 1°C$ for 1 hour. Then, dish is taken out from the oven and kept in desiccator for cooling after closing the lid. Further, sample is weighed and noted down. The above process is repeated until a constant weight is achieved for single sample.

Similarly, Ash contents of turmeric root and carrot seed are determined using the method ISO-749. For this purpose, moisture free samples of quantity 2 ± 0.1 g are taken and kept in preheated electric furnace at $550 \pm 10°C$ until a constant weight is achieved. Moisture and ash content are computed using equation 3.2.

$$\text{Moisture/Ash Content (\%)} = \frac{\text{Loss of Weight}}{\text{Initial Weight Taken}} \times 100 \tag{3.2}$$

81

3.7 Characterization of Raw Materials and Extracted Oils

Characterization of raw materials is performed using different techniques as:

Fourier transform infrared (FTIR) spectrometer purchased from Thermo Nicolet, Madison, WI, USA is used to study the presence of functional groups, chemical nature of turmeric root, carrot seed and extracted oil using KBr pressing technique over a spectral range of $500-4000$ cm^{-1}.

Morphologies of turmeric root and carrot seed are observed using LEO-1550 Scanning electron microscope (SEM). Pre and post extraction samples of both raw materials are coated with gold–palladium alloy using gold spurting prior to scan through SEM.

To study thermal stability of turmeric root and carrot seed, differential thermal and thermo gravimetric analysis (DTA and TGA) are carried out under nitrogen atmosphere. Nitrogen with a flow of 200 ml/min and heating rate of 20 °C/min is used from 25°C to 700 °C temperature range. Aluminum is used as a reference material.

To study the melting and crystalline characteristics of extracted oil, differential scanning calorimeter purchased from DSC 131 evo, SETARAM Instrumentation, KEP Technologies is used. Oil is scanned over a range of -60°C to 50°C for melting and crystalline profiles. Oil sample of around 10 mg is placed inside high pressure alumina crucible, which is tightly closed. An empty crucible is also placed as a reference. Liquid nitrogen is used to achieve cooling temperature of sample to -60°C.

3.8 Application of Design of Experiment (DOE)

In the present work, DOE technique is employed to optimize the SFE process. As a matter of fact, optimization of several operating parameters can be carried out while varying one factor at a time and considering other factors as constant. However, it gives a large number of experimental runs to perform, which is a time-consuming method and not economically feasible as well, especially when large numbers of variables are involved. In addition, the study based on interaction of operating parameters is not possible with this approach. It also provides a correlation between input parameters and output parameter/s, which can be used to find output at different input values without performing experimental run. Further, DOE allows the user to perform screening of operating parameters, which gives most and least influential parameters of the process with minimum number of experimental runs. Hence, least influential parameters can be eliminated and optimization of remaining operating parameters can be performed with reduced number of experimental runs. Therefore, statistical analysis using DOE is found to be very efficient tool for estimating the effect of multiple operating parameters on output parameters. Several operating

parameters affecting the extraction yield directly or indirectly are; extraction temperature, extraction pressure, particle size, extraction time, solvent flow rate, amount of co-solvent (modifier), bed void fraction and moisture content and pretreatment of solute (Doker et al., 2004; Koga et al., 1996; Mitra et al., 2009; Reverchon, 1997; Taher et al., 2014). Amongst several DOE techniques, RSM is widely used and well adapted technique to optimize the SFE process as concluded in Chapter 2. Face centered centre composite design (CCD) is the highly adopted design under response surface methodology (RSM) as it is very efficient, flexible and simpler one since it requires only three levels of each variable in contrast to other five levels designs.

In the present work, to avoid a huge number of experimental runs, five operating parameters are chosen for the optimization. Effect of these parameters on the output parameter i.e., extraction yield is studied. Screening and optimization of operating parameters is performed using screening design and CCD under RSM. For this purpose, Design Expert 8.0.1, Design Expert 10 and Quantum XL software are used.

3.8.1 Raw material-I (turmeric root)

To study SFE of turmeric root, operating parameters considered are extraction pressure (X_1), extraction temperature (X_2), solvent flow rate (X_3), raw material particle size (X_4), and amount of modifier/Co-solvent (X_5) to examine effects of these on the extraction yield. These parameters are varied as 200-400 bar, 40-60 °C, 5-15 g/min, 0.2-7.3 mm and 0-15% of solvent flow rate. Other parameters such as extraction time and raw material amount are kept constant at 260 min and 100 g, respectively, to achieve higher extraction yield. CCD is employed to design the set of experimental runs with different values of operating parameters. Values and levels of five inputs for SFE are reported in Table 3.1. It shows minimal (Xi, min), middle (Xi, mid) and maximal (Xi, max) values used for each parameter, which corresponds to -1, 0 and +1 levels, respectively. Design and analysis of RSM was carried out using Design Expert 7.0.3 Software (DE7). A full face CCD design provides 50 different combinations of five input parameters. It consists of 32 factorial points, 10 axial points and 8 center points. All these 50 experiments were performed and results based on the extraction yield are discussed in chapter 6.

Table 3.1 Set of operating parameters for SFE of turmeric root using CCD.

St. order	X_1: Pressure (bar)	X_2:Temp(°C)	X_3: Solvent flow rate (g/min)	X_4: Particle size(mm)	X_5: Co-solvent
1	200	40.00	5.00	0.20	0.00
2	400	40.00	5.00	0.20	0.00
3	200	60.00	5.00	0.20	0.00
4	400	60.00	5.00	0.20	0.00
5	200	40.00	15.00	0.20	0.00
6	400	40.00	15.00	0.20	0.00
7	200	60.00	15.00	0.20	0.00
8	400	60.00	15.00	0.20	0.00
9	200	40.00	5.00	0.73	0.00
10	400	40.00	5.00	0.73	0.00
11	200	60.00	5.00	0.73	0.00
12	400	60.00	5.00	0.73	0.00
13	200	40.00	15.00	0.73	0.00
14	400	40.00	15.00	0.73	0.00
15	200	60.00	15.00	0.73	0.00
16	400	60.00	15.00	0.73	0.00
17	200	40.00	5.00	0.20	15.00
18	400	40.00	5.00	0.20	15.00
19	200	60.00	5.00	0.20	15.00
20	400	60.00	5.00	0.20	15.00
21	200	40.00	15.00	0.20	15.00
22	400	40.00	15.00	0.20	15.00
23	200	60.00	15.00	0.20	15.00
24	400	60.00	15.00	0.20	15.00
25	200	40.00	5.00	0.73	15.00
26	400	40.00	5.00	0.73	15.00
27	200	60.00	5.00	0.73	15.00
28	40	60.00	5.00	0.73	15.00
29	200	40.00	15.00	0.73	15.00
30	400	40.00	15.00	0.73	15.00
31	200	60.00	15.00	0.73	15.00
32	400	60.00	15.00	0.73	15.00
33	200	50.00	10.00	0.45	7.50
34	400	50.00	10.00	0.45	7.50
35	300	40.00	10.00	0.45	7.50
36	300	60.00	10.00	0.45	7.50
37	300	50.00	5.00	0.45	7.50
38	300	50.00	15.00	0.45	7.50
39	300	50.00	10.00	0.20	7.50
40	300	50.00	10.00	0.73	7.50
41	300	50.00	10.00	0.45	0.00
42	300	50.00	10.00	0.45	15.00
43	300	50.00	10.00	0.45	7.50

44	300	50.00	10.00	0.45	7.50
45	300	50.00	10.00	0.45	7.50
46	300	50.00	10.00	0.45	7.50
47	300	50.00	10.00	0.45	7.50
48	300	50.00	10.00	0.45	7.50
49	300	50.00	10.00	0.45	7.50
50	300	50.00	10.00	0.45	7.50

3.8.2 Raw material-II (carrot seed)

In this section, DOE applied on SFE of carrot seed is explained. It requires 50 experimental run to perform, if five operating parameters are considered for the optimization as explained in section 3.8.1 for turmeric root. It is observed that screening of operating parameters can be performed to reduce number of experimental runs. Therefore, screening design is applied on the SFE of carrot seed prior to optimization. The key objective of the screening design is to find most influential input parameter related to desired output amongst all potential parameters (Sharif et al., 2014).

In the present study, five operating parameters such as pressure, temperature, particle size, flow rate and addition of co-solvent are considered as input parameters for screening design, which are varied as 100-300 bar, 40-60 °C, 0.3-0.9 mm, 10-20 g/min and 0-10% of solvent flow rate. Design Expert 10 was used for screening purpose, which suggested 10 numbers of experimental runs using minimum run resolution (iv) varying operating parameters into two levels only as shown in Table 3.2. Based on this design, SFE experiments are performed and results are generated as explained in chapter 6.

Table 3.2 Screening design for the SFE of carrot seed oil.

Run	X_1:Press bar	X_2:Temp °C	X_3:Particle Size, mm	X_4:Flow rate, g/min	X_5:Co-solvent, %
1	300(1)	40(-1)	0.3(-1)	10(-1)	10(1)
2	300(1)	60(1)	0.9(1)	10(-1)	0(-1)
3	100(-1)	40(-1)	0.3(-1)	20(1)	10(1)
4	100(-1)	60(1)	0.9(1)	20(1)	0(-1)
5	100(-1)	60(1)	0.9(1)	10(-1)	10(1)
6	300(1)	40(-1)	0.9(1)	20(1)	10(1)
7	100(-1)	60(1)	0.3(-1)	10(-1)	0(-1)
8	300(1)	40(-1)	0.3(-1)	20(1)	0(-1)
9	100(-1)	40(-1)	0.9(1)	10(-1)	0(-1)
10	300(1)	60(1)	0.3(-1)	20(1)	10(1)

Table 3.3 CCD design for the SFE of carrot seed oil (Particle size: 0.3mm)

Run	Space type	A:Pressure (bar)	B:Temperature (°C)	C:Flow rate (g/min)	D: Co-solvent (%)
1	Factorial	200	70	15	0
2	Factorial	400	70	5	10
3	Factorial	200	70	15	10
4	Factorial	400	50	15	0
5	Center	300	60	10	5
6	Axial	300	70	10	5
7	Center	300	60	10	5
8	Center	300	60	10	5
9	Factorial	400	50	5	0
10	Axial	200	60	10	5
11	Factorial	200	50	5	0
12	Factorial	400	70	15	10
13	Factorial	200	50	15	0
14	Axial	300	60	15	5
15	Axial	300	60	5	5
16	Factorial	400	50	15	10
17	Factorial	400	50	5	10
18	Center	300	60	10	5
19	Factorial	200	50	15	10
20	Factorial	200	50	5	10
21	Factorial	400	70	5	0
22	Axial	300	60	10	0
23	Factorial	200	70	5	10
24	Axial	300	50	10	5
25	Factorial	400	70	15	0
26	Axial	300	60	10	10
27	Center	300	60	10	5
28	Axial	400	60	10	5
29	Factorial	200	70	5	0
30	Center	300	60	10	5

Screening study of carrot seed provides the most influential parameters for the optimization study. Therefore, full face CCD is employed to design the set of experimental runs for reduced four operating parameters. Effect of four operating parameters such as pressure (A), temperature (B), solvent flow rate (C) and amount of co-solvent (D) on the extraction yield is studied. Optimization

study of SFE of carrot seed was performed using Quantum XL 2016 (Sigma Zone), which suggested total 30 experimental runs as tabulated in Table 3.3. CCD provides 16 factorial, 8 axial and 6 centre points. All sets of experimental runs are performed to generate results, which are discussed in chapter 6.

3.9 Industrial-scale Economic Evaluation of SFE Process

In this section, economic evaluation of SFE process to extract oil from turmeric root and carrot seed at industrial scale is performed, which includes fixed cost investment (FCI), operating cost (OC), cost of manufacturing (COM) and selling cost (SC) of the product.

FCI comprised of equipment and land costs which were estimated through sizing the set-up for required production capacity. Extraction vessels of 1 L, 5 L and 10 L capacities were considered and respective equipment cost, land requirement and power consumption data were collected from supplier i.e. Waters Corporation, Massachusetts, USA, as reported in Table 3.4. These parameters are plotted in Fig. 3.12. It shows that equipment cost, land requirement and power consumption are increasing almost linearly providing increment factors as 0.32, 0.56 and 0.27, respectively, per L of the product. Hence, equipment cost, land requirement and power consumption were computed for required production capacity using respective factor of increment. Cost of equipment includes costs of CO_2 recycler and chiller. Straight-line depreciation was considered for 20 years plant life to estimate the annual equipment and land costs.

OC of the process includes costs of raw materials (CRM), labor (COL) and utilities (CUT). CRM is the summation of costs of feedstock (turmeric root or carrot seed), ethanol and CO_2. These are found through local suppliers. Recoveries of CO_2 and ethanol were considered as 80% and 85%, respectively, of required quantity, as suggested by the supplier of SFE setup i.e. Waters Corporation, Massachusetts, USA. Therefore, CRM comprises only costs of used CO_2 and ethanol in the process. Operation time for the plant was considered as 300 days in a year. COL was calculated considering two labors per shift whereas one labor was paid Rs 500/- per day as per Indian rates. CUT was computed based on cost of electricity per kWh, as per Indian rates, and total electricity consumption in the process.

COM was predicted using Equation (3.3) (Turton et al., 1998)

$$COM = 0.304 FCI + 2.73 COL + 1.23 (CUT + CWT + CRM)$$
(3.3)

Where, CWT is cost of waste treatment, which is considered as zero in this study.

Annual production capacity of the plant was considered as 60 and 120 t/y for turmeric root oil and carrot seed oil, respectively. Based on optimum oil yield predicted through DOE, 1,200 t/y of turmeric root and 850 t/y of carrot seed oil were utilized as raw materials to meet the production capacity. Product cost of turmeric oil and carrot seed oil were taken as Rs. 12,500 and Rs. 15,599 per kg, respectively, considering actual selling price provided by local sellers. SC of the product was estimated considering 18% GST (Goods & services tax) as per Indian government norms on the selling price.

Table 3.4 Classification of fixed cost for SFE setup of different vessel capacities.

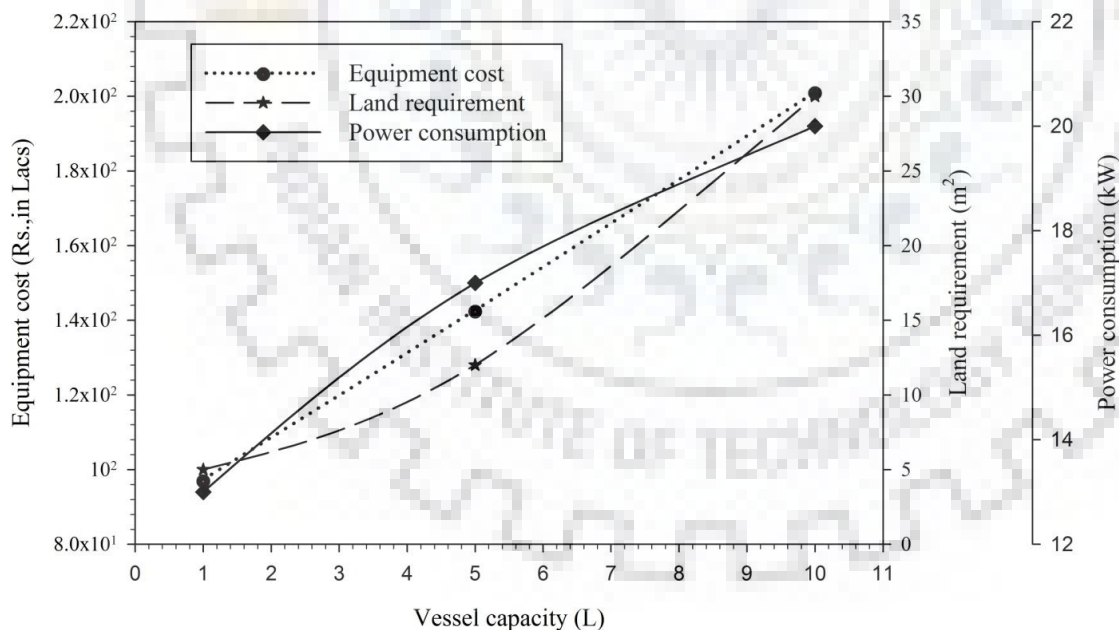| Vessel capacity (L)	Equipment cost (Rs., in Lacs)	Land requirement (m²)	Power consumption (kW)
1	97.33	5	13
5	142.75	12	17
10	201.15	30	20

Fig. 3.12 Comparison of equipment cost, land requirement and power consumption for different extraction vessel capacity.

CHARACTERIZATION AND ANALYSIS OF EXTRACTED OIL

In this chapter, methods and techniques to characterize products of supercritical fluid extraction (SFE) process i.e. turmeric root oil and carrot seed oil are presented. Further, physical and chemical properties of extracted oils are investigated. In addition, techniques for qualitative and quantitative analyses of extracted oils are also discussed.

4.1 Moisture Content of Extracted Oils

Moisture content of extracted oil using SFE technique was obtained with the method discussed in Section 3.6. Oil sample of 5.0 ± 0.001 gm was taken into a dried dish and kept in to the oven at 105 ± 1°C for 1 hour. Then, dish was removed from the oven and lid was closed to avoid losses. Dish was kept inside the desiccator to cool down before weighing it. Further, sample was again heated inside the oven for 1 hour, cooled and weighed. Same process was repeated until change in weight of sample between two successive observations did not exceed 1 mg. The moisture content of oil was calculated using equation 3.3. In the present study, moisture contents of turmeric oil and carrot seed oil were found to be 6.8% and 5.31%, respectively.

4.2 Physical Properties of Oils

In this section, physical properties of turmeric oil and carrot seed oil extracted from SFE process are estimated.

4.2.1 Refractive index

The refractive indices of turmeric oil and carrot seed oil were measured using refractometer as suggested by official method of AOAC 921.08 (AOAC International, 1998). Refractometer was calibrated using distilled water having refractive index of 1.32 at 20 °C and 1.33 at 40 °C. Moisture free oil samples (1-2 drops) were placed on clean and dry prisms. Then, instrument and light were adjusted and refractive indices were determined.

The refractive index at the specified temperature was calculated as:

$$R = R_1 + K(T_1 - T)$$
(5.1)

4.2.2 Specific gravity

The specific gravity of oil samples at 30 °C was obtained as suggested by the official method 920.212 by AOAC (AOAC International, 1998). Moisture free and filtered oil samples were taken in a clean and dry pycnometer fitted with a thermometer of 1°C least count. The instrument was

filled with distilled water, which was already cooled to about 30°C and placed in a constant temperature bath maintained at 30°C for 30 min. After 30 min, water level was maintained to a proper point on the pycnometer and stopper was inserted. Further, water filled pcynometer was removed from the bath, cleaned with cloth and weighed. Similar procedure was repeated for each oil sample by filled oil instead of distilled water. The specific gravity of each oil sample was computed as:

$$\text{Specific Gravity at } 30°C = \frac{(A - B)}{(C - B)} \qquad (5.2)$$

4.3 Chemical Properties of Oils

Chemical properties of turmeric oil and carrot seed oil extracted from SFE process are discussed in this section.

4.3.1 Peroxide value

The peroxide value of oil sample, referred as milli equivalents of active oxygen per kg of oil, was determined using the approach suggested by the AOAC official method 965.33 (AOAC International, 1998).

Oil sample ($5.00 \pm 0.05 \, g$) was taken into a 250 ml conical flask fitted with a ground-glass stopper. 30 ml of a mixture of chloroform and glacial acetic acid (2:3) was added in conical flask containing oil and was shaken properly. Further, 0.5 ml of saturated potassium iodide solution was added to conical flash and shaken for exactly 1 min and then, 30 ml of distilled water was added to it. Then, the mixture was titrated with 0.01N sodium thio-sulphate solution until yellow color was disappeared. Further, 0.5 ml of starch solution was added to the solution, shaken vigorously and titrated until the color was disappeared. A blank test was also performed under similar conditions. The peroxide value was predicted using as:

$$\text{Peroxide value(mili equivalent/kgoil)} = \frac{S \times N \times 1000}{\text{gm of oil sample taken}} \qquad (5.3)$$

4.3.2 Iodine value

Iodine values of turmeric oil and carrot seed oil were determined using the procedure explained in the official method 993.20 of AOAC (AOAC International, 1998). Iodine value of any oil implies towards the amount of un-saturation in fatty acids. Clean and dried oil sample (1 gm) was taken in to 500 ml conical flask and 10 ml of carbon tetrachloride was added in the oil. Simultaneously, a

blank sample, without oil was also prepared. Wij's solution (20 ml) was added and swirled for proper mixing before flasks were kept in dark for two hours. After two hours, 10 ml of potassium iodide solution was added with 100 ml of recently boiled and cooled water. Liberated iodine was titrated with sodium thio-sulphate solution adding starch as indicator. Mixture was titrated until the blue color disappeared and blank sample was also titrated in similar way. Iodine value was estimated using following formula:

$$\text{Iodine value} = \frac{12.69 \times (B - S) \times N}{W} \tag{5.4}$$

4.3.3 Acid value

Acid value of any oil is defined as the amount of potassium hydroxide (mg) required to neutralize the free fatty acid present in 1 gm of oil. Acid values of turmeric oil and carrot seed oil samples were obtained using AOAC method 940.28 (AOAC International, 1998). Oil sample of 1 ± 0.001 gm was taken in a conical flask and 10-20 ml of freshly prepared neutralized ethyl alcohol with 2 ml of phenolphthalein indicator was mixed with the oil sample. The mixture was boiled for 5 min and titrated with 0.5 N KOH. The solution was shaken vigorously during the titration. Further, the acid value was computed as:

$$\text{Acid value} = \frac{56.1 \times V \times N}{W} \tag{5.5}$$

Where,

The acidity can be expressed as free fatty acid content:

$$\text{Free fatty acids as oleic acid (wt\%)} = \frac{28.2 \times V \times N}{W}$$

Acid value = %fatty acid (as oleic) x 1.99 (5.6)

4.3.4 Saponification value

The saponification value is referred to the number of mg of potassium hydroxide required to saponify 1 gm of oil/fat under specified conditions. In the present study, saponification value of turmeric oil and carrot seed oil was obtained as suggested by official method 920.160 by AOAC (AOAC, 2000). Oil sample (1 or 2 gm) was taken in a 250 ml Erlenmeyer flask and mixed with 25 ml of alcoholic potassium hydroxide solution. It was prepared by refluxing 1.2 litre alcohol with 10 gm KOH and 6 gm aluminium foil for 30 minutes. Mixture was distilled and collected (1 litre) after discarding first 50 ml. Then, 40 g of potassium hydroxide was dissolved in 1 litre ethyl

alcohol while maintaining temperature below 15° C. Mixture was kept in dark overnight before clear liquid was transferred and kept in a bottle tightly closed with rubber stopper.

Similarly, 25 ml alcoholic potassium hydroxide solution was taken in to another flask for blank titration. Both flasks, connected with air condensers, were kept inside the water bath for approximately 1 h. Absence of any oily matter and appearance of clear solution indicated that the saponification was complete. Condensers and flasks were washed with freshly prepared neutralized ethyl alcohol and excess potassium hydroxide was titrated with 0.5N hydrochloric acid in the presence of 1 ml phenolphthalein indicator. The Saponification value was calculated as:

$$\text{Saponification Value} = \frac{56.10 \times (B - S) \times N}{W} \tag{5.7}$$

4.3.5 Unsaponifiable matter

The unsaponification value was obtained using the procedure suggested by official method 933.08 of AOAC (AOAC International, 1998). Unsaponifiable matter is defined as compounds present in oil, which cannot be saponified using potassium hydroxide. Oil sample (1 gm) was taken in a 250 ml conical flask and mixed with 10 ml alcoholic potassium hydroxide solution. Mixture was boiled under reflux air condenser for 1 hour. Air condenser was washed with 10 ml ethyl alcohol and saponified mixture was transferred to a separating funnel. The saponification flask was rinsed with ethyl alcohol and 10 ml of cold distilled water. After that, 10 ml of petroleum ether was added into the separating funnel, shaken vigorously, and layers were allowed to separate. The lower soap layer was collected into another separating funnel and ether extraction was repeated using 10 ml petroleum ether for 3 times. Total ether extract was washed three times with 10 ml alcohol followed by washing with 10 ml distilled water to ensure that the ether extract was free of alkali. Then, solution was transferred to a beaker and evaporated to about 5 ml. Again, some small portions of ether were transferred to a 50 ml dried Erlenmeyer flask and ether was evaporated. Further, 2-3 ml acetone was added and heated on a water bath to remove the solvent completely. Further, sample was dried at 100ºC for 30 minutes to remove the traces of ether. Then, 10 ml of neutralized ethanol was added to dissolve the residue and titrated with 0.02N NaOH.

Weight of free fatty acid in the extract as oleic acid = 0.282 V×N (5.8)

$$\text{Unsaponifiable matter} = \frac{(A - B)}{W} \times 100 \tag{5.9}$$

4.4 Composition of Oils

In this section, quantification and qualification process of turmeric oil and carrot seed oil is discussed. Essential oil and fatty acid analyses of both oils are performed.

4.4.1 Essential oil analysis of turmeric oil

Essential oil analysis of turmeric oil was performed using Mass spectrometry (MS), Gas chromatography (GC), and UV spectroscopy.

4.4.1.1 Sample preparation

Sample for MS and GC analysis was prepared while diluting turmeric oil with acetone in a ratio of 1:5. Diluted sample was filtered with syringe filter (0.2 μm) before injection (Raina et al., 2002). Similar method was employed to prepare standard turmerone solution for analysis.

For UV analysis, stock solution was made by dissolving 2 mg of standard curcumin into methanol to prepare a final concentration of 400 μg/ml. From stock solution, concentrations of 0.1, 0.3, 0.5, 0.8, 1.3, 1.7, 2, 2.4 and 3.2 μg/ml were prepared and a calibration curve was plotted (Singh and Jain, 2011). To prepare turmeric oil sample, 10 mg of oil was dissolved in 10 ml methanol and a concentration of 1 mg/ml was prepared. Sample was analyzed using UV-spectrophotometer and while comparing with the calibration curve, the actual concentration of curcumin was predicted (Singh and Jain, 2011).

4.4.1.2 MS, GC and UV analysis conditions

Mass-Spectra (MS) analysis of turmeric oil was carried out to identify compounds present in essential oil. MS analysis was performed (Perkin-Elmer mass spectrometer) at 70 eV and 250 °C whereas column used for the analysis was DB-5MS (Agilent Technologies: 60 m, 0.25 mm i.d, film thickness 0.25 μm). Initial temperature was 70 °C for 5 min and then heated to 120 °C at 2 °C/min and held isothermally for 2 min. Temperature was then increased from 120 °C to 240 °C at 2 °C/min and maintained for 3 min. Carrier gas was helium and m/z ratio was taken from 45 to 350 (Raina et al., 2002).

GC analysis of essential oil of turmeric root was performed using a Perkin-Elmer GC with a fused capillary column (Clarus 680, 30 m, 0.32 mm i.d, film thickness 0.25 μm), coated with dimethyl siloxane (Elite-1). Oven temperature was programmed from 60 °C for 1 min to 220 °C at the rate of 5 °C/min where column was maintained for 15 min. Amount of sample injected was 1 μL. Injector port temperature was 250 °C with FID detector temperature at 300 °C and split ratio of nitrogen as a carrier gas was 1:80 (Raina et al., 2002).

Curcumin content was found through UV-spectrophotometer (HACH, DR 5000, USA) with 1mL cuvette. The wavelength corresponding to maximum absorbance (λmax) was found to be 420 nm and total curcumin content was computed using a standard curve. Analysis of each sample was carried out in triplicate.

4.4.2 Essential oil analysis of carrot seed oil

Essential oil analysis of carrot seed oil was performed using coupled Gas chromatography-Mass spectrometry (GC-MS).

4.4.2.1 Sample preparation

Sample for GC-MS analysis was prepared while diluting carrot seed oil with methanol in a ratio of 1:10. Diluted sample was filtered with syringe filter (0.2 μm) before injection.

4.4.2.2 GC-MS analysis conditions

GC-MS analysis of carrot seed oil was carried out using a GC-MS (Agilent, Santa Clara, CA, USA) equipped with the capillary column (DB- 5MS; dimensions 30 mm 0.25 mm, ID and 0.25 mm film thickness). Initially, GC oven temperature was at 60°C and maintained isothermally for 2 min. Then, oven was heated up to 285°C at a rate of 3°C/min and held constant for 3 min. Helium was used as carrier gas, which was injected at 250°C through splitless injection mode. On the other hand, MS scan conditions were maintained while considering MS source temperature, ionization energy and m/z ratio as 230°C, 70 eV and 40-500, rsepectively.

4.4.3 Fatty acid analyses of turmeric oil and carrot seed oil

Fatty acids, present in turmeric oil and carrot seed oil, were first converted into esters and fatty acid methyl esters (FAME) were prepared.

4.4.3.1 Sample preparation

To analyze fatty acid contents of turmeric oil and carrot seed oil, FAME were prepared for each sample of turmeric oil using the method recommended by Rai et al. (2015). Oil sample (50 ± 0.005 mg) was taken in a glass tube then 1 ml of toluene and 2 ml of 1% sulfuric acid in methanol solution was added. Mixture was then heated at 70°C for two hours in a water bath equipped with total reflux system, which prevented any loss of mixture vapor. After two hours, 1 ml of freshly prepared 5% sodium chloride solution and 5 ml of n-hexane was added and stirred well to get the converted FAME. Upper n-hexane layer was separated with the help of Pasteur pipette and washed with 4 ml of freshly prepared 2% potassium bicarbonate solution and dried over anhydrous sodium sulfate. FAME layer was again separated and solvent was removed under reduced pressure through

rotary vacuum evaporator. Prepared FAME was then dissolved in 2 ml of n-hexane and analyzed using Gas chromatography.

4.4.3.2 GC conditions for FAME analysis

Identification and quantification of fatty acids from FAME of turmeric and carrot seed oils were carried out using Thermo Trace Ultra Gas chromatograph purchased from Thermo Scientific, USA. Flame ionization detector and fused silica capillary column (HP-88) of 30 m height, 0.25 mm i.d. and 0.20 μm film thickness purchased from Agilent Technologies, USA was used for fatty acid analysis. Initially, column temperature was maintained at 120°C for 1 min and then increased up to 145°C at a rate of 5 °C/min and held for 1 min. Oven temperature again increased from 145°C to 220°C from a rate of 2°C/min and maintained for 2 min. Injector and detector temperature was set at 250°C and split ratio was set at 50:1 with total run time 45.5 minute. Nitrogen gas was used as a makeup gas with a flow rate of 30 ml/min whereas, hydrogen and air flow rates were maintained at 35 ml/min and 350 ml/min, respectively (Rai et al., 2015). Fatty acid peaks were identified using a standard 37 FAME mixture (Supelco 37 component FAME mix, Supelco, Bellefonte, PA), purchased from Sigma-Aldrich.

MATHEMATICAL MODELING OF SFE PROCESS

In this chapter, mathematical models available in the literature for supercritical fluid extraction (SFE) process, which are used in the present work, are explained briefly. In addition, solution technique used in the present work to solve these models is also discussed.

SFE of natural products strongly depends upon type of seed matrix or morphological structure of seed and availability of oil inside the seed. Many investigators observed that oil particles are bound by channels, which can be broken through milling. Consequently, a few channels can be broken and oil can be easily accessible (Sovova et al., 1994a). However, extraction of oil from intact channels is difficult because of intermolecular resistance. Each type of seed has different type of matrix and it shows different type of inside mechanism for extraction of oil. Type of seed matrix or type of oil availability helps to decide particle sizes of seed for SFE of seed and its inside mechanism helps to predict resistances working on extraction and based on these assumptions a model can be proposed (Misic et al., 2008; Sovova et al., 1994a).

Modeling of SFE of essential oils is difficult due to complexity of the vegetable structure and lack of reliable experimental data on yield of the process (Reverchon, 1996). It is evident that the various models differ not only from a mathematical point of view, but also due to mass transfer mechanisms, which control the supercritical extraction process of different matrices. Thus, a single model cannot describe all experimental results (Sovova et al., 1994a). It is discussed in section 2.6.4 that more than 60 models are proposed by various authors to simulate the supercritical extraction process for different type of species such as seeds, roots, flowers, stems, meat, etc. All types of matrices need mathematical model with different mass balance equations and resistances. However, there is possibility that a single model can fit more than one type of matrices. Solution of these mathematical models is also a concern because of complex mass balance equations. To find an easy and accurate method to solve these mathematical models is also a challenge.

In this section, some mathematical models are taken into consideration to discuss its mass balance equations and solution techniques. Further, solution technique used in the present study is also discussed.

5.1 Mathematical Models Used in SFE and Solution Techniques

Several mathematical models for SFE process have been proposed by different authors as discussed in section 2.6.4 and a few amongst these models are discussed in this section.

5.1.1 Mathematical model-1

A mathematical model was developed by Reverchon (1996) for the extraction of essential oil from leaves. Proposed model was based on differential mass balances performed along the extraction bed while neglecting external mass transfer coefficient. Goto et al. (1993) proposed a hypothesis that essential oil is absorbed on leaf waxes and fraction of essential oil available on particle surface is significant. However, Reverchon (1996) assumed that extraction of essential oil from leaves does not support the hypothesis proposed by Goto et al. (1993) and only internal mass transfer resistance controls the extraction. Further, assumptions taken were: essential oil was considered as a single compound, negligible axial dispersion and solvent density and flow rate were constant along the bed. Solvent phase and solid phase mass balance equations with initial and boundary conditions are provided in Table 5.1. An equilibrium relationship and internal diffusion time equation are also required to solve these equations, which are also shown in Table 5.1. The author proposed two methods to solve mass balance equations with two boundary conditions and an equilibrium relationship. First, model can be solved numerically using the method of characteristics. In other method, fixed bed can be divided in n stages with uniform fluid and solid phase compositions in each stage. This pattern represents the plug-flow extractor through a series of mixed extractors and mass balance equations can be rewritten as a set of 2n equations. Then, equations can be solved numerically using fourth order Runge - Kutta method.

5.1.2 Mathematical model-2

A mathematical model for the extraction of flower concrete was developed by Reverchon and Poletto (1996). In fact, it appears that it is the first model to simulate extraction process of flower. In this work, authors studied microphotographs of rose and tuberose and found that solute is available in oily phase and can be extracted without any mass transfer resistance. For the extraction of flower concrete, rose and tuberose concretes were melted and mixed with 2 mm glass beads. A mathematical model was developed while considering following assumptions: (1) The concrete was uniformly distributed on surface of the glass spheres and occupied a finite volume fraction of the extractor, (2) Solvent flow rate, with superficial velocity U, was uniformly distributed in every section of the extractor. Pressure drops as well as temperature gradients within the column along with axial dispersion were negligible, (3) several components involved in the extraction process could be described through a single pseudo-component, which was called the 'solute'. Two mass balance differential equations were written for solvent as well as solute phases considering extraction time 't' and axial co-ordinate 'x' as independent variables as given in Table 5.1. Solution

of these equations with initial and boundary conditions was obtained with a single step of an ODE integration. They used fourth-order Runge-Kutta algorithm. Reverchon and Poletto (1996) found that the model with constant mass transfer coefficients was inadequate for a satisfactory description of the extraction process in comparison to the case of a variable resistance to mass transfer.

5.1.3 Mathematical model-3

Reverchon and Marrone (1997) isolated the clove essential oil from the SFE of clove bud and developed model was validated with experimental data. Assumptions made were: (1) the extract can be described as a single pseudo compound, (2) The interstitial fluid velocity *u/e,* is constant. Fluid phase mass balance differential equation contains axial dispersion term if axial dispersion does not assume to be negligible and Danckwerts' boundary conditions at inlet and outlet of the column are used to solve the model as provided in Table 5.1. Reverchon and Marrone (1997) solved model equations with equilibrium model and initial and boundary condition while assuming negligible axial dispersion as given in Table 5.1. Model equations were solved while integrating equations using Crank Nicholson method with the help of Mathematica *2.23* *TM* (Wolfram Research) software.

5.1.4 Mathematical model-4

In addition to models for the extraction of leaves and flower concrete, Reverchon et al. (2000) also proposed a mathematical model for the extraction of oil from flower seed. Before this study, broken and intact cells model, developed by Sovova (1994) was used for the modeling of supercritical extraction of seeds. Reverchon et al. (2000) found that broken and intact cells model cannot be used for the extraction of hiprose seed. Though hiprose seed contains broken and intact cells, however oil inside the intact channels is not accessible. SEM images of hiprose seed suggested that an increasing resistance was experienced by supercritical solvent as extraction proceeds in channels at an increasing depth. Considering this fact, authors included an internal mass transfer resistance term in the model, which was increasing linearly till oil contained in channels was extracted. Assumptions made for the development of model were same as given by Reverchon and Poletto (1996) and discussed in section 4.1.2. Reverchon et al. (2000) omitted a partial differential equation for the extraction of oil in intact cells from the standard broken and intact cells model and considered only two differential equations (oil in broken cells and oil in fluid phase) with initial and boundary conditions as shown in Table 5.1. Only adjustable parameter in this model was internal mass transfer coefficient, which varied linearly with asymptotic value of

oil yield and initial and final values of mass transfer coefficients. They solved model using a finite difference method where an explicit numerical cell was implemented.

5.1.5 Mathematical model-5

Nobre et al. (2006) proposed a model for the supercritical extraction of pigments from *Bixa orellana* seeds based on similar assumptions as considered by Reverchon (1996) and discussed in section 4.1.1. They assumed that intra-particle resistance to mass transfer controls the extraction if it was carried out using pure CO_2. However, for the case of ethanol and CO_2, it was assumed that the solvent film controls extraction process. Mass balance equations for solvent and solid phases, as reported in Table 5.1, were solved with initial and boundary conditions. Two different overall mass transfer rate equations were considered: an internal one for the extraction with pure CO_2 and an external for the system with ethanol. Nobre et al. (2006) employed same solution techniques as used by Reverchon (1996).

5.1.6 Mathematical model-6

All models discussed from section 4.1.1 to 4.1.5 are based on two extraction periods only: (a) Fast extraction period and (b) constant extraction period. In contrast to these models, Sovova (1994) proposed a model assuming three extraction periods for the supercritical extraction of any solute matrix. Sovova (1994) compared equations of models (solvent and solid phase mass transfer coefficients) developed by several authors (Cygnarowicz-Provost et al., 1992; Lee et al., 1986; Lack, 1985; Pekhov and Goncharenko, 1968) and combined into a new model containing both mass transfer coefficients. Sovova (1994) model is also called "extended Lack model". The proposed model was one-dimensional, unsteady state mathematical model to obtain oil concentration profiles in solvent and solid phases, and to determine the overall volumetric mass transfer coefficients, K. The model was based on following assumptions: (i) plug flow existed in the bed, (ii) axial dispersion in the bed was negligible, (iii) fluid flow rate, temperature, pressure and bed properties were constant, (iv) solvent was oil-free at the entrance of the extractor and (v) all seeds contained same initial oil content. The model proposed by Lack, 1985 was a general mathematical model for fast as well as slow extraction period whereas (Helena Sovova, 1994) extended it considering transition period between fast and slow extraction period. The author described that easily accessible solute exhausted at the solvent entrance to the solvent phase at time, t_m, when a transition period occurred as shown in Fig. 5.1. In this period, easily accessible solute was still extracted in one section of the fixed bed, while the extraction from the inside of particles occurred in another section. The author referred transition period as a layer between both

extraction periods, which passed through the bed until it reached its end. Sovova (1994) solved mass balance equations, given in Table 5.1, analytically. Sovova (1994) reported the solution of model in terms of concentration profiles in solid and solvent phases for three extraction periods separately.

5.1.7 Mathematical model-7

Goto et al. (1996) reported that the extraction or leaching of a solute from a solid material involves mass transfer in solid matrix. They developed a shrinking-core model for the modelling of the extraction process, which included axial dispersion in the extraction column. The model includes desorption followed by diffusion in the porous solid through pores. The mass transfer rate of the solute in the non-extracted inner part is much slower than that in the outer part where most of the solute is extracted, or the solute concentration is much higher than the solubility of solute in the solvent phase. A sharp boundary may exist between outer and inner regions and the core of inner region, shrinks with the progress of the extraction.

These situations were formulated using shrinking core model with following assumptions: (i) Solvent flowed axially with interstitial velocity, v, through a packed bed in a cylindrical extractor of height, (ii) Pure solvent entered the bed and the process was isothermal, (iii) Axial dispersion was considered. Based on these assumptions, material balance on bulk fluid-phase inside the extractor was predicted. In addition, time variation of solid phase concentration or average oil concentration in a particle was equated with the rate of mass transfer of solute within external film surrounding the particle. Diffusion in outer layer equation with initial as well as Danckwert's boundary conditions was considered to complete the model. Further, Goto et al. (1996) transformed all equations into non-dimensional form as reported in Table 5.1 and solved using Crank Nicholson's method.
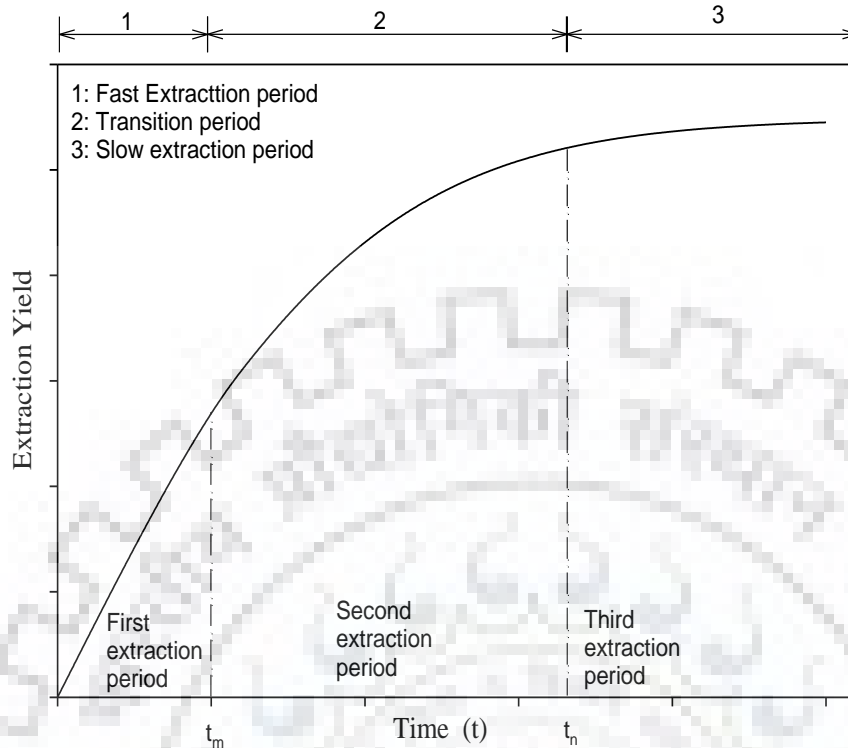
Fig. 5.1 Extraction periods during extraction process

5.2 Solution of models Using COMSOL Multiphysics 5.3

In the literature, mathematical models proposed by different authors are based on mass balance equations for solid and liquid phases. These are partial differential equations with some initial and boundary conditions, which are very difficult to solve manually. Authors solve these equations employing numerical methods i.e. Runge-Kutta method, integration using a finite differences. To get the solution of these complex model equations by numerical techniques, a few software such as MATLAB, C++, Mathematica 2.23 TM require coding of numerical procedure, which is difficult and time consuming. Therefore, in the present work, COMSOL Multiphysics 5.3 software is employed to solve mathematical models using "equation based modelling" approach. This software does not require manual coding. Fig. 5.2 depicts a flow chart of solution steps to solve mathematical equations using COMSOL Multiphysics 5.3. Model equations are solved considering "1D" geometry under "Model wizard" window on COMSOL desktop and further steps for solving the model are:

Step 1: Under "Select Physics" wizard, required module can be selected depending upon the nature of work such as "Mathematics" module is selected for the present study as shown in appendix-B.1.

Step 2: Type of equations and number of dependent variables can be added under the subgroup of selected module based upon the nature of equations to be solved. In the present study, "Coefficient form PDE" under "PDE interfaces" and "Domain ODEs and DAEs" under "ODE and DAE interfaces" are selected for solvent and solid phase equations, respectively. Dependent variable for both equations are defined in respective interfaces, a sample picture is shown in appendix-B.1.

Step 3: Type of study can be selected among stationary or time dependent studies. In the present work, "Time dependent study" is used as shown in appendix-B.2.

Step 4: Geometry can be created while entering all measurements of geometry under "Geometry" wizard in Model builder window. In the present study, 1D geometry is selected therefore, interval node is added and height of bed is inserted as a length of geometry as shown in appendix-B.3.

Step 5: Constants parameters of the model are added in "parameters" node under "Global definition" whereas, variable parameters of the model are added in "Variables" node under "Definitions" option of "Component 1". A sample picture is shown in appendix-B.4 and B.5 for Sovova (1994) model.

Step 6: Values of coefficients are inserted comparing equations with default equations of selected interface while adding initial and boundary values also. In the present study, coefficients of solvent and solid phase equations with initial and boundary values are inserted in respective interfaces as shown in appendix-B.6 and B.7.

Step 7: A range of time value can be given for the solution of equations in "Time dependent wizard" under "study" setting as shown in appendix-B.8. However, for the stationary i.e. steady state study, no need to add range of time.

 Step 8: Meshing was built and model was computed to get results as shown in appendix-B.9.

Computation time of COMSOL multiphysics is in seconds, which is far lesser than other software packages. Further, larger memory usage also requires for other numerical methods i.e. Runge-Kutta method.
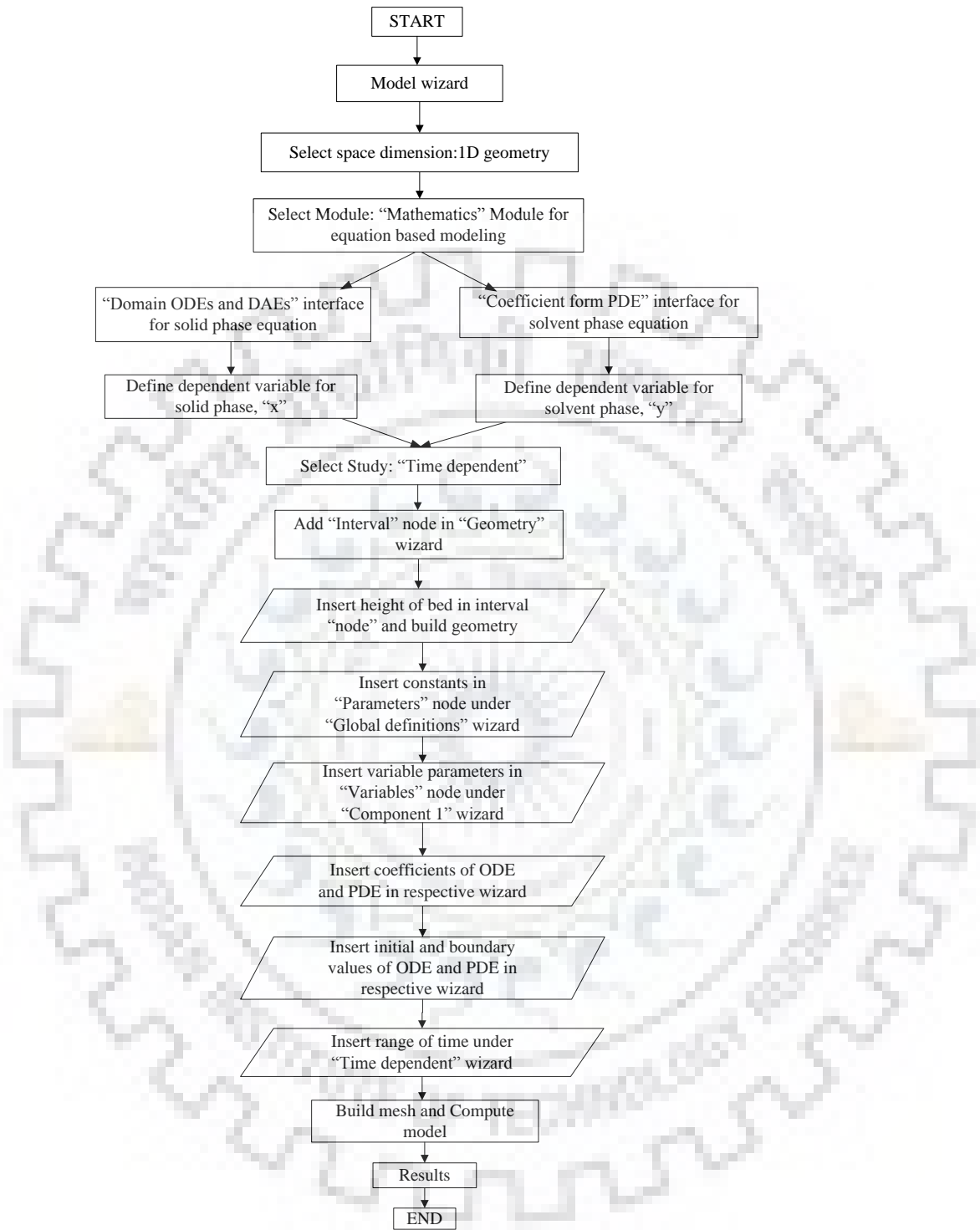
```
┌─────────┐
│  START  │
└────┬────┘
     ▼
┌──────────────┐
│ Model wizard │
└──────┬───────┘
       ▼
┌──────────────────────────────────┐
│ Select space dimension:1D geometry│
└──────────────┬───────────────────┘
               ▼
┌──────────────────────────────────┐
│ Select Module: "Mathematics" Module for │
│     equation based modeling       │
└──────────────┬───────────────────┘
```

"Domain ODEs and DAEs" interface for solid phase equation

"Coefficient form PDE" interface for solvent phase equation

Define dependent variable for solid phase, "x"

Define dependent variable for solvent phase, "y"

Select Study: "Time dependent"

Add "Interval" node in "Geometry" wizard

Insert height of bed in interval "node" and build geometry

Insert constants in "Parameters" node under "Global definitions" wizard

Insert variable parameters in "Variables" node under "Component 1" wizard

Insert coefficients of ODE and PDE in respective wizard

Insert initial and boundary values of ODE and PDE in respective wizard

Insert range of time under "Time dependent" wizard

Build mesh and Compute model

Results

END

Fig. 5.2 Flow chart of solution technique to solve models using COMSOL Multyphyscis 5.3.

Table 5.1 Mathematical models used in SFE process.

Reference	Model Description	Input parameters	Nomenclature
Reverchon(1996)	The differential mass balance equation $$uV\frac{\partial c}{\partial h}+\varepsilon V\frac{\partial c}{\partial t}+(1-\varepsilon)V\frac{\partial q}{\partial t}=0$$ $$(1-\varepsilon)V\frac{\partial q}{\partial t}=-A_pK(q-q^*)$$ IC at $t=0$, $c=0$ and $q=0$ BC at $h=0$, $c(0,t)=0$ A linear relationship was used due to lack of experimental data. $$c=k_p\cdot q^*$$ Considering internal diffusion time $$t_i=\frac{(1-\varepsilon)V}{A_pK}$$	1. Solvent density, 2. Seed density, 3. Initial conc of solute in solid phase, 4. Porosity, 5. Superficial velocity, 6. Height of extractor, 7. Volume of extractor, 8. Diameter of particle, 9. Diffusivity, 10. Internal mass transfer coefficient, 11. Partition coefficient	ρ/ρ_f = Solvent density (kg/m^3), ρ_s= Seed density (kg/m^3), y= Solute mass fraction in solvent phase (kg/kg), x= Solute mass fraction in solid phase (kg/kg), c= Concentration of solute in solvent phase (kg/m^3), q= Concentration of solute in solid phase (kg/m^3), k_fa_0=Solvent phase mass transfer coefficient (m^3/s), k_sa_0=Solid phase mass transfer coefficient (m^3/s), x_0= Initial fraction of solute in solid phase (kg/kg), x_k= Easily accessible fraction of solute (kg/kg), y_r= Solubility (kg/kg solvent), ε= Porosity, U/u= superficial velocity (m/s), L= Height of extractor (m), V= Volume of extractor (m^3), A_p=Total surface of particle (m^2), K= Internal mass transfer coefficient (m/s),
(Reverchon and Poletto (1996)	The differential mass balance equation $$\rho_f.\varepsilon\left(\frac{\partial y}{\partial t}+u\frac{\partial y}{\partial z}\right)=J$$ $$\rho_s.\varepsilon_c\frac{\partial x}{\partial t}=-J$$ IC at $t=0, x=x_0, y=y^*(x_0)=y_0$ BC at $x=0, y(0,t)=0$ In case of variable mass transfer coefficient	1. Solvent density, 2. Seed density, 3. Concrete density, 4. Initial fraction of solute in solid phase, 5. Asymptotical solute yield, 6. initial solute fraction in the solvent, 7. Solute fraction in the concrete at exit, 8. Proportionality constant, 9. Porosity, 10. superficial velocity,	

	$J = \dfrac{A_p h_0 \rho_f (y_0 - y)}{\left(\dfrac{x_t - x}{x_t} + \dfrac{\delta}{\delta_0}\right)}$	11. Height of extractor, 12. Volume of extractor, 13. Diameter of particle, 14. Porosity of concrete, 15. specific surface of glass filling	q^*=Concentration at solid phase interface (kg/m^3), k_p=Partition coefficient, t_i= Internal diffusion time (s), P_e= Peclet number,
Reverchon and Marrone (1997)	$\dfrac{\partial c}{\partial t} + \dfrac{u}{\varepsilon}\dfrac{\partial c}{\partial z} + \dfrac{1-\varepsilon}{\varepsilon}\dfrac{\rho_s}{\rho} K \dfrac{\partial c}{\partial t} = 0$ $\dfrac{\partial q}{\partial t} = -f(c,q)$ If only fluid phase mass transfer controls the mass transfer process: $f(c,q) = -k_e a(c^* - c) = -k_e a\left(\left(\dfrac{q}{K}\right) - c\right)$ IC at $t = 0$, $q = q_0$, c $= c_0$ BC at $z = 0$, $c = 0$	1. Solvent density, 2. Seed density, 3. Initial fraction of solute in solid phase, 4. initial solute fraction in the solvent, 5. External mass transfer coefficient, 6. Porosity, 7. Superficial velocity, 8. Height of extractor, 9. Volume of extractor, 10. Diameter of particle, 11. Equilibrium Constant	B_i= Biot number, dp= Particle diameter (m), R= Particle radius (m), D_e= Effective diffusivity (m^2/s), C_{sat}= saturation concentration (kg/m^3), Θ= Dimensionless time, Z= Axial coordinate of extractor, ζ_c= Dimensionless radius of unleached core, ε_c=Concrete volume fraction, y*= Solute fraction in the solvent in equilibrium with the concrete (kg/kg),
Reverchon et al. (2000)	$\dfrac{\partial c}{\partial t} + \dfrac{u}{\varepsilon}\dfrac{\partial c}{\partial z} + \dfrac{1-\varepsilon}{\varepsilon}\dfrac{\rho_s}{\rho_f}\dfrac{\partial q}{\partial t} = 0$ $\dfrac{\partial q}{\partial t} = -K_i(Y) a (q - q^*)$ $q^* = K_{eq}.c$ IC and BC $c = c_0$ at $t = 0$ for each z $q = q_0$ at $t = 0$ for each z $c = 0$ at $z = 0$ for each t Internal mass transfer coefficient:	1. Solvent density, 2. Seed density, 3. Initial fraction of solute in solid phase, 4. Initial solute fraction in the solvent, 5. Initial mass transfer coefficient, 6. Porosity, 7. Superficial velocity, 8. Height of extractor, 9. Volume of extractor, 10. Diameter of particle, 11. Asymptotic yield, 12. Equilibrium constant	h_0= Proportionality constant, x_t= Solute fraction in the concrete at the transition extraction regime at solid phase interface (kg/kg), δ= Thickness of concrete film (m), δ_0= Thickness of the fictitious external layer in the film (m), K= Equilibrium constant in model [12], ke= External mass transfer coefficient (m/s), a= Particle surface (m^2), c*=Solvent phase interface concentration (kg/m^3),

	$K_i(Y) = K_{i0}\left(1 - \dfrac{y}{y_f}\right)$		K_{eq}=Equilibrium constant, K_{i0}= Initial mass transfer coefficient (m/s), y_f= Asymptotic value of yield, A_pK_s=Overall internal mass transfer coefficient (m³/s),
Nobre et al. (2006)	$\rho u \dfrac{\partial y}{\partial h} + \rho\varepsilon \dfrac{\partial y}{\partial t} = R\{x, y\}$ $(1-\varepsilon)\rho_s \dfrac{\partial x}{\partial t} = -R\{x, y\}$ For internal mass transfer system: $R\{x, y\} = A_p K_s \rho_s (x - x^*)$ IC at $x = x_0$ for $t = 0$ any h BC at $y = 0$ for $h = 0$ any t	1. Solvent density, 2. Seed density, 3. Initial Conc of solute in solid phase, 4. Partition coefficient, 5. Overall internal mass transfer coefficient, 6. Porosity, 7. Superficial velocity, 8. Height of extractor, 9. Volume of extractor, 10. Diameter of particle	
Sovova (1994)	The material balance for an element of the bed are given by $\rho\varepsilon \dfrac{\partial y}{\partial t} + \rho U \dfrac{\partial y}{\partial h} = J(x, y)$ $-\rho_s(1-\varepsilon)\dfrac{\partial x}{\partial t} = J(x, y)$ $J(x,y)$ is a function of the difference in concentration using a local mass transfer coefficient for both phases. $J(x > x_{k,y}) = k_f a_0 \rho(y_r - y)$ $J(x \leq x_{k,y}) = k_s a_0 \rho_s x\left(1 - \dfrac{y_r}{y}\right)$ IC at $t = 0$, $y = 0$ and $x = x_0$ BC at $h = 0$, $y = 0$	1. Solvent density, 2. Seed density, 3. Solvent phase mass transfer coefficient, 4. Solid phase mass transfer coefficient, 5. Initial fraction of solute in solid phase, 6. Easily accessible fraction of solute, 7. Solubility, 8. Porosity, 9. Superficial velocity, 10. Height of extractor, 11. Volume of extractor	

| Goto et al. (1996) | The dimensionless solid and fluid phase mass balance are $$\frac{\partial x}{\partial \theta} + a\frac{\partial x}{\partial Z} = \frac{a}{Pe}\frac{\partial^2 x}{\partial Z^2} - \frac{1-\varepsilon}{\varepsilon}\frac{3Bi(x-1)}{1-Bi\left(1-\frac{1}{\xi_c}\right)}$$ $$\frac{\partial \xi_c}{\partial \theta} = \frac{bBi(x-1)}{\xi_c^2\left[1-Bi\left(1-\frac{1}{\xi_c}\right)\right]}$$ The initial and boundary conditions are $\xi_c = 1$ at $\theta = 0$ $x = 0$ at $\theta = 0$ $x - \frac{1}{Pe}\frac{\partial x}{\partial Z} = 0$ at $Z = 0$ $\frac{\partial x}{\partial Z} = 0$ at $Z = 1$ $a = \frac{vR^2}{D_e L}, b = \frac{C_{sat}}{q_0}$ | (i)   Solvent density,
(ii)   Seed density,
(iii) Initial fraction of solute in solid phase,
(iv) Saturated solute fraction in solvent,
(v)   Film mass transfer coefficient,
(vi) Porosity,
(vii) superficial velocity,
(viii) Height of extractor,
(ix) Volume of extractor,
(x)   Effective diffusivity,
(xi) Diameter of particle,
(xii) Axial dispersion coefficient | |

RESULTS AND DISCUSSION

This chapter embodies the results obtained from the experimental and modeling studies for SFE of natural matrices i.e. turmeric root and carrot seed. For this purpose, preparation of raw materials and selection of operating parameters to design the sets of experimental runs are described in Sections 3.1 and 3.2. Experimental setup and procedure to perform SFE of raw materials (turmeric root and carrot seed) are explained in sections 3.3 and 3.4 whereas; characterization techniques of raw materials based on standard methods are presented in sections 3.5 to 3.7. Design of experiment technique is used to design the experimental runs using Design expert 7.0.3 Software (DE7) and Quantum XL 2016 for turmeric root and carrot seed, respectively, as discussed in section 3.8. Industrial-scale economic assessment of the SFE process is discussed in section 3.9 considering turmeric root oil and carrot seed oil as products. Further, physical and chemical properties of extracted oils are determined using available standard methods described in section 4.1 to 4.3. Essential oil and fatty acid composition of extracted oil is investigated using gas chromatography, mass spectroscopy and UV-spectroscopy where the procedures are provided in section 4.4. The chromatograms of all samples of the extracted oil are given in Appendix (C). Modeling and simulation study of SFE process is discussed in chapter 5. Various mathematical models available in literature and their solution techniques are discussed in section 5.1, which are solved using COMSOL multiphysics 5.3 as explained in section 5.2.

Further, in the subsequent paragraphs results related to characterization of turmeric root and carrot seed, essential oil and fatty acid analyses of extracted oils, physico-chemical characteristics of turmeric root oil and carrot seed oil, regression analysis of both the raw materials and effects of parameters on the responses, solution of various mathematical models available in literature using COMSOL multiphysics 5.3, fitting of experimental data of turmeric root and carrot seed into different models and economic analysis are discussed in detail.

6.1 Raw Material-I

Based on the literature review carried out in Chapter 2, two raw materials are selected to be extracted through SFE process. Turmeric root is selected as first raw material from the root category.

6.1.1 Initial oil

Soxhlet extraction method is used to estimate total initial oil content of turmeric root using the method explained in section 3.5. Total initial oil content in turmeric root is estimated as 5.954% of turmeric powder, which is closed to the results reported in literature where it is 5% to 7% (Gopalan et al., 2000).

6.1.2 Moisture and ash content

Moisture and ash contents of turmeric root are estimated using the method explained in section 3.6 and found to be approximately 6.93% and 4.64%, respectively.

6.1.3 Fourier-transform infrared spectroscopy (FTIR) Analysis

FTIR spectra of turmeric oil and turmeric root (pre and post extraction) are measured in a range of 500-4000 cm^{-1} wave numbers as shown in Fig. 6.1. The strong peak at 3414 cm^{-1} shows the presence of O-H bond stretching due to availability of fatty acids, proteins and carbohydrates (Sahu & Saxena , 2014; Pawar et al., 2014; Rohman, 2012; Rai et al., 2015, 2016). Further, peak at 2926 cm^{-1} is due to stretching of aliphatic compound (C-H) present in fatty acids. The peak at wave number of 1638 cm^{-1} is assigned to the stretching of aromatic rings (C=C) and vibration frequency of carbonyl group of amides present in the protein portion (Sahu & Saxena, 2014; Pawar et al., 2014; Rohman, 2012; Rai et al., 2015, 2016). A peak at 1515 cm^{-1} may be because of C=O stretching, which supports the presence of sesquiterpens (turmerone) and peaks at 1377 and 1321 cm^{-1} confirmed the availability of alkanes or CH_3 bending due to presence of curcuminoid (curcumin). Peaks observed at 1158 and 1025 cm^{-1} are due to C=O stretching of ester groups and those found at wave numbers 767, 707 and 614 cm^{-1} are confirming the presence of C-H bending (bending of aromatic H) (Began et al., 2000; Bimakr et al., 2012; Gopalan et al., 2000; Mukhopadhyay, 2009). FTIR spectra for turmeric oil and pre-extraction turmeric powder are almost similar with only change in the intensities of peaks of turmeric oil. Intensities of peaks for the turmeric oil are higher because of pure oil and the waste material of turmeric powder does not affect transmittance. FTIR spectrum of post-extraction turmeric powder favors the extraction of turmeric oil as some peaks are vanished due to extraction of oil compounds. However, few peaks are still visible at lower intensity, which shows the residual amount of oil in the turmeric sample.
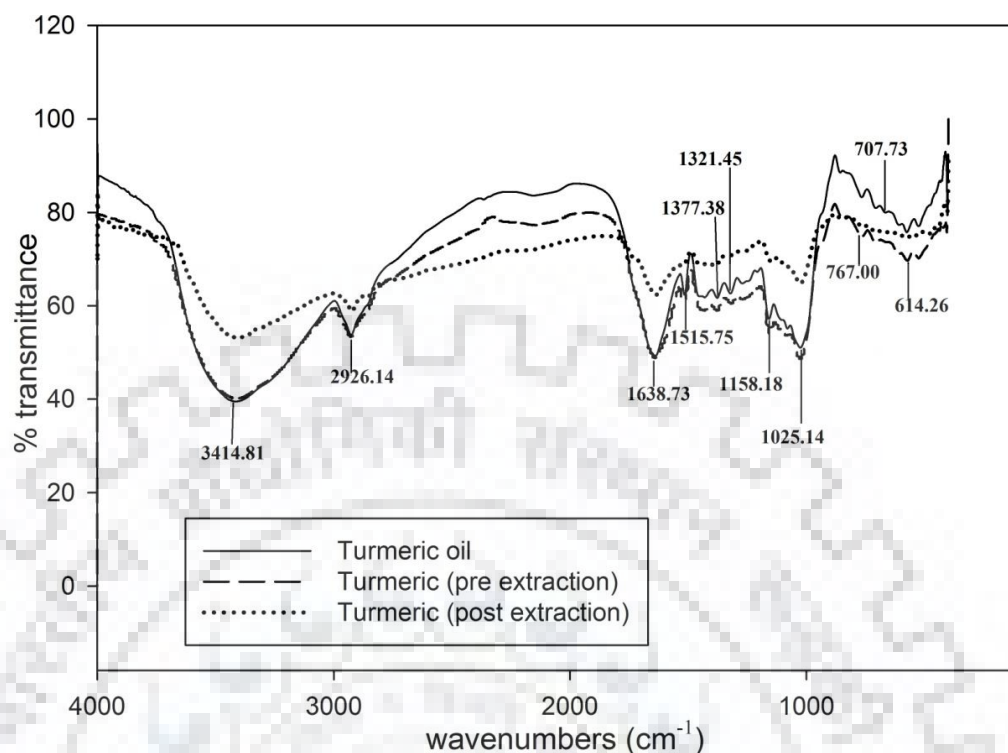
Fig. 6.1 FTIR spectra of Turmeric oil and turmeric powder.

6.1.4 Scanning electron microscopy (SEM) Analysis

Morphological structure of turmeric powder is studied using SEM images. These images of turmeric powder (pre-extraction and post-extraction) are presented in Fig. 6.2. From Fig. 6.2(a), it can be noticed that milled particle of turmeric powder is in cellular structure and oil is found inside the Secretory cells and layers, as reported in the literature (Braga et al., 2006; Danh et al., 2009). On the other hand, cells present inside the turmeric root, found through post-extraction, are destroyed by means of high pressure and no more cellular structure with oil is visible in Fig. 6.2(b). It is in well agreement with TGA profile of post -extraction sample, shown in Fig. 6.3. It is visible from Fig. 6.2(a) that turmeric root consists of secretory cells containing oil and husk as a waste material whereas, in post-extraction sample only husk remains as shown in Fig. 6.2(b). Therefore, it can be concluded that particle size of the turmeric root should be large enough to contain oil cells for extraction.
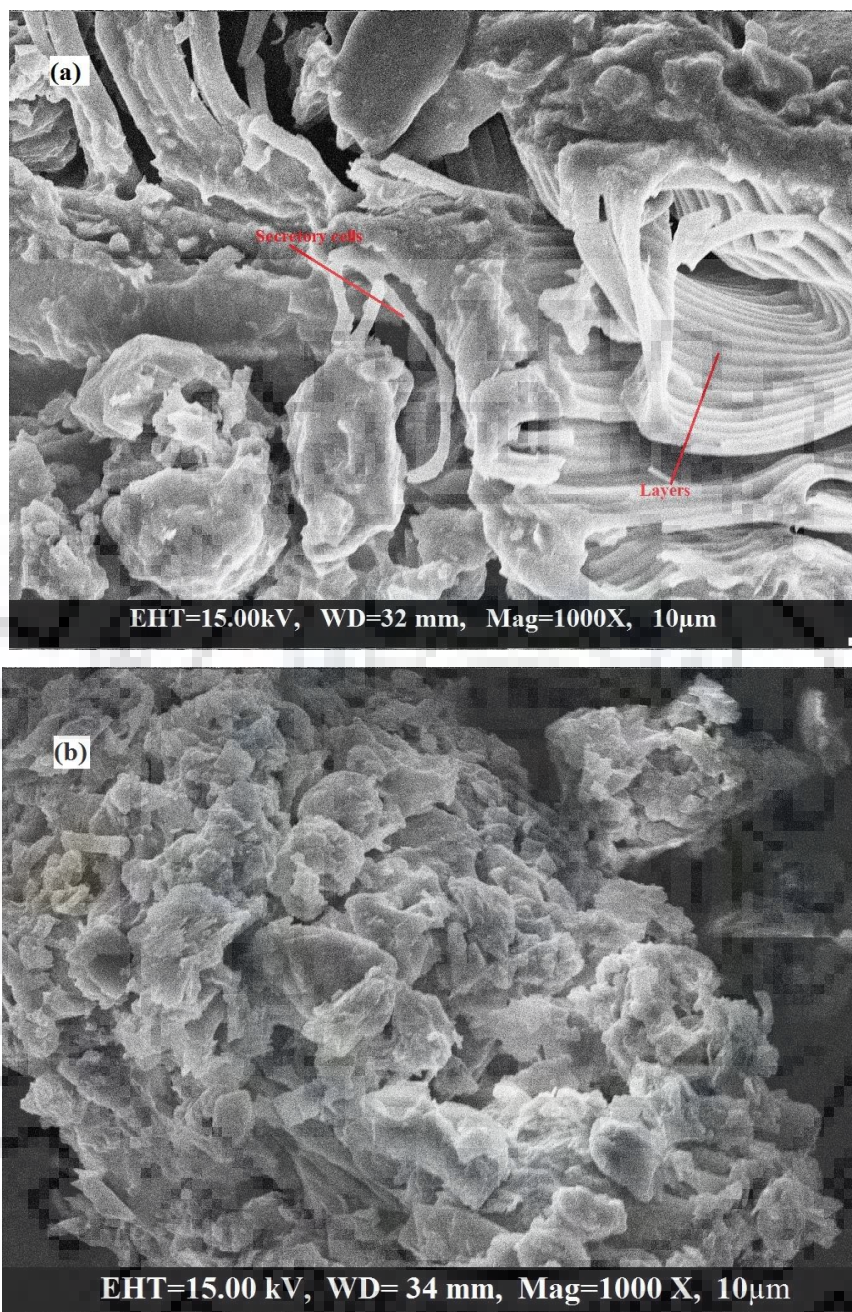
Fig. 6.2 SEM Image of turmeric root (a) pre-extraction (b) post-extraction.

6.1.5 Thermo-gravimetric analysis (TGA)/Differential thermal analysis (DTA)

TGA and DTA of turmeric root (pre-extraction and post-extraction) are shown in Fig. 6.3. TGA curve shows three zones of mass loss. These are from 50 to 200 °C (7.64% loss), 200 to 400 °C (48.2% loss) and 400 to 500 °C (19.69% loss), which are due to moisture removal, decomposition of organic matter and carbonaceous matter/husk, respectively. Three mass loss zones can also be identified within similar temperature ranges in post-extraction sample, which contribute mass

losses of 10.95%, 49.83% and 29.26%. These zones of post-extraction sample are responsible for removal of moisture, decomposition of residual oil and carbonaceous matter. TGA curve of post-extraction sample also approves the extraction of turmeric oil due to which curve is shifted downward to that of pre-extraction sample. In DTA analyses, exothermic peaks are responsible for oxidation reaction. As can be seen from Fig. 6.3, two exothermic peaks are visible in pre-extraction sample, which are due to oxidation of organic matter i.e., fatty acids and husk material. Similarly, two exothermic peaks are also visible in post-extraction sample because of oxidation of residual organic matter and husk material. First exothermic peak is due to degradation of unsaturated fatty acids (USFA) i.e. Mono-unsaturated fatty acid (MUFA) and Poly-unsaturated fatty acid (PUFA) whereas last exothermic peak corresponds to decomposition of saturated fatty acid (SFA) (Asep et al., 2013). However, DTA peaks of pre-extraction sample are higher than that of post-extraction sample, which support the presence of organic compounds i.e. fatty acids in pre-extraction sample. Thus, it can be concluded that turmeric root is thermally stable between 50 to 100 °C as also observed in literature (Masek et al., 2013). Therefore, it is observed from above discussion that extraction temperature for the SFE of turmeric root can be considered up to 100 °C.
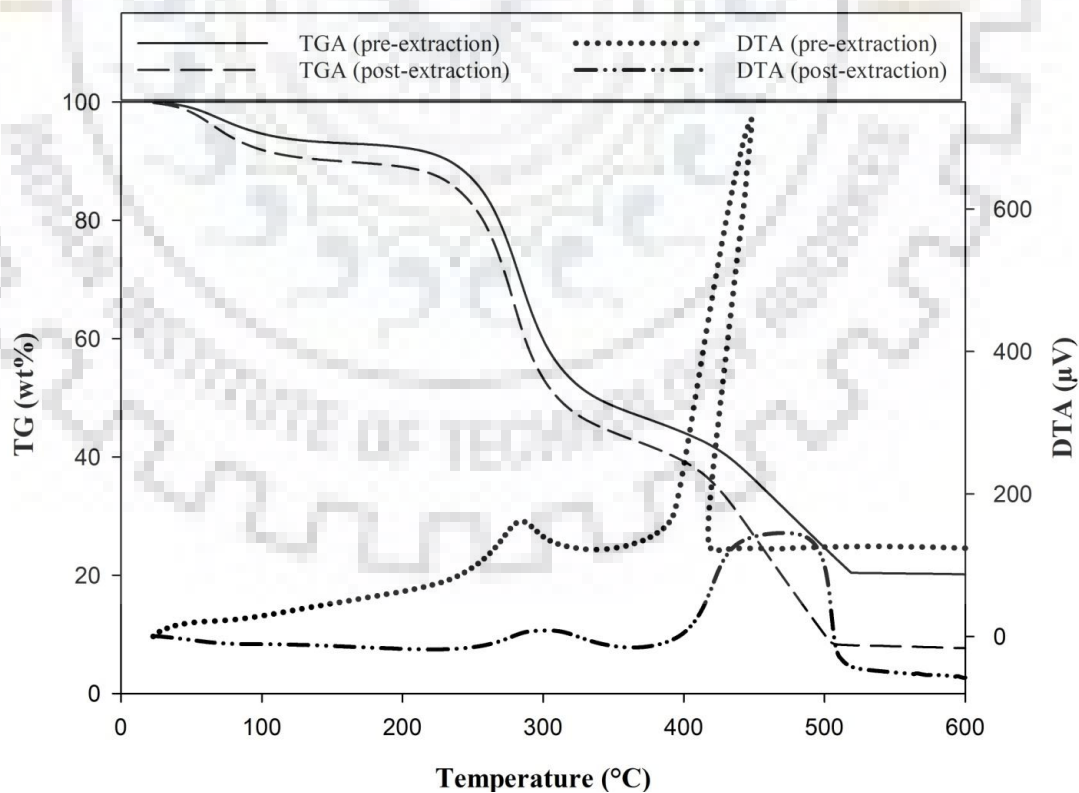
Fig. 6.3 Thermo-gravimetric analysis of Turmeric root powder.

6.2 Raw Material-II

Carrot seed is considered as second raw material to be extracted using SFE process under seed category.

6.2.1 Initial oil

Soxhlet extraction method is employed to estimate total oil content of carrot seed using the method discussed in section 3.5 and found as 13.5% of carrot seed.

6.2.2 Moisture and ash contents

Moisture and ash contents of carrot seed are found as 7.19% and 10.92%, respectively, using the method explained in section 3.6.

6.2.3 FTIR analysis

FTIR spectra of carrot seed and oil are measured from 400 to 4000 cm^{-1} as reported in Fig. 6.4. All peaks in both spectra are at same wave numbers, which indicates that functional groups are same in both samples while the intensities of peaks are varying. Higher intensities of peaks represent the higher concentration of particular functional group and can be seen from Fig. 6.4 that spectrum of carrot seed oil shows high- intensity peaks. Carrot seed oil contains pure chemicals compounds with a high concentration due to which spectrum of oil is shifted above than that of carrot seed (pre and post-extraction). Further, spectrum of carrot seed (post-extraction) supports the extraction of oil, as less intensity peaks of residual oil content and carbonaceous material are visible. In the study of IR peaks, the first peak is found at 3471.6 cm^{-1}, which is due to stretching of O-H bonds present in fatty acids, carbohydrates, and proteins (Masek et al., 2013; Pourmortazavi and Hajimirsadeghi, 2007). IR peaks at 2923.46 and 2857.69 cm^{-1} show the presence of Carotol and -CH_2 available in fatty acids (Chahal et al., 2016). Further, peaks at 1742.71 and 1456.22 cm^{-1} are attributed due to the carbonyl component present in lipids or ester and Daucol, respectively (Chahal et al., 2016). Peaks at a wavelength of 1372.71 to 1153.48 cm^{-1} support the C=O bonds of ester groups (Allam and Hamed, 2007). In addition, peaks at 721.7 to 466.77 cm^{-1} correspond to Carotol amide group present in carrot seed oil (Chahal et al., 2016).
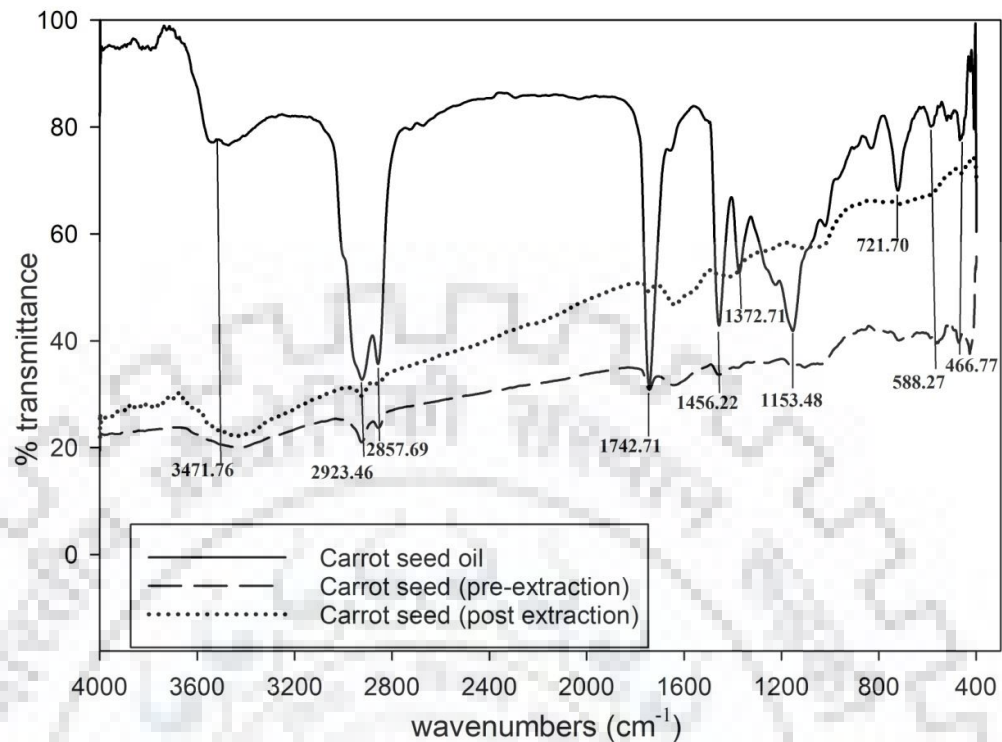
Fig. 6.4 FTIR spectra of carrot seed and oil.

6.2.4 SEM analysis

Morphology of carrot seed (pre- and post-extraction) is studied using SEM images as shown in Fig. 6.5. From SEM image of pre-extraction sample, it can be seen that carrot seed contains secretory cavities as well as glandular trichomes. Due to milling, some part of oil is easily available for extraction as oil containing cavities and trichomes are broken. Oil is uniformly spread over the non-extractable solid structure, which provides lower external mass transfer resistance to the extraction of oil. However, some part of oil is still inaccessible because it is bounded through intact structure as can be noticed from Fig. 6.5 (a). It indicates high internal mass transfer resistance, which makes the extraction of oil from the inside of intact structure difficult. Fig. 6.5 (b) represents the SEM image of post-extraction carrot seed, which supports the extraction of oil as structure seems to be porous and deflated. In addition, application of high pressure also ruptured the structure of carrot seed, which can be seen from post-extraction sample. Although, few intact structures are still visible, mainly glandular trichomes, which clearly show the presence of residual oil in post-extraction sample. Further, empty cavities are also visible in post-extraction sample due to extraction of oil in SFE process.
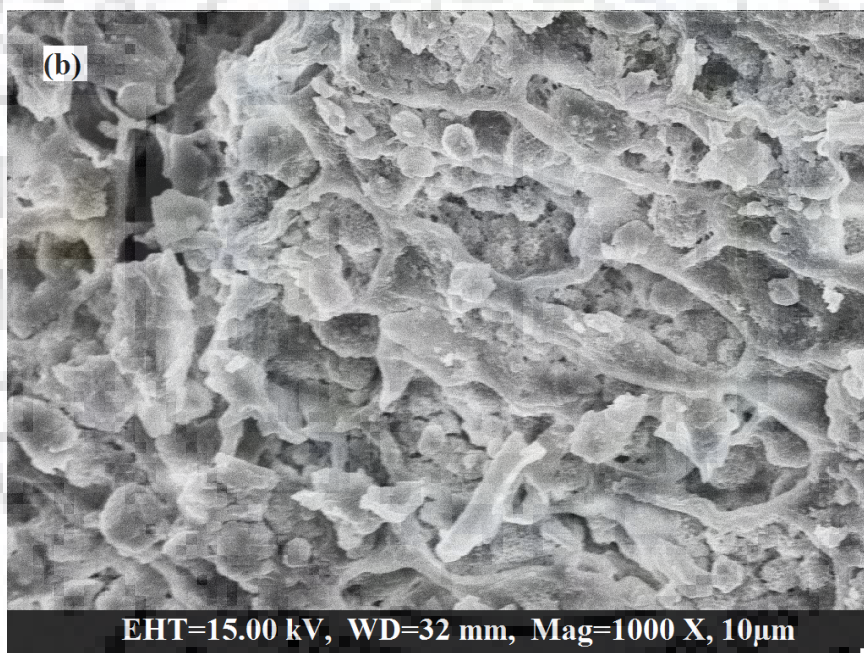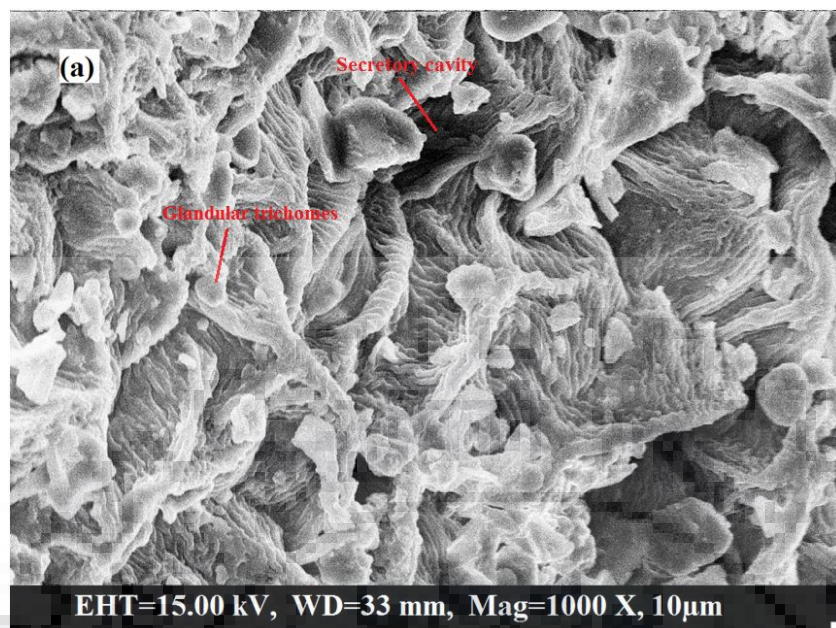
Fig. 6.5 SEM image of carrot seed (a) pre-extraction, (b) post-extraction.

6.2.5 TGA/DTA analysis

Thermal properties of carrot seed are investigated with the help of TG and DT analyses as shown in Fig. 6.6. Thermo gram of carrot seed contains three temperature zones of weight loss as from 23.7 to 200 °C, 200 to 500 °C and 500 to 700 °C. These zones depict weight loss of 7.9%, 79.4% and 3.3%, which correspond to moisture removal, degradation of organic matter and degradation of remaining carbonaceous matter, respectively. As can be seen from Fig. 6.6, 9.4% residue is left

at 700 °C due to presence of inorganic oxides of ash content. Major weight loss zone is from 200 to 500 °C due to loss of fatty acids (PUFA, MUFA AND SFA) (Gao and Birch, 2016). DTA curve of carrot seed indicates three exothermic peaks inside the second weight loss zone i.e. from 200 to 500 °C, as shown in Fig. 6.6, which are the measure of crystallization. First two exothermic peaks are due to crystallization of unsaturated fatty acids (MUFA and PUFA) whereas last and large exothermic peak corresponds to saturated fatty acid (SFA) (Asep et al., 2013). Hence, TGA and DTA study shows the presence of USFA as well as SFA in carrot seed and concludes that carrot seed is thermally stable only up to 100 °C. Therefore, the extraction temperature should be below 100 °C.
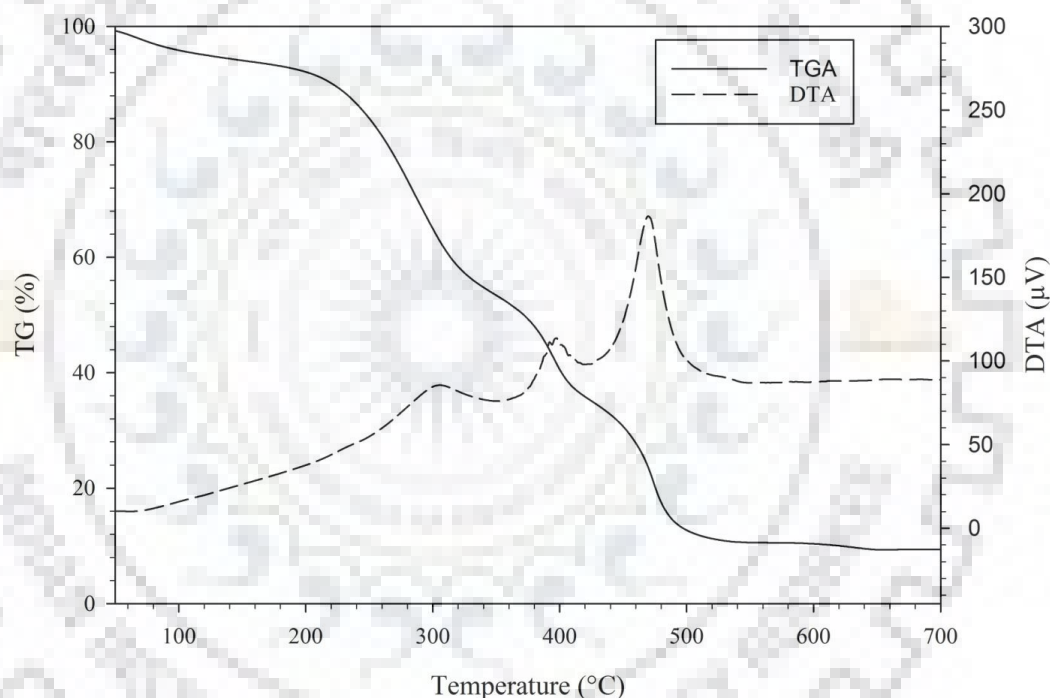
Fig. 6.6 TGA and DTA of carrot seed.

6.2.6 Differential scanning calorimetry (DSC) analysis

DSC is a widely used technique to access thermal stability of carrot seed oil through melting and crystallization profiles as shown in Fig. 6.7. Melting profile is provided between a range of -60 °C to 40 °C, where two endothermic/melting peaks are observed at -16.64±0.35 °C and 19.43±0.25 °C. Gao et al. (2016) also observed two melting peaks for carrot seed oil though first melting peak was at -30.61 °C, which is slightly different than that for present study whereas second peaks is at same temperature. Melting enthalpy is a measure of energy required to melt 1 g of carrot seed oil

at its melting point, which is proportional to the area under the melting curve (Liu et al., 2008). Total melting enthalpy for carrot seed oil is 49.19±5.6 J/g. As can be seen from Fig. 6.7, melting enthalpy of the first peak (5.208±2.4 J/g) is lower than that of the second peak (43.985±3.2 J/g) as the first region is due to melting of MUFA and PUFA followed by melting of SFA in the second region. Melting of PUFA and MUFA require less energy because of their cis double bonds (Gao et al., 2016). Similar behavior was also observed in TGA/DTA curves of carrot seed shown in Fig. 6.6 as three exothermic peaks are shown due to decomposition of PUFA, MUFA and SFA respectively. Glass transition temperature (T_g) can also be investigated through DSC heating curve, which is a measure of a point where heating curve shifts downward suddenly. It is visible from Fig. 6.7 that T_g for carrot seed oil is found to be -48.91 °C.

Crystallization profile of carrot seed oil is shown in Fig. 6.7 that varies from -60 °C to 40 °C. Single exothermic region is found in crystallization profile, which is at -33.32±0.43 °C, and total crystallization enthalpy is -46.205±2.7 J/g. Total enthalpy of melting and crystallization does not differ significantly in magnitude. However, crystallization enthalpy carries negative sign due to release of heat during phase transition of oil to solid state. It can be concluded from above estimation that melting process is compatible with the crystallization process, which is observed by Gao et al. (2016) also.

Solid fat content (SFC) is used to evaluate fat of oil and predicted using DSC melting curve. SFC of carrot seed oil is given in Fig. 6.7 and considered as equivalent to melting integral curve. SFC is calculated on the basis of area under the integration line of melting profile of carrot seed oil as shown in Fig. 6.7 and can be noticed that % SFC is started to drop rapidly beyond 5 °C. It is further started to decrease rapidly from 17 °C to the no-fat level. Oils with higher content of USFA are easier to melt as compared to ones with higher SFA (Gao et al., 2016). Carrot seed oil has a higher melting temperature i.e. 30 °C as shown in Fig. 6.7 than sunflower oil (<5 °C) though it is less than palm oil (>40 °C) (Gao et al., 2016).
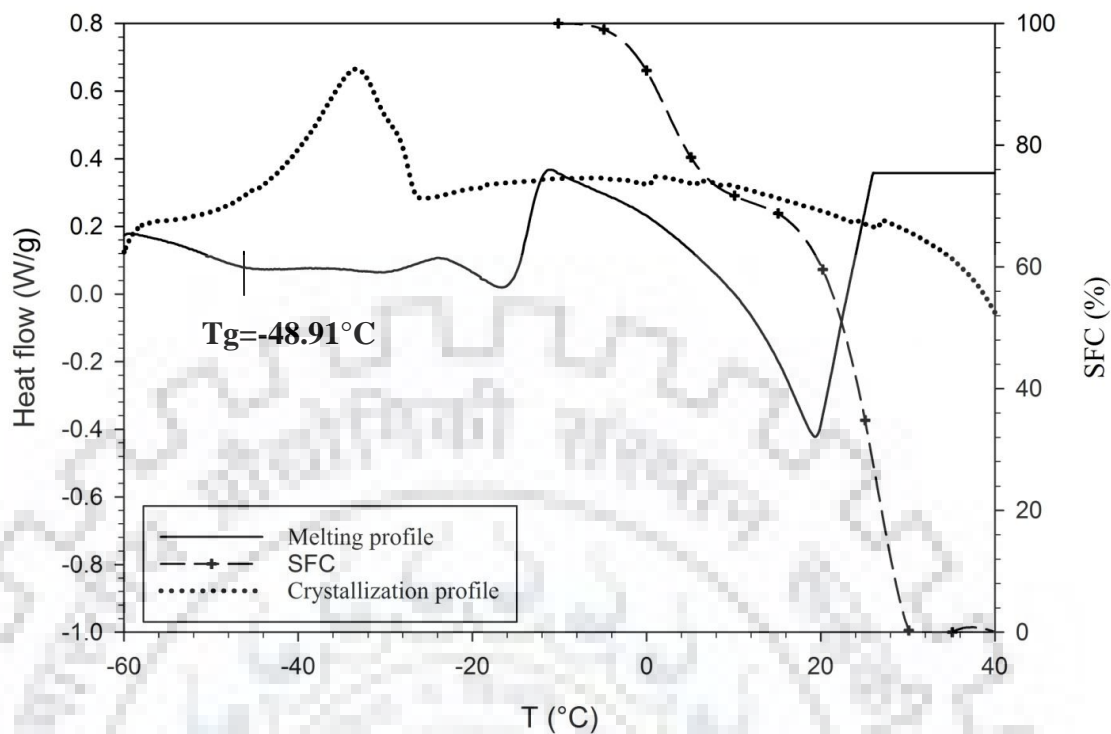
Fig. 6.7 Melting, Crystallization and solid fat content profile of carrot seed oil.

6.3 Qualitative and Quantitative Analyses of Extracted Oil

6.3.1 Raw material-I: turmeric root

Qualitative and quantitative analyses of turmeric oil were carried out using UV spectrometry, GC and MS as shown in Table 6.1 and 6.2.

6.3.1.1 GC-MS and UV analyses of turmeric oil

Major bioactive compound of turmeric oil is Turmerone, which is identified using standard Turmerone. A sample gas chromatogram of turmeric oil is shown in Fig. 6.8 and reveals the presence of several bioactive compounds including turmerone as tabulated in Table 6.1. Gas chromatograms of all experimental runs are shown in Appendix C. GC and MS analyses of turmeric oil result total 14 bioactive compounds present in turmeric oil. Major compounds of turmeric oil are sesquiterpenes (ar-Turmerone, β-Turmerone and α-Turmerone) and constitute 0 to 302.97 mg per g of turmeric oil, respectively. Turmerones protect cells from damage, enhance wound healing capacities, controls type 2 diabetes symptoms, inhibit the replication of HIV (human immunodeficiency virus), conceal the formation of tumors and protect liver damage. Ar-turmerone plays an important role in self-repair and recovery of brain function in neurodegenerative diseases.

Curcumin is analyzed using UV Spectrophotometer where content varies from 0.09 to 2.2 mg/ml as shown in Table 6.1. In the present work, curcumin content of turmeric oil showed a good agreement with the value reported by Priyadarsini (2014). Curcumin is beneficial to human health in many ways due to its anti-inflammatory, antioxidant, antifungal, anticarcinogenic, antiviral, antimutagenic, anticoagulant, antidiabetic, antibacterial, antiprotozoal, antifibrotic, antifertility, hypotensive and hypocholesteremic properties (Bagchi, 2012). Curcumin (detected by UV spectrophotometer) should not be confused with Curcumene (detected by GC-MS) as reported in Table 6.1.
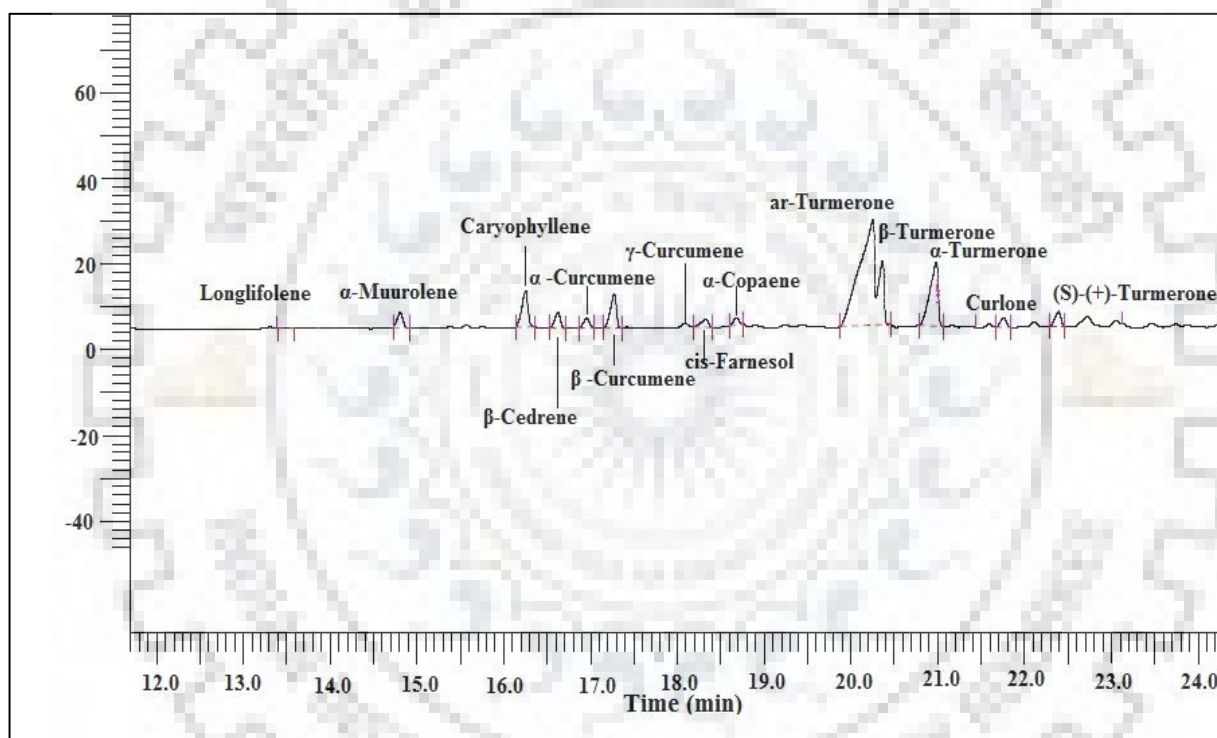
Fig. 6.8 Gas chromatograph of essential oil composition of turmeric.

Table 6.1 Essential oil composition of Turmeric oil

Compound	RT	Standard Order																
		1	2	3	4	5	6	7	8	9	10	11	12	13	14	15	16	17
Longifolene	13.2	0.3	0.4	0.3	0.4	0.7	0.7	0.3	0.3	0	0.3	0.7	0.4	0.5	0.6	0.4	0.2	0.0
α-Muurolene	14.7	2.5	3.1	2.6	3.5	0.6	0.5	2.4	3.3	0	1.8	0.0	3.4	0.3	0.4	2.2	1.9	1.4
Caryophyllene	15.6	2.4	5.3	2.2	3.9	2.3	0.9	2.7	4.4	0	0.6	0.0	4.9	1.4	1.6	4.7	2.4	5.0
β-Cedrene	16.2	6.4	5.2	6.8	6.1	4.3	5.5	6.2	5.0	0	8.8	6.0	5.7	4.2	4.3	5.7	5.7	3.1
α -Curcumene	16.9	1.8	1.9	1.9	1.9	1.1	1.1	1.8	1.7	0	1.8	0.9	1.9	0.8	1.0	1.7	1.6	1.2
β -Curcumene	17.2	5.5	6.1	5.6	5.8	3.3	3.3	5.7	5.3	0	5.1	3.0	5.9	2.9	3.2	5.6	5.4	4.8
γ-Curcumene	17.7	0.1	0.2	0.2	0.1	0.3	0.2	0.1	0.1	0	0.0	0.0	0.1	0	0.3	0.0	0.2	0.0
cis-Farnesol	18.2	2.1	1.4	2.1	1.7	0.8	0.9	2.0	0.7	0	3.6	0.0	1.3	0.5	0.9	0.2	1.8	0.0
α-Copaene	18.6	0.3	0.8	1.4	1.0	0.8	1.9	0.1	0.2	0	0.2	0.0	0.9	0	1.8	1.2	1.5	0.0
ar-Turmerone	20.1	43	31	44	34	51	56	42	39	0	53.3	65	32	52	52	49	42	31
β-Turmerone	20.2	10	22	11	18	11	6.0	14	17	0	3	1.9	21	12.7	13	1.1	12	33
α-Turmerone	20.8	15	15	15	14	18	18	16	14	0	13	16	14	18	20	21.3	16	16
Curlone	21.4	2	0.5	0.6	1.4	0.3	0.3	0.6	1.2	0	1.7	2.1	0.5	2.5	1.2	1.4	1.5	0.4
(S)-(+)-Turmerone	22.2	3	2.2	2.9	2.5	2.6	2.4	2.5	2.3	0	2.3	2.0	2.3	2.3	2.5	3.0	2.8	2.7
UV spectrophotometer																		
Curcumin		0.58	0.63	0.1	0.29	0.19	0.16	0.51	0.44	0.1	0.38	0.21	0.55	0.09	0.3	0.6	0.29	2.1

Compound	RT	Standard Order																
		18	19	20	21	22	23	24	25	26	27	28	29	30	31	32	33	34
Longifolene	13.2	0.0	0.2	0.3	0.4	0.5	0.3	0.0	0.3	0.4	0.4	0.0	0.0	0	0	0.0	0.2	0
α-Muurolene	14.7	1.3	1.2	1.0	1.6	1.2	1.5	0.0	2.5	2.4	2.1	0.0	1.7	0.8	0	0.0	0.9	0
Caryophyllene	15.6	2.7	2.4	2.3	4.5	3.8	5.0	0.0	5.0	4.7	4.7	2.0	4.6	1.7	0	4.7	2.7	0
β-Cedrene	16.2	3.9	3.6	3.3	3.3	3.1	3.3	0.0	4.4	4.6	4.2	2.3	3.9	1.9	0	1.8	2.9	0
α -Curcumene	16.9	1.1	1.2	0.9	1.3	1.2	1.4	0.0	1.7	1.6	1.6	0.0	0.0	0	0	0.0	0.9	0
β -Curcumene	17.2	3.2	2.9	2.6	4.7	4.2	4.8	0.0	5.9	5.7	5.5	2.2	3.9	0	0	4.2	3.0	0
γ-Curcumene	17.7	0.0	0.1	0.1	0.1	0.1	0.1	0.0	0.1	0.1	0.1	0.0	0.0	0	0	0.0	0.0	0
cis-Farnesol	18.2	0.0	0.6	0.5	0.7	0.5	0.5	0.0	0.7	0.7	0.6	0.0	0.0	0	0	0.0	0.1	0
α-Copaene	18.6	0.0	0.2	0.2	0.2	0.2	0.4	0.0	0.7	0.2	0.2	0.0	0.0	0	0	0.0	0.3	0
ar-Turmerone	20.1	46	45	45	33	34	29	51	29	31	34	47	41	47.3	0	31.1	40.7	67.1
β-Turmerone	20.2	22	20	22	26	28	32	49	26	24	23	27	27	25.3	0	37.9	25.3	32.9
α-Turmerone	20.8	14	14	14	17	17	15	0.0	15	16	17	14	11	14.3	0	16.5	16.4	0
Curlone	21.4	0.6	0.9	1.5	1.4	0.5	1.3	0.0	1.4	1.4	0.5	0.0	2.4	1.2	0	0.0	1.3	0
(S)-(+)-	22.2	2.3	2.6	2.5	2.5	2.4	2.5	0.0	2.4	2.2	2.4	2.8	2.4	2.9	0	2.6	2.7	0

Compound	RT	35	36	37	38	39	40	41	42	43	44	45	46	47	48	49	50	
Turmerone																		
UV spectrophotometer analysis																		
Curcumin		1.86	1.49	2.11	2.1	2.2	2.0	2.1	2.1	2.1	2.12	2.12	2.12	2.11	2.1	2.13	2.06	2.1
Compound	**RT**	Standard order																
		35	**36**	**37**	**38**	**39**	**40**	**41**	**42**	**43**	**44**	**45**	**46**	**47**	**48**	**49**	**50**	
Longifolene	13.2	0.3	0.3	0	0	0.0	0	0	0	0.0	0.0	0.0	0.0	0.0	0.0	0.0	0.0	
α-Muurolene	14.7	1.0	1.9	0	0	1.8	0	0	0	1.1	1.1	1.1	1.1	1.1	1.1	1.1	1.1	
Caryophyllene	15.6	2.5	4.4	0	0	3.3	0	0	0	3.4	3.4	3.4	3.4	3.4	3.4	3.4	3.4	
β-Cedrene	16.2	3.2	3.5	0	0	4.6	0	0	0	2.7	2.7	2.7	2.7	2.7	2.7	2.7	2.7	
α -Curcumene	16.9	1.0	1.3	0	0	0.9	0	0	0	0.8	0.8	0.8	0.8	0.8	0.8	0.8	0.8	
β -Curcumene	17.2	2.9	4.6	0	0	3.6	0	0	0	3.6	3.6	3.6	3.6	3.6	3.6	3.6	3.6	
γ-Curcumene	17.7	0.1	0.2	0	0	0.0	0	0	0	0.0	0.0	0.0	0.0	0.0	0.0	0.0	0.0	
cis-Farnesol	18.2	0.5	0.6	0	0	0.0	0	0	0	0.0	0.0	0.0	0.0	0.0	0.0	0.0	0.0	
α-Copaene	18.6	0.2	0.4	0	0	0.0	0	0	0	0.0	0.0	0.0	0.0	0.0	0.0	0.0	0.0	
ar-Turmerone	20.1	43.5	32.9	0	0	46.4	0	0	49.6	38	38	38	38	38	38	38	38	
β-Turmerone	20.2	21.1	25.2	0	0	22.3	0	0	31	2	2	2	2	2	2	2	2	
α-Turmerone	20.8	15.9	16.7	0	0	13.1	0	0	17.2	18	18	18	18	18	18	18	18	
Curlone	21.4	1.5	1.3	0	0	0.0	0	0	0	1.2	1.2	1.2	1.2	1.2	1.2	1.2	1.2	
(S)-(+)-Turmerone	22.2	2.6	2.5	0	0	2.1	0	0	1	2.6	2.6	2.6	2.6	2.6	2.6	2.6	2.6	
UV spectrophotometer analysis																		
Curcumin		1.83	2.1	1.56	2.12	2.1	2.11	0.44	2.1	2.11	2.11	2.11	2.1	2.1	2.1	2.1	2.1	

6.3.1.2 Fatty acid analysis of turmeric oil

Saturated and unsaturated fatty acid contents of turmeric oil are found using gas chromatography as explained in section 4.4.3 and shown in Fig. 6.9 and Table 6.2. It can be seen from Table 6.2 that turmeric oil contains saturated (SFA) and unsaturated fatty acids (USFA) as well. Gas chromatograms of all experimental runs are presented in Appendix C. SFA identified in the turmeric oil are: Butyric acid, Caproic acid, Caprylic acid, Undecylic acid, Lauric acid, Myristic acid, Pentadecylic acid, Palmitic acid and Arachidic acid whereas USFA are: cis-10- Pentadecylic acid, cis-10-Heptadecenoic acid, trans-9- Oleic acid, cis-9-Oleic acid, Linoleic acid, Linolenic acid, cis-11,14,17-eicosatrienoic acid and cis-5,8,11,14-Eicosatetraenoic acid. Both SFA and USFA are necessary for the human body; however, USFA should be in higher proportion to promote good cholesterol. Oleic acid (cis and trans) is the major monounsaturated fatty acid (MUFA) found in turmeric oil. In the present work, it comprises of 2.9 to 61.5% of turmeric oil, which shows a good agreement with values reported by Paul et al. (2011). Oleic acid content of turmeric oil (61.5%) is comparable with the other oleic acid rich compounds such as olive oil (66.4%), sunflower oil (56%), sesame oil (41.5%), almond oil (67.2%) and peanut oil (71.1%) (Orsavova et al., 2015 ;Rai et al., 2016). Oleic acid is a monounsaturated (omega-9) fatty acid, which has several health benefits such as boosts immune system, fights cancer, acts as anti-inflammatory, regulates blood sugar, supports cardiovascular health and fights free radical damage (Orsavova et al., 2015). Turmeric oil is used in several beauty and heath products such as moisturizer, hair growth serum, anti aging creams, anti-dandruff products and anti-fungal lotion due to its richness of oleic acid. Other than oleic acid, Linoleic acid (22.56%) and Linolenic acid (21.3%) are also major omega-6 unsaturated fatty acids found in turmeric oil. Both types of omega-6 fatty acids include several benefits such as enhance metabolism, increase hair growth, maintain the reproductive system and help in growth of brain and muscle (Rai et al., 2016a). Composition of each fatty acid present in turmeric oil for each experimental run is reported in Table 6.2.

It can be concluded from above discussion that turmeric oil can be consumed at a very high dose without any toxic effects. It is usually side effects free in most healthy adults. However, mild and temporary side effects may occur such as diarrhea, nausea, insomnia, headache and vomiting. Thus, turmeric has high potential for the development of modern medicine to treat various diseases.
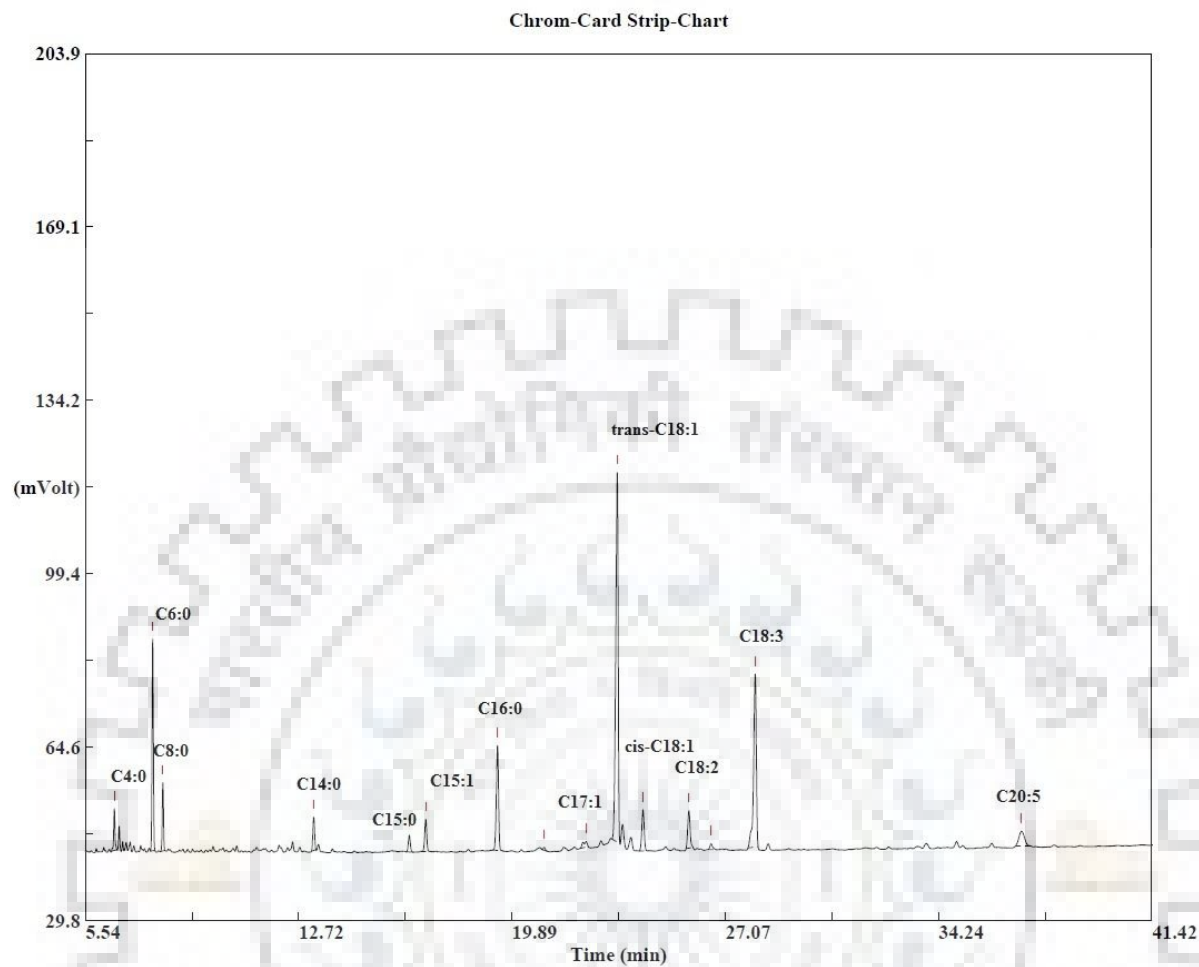
Fig. 6.9 Gas chromatograph of fatty acid mixture of turmeric oil.

Table 6.2 Fatty acid composition of Turmeric oil.

Lipid number	Standard order															
	1	2	3	4	5	6	7	8	9	10	11	12	13	14	15	16
C4:0	2.77	3.28	2.09	4.63	2.21	1.10	2.88	4.26	1.02	2.04	-	3.71	2.77	1.12	1.10	1.81
C6:0	6.13	10.03	4.09	12.26	11.16	5.04	4.24	12.67	4.10	5.09	2.23	11.58	6.13	6.12	8.04	4.79
C8:0	3.78	3.25	4.66	4.67	3.43	3.23	4.21	4.20	3.93	6.84	3.03	4.94	3.78	2.23	3.23	4.05
C11:0	-	0.59	-	1.50	-	-	-	0.82	0.58	-	-	0.67	-	-	-	-
C12:0	0.54	0.24	-	1.03	-	0.62	-	-	2.45	-	-	0.24	0.54	-	0.62	-
C14:0	3.07	2.17	5.39	3.84	2.23	3.33	5.17	4.40	1.25	5.30	2.32	2.77	3.07	2.10	3.33	2.32
C15:0	0.58	7.10	4.64	0.98	1.34	1.59	3.69	0.95	2.29	0.57	0.94	-	0.58	0.46	1.59	-
C15:1	1.72	6.77	2.29	3.27	2.61	2.89	4.39	2.36	5.61	2.25	8.48	2.09	1.72	2.09	3.89	4.50
C16:0	6.40	1.91	2.86	8.35	9.47	5.42	2.68	8.76	1.02	3.36	2.54	8.68	6.40	6.82	5.42	4.86
C17:1	1.50	3.60	-	-	1.19	1.67	-	-	-	-	2.12	-	1.50	-	1.67	1.05
trans-C18:1-ω-9	46.85	14.64	37.70	29.56	36.44	40.93	38.03	26.70	44.65	43.18	37.89	29.52	46.85	32.64	45.93	37.32
cis-C18:1--ω-9	2.65	2.91	1.14	3.60	3.91	2.19	-	3.79	2.37	2.10	-	3.66	2.65	1.55	2.19	2.10
C18:2-ω-6	1.87	9.50	3.82	6.10	3.57	4.62	6.92	5.26	3.49	4.76	22.56	4.92	1.87	2.40	4.62	5.77
C18:3-ω-6	21.03	3.28	21.37	18.03	19.14	21.14	18.75	16.11	23.35	22.61	18.2	15.95	21.03	25.29	19.14	16.85
C20:0	-	1.22	-	1.26	-	-	1.35	0.95	-	1.11	17.89	0.87	-	-	-	1.11
C 20:5-ω-3	0.47	-	1.37	-	-	-	1.26	-	0.66	0.80	-	0.56	0.47	-	-	0.32
C 20:5-ω-3	0.42	2.71	8.53	0.85	3.25	6.24	6.44	8.78	4.25	-	-	7.87	0.42	3.03	6.24	13.16

Lipid number	Standard order																
	17	18	19	20	21	22	23	24	25	26	27	28	29	30	31	32	33
C4:0	4.65	2.45	2.02	1.77	3.99	3.36	3.14	3.16	2.67	4.85	4.34	1.78	3.57	1.29	3.46	3.77	2.55

125

C6:0	23.06	13.37	15.25	13.57	21.41	21.07	15.03	23.25	9.39	13.66	17.33	15.50	16.21	15.86	17.36	20.00	17.71
C8:0	2.96	2.47	2.44	1.81	2.42	2.95	2.39	2.07	4.32	3.74	3.30	1.75	2.25	1.46	1.94	1.54	2.04
C11:0	-	-	-	-	-	-	-	-	0.88	-	-	-	-	-	-	0.89	-
C12:0	-	-	-	-	0.76	0.31	-	-	-	-	-	-	-	-	-	0.86	0.23
C14:0	1.89	3.11	1.64	2.77	1.28	1.34	2.41	2.17	2.96	2.96	2.31	1.64	2.14	1.78	2.50	0.97	1.98
C15:0	1.00	0.86	0.62	-	0.60	3.10	0.86	-	-	2.89	0.42	0.51	0.84	-	0.65	0.56	-
C15:1	3.12	4.06	3.71	4.58	3.57	-	3.74	3.45	2.30	-	2.60	3.63	3.73	4.27	2.97	3.12	3.38
C16:0	15.08	9.69	10.65	7.74	13.64	10.79	10.34	14.86	7.26	10.76	11.55	11.91	11.80	11.27	12.94	14.87	11.93
C17:1	-	1.62	-	-	3.55	-	-	-	0.06	-	-	-	-	-	-	-	0.44
trans-C18:1-ω-9	31.82	31.20	29.27	25.58	5.90	26.99	25.57	23.82	34.75	30.49	24.89	28.59	27.53	30.62	25.93	20.06	29.25
cis-C18:1-ω-9	2.22	4.20	4.90	3.99	5.98	5.97	4.54	6.70	3.50	4.68	5.01	5.23	5.39	5.12	5.60	6.44	5.29
C18:2-ω-6	6.59	7.56	8.12	8.01	0.76	5.23	7.29	6.31	3.72	4.95	4.79	8.54	6.72	7.97	5.69	7.28	6.25
C18:3-ω-6	6.88	16.55	16.87	16.63	12.23	14.64	15.22	12.61	19.91	17.28	13.02	15.24	13.21	13.52	14.04	10.67	14.96
C20:0	-	1.66	1.50	2.15	1.47	1.30	1.41	1.61	-	1.39	1.54	2.17	1.98	2.21	1.76	2.12	1.26
C 20:5-ω-3	-	-	-	-	-	-	-	-	-	-	-	-	-	-	-	-	-
C 20:5-ω-3	-	0.48	-	-	-	-	-	-	0.50	-	-	-	-	-	-	-	-

	Standard order																
Lipid number	34	35	36	37	38	39	40	41	42	43	44	45	46	47	48	49	50
C4:0	2.41	2.46	3.86	3.47	3.00	2.58	2.04	3.05	1.71	3.96	3.96	3.96	3.96	3.96	3.96	3.96	3.96
C6:0	17.27	14.72	18.04	15.12	15.67	13.21	14.84	17.86	14.66	18.25	18.25	18.25	18.25	18.25	18.25	18.25	18.25
C8:0	2.36	2.00	2.25	2.73	1.69	2.98	1.49	2.69	1.26	2.86	2.86	2.86	2.86	2.86	2.86	2.86	2.86

C11:0	0.48	0.56	-	-	-	-	-	-	-	-	-	-	-	-	-	-	-
C12:0	1.02	0.27	-	-	-	-	-	-	-	-	-	-	-	-	-	-	-
C14:0	1.85	2.23	1.18	3.50	0.60	1.72	1.27	1.60	1.79	2.00	2.00	2.00	2.00	2.00	2.00	2.00	2.00
C15:0	0.85	0.74	-	-	1.74	0.41	-	1.04	0.71	-	-	-	-	-	-	-	-
C15:1	2.82	3.34	2.32	2.71	0.65	2.75	2.29	0.65	3.62	3.83	3.83	3.83	3.83	3.83	3.83	3.83	3.83
C16:0	11.97	10.44	11.75	10.29	2.84	9.38	10.06	2.84	10.39	13.86	13.86	13.86	13.86	13.86	13.86	13.86	13.86
C17:1	-	4.08	-	-	0.76	-	-	0.76	-	-	-	-	-	-	-	-	-
trans-C18:1-ω-9	27.53	4.42	21.75	30.23	33.98	27.50	22.23	30.98	25.67	29.82	29.82	29.82	29.82	29.82	29.82	29.82	29.82
cis-C18:1--ω-9	5.20	6.06	4.61	4.93	5.78	4.07	4.27	5.78	4.46	5.85	5.85	5.85	5.85	5.85	5.85	5.85	5.85
C18:2-ω-6	5.33	15.09	4.39	5.76	6.19	6.03	4.81	7.19	7.32	5.31	5.31	5.31	5.31	5.31	5.31	5.31	5.31
C18:3-ω-6	16.13	1.35	11.32	17.77	13.03	14.37	11.36	13.03	13.96	10.68	10.68	10.68	10.68	10.68	10.68	10.68	10.68
C20:0	1.27	2.46	0.88	1.25	1.54	1.35	-	1.54	1.87	1.82	1.82	1.82	1.82	1.82	1.82	1.82	1.82
C 20:5-ω-3	-	-	-	-	-	-	-	-	-	-	-	-	-	-	-	-	-
C 20:5-ω-3	3.51	2.23	17.64	2.27	-	13.66	25.33	-	12.58	-	-	-	-	-	-	-	-

6.3.2 Raw material-II: carrot seed

6.3.2.1 GC-MS analysis of carrot seed oil

Carrot seed oil, extracted through Soxhlet and SFE, is analyzed using coupled GC-MS. Sample preparation method and analysis conditions are explained in section 4.4.2.
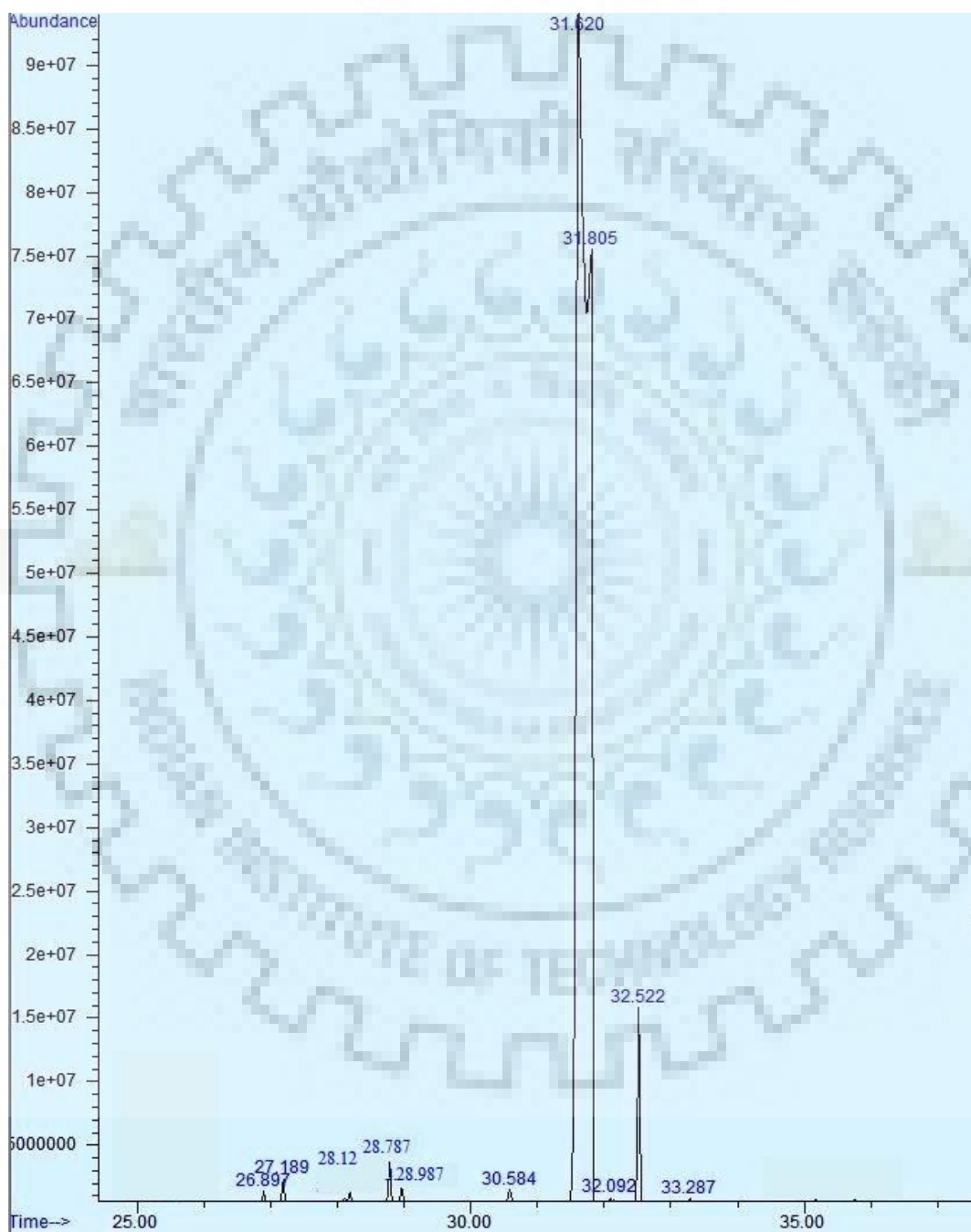
Fig. 6.10 Gas chromatograph of essential oil composition of carrot seed oil.

128

Essential oil content of carrot seed oil comprises of seven bioactive compounds such as α -Farnesene, cis-β-Farnesene, α-Cubebene, γ-Muurolene, β-Bisabolene, Carotol and Daucol, which are in well agreement with those reported in literature (Chahal et al., 2016). Concentrations of these compounds with respective retention time are given in Table 6.3 whereas a sample chromatogram is shown in Fig. 6.10. Gas chromatograms of all experimental runs as well as Soxhlet are provided in Appendix C. Carrot seed essential oil is a common fragrance component in cosmetics and perfumes (up to 0.4% in perfumes) (Sieniawska et al., 2016). It is used in food products as a flavor ingredient (mainly in beverages, desserts, sweets and meat products). It is approved as GRAD (generally regarded as safe) by Food and Drug Administration when ingested in commonly used amounts as food additives or food flavoring (Sieniawska et al., 2016). As can be seen from Table 6.3 and Fig. 6.10, Carotol (RT=31.62 min) is found to be primary compound of carrot seed oil, which contributes around 82.19 to 94.09 % of carrot seed oil. Carotol is a type of sesquiterpene alcohol, which is responsible for the excellent antifungal activity of carrot seed oil. Its activity is nearly as strong as of the commercially available fungicide, Funaben T, (85%) (Jasicka-Misiak et al., 2004). It has moderate cytotoxicity and can be used for fragrance synthesis (Sieniawska et al., 2016). Other than Carotol, Daucol is also a type of sesquiterpene alcohol. It contributes major amount of carrot seed essential oil i.e. 0.53 to 5.85 % of extracted carrot seed oil as reported for each experimental run in Table 6.3. It also can be used as antifungal agent with Carotol (Jasicka-Misiak et al., 2004).

In addition, carrot seed essential oil contains α-Farnesene, cis-β-Farnesene, α-Cubebene, γ-Muurolene and β-Bisabolene also where concentrations of these vary as 0.08 to 0.51, 0.05 to 0.43, 0.05 to 0.38, 0.09 to 0.25 and 0.20 to 0.68 % of carrot seed oil, respectively.

6.3.2.2 Fatty acid analysis of carrot seed oil

Identification and compositions of fatty acids present in carrot seed oil extracted from SFE and Soxhlet are tabulated in Table 6.4 and a sample Gas chromatogram is shown in Fig. 6.11. Gas chromatograms of all experimental runs are shown in Appendix C. Table 6.4 shows that carrot seed oil comprises SFA as well as USFA, which contribute 36 to 84% and 13 to 64%, respectively. SFA identified in the carrot seed oils are C 4:0, C 6:0, C 8:0, C 11:0, C16:0, C18:0 and C20:0 whereas USFA are C15:1, C17:1, C 18:1 ω-9, C 18:3 ω-6, C 20:1and C20:5 ω-3, which support the published literature (Ozcan and Chalchat,2007). The human body requires both types of fatty acids (SFA and USFA); however, the presence of USFA should be high in comparison to SFA to promote good cholesterol.

Table 6.3 Essential oil composition of carrot seed oil.

RT Run	Name of compounds						
	α -Farnesene	cis-β-Farnesene	α - Cubebene	γ-Muurolene	β-Bisabolene	Carotol	Daucol
	26.89	27.18	27.8	28.19	28.79	31.62	32.52
Soxhlet	0.16	0.52	0.24	0.19	0.57	94.5	1.97
1	0.38	0.43	0.38	0.25	0.68	84.6	2.67
2	0.25	0.18	0.35	0.15	0.56	86.8	2.89
3	0.18	0.13	0.09	0.09	0.32	92.05	3.46
4	0.18	0.21	0.15	0.15	0.29	89.25	3.28
5	0.51	0.21	0.05	0.09	0.24	91.23	4.82
6	0.49	0.13	-	0.16	0.21	89.93	5.83
7	0.51	0.21	0.05	0.09	0.24	91.23	4.82
8	0.51	0.21	0.05	0.09	0.24	91.23	4.82
9	0.08	0.05	-	0.18	0.57	94.50	2.90
10	0.42	0.09	0.08	0.25	0.58	82.19	4.13
11	0.38	0.18	0.19	0.14	0.45	83.50	3.50
12	0.09	0.15	0.07	0.14	0.20	90.99	0.53
13	0.08	0.21	-	0.25	0.35	93.82	1.25
14	0.28	0.25	0.24	0.19	0.28	88.37	2.97
15	0.17	0.15	0.05	0.20	0.21	92.31	2.35
16	0.19	0.09	-	0.05	0.29	91.29	0.59
17	0.12	0.05	-	0.18	0.32	90.98	1.63
18	0.51	0.21	0.05	0.09	0.24	91.23	4.82
19	0.13	0.18	0.17	0.14	0.23	96.03	0.52
20	0.13	0.09	0.05	0.07	0.24	86.37	5.09
21	0.25	0.05	0.35	0.26	0.48	87.05	3.59
22	0.36	0.15	0.28	0.08	0.39	82.61	4.27
23	0.05	0.12	0.15	0.18	0.28	93.56	4.39
24	0.06	0.16	0.08	0.12	0.32	94.09	3.28
25	0.46	0.20	0.05	0.18	0.22	80.20	1.67
26	0.26	0.07	0.24	0.09	0.38	83.56	3.69
27	0.51	0.21	0.05	0.09	0.24	91.23	4.82
28	0.08	0.18	-	0.17	0.51	93.95	2.57
29	0.18	0.20	-	0.25	0.41	91.09	1.25
30	0.51	0.21	0.05	0.09	0.24	91.23	4.82

Primary USFA of carrot seed oil is cis-oleic acid (C18:1 ω-9), which contributes 28 to 78% of carrot seed oil as reported in literature also (Gao and Birch, 2016). Cis-oleic acid is a monounsaturated omega-9 fatty acid (MUFA), which has several health benefits such as treatment and prevention of heart disease, decrease the chances of cardiovascular disease because of its stability (Rai et al., 2016a). Other than cis-oleic acid, Pentadecylic acid (C15:1), Margaric acid (C17:1), γ-Linolenic acid (C18:3 ω-6), cis-Arachidic acid (C 20:1) and cis-eicosatetraenoic acid (C20:5 ω-3) are also available in a small amount as compared to oleic acid. Carrot seed oil contains a lower level of Polyunsaturated fatty acid (PUFA) as reported by Gao and Birch (2016).

Linoleic acid is also an important omega-6 (PUFA), which controls metabolism and maintains the reproductive system. It is good for skin, bone, hair, brain and muscle growth (Rai et al., 2015). It is also evident from Table 6.4 that oil extracted from SFE and Soxhlet have the similar composition of fatty acids, however, oil extracted from SFE is pure and solvent free.
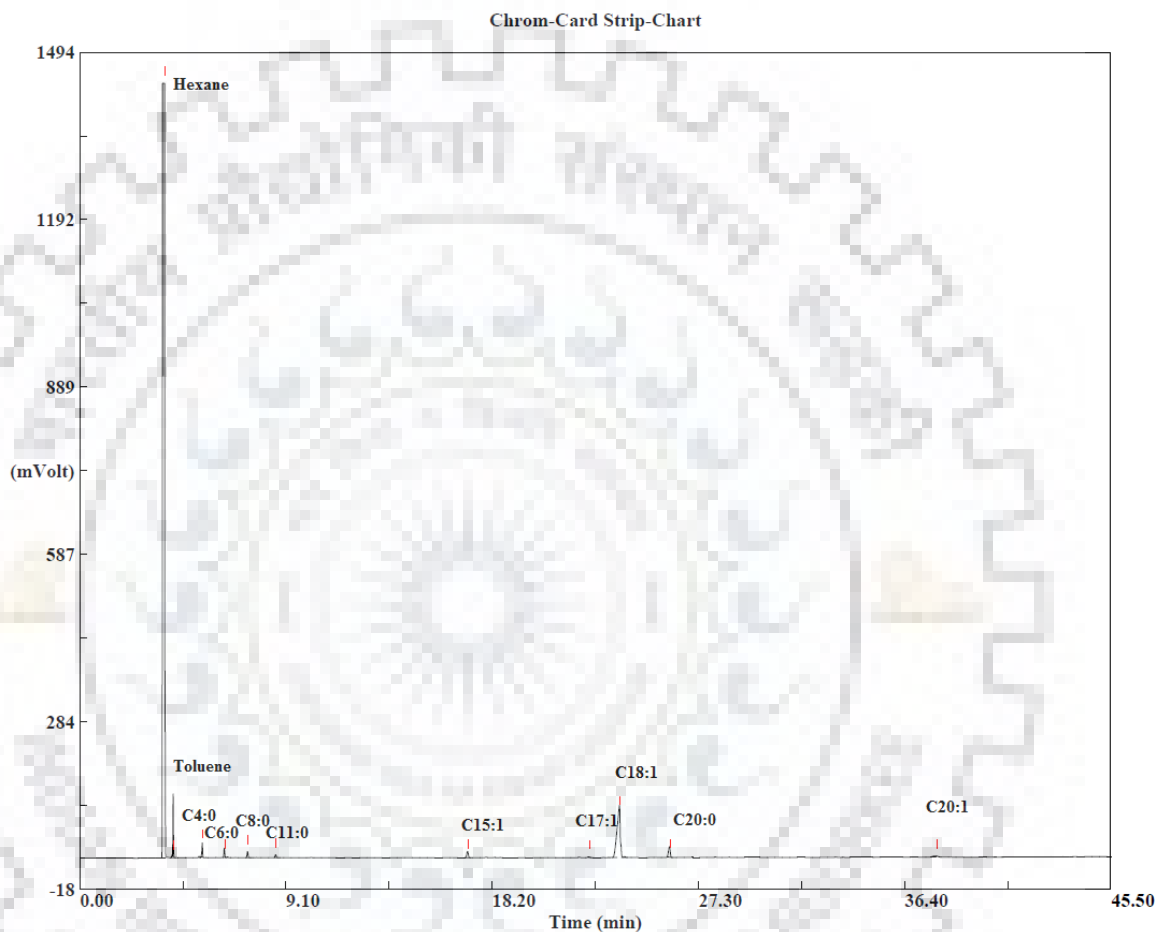
Fig. 6.11 Gas chromatograph of fatty acid mixture of carrot seed oil.

Table 6.4 Fatty acid composition of carrot seed oil.

Run	Name of Fatty acid													Type of saturation	
	C 4:0	C 6:0	C 8:0	C 11:0	C 15:1	C 16:0	C 17:1	C 18:0	C 18:1 ω-9	C 18:3 ω-6	C 20:0	C 20:1	C20:5 ω-3	SFA	USFA
Soxhlet	3.15	1.83	1.15	0.44	4.16	-	1.68	0.81	75.76	-	8.55	-	2.45	24.22	75.78
1	1.29	8.75	5.05	0.80	4.66	-	1.40	0.58	59.62	-	7.75	0.79	9.31	22.79	77.21
2	5.47	5.67	2.77	-	4.41	-	1.00	-	71.80	-	8.88	-	-	20.35	79.64
3	4.90	4.44	2.25	-	4.76	-	1.39	0.86	70.68	0.65	7.90	0.28	1.88	15.82	84.16
4	0.55	3.10	1.88	0.26	4.22	0.24	-	0.75	76.98	0.44	9.04	0.23	2.29	17.78	82.21
5	3.83	2.92	1.13	-	4.53	-	-	0.79	77.19	0.49	9.11	-	-	13.64	86.35
6	3.25	1.89	1.32	0.17	4.12	-	1.47	0.80	67.12	0.49	6.21	-	13.15	17.78	82.21
7	3.83	2.92	1.13	-	4.53	-	-	0.79	77.19	0.49	9.11	-	-	17.78	82.21
8	3.83	2.92	1.13	-	4.53	-	-	0.79	77.19	0.49	9.11	-	-	22.79	77.21
9	5.47	5.67	2.77	-	4.41	-	1.00	-	71.80	-	8.88	-	-	20.15	84.25
10	5.66	4.89	2.55	-	5.41	-	7.97	-	70.87	-	7.05	-	-	30.1	69.9
11	8.10	8.11	4.10	1.12	3.79	0.23	1.63	0.69	59.78	0.31	7.75	-	4.39	39.59	60.41
12	2.84	18.88	10.33	-	3.43	0.35	1.27	1.31	51.47	0.69	5.88	0.42	3.13	63.65	36.36
13	26.35	19.91	9.77	3.54	2.83	-	1.95	-	28.17	-	4.08	-	3.41	16.21	83.79
14	2.66	2.59	1.35	-	4.13	0.22	-	0.79	73.51	0.38	8.6	-	5.77	18.68	81.35
15	4.59	3.33	1.86	-	4.66	-	1.04	0.86	75.24	0.41	8.04	-	-	26.64	73.36
16	1.24	10.04	5.41	0.68	4.87	-	1.74	0.55	66.2	-	8.72	0.55	-	25.76	74.24
17	7.53	5.84	3.48	0.56	4.04	0.16	1.38	0.57	58.61	0.78	7.62	0.28	9.15	17.78	82.21
18	3.83	2.92	1.13	-	4.53	-	-	0.79	77.19	0.49	9.11	-	-	16.36	83.64
19	3.37	2.19	1.39	0.21	4.12	-	0.77	-	76.08	0.45	9.20	-	2.22	19.34	80.64
20	4.88	3.80	2.25	-	5.00	-	1.81	0.86	69.72	0.61	7.55	-	3.50	19.49	85.35
21	5.45	3.17	1.97	-	4.31	-	6.29	-	74.11	-	8.9	-	0.64	25.76	74.24
22	7.53	5.84	3.48	0.56	4.04	0.16	1.38	0.57	58.61	0.78	7.62	0.28	9.15	16.3	83.5
23	3.53	3.00	1.57	-	4.55	-	0.22	-	76.49	-	8.20	-	2.24	13.56	77.04
24	2.54	2.15	1.14	-	4.24	-	1.15	-	71.26	0.39	7.73	-	-	14.52	85.47
25	2.44	2.18	0.98	-	3.85	-	-	0.24	73.45	0.28	8.68	0.27	7.62	26.64	73.36
26	1.24	10.04	5.41	0.68	4.87	-	1.74	0.55	66.2	-	8.72	0.55	-	17.78	82.21
27	3.83	2.92	1.13	-	4.53	-	-	0.79	77.19	0.49	9.11	-	-	18.68	81.35
28	4.59	3.33	1.86	-	4.66	-	1.04	0.86	75.24	0.41	8.04	-	-	39.6	60.38
29	2.85	18.94	10.37	1.54	1.54	-	1.27	-	51.66	-	5.90	-	5.91	17.78	82.21
30	3.83	2.92	1.13	-	4.53	-	-	0.79	77.19	0.49	9.11	-	-	24.22	75.78

6.4 Physico -chemical properties of extracted oil

In this section, physical and chemical properties of extracted turmeric root oil and carrot seed oil through Soxhlet extraction and SFE are discussed.

6.4.1 Raw material-I: turmeric root oil

Physico-chemical properties of turmeric root oil such as refractive index, specific gravity, peroxide value, iodine value, saponfication value and unsaponifiable matter are shown in Table 6.5. These values are estimated for each experimental run of SFE as well as Soxhlet extraction using the methods explained in sections 4.2 and 4.3. Refractive indexes of all samples extracted from SFE are varied from 1.428 to 1.465 whereas it is 1.465 for Soxhlet extraction as given in Table 6.5. These values are in well agreement with that reported in the literature (Paul et al., 2011).The presence of double bonds in large numbers indicates high values of refractive index (Khoddami et al., 2014; Paul et al., 2011).

Specific gravity of turmeric oil samples, shown in Table 6.5, are ranged as 0.892 to 0.919 for SFE whereas, it is 0.921 for Soxhlet extraction, which show well accordance with value reported in the literature (Survase et al., 2011). It indicates that the turmeric root oil contains fatty acids of higher molecular weight similar to that available in olive oil (0.914 - 0.918) and cotton seed oil (0.917 - 0.918) (Paul et al., 2011).

The peroxide value of turmeric root oil varies from 4.195 to 4.246 (meq O_2/ kg oil) for SFE process whereas its value is 4.301 (meq O_2/ kg oil) for Soxhlet extraction. Peroxide values reported in literature support the values found in the present work (Survase et al., 2011). Oils with high peroxide value such as greater than 9 meq O_2/kg oil can cause undesirable health problems by increasing reactive oxygen species as well as secondary products of lipid peroxidation that stimulate cardiovascular and inflammatory diseases (Konuskan et al., 2018).

Iodine value and acid value of turmeric root oil extracted using SFE are varied as 79.39 to 81.05 g I/100 g oil and 10.96 to 11.35 mg KOH/g oil, respectively. However, for Soxhlet extraction values are 81.51 g I/100 g oil and 11.08 mg KOH/g oil, respectively. Iodine and acid values estimated in the present work are in well accordance with in the published literature (Paul et al., 2011). The iodine value of oil indicates the amount of unsaturated fatty acid present in oil whereas acid value is a measure of the free fatty acids (Konuskan et al., 2018).

Table 6.5 Physico-chemical properties of Turmeric root oil.

Run	Refractive Index (30 °C)	Specific Gravity	Peroxide value (meq O$_2$/ kg oil)	Iodine Value (g I /100 g)	Acid Value (mg KOH/g)	Saponification Value (mg KOH/ g)	Unsaponifiable matter (%)
Soxhlet	1.465	0.921	4.301	81.51	11.08	205.39	11.29
1	1.462	0.893	4.205	80.32	10.98	199.57	14.57
2	1.451	0.896	4.241	80.69	11.06	198.93	13.51
3	1.456	0.896	4.195	81.05	11.14	201.37	14.83
4	1.452	0.909	4.195	79.96	11.18	201.83	12.78
5	1.438	0.912	4.246	80.27	10.98	199.57	13.51
6	1.428	0.893	4.205	80.59	11.12	201.37	14.57
7	1.445	0.892	4.192	80.32	11.06	203.12	14.83
8	1.453	0.912	4.195	79.90	11.09	199.57	12.78
9	1.452	0.909	4.231	80.36	10.98	203.12	13.52
10	1.442	0.893	4.241	79.91	11.12	202.58	14.05
11	1.438	0.895	4.246	80.32	11.11	198.27	14.57
12	1.452	0.892	4.235	79.99	11.02	202.58	13.51
13	1.448	0.896	4.205	80.55	11.06	201.37	12.78
14	1.453	0.909	4.235	81.05	10.98	202.58	13.52
15	1.451	0.912	4.240	80.83	11.14	199.57	14.83
16	1.449	0.893	4.241	80.32	11.15	203.12	13.97
17	1.456	0.909	4.240	81.25	11.14	198.27	15.01
18	1.443	0.895	4.205	79.81	11.05	198.93	14.57
19	1.452	0.919	4.193	80.29	11.25	201.37	13.52
20	1.450	0.896	4.246	81.01	11.30	198.27	15.01
21	1.452	0.916	4.195	80.29	10.98	199.57	14.05
22	1.449	0.896	4.215	80.32	11.35	201.83	12.78
23	1.451	0.919	4.243	81.05	11.28	198.27	13.51
24	1.435	0.912	4.205	79.27	11.05	201.37	13.97
25	1.450	0.916	4.220	80.67	11.35	202.58	14.05
26	1.442	0.893	4.238	80.60	11.36	199.23	14.83
27	1.456	0.897	4.195	79.96	11.06	199.57	13.97
28	1.448	0.909	4.235	79.57	10.98	203.12	14.57
29	1.451	0.897	4.241	81.06	11.05	201.37	12.78
30	1.450	0.895	4.239	82.00	11.35	199.23	14.05
31	1.438	0.919	4.246	80.32	11.14	198.93	14.83
32	1.435	0.896	4.239	80.24	11.29	201.83	13.52
33	1.446	0.892	4.205	79.96	11.23	199.23	13.97
34	1.452	0.897	4.243	79.28	11.05	201.37	14.05
35	1.453	0.912	4.220	80.62	11.31	199.23	14.57
36	1.451	0.902	4.195	79.39	10.98	199.57	14.83
37	1.445	0.893	4.192	80.06	10.96	199.85	12.78
38	1.448	0.892	4.205	80.32	11.02	199.89	13.52
39	1.512	0.895	4.245	80.24	11.05	201.85	13.51
40	1.449	0.909	4.243	80.05	11.06	198.93	14.05

41	1.438	0.905	4.241	81.09	11.14	199.23	13.97
42	1.441	0.905	4.245	80.24	11.19	201.82	13.57
43	1.465	0.892	4.215	80.26	11.07	199.58	13.27
44	1.465	0.892	4.215	80.26	11.07	199.58	13.27
45	1.465	0.892	4.215	80.26	11.07	199.58	13.27
46	1.465	0.892	4.215	80.26	11.07	199.58	13.27
47	1.465	0.892	4.215	80.26	11.07	199.58	13.27
48	1.465	0.892	4.215	80.26	11.07	199.58	13.27
49	1.465	0.892	4.215	80.26	11.07	199.58	13.27
50	1.465	0.892	4.215	80.26	11.07	199.58	13.27

Saponification values of turmeric root oil are found within 198.27 to 203.12 mg KOH/g oil for SFE process; however, it is 205.39 mg KOH/ g oil for Soxhlet extraction process. High saponification value depicts the presence of higher molecular weight fatty acids in oil. In addition, unsaponifiable matter is a measure of various compounds such as, alcohols, tocopherols, sterols, waxes present in the oil, which varies within 12.78 to 15.01% for SFE. However, unsaponifiable matter is found as 11.29% using Soxhlet extraction process. Both the values are in well agreement with the that reported in the literature (Paul et al., 2011).

6.4.2 Raw material-II: carrot seed oil

Carrot seed oil samples extracted through Soxhlet extraction and SFE process are analyzed to estimate their physico-chemical properties using the methods as explained in sections 4.2 and 4.3, which are provided in Table 6.6. It shows that refractive indexes for all experimental runs of SFE are ranged between 1.468 and 1.472 whereas it has a value of 1.473 for the oil extracted through Soxhlet process. Ozcan & Chalchat (2007) estimated physical and chemical characteristics of carrot seed oil extracted through Soxhlet process using petroleum ether as a solvent. They reported the refractive index of carrot seed oil as 1.473, which supports well the value estimated through Soxhlet extraction in the present work. The oil samples (run 1-30) extracted through SFE have lower refractive indexes than that of Soxhlet; however, it does not differ much.

Specific gravity and peroxide values of oil extracted through Soxhlet process are estimated as 0.981 and 2.51 meq O_2/ kg oil respectively. For SFE process, these values are ranged between 0.979 to 0.981 and 2.46 to 2.50 meq O_2/ kg oil. specific gravity values show well accordance with that provided by Ozcan & Chalchat (2007) i.e. 0.9811, whereas peroxide values are not matching at all as it is reported quite high i.e. 16.0 meq O_2/ kg oil (Ozcan and Chalchat, 2007). However, the peroxide values of carrot seed oil are in well agreement with that provided by Gao et al. (2016) i.e. 2.47 meq O_2/ kg oil. Peroxide value depends on fatty acid composition and oxidation conditions of

the oil. Oils having low peroxide value are desirable due to less oxidation of oil occurs (Gao et al., 2016).

Table 6.6 Physico-chemical properties of Carrot seed oil.

Run	Refractive Index (30 °C)	Specific Gravity	Peroxide value (meq O_2/ kg oil)	Iodine Value (g I /100 g)	Acid Value (mg KOH/g)	Saponification Value (mg KOH/ g)	Unsaponifiable matter (%)
Soxhlet	1.473	0.981	2.51	85.6	1.61	143.6	0.930
1	1.471	0.979	2.49	83.4	1.63	143.1	0.950
2	1.472	0.981	2.46	83.9	1.63	143.2	0.951
3	1.469	0.981	2.50	84.2	1.62	143.0	0.956
4	1.468	0.979	2.48	83.9	1.62	143.1	0.931
5	1.470	0.980	2.47	82.6	1.65	143.5	0.951
6	1.472	0.981	2.46	83.4	1.63	143.2	0.942
7	1.470	0.980	2.47	82.6	1.65	143.5	0.951
8	1.470	0.980	2.47	82.6	1.65	143.5	0.951
9	1.469	0.981	2.49	84.2	1.64	143.0	0.934
10	1.472	0.978	2.50	83.9	1.63	143.2	0.931
11	1.468	0.978	2.48	83.4	1.62	143.1	0.935
12	1.471	0.979	2.46	83.9	1.63	143.2	0.938
13	1.468	0.981	2.48	83.6	1.62	143.0	0.942
14	1.469	0.978	2.50	83.4	1.63	143.1	0.945
15	1.472	0.978	2.49	84.5	1.64	143.2	0.938
16	1.468	0.981	2.48	84.2	1.63	142.9	0.935
17	1.471	0.979	2.50	83.4	1.64	143.1	0.938
18	1.470	0.980	2.47	82.6	1.65	143.5	0.951
19	1.471	0.981	2.48	84.2	1.63	142.9	0.942
20	1.472	0.978	2.46	83.9	1.64	143.2	0.935
21	1.473	0.980	2.47	83.4	1.64	143.1	0.938
22	1.471	0.979	2.49	84.6	1.62	142.8	0.934
23	1.469	0.981	2.50	83.9	1.63	143.2	0.936
24	1.469	0.978	2.48	83.4	1.62	142.9	0.942
25	1.472	0.979	2.46	84.2	1.64	143.1	0.935
26	1.470	0.981	2.49	84.2	1.62	142.9	0.938
27	1.470	0.980	2.47	82.6	1.65	143.5	0.951
28	1.471	0.979	2.50	84.6	1.63	142.9	0.932
29	1.471	0.981	2.48	83.4	1.62	143.1	0.942
30	1.470	0.980	2.47	82.6	1.65	143.5	0.951

Iodine values and acid values of carrot seed oil are ranged as 82.6 to 84.6 g I /100 g and 1.61 to 1.65 mg KOH/ g for the SFE process, whereas theses are 85.6 g I /100 g and 1.61 mg KOH/ g, respectively, through Soxhlet extraction. Iodine value of carrot seed oil is not reported in literature; however, it is quite close to that of Olive oil (80.03 g I /100 g) whereas, much lower than that of

Mustard (94.51 g I /100 g), Rapeseed (107.51 g I /100 g), Sunflower (102.02 g I /100 g) and Peanut (111.19 g I /100 g) (Konuskan et al., 2018). Acid values of all oil samples are in well accordance with that provided by Gao et al. (2016) i.e.1.65 mg KOH/ g, which indicates that quality of carrot seed oil is good as it is less than the standard of 4.0 mg KOH/g (Gao et al., 2016). Saponification value and unsaponifiable matter of carrot seed oil extracted through Soxhlet extraction are as 143.6 mg KOH/ g and 0.930%, respectively, while these vary as 142.8 to 143.5 mg KOH/ g and 0.932 to 0.951% for SFE of carrot seed oil. Saponification values are matching well with that reported by Ozcan & Chalchat (2007); however, considerably lower than that reported by Abdulrasheed et al. (2015). Further, unsaponifiable matter of carrot seed oil are matching well with that provided by Ozcan & Chalchat (2007) whereas larger than that of suggested by Gao et al. (2016). However, unsaponifiable matter of all oil samples, as given in Table 6.6, are less than the maximum limit of 1% because low unsaponifiable matter is required to maintain the quality and shelf life of oil (Gao et al., 2016).

6.5 Design of Experiment (DOE)

6.5.1 Raw material-I

In order to optimize operating parameters of SFE process and to predict its correlation with responses (OY, TC and TT), experimental results are analyzed using Analysis of variance (ANOVA). Available models such as linear, two-factor interaction model (2FI) and quadratic are tested for ANOVA and discussed in this section.

6.5.1.1 Response surface analysis of operating parameters

Various operating parameters affecting extraction yield of oil and its bioactive compounds directly or indirectly are temperature, pressure, particle size, extraction time, solvent flow rate, amount of co-solvent (modifier), bed void fraction and moisture content and pretreatment of solute (Rai et al., 2015). In the present work, pressure (X_1), temperature (X_2), solvent flow rate (X_3), particle size (X_4), and amount of co-solvent (X_5) are considered to examine effects of these on the extraction yield of essential oil and total curcuminoid (curcumin) and sesquiterpene (turmerone) contents of raw material-1 i.e. turmeric root. Other parameters such as extraction time and feed material are fixed at 260 min and 100 g, respectively, for all experimental runs. Values of five operating parameters at three levels i.e. -1, 0 and +1 are reported in Table 6.7. Design and analysis of RSM is carried out using Design Expert 7.0.3 Software (DE7).

Table 6.7 CCD for SFE of turmeric root.

St. run	Input Factors					Responses		
	X_1: Pressure (bar)	X_2: Temp (°C)	X_3: Flow rate (g/min)	X_4: Particle size(mm)	X_5: Co-solvent (% of CO_2)	OY* (goil/g feed) ±0.02	TC* (mg/g oil) ±0.05	TT* (mg/g oil) ±0.05
1	200(-1)	40(-1)	5(-1)	0.2(-1)	0(-1)	0.034	0.58	184.62
2	400(1)	40(-1)	5(-1)	0.2(-1)	0(-1)	0.037	0.63	97.02
3	200(-1)	60(1)	5(-1)	0.2(-1)	0(-1)	0.036	0.1	103.31
4	400(1)	60(1)	5(-1)	0.2(-1)	0(-1)	0.041	0.29	41.73
5	200(-1)	40(-1)	15(1)	0.2(-1)	0(-1)	0.037	0.19	302.97
6	400(1)	40(-1)	15(1)	0.2(-1)	0(-1)	0.043	0.16	119.60
7	200(-1)	60(1)	15(1)	0.2(-1)	0(-1)	0.045	0.51	65.75
8	400(1)	60(1)	15(1)	0.2(-1)	0(-1)	0.045	0.44	184.62
9	200(-1)	40(-1)	5(-1)	0.73(1)	0(-1)	0.024	0.1	0.00
10	400(1)	40(-1)	5(-1)	0.73(1)	0(-1)	0.021	0.38	20.45
11	200(-1)	60(1)	5(-1)	0.73(1)	0(-1)	0.030	0.21	14.67
12	400(1)	60(1)	5(-1)	0.73(1)	0(-1)	0.028	0.55	83.79
13	200(-1)	40(-1)	15(1)	0.73(1)	0(-1)	0.020	0.09	23.56
14	400(1)	40(-1)	15(1)	0.73(1)	0(-1)	0.023	0.3	134.54
15	200(-1)	60(1)	15(1)	0.73(1)	0(-1)	0.030	0.6	23.55
16	400(1)	60(1)	15(1)	0.73(1)	0(-1)	0.032	0.29	65.50
17	200(-1)	40(-1)	5(-1)	0.2(-1)	15(1)	0.033	2.1	8.97
18	400(1)	40(-1)	5(-1)	0.2(-1)	15(1)	0.028	1.86	11.62
19	200(-1)	60(1)	5(-1)	0.2(-1)	15(1)	0.036	1.49	109.74
20	400(1)	60(1)	5(-1)	0.2(-1)	15(1)	0.029	2.11	62.38
21	200(-1)	40(-1)	15(1)	0.2(-1)	15(1)	0.036	2.1	111.04
22	400(1)	40(-1)	15(1)	0.2(-1)	15(1)	0.036	2.2	62.17
23	200(-1)	60(1)	15(1)	0.2(-1)	15(1)	0.038	2	31.09
24	400(1)	60(1)	15(1)	0.2(-1)	15(1)	0.047	2.1	0.17
25	200(-1)	40(-1)	5(-1)	0.73(1)	15(1)	0.034	2.1	42.60
26	400(1)	40(-1)	5(-1)	0.73(1)	15(1)	0.035	2.09	45.47
27	200(-1)	60(1)	5(-1)	0.73(1)	15(1)	0.047	2.12	127.03
28	400(1)	60(1)	5(-1)	0.73(1)	15(1)	0.043	2.12	3.70
29	200(-1)	40(-1)	15(1)	0.73(1)	15(1)	0.033	2.12	3.17
30	400(1)	40(-1)	15(1)	0.73(1)	15(1)	0.033	2.11	5.73
31	200(-1)	60(1)	15(1)	0.73(1)	15(1)	0.043	2.11	0.00
32	400(1)	60(1)	15(1)	0.73(1)	15(1)	0.050	2.13	1.98
33	200(-1)	50(0)	10(0)	0.45(0)	7.5(0)	0.041	2.06	24.13
34	400(1)	50(0)	10(0)	0.45(0)	7.5(0)	0.050	2.1	0.21
35	300(0)	40(-1)	10(0)	0.45(0)	7.5(0)	0.040	1.83	117.76
36	300(0)	60(1)	10(0)	0.45(0)	7.5(0)	0.050	2.1	90.21
37	300(0)	50(0)	5(-1)	0.45(0)	7.5(0)	0.047	1.56	0.00
38	300(0)	50(0)	15(1)	0.45(0)	7.5(0)	0.053	2.12	0.00
39	300(0)	50(0)	10(0)	0.2(-1)	7.5(0)	0.036	2.1	4.13
40	300(0)	50(0)	10(0)	0.73(1)	7.5(0)	0.032	2.11	0.00
41	300(0)	50(0)	10(0)	0.45(0)	0(-1)	0.043	0.44	0.00
42	300(0)	50(0)	10(0)	0.45(0)	15(1)	0.052	2.1	0.78

43	300(0)	50(0)	10(0)	0.45(0)	7.5(0)	0.050	2.11	12.71
44	300(0)	50(0)	10(0)	0.45(0)	7.5(0)	0.049	2.11	12.71
45	300(0)	50(0)	10(0)	0.45(0)	7.5(0)	0.049	2.11	12.71
46	300(0)	50(0)	10(0)	0.45(0)	7.5(0)	0.050	2.1	12.71
47	300(0)	50(0)	10(0)	0.45(0)	7.5(0)	0.049	2.1	12.71
48	300(0)	50(0)	10(0)	0.45(0)	7.5(0)	0.049	2.1	12.71
49	300(0)	50(0)	10(0)	0.45(0)	7.5(0)	0.049	2.1	12.71
50	300(0)	50(0)	10(0)	0.45(0)	7.5(0)	0.049	2.1	12.71

*OY-Oil yield, TC-Total curcuminoids, TT-Total Turmerone

CCD is used to study the effect of interactions parameters on the responses such as, extraction yield of oil, total curcuminoid content and sesquiterpene content of oil. A full-face centered CCD gives 50 different combinations of five input parameters. It consists of 32 factorial points, 10 axial points and 8 center points. All these 50 experiments were performed and responses are reported in Table 6.7.

6.5.1.2 Development of correlation between operating parameters and responses

Response-1: oil yield (OY) from SFE of turmeric root

Linear and 2FI model

Firstly, experimental data of all input parameters are fitted in regressed linear and two factor interaction (2FI) models to find the oil yield response as shown through equation 6.1 and 6.2, respectively. ANOVA analysis is carried out to establish relative significance of the individual terms and found X_2 as significant term over X_1, X_3, X_4 and X_5 for linear model. For 2FI model, X_2 and X_4X_5 are only significant terms. Basis for above conclusion is that p-values of terms less than 0.0001 indicate a significant model terms. P-values of both models are less than 0.0001, which show that model fitting is significant. For these models, correlation coefficients are very less as shown in Table 6.8. Thus, linear as well as 2FI models are not suitable for the SFE of turmeric oil.

$$OY = 0.039 + 6.922 \times 10^{-4}. X_1 + 3.751 \times 10^{-3}. X_2$$
$$+ 1.75 \times 10^{-3}. X_3 - 2.25 \times 10^{-3}. X_4 + 2.487 \times 10^{-3}. X_5 \tag{6.1}$$

$$OY = 0.039 + 6.922 \times 10^{-4}. X_1 + 3.751 \times 10^{-3}. X_2 + 1.75 \times 10^{-3}. X_3 - 2.25 \times 10^{-3}. X_4 + 2.487 \times 10^{-3}. X_5$$
$$+ 1.705 \times 10^{-4}. X_1 X_2 + 1.157 \times 10^{-3}. X_1 X_3 - 2.058 \times 10^{-4}. X_1 X_4 - 3.340 \times 10^{-4}. X_1 X_5$$
$$+ 7.3727 \times 10^{-4}. X_2 X_3 + 1.484 \times 10^{-3}. X_2 X_4 + 5.272 \times 10^{-4}. X_2 X_5 - 1.591 \times 10^{-3}. X_3 X_4$$
$$+ 2.225 \times 10^{-4}. X_3 X_5 + 4.493 \times 10^{-3}. X_4 X_5 \tag{6.2}$$

Table 6.8 Correlation coefficients of Linear, 2FI and quadratic models.

Model	R-squared			Adjusted R-squared			Predicted R-squared		
	OY	TC	TT	OY	TC	TT	OY	TC	TT
Linear	0.25	0.73	0.27	0.17	0.70	0.20	0.05	0.68	0.03
2FI	0.47	0.74	0.63	0.24	0.63	0.47	0.003	0.50	0.12
Quadratic	0.96	0.98	0.85	0.92	0.97	0.74	0.84	0.92	0.42

Quadratic model

Quadratic model is used to fit experimental data of SFE of turmeric root as shown in equation 6.3. ANOVA results for quadratic model are shown in Table 6.9. It indicates that the individual and second order interaction terms such as X_2, X_3, X_4, X_5, X_4^2, X_1X_3, X_2X_4, X_3X_4 and X_4X_5 were significant. Predicted R-Squared of quadratic model is in reasonable agreement with the adjusted R-Squared as shown in Table 6.8. Adequate precision is a measure of signal to noise ratio and its value greater than 4 is desirable for fitting. For equation 6.3, "adeq precision" value is 21.348, which indicates an adequate signal. Lack of fit and p-value for the quadratic model are less than 0.0001, which show significant fitting as reported in Table 6.9. Thus, quadratic model is most suitable model for SFE of turmeric root in comparison to linear and 2FI models. Parity plot of quadratic model for the prediction of OY is shown in Fig. 6.12 with an error band of ± 2.9%. Therefore, OY predicted through quadratic model lie within ± 2.9% of experimental values.
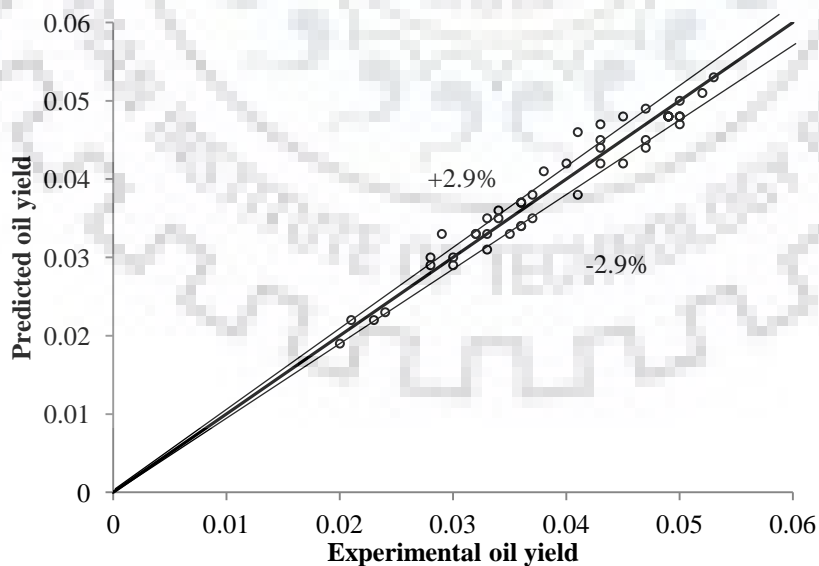
Fig. 6.12 Parity plot of quadratic model developed for the prediction of oil yield.

Table 6.9 ANOVA for RSM variables fitted to quadratic model.

Source	Sum of squares	df	Mean square	F-value	p-value	Significance
Model	3.735×10^{-3}	20	1.868×10^{-4}	30.39	< 0.0001	Significant
X_1: Pressure	1.629×10^{-5}	1	1.629×10^{-5}	2.65	0.1143	Insignificant
X_2: Temperature	4.784×10^{-4}	1	4.784×10^{-4}	77.84	< 0.0001	Significant
X_3:Flow rate	1.042×10^{-4}	1	1.042×10^{-4}	16.95	0.0003	Significant
X_4:Particle Size	1.721×10^{-4}	1	1.721×10^{-4}	28.01	< 0.0001	Significant
X_5:Co-solvent (%)	2.104×10^{-4}	1	2.104×10^{-4}	34.23	< 0.0001	Significant
X_1^2	5.272×10^{-6}	1	5.272×10^{-6}	0.86	0.3620	Insignificant
X_2^2	1.380×10^{-5}	1	1.380×10^{-5}	2.25	0.1448	Insignificant
X_3^2	2.179×10^{-5}	1	2.179×10^{-5}	3.55	0.0698	Insignificant
X_4^2	4.165×10^{-4}	1	4.165×10^{-4}	67.77	< 0.0001	Significant
X_5^2	1.569×10^{-6}	1	1.569×10^{-6}	0.26	0.6172	Insignificant
X_1X_2	9.306×10^{-7}	1	9.306×10^{-7}	0.15	0.7000	Insignificant
X_1X_3	4.287×10^{-5}	1	4.287×10^{-5}	6.98	0.0132	Significant
X_1X_4	1.356×10^{-6}	1	1.356×10^{-6}	0.22	0.6421	Insignificant
X_1X_5	3.569×10^{-6}	1	3.569×10^{-6}	0.58	0.4522	Insignificant
X_2X_3	1.739×10^{-5}	1	1.739×10^{-5}	2.83	0.1033	Insignificant
X_2X_4	7.047×10^{-5}	1	7.047×10^{-5}	11.47	0.0021	Significant
X_2X_5	8.895×10^{-6}	1	8.895×10^{-6}	1.45	0.2387	Insignificant
X_3X_4	8.104×10^{-5}	1	8.104×10^{-5}	13.19	0.0011	Significant
X_3X_5	1.584×10^{-6}	1	1.584×10^{-6}	0.26	0.6155	Insignificant
X_4X_5	6.459×10^{-4}	1	6.459×10^{-4}	105.10	< 0.0001	Significant
Residual	1.782×10^{-4}	29	6.146×10^{-6}			
Lack of Fit	1.769×10^{-4}	22	8.040×10^{-7}	41.53	< 0.0001	significant
Pure Error	1.355×10^{-6}	7	1.936×10^{-7}			
Cor Total	3.913×10^{-3}	49				

$$OY = 0.048 + 6.922 \times 10^{-4}.X_1 + 3.751 \times 10^{-3}.X_2 + 1.75 \times 10^{-3}.X_3 - 2.25 \times 10^{-3}.X_4 + 2.487 \times 10^{-3}.X_5$$
$$- 1.460 \times 10^{-3}.X_1^2 - 2.362 \times 10^{-3}.X_2^2 + 2.968 \times 10^{-3}.X_3^2 - 0.013.X_4^2 + 7.965 \times 10^{-4}.X_5^2$$
$$+ 1.705 \times 10^{-4}.X_1X_2 + 1.157 \times 10^{-3}.X_1X_3 - 2.058 \times 10^{-4}.X_1X_4 - 3.340 \times 10^{-4}.X_1X_5$$
$$+ 7.3727 \times 10^{-4}.X_2X_3 + 1.484 \times 10^{-3}.X_2X_4 + 5.272 \times 10^{-4}.X_2X_5$$
$$- 1.591 \times 10^{-3}.X_3X_4 + 2.225 \times 10^{-4}.X_3X_5 + 4.493 \times 10^{-3}.X_4X_5 \quad (6.3)$$

Response-2: Total curcuminoid (TC) content from SFE of turmeric root

Curcuminoids are one of the major bioactive compounds present in turmeric oil other than sesquiterpenes. Principal curcuminoid of turmeric oil is curcumin (mg/g oil), which is found using UV-spectroscopy as reported in Table 6.7. Analysis data is fitted into three models in a similar way as carried out for OY to evaluate the significance of operating parameters. The p-values for linear

and quadratic models are less than 0.0001 though it is greater for 2FI model. However, regression coefficient of quadratic model, found as 0.98, shows very good fitting of experimental data for TC content as reported in Table 6.8. Therefore, quadratic model is recommended for TC content and its correlation with operating parameters is:

$$
\begin{aligned}
TC = {}& 2.06 + 0.038 \times X_1 + 9.706 \times 10^{-3} \times X_2 + 0.035 \times X_3 + 0.017 \times X_4 + 0.86 \times X_5 + 0.054 \times X_1^2 \\
& - 0.061 \times X_2^2 - 0.91 \times X_3^2 + 0.079 \times X_4^2 - 0.76 \times X_5^2 + 0.017 \times X_1 X_2 - 0.038 \times X_1 X_3 \\
& - 6.25 \times 10^{-3} \times X_1 X_3 - 2.5 \times 10^{-3} \times X_1 X_4 + 0.055 \times X_2 X_3 + 0.051 \times X_2 X_4 - 0.033 \times X_2 X_5 \\
& - 0.014 \times X_3 X_4 + 0.036 \times X_3 X_5 + 0.041 \times X_4 X_5
\end{aligned} \tag{6.4}
$$

Response-3: Total Turmerone (TT) content from SFE of turmeric root

Turmeric oil majorly contains Sesquiterpenes, which are different types of Turmerone such as ar-turmerone, α-turmerone and β-turmerone. Sesquiterpenes content of the turmeric oil is identified using MS spectra and concentrations are computed through GC analysis. Standard turmerone is used to estimate the amount of turmerone extracted for all the experimental runs as reported in Table 6.7. Experimental data for TT content is fitted into three models i.e. Linear, 2FI and quadratic and regression analysis is carried out. It shows that only quadratic model is most suitable because of its low p-value and good regression coefficients which are <0.0001 and 0.85, respectively, as reported in Table 6.8. A correlation between TT content and operating parameters is derived in equation (6.5).

$$
\begin{aligned}
TT = {}& 12.77 + 2.13 \times X_1 - 10.02 \times X_2 + 6.97 \times X_3 - 28.35 \times X_4 - 26.37 \times X_5 - 0.66 \times X_1^2 \\
& + 91.15 \times X_2^2 - 12.83 \times X_3^2 - 10.77 \times X_4^2 - 12.44 \times X_5^2 - 4.97 \times X_1 X_2 + 17.06 \times X_1 X_3 \\
& + 4.9 \times X_1 X_3 - 18.04 \times X_1 X_4 - 18.26 \times X_2 X_3 + 12.58 \times X_2 X_4 + 12.62 \times X_2 X_5 \\
& - 12.39 \times X_3 X_4 - 19.67 \times X_3 X_5 + 19.52 \times X_4 X_5
\end{aligned} \tag{6.5}
$$

6.5.1.3 Effect of individual parameter on OY

SFE process is affected by various operating parameters such as pressure (X_1), temperature (X_2), solvent flow rate (X_3), particle size (X_4) and co-solvent (X_5). Effect of individual parameter on OY can be explained through perturbation plot shown in Fig. 6.13. It indicates that while increasing pressure from 200 to 400 bar and keeping other factors at base values shown in Fig. 6.13, OY increases slightly. The increment in OY with increasing pressure is due to increase in solubility of oil in solvent (Sodeifian et al., 2016a; Zaghdoudi et al., 2016). Similarly, temperature is also showing positive effect and OY is increasing with temperature from 40 °C to 60 °C. Mass transfer coefficient as well as mass transfer rate of solute to bulk liquid phase increases with increasing

temperature due to high diffusivity of oil in solvent (Nyam et al., 2011; Rai et al., 2015). Solvent flow rate is showing a moderate effect on OY as can be seen from Fig. 6.13. At high solvent rate, mass transfer resistance surrounding the solid particles reduces or thickness of film layer around the solid particle reduces (Pourmortazavi & Hajimirsadeghi, 2007), which increases OY. A steep slope is noticed through Fig. 6.13 while varying the particle size of turmeric root. It reflects that OY is highly sensitive towards particle size in comparison to other factors. OY is increasing for the particle size varying from 0.2 to 0.45 mm and further decreasing as particle size is increased to 0.73 mm. Generally, OY should increase for lowest particle size due to smaller intra-particle diffusion as cell walls are disrupted by grinding (Braga et al., 2006; Danh et al., 2009; Masek et al., 2013; Pourmortazavi and Hajimirsadeghi, 2007). If the particle size is too small, fluid channeling can happen inside the fixed bed resulting in inhomogeneous extraction. Re-adsorption of solute on the matrix surfaces can occur, which hinders the extraction (Allam and Hamed, 2007; Rai et al., 2016a, 2015). The probable reason for lowering the oil yield at 0.2 mm could be the re-adsorption of oil on the solid surface of turmeric root. On the other hand, for larger particle size, cell walls are not ruptured where oil is enclosed. Thus, a moderate particle size is suitable to maximize OY. Therefore, a moderate size of particle (0.45 mm) favors the extraction of oil from turmeric root as similar fact was also observed by Chang et al. (2006). Further, the effect of addition of modifier/co-solvent is studied through Fig. 6.13, which shows that OY is increasing significantly while increasing amount of co-solvent. It enhances solvent polarity and specific interaction whereas the sensitivity of solubility with respect to pressure and temperature remains unaltered (Mukhopadhyay, 2000). Thus, it can be concluded that pressure is not affecting the OY significantly while temperature, solvent flow rate and addition of co-solvent show significant positive effects on the OY. Apart from this, particle size is highly sensitive towards OY. Based on above discussion, optimized values of operating parameters are investigated as 255 bar pressure, 53.72 °C temperature, 13.6 g/min solvent flow rate, 0.54 mm particle size and 7.85 % co-solvent, which provide an OY of 5.5 wt% for SFE of turmeric root as shown Table 6.10.
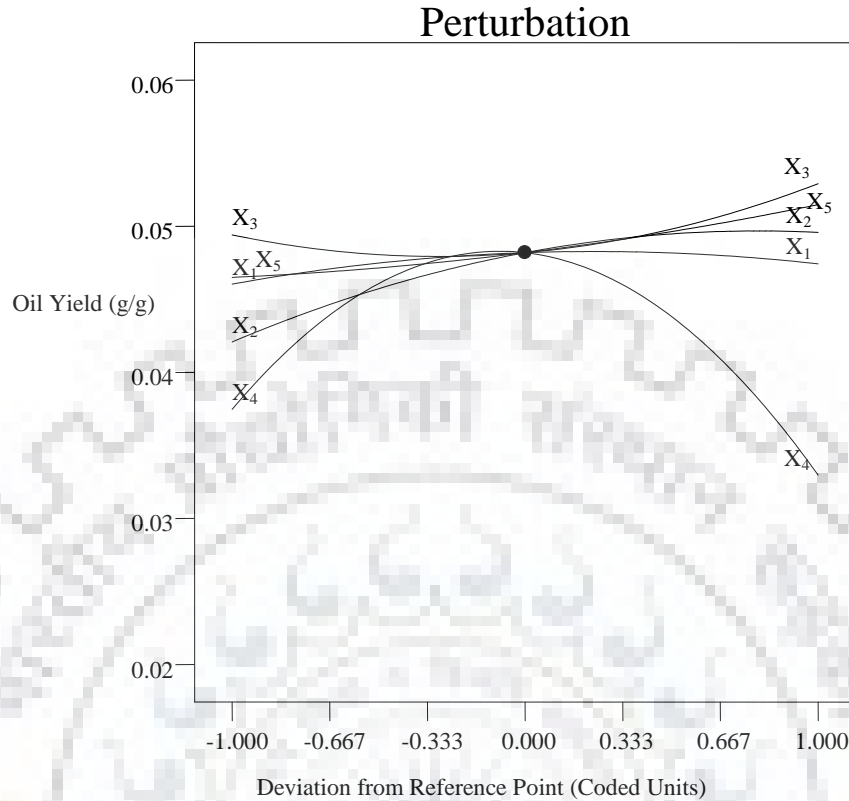
Fig. 6.13 Effect of individual parameters on the oil yield of turmeric oil.

6.5.1.4 Effect of two-parameter interactions on OY

Two-parameter interaction response surface plots as shown in Fig. 6.14 (a) to (j) are drawn for different input parameters while considering other parameters as constant at the base case (Fig. 6.13). Simultaneous effects of four input parameters such as temperature, solvent flow rate, particle size and co-solvent with the pressure are shown in Fig. 6.14 (a) to (d), which indicate that pressure does not show significant effect on OY as compared to other parameters. OY is increasing with pressure and temperature simultaneously, which is due to increase in mass transfer coefficient as discussed in section 6.5.1.3. In comparison to any other combination of parameter interactions, OY is minimum for combining effect of pressure and temperature. In Fig. 6.14 (b), OY is increasing with pressure and solvent rate and can be explained as: higher pressure enhances the solvent density and thus, interaction between oil and solvent molecules increases, which leads to increase of oil solubility in solvent.

On the other hand, combined effect of pressure and particle size is larger as shown in Fig. 6.14 (c). It can be observed that OY depends on particle size only. OY is first increasing with particle size

144

upto 0.45 mm then decreasing till 0.73 mm and reason is discussed in section 6.5.1.3. Further, Fig.s 6.14 (d) and (i) show that combined effect of co-solvent with pressure and flow rate are similar to that is observed in Fig. 6.14 (b). Co-solvent is added to enhance the solvent characteristics, such as polarity and specific interactions, without significantly affecting density and compressibility of solvent. For the extraction of oil from solid material, solvent penetrates inside solid material where oil is dissolved in it. Further, co-solvent is added, which is mixed with solvent and enhances extraction efficiency of solvent. The hydroxyl group present in ethanol may lead to form hydrogen bond with solvent to increase the solubility of oils (Asep et al., 2013). Fig.s 6.14 (e) and (g) present the interaction of solvent rate and co-solvent with temperature where OY increases with temperature, solvent rate and co-solvent. An increase in solvent flow rate reduces thickness of the film layer around solid particles and consequently, mass transfer resistance decreases, which enhances OY. Interaction of particle size with temperature, flow rate and addition of co-solvent are presented in Fig.s 6.14 (f), (h) and (j), respectively. Extraction of oil from solid matrix is affected by two types of mass transfer resistances: internal as well as external. Particle size strongly affects OY if internal mass transfer mechanism is a controlling factor during extraction process. Moreover, extraction from solid matrix largely depends on length of diffusion path. On the other hand, if external mass transfer is the controlling factor in process, particle size does not affect OY considerably (Reverchon, 1997). Larger particle size leads to larger diffusion path, which decreases OY and this may be a reason behind negative effect of larger size particle on OY. Further, particle of very small size offers low diffusion path; however, turmeric root of smaller particle size contains husk material with oil. Therefore, at 0.2 mm, availability of oil is very less than that of larger particle size.

146
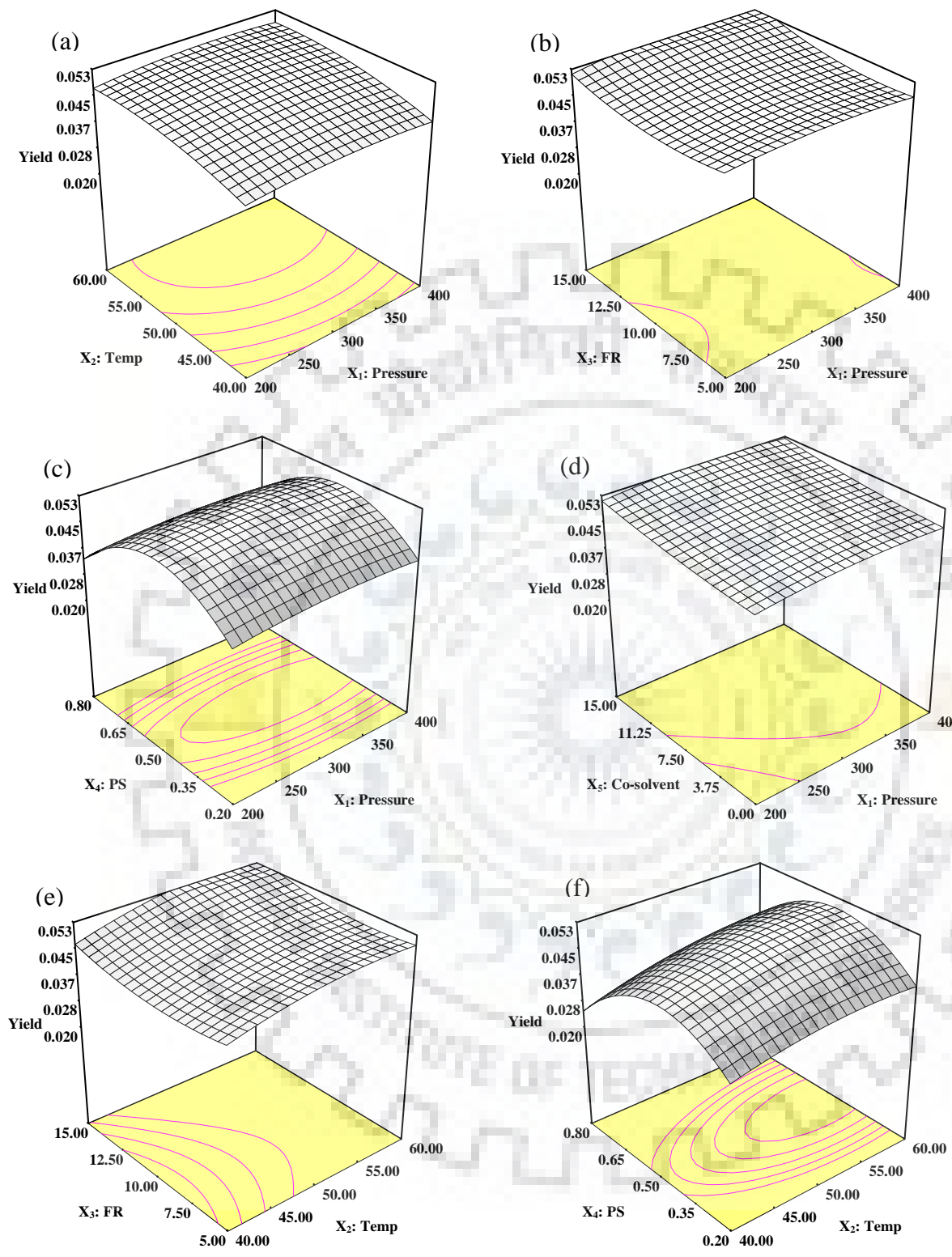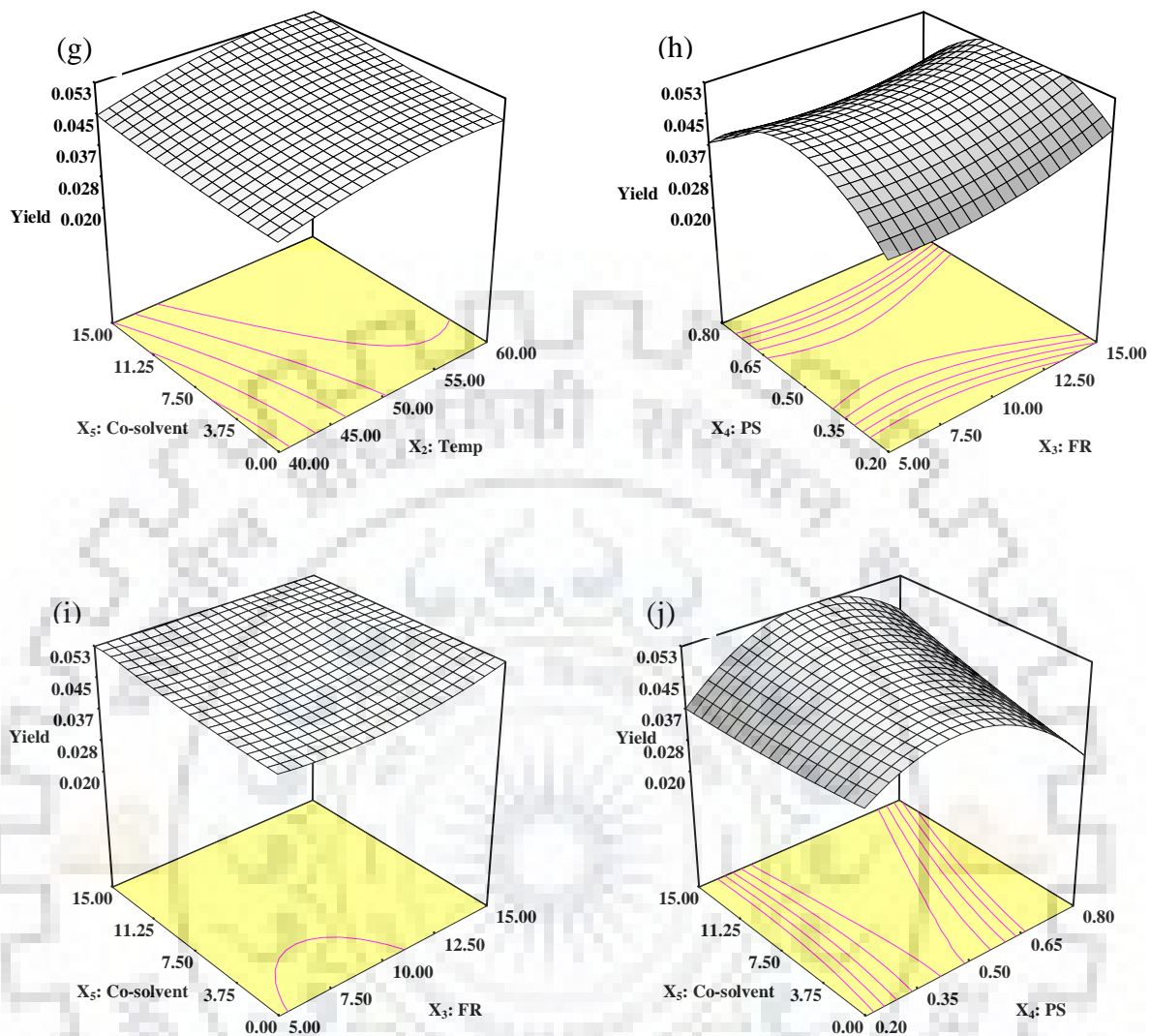
Fig. 6.14 Effect of two parameter interaction on the Oil yield of turmeric.

6.5.1.5 Effect of individual parameters on TC

A perturbation plot showing effect of operating parameters on extraction of TC is drawn in Fig. 6.15 (a). It indicates that no operating parameter other than addition of co-solvent is significantly affecting extraction of TC where it is increasing with addition of co-solvent. Curcumin is found to be a liposoluble compound having less polar properties and thus, it is easily dissolved into organic solvent such as methanol, ethanol and acetone (D. Liu et al., 2008). Ethanol is used as co-solvent in this study due to its higher solubility of curcumin, which results increase in extraction of TC with addition of ethanol from 0 to 15% (Nabati et al., 2014; Popuri and Pagala, 2013). Based on the above study, optimum values of parameters are 360 bar pressure, 54.63 °C temperature, 10.65

g/min solvent flow rate, 0.60 mm particle size and 8.89 % co-solvent, which provide TC content of 2.26 mg/g oil as shown in Table 6.10.

6.5.1.6 Effect of individual parameters on TT

Effects of various operating parameters on extraction of TT content are explained through perturbation curve as shown in Fig. 6.15 (b). It indicates that pressure is not affecting the extraction of TT significantly. In case of temperature, TT content decreases with increase in temperature from 40 to 50 °C and further, increases up to 60 °C. Increase in temperature decreases density of solvent and increases vapor pressure as well as volatility of solute (Rai et al., 2015). Therefore, it can be noticed from Fig. 6.15 (b) that density effect is dominant from 40-50 °C, which decreases the TT content; whereas, from 50-60 °C, vapor pressure dominates that shows higher TT content. On the other hand, TT content is increasing when solvent rate varies from 5 to 10 g/min due to the reason explained in section 6.5.1.3. Further, it decreases at 15 g/min due to lesser contact time of CO_2 and turmerone. However, an increase in particle size results a slight decrease in TT content as evident from Fig. 6.15(b). This may be due to increase in the intra-particle mass transfer resistance with increasing size of particle (Masek et al., 2013; Pourmortazavi and Hajimirsadeghi, 2007). Similarly, addition of co-solvent is also showing a negative effect on the TT content as slight decrease in TT content is visible with increasing co-solvent addition. As discussed in section 6.3.1.1, Turmerone's are basically sesquiterpenes, which are moderately soluble in alcohol, ethanol in the present work (Guenther, 2008) and thus, hinders the extraction of turmerone from solid sample. This may be the reason behind the low TT content with increasing addition of ethanol as co-solvent. As shown in Table 6.10, optimized values of operating parameters i.e. pressures, temperature. solvent flow rate, particle size and co-solvent to find maximize the TT content of 214.32 mg/g oil are 240 bar, 40 °C, 13.6 g/min, 0.20 mm and 0 % of solvent flow rate, respectively.
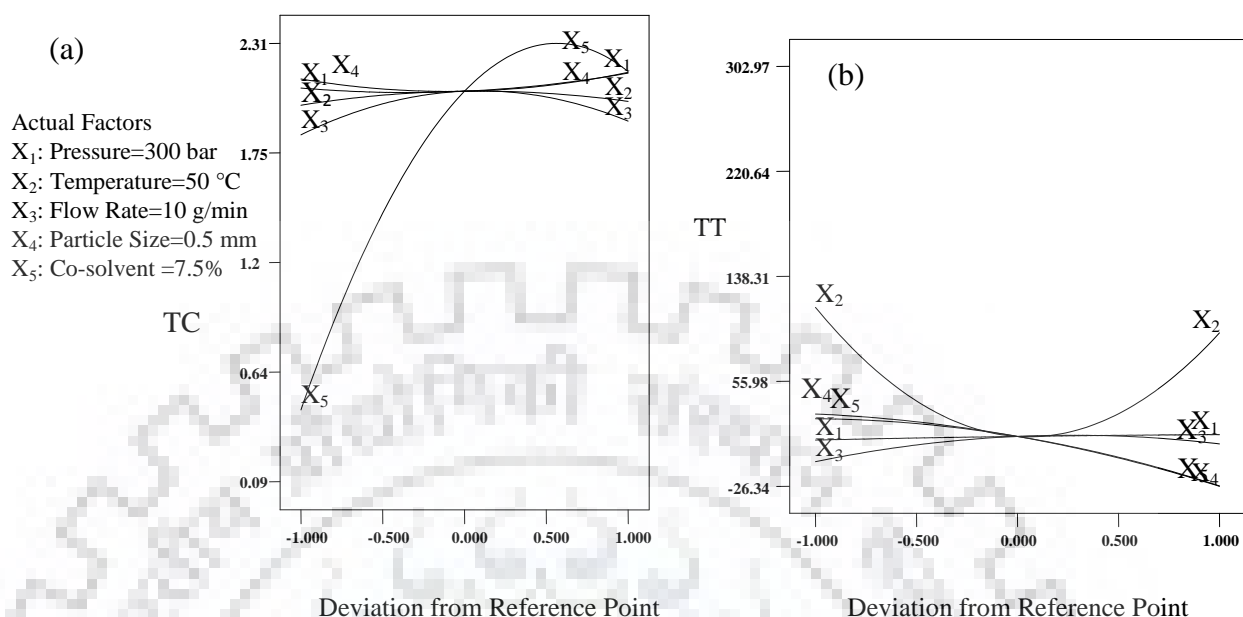
Fig. 6.15 Effect of individual parameters on the TC and TT content.

Table 6.10 Optimum points of operating parameters to maximize the responses.

Responses		P (bar)	T (°C)	FR (g/min)	PS (mm)	CS (%)
Name	Maximum value					
OY	0.055	255	53.72	13.60	0.54	14.67
TC	2.26	360	54.63	10.65	0.60	8.89
TT	214.32	240	40.00	13.6	0.20	0.00

6.5.2 Raw material –II

6.5.2.1 Screening design of operating parameters

Screening design was performed while selecting five operating parameters to estimate the effect of each on the extraction oil yield (EOY). Design Expert 10 suggested 10 numbers of experimental runs using minimum run resolution (iv), as discussed in Section 3.8.2, and values with levels of 10 runs for SFE of carrot seed oil are reported in Table 6.11. Experimental runs, provided in Table 6.11, were performed and the response was used to evaluate the effect of different terms (individual and interaction parameters) available in Main effect model as represented in equation (6.6). R-squared and p-values are found as 0.91 and 0.041, respectively, which proves the efficacy of the model. %contribution of each term to maximize EOY is tabulated in Table 6.12 with the

149

sum of squares values and standardized effect. Main effect model (equation 6.6) does not contain aliased terms as shown in Table 6.12.

Table 6.11 Screening design for the SFE of carrot seed oil.

Run	X_1:Press bar	X_2:Temp °C	X_3:Particle Size, mm	X_4:Flow rate, g/min	X_5:Co-sol, %	EOY (g/100g solid)
1	300(1)	40(-1)	0.3(-1)	10(-1)	10(1)	13.3465
2	300(1)	60(1)	0.9(1)	10(-1)	0(-1)	7.9397
3	100(-1)	40(-1)	0.3(-1)	20(1)	10(1)	7.789
4	100(-1)	60(1)	0.9(1)	20(1)	0(-1)	2.898
5	100(-1)	60(1)	0.9(1)	10(-1)	10(1)	10.2748
6	300(1)	40(-1)	0.9(1)	20(1)	10(1)	8.0938
7	100(-1)	60(1)	0.3(-1)	10(-1)	0(-1)	2.1419
8	300(1)	40(-1)	0.3(-1)	20(1)	0(-1)	3.4826
9	100(-1)	40(-1)	0.9(1)	10(-1)	0(-1)	4.7499
10	300(1)	60(1)	0.3(-1)	20(1)	10(1)	12.7232

Sum of squares of a term is considered as amount of variation caused by deviation in any term whereas, the standardized effect is the change in response related to the change in term's factors. In Table 6.12, sum of squares and standardized effect values for term X_5 are much higher than that of term X_3. This fact can be explained as variation in term X_3 does not lead to significant deviation in response whereas, that in term X_5 results a drastic deviation in response. As can be noticed from Table 6.12, term X_5 i.e. addition of co-solvent shows highest contribution (69.4%) followed by X_1, X_4, X_1X_3, X_2, X_1X_2, X_1X_4, X_3X_5, X_3. %contribution of particle size is almost negligible i.e. 8.77×10^{-3} and shows that this term does not affect EOY significantly. Thus, particle size can be fixed at a constant value i.e. 0.3 mm.

$$EOY = 7.34 + 1.49 \times X_1 + 0.54 \times X_2 + 0.035 \times X_3 - 1.16 \times X_4 + 3.15 \times X_5$$

(6.6)

To evaluate the significance of each term on EOY, a student's t-test was performed and plotted as a Pareto chart shown in Fig. 6.16. It indicates t-value of effect and rank of each term. A large t-value of a term indicates its higher significance to EOY (Haider and Pakshirajan, 2007). This can be concluded from Table 6.12 and Fig. 6.16 that value for particle size of carrot seed can be considered as fixed and same will be used for optimization study for SFE of carrot seed oil.
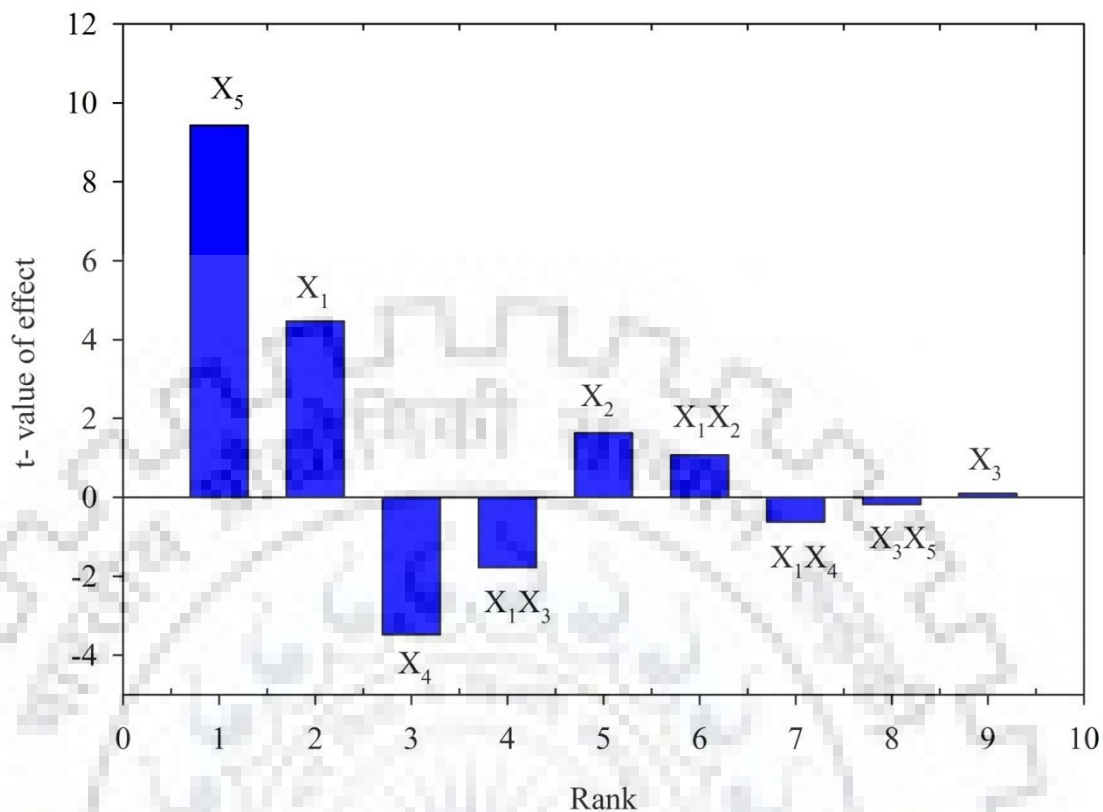
Fig. 6.16 Pareto chart of screening design of carrot seed oil.

Table 6.12 %contribution of the terms to maximize the EOY of carrot seed oil.

Term	Sum of squares	Standardized effect	%contribution
X_1-pressure	19.99	2.98	15.5271
X_2-Temperature	2.63	1.08	2.04
X_3-Particle size	0.011	0.071	8.77×10^{-3}
X_4- Flow rate	12.10	-2.32	9.4
X_5-Co-solvent	89.34	6.3	69.40
$X_1 X_2$	1.13	0.708	0.877
$X_1 X_3$	3.1	-1.174	2.409
$X_1 X_4$	0.3949	-0.42	0.3067
$X_1 X_5$	-	-	Aliased
$X_2 X_3$	-	-	Aliased
$X_2 X_4$	-	-	Aliased
$X_2 X_5$	-	-	Aliased
$X_3 X_4$	-	-	Aliased
$X_3 X_5$	0.03148	-0.118	0.0245
$X_4 X_5$	-	-	Aliased

151

6.5.2.2 Response surface analysis of reduced operating parameters

Full face CCD was used for the optimization of four operating parameters after applying screening design. Effects of four parameters such as pressure (A), temperature (B), solvent flow rate (C) and amount of co-solvent (D) on EOY (response) were studied. Optimization study of SFE of carrot seed was carried out using Quantum XL 2016 (Sigma Zone), which suggested total 30 experimental runs as tabulated in Table 6.13.

Table 6.13 CCD design for the SFE of carrot seed oil (Particle size: 0.3 mm).

Run	Space type	Input parameters				Responses	
		A:Pressure (bar)	B:Temperature (°C)	C:Flow rate (g/min)	D: Co-solvent (%)	EOY(g/100g solid)	CC (%)
1	Factorial	200	70	15	0	2.813	84.6
2	Factorial	400	70	5	10	11.73	86.8
3	Factorial	200	70	15	10	9.8994	92.05
4	Factorial	400	50	15	0	6.2538	89.25
5	Center	300	60	10	5	9.0205	91.23
6	Axial	300	70	10	5	12.1434	89.93
7	Center	300	60	10	5	8.9802	91.23
8	Center	300	60	10	5	9.00	91.23
9	Factorial	400	50	5	0	6.7965	94.50
10	Axial	200	60	10	5	6.9505	82.19
11	Factorial	200	50	5	0	4.4001	83.50
12	Factorial	400	70	15	10	9.515	90.99
13	Factorial	200	50	15	0	1.977	93.82
14	Axial	300	60	15	5	7.5457	88.37
15	Axial	300	60	5	5	7.9966	92.31
16	Factorial	400	50	15	10	7.825	91.29
17	Factorial	400	50	5	10	7.7521	90.98
18	Center	300	60	10	5	8.9905	91.23
19	Factorial	200	50	15	10	7.7221	96.03
20	Factorial	200	50	5	10	7.3667	86.37
21	Factorial	400	70	5	0	11.03	87.05
22	Axial	300	60	10	0	7.0252	82.61
23	Factorial	200	70	5	10	6.9831	93.56
24	Axial	300	50	10	5	8.89	94.09
25	Factorial	400	70	15	0	8.5793	80.20
26	Axial	300	60	10	10	10.0958	83.56
27	Center	300	60	10	5	9.0205	91.23
28	Axial	400	60	10	5	12.919	93.95
29	Factorial	200	70	5	0	4.8884	91.09
30	Center	300	60	10	5	8.9985	91.23

CCD consists of 16 factorial, 8 axial and 6 centre points and all the set of experimental runs were performed using SFE setup as explained in section 3.3. Quantum XL uses Ordinary Least Squares Regression as a primary method of analysis for quantitative outputs. It also supports Binary Logistic Regression for Binary output and Nominal Logistic Regression for Nominal Outputs. Quantum XL automatically selects correct type of regression for any type of model. In this paper, response/output is quantitative so Least Squares Regression method is used for regression.

6.5.2.3 Development of correlation between operating parameters and responses

Response-1: Extraction oil yield (EOY) from SFE of carrot seed oil

Regression results for experimental runs of SFE of carrot seed oil are reported in Table 6.14. It shows that model includes individual parameters, 2-way interaction, 3-way interaction, 4-way interaction and quadratic terms as represented through equation (6.7). Coefficients of all parameters are shown in Table 6.14 that results into a correlation between response and these parameters. SE, T, P, VIF, Seq SS, Adj SS, df, Adj MS and F stand for standard error, T statistic (Coeff/SE or signal to noise ratio), p-value, variance inflammation factor, sequential sum of squares, adjusted sum of squares, degree of freedom, adjusted mean square and F-statistic for the terms, respectively. For significant model terms, T statistic should be higher and p-value should be less than 0.5. VIF is a measure of multicolinearity and its value equal to 1 indicates an orthogonal term. VIF values greater than 1 show that term is correlated with other input parameters and tolerance is considered as a reverse of VIF i.e. Tol=1/VIF. Seq SS is a type I error and is a measure of reduction in sum of squares of the model if the term is sequentially removed from the model. Adj SS is a type III error, which indicates the reduction in the sum of squares of the model. It happens when a term is sequentially removed from the model while considering all other terms in the model. For orthogonal model, VIF is 1, where Seq SS=Adj SS. However, Adj SS is preferred over Seq SS as Seq SS is order dependent. Regression coefficients as shown in Table 6.14 are found as R^2=0.9601, Adj R^2=0.8913, which indicate appreciable fitting of the model. Std error of model indicates variation in data of the model. F, Sig F, F_{LOF} and Sig F_{LOF} refer to F statistic for the model, the significance for F statistic, F statistic of lack of fit and significance of F_{LOF} statistic, respectively. For the prediction of significant model, F value should be higher and Sig F value should be less than 0.5. As F_{LOF} increases, the model has more lack of fit and Sig F_{LOF} <0.5 indicates that model has lack of fit, which can be reduced while removing insignificant terms of the model shown in Table 6.14. As far as R^2 value is near to unity, no need to reduce the model and that can be further used to predict other results explained in subsequent section.

Optimal operating conditions for SFE of carrot seed oil were investigated through model reported in equation (6.7) and experimental run was performed at these values.

$$EOY = 9.3422 + 1.6333 \times A + 1.0332 \times B + -0.3888 \times C + 1.3958 \times D + 0.5694 \times AB - 0.2443 \times AC$$
$$- 0.8581 \times AD - 0.0804 \times BC - 0.0263 \times BD + 0.5389 \times CD - 0.4441 \times ABC - 0.0851 \times ABD$$
$$- 0.4325 \times ACD + 0.1146 \times BCD - 0.162 \times ABCD + 0.198 \times A^2 + 0.78 \times B^2 - 1.8739 \times C^2$$
$$- 1.1762 \times D^2$$

$$(6.7)$$

Table 6.14 Regression results of SFE of carrot seed oil.

Factor	Coeff	SE	T	P	VIF	Seq SS	Adj SS	DF	Adj MS	F
Main						105		4		
Const	9.3422	0.2373	39.367	**0.000**						
P (A)	1.6333	0.1886	8.6622	**0.000**	1.0	48.02	48.02	1	48.02	75.034
T (B)	1.0332	0.1886	5.4795	**0.000**	1.0	19.215	19.215	1	19.215	30.025
FR (C)	-0.3888	0.1886	-2.062	**0.064**	1.0	2.7206	2.7206	1	2.7206	4.2511
CS (D)	1.3958	0.1886	7.4026	**0.000**	1.0	35.069	35.069	1	35.069	54.798
2 - way						22.685		6		
AB	0.5694	0.2	2.847	**0.016**	1.0	5.1872	5.1872	1	5.1872	8.1054
AC	-0.2443	0.2	-1.221	0.247	1.0	0.9546	0.9546	1	0.9546	1.4917
AD	-0.8581	0.2	-4.291	**0.001**	1.0	11.782	11.782	1	11.782	18.41
BC	-0.0804	0.2	-0.402	0.695	1.0	0.1035	0.1035	1	0.1035	0.1617
BD	-0.0263	0.2	-0.132	0.898	1.0	0.0111	0.0111	1	0.0111	0.0173
CD	0.5389	0.2	2.6947	**0.021**	1.0	4.647	4.647	1	4.647	7.2613
3 - way						6.474		4		
ABC	-0.4441	0.2	-2.2206	**0.048**	1.0	3.1558	3.1558	1	3.1558	4.9311
ABD	-0.0851	0.2	-0.4256	0.679	1.0	0.1159	0.1159	1	0.1159	0.1811
ACD	-0.4325	0.2	-2.1624	**0.053**	1.0	2.9924	2.9924	1	2.9924	4.6758
BCD	0.1146	0.2	0.5728	0.578	1.0	0.2099	0.2099	1	0.2099	0.3281
4 - way						0.4198		1		
ABCD	-0.162	0.2	-0.81	0.435	1.0	0.4198	0.4198	1	0.4198	0.656
Quadratic						34.908		4		
AA	0.198	0.4966	0.3988	0.698	2.9086	16.325	0.1018	1	0.1018	0.159
BB	0.78	0.4966	1.5706	0.145	2.9086	0.9104	1.5788	1	1.5788	2.4669
CC	-1.8739	0.4966	-3.773	**0.003**	2.9086	14.082	9.1127	1	9.1127	14.239
DD	-1.1762	0.4966	-2.369	**0.037**	2.9086	3.5905	3.5905	1	3.5905	5.6103
Regression coefficients										
R^2	Adj R^2	Std Error	F	Sig F	F_{LOF}	Sig F_{LOF}				
0.9601	0.8913	0.8	13.941	0.0	6121.98	0.0				

Response-2: Carotol content (CC) from SFE of carrot seed oil

Carotol is found as a principal bioactive compound in the carrot seed oil, which comprises of 82.19 to 94.09% of carrot seed oil as shown in Table 6.13. A regression analysis is carried out considering the CC of carrot seed oil as second responses. Regression results are reported in Table 6.15 where correlation between operating parameters and CC is shown through equation 6.8. Coefficients of all model terms are provided in Table 6.15.

Table 6.15 Regression results for CC of carrot seed oil.

Factor	Coeff	SE	T	P	VIF	Seq SS	Adj SS	DF	Adj MS	F
Main						1,703.9		4		
Const	90.588	1.0204	88.78	**0.000**						
P (A)	3.4495	0.8107	4.2548	**0.001**	214.18	214.18	1	214.18	18.103	75.034
T (B)	-5.6395	0.8107	-6.956	**0.000**	572.467	572.467	1	572.467	48.386	30.025
FR (C)	-4.2267	0.8107	-5.2134	**0.000**	321.57	321.57	1	321.57	27.18	4.2511
CS (D)	5.7528	0.8107	7.0958	**0.000**	595.707	595.707	1	595.707	50.35	54.798
2 - way						2,471.0		6		
AB	3.7257	0.8599	4.3326	**0.001**	222.089	222.089	1	222.089	18.771	8.1054
AC	3.1594	0.8599	3.6741	**0.004**	159.71	159.71	1	159.71	13.499	1.4917
AD	-4.8894	0.8599	-5.6859	**0.000**	382.502	382.502	1	382.502	32.33	18.41
BC	-6.5344	0.8599	-7.5989	**0.000**	683.177	683.177	1	683.177	57.743	0.1617
BD	5.8994	0.8599	6.8605	**0.000**	556.849	556.849	1	556.849	47.066	0.0173
CD	5.4007	0.8599	6.2805	**0.000**	466.674	466.674	1	466.674	39.444	7.2613
3 - way						1,545.89		4		
ABC	5.6307	0.8599	6.5479	**0.000**	507.27	507.27	1	507.27	42.875	4.9311
ABD	-4.7132	0.8599	-5.481	**0.000**	355.422	355.422	1	355.422	30.041	0.1811
ACD	-4.5144	0.8599	-5.2498	**0.000**	326.079	326.079	1	326.079	27.561	4.6758
BCD	4.7244	0.8599	5.4941	**0.000**	357.121	357.121	1	357.121	30.185	0.3281
4 - way						345.687		1		
ABCD	-4.6482	0.8599	-5.4054	**0.000**	345.687	345.687	1	345.687	29.218	0.656
Quadratic						291.577		4		
AA	-1.605	2.1352	-0.7517	0.468	169.324	6.6851	1	6.6851	0.565	0.159
BB	1.215	2.1352	0.569	0.581	4.2327	3.8311	1	3.8311	0.3238	2.4669
CC	1.22	2.1352	0.5714	0.579	1.6981	3.8627	1	3.8627	0.3265	14.239
DD	-6.695	2.1352	-3.1356	**0.009**	116.322	116.322	1	116.322	9.8318	5.6103
Regression coefficients										
R^2	Adj R^2	Std Error	F	Sig F	F_{LOF}	Sig F_{LOF}				
0.9799	0.9453	3.4397	28.284	0.0	NA	NA				

As discussed in section 6.5.2.3, T statistic should be higher and p-value should be less than 0.05 for significant model terms.

(6.8)

Therefore, it can be noticed from Table 6.15 that all the model terms are significant except A^2, B^2 and C^2 because p-values are considerably higher. Regression coefficients are found as $R^2=0.9799$ and Adj $R^2=0.9453$ as shown in Table 6.15, which indicate the model fits with experimental data very well.

$$CC = 90.588 + 13.4495 \times A + -5.6395 \times B - 4.2267 \times C + 5.7528 \times D + 3.7257 \times AB + 3.1594 \times AC$$
$$- 4.8894 \times AD - 6.5344 \times BC + 5.8994 \times BD + 5.4007 \times CD + 5.6307 \times ABC - 4.7132 \times ABD$$
$$- 4.5144 \times ACD + 4.7244 \times BCD - 4.6482 \times ABCD - 1.605 \times A^2 + 1.215 \times B^2 + 1.22 \times C^2$$
$$- 6.695 \times D^2$$

6.5.2.4 Effect of individual parameter on EOY

Effect of the individual operating parameter on EOY can be explained by Main effects plot shown in Fig. 6.17. Fig. 6.17(a) depicts the effect of change in pressure on EOY and can be noticed that EOY is increasing rapidly with increasing pressure from 200 to 400 bar. It is due to the fact that increase in pressure leads to increase in solvent density and causes high EOY due to enhancement in solubility of supercritical fluid (Masek et al., 2013; Pourmortazavi and Hajimirsadeghi, 2007). Effect of temperature on EOY is shown in Fig. 6.17 (b) where it increases while varying temperature from 50 to 70 °C. Effect of temperature on EOY is very complex due to its opposite effects: (i) increase in temperature results decrease in density and consequentially EOY decreases, (ii) rise in temperature leads to increase in vapor pressure, which increases solubility of oil in supercritical fluid and thus, EOY enhances (Ruan et al., 2017; Wang et al., 2016). Therefore, effect of temperature on EOY can be explained through dominancy of both effects (density or vapor pressure effects). In the present work, only vapor pressure effect is dominating as EOY is increasing continuously with temperature. On the other hand, rise in temperature increases mass transfer rate along with mass transfer coefficients due to high diffusivity of solute in the solvent (Asep et al., 2013; Mukhopadhyay, 2009).

Effect of solvent flow rate on the EOY is shown in Fig. 6.17 (c), which represents that EOY is increasing with solvent flow rate from 5 to 10 g/min and then decreasing with further increase in solvent flow rate up to 15 g/min. Increase in solvent flow rate reduces film thickness around the particle due to which mass transfer resistance surrounding the particle decreases and consequently, EOY is enhanced (Sodeifian et al., 2016a). High solvent flow rate decreases EOY due to low

residence time of solvent in the extractor, which limits the available time for solutes to get soluble into the solvent (Haider and Pakshirajan, 2007; Zaghdoudi et al., 2016).

In this work, ethanol is used as a co-solvent and its concentration varies from 0 to 10% of solvent flow rate. Effect of addition of co-solvent is shown in Fig. 6.17 (d). It indicates that EOY is continuously increasing when co-solvent is added from 0 to 10% of solvent flow rate due to solubility enhancement (Sharif et al., 2015; Zaghdoudi et al., 2016). In the present study, optimum values provided through Quantum XL for pressure, temperature, flow rate and addition of co-solvent are 400 bar, 70 °C, 8.53 g/min and 5.87% of solvent flow rate, respectively, to find maximum EOY as 14.23% as shown in Table 6.16.
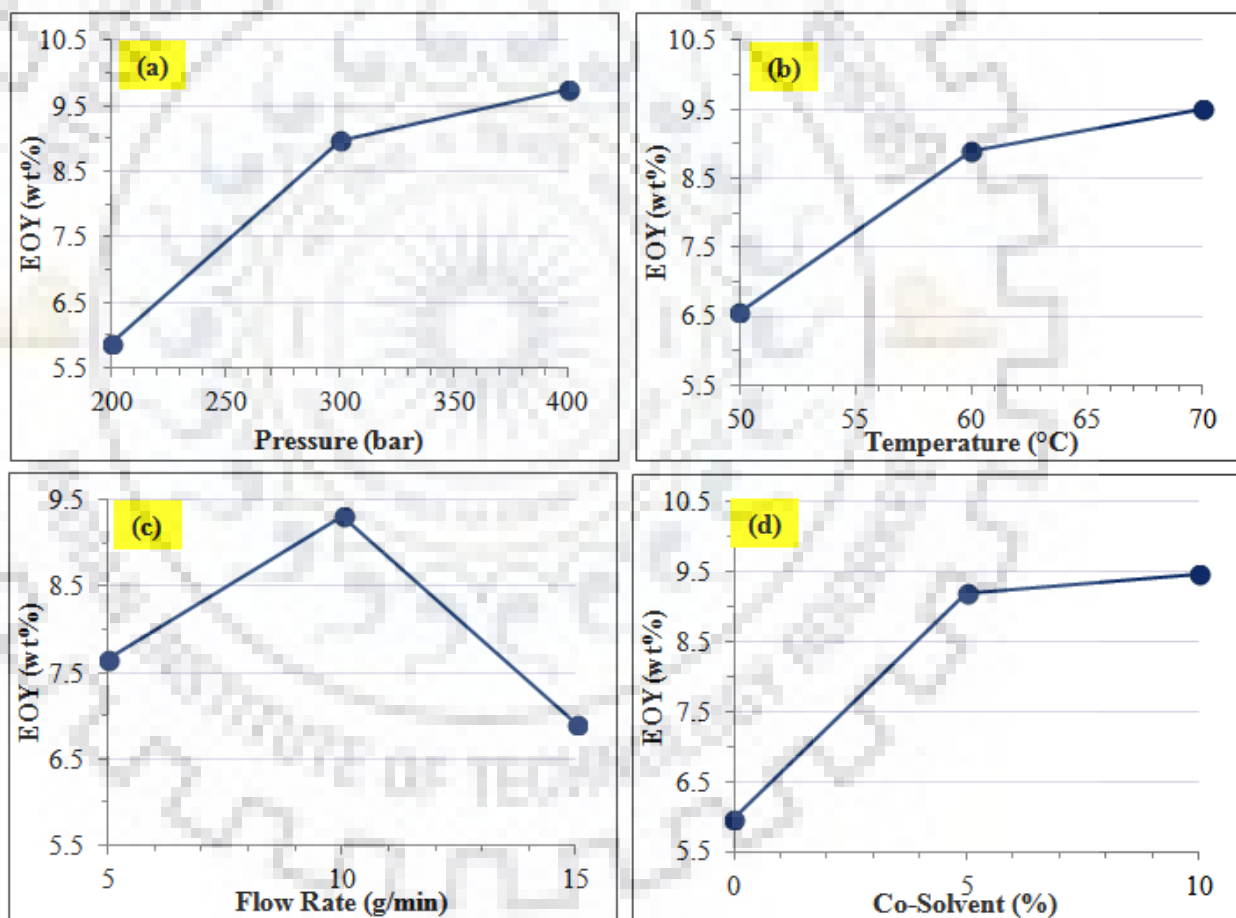
Fig. 6.17 Main effects plot of CCD of carrot seed oil.

6.5.2.5 Effect of two-parameter interactions on EOY

In this section, the effect of interaction of two independent parameters is studied on EOY while keeping other two parameters at the fixed values. Interaction plots and corresponding response

surface plots of operating parameters are shown in Fig. 6.18 and 6.19. Fig.s 6.18(a) and 6.19(a) show the effect of interaction of pressure and temperature on EOY and can be noticed that at lower pressure level (200 bar), increase in temperature does not affect EOY significantly due to low solubility at low pressure. At intermediate pressure level (300 bar), EOY first decreases and then increases while increasing temperature. Solubility at 300 bar is higher than 200 bar, which results in higher EOY than that found at 200 bar. However, due to opposite effect of temperature, the trend of EOY is very complex to explain. At 300 bar, increase in temperature from 50 to 60 °C decreases density of solvent and thus, density effect is prevailing till 60 °C, which results in lower EOY. However, high temperature increases mass transfer rate of solute to bulk liquid phase and thus, EOY is increasing at 70 °C. At pressure 400 bar, enhanced mass transfer rate is achieved due to increase in temperature from 50 to 60 °C, which increases EOY. However, at elevated pressure, a repulsion force acts between solute–solvent due to highly compressed CO_2 with a further increase in temperature from 60 to 70 °C, which consequently decreases EOY. It can be concluded that best combination of pressure and temperature is high pressure i.e. 400 bar and intermediate temperature 60 °C to maximize EOY as can be seen in Fig. 6.19 (a).

Interaction effect of pressure and flow rate is shown in Fig.s 6.18 (b) and 6.19(b), which depict an increase in EOY with pressure and flow rate. However, further increase in both independent parameters decreases in EOY. Individually, EOY is continuously increasing with pressure whereas, EOY first increases and then decreases while increasing flow rate as discussed in Section 6.5.2.4. Interaction of pressure and flow rate does not alter individual effects of these on EOY, which are explained in Section 6.5.2.4. Similar trend can be observed in the response surface plot shown in Fig. 6.19 (b). Hence, high pressure i.e. 400 bar with moderate flow rate i.e. 10 g/min can be a good combination to maximize EOY.

In case of SFE of carrot seed oil, EOY is highly sensitive toward the addition of co-solvent and its interaction effect with pressure is shown in Fig.s 6.18(c) and 6.19(c). Co-solvent and pressure show a positive effect on EOY because both are responsible for the enhancement of solubility of solute in the solvent and same can be noticed from Figs. 6.18 (c) and 6.19(c). EOY is increasing with co-solvent for 200 and 300 bar as both curves are like parallel lines. However, at elevated pressure, EOY is first increasing from 0 to 5% co-solvent then decreasing till 10% due to reduction in interactions between solute and solvent. Thus, it can be concluded that high pressure i.e. 400 bar and intermediate co-solvent concentration i.e. 5% will give maximum EOY as supported by response surface plot in Fig. 6.19(c).

Interaction effect of temperature with solvent flow rate and co-solvent on EOY is shown in Figs. 6.18(d) and (e). Corresponding response surface plots are shown in Fig. 6.19 (d) and (e). These figures represent that for temperature 50 and 70 °C, extraction curves are similar with increasing flow rate and co-solvent. EOY is increasing up to 10 g/min and 5%. Further, it decreases until 15 g/min and 10%. It is because the resistance surrounding the solute particle decreases first; however, a further increase in flow rate decreases the residence time of solvent with solute in the extractor. Addition of co-solvent increases the polarity of solvent and hence, EOY is increased. Further, the addition of co-solvent results a slight decrease in EOY and this may be due to excess amount of ethanol added to the solvent. It may lead to an excessive polarity of the solvent, which is not suitable for extraction and interactions between solvent and matrix can also be reduced (Liu et al., 2011). For 5% co-solvent, EOY is continuously increasing, which shows an appropriate amount of co-solvent to increase the polarity of the solvent. It can also be noticed that individual effect of temperature on EOY suggests high EOY at 70 °C and same behavior is shown in interaction plots of temperature with pressure, flow rate and co-solvent as given in Figs. 6.19 (a), (d) and (e). For temperature at 60 °C, EOY is between that found at 50 and 70 °C, which shows that vapor pressure effect of temperature is prevailing in this case. It can be concluded that high temperature i.e. 70 °C with intermediate co-solvent addition i.e. 5% is suitable to maximize EOY. Figs. 6.18(f) and 6.19(f) show the interaction effect of solvent flow rate and the addition of co-solvent on EOY and depict that rise in flow rate with co-solvent leads to an increase in EOY except for solvent flow rate of 5 g/min. Co-solvent is added to increase the extraction efficiency of solvent, which increases EOY and combined effect of both independent parameters shows positive effects of these on EOY. As can be seen from Fig. 6.18(f), extraction curve of 10 g/min is higher than that of 15 g/min due to less residence time between solute and solvent. However, increase in co-solvent enhances EOY continuously except for 5 g/min flow rate. In fact, at low flow rate and high co-solvent, amount of co-solvent is increased in the solvent-co-solvent mixture, which may hinder the interaction between solute and solvent. It can be concluded that an optimum values of solvent i.e.10 g/min and co-solvent i.e. 5% in the mixture is required to maximize EOY.
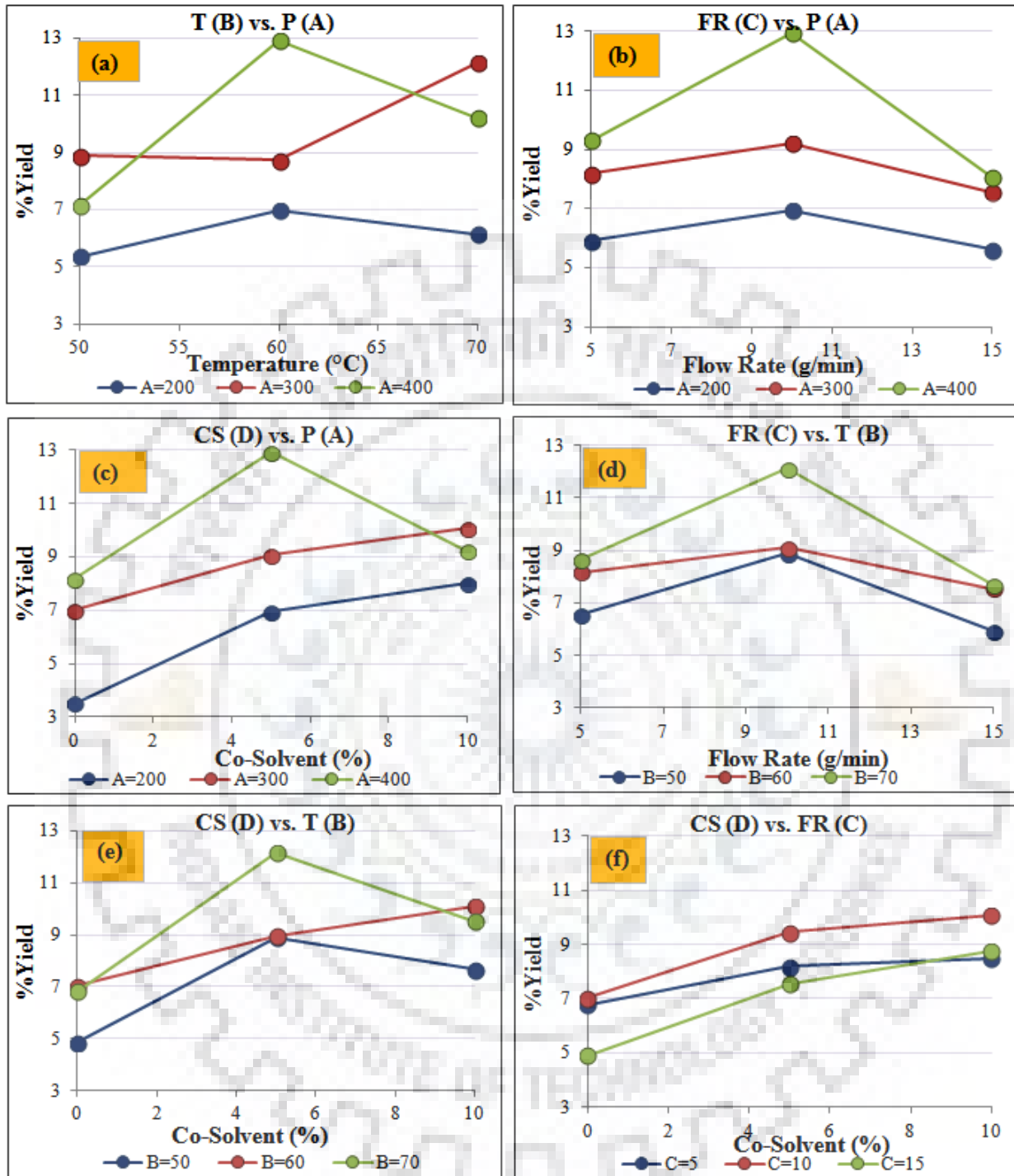
Fig. 6.18 Interaction plots of CCD of carrot seed oil.
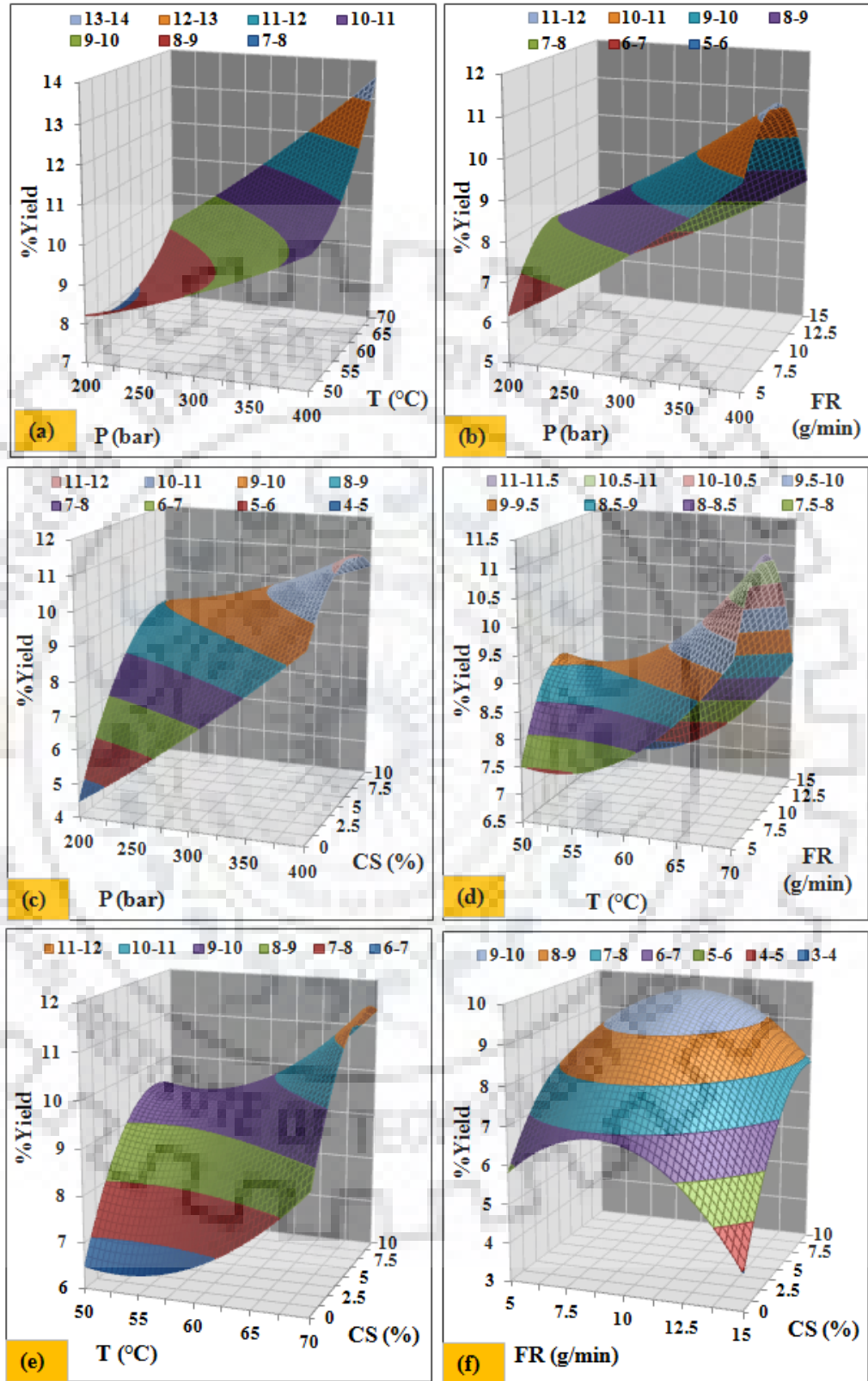
Fig. 6.19 Response surface plots of CCD of carrot seed oil.

161

6.5.2.6 Effect of individual parameters on CC

In this section, individual effects of operating parameters on CC content of carrot seed oil are studied as shown in Fig. 6.20 (a) to (d). Fig. 6.20 (a) depicts that CC is increasing with pressure from 200 to 400 bar due to enhancement in solvent density as well as solubility of supercritical fluid as discussed in section 6.5.2.4 (Masek et al., 2013; Pourmortazavi and Hajimirsadeghi, 2007). However, temperature, shown in Fig. 6.20 (b), follows negative trend on the extraction of CC as it is decreasing with increasing temperature from 50 to 70 °C. It is known fact that rise in temperature results a decrease in density as well as solubility which consequently decreases the extraction of CC from carrot seed (Rai et al., 2015). Similar to effect of temperature, increasing solvent flow rate also decreases CC content as shown in Fig. 6.20 (c). The reason for this trend is explained in section 6.5.2.4 (Haider and Pakshirajan, 2007; Zaghdoudi et al., 2016). Fig. 6.20 (d) represents the effect of co-solvent addition on the extraction of CC from carrot seed. It depicts that CC is increasing with co-solvent concentration from 0 to 5% of solvent flow rate due to enhancement of solubility as explained in section 6.5.2.4 (Sharif et al., 2015; Zaghdoudi et al., 2016). However, further increase in co-solvent concentration up to 10 % of solvent flow rate slightly decreases the extraction of CC from carrot seed. As discussed in section 6.3.2.1, Carotol is a sesquiterpene alcohol, which is moderately soluble in alcohol i.e. ethanol in present work (Guenther, 2008). This may be the reason behind the reduction in the extraction of CC from carrot seed with increasing co-solvent concentration as discussed in section 6.5.1.6. Based on optimization of operating parameters, Quantum XL predicts the optimum condition for the maximum extraction of CC as 376.68 bar pressure, 50 °C temperature, 5 g/min solvent flow rate and 4.82% co-solvent. Corresponding maximum CC content is 95.88% of extracted carrot seed oil as shown in Table 6.16.

Table 6.16 Optimum operating parameters to maximize EOY and CC of carrot seed oil.

Responses		P (bar)	T (°C)	FR (g/min)	CS (%)
Name	Maximum value				
EOY	14.23%	400	70	8.53	5.87
CC	95.88%	376.68	50	5	4.82
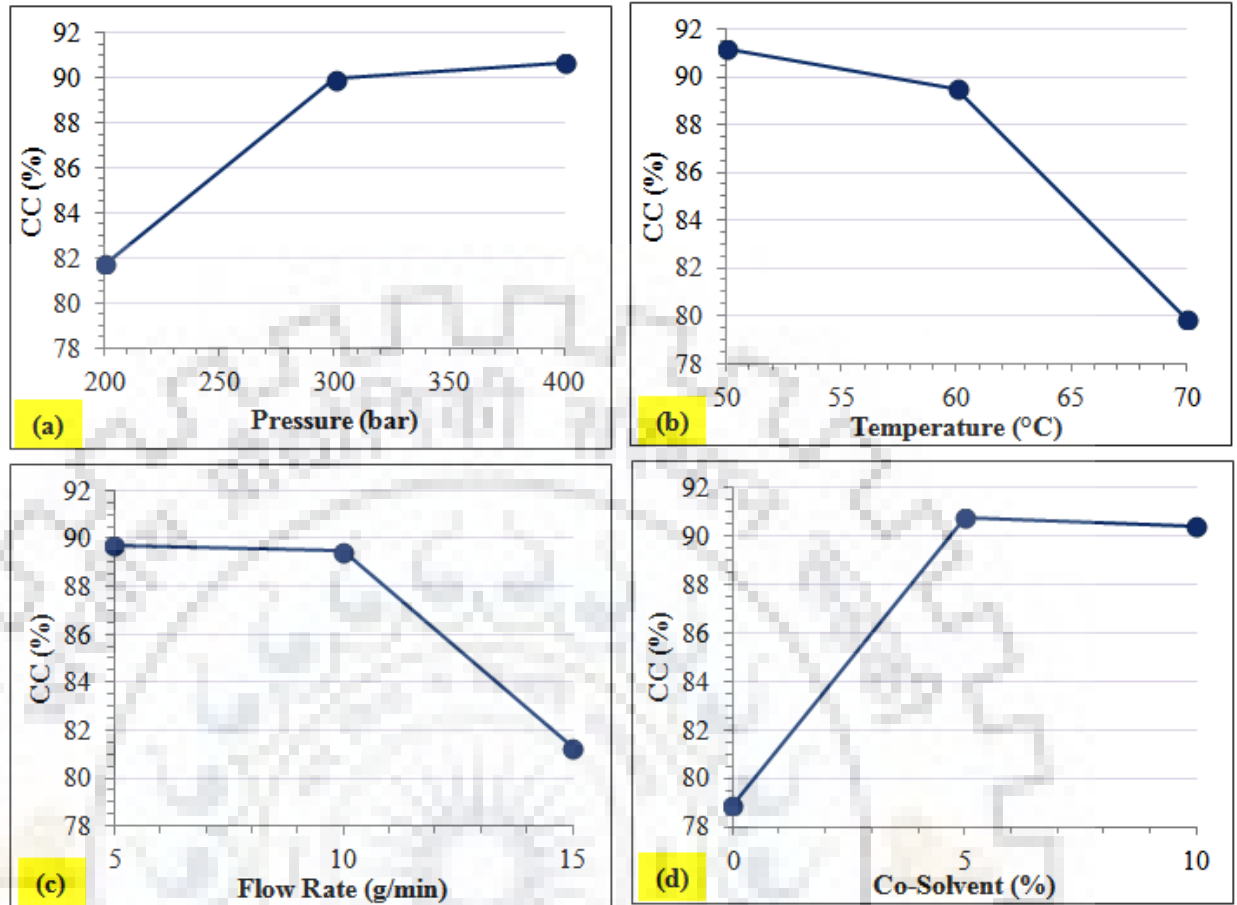
Fig. 6.20 Effect of individual parameters on the CC of carrot seed oil.

6.6 Application of COMSOL Multiphysics 5.3

6.6.1 Solution and validation of different models of SFE

Several mathematical models on SFE process are proposed by different authors as discussed in section 2.6.4. A few amongst these are solved using COMSOL multiphysics 5.3 software. The solution technique is provided in section 5.2.

6.6.1.1 Mathematical model-1

Reverchon (1996) developed a mathematical model for the extraction of essential oil from Sage leaves, which was discussed thoroughly in section 5.1.1. Proposed model was solved using COMSOL multiphysics 5.2 software. For the validation of results, extraction curves found through experiment and software were compared in Fig. 6.21 where average absolute relative deviation (AARD) is 1.64%. Thus, results found for model proposed by Reverchon (1996) while solving it through COMSOL multiphysics 5.3 software validate the experimental data very well.
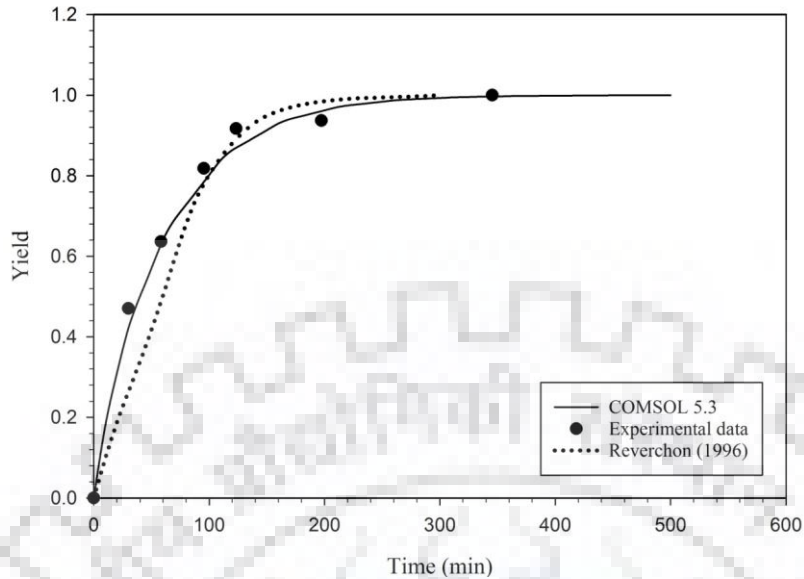
Fig. 6.21 Comparison of results for the SFE of Sage leaves using model proposed by Reverchon (1996).

6.6.1.2 Mathematical model-2

A mathematical model for the extraction of Rose flower concrete was developed by Reverchon and Poletto (1996) and explained in detail in section 5.1.2. Experimental extraction curve was compared with the extraction curve of model solved by COMSOL multyphysics 5.2 and shown in Fig. 6.22. The model proposed by Reverchon and Poletto (1996) showed a good agreement with the experimental data with AARD value of 2.21%.
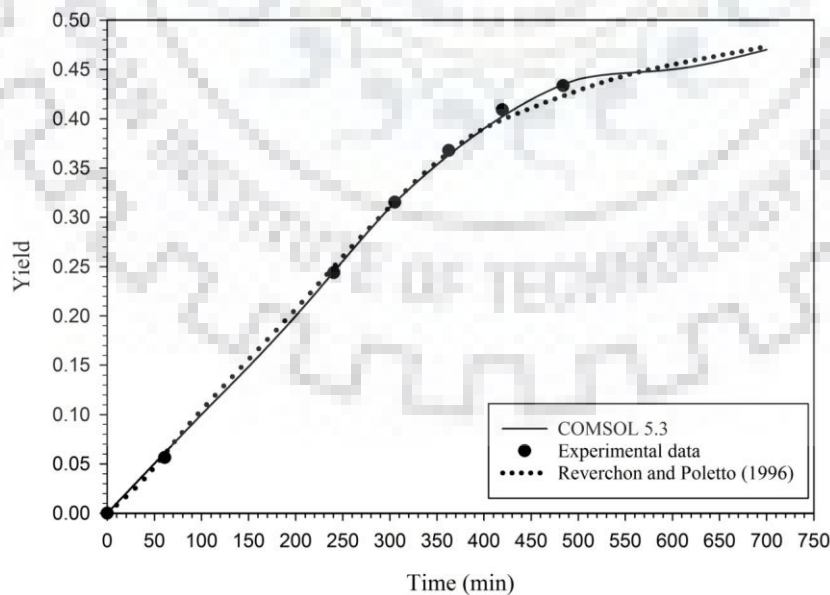
Fig. 6.22 Comparison of results for the SFE of Rose flower concrete using model proposed by Reverchon and Poletto (1996).

164

6.6.1.3 Mathematical model-3

Reverchon and Marrone (1997) developed a mathematical model for the SFE of clove essential oil from clove bud. In the present work, model was solved using COMSOL multyphysics 5.2 and extraction curves were compared with the experimental extraction curve in Fig. 6.23. It depicts that COMSOL solves the model faultlessly with AARD as 5.6%.
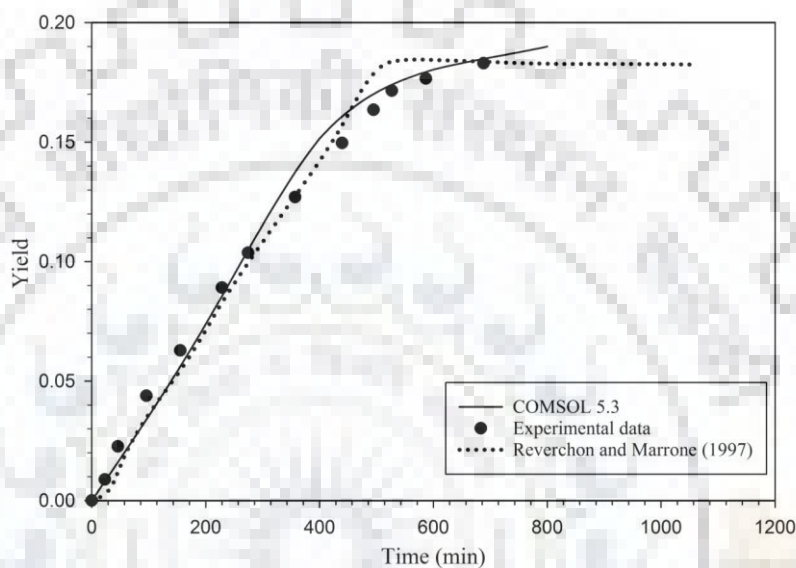
Fig. 6.23 Comparison of results for the extraction of Clove bud using model proposed by Reverchon and Marrone (1997).

6.6.1.4 Mathematical model-4

In sections 6.6.1.2 and 6.6.1.3, models for extraction of leaves and flower concrete were discussed. Reverchon et al. (2000) also proposed a mathematical model for the SFE of oil from flower seed i.e. Hiprose seed. COMSOL multyphysics 5.2 was used to solve the model proposed by Reverchon et al. (2000) and extraction curves were compared in Fig. 6.24. It is clear from Fig. 6.24 that COMSOL solves the model perfectly and shows an AARD of 0.41% from the experimental data.
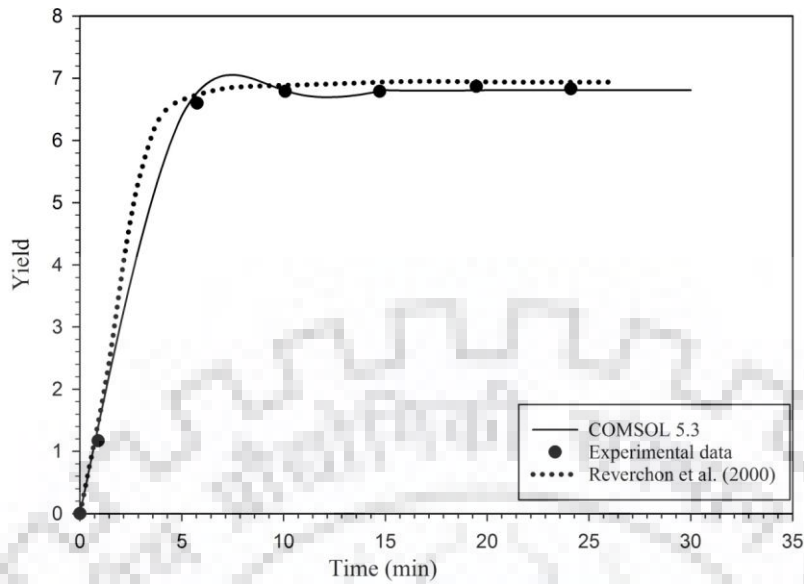
Fig. 6.24 Comparison of results for the extraction of Hiprose seed using model proposed by Reverchon et al. (2000).
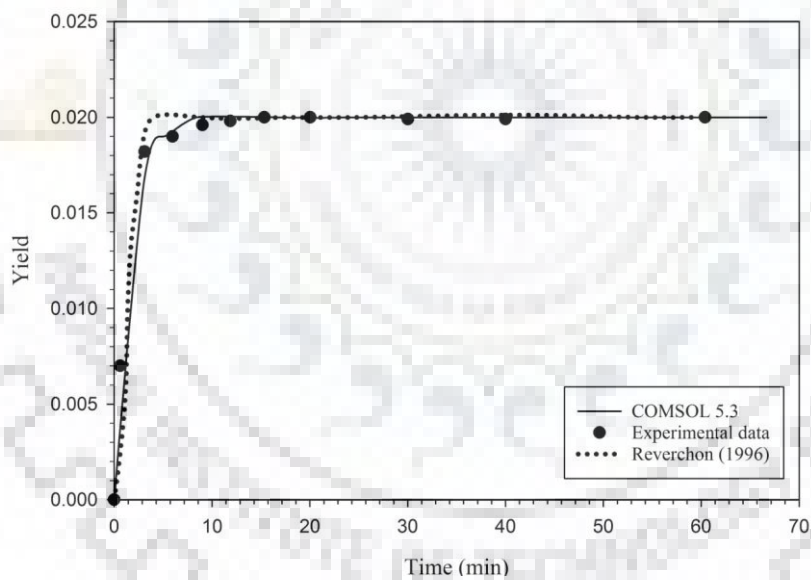
Fig. 6.25 Comparison of results for the extraction of *Baccharis trimera* plant using model proposed by Reverchon (1996).

6.6.1.5 Mathematical model-5

Vargas et al. (2006) extracted the *carqueja* essential oil from the SFE of *Baccharis trimera* plant. They used the model proposed by Reverchon (1996) to model the extraction process with certain modification in geometry as discussed in section 5.1.5. This model was solved using COMSOL multyphysics 5.2 and compared with the experimental extraction curve as shown in Fig. 6.25. It

shows that extraction curve solved through COMSOL compares very well with the experimental data with 1.07% AARD value.

6.6.1.6 Mathematical model-6

Nobre et al. (2006) extracted the pigments from *Bixa orellana* seed using SFE process and proposed a model for the same. In the present work, COMSOL multyphysics 5.2 was used to solve the model equations and results were compared with that of published work in Fig. 6.26. It shows that trends of both curves are almost similar with 2.15% AARD value.
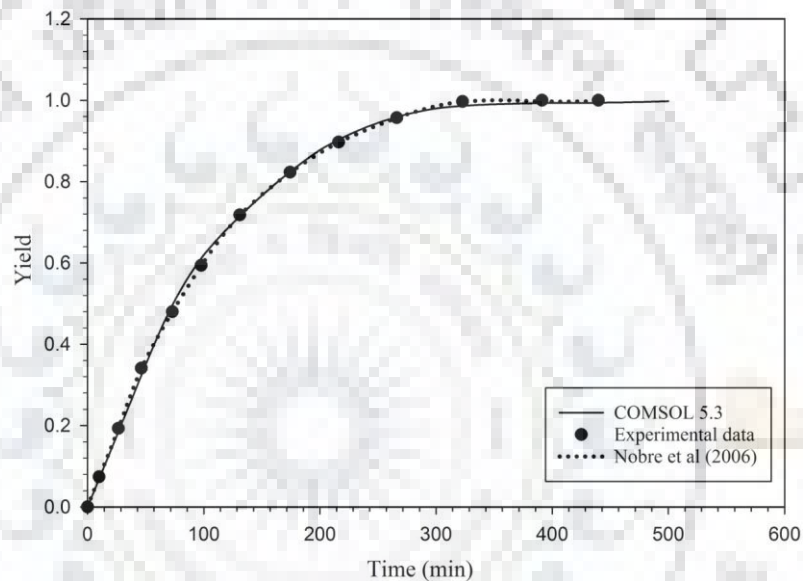
Fig. 6.26 Comparison of results for the extraction of *Bixa orellana* seed using model proposed by Nobre et al. (2006).

6.6.1.7 Mathematical model-7

Sovova (1994) proposed a model assuming three extraction periods for the SFE. Pederssetti et al. (2011) used the model proposed by Sovova (1994) to simulate the SFE process of Canola seed. The model proposed by Sovova (1994) was solved using COMSOL multyphyscis 5.2 and results were compared with the experimental data of Canola seed as given in Pederssetti et al. (2011). Fig. 6.27 represents the comparison of extraction curves and shows very good fitting between experimental results and that found through software. The value of AARD is 1.70%.
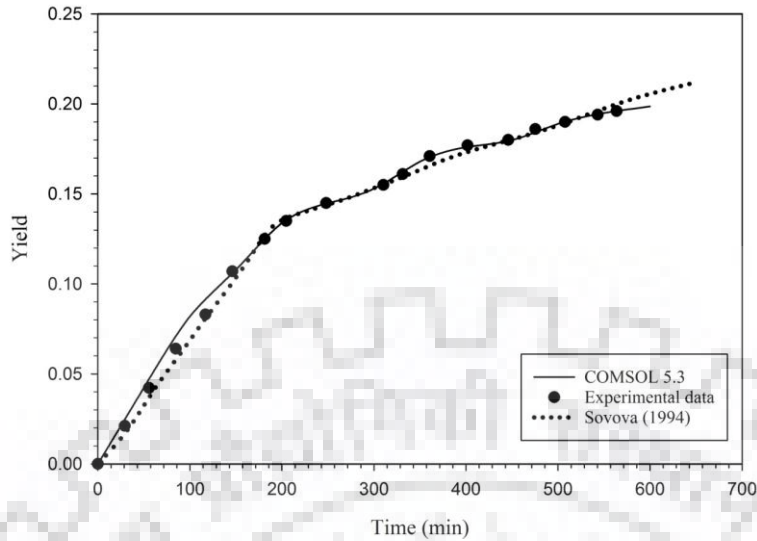
Fig. 6.27 Comparison of results for the extraction of Canola seed using model proposed by Sovova (1994).

6.6.1.8 Mathematical model-8

Goto et al. (1996) developed a shrinking-core model for the modelling of the SFE process while including axial dispersion in the extraction column. Salgin et al. (2006) used the model proposed by Goto et al. (1996) for the modeling of SFE of sunflower seed, which was solved using COMSOL multyphysics 5.2. Results of the model are compared in Fig. 6.28 with that of experiment carried out by Salgin et al. (2006). It shows excellent fitting of extraction curves with AARD of 1.4%.
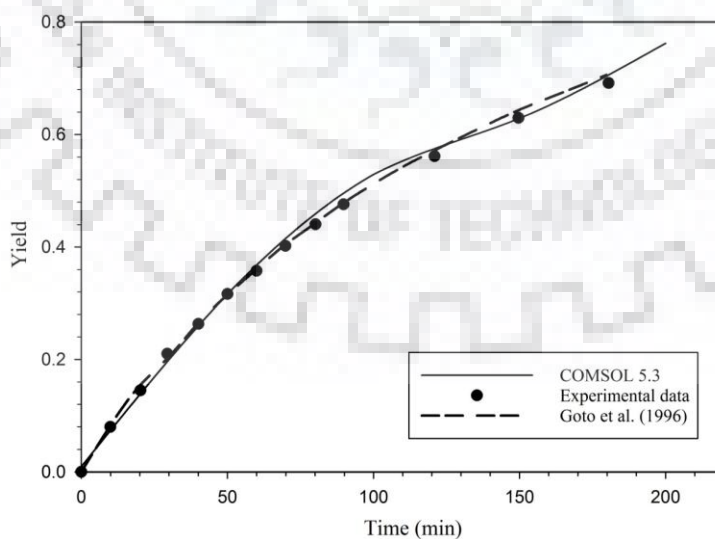
Fig. 6.28 Comparison of results for the extraction of Sunflower seed using model proposed by Goto et al. (1996).

6.6.2 Investigation of best fit model for different type of matrices

In this section, experimental data of different types of solute matrices are fitted in various mathematical models to study the effect of matrix on extraction yield. Input parameters of different matrices such as pressure, temperature, particle size, solvent flow rate, initial oil content, solvent and raw material density and solubility are considered to solve these models as shown in Table 6.17. On the other hand, for these matrices, a few parameters are tuned to acquire desired results and values of these tuning parameters with respective model no. are reported in Table 6.18.

6.6.2.1 Raw material matrix-1: Leaves

The most suitable model for SFE of leaves type of matrix was investigated while fitting the experimental data of sage leaves into different models. Experimental conditions used in present work were the optimum extraction conditions as reported by Reverchon (1996) and shown in Table 6.17. Reverchon (1996) developed a mathematical model for the extraction of natural products while predicting mass balance equations for both solvent as well as solid phase. Experimental data of the extraction of sage leaves oil were fitted in the model and found around 100% yield of oil, which was well suited with the experimental yield as shown in Fig. 6.29. Experimental data of sage leaves are also fitted in different models, discussed in section 6.6.1, to find out the relation between type of matrix and model as shown in Fig. 6.29. It can be noticed from Fig. 6.29 that other than Reverchon (1996), model proposed by Sovova (1994) also shows similar trend, and gives an error band from 0 to +10% as shown in Table 6.19. Thus, Sovova (1994) model is best fitted for sage leaves. Results from the other models are also approaching to the experimental yield though extraction time and trend of extraction curves are different. The only model which does not suit the experimental results of sage leaves at all is proposed by Reverchon et al. (2000) as can be seen in Fig. 6.29. Above results can be explained by the SEM images of sage leaves shown in Table 6.19 (Akalın et al., 2015). The essential oil adsorbed on leaf waxes does not seem to support the configuration of vegetable matter (Reverchon,1996) . Sage leaf has a linear string of cells with hairy-like structures also called glandular trichomes and the trichomes secrete globules of essential oils (Akalın et al., 2015). The freely available oil on the particle surface was not significant in the case of leaves because of low oil content and oil bound structure of leaves (Reverchon,1996). Reverchon (1996) also solved the model assuming that geometry of sage leaf was slab-like as results for spherical geometry were not suitable for the experimental results. Therefore, it can be concluded from above facts that the extraction of leaves should be only controlled by internal diffusion. Other than these explanations, when experimental data for sage leaves was fitted in the

model of Sovova (1994) it required external mass transfer coefficient value to complete the model, which might be any small value such as 6.7×10^{-4} s^{-1} to find same results as experimental data for sage leaves and thus, it was considered as tuning parameter. Hence, it can be concluded that models proposed by Reverchon (1996) as well as Sovova (1994) can be used for modelling of SFE extraction of leaves.

6.6.2.2 Raw material matrix-2: Flower concrete

In this section, type of solute matrix considered is flower concrete. The experimental results were fitted in different models to investigate the most suitable model for the Rose flower concrete. Reverchon and Poletto (1996) extracted the Rose flower concrete by SFE and proposed a mathematical model also for this. Reverchon and Poletto (1996) considered optimum extraction conditions for the extraction of rose flower concrete as optimized by Reverchon et al. (1995) and reported in Table 6.17.

Reverchon and Poletto (1996) proposed a model and fitted it with the experimental data for SFE of rose flower concrete. Further, different models were fitted on the experimental data of rose flower concrete as shown in Fig. 6.30. Extraction yield by fitting in their own model was around 50% whereas it was decreased for all other models. Based on microphotographs of rose flower concreteand SEM images of rose petal as shown in Table 6.19, it was observed that flower concrete consisted of two phases: an oily one (darker) mainly constituted by liquid compounds that are soluble in supercritical CO_2 and a waxy phase (lighter) where insoluble waxes are predominant. Reverchon and Poletto (1996) developed the model equation considering the inside structure of flower concrete as they assumed that oily phase in concrete is easily available. Further, they assumed that the extraction of waxy phase experienced a mass transfer resistance and considered in mass balance equations. Hence, it can be concluded from the Fig. 6.30 that the solute matrix (flower concrete), which contains soluble oil and insoluble wax can be modelled using the model proposed by Reverchon and Poletto (1996), with error band from -7.5% to 2.5% as shown in Table 6.19. Further, it can be observed from Fig. 6.30 that initially the model of Reverchon et al. (2000) follows similar trend as that of Reverchon and Poletto (1996). However, for complete extraction process it behaves far different than the proposed model (Reverchon and Poletto, 1996). Extraction yields of the models proposed by Reverchon and Marrone (1997), Goto et al. (1996), Sovova (1994), Reverchon (1996), Nobre et al. (2006) and Vargas et al. (2006) are much lesser than that of experimental as can be noticed from Fig. 6.30. However, amongst these models, significantly less yields of 0.06%, 0.6% and 0.07% are obtained for models of Reverchon (1996),

Nobre et al. (2006) and Vargas et al. (2006), respectively. These models considered only internal mass transfer coefficient and this might be a reason for almost negligible extraction yield for these models.
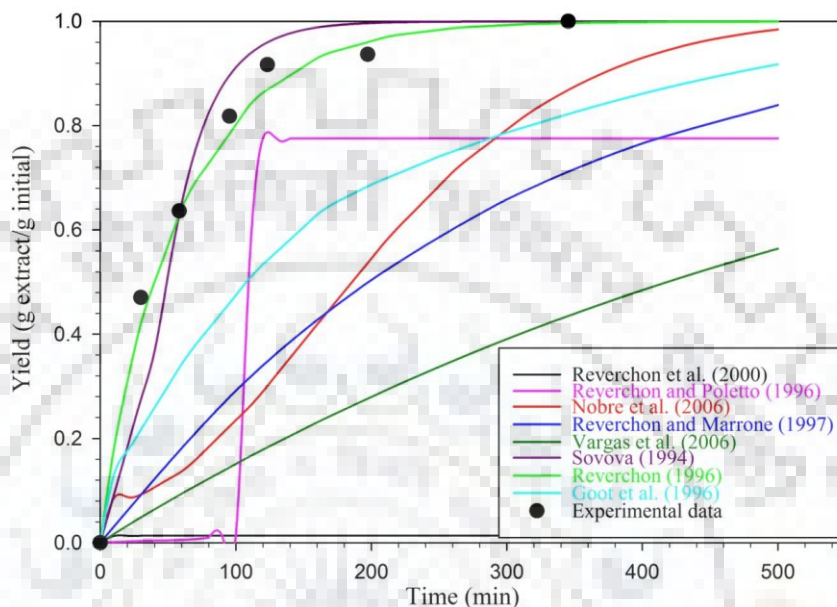
Fig. 6.29 Effect of Leaves matrix on different models.
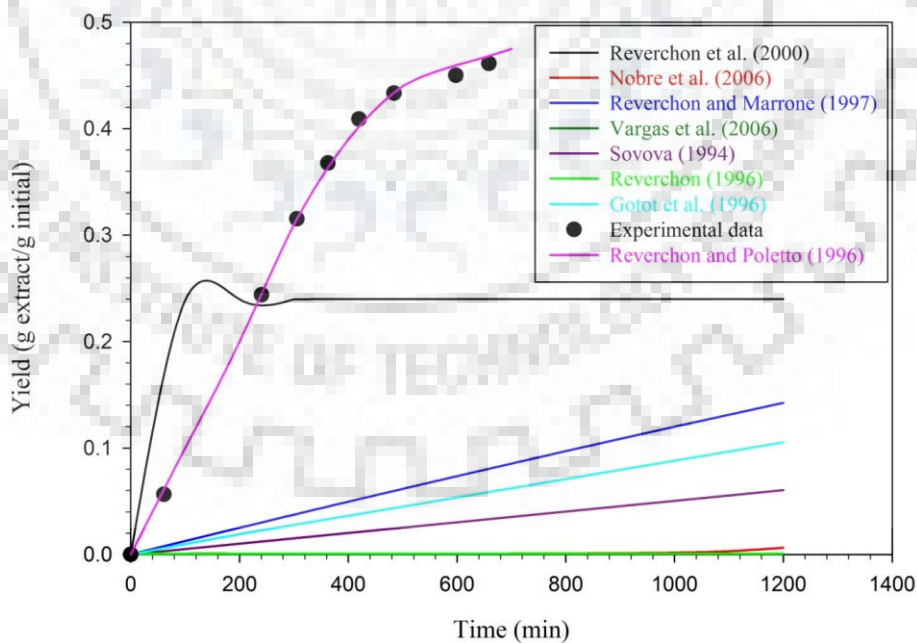
Fig. 6.30 Effect of flower concrete matrix on different models.

On the other hand, models proposed by Reverchon and Marrone (1997) and Goto et al. (1996) are also showing linear trend of extraction curve though extraction yield values are significant as mass balance equations of these models are dominated by external mass transfer coefficient. For models proposed by Reverchon and Marrone (1997) and Goto et al. (1996) external mass transfer coefficients are 7.56×10^{-4} and 3.6×10^{-7}, respectively as reported in Table 6.18. As can be seen from Table 6.18 that high external mass transfer coefficient value for Reverchon and Marrone (1997) results a low external mass transfer resistance to extraction of oil followed by high extraction yield in comparison to Goto et al. (1996). The trend of extraction curve from the model proposed by Sovova (1994) can be explained by the combination of solubility and external mass transfer coefficient. Sovova (1994) modeled the mass balance equations considering both mass transfer resistances (solvent and solid phase) with the solubility term though in the present case, no mass transfer coefficient was affecting the yield. Further, Fig. 6.30 shows that extraction curve is linear till the end of extraction time and the only yield of oil is due to solubility of solute in solvent. It is observed that only easily accessible oil, can be extracted by above mentioned models. The model proposed by Reverchon and Poletto (1996) considered the variable mass transfer coefficient and were able to extract easily accessible oil with waxy phase also. Thus, for flower concrete, model proposed by Reverchon and Poletto (1996) is most suitable.

6.6.2.3 Raw material matrix-3: Flower bud

In this section, different models were fitted with the SFE data of flower bud to find out the best suitable model for this type of solute matrix. SFE of Clove bud was performed by Reverchon and Marrone (1997) and fitted their own model. Reverchon and Marrone (1997) used optimum pressure and temperature values as reported in literature and vary the solvent flow rate and bed height to optimize both parameters. Experimental conditions selected in the present work for the extraction of rose flower are the optimized conditions as reported in Table 6.17.

Fig. 6.31 (a) and (b) showed the extraction curves while fitting the experimental data of clove bud into different models. However, model of Reverchon and Marrone (1997) showed a extraction curve trend, which was absurd and unexplainable. In fact, they developed model for the flower concrete and required additional information such as density of glass fiber and porosity of concrete for the model execution, which were not available for clove bud. Dotted portion of Fig. 6.31(a) was enlarged in Fig. 6.31 (b) for the clarity. SEM analysis of clove bud was shown in literature and reproduced in Table 6.19. It shows that a series of cavities that are probably the essential oil bearing cells in clove buds (Reverchon and Marrone, 1997; Zizovic et al., 2012). The vegetable

structure, thus, presents easily accessible essential oil sites reinforcing the hypothesis that only small mass transfer resistances should be encountered in the SFE process. Reverchon and Marrone (1997) solved the model considering internal and external mass transfer rate equations separately. Results of external mass transfer rate equation were in a good agreement with experimental results and showed an error band from -5% to +4% as provided in Table 6.19. However, while considering the internal mass transfer rate equation, poor fitting was observed due to its insensitiveness towards solvent flow rate. From the model of Reverchon and Marrone (1997), it was observed that only the external mass transfer resistance was taken into account to model the extraction of clove bud as these particles were highly agglomerated and thus, oil available in the deep inside of the cavities was not extractable (Abdali and Ajji, 2015). Extraction yield for the clove bud from the model proposed by Reverchon and Marrone (1997) was around 20% and was in well support with the experimental yield. Model proposed by Reverchon (1996) is also showing somewhat similar trend of extraction curve with extraction yield almost equal to experimental yield.

The model proposed by Sovova (1994) is also showing same extraction yield though extraction time is less in comparison to experimental time as can be observed from Fig. 6.31(a). Sovova (1994) proposed the model considering three extraction period. However, in the case of clove bud, fast extraction and transition periods were combined due to less value of solubility. Extraction yield due to solubility factor and external mass transfer coefficient was covered in first extraction period. The model developed by Reverchon et al. (2000) was proposed for flower hip seed. It provided two times higher extraction yield than that of experiment as internal mass transfer resistance was considered in this model. The models proposed by Reverchon (1996) and Vargas et al. (2006) assumed that extraction of solute was due to diffusion of oil, which was considered by Reverchon and Marrone (1997) though did not find suitable for Clove bud. On the other hand, Nobre et al. (2006) considered both internal and external mass transfer resistances working together on extraction process. Three models such as Reverchon (1996), Nobre et al. (2006) and Vargas et al. (2006) were showing that yield was around 100% hence all the oil available in clove bud was extracted and reasons were discussed above. It is clear from above discussion that the model proposed by Reverchon and Marrone (1997) is most suitable model for flower bud matrix.
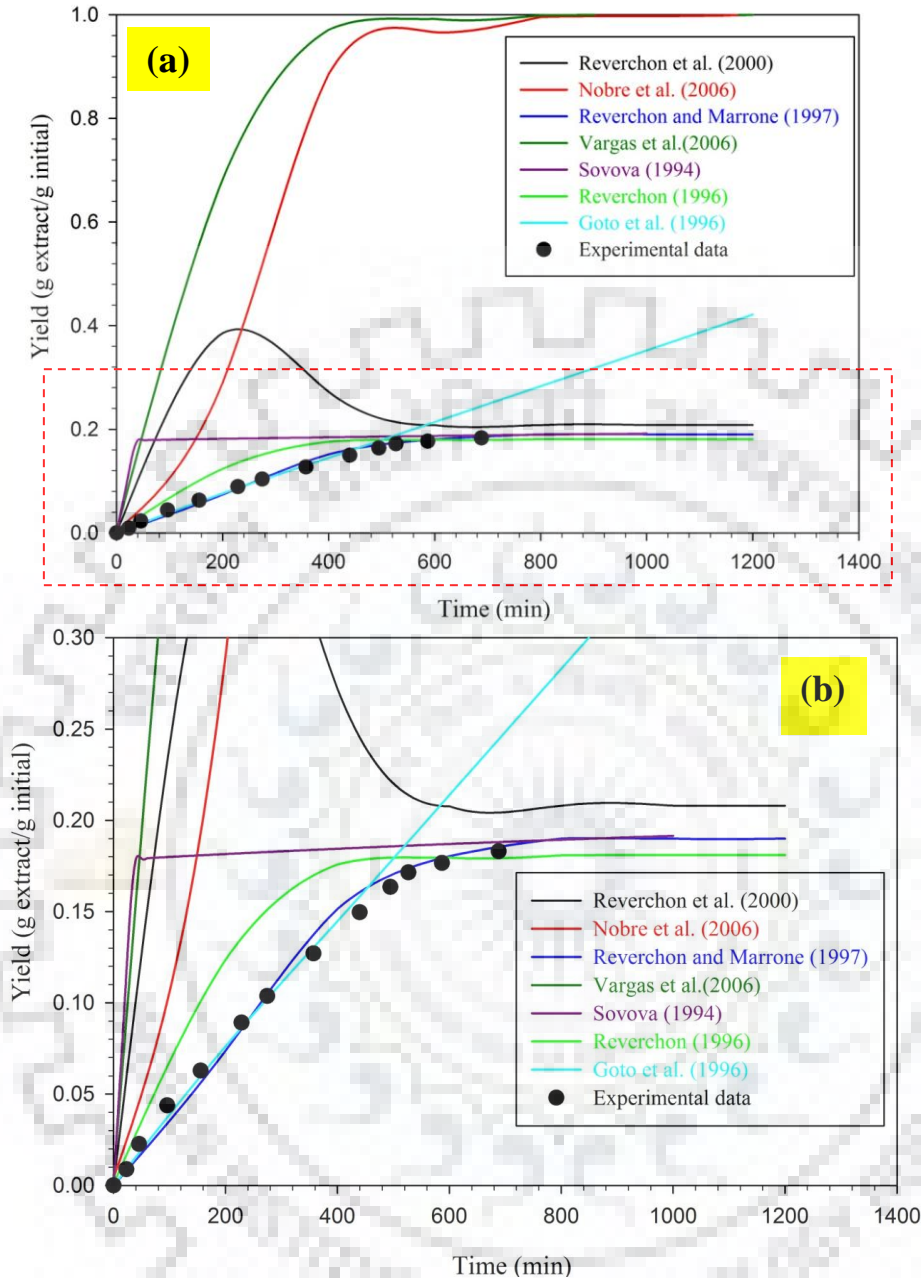
Fig. 6.31 (a) Effect of flower bud matrix on different models and (b) Dotted portion of Fig. 6.31(a).

6.6.2.4 Raw material matrix-4: Flower hip seed

In this section, solute matrix of flower hip seed is considered for the selection of best suited mathematical model for it. Hiprose seed was extracted at various pressure, temperature and solvent flow rates by the Reverchon et al. (2000) to study the effect of various operating parameters on the SFE of hiprose seed and a model was also developed for this process. In the present work,

optimum operating conditions proposed by Reverchon et al. (2000) are accounted to fit the model as reported in Table 6.17.

Reverchon et al. (2000) developed the mathematical model and experimental data for Hiprose seed were fitted well as shown in Fig. 6.32. Further, results are found with an error band from -4% to +4% as indicated in Table 6.19. Fig. 6.32 also shows results of other models when experimental data of the extraction of hiprose seed are fitted in these. As can be seen from the Fig. 6.32 that model developed by Reverchon et al. (2000) gave the yield of around 7%, which was well fitted with the experimental yield of hiprose seed. A few other models: Reverchon and Marrone (1997), Sovova (1994), Reverchon (1996), Nobre et al. (2006) and Vargas et al. (2006) show approximately 100% yield with an appropriate trend of extraction curve though do not support experimental results. The model proposed by Goto et al. (1996) was also not supported well by the experimental data of hiprose seed. SEM images of hiprose seed, presented in Table 6.19, also help in understanding the inside structure of seed and predicting mass transfer resistances of hiprose seed. SEM analysis of hiprose seed, as incorporated in Table 6.19, shows that essential oil is available in channels of different diameter and length (Reverchon et al., 2000). In SEM images, lignin structure protects the unbroken channels and makes too compact to allow an effective diffusion of the supercritical solvent in a reasonable extraction time. Due to above reasons, intact and broken cells model of Sovova (1994) cannot be used to study the extraction of Hiprose seed, which includes broken and intact cells though oil near to intact cell is not accessible. SEM images showed that the oil near the opening of the channel was readily available for the extraction whereas the supercritical solvent faced an increasing resistance due to diffusion in channels at an increasing depth to extract the oil from inside channels. Reverchon et al. (2000) accounted an internal mass transfer resistance that increased linearly in the model till the oil contained in the channels was extracted and model satisfied the experimental results well. If experimental yield can be increased by adding co-solvent or any other modification in process like pretreatment of seed, small particle size, then models of Sovova (1994), Goto et al. (1996), Reverchon (1996), Reverchon and Marrone (1997), Nobre et al. (2006) and Vargas et al. (2006) may give high yield for the extraction of hiprose seed. However, all models discussed above showing good results apart from that of Reverchon and Poletto (1996), which is absurd as can be evident from Fig. 6.32. The reason behind it is that the model developed by Reverchon and Poletto (1996) is for flower concrete and requires additional data like density of glass fiber and porosity for concrete for the model

175

execution. Therefore, the model proposed by Reverchon et al. (2000) is found most suitable model for flower hip seed matrix**.**
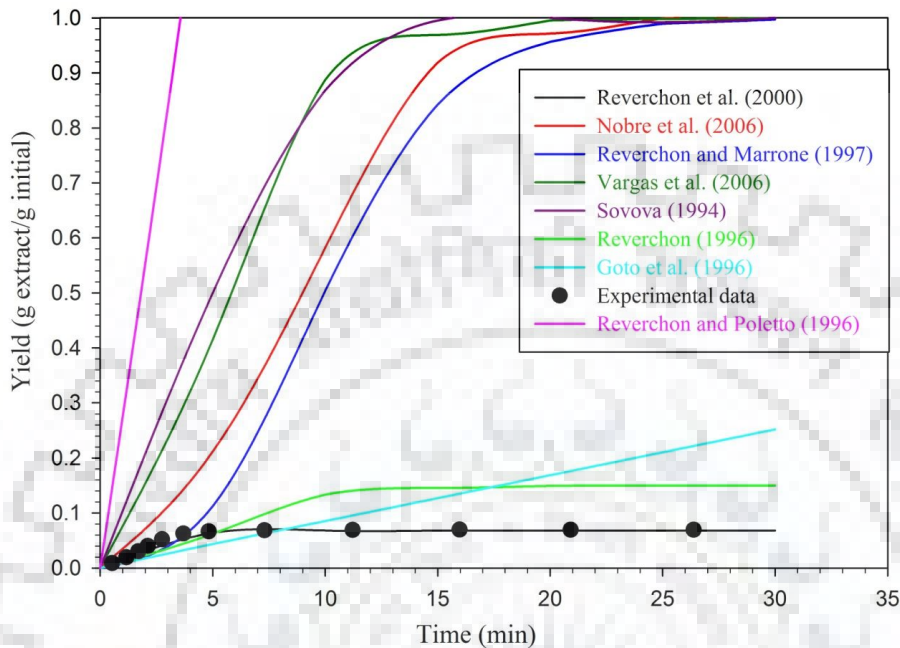
Fig. 6.32 Effect of flower hip seed matrix on different models.

6.6.2.5 Raw material matrix-5: *Baccharis trimera* **Plant**

In this section, type of matrix accounted is leaves and twigs of the *Baccharis trimera* plant and experimental data is fitted in different models. SFE of *Baccharis trimera* plant was performed by Vargas et al. (2006) at different operating temperatures while other parameters were fixed and model used for the modeling was Reverchon (1996). Optimum conditions providing in Vargas et al. (2006) were used to fit different models and shown in Table 6.17.

Fittings of experimental data of the extraction of leaves and twigs of *Baccharis trimera* plant in different models are shown in Fig. 6.33 (a) and (b). Enlarged view of dotted portion of Fig. 6.33 (a) is presented in Fig. 6.33 (b) for clarity. As reported in literature (Vargas et al., 2006), extraction yield was 2%, which was in support with the results of model proposed by Reverchon (1996). An error band from -2% to +4% was found through model of Reverchon (1996), which can be observed through Table 6.19. Results from the models proposed by Goto et al. (1996) and Nobre et al. (2006) were also close to experimental results but not fitting well. While fitting the experimental data for extraction of *Baccharis trimera* plant into other models such as Sovova (1994) and Reverchon and Marrone (1997), higher yield of around 65% and 100% was found,

176

whereas a few models such as Reverchon and Poletto (1996) and Reverchon et al. (2000) showed absurd results. Extraction of leaves and twigs of *Baccharis trimera* plant can be studied well through model proposed by Reverchon (1996), which was best for leaves.
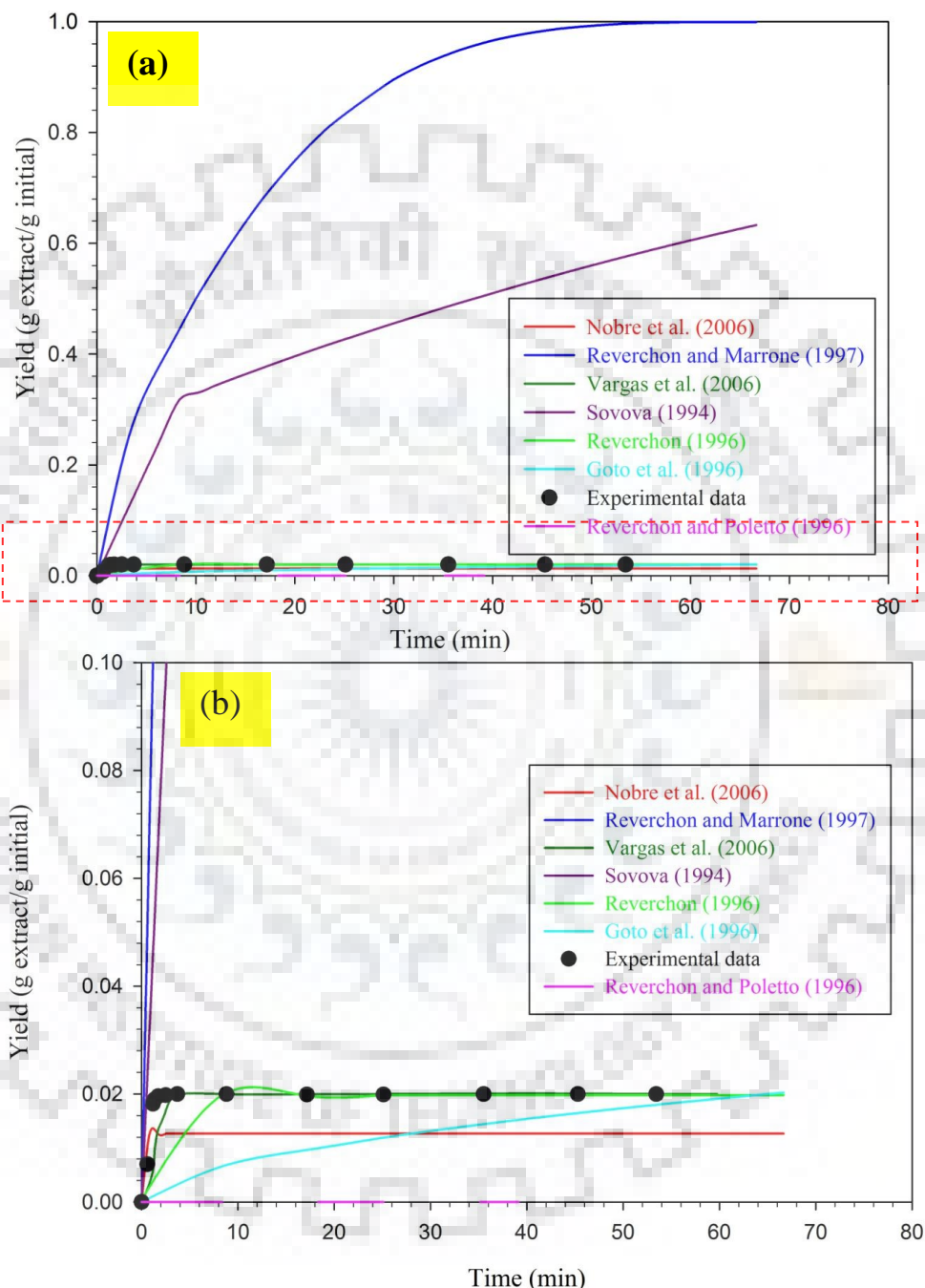
Fig. 6.33(a) Effect of Herb plant matrix on different models and (b) Dotted portion of Fig. 6.33(a).

6.6.2.6 Raw material matrix-6: Shrub seed

SFE of *Bixa orellana* seed was done by Nobre et al. (2006) while varying pressure, temperature and solvent flow rate to investigate the optimum points. Further, they developed model to fit the experimental data at optimum points, which are reported in Table 6.17.

Nobre et al. (2006) developed a differential mass balance model and fitted the extraction data of Shrub seed (*Bixa orellana* seed) and observed 1% extraction yield of oil. The experimental data for the extraction of *Bixa orellana* seed were fitted in other models and results are complied in Fig. 6.34(a) and (b). For clarity, dotted portion of Fig. 6.34 (a) is further enlarged in Fig. 6.34 (b). Other than the model developed by Nobre et al. (2006), a few models such as Sovova (1994), Reverchon (1996), Reverchon and Marrone (1997) and Vargas et al. (2006) are also showing same extraction yield. Trends of extraction curves are same for models proposed by Reverchon (1996) and Vargas et al. (2006) whereas, these are slightly different for Reverchon and Marrone (1997) and Sovova (1994). The error band while comparing experimental data with data of model proposed by Vargas et al. (2006) varies from -11% to 0% as evident through Table 6.19. The models developed by Reverchon and Poletto (1996) and Goto et al. (1996) show an extraction yields of around 10% and 5%, respectively, which are increasing continuously. On the other hand, model proposed by Reverchon et al. (2000) predicts the extraction yield below 0.1%, which is very less.

Model proposed by Sovova (1994) showed 1.2% yield for *Bixa orellana* seed. Up to 300 min the extraction curve found through Sovova (1994) model is sloppy whereas, beyond it, curve is flat. This trend can be explained as: Internal mass transfer coefficient is very low in comparison to external, which results very high mass transfer resistance in solid phase. Consequently, the low extraction yield and flat extraction curve are found. On the other hand, initial slope i.e. linear portion of extraction curve is due to solubility and external mass transfer coefficient value, which is higher than internal mass transfer coefficient as can be seen from Table 6.18. Therefore, extraction curve is almost constant after the effect of solubility and external mass transfer coefficient. All results in Fig. 6.34(a) can be justified with the SEM images of *Bixa orellana* seed presented in Table 6.19 (Taham et al., 2016). It shows that *Bixa orellana* seed structure is intact and many small globules can be found, which made extraction oil very difficult. Through SEM images, it can be assumed that the intra-particle resistance to mass transfer controls the extraction and low extractable pigment caused less extraction yield. Therefore for shrub seed, the model proposed by Nobre et al. (2006) is the most suitable model though that proposed by Vargas et al. (2006) can also be considered for shrub seed.
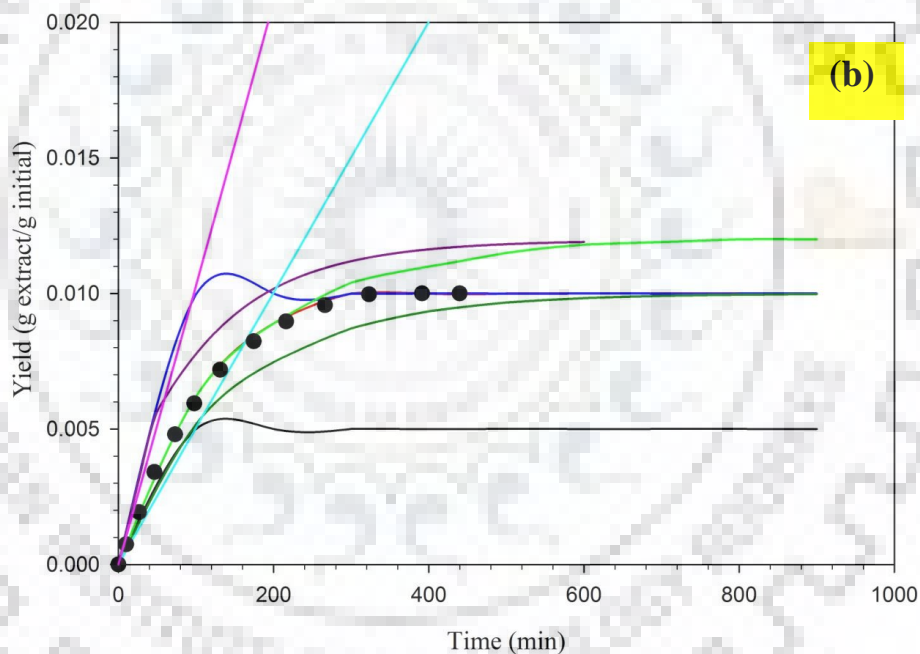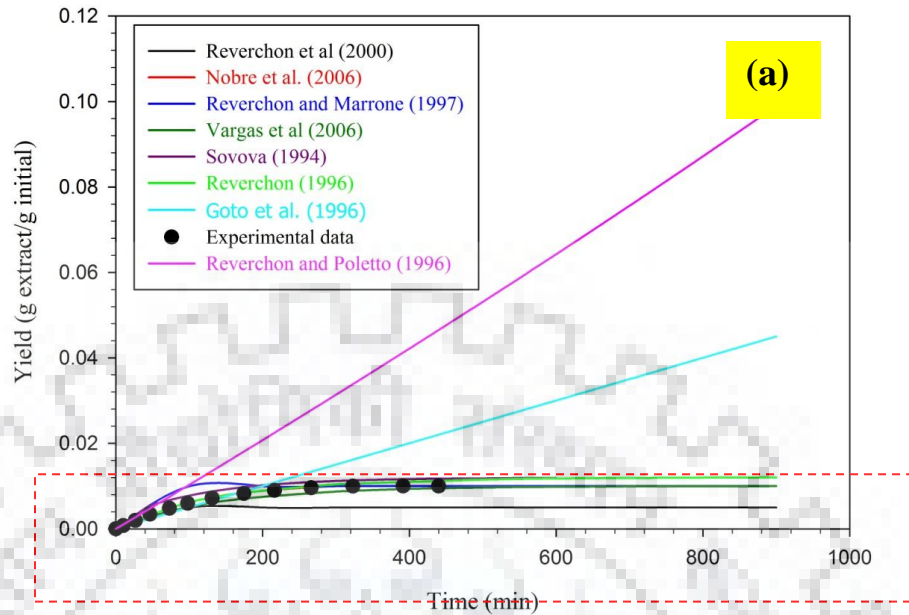
Fig. 6.34(a) Effect of Shrub seed matrix on different models and (b) Dotted portion of Fig. 6.34(a).

6.6.2.7 Raw material matrix-7: Vegetable matter-1

In this section, experimental data of SFE of vegetable seed is used to fit in different models to select the best fit model. Pederssetti et al. (2011) investigated the SFE of Canola seed and data were fitted in the model proposed by Sovova (1994).

Sovova, 1994 proposed a modified model from that developed by Lack (1985) while considering three extraction periods in the whole extraction process of any solute matrix. Pederssetti et al. (2011) extracted canola oil while varying pressure, temperature and type of solvent (carbon

179

dioxide, propane) and the model proposed by Sovova (1994) was used for fitting of extraction data of Canola seed. Extraction conditions considered for fitting in models were optimum conditions for the extraction of canola seed using supercritical CO_2 as reported by Pederssetti et al. (2011). This data is fitted in other models and extraction curves are compared in Fig. 6.35. It shows that the model proposed by Sovova (1994) gives a yield of 19%, which matches well with the experimental yield having error band from -4% to 0% as reported in Table 6.19. All other models show lesser yields than Sovova (1994) hence, not fitting well with experimental data of canola seed except models proposed by Goto et al. (1996) and Vargas et al. (2006). These models predict the extraction yield similar to experimental though trends were continuously increasing. Canola seed has a vegetable structure and contains a good amount of vegetable oil bounded inside the cavities or cells. Intact cells were broken through milling to make the oil accessible; however, a few were still intact as evident from SEM images shown in Table 6.19 (Kouba et al., 2016; Qaderi et al., 2007). The model developed by Sovova (1994) was based on intact and broken cells theory where first solvent phase mass transfer resistance was responsible for the extraction of easily accessible oil from broken cells and then oil was extracted from intact cells where solid phase mass transfer resistance dominated. Hence, it can be concluded that Sovova (1994) is the best suited model for the vegetable matter, which contains oil inside broken and intact cells.

6.6.2.8 Raw material matrix-8: Vegetable matter-2

Salgin et al. (2006) extracted the sunflower seed through SFE process and experimental data were fitted in the Shrinking core model proposed by Goto et al. (1996).

Salgin et al. (2006) extracted the oil from sunflower seed while varying four extraction parameters such as temperature, pressure, particle size and solvent flow rate. The SFE process was modeled using Shrinking core model at the optimum operating conditions, shown in Table 6.17. The model was fitted well with almost 100% extraction yield as can be seen from Fig. 6.36. It is observed by Goto et al. (1996) that when a sharp boundary exists inside the particle between extracted and non-extracted part, shrinking core model is useful. It is evident from SEM images of sunflower seed shown in Table 6.19 (Rai et al., 2016a) that surface of the particle is formed by a sequence of layers.
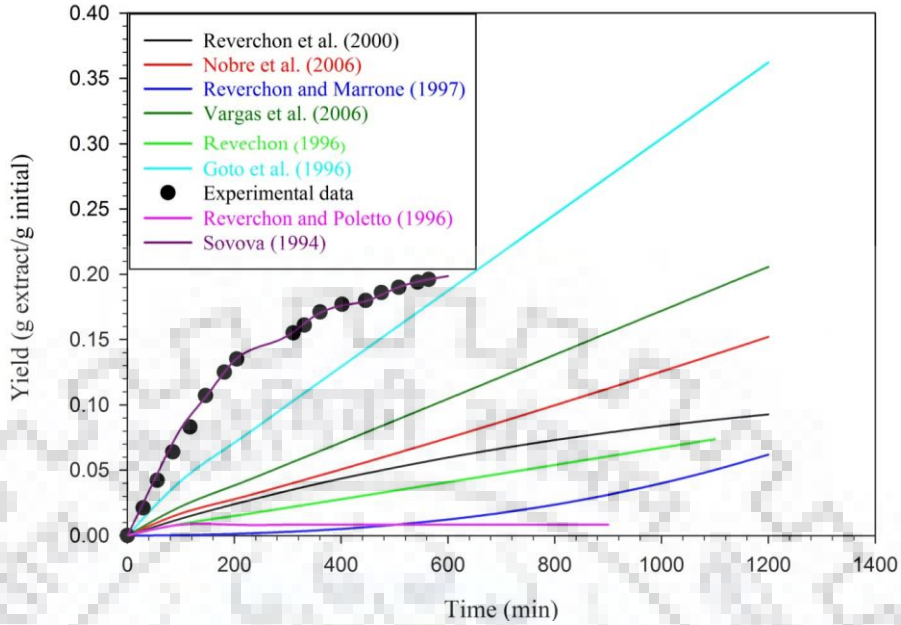
Fig. 6.35: Effect of seed matrix-I on different models.
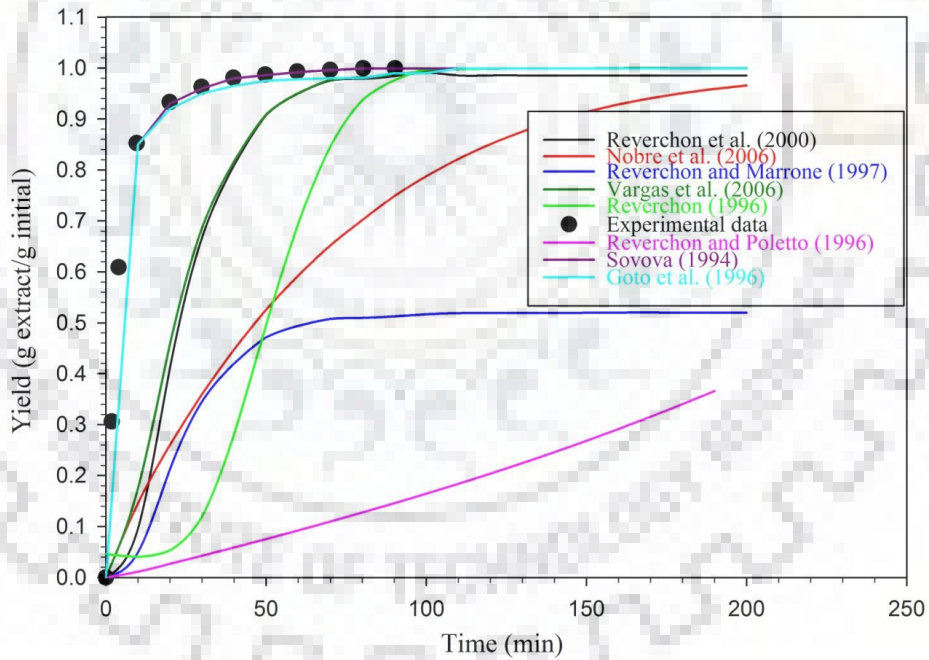
Fig. 6.36: Effect of seed matrix-II on different models.

Oil is uniformly distributed in each layer where extracted and non-extracted parts of solids are closely interpenetrating. SEM images of sunflower seed are in well support to use the shrinking core model proposed by Goto et al. (1996).It can be observed from Fig. 6.36 that the model proposed by Sovova (1994) is also fitting well with the experimental data. The solid phase mass

181

transfer coefficient is the tuning parameter and solvent phase mass transfer coefficient is not showing any effect on extraction curve. The behavior of extraction curve from Sovova (1994) is also matching well with the experimental extraction curve having an error band from -2.5% to 0% as shown in Table 6.19. The model developed by Sovova (1994) was based on the theory discussed in section 5.1.6. This can be a reason for the well fitting of experimental data of sunflower seed into the model proposed by Sovova (1994). Apart from Sovova (1994), the model proposed by Reverchon et al. (2000), Nobre et al. (2006) and Vargas et al. (2006) are also resulting same extraction yield though do not follow the trend of extraction curve as can be observed from Fig. 6.36. Other models such as Reverchon (1996), Reverchon and Poletto (1996) and Reverchon and Marrone (1997) are showing good results but not matching with the experimental data as shown in Fig. 6.36. It can be concluded that if oil is distributed in layers and a very sharp boundary exists between the extracted and non-extracted part then the model proposed by Sovova (1994) and Goto et al. (1996) can be used for the modeling of SFE process.

6.6.2.9 Consolidated results of effects of matrices

In this section, different facts discussed in sections 6.6.2.1 to 6.6.2.8 are complied in Table 6.19 and Table 6.20. From Table 6.19, it can be noticed that for *Baccharis trimera* plant, the model proposed by Goto et al. (1996) and Nobre et al. (2006) also predict same extraction yield as experimental yield along with other models such as Reverchon (1996) and Vargas et al. (2006). However, the trends of experimental curve for the models of Goto et al. (1996) and Nobre et al. (2006) are not matching well and hence, these models cannot be suggested for Herb seed. Similarly, the extraction yield found through the model proposed by Reverchon and Marrone (1997) is same as the experimental yield of *Baccharis orellana* seed. However, this model cannot be suggested for the modeling of Shrub seed as desired behavior of experimental curve is not found. If two solutes have same type of matrix, best fitted model may be same for both. From Table 6.20, it can be noticed that leaf and herb plant are having similar type of matrices and best fitted model is Reverchon (1996) for both. Similarly for seed category, Canola and sunflower seeds follow same matrices and thus, the best fitted model is also same i.e. the model proposed by Sovova (1994). Thus, it can be concluded from Table 6.19 and 6.20 that for best fitting of model for any type of solute matrix, extraction yield and behavior of extraction curve should be matched well with the experimental results. Secondly, same model can be used for the modeling of SFE process of any solute if solute matrices are same.
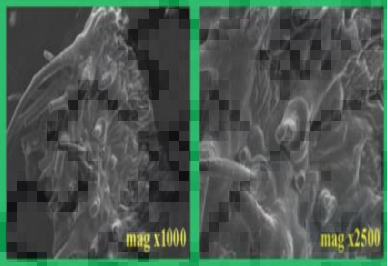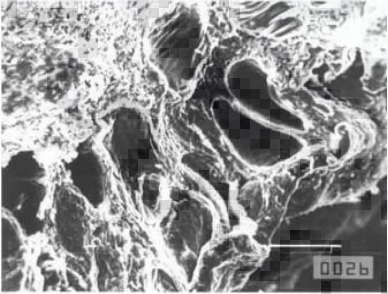
Table 6.17 Input parameters/experimental data of different matrices
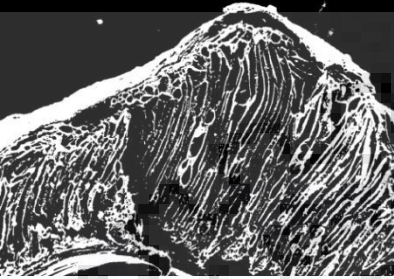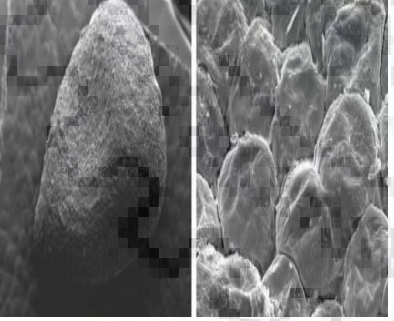
Reference	Raw material	Matrix	P (bar)	T (°C)	u (m/s)	V (m³)	ε	dp (mm)	P_f (kg/m³)	ρ_s (kg/m³)	x_0 (kg/m³)	x_0 (g/g)	y_0(g/g)	y_r (g/g)
Reverchon (1996)	Sage leaf	Leaves	90	50	$4.55*10^{-4}$	$4*10^{-4}$	0.4	0.25	285	413.25	9	0.022	0.0044	0.064
Reverchon and Poletto (1996)	Rose flower	Flower concrete	80	40	$4.33*10^{-4}$	$2*10^{-4}$	0.3	2	280	759	587	0.96	0.0014	0.0014
Reverchon and Marrone (1997)	Clove bud	Flower bud	90	50	$4.56*10^{-4}$	$2*10^{-4}$	0.49	0.37	629	1290	233.49	0.208	0.0049	0.0049
Reverchon et al. (2000)	Hiprose seed	Flowerhip seed	690	40	$9.54*10^{-4}$	$2.5*10^{-5}$	0.48	0.42	629	1000	150	0.15	0.04	0.04
Vargas et al. (2006)	Baccharis trimera Plant	Herb plant	90	40	$3.515*10^{-4}$	$7.1*10^{-6}$	0.67	1.02	690	1087.2	27	0.025	$2.5*10^{-4}$	$2.48*10^{-4}$
Nobre et al. (2006)	Bixa orellana Plant seed	Shrub seed	200	40	$4.49*10^{-4}$	$5*10^{-6}$	0.65	3.5	840.5	1145	13.7	0.012	0.008	$1.2*10^{-4}$
Pederssetti et al, (2011)	Canola seed	Vegetable matter-I	250	60	$1*10^{-4}$	$1.5*10^{-4}$	0.73	0.75	724	967	377.13	0.39	0.0024	$5.44*10^{-3}$
(Salgin et al., 2006)	Sunflower seed	Vegetable matter-II	600	80	$3.67*10^{-4}$	$1*10^{-5}$	0.62	0.23	924	922	479.44	0.52	0.0282	0.0282

Table 6.18 Tuning parameters of different models by fitting the experimental data of different matrices.

Model No.	Parameters	Type of matrix							
		Leaves	Flower concrete	Flower bud	Flowerhip seed	Herb plant	Shrub seed	Vegetable matter-I	Vegetable matter-II
[1]	ApK (m³/s)	-	$1.5*10^{-7}$	$4.09*10^{-6}$	$3.52*10^{-6}$	$1.32*10^{-7}$	$2.5*10^{-10}$	$3.95*10^{-10}$	$6.15*10^{-5}$
	k_p*10^3	-	1.4	23.6	270	10	667	6	23
[2]	x_{ti} (g/g)	$7.56*10^{-3}$	-	0.0715	0.053	0.0086	0.0041	0.134	0.179
	y_i (g/g)	0.012	-	0.106	0.075	0.0128	0.0061	0.199	0.27
	Aph_0 (1/s)	$3.45*10^{-4}$	-	0.0204	0.14114	2.2537	$2.16*10^{-4}$	0.0065	$9.83*10^{-4}$
[3]	ApK_e (1/s)	$3.45*10^{-4}$	$7.56*10^{-4}$	-	0.141	0.0037	$4.7*10^{10}$	0.0082	0.0065
	K	5	235.7	-	3.75	1.23	172.2	1.5	162.5
[4]	K_{io} (m/s)	$5.4*10^{-8}$	$3.6*10^{-7}$	$2.5*10^{-6}$	-	$6.1*10^{-4}$	$8.33*10^{-8}$	$1.22*10^{-9}$	$4.77*10^{-6}$
	y_f (g/g)	0.0132	0.24	0.025	-	0.012	0.005	0.13	0.364
	k_{eq}	3	0.67	0.024	-	0.01	0.667	54.17	172.2
[5]	ApK (m³/s)	$6.9*10^{-9}$	$1.51*10^{-7}$	$4.09*10^{-6}$	$3.52*10^{-6}$	-	$2.5*10^{-10}$	$3.95*10^{-10}$	$6.15*10^{-5}$
	$kp*10^3$	200	1.4	23.6	270	-	667	6	23
[6]	ApK_s (m³/s)	$3.45*10^{-4}$	$7.56*10^{-4}$	0.0204	0.14	0.0037	-	$2.63*10^{-6}$	$9*10^{-3}$
	$kp*10^3$	200	0.4	23.6	270	10	-	6	5.8
[7]	kf_{a0} (1/s)	$6.7*10^{-4}$	$7.6*10^{-4}$	0.0204	0.39	0.05	0.0081	-	$4.16*10^{-5}$
	ks_{a0} (1/s)	$3.45*10^{-4}$	$6.87*10^{-5}$	$5*10^{-6}$	0.141	$6.22*10^{-5}$	$5*10^{-5}$	-	0.364
	x_k (g/g)	0.013	0.33	0.029	0.024	0.017	0.006	-	0.003
[8]	D_e (m²/s)	$6.1*10^{-13}$	$6.15*10^{-9}$	64.55	0.454	$4.3*10^{-14}$	27.71	0.304	-
	C_{sat} (g/g)	0.003	0.0014	0.0049	0.04	$2.4*10^{-4}$	$1.19*10^{-4}$	0.0024	-
	k_f (m/s)	$7.6*10^{-4}$	$3.6*10^{-7}$	$2.5*10^{-8}$	$4*10^{-8}$	$6.16*10^{-4}$	$5.05*10^{-8}$	$7.92*10^{-7}$	-
	D_L (m²/s)	$1.75*10^{-13}$	$1.75*10^{-10}$	$1.7*10^{-5}$	1.75	$5.25*10^{8}$	$1.75*10^{-5}$	1.75	-

Table 6.19 Consolidated results of the effects of matrices (Priyanka and Khanam, 2018)

Reference	Raw material	SEM Images	Matrix type	Model applied	Yield obtained		Suitable model		Error band
					Exp.	Model	Model	Yield	
Reverchon (1996)	Sage Leaves		Linear string of cells with hairy-like structures/ Glandular trichomes		100%	[7]100% [8]100% [1]100% [2]78% [3]83% [4]1.3% [5]56% [6]98%	[7], [8],[1]	100%	0-10% [7]
	Rose flower concrete		A soluble oily liquid compounds phase (darker) and an insoluble waxy phase (lighter)		50%	[7]6% [8]10% [1]0.06% [2]52% [3]14% [4]24% [5]0.07% [6]0.6%	[2]	52%	-7.5- +2.5% [2]
Reverchon and Poletto (1996)	Clove bud		A series of cavities/ Essential oil bearing organules		20%	[7]19% [8]42% [1]18.1% [2]NA [3]20% [4]38% [5]100% [6]100%	[7] [1] [3]	20.7 %, 18.1 % 19%	-5.0- +4.0% [3]

185

Revercho n et al. (2000)	Hiprose seed		Oil is available in channels of different diameter and length. Lignin structure protects the unbroken channels and makes too compact to allow an effective diffusion.	1-8	7%	[7]100% [8]25% [1]100% [2]NA [3]100% [4]7.4% [5]100% [6]100%	[4]	7.4%	±4% [4]
Vargas et al. (2006)	*Baccharis trimera* Plant	-	Linear string of cells with hairy-like structures/ Glandular trichomes		2%	[7]63% [8]2% [1]2% [2]NA [3]100% [4]NA [5]2% [6]1.4%	[1], [5],	2%	-2.0- +4.0% [1]
Nobre et al. (2006)	*Bixa orellana* Plant seed		Structure is intact and many small globules are observed		1.1%	[7]1.2% [8]4.5% [1]1.2% [2]10% [3]1% [4]0.5% [5]1% [6]1%	[7], [1], [5], [6]	1.2%	-11.0- 0% [5]
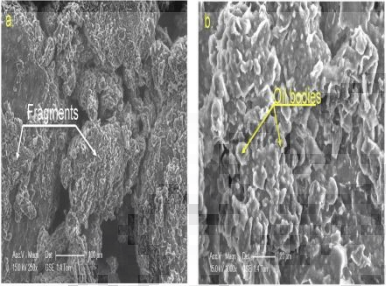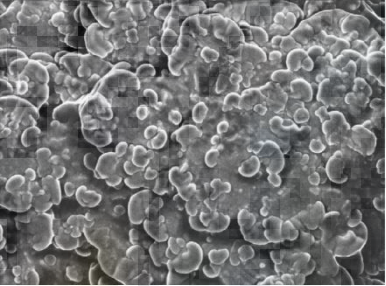
Pederssetti et al. (2011)	Canola seed		Oil enclosed inside broken and intact cells		20%	[7]19.9% [8]36% [1]2.6% [2]0.8% [3]6.1% [4]9.2% [5]1.7% [6]15%	[7]	19.9%	-4.0-0% [7]
Salgin et al. (2006)	Sunflower Seed		Oil is enclosed in layers		100%	[7]100% [8]100% [1]99% [2]40% [3]52% [4]100% [5]100% [6]95%	[7], [8]	100%	-2.5-0% [7]

Table 6.20 Best suited model for different type of matrices.

Matrix	Type of matrix	Suitable model/s
Leaf	Linear string of cells with hairy-like structures/ Glandular trichomes	Sovova (1994) Reverchon (1996)
Flower	Secretory duct	Reverchon and Poletto (1996)
Flower bud	Oil in Cavities	Sovova (1994) Reverchon (1996) Reverchon and Marrone (1997)
Flowerhip seed	Oil inside the cells and protected by lignin structure	Reverchon et al (2000)
Herb plant	Linear string of cells with hairy-like structures/ Glandular trichomes	Reverchon (1996) Vargas et al. (2006)
Shrub seed	Intact globules	Sovova (1994) Reverchon (1996) Nobre et al. (2006) Vargas et al. (2006)
Seed	Intact cells	Sovova (1994)
Flower seed	In layers	Sovova (1994) Goto et al. (1996)

6.6.3 Mathematical model and experimental results

6.6.3.1 Raw material-I: Turmeric root

In this section, experimental data of turmeric root are fitted in the model proposed by Sovova (1994) and effects of various operating parameters on the extraction yield are studied.

Pressure effect on yield of turmeric root

To study the effect of pressure on oil yield (g oil/g feed) of turmeric root, temperature, solvent flow rate, particle size and addition of co-solvent are fixed at 50 °C, 10 g/min, 0.45 mm and 7.5% of solvent flow rate, respectively. Extraction curve is plotted between % yield of oil and time (min) as shown in Fig. 6.37 where pressure varies from 200 to 400 bar to explore its effect on yield. Experimental extraction curve is compared with that obtained from the model proposed by Sovova (1994).

Following facts are observed from Fig. 6.37:

1. Firstly, the yield is increasing with pressure from 200 to 300 bar and then decreasing for 400 bar.

2. For three pressure levels (200,300 and 400 bar), the yield of initial part of extraction curve is similar for all three pressures.

Dual effect of pressure mentioned in point 1 can be explained through the facts: (i) increase in pressure leads to increase in extraction rate due to enhancement in solubility, which in turn increases the yield (Gopalan et al., 2000; Liu et al., 2009; Pilavtepe and Yesil-Celiktas, 2013; Sodeifian et al., 2016a), (ii) Increase in pressure results a decrease in mass transfer coefficient, which results a decrease in yield (Liu et al., 2009; Pilavtepe and Yesil-Celiktas, 2013; Sodeifian et al., 2016a). Similar results were obtained for SFE of P. khinjuk fruit, Passiflora seed and P. oceanica leaves by Sodeifian et al. (2016), Liu et al. (2009) and Pilavtepe and Yesil-Celiktas (2013), respectively.

Solubility of supercritical CO_2 is increased with pressure due to rise in density of solvent from 805 kg/m^3(200 bar) to 850 kg/m^3 (300 bar) as shown in Table 6.21, which leads to high salvation power for dissolving solute. Further, increase in pressure to 400 bar also increases the density (920 kg/m^3) of solvent however decreases the solubility and yield. The reason for reduced yield is higher mass transfer resistance due to less value of coefficient. At elevated pressure (400 bar), solute-solvent repulsion occurs from the highly compressed CO_2 which causes high mass transfer resistance to the extraction of solute (Liu et al., 2009; Sodeifian et al., 2016a). Solvent phase mass transfer coefficient ($k_f a_0$) and solid phase mass transfer coefficient ($k_s a_0$) for different pressure values are reported in Table 6.21. The $k_f a_0$ first decreases from 200 to 300 bar and then increases from 300 to 400 bar. Consequently, yield should be decreased and then increased. However, this behavior is just reverse as depicted by $k_s a_0$ for three different pressures as well as trend shown in Fig. 6.37. It indicates that extraction of turmeric oil is dominated by $k_s a_0$ irrespective to $k_f a_0$. The $k_s a_0$ at 400 bar is 2.17×10^{-5} (s^{-1}) which is far lesser than that at 300 bar (3.67×10^{-5} s^{-1}) and supports the solute-solvent repulsion phenomena of highly compressed CO_2. % yield of turmeric oil is increased by 1.4 times while pressure rises from 200 to 300 bar whereas, it is reduced by 1.16 times with a further increase in pressure (400 bar).

It can be noticed from Fig. 6.37 that yield of the initial part of extraction curve is almost same for all three pressures i.e. 200, 300 and 400 bar. The initial part of extraction curve is reported as fast extraction period by Sovova (1994), which is due to the extraction of easily accessible oil and solubility of oil in solvent. Easily accessible oil (x_k) is same for all three pressures and this can be a reason for a similar yield of fast extraction periods.

At 300 bar, final yield is about 83.2% of initial oil content after 260 minutes whereas 77.64% of the initial oil content is extracted within first 170 minutes of the experiment. The mathematical model proposed by Sovova (1994) supports the experimental data of intermediate pressure (300

bar) very well with the average relative error of 5.47%. It can be concluded that operating pressure at 300 bar is appropriate to maximize the yield because at pressures higher than 300 bar, the adverse effect of pressure becomes dominant and yield is reduced. Similar value of operating pressure is obtained through Design of experiment study mentioned in section 6.5.1.3.
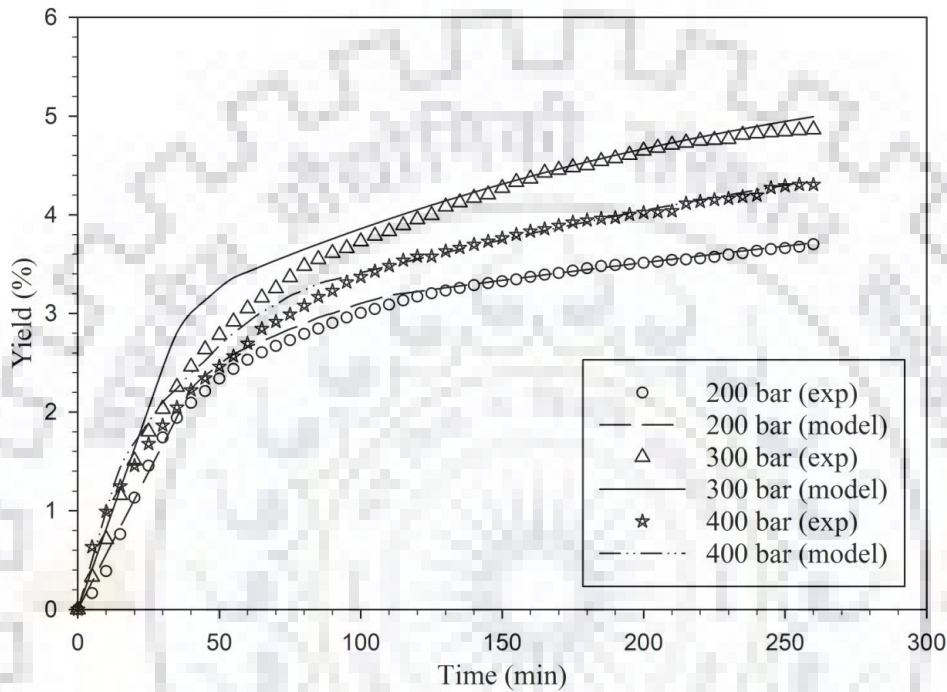
Fig. 6.37 Effect of pressure on oil yield of turmeric root at 50 °C, 10 g/min, 0.45 mm and 7.5%.

Table 6.21 Solvent and solid phase mass transfer coefficients at different pressures (50 °C, 10 g/min, 0.45 mm and 7.5 %).

P (bar)	y_r (g oil/g CO_2)	ρ_f (kg/m^3)	x_k (g/g)	$k_s a_0$ (s^{-1})	$k_f a_0$ (s^{-1})	AARD (%)
200	0.013	805	0.03	1.08×10^{-5}	5.17×10^{-4}	4.22
300	0.02	850	0.03	3.67×10^{-5}	4.67×10^{-4}	5.47
400	0.007	920	0.031	2.17×10^{-5}	1.51×10^{-3}	3.48

Temperature effect on yield of turmeric root

Effect of temperature on oil yield (g oil/g feed) of turmeric root is investigated using three different temperatures values i.e. 40, 50 and 60 °C and shown in Fig. 6.38. Other operating parameters such as pressure, solvent flow rate, particle size and addition of co-solvent are considered constant at 300 bar, 10 g/min, 0.45 mm and 7.5% solvent flow rate, respectively.

Following facts are observed from Fig. 6.38:

1. As temperature rises, oil yield (g oil/g feed) of turmeric root increases.

2. Oil yield and extraction time of initial part of extraction curve are similar for three temperature levels.
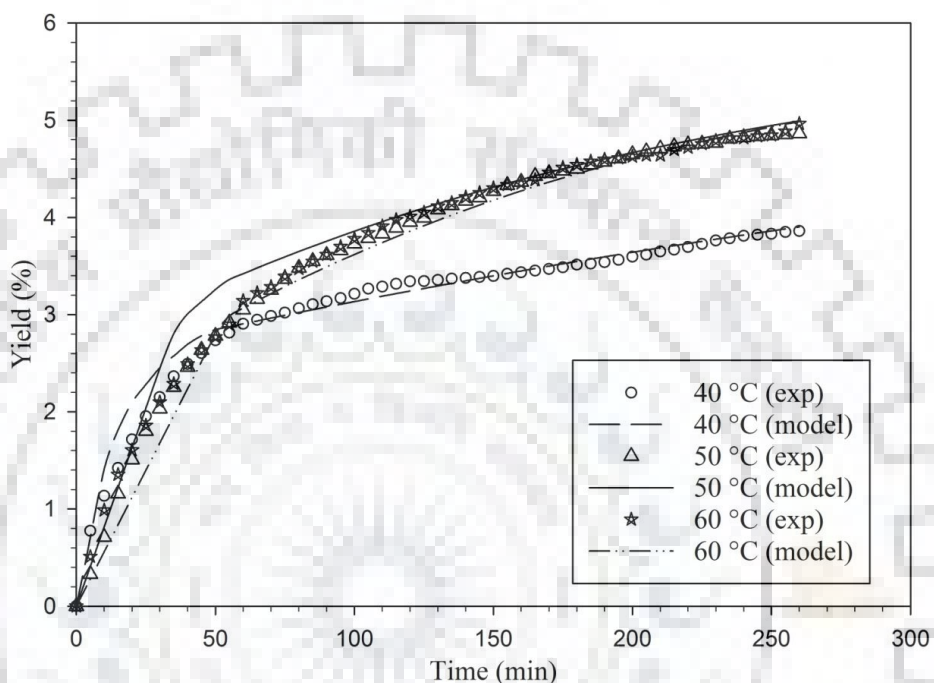
Fig. 6.38 Effect of temperature on oil yield of turmeric root at 300 bar, 10 g/min, 0.45 mm and 7.5%.

It is evident from Fig. 6.38 that oil yield of turmeric root is increased with temperature and probable reason can be an increase in solubility due to increase in volatility of solute (Mukhopadhyay, 2000). Solubility is a key factor in SFE process because higher solubility of solute in solvent results the higher dissolution of solute in solvent. Extraction of solute due to solubility is represented through the initial part of extraction curve, which is termed as "fast extraction period" (Sovova, 1994). An isobaric increase in temperature leads to decrease in density of solvent and consequently decrease in solubility (Mukhopadhyay, 2000; Salgin et al., 2006). However, increase in temperature is also responsible for increase in volatility of solute and hence, solubility increases (Mukhopadhyay, 2000). Increase in solubility values at different temperatures as reported in Table 6.22. Therefore, it can be stated that the volatility effect is more

pronounced than the density effect when temperature is increased from 40 to 60 °C for SFE of turmeric root.

Mass transfer coefficients are responsible for the transition and constant extraction period of extraction curves. Mass transfer coefficients (solvent and solid phase) as well as mass transfer rate of solute to bulk liquid phase are increased with increasing temperature due to high diffusivity of oil in solvent (Rai et al., 2015) as reported in Table 6.22. The $k_f a_0$ values for three different temperatures are comparatively larger in magnitude than $k_s a_0$. Solvent phase mass transfer becomes active when mass transfer rate is controlled by diffusion of easily accessible solute (intra-particle diffusion) into solvent whereas, $k_s a_0$ is responsible for the diffusion of solute from interior of solid matrix (Rai et al., 2016; Sovova et al., 1995). In the present work, $k_f a_0$ values are decreasing with increasing temperature, which increase solvent phase mass transfer coefficients. However, $k_s a_0$ values are increasing with temperature providing the oil yield greater at higher temperature. As can be seen from Fig. 6.38, higher oil yield is available at 60 °C, which depicts that mass transfer rate is controlled by solid phase mass transfer coefficient for the SFE of turmeric oil.

Similar to effect of pressure on oil yield of turmeric oil as discussed in section 6.6.3.1, fast extraction period (initial part of extraction curve) is equal for different temperatures such as 40, 50 and 60 °C. This period ends at 50 min and shows 2.85 wt% of oil yield due to equal amount of easily accessible oil content for all temperature levels as given in Table 6.22. Solubility at 40 °C is far lesser than that at 50 and 60 °C as shown in Table 6.22, which should lead to the lesser oil yield in fast extraction period for 40 °C. However, greater value of $k_f a_0$ at 40 °C compensates the solubility effect and consequently, increases the oil yield.

Table 6.22 Solvent and solid phase mass transfer coefficients at different temperatures (300 bar, 10 g/min, 0.45 mm and 7.5%).

T (°C)	y_r (g oil/g CO_2)	ρ_f (kg/m^3)	x_k (g/g)	$k_s a_0$ (s^{-1})	$k_f a_0$ (s^{-1})	AARD (%)
40	0.013	910	0.03	1.5×10^{-5}	1.17×10^{-3}	3.74
50	0.02	850	0.03	3.67×10^{-5}	4.67×10^{-4}	5.47
60	0.04	830	0.03	4.14×10^{-5}	1.63×10^{-4}	6.25

Oil yield at 40 °C is 3.86 wt%, approximately 64.83% of initial oil content. However, it does not differ significantly for 50 and 60 °C i.e. 4.8 wt%, which is approximately 83.30% of initial oil

content of turmeric root and 1.3 times of that at 40 °C. It can be seen from Table 6.22 that the magnitude of $k_f a_0$ and $k_s a_0$ for three different temperatures were in well agreement with the yield in fast, transition and constant extraction periods. Mathematical model proposed by Sovova (1994) supported the experimental data of 40, 50 and 60 °C with the average relative error of 3.74, 5.47 and 6.25%, respectively. Therefore, it can be concluded that operating temperature at 50 °C is appropriate to maximize the yield of turmeric oil. However, optimized value of temperature suggested through DOE is 53.72 °C as shown in section 6.5.1.3, which is quite close to that predicted through the model proposed by Sovova (1994).

Solvent flow rate effect on yield of turmeric root

The effect of solvent flow rate on yield of turmeric root is studied using three different flow rates of supercritical CO_2 while keeping other operating parameters constant as shown in Fig. 6.39. Solvent flow rate varies at three different levels i.e. 5, 10 and 15 g/min while pressure, temperature, particle size and addition of co-solvent are fixed at 300 bar, 50 °C, 0.45 mm and 7.5% of solvent flow rate, respectively.

Following facts are observed from Fig. 6.39:

1. Oil yield (g oil/g feed) of turmeric root increases with solvent flow rate.

2. Duration of fast extraction period reduces with increasing solvent flow rate.

It is clear from Fig. 6.39 that oil yield of turmeric root increases with solvent flow rate due to reduction in film thickness around the solid particle (Ozkal et al., 2005b; Rai et al., 2016b). Values of mass transfer coefficients ($k_f a_0$ and $k_s a_0$), shown in Table 6.23, are increasing with solvent flow rate. As solvent flow rate increases, mass transfer resistances decrease and hence, mass transfer rate as well as mass transfer coefficients are increased.

Mechanism of SFE of solute from solid materials can be explained using following steps (Mukhopadhyay, 2000):

(xiii) Diffusion of supercritical fluid inside the solid matrix,

(xiv) Formation of thin liquid film surrounding the solid particle due to transport of solute into outer layer,

(xv) Dissolution of solute in supercritical fluid and transport of solute to the bulk liquid phase by means of convection.

It is clear from step 1 that solvent first penetrates inside the solid pores and if solvent flow rate is increased sufficiently, number of molecules per unit volume of solvent entering to the extractor is increased. Consequently, surface renewal of solid particles occurs more rapidly and

hence, the inter-molecular interaction between solvent and solute is increased. This increment of inter-molecular interaction causes an increase in oil yield at high solvent flow rate.
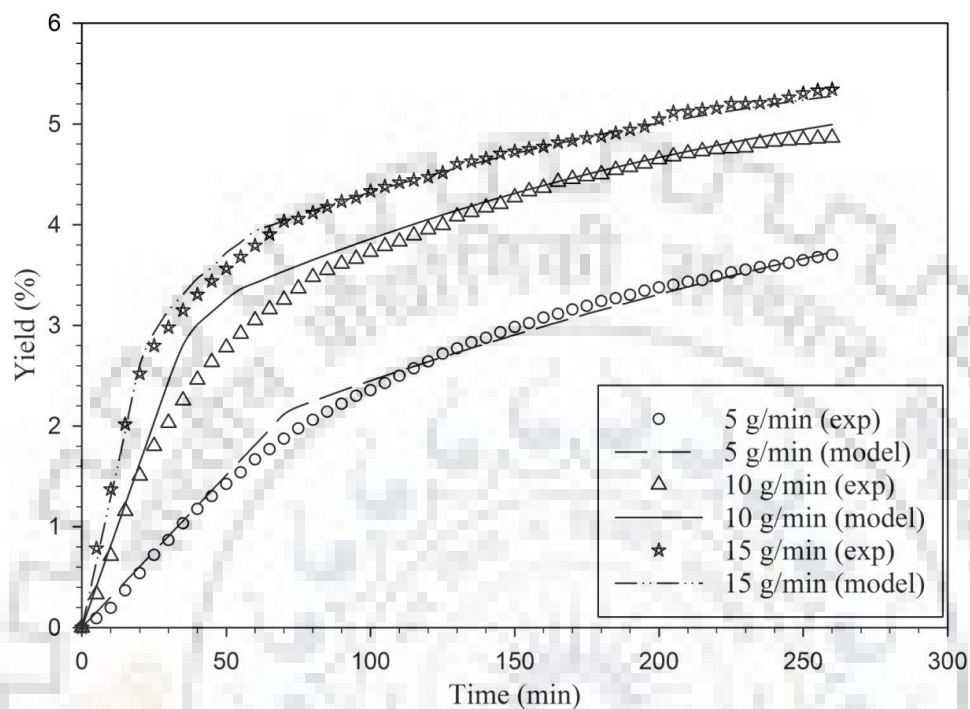
Fig. 6.39 Effect of solvent flow rate on oil yield of turmeric root at 300 bar, 50 °C, 0.45 mm and 7.5%.

It can be seen from Fig. 6.39 that duration of fast extraction period is decreased as flow rate increases from 5 to 15 g/min. However, oil yield in fast extraction period is increased with solvent flow rate. Fast extraction period are 95, 60 and 40 min for 5, 10 and 15 g/min solvent flow rate, respectively, whereas oil yield in fast extraction period are 38.6%, 51.2% and 55.5% of initial oil content, respectively. This behavior may be attributed due to increment in the solubility with increasing solvent flow rate. Similar behavior was also reported by Ozkal et al. (2005) for the SFE of apricot kernel.

The trend of extraction curves in transition period and constant extraction period can be explained through magnitudes of $k_f a_0$ and $k_s a_0$ as reported in Table 6.23. Values of $k_f a_0$ and $k_s a_0$ are increasing rapidly if solvent flow rate is increased from 5 to 10 g/min. As a result, the trend of extraction curve of 10 g/min is also increasing drastically compared to that of 5 g/min. However, extraction curve of 15 g/min is slightly higher than that of 10 g/min, which is supported by the values of $k_f a_0$ and $k_s a_0$ for 10 and 15 g/min also. These values for 15 g/min are slightly higher than that of 10 g/min as found in Table 6.23.

194

Final oil yield for 5, 10 and 15 g/min were 62.1%, 81.7% and 89.74% of initial oil content, respectively. At 10 and 15 g/min of solvent flow rate, oil yield of turmeric oil does not differ significantly, which is around 1.3 and 1.4 times of oil yield at 5 g/min, respectively. The AARD values of all three flow rate levels are 6.135%, 5.47% and 1.72% as reported in Table 6.23, which shows that fitting of experimental data for 15 g/min fits well with the model proposed by Sovova (1994). Therefore, solvent flow rate of 15 g/min can be taken as optimum solvent flow rate corresponding to maximum oil yield, which is in well agreement to that predicted through DOE as reported in section 6.5.1.3 i.e. 13.6 g/min.

Table 6.23 Solvent and solid phase mass transfer coefficients at different flow rate (300 bar, 50 °C, 0.45 mm and 7.5%).

FR (g/min)	y_r (g oil/g CO_2)	ρ_f (kg/m^3)	x_k (g/g)	$k_s a_0$ (s^{-1})	$k_f a_0$ (s^{-1})	AARD (%)
5	0.015	850	0.038	2.17×10^{-5}	1.15×10^{-4}	6.13
10	0.02	850	0.03	3.67×10^{-5}	4.67×10^{-4}	5.47
15	0.03	850	0.024	4.16×10^{-5}	4.97×10^{-4}	1.72

Particle size effect on yield of turmeric root

The effect of particle size on oil yield of turmeric root is shown in Fig. 6.40, which is investigated using three different values of particle size, i.e. 0.2, 0.45 and 0.73 mm. For such investigation pressure, temperature, flow rate and addition of co-solvent values are constant at 300 bar, 50 °C, 10 g/min and 7.5% of solvent flow rate, respectively.

Following facts are observed from Fig. 6.40:

1. As particle size of solid feed decreases, oil yield (g oil/g feed) of turmeric root is increased and then decreased.

2. Oil yield of fast extraction period for 0.45 mm particle size is higher while duration is almost same.

It is depicted from Fig. 6.40 that the oil yield of turmeric root is increasing when particle size is decreased from 0.73 mm to 0.45 mm. However, further reduction in particle size leads to a decrease in oil yield also. It is reported by various researchers that large particles of solid materials are broken into smaller one through milling and hence, intra-particle diffusion resistance is reduced due to shorter diffusion path (Gopalan et al., 2000). Intact cells are ruptured by means of milling and ratio of broken to intact cells is increased. Consequently, more oil molecules are released for

extraction (Ozkal et al., 2005b). Oil yield of larger particle size (0.73 mm) is far lesser than that of 0.45 mm as oil is not easily transported from inside of intact cells. Particle size of solid material should be sufficiently small so that the oil can be rapidly transported from solid matrix to the bulk solvent phase (Goto et al., 1996; Mukhopadhyay, 2000). However, this trend is reversed, if particle size is further reduced to 0.2 mm as can be seen from Fig. 6.40. If the particle size is too small, fluid channeling may occur inside the fixed bed resulting in inhomogeneous extraction. Re-adsorption of solute on the matrix surfaces can occur, which hinders the extraction (Liu et al., 2011). Similar trend was also observed by Liu et al. (2011) for the SFE of *Maydis stigma*. Therefore, particle size for SFE of turmeric root should be sufficiently small but precisely, not too small.
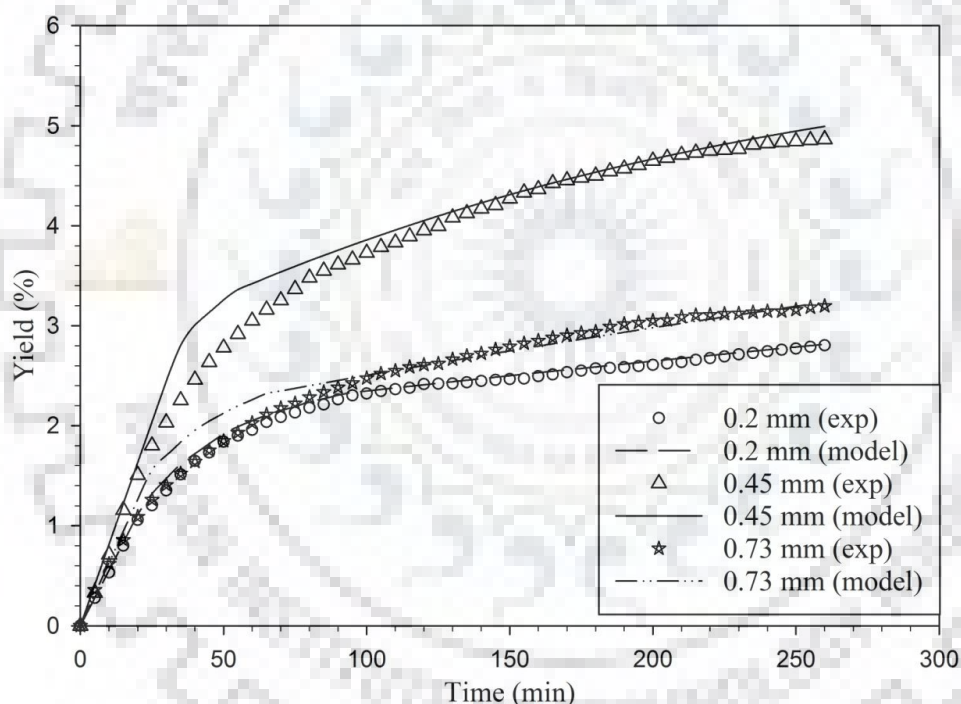
Fig. 6.40 Effect of particle size on oil yield of turmeric root at 300 bar, 50 °C, 10 g/min and 7.5%.

Smaller particle size offers reduced mass transfer resistances and increased surface area for extraction of oil. The $k_f a_0$ and $k_s a_0$ values for three different particle sizes are reported in Table 6.24. It shows that $k_s a_0$ for 0.45 mm is considerably large (3.67×10^{-5} s^{-1}) than that of any other size while, $k_s a_0$ is responsible for the diffusion of inaccessible oil from the inside of matrix (Ozkal et al., 2005). Larger value of $k_s a_0$ for 0.45 mm shows that solvent is able to penetrate inside the solid matrix and

196

hence, unreleased oil of turmeric root can be extracted. Similarly, k_fa_0 is increasing with decreasing particle size from 0.73 to 0.45 mm. However, it is decreasing with further decrease in particle size from 0.45 mm to 0.2 mm, which depict that released oil (through milling) is extracted completely. Duration of fast extraction period for all three particle sizes is almost similar i.e. 60 min while oil yield for 0.45 mm is higher in comparison to 0.2 and 0.73 mm. It can be explained through the magnitude of x_k parameter as shown in Table 6.24. For 0.45 mm, it is 0.03, which is greater than these values for other particle sizes and gives an oil yield as 51.2% of initial oil content. However, oil yield in fast extraction period for 0.2 and 0.73 mm is around 34% of initial oil content because x_k is same for both particle sizes. Final oil yield for 0.2, 0.45 and 0.73 mm was 47.07%, 81.71% and 53.71%, respectively where final oil yield of 0.45 mm is 1.73 and 1.5 times than that of 0.2 and 0.73 mm, respectively, particle size. In case of fitting of experimental data with the model proposed by Sovova (1994), experimental data of 0.2 mm is fitted well with AARD of 2.17%, which is very less. However, AARD of 0.45 mm is larger in comparison to other sizes i.e. 5.47%, which is acceptable. Therefore, particle size of 0.45 mm is recommended as optimum value to maximize oil yield. This can also be suggested that to maximize oil yield, particle size should be neither too small nor too large. Optimum value for particle size obtained through DOE is 0.54 mm as reported in section 6.5.1.3 which is in well support to that obtained through the fitting of model proposed by Sovova (1994).

Table 6.24 Solvent and solid phase mass transfer coefficients at different particle size (300 bar, 50 °C, 10 g/min and 7.5%).

PS (mm)	y_r (g oil/g CO_2)	ρ_f (kg/m^3)	x_k (g/g)	k_sa_0 (s^{-1})	k_fa_0 (s^{-1})	AARD (%)
0.2	0.02	850	0.02	5.83×10^{-6}	3.17×10^{-4}	2.17
0.45	0.02	850	0.03	3.67×10^{-5}	4.67×10^{-4}	5.47
0.73	0.02	850	0.02	1.25×10^{-5}	4.17×10^{-4}	5.04

Co-solvent effect on yield of turmeric root

To study the effect of addition of co-solvent i.e. ethanol on yield of turmeric root, three different concentrations of co-solvent are used i.e. 0, 7.5% and 15% of solvent flow rate. Pressure, temperature, solvent flow rate and particle size are fixed at 300 bar, 50 °C, 10 g/min and 0.45 mm. Fig. 6.41 depicts the extraction curve for three different concentrations of co-solvent through which

following fact is observed: Oil yield (g oil/g feed) of turmeric root first increases and then decreases while increasing the addition of co-solvent.

Co-solvent is mixed with solvent to increase the polarity and solvent strength while, sensitiveness of solubility towards pressure and temperature remains unaltered (Mukhopadhyay, 2000).

It can be observed from Fig. 6.41 that oil yield of turmeric root increases by 12% when co-solvent is added with a concentration of 7.5% of solvent flow rate. However, further increase in concentration of co-solvent to 15% reduces oil yield. The plausible reason could be the excessive polarity of solvent due to addition of excess amount of co-solvent (Liu et al., 2011). Co-solvent is soluble in solvent up to an extent and this limitation may increase the mass transfer resistance and hence, oil yield is decreased (Liu et al., 2011).

Solubility at different concentrations of co-solvent is mentioned in Table 6.25, which shows that solubility of 7.5% co-solvent is highest and thus, maximum oil yield is found at this concentration. Similar behavior was observed by Guindani et al. (2016) and Lin et al. (2015) for the SFE of *Schisandra chinensis* seed and Chia seed, respectively.
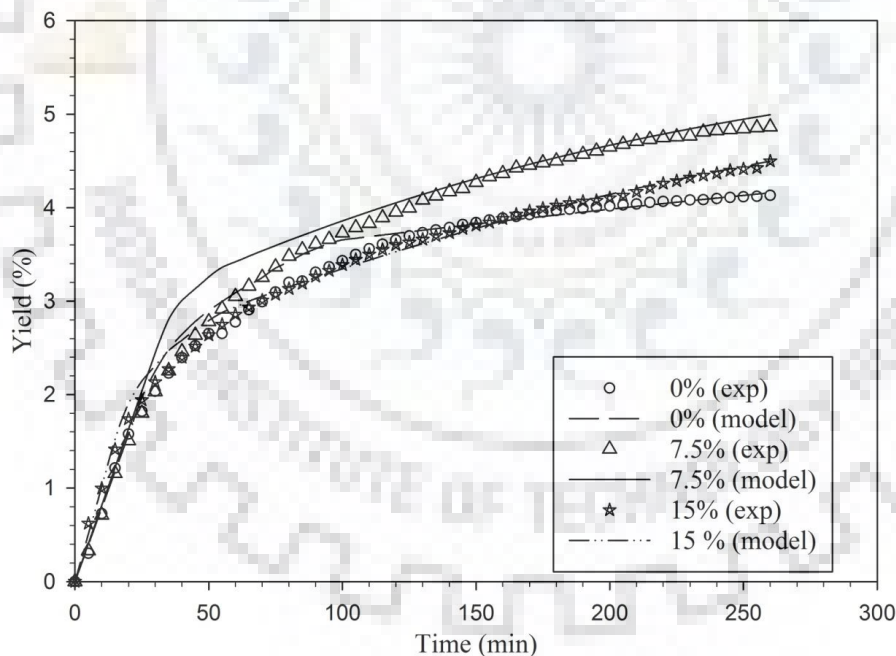
Fig. 6.41 Effect of co-solvent on oil yield of turmeric root at 300 bar, 50 °C, 10 g/min and 0.45 mm.

Mass transfer coefficients for all three different concentrations of co-solvent are given in Table 6.25 and show that value of $k_f a_0$ increases when co-solvent is added to the solvent. The $k_f a_0$ value is responsible for transition period of extraction, which shows the extraction of accessible (through

milling) oil. Higher value of $k_f a_0$ for 15% co-solvent indicates that solvent phase mass transfer resistance is decreased due to higher concentration of co-solvent. However, value of $k_s a_0$ for 7.5% co-solvent is higher than that for other concentrations reported in Table 6.25, which promotes the extraction of polar compounds from inside the solid particles. The value of $k_s a_0$ for 15% co-solvent is 2.73×10^{-5} s^{-1} which is lesser than 7.5% co-solvent i.e. 3.67×10^{-5} s^{-1} however, higher than 0% co-solvent i.e. 1.17×10^{-5} s^{-1}. Therefore, combined effect of $k_f a_0$ and $k_f a_0$ increases the yield when 7.5% co-solvent is added. The main aspect of adding co-solvent is the reduction of the thickness of the boundary layer for mass transfer (Lin et al., 2015). It is clear from the values of $k_f a_0$ and $k_s a_0$ that oil yield is increasing in transition and constant extraction periods with the addition of 7.5% co-solvent. From above discussion, it can be concluded that higher concentration of co-solvent does not mean high oil yield though only a little amount of co-solvent is enough for extraction.

Final oil yield at different co-solvent concentrations i.e. 0%, 7.5% and 15% of solvent flow rate are 69.37%, 81.7% and 75.5% of initial oil content, respectively. Therefore, co-solvent concentration of 7.5% of solvent flow rate can be considered as optimized value for maximum oil yield and its experimental data is fitted well in the model proposed by Sovova (1994) with AARD value of 5.47%. In section 6.5.1.3, optimized concentration of co-solvent is predicted as 7.85%, which is in well agreement with the co-solvent concentration obtained through model fitting.

Table 6.25 Solvent and solid phase mass transfer coefficients at different amount of co-solvent (300 bar, 50 °C, 10 g/min and 0.45 mm).

CS(%)	y_r (g oil/g CO_2)	ρ_f (kg/m³)	x_k (g/g)	$k_s a_0$ (s^{-1})	$k_f a_0$ (s^{-1})	AARD (%)
0	0.015	850	0.025	1.17×10^{-5}	4.5×10^{-4}	4.26
7.5	0.02	850	0.03	3.67×10^{-5}	4.67×10^{-4}	5.47
15	0.016	850	0.034	2.73×10^{-5}	5.83×10^{-4}	2.45

Selection of suitable model/s for the SFE of turmeric oil

The parametric study on the SFE of turmeric oil is investigated through the fitting of experimental data in the model proposed by Sovova (1994). Based on this study, optimum values for five operating parameters are obtained as 300 bar, 60 °C, 15 g/min, 0.45 mm and 7.5% of solvent flow rate. Optimized oil yield of turmeric root is found as 5.56 wt % at these optimum values.

In this section, experimental data of turmeric oil at these optimum values are fitted in models proposed by different researchers such as Nobre et al. (2006), Reverchon (1996), Reverchon et al.

(2000), Reverchon and Marrone (1997), Reverchon and Poletto (1996), Goto et al. (1996), Sovova (1994), Vargas et al. (2006) to investigate the most suitable model. Experimental extraction curve is compared with the predicted curves of different models as shown in Fig. 6.42 where tuning parameters of each model are reported in Table 6.26. It is depicted from Fig. 6.42 that the models proposed by Sovova (1994) and Goto et al. (1996) are fitted well with the experimental data as AARD values are 3.4% and 5.87%, respectively, as shown in Table 6.26. Other models do not fit the experimental data properly as can be seen from Fig. 6.42 and AARD values reported in Table 6.26. Models proposed by Reverchon et al. (2000) and Reverchon and Marrone (1997) provide similar oil yield and trend of extraction curves are somewhat following the experimental curve pattern. However, AARD for both models are 15.69% and 9.02%, respectively, which is quite high for acceptable fitting of model. Further, final oil yields predicted through models Vargas et al. (2006), Nobre et al. (2006) and Reverchon (1996) are same as experimental one. However, trends of experimental curves differ drastically as AARD values are vey large due to poor fitting.
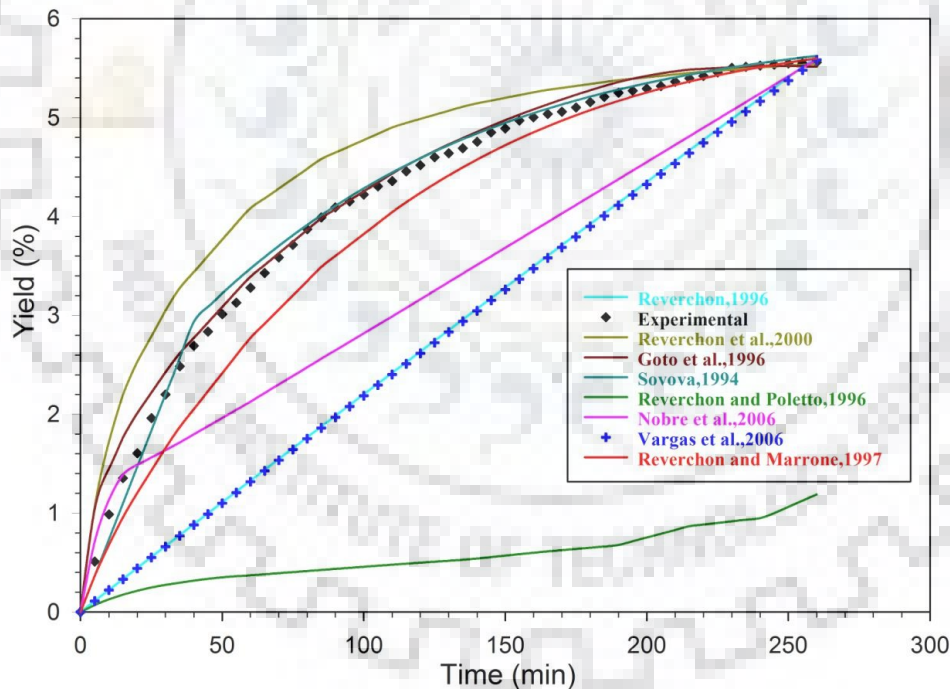
Fig. 6.42 Comparison of different model/s for the SFE of turmeric oil.

As can be seen from Fig. 6.42, the model proposed by Reverchon and Poletto (1996) does not fit the experimental data at all, which gives AARD of 86.87%. Reverchon (1996) and Reverchon et al. (2000) proposed the model equations with negligible external mass transfer resistance. Vargas

et al. (2006) used the model proposed by Reverchon (1996) with modified geometry. Sovova (1994) and Goto et al. (1996) assumed that external mass transfer resistance exists during extraction of solute. However, Reverchon and Marrone (1997) and Nobre et al. (2006) modeled the mass balance eaquation considering external mass transfer resistance. The model proposed by Nobre et al. (2006) considers fluid phase solute concentration to be zero at the entrance of extractor, which must be a reason behind poor fitting of model as this assumption is not followed in the SFE of turmeric oil. Therefore, it can be concluded that models proposed by Sovova (1994) and Goto et al. (1996) are found as suitable models to simulate the SFE of turmeric root. Further, in section 6.6.2.9, the model proposed by Sovova (1994) and Goto et al. (1996) are found best suitable models for the solute matrix, which contains oil inside the cells and layers. SEM images of turmeric root reveals that oil is enclosed inside the cells and layers as discussed in section 6.1.4 and thus, Sovova (1994) and Goto et al. (1996) models are also found suitable for turmeric root.

Table 6.26 Tuning parameters of different models for SFE of turmeric oil.

Model	Parameter	Values	AARD (%)
Reverchon (1996)	A_pK (m^3/s)	1.09×10^{-9}	38.38
	k_p	2.5	
Reverchon and Poletto (1996)	x_{ti} (g/g)	0.02	86.87
	y_i (g/g)	0.02	
	A_ph_0 (1/s)	8.01×10^{-4}	
Reverchon and Marrone (1997)	k_e (m/s)	2.5×10^{-8}	9.02
	K	0.6	
Reverchon et al. (2000)	K_{io} (m/s)	1.51×10^{-7}	15.69
	y_f (g/g)	0.06	
	k_{eq}	0.1	
Vargas et al. (2006)	A_pK (m^3/s)	1.09×10^{-9}	38.76
	k_p	1.8	
Nobre et al. (2006)	A_pk_f (1/s)	1.1×10^{-3}	22.15
	y^*	0.02	
Sovova (1994)	k_fa_0 (1/s)	4.3×10^{-3}	3.4
	k_sa_0 (1/s)	7.47×10^{-5}	
	x_k (g/g)	0.03	
Goto et al. (1996)	D_e (m^2/s)	1.36×10^{-7}	5.87
	C_{sat} (g/g)	0.013	
	k_f (m/s)	9.07×10^{-5}	
	D_L (m^2/s)	1.35×10^{-6}	

6.6.3.2 Raw material-II: Carrot seed

In this section, experimental data of carrot seed are fitted in the model proposed by Sovova (1994) and effects of various operating parameters on the extraction yield are studied.

Pressure effect on yield of carrot seed

To investigate pressure effect on the oil yield of carrot seed, three different pressure values are used i.e. 200, 300 and 400 bar. Other operating parameters such as temperature, solvent flow rate and addition of co-solvent are considered constant at 60 °C, 10 g/min and 5% of solvent flow rate. Extraction curves at three different pressures are compared to study the effect of pressure on yield of carrot seed and given in Fig. 6.43. It shows that

  1.Oil yield (g oil/g feed) of carrot seed increases with pressure.

  2.At 400 bar, extraction of carrot seed oil is almost completed.

It is depicted from Fig. 6.43 that oil yield of carrot seed is increasing with pressure and hence, maximum yield is found at 400 bar. Isothermal increase in yield with pressure can be explained through enhanced salvation power of solvent due to increase in solvent density. Density and solubility for 200, 300 & 400 bar are 790, 830 & 900 kg/m^3 and 0.015, 0.03 & 0.035 g oil/g CO_2, respectively, as reported in Table 6.27. At elevated pressure (400 bar), high solvent density as well as high solubility results a maximum oil yield of carrot seed. Oil yield at 400 bar is 94.9% of initial oil content, which is around 1.76 and 1.41 times of yield obtained at 200 and 300 bar, respectively.
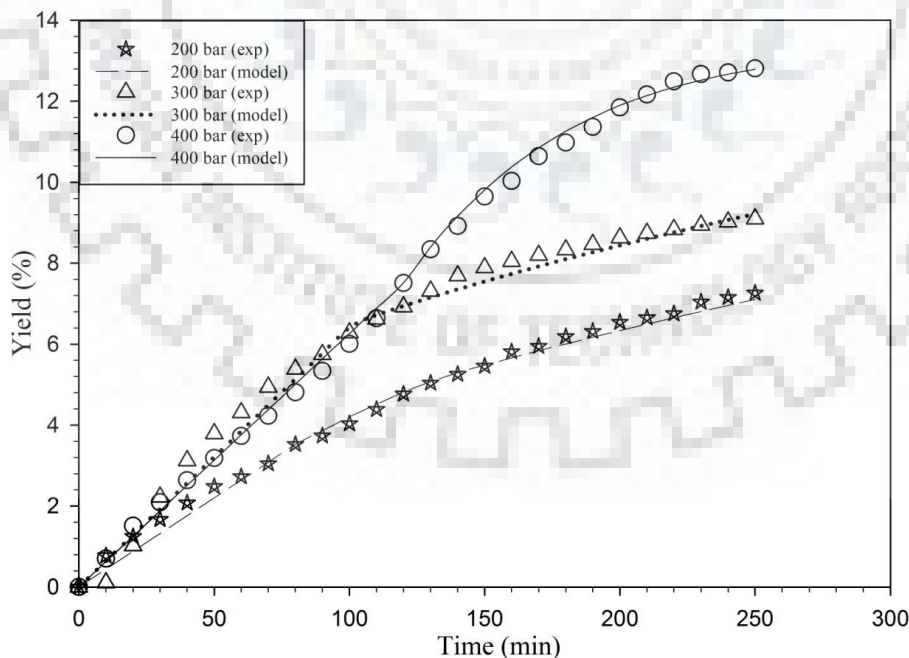
Fig. 6.43 Effect of pressure on oil yield of carrot seed at 60 °C, 10 g/min and 5%.

Duration of fast extraction period for 200 bar is 130 min, which decreases with increasing pressure as it is 90 min for 300 bar as well as for 400 bar. During fast extraction period, extraction curves of 300 and 400 bar are overlapping to each other due to almost equal magnitude of easily accessible oil content (x_k) for both the pressure levels. Although, easily accessible oil content at 200 bar is comparatively larger i.e. 0.089 g oil/g solid, lower oil yield is obtained in fast extraction period due to low solubility at 200 bar.

The value of $k_f a_0$ for 200, 300 and 400 bar are 1.85×10^{-4}, 1.1×10^{-4} and 9.9×10^{-5} s^{-1}, respectively, which show that solvent phase mass transfer resistance is higher for 400 bar. The probable reason can be the solute-solvent repulsion from the highly compressed CO_2 which causes high mass transfer resistance to the extraction of solute (Liu et al., 2009; Sodeifian et al., 2016a). However, reduction in oil yield due to $k_f a_0$ is compensated by $k_s a_0$ as high pressure reduces the solid phase mass transfer resistance. The $k_s a_0$ values for 200, 300 and 400 bar are 1.17×10^{-5}, 1.68×10^{-5} and 8.17×10^{-5} s^{-1}, respectively, which show that high value of $k_s a_0$ results low solid phase mass transfer resistance for 400 bar. High pressure allows the extraction of non-accessible oil from inside the solid matrix due to reduced solid phase mass transfer resistance. Hence, carrot seed is almost exhausted as major amount of oil is extracted. In fast extraction period (90 min), 39.57% of initial oil content is extracted whereas, rest 54.39% of initial oil content is extracted in next 160 min for 400 bar. It can be observed that solid phase mass transfer coefficient governs the extraction of oil from carrot seed at high pressure. Experimental data of all three pressure levels are fitted in the model proposed by Sovova (1994) and AARD of 400 bar is feasible i.e. 3.39% as shown in Table 6.27. To extract maximum carrot seed oil, 400 bar is predicted as optimum value through simulation as well as through DOE, which is discussed in section 6.5.2.4.

Table 6.27 Solvent and solid phase mass transfer coefficients at different pressures (60 °C, 10 g/min and 5%).

P (bar)	y_r (g oil/g CO_2)	ρ_f (kg/m^3)	x_k (g/g)	$k_s a_0$ (s^{-1})	$k_f a_0$ (s^{-1})	AARD (%)
200	0.015	790	0.089	1.17×10^{-5}	1.85×10^{-4}	6.48
300	0.03	830	0.07	1.68×10^{-5}	1.1×10^{-4}	4.82
400	0.035	900	0.07	8.17×10^{-5}	9.9×10^{-5}	3.39

Temperature effect on yield of carrot seed

To study the temperature effect on the oil yield of carrot seed, three different temperature levels are considered i.e. 50, 60 and 70 °C. Other operating parameters i.e. pressure, solvent flow rate and co-solvent remain constant at 300 bar, 10 g/min and 5% of solvent flow rate, respectively. Extraction curves of all three-temperature levels are compared in Fig. 6.44 to investigate the effect of temperature on oil yield of carrot seed.

Following observations are drawn from Fig. 6.44:

1. As temperature increases from 50 to 70 °C, oil yield (g oil/g feed) of carrot seed is also increased.

2. Final oil yield of carrot seed is equal for temperature of 50 and 60 °C.

Solubility is directly proportional to the vapor pressure and density so, increase in both the terms increases the solubility and vice-versa. An increase in temperature shows positive effect on vapor pressure and negative effect on density and hence, temperature affects the solubility in the similar manner. As can be noticed from Table 6.28, solvent density decreases from 890 to 810 kg/m^3 with increasing temperature from 50 to 70 °C. Solubility is also decreasing with density for 50 to 70 °C. It can be identified that density effect is dominating from 50 and 70 °C. Similarly, x_k first decreases from 50 to 60 °C and then increases up to 70 °C as reported in Table 6.28.

Duration of fast extraction period for 60 and 70 °C is almost same (90 min) whereas, it increases for 50 °C (200 min) due to extraction of easily accessible oil content (0.08 g oil/g feed) only. Oil yield of fast extraction period for 50 °C is the final oil yield as extraction is limited to fast extraction period only. For 50, 60 and 70 °C, oil yield are 80.2%, 62.8% and 85.6%, respectively, in fast extraction period, which are in the well accordance with the easily accessible oil content at respective temperature levels as reported in Table 6.28.

Values of $k_f a_0$ for 50, 60 and 70 °C are 9.26×10^{-5}, 1.1×10^{-4} and 5.35×10^{-4} s^{-1}, respectively, which show high mass transfer rate as well as high yield at 70 °C followed by 60 °C and 50 °C. In transition period, mass transfer rate is governed by convective transport as well as intra-particle diffusion. The $k_s a_0$ for 50, 60 and 70 °C are 2.0×10^{-5}, 1.68×10^{-5} and 4.5×10^{-5} s^{-1}, respectively, which support the trend shown by extraction curves in Fig. 6.44. According to the magnitude of $k_s a_0$, solid phase mass transfer resistance is higher at 60 °C in comparison that at 50 and 70 °C. Hence, lowest oil yield is obtained at 60 °C in constant extraction period, which is governed by intra-particle diffusion only. Due to larger values of $k_f a_0$ and $k_s a_0$, highest yield is obtained at 70 °C for all three extraction period in total extraction time of 250 min.
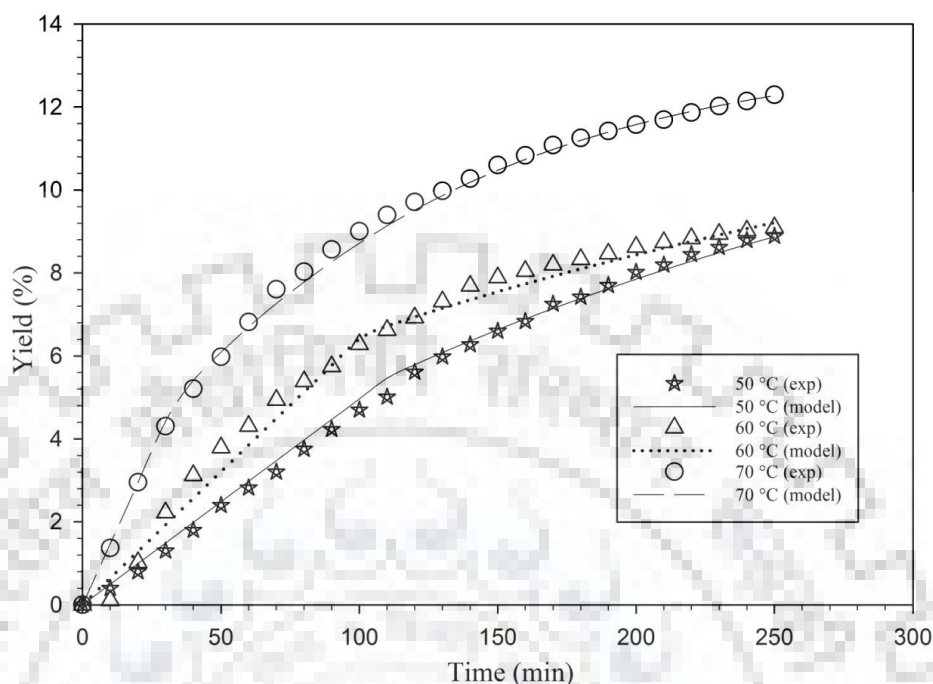
Fig. 6.44 Effect of temperature on oil yield of carrot seed at 300 bar, 10 g/min and 5%.

Final oil yield of carrot seed at 50, 60 and 70 °C are 65.8, 67.39 and 91.06% of initial oil content, respectively, in extraction time of 250 min. Experimental data of all three different temperature levels are fitted well with the model proposed by Sovova (1994) and AARD values are shown in Table 6.28, which is minimum i.e. 1.74% for 70 °C. Therefore, it can be concluded that highest temperature i.e. 70 °C is suitable for maximum oil yield from carrot seed. Similar value of optimum temperature is predicted through DOE also as discussed in section 6.5.2.4.

Table 6.28 Solvent and solid phase mass transfer coefficients at different temperatures (300 bar, 10 g/min and 5%).

T (°C)	y_r (g oil/g CO_2)	ρ_f (kg/m^3)	x_k (g/g)	$k_s a_0$ (s^{-1})	$k_f a_0$ (s^{-1})	AARD (%)
50	0.035	890	0.08	2.0×10^{-5}	9.26×10^{-5}	5.43
60	0.03	830	0.07	1.68×10^{-5}	1.1×10^{-4}	4.82
70	0.017	810	0.086	4.5×10^{-5}	5.35×10^{-4}	1.74

Solvent flow rate effect on yield of carrot seed

Solvent flow rate effect on the yield of carrot seed is studied by comparing the extraction curves for three different solvent flow rates while considering other parameters constant. Pressure, temperature and addition of co-solvent are taken constant at 300 bar, 60 °C and 5% of solvent flow rate, respectively. Experimental runs are performed while varying solvent flow rate to three different levels i.e. 5, 10 and 15 g/min and corresponding extraction curves are shown in Fig. 6.45, which indicates that oil yield (g oil/g feed) of carrot seed is first increasing from 5 to 10 g/min and then decreasing at 15 g/min.

It can be seen from Fig. 6.45 that final oil yield of carrot seed is increasing with solvent flow rate from 5 to 10 g/min and reason can be that high solvent flow rate facilitates more molecules of solvent for the interaction with the solute. Increase in solvent flow rate reduces film thickness around the particle due to which mass transfer resistance surrounding the particle becomes smaller and consequently yield is enhanced (Sodeifian et al., 2016a). However, further increase in solvent flow rate up to 15 g/min shows a negative effect on oil yield of carrot seed. A very high solvent flow rate reduces the residence time for solute to get soluble into the solvent, which is also observed by Zaghdoudi et al. (2016) for extracting carotenoids from persimmon fruits.
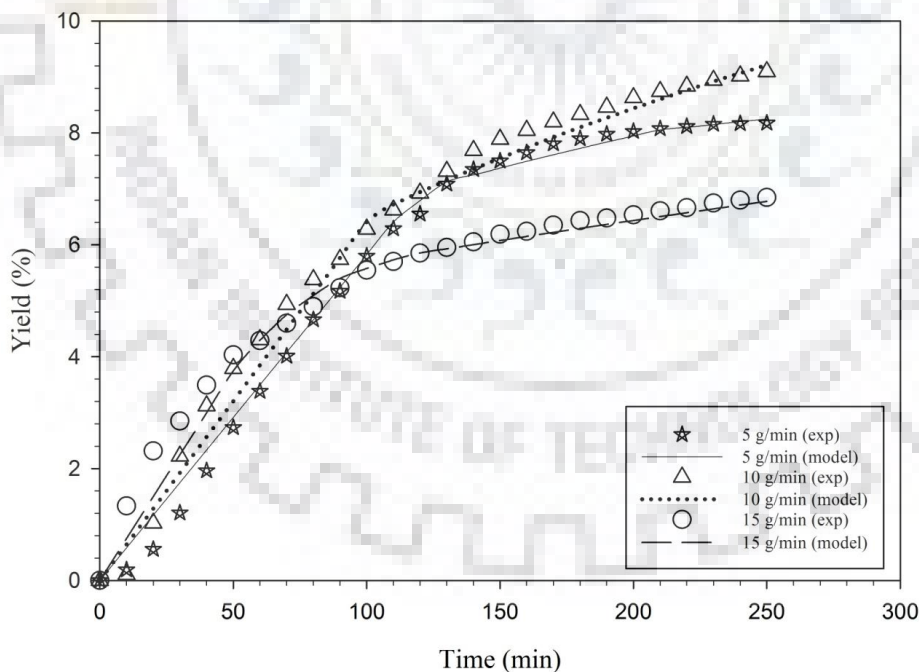
Fig. 6.45 Effect of flow rate on oil yield of carrot seed at 300 bar, 60 °C and 5%.

The values of $k_f a_0$ are 2.5×10^{-4}, 1.1×10^{-4} and 1.02×10^{-4} s^{-1} for solvent flow rate of 5, 10 and 15 g/min, respectively, as shown in Table 6.29. It indicates that solvent phase mass transfer resistance is highest for 15 g/min, which reduces oil yield. The reason can be the less available time for the interaction between solute and solvent.

The $k_s a_0$ are 1.01×10^{-5}, 1.68×10^{-5} and 4.97×10^{-6} s^{-1} for solvent flow rates of 5, 10 and 15 g/min, respectively, and showing the similar pattern as in case of solvent phase mass transfer coefficient. Extraction curves of all three solvent flow rates shown in Fig. 6.45 also support the same fact. The probable reason for increasing yield with solvent flow rate is explained in section 6.6.3.1. However, increase in solvent rate from 10 to 15 g/min leads to a decrease in yield as at high flow rate, penetration of solvent inside the solid matrix is not possible to extract the unreleased oil.

Final oil yield of carrot seed for three different solvent flow rates i.e. 5, 10 and 15 g/min are 60.6%, 67.38% and 50.7% of initial oil content. The model proposed by Sovova (1994) is employed to fit the experimental data of extraction curves with three different flow rates and corresponding AARD values are reported in Table 6.29. Therefore, it is clear from above discussion that solvent flow rate of 10 g/min is appropriate for maximization of oil yield through SFE of carrot seed. This optimum value of temperature is in well accordance with that predicted through DOE in section 6.5.2.4 i.e. 8.53 g/min.

Table 6.29 Solvent and solid phase mass transfer coefficients at different solvent flow rate (300 bar, 60 °C and 5%).

FR (g/min)	y_r (g oil/g CO_2)	ρ_f (kg/m^3)	x_k (g/g)	$k_s a_0$ (s^{-1})	$k_f a_0$ (s^{-1})	AARD (%)
5	0.03	830	0.065	1.01×10^{-5}	2.5×10^{-4}	6.83
10	0.03	830	0.07	1.68×10^{-5}	1.1×10^{-4}	4.82
15	0.03	830	0.065	4.97×10^{-6}	1.02×10^{-4}	6.05

Co-solvent effect on yield of carrot seed

SFE of carrot seed oil is carried out at three different co-solvent concentrations i.e. 0%, 5% and 10% of solvent flow rate to study its effect on yield of carrot seed. However, other operating parameters i.e. pressure, temperature and solvent flow rate are set at 300 bar, 60 °C and 10 g/min, respectively. Extraction curves at three different concentrations of co-solvent are drawn in Fig. 6.46.

Following observations are identified from Fig. 6.46:

1. Oil yield (g oil/g feed) of carrot seed increases with addition of co-solvent.

2. The magnitude of final oil yield of 5% and 10% co-solvent concentration does not differ significantly.

Fig. 6.46 is showing variation in extraction curves with the change in concentration of co-solvent. It is visible from Fig. 6.46 that oil yield of carrot seed is increased by 14.6% when 5% co-solvent is added with pure CO_2 due to enhancement in polarity of solvent, which in turn gives a rise to solubility also. This increment in solubility with addition of co-solvent is noticeable from Table 6.30 as solubility of 5% is increased considerably in comparison to pure CO_2. However, further increase in co-solvent concentration reduces solubility and so, the yield. This can be seen through the trends of extraction curves in fast extraction period: initial part of extraction curve increases from 0 to 5% co-solvent then decreases at 10% co-solvent. The probable reason is explained in section 6.6.3.1. Co-solvent may penetrate the solid matrix, which enhances the polarity as well as the solid-phase oil interaction of supercritical solvent.
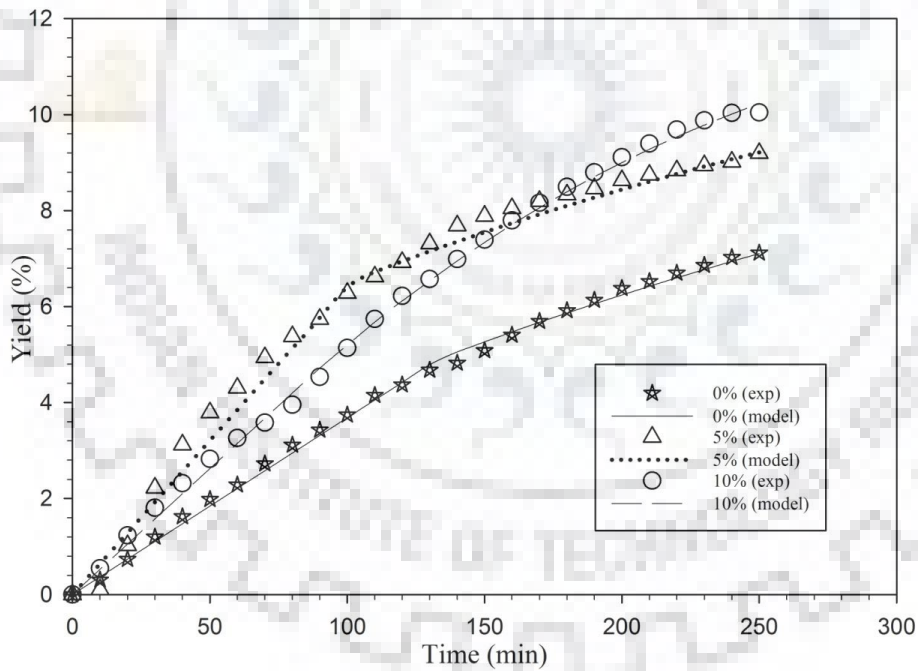
Fig. 6.46 Effect of co-solvent on oil yield of carrot seed at 300 bar, 60 °C and 10 g/min.

The magnitude of $k_f a_0$ and $k_s a_0$, reported in Table 6.30, for all three levels are increasing with addition of co-solvent, which offer less solvent and solid phase mass transfer resistance to the extraction of oil. Similar trends can be observed in extraction curves shown in Fig. 6.46. For 10%

co-solvent, values of $k_f a_0$ and $k_s a_0$ are considerably higher, which increases oil yield as can be observed from Fig. 6.46 also. Therefore, it is evident that high amount of co-solvent facilitates the extraction of polar compounds from inside of solid matrix as can be seen through extraction curve of 10% co-solvent.

Final oil yield of carrot seed are 52.7%, 67.39% and 75.77% of initial oil content for 0%, 5% and 10%, respectively, co-solvent concentrations. The model proposed by Sovova (1994) is used to fit the experimental data of extraction curves for three different co-solvent concentrations and AARD values are reported in Table 6.30. Final oil yield of carrot seed after adding high amount of co-solvent (10%) does not differ much with that at 5% co-solvent addition. Therefore, it can be concluded that 5% co-solvent addition is suitable and appropriate for the extraction of polar compounds. Similar value of co-solvent is also investigated through the prediction based on DOE i.e. 5.87% as discussed in section 6.5.2.4.

Table 6.30 Solvent and solid phase mass transfer coefficients at different co-solvent concentrations (300 bar, 60 °C and 10 g/min).

CS (%)	y_r (g oil/g CO_2)	ρ_f (kg/m^3)	x_k (g/g)	$k_s a_0$ (s^{-1})	$k_f a_0$ (s^{-1})	AARD (%)
0	0.017	830	0.086	1.3×10^{-5}	1.0×10^{-4}	3.64
5	0.03	830	0.07	1.68×10^{-5}	1.1×10^{-4}	4.82
10	0.015	830	0.08	3.17×10^{-5}	2.1×10^{-4}	3.25

Selection of suitable model/s for the SFE of carrot seed oil

To investigate the suitable model/s for the SFE of carrot seed oil, various models discussed in section 6.6.1 are used to simulate the experimental data of carrot seed at optimum parameters. These are 400 bar, 70 °C, 10 g/min and 5% of co-solvent found through parametric study using DOE and model proposed by Sovova (1994) which gives oil yield of 13.8 wt%. The models proposed by Nobre et al. (2006), Reverchon (1996), Reverchon et al. (2000), Reverchon and Marrone (1997), Reverchon and Poletto (1996), Goto et al. (1996), Sovova (1994), Vargas et al. (2006) are employed to fit the experimental data and extraction curves are compared in Fig. 6.47. Tuning parameters of each model as well as AARD values are reported in Table 6.31. Fig. 6.47 depicts that the models proposed by Sovova (1994) and Reverchon and Marrone (1997) are fitted well with the experimental data as AARD values are 3.54% and 3.85%, respectively, as shown in Table 6.31. Other models, shown in Fig. 6.47, do not fit the experimental data properly. Although,

the models proposed by Goto et al. (1996), Vargas et al. (2006), Nobre et al. (2006) and Reverchon (1996) show similar extraction yield as found through experiment. However, trends of extraction curves do not follow that of experiment at all. As discussed in section 6.6.3.6,the model proposed by Reverchon (1996) does not include external mass transfer resistance whereas, Reverchon and Marrone (1997) and Sovova (1994) account this during the extraction of solute. However, Goto et al. (1996) and Nobre et al. (2006) modeled the mass balance eaquation considering external mass transfer resistance. Similar to turmeric oil extraction, predicted extraction curve of Nobre et al. (2006) deviates drastically from the experimental data as AARD value is quite high i.e. 85.01%. They assumed that solvent-phase solute concentration is zero at the entrance of extractor, which may not be applicable for SFE of carrot seed. Similarly, Goto et al. (1996) proposed the model considering axial dispersion in model equations, which might not present in the case of carrot seed and hence, model fitting is poor with high AARD value as shown in Table 6.31.
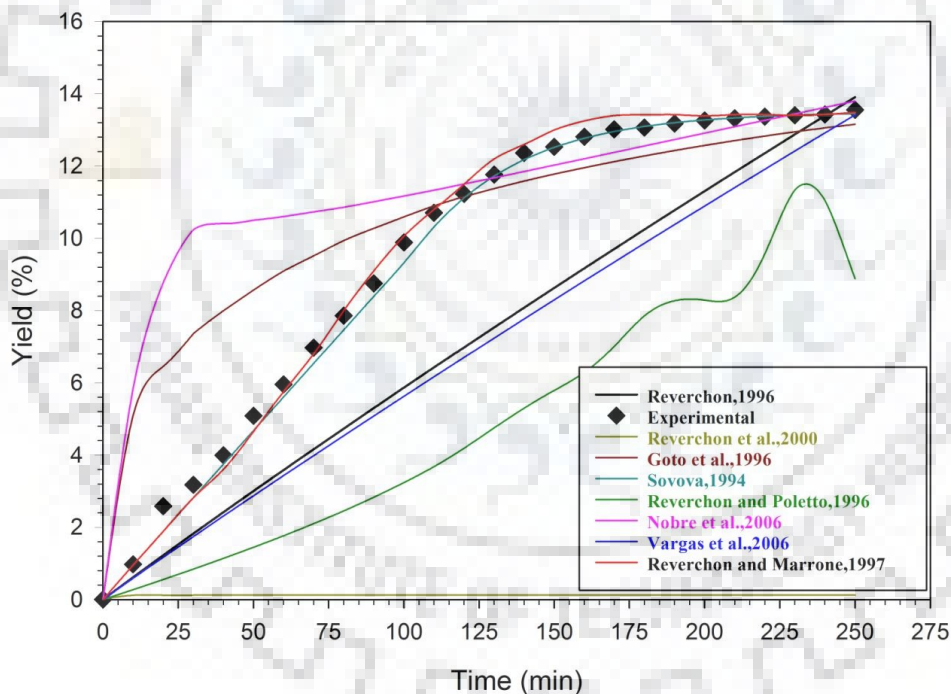
Fig. 6.47 Comparison of different model/s for the SFE of carrot seed oil.

Table 6.31 Tuning parameters of different models for SFE of carrot seed oil.

Model	Parameter	Values	AARD (%)
Reverchon (1996)	A_pK (m^3/s)	$2.03*10^{-9}$	29.31
	k_p	0.37	
Reverchon and Poletto (1996)	x_{ti} (g/g)	0.06	54.88
	y_i (g/g)	0.119	
	A_ph_0 $(1/s)$	$2.01*10^{-5}$	
Reverchon and Marrone (1997)	k_e (m/s)	$2.5*10^{-5}$	3.85
	K	1.6	
Reverchon et al. (2000)	K_{io} (m/s)	$8.95*10^{-5}$	$7.8*10^3$
	y_f (g/g)	0.119	
	k_{eq}	$5.2*10^{-6}$	
Vargas et al. (2006)	A_pK (m^3/s)	$1.95*10^{-9}$	31.88
	k_p	3	
Nobre et al. (2006)	A_pk_f $(1/s)$	$9.3*10^{-4}$	85.01
	$y*$	5	
Sovova (1994)	k_fa_0 $(1/s)$	$6.6*10^{-3}$	3.54
	k_sa_0 $(1/s)$	$9.2*10^{-3}$	
	x_k (g/g)	0.04	
Goto et al. (1996)	D_e (m^2/s)	$5.04*10^{-8}$	$3.85*10^2$
	C_{sat} (g/g)	0.05	
	k_f (m/s)	$1.47*10^{-4}$	
	D_L (m^2/s)	$6.75*10^{-6}$	

Therefore, it can be concluded that models proposed by Sovova (1994) and Reverchon and Marrone (1997) are found as suitable models to simulate the SFE of carrot seed. Similar models are also suggested in the Table 6.20 for the solute matrix, which contains oil inside the broken and intact cavities. It is visible from SEM images of carrot seed that its oil is bound inside the scattered cavities as discussed in section 6.2.4.

6.7   Comparison of Optimum Points

In this section, optimum points of operating parameters predicted through DOE (individual effect study and interaction effect study) and mathematical model (Sovova et al., 1994a) are compared. Optimum values of operating parameters for SFE of turmeric root oil are provided in Table 6.32, which shows that OY does not differ significantly. Operating parameters such as pressure, temperature, solvent flow rate and particle size also show similar values while co-solvent concentration through interaction effect is quite high in comparison to others.

For SFE of carrot seed oil, EOY has maximum value through individual effect prediction as reported in Table 6.32. However, EOY predicted through mathematical modeling is also closer to

that of individual effect while it is less for interaction effects. Optimum values of operating parameters for SFE of carrot seed oil are comparable except operating temperature. It is 70 °C, predicted through individual effects and mathematical modeling while it has optimum value of 60 °C through interaction effects.

Table 6.32 Comparison of optimum points for SFE of turmeric root oil and carrot seed oil.

| Parameters | Turmeric root | | |
	Individual effects	Interaction effects	Mathematical modeling (Sovova,1994)
P (bar)	255	300	300
T (°C)	53.72	50	60
FR (g/min)	13.6	15	15
PS (mm)	0.54	0.45	0.45
CS (%)	7.85	15	7.5
OY	5.5%	5.53%	5.56%
Carrot seed			
P (bar)	400	400	400
T (°C)	70	60	70
FR (g/min)	8.53	10	10
CS (%)	5.87	5	5
EOY	14.23	12.92%	13.8%

Therefore, it can be concluded from Table 6.32 that optimum parameters for turmeric root are 300 bar, 60 °C, 15 g/min, 0.45 mm and 5.56% whereas, for carrot seed, these are 400 bar, 70 °C, 5.53 g/min, and 5.87%.

6.8 Industrial-scale Economic Evaluation of SFE Process

In this section, industrial-scale economic assessment for extraction of turmeric root oil and carrot seed oil using SFE process is presented based on the procedure explained in section 3.9.

6.8.1 Raw material-I: Turmeric root oil

Economic assessment of SFE of turmeric oil at industrial scale is presented for annual production capacity of 60 t. Cost estimation of different factors for the economic evaluation is shown in Table 6.33. Annual cost of equipment is Rs. 2,550 lacs for 800 kg feedstock per experimental run or 1,200t/y, which in turn converts into FCI of Rs. 2,573 lacs per year. It also includes cost of land as Rs. 23 lacs per year as shown in Table 6.33. Rosa and Meireles (2005) reported the cost of equipment as USD 2,000,000 (Rs. 12,98 lacs) for approximately 420 kg of clove bud and 280 kg ginger per run. Equipment cost, found in the present study, is in well accordance with that

provided by Rosa and Meireles (2005). Todd and Baroutian (2017) provided equipment cost as USD 6,537,750 (Rs. 42,420 lacs) for the feedstock of 8,000 t/y. Land requirement for the present plant is 13,000 m^2 where land costs 3,560 Rs./m^2 as per local rates. CRM is computed as Rs. 6,925 lacs per year while adding costs of feedstock, CO_2 and ethanol as provided in Table 6.33. Cost of CO_2 and ethanol is computed based on the used amount as recoveries of CO_2 and ethanol were considered as 80% and 85%, respectively. It was suggested by the supplier of SFE setup i.e. Waters Corporation, Massachusetts, USA and SFE setup with recycle stream is shown in Fig. 6.48. OC is the sum of CRM, CUT and COL, which is found to be Rs. 7,259 lacs per year. COM of the process, computed using equation (3.3), is Rs. 9,724 lacs per year. SC of product (turmeric oil) is estimated to be Rs. 8,850 lacs per year considering market price as 12,500 Rs. per kg and 18% GST. In the present study, OC is less than SC for the production of 60 tonne turmeric oil per year. Hence, SFE process can be considered as profitable method for the extraction of turmeric root oil. Rosa and Meireles (2005), Moncada et al. (2016) and Todd and Baroutian (2017) also suggested the SFE as feasible method considering the feedstock as clove bud and ginger, Oregano and Rosemary and Grape marc.

Table 6.33 Cost indicators for SFE of turmeric root oil.

Particulars	Cost per unit (Rs.)	Quantity used	Annual cost (Rs. per year, in Lacs)
SFE equipment	-	-	2,550.00
Land	3,560 (per m^2)	13,000 (m^2)	23.00
FCI (Approx.)			2,573.00
Turmeric root	80 (per kg)	12,00,000 (kg)	960.00
CO_2	44 (per kg)	6,910,000 (kg)	3,040.00
Ethanol	640 (per L)	4,57,000 (L)	2,925.00
CRM (Approx.)			6,925.00
COL	500 (per labor)	1,800 labor	9.00
CUT	5 (per kWh)	6,500,000 (kW)	325.00
CRM			6,925.00
OC (Approx)			7,259.00
COM(Approx)			9,724.00
Turmeric oil (Approx)	12,500 (per kg)	60,000 (kg)	7,500,.00
SC (18% GST)			8,850.00
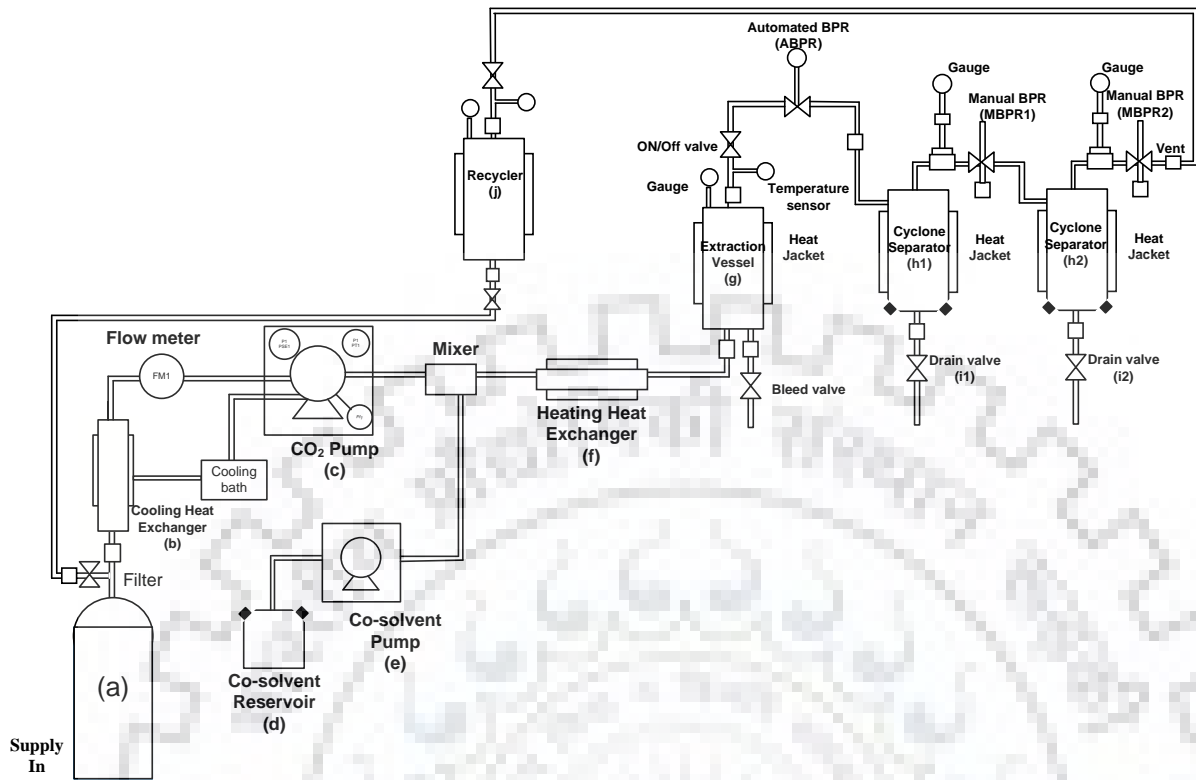
Fig. 6.48 Industrial-scale SFE setup with CO_2 recycler.

6.8.2. Raw material-II: Carrot seed oil

An industrial scale economic assessment for SFE of carrot seed oil is carried out considering four components such as FCI, OC, COM and SC. These are computed for the carrot seed oil production capacity of 120 t/y, which are shown in Table 6.34. To meet the production capacity of carrot seed oil, 560 kg of raw material need to be loaded per experimental run, which in turn can be converted as 850 ton of raw material per year. For this, equipment cost is computed as Rs. 1,791 lacs per year using the procedure explained in section 3.9 while considering 20 years period of service for the plant. Similarly, land requirement to fulfil the production demand is estimated as 9300 m², which results the land cost of Rs. 16 lacs per year at the rate of Rs. 3,560 per m² of land. FCI is computed as Rs. 1,807 lacs per year while adding annual cost of equipment and land. Equipment cost estimated in the present work for carrot seed oil is in well accordance with those provided by Rosa and Meireles (2005), who reported the cost of equipment as USD 2,000,000 (Rs. 12,98 lacs) for approximately 420 kg of clove bud and 280 kg ginger per run. Further, OC is estimated, which is the summation of CRM, CUT and COL whereas; CRM is the summation of cost of feed stock (carrot seed), solvent

214

(CO_2) and co-solvent (ethanol) utilized in the process. Quantities of carrot seed, CO_2 and ethanol, consumed in the process, are 845 t, 4,120 t and 203 kL respectively considering the recycling of CO_2 and ethanol. Cost of carrot seed, CO_2 and ethanol are computed as Rs. 718, 1,813 and 1,299 lacs at the rate 85 Rs. per kg, 44 Rs. per kg and 640 Rs. per L respectively. Summation of these cost results the CRM as Rs. 3,184.00 lacs per year. COL and CUT are estimated as Rs. 9 and 227 lacs per year for the requirement of 1,800 labor and 4,550,000 kW of electricity. OC for the required production capacity of carrot seed oil is computed as Rs. 3,420 lacs per year, which is the summation of CRM, COL and CUT. COM for the carrot seed oil extraction is estimated as Rs. 4,770 lacs per year of oil using equation (3.3) discussed in section 3.9. SC of carrot seed oil is estimated as Rs. 22,088 lacs per year considering 18% GST on the selling price of Rs. 15,599 per kg for carrot seed oil. As can be noticed from Table 6.34, OC is far lesser than the SC, approximately six times lesser, for the production of 120 t carrot seed oil per year. This must be due to the extraction of high-valued product (carrot seed oil) from the low-cost material (carrot seed) and recycling of solvent and co-solvent makes it cheaper. Hence, SFE process can be considered as economically feasible for the extraction of carrot seed oil and profit can be made while selling the product at market price.

Table 6.34 Cost indicators for the SFE of carrot seed oil.

Particulars	Cost per unit (Rs.)	Quantity used	Annual cost (Rs. per year, in Lacs)
SFE equipment	-	-	1,791.00
Land	3,560 (per m^2)	9,300 (m^2)	16.00
FCI (Approx.)			1,807.00
Carrot seed	85 (per kg)	845,000 (kg)	718.00
CO_2	44 (per kg)	4,120,000 (kg)	1,813.00
Ethanol	640 (per L)	203,000 (L)	1,299.00
CRM (Approx.)			3,184.00
COL	500 (per labor)	1,800 labor	9.00
CUT	5 (per kWh)	4,550,000 (kW)	227.00
CRM			3,184.00
OC (Approx.)			3,420.00
COM (Approx.)			4,770.00
Carrot seed oil (Approx.)	15599 (per kg)	120,000 (kg)	18,718.00
SC (18% GST)			22,088.00

CONCLUSIONS AND RECOMMENDATIONS

This Chapter includes the salient conclusions drawn from the present work along with recommendations for future work.

7.1 Conclusions

In the present work, turmeric root and carrot seed are selected as raw materials and extracted using supercritical fluid extraction (SFE). Design of experiment technique is used to design the experimental runs and optimize the operating parameters. Further, characterization of raw materials and extracted oil is performed using various techniques as discussed in chapter 3 and 4. Compositions of extracted oils are also analyzed using Gas chromatography-Mass spectroscopy (GC-MS), Gas chromatography (GC) and UV-Spectroscopy. In addition, simulation of SFE process is carried out using mathematical models available in literature and suitable model is proposed for particular type of solute matrix. Based on results and discussion presented in Chapter 6, salient conclusions are drawn for three different types of investigations carried out in the present work as:

7.1.1 Characterization of raw materials

- Moisture and ash content of turmeric root are 6.93% and 4.64%, respectively, whereas, for carrot seed these are 7.19% and 10.92%.

- Fourier-transform infrared spectroscopy (FTIR) analyses of turmeric root and carrot seed confirm the presence of fatty acids, protein and carbohydrates. In addition, turmeric oil also contains Turmerone and Curcumin whereas carrot seed oil comprises of Carotol and Daucol.

- Scanning electron microscopy (SEM) analyses show that turmeric root oil is enclosed inside secretory cells and layers whereas carrot seed oil is available inside secretory cavities as well as glandular trichomes. Further, structure of both raw materials can be broken through milling and oil from inside solid particles can be extracted at high pressure.

- Thermo-gravimetric (TG) analysis of turmeric root shows the presence of 7.64 moisture,

48.2 organic matter, 19.69 decomposition of carbonaceous matter and 24.47 wt% ash. On the other hand, Differential thermal (DT) analysis of turmeric root indicates exothermic peaks due to oxidation of organic matter/oil.

- It is depicted from TG plot of carrot seed that moisture, organic matter, decomposition of carbonaceous matter and ash content contribute 7.9, 79.4, 3.3 and 9.4 wt%, respectively. Further, DT analysis of carrot seed shows three exothermic peaks due to crystallization of Mono-unsaturated fatty acid (MUFA) ,Poly-unsaturated fatty acid (PUFA) and saturated fatty acid (SFA).

- Differential scanning calorimetry (DSC) analysis of carrot seed oil depicts two melting peaks and single crystallization peak at -16.64±0.35 °C, 19.43±0.25 °C and 33.32±0.43 °C. Glass transition temperature (Tg) of carrot seed oil is at -48.91 °C.

- GC-MS analyses of turmeric root oil show that sesquiterpenes (ar-Turmerone, β-Turmerone and α-Turmerone) are the principle compounds of turmeric essential oil. Concentrations of these in the turmeric oil are varied from 0 to 302.97 mg per gm of oil. UV spectrophotometer analysis indicates that turmeric essential oil also contains curcumin (0.09 to 2.2 mg/ g oil), which acts as anti-inflammatory, antioxidant, antifungal, anticarcinogenic, antiviral etc.

- Fatty acid analysis of turmeric oil shows the presence of Oleic acid (2.9 to 61.5%) as major MUFA whereas, Linoleic acid (22.56%) and Linolenic acid (21.3%) are available as major omega-6 unsaturated fatty acid (USFA), which are very beneficial for human health.

- Essential oil analysis of carrot seed reveals the presence of Carotol and Daucol as primary compounds through GC-MS analyses. Both compounds contribute 82.19 to 94.09% and 0.53 to 5.85%, respectively, of carrot seed oil.

- Carrot seed oil comprises of 28 to 78% Oleic acid, which is the major MUFA of carrot seed oil. In addition, Pentadecylic acid, Margaric acid, γ-Linolenic acid, cis-Arachidic acid and

cis-eicosatetraenoic acid are the USFA found in carrot seed oil.

- Physico-chemical analyses of turmeric root and carrot seed oil such as, refractive index, acid value, iodine value, peroxide value, specific gravity, saponification value, unsaponification matter suggest that oil can be used for medicinal and cosmetic purpose.

7.1.2 Response Surface analyses of raw materials

- From regression analysis of turmeric root, it is evident that quadratic model is most suitable with all three responses i.e. Oil yield (OY), Total Curcumin (TC) and Total Turmerone (TT) contents as p-value of quadratic model is less than < 0.0001.

- Pressure, temperature, solvent flow rate and co-solvent addition are affecting the OY positively and consequently, OY increases. However, increase in particle size first increases then decreases the OY.

- Effect of two parameter interaction is also studied for the SFE of turmeric root, which depicts that pressure-temperature interaction does not increase the OY appreciably. It provides minimum OY of turmeric root in comparison to any other combination.

- For TC content of turmeric oil, no operating parameter is showing significant effect on the extraction of TC except co-solvent. Addition of co-solvent increases the TC content drastically.

- Pressure does not affect the extraction of TT content; however, increase in temperature first decreases TT content and then increases. On other hand, TT content first increases and then decreases with increasing solvent flow rate. Further, increase in particle size and addition of co-solvent decrease the extraction of TT content.

- Screening design of all five operating parameters (pressure, temperature, flow rate, particle size and addition of co-solvent) shows particle size as a least influential parameter for SFE of carrot seed.

- Least square regression model fits well with the experimental results of carrot seed for two responses i.e. extraction oil yield (EOY) and Carotol content (CC).

- Pressure, temperature and addition of co-solvent are showing positive effects on EOY, which give the maximum EOY at higher levels. However, increase in solvent flow rate first increases EOY and then decreases, which results maximum EOY at intermediate solvent flow rate.

- Interaction of operating parameters (2-way, 3-way and 4-way) is observed on the SFE of carrot seed. Effect of two-parameter interaction is studied on EOY, which indicates that pressure-co-solvent interaction affects EOY significantly as compared to any other interaction.

- For CC of carrot seed oil, it is increasing with pressure and addition of co-solvent whereas it decreases with increase in temperature and solvent flow rate.

7.1.3 Mathematical modeling of SFE process

Selection of suitable model for the different type of solute matrices and effect of matrices on the extraction yield are studied. Suitable model/s for the SFE of turmeric root and carrot seed oil are also predicted. Following salient conclusions are drawn from the model fitting:

- Solute matrices such as leaf, flower, flower bud, flowerhip seed, herb plant, shrub seed and vegetable matter are taken into consideration to investigate the best-suited model. Model proposed by Reverchon (1996) and Sovova (1994) are found as suitable models for leaf whereas Reverchon and Poletto (1996) and Reverchon et al (2000) are suitable models for flower and flowerhip seed, respectively. For flower bud, Reverchon (1996), Reverchon and Marrone (1997) and Sovova (1994) models are found suitable. Further, Reverchon (1996) is well suited model for herb plant also. Model proposed by Reverchon (1996), Sovova (1994) and Nobre et al. (2006) are suitable models for shrub seed while, for vegetable matter, Sovova (1994) and Goto et al. (1996) are well suited model.

- If two or more solutes show same type of matrix/morphological structure, best suited model found for these is same.

- Oil yield (g oil/g feed) of turmeric root is increasing with pressure from 200 to 300 bar and then decreasing for 400 bar. It is increasing with temperature from 40 to 50 °C and then no significant effect is visible up to 60 °C as extraction curves of 50 and 60 °C are overlapping.

- Oil yield (g oil/g feed) of turmeric root is increasing with solvent flow rate whereas it is first increasing and then decreasing with increase in particle size. Similar to the effect of particle size, oil yield of turmeric root first increases and then decreases with increase in addition of co-solvent.

- Models proposed by Sovova (1994) and Goto et al. (1996) are investigated as most suitable models for the SFE of turmeric root oil while fitting the experimental data of optimum points into different models.

- Experimental data of carrot seed oil is fitted in model proposed by Sovova (1994), which indicates that oil yield of carrot seed in increasing continuously with pressure and temperature from 200 to 400 bar and 50 to 70 °C, respectively. Extraction of carrot seed oil is complete at elevated pressure as oil yield approaches to that found through Soxhlet.

- For Sovova (1994) model, oil yield of carrot seed increases with increase in solvent flow rate from 5 to 10 g/min; however, it decreases with further increase in solvent flow rate up to 15 g/min. Oil yield of carrot seed also increases with the addition of co-solvent from 0 to 10 wt% of solvent flow rate.

- Experimental data of optimum points for the SFE of carrot seed oil, predicted through Sovova (1994), is fitted into different models and the models proposed by Sovova (1994) and Reverchon and Marrone (1997) are found most suitable model.

- Optimal values of parameters along with oil yield for SFE of turmeric root oil, predicted through DOE (individual and interaction effects) and Sovova (1994) model are comparable.

- For SFE of carrot seed oil, optimum points of operating parameters predicted through DOE (individual and interaction effects) and Sovova (1994) model are in well accordance.

- Industrial-scale economic evaluations of SFE of turmeric root oil and carrot seed oil reveal that SFE can be considered as profitable and feasible extraction technology.

7.2 Recommendations

Based on the present work, following recommendation for future work is proposed:

- Other models such as Reverchon (1996), Goto et al. (1996), Rverchon and Poletto (1996), Reverchon and Marrone (1997), Reverchon et al. (2000) can be used for the fitting of experimental data to check their suitability for different ranges of various operating parameters.

- A correlation can be formulated to predict the effect of temperature on extraction yield considering the dual effect of temperature on solubility and vapor pressure.

- Ficus glomerata berries and seeds can be considered as raw material for SFE as no research article is available on it.

- Other solvents such as propane and water can also be utilized as supercritical fluid to study SFE process.

REFERENCES

A-1.   Abaroudi, K., Trabelsi, F., Calloud-Gabriel, B., Recasens, F., 1999a. Mass Transport Enhancement in Modified Supercritical Fluid. Ind. Eng. Chem. Res 38, 3505–3518. doi:10.1021/ie990105e

A-2.   Abbas, K.A., Mohamed, A., Abdulamir, A.S., Abas, H.A., 2008. A Review on Supercritical Fluid Extraction as New Analytical Method. Am. J. Biochem. Biotechnol. 4, 345–353. doi:10.3844/ajbbsp.2008.345.353

A-3.   Abdali, H., Ajji, A., 2015. Development of antibacterial structures and films using clove bud powder. Ind. Crops Prod. 72, 214–219. doi:10.1016/j.indcrop.2014.09.050

A-4.   Abdulrasheed, A., Aroke, U.O., Sani, I.M., 2015. Parametric Studies of Carrot Seed Oil Extract for the Production of Medicated Soap. Int. J. Recent Dev. Eng. Technol. 4, 1–5.

A-5.   Acimovic, M., Stankovic, J., Cvetkovic, M., Ignjatov, M., Nikolic, L., 2016. Chemical characterization of essential oil from seeds of wild and cultivated carrots from Serbia. Bot. Serbica 40, 55–60. doi:10.5281/zenodo.48861

A-6.   Ahmed, Z., Abdeslam-Hassan, M., Ouassila, L., Danielle, B., 2012. Extraction and modeling of Algerian Rosemary essential oil using supercritical CO_2: Effect of pressure and temperature. Energy Procedia 18, 1038–1046. doi:10.1016/j.egypro.2012.05.118

A-7.   Akalin, M.K., Karagöz, S., Akyüz, M., 2013. Supercritical ethanol extraction of bio-oils from German beech wood: Design of experiments. Ind. Crops Prod. 49, 720–729. doi:10.1016/j.indcrop.2013.06.036

A-8.   Akalın, M.K., Tekin, K., Akyüz, M., Karagöz, S., 2015. Sage oil extraction and optimization by response surface methodology. Ind. Crops Prod. 76, 829–835. doi:10.1016/j.indcrop.2015.08.005

A-9.   Aladic, K., Jarni, K., Barbir, T., Vidović, S., Vladić, J., Bilić, M., Jokić, S., 2015. Supercritical CO_2 extraction of hemp (Cannabis sativa L.) seed oil. Ind. Crops Prod. 76, 472–478. doi:10.1016/j.indcrop.2015.07.016

A-10.   Aladic, K., Jokic, S., Moslavac, T., Tomas, S., Vidovic, S., Vladic, J., Subaric, D., 2015. Cold Pressing and Supercritical CO_2 Extraction of Hemp (Cannabis sativa) Seed Oil. Chem. Biochem. Eng. Q. J. 28, 481–490. doi:10.15255/CABEQ.2013.1895

A-11.   Alcázar-Alay, S.C., Osorio-Tobón, J.F., Forster-Carneiro, T., Meireles, M.A.A., 2017. Obtaining bixin from semi-defatted annatto seeds by a mechanical method and solvent

extraction: Process integration and economic evaluation. Food Res. Int. 99, 393–402. doi:10.1016/j.foodres.2017.05.032

A-12. Allam, M.A., Hamed, S.F., 2007. Application of FTIR spectroscopy in the assessment of olive oil adulteration. J. Appl. Sci. Res. 18, 102–108.

A-13. Allawzi, M., Al-Otoom, A., Allaboun, H., Ajlouni, A., Al Nseirat, F., 2011. CO_2 supercritical fluid extraction of Jordanian oil shale utilizing different co-solvents. Fuel Process. Technol. 92, 2016–2023. doi:10.1016/j.fuproc.2011.06.001

A-14. Almeida, R.N., Neto, R.G., Barros, F.M.C., Cassel, E., von Poser, G.L., Vargas, R.M.F., 2013. Supercritical extraction of Hypericum caprifoliatum using carbon dioxide and ethanol+water as co-solvent. Chem. Eng. Process. Process Intensif. 70, 95–102. doi:10.1016/j.cep.2013.05.002

A-15. Ameer, K., Chun, B.S., Kwon, J.H., 2017. Optimization of supercritical fluid extraction of steviol glycosides and total phenolic content from Stevia rebaudiana (Bertoni) leaves using response surface methodology and artificial neural network modeling. Ind. Crops Prod. 109, 672–685. doi:10.1016/j.indcrop.2017.09.023

A-16. Andrade, K.S., Gonalvez, R.T., Maraschin, M., Ribeiro-Do-Valle, R.M., Martínez, J., Ferreira, S.R.S., 2012. Supercritical fluid extraction from spent coffee grounds and coffee husks: Antioxidant activity and effect of operational variables on extract composition. Talanta 88, 544–552. doi:10.1016/j.talanta.2011.11.031

A-17. Andrich, G., Balzini, S., Zinnai, A., Silvestri, S., Venturi, F., 2001. Supercritical fluid extraction in sunflower seed technology. Eur. J. Lipid Sci. Technol. 103, 151–157.

A-18. Anggrianto, K., Salea, R., Veriansyah, B., Tjandrawinata, R.R., 2014. Application of Supercritical Fluid Extraction on Food Processing Black eyed Pea (Vigna Unguiculata) and Peanut (Arachis Hypogaea). Procedia Chem. 9, 265–272.

A-19. AOAC International, 1998. Official Method of Analysis of the AOAC international, 16th ed. AOAC international.

A-20. Ara, K.M., Karami, M., Raofie, F., 2014. Application of response surface methodology for the optimization of supercritical carbon dioxide extraction and ultrasound-assisted extraction of Capparis spinosa seed oil. J. Supercrit. Fluids 85, 173–182. doi:10.1016/j.supflu.2013.10.016

A-21. Araujo, J.M.A., Sandi, D., 2006. Extraction of coffee diterpenes and coffee oil using supercritical carbon dioxide. Food Chem. 101, 1087-1094.

doi:10.1016/j.foodchem.2006.03.008

A-22. Arnaiz, E., Bernal, J., Martin, M.T., Nozal, M.J., Bernal, J.L., Toribio, L., 2012. Supercritical fluid extraction of free amino acids from broccoli leaves. J. Chromatogr. A 1250, 49–53. doi:10.1016/j.chroma.2012.04.066

A-23. Asep, E.K., Jinap, S., Jahurul, M.H.A., Zaidul, I.S.M., Singh, H., 2013. Effects of polar cosolvents on cocoa butter extraction using supercritical carbon dioxide. Innov. Food Sci. Emerg. Technol. 20, 152–160. doi:10.1016/j.ifset.2013.06.010

A-24. Asghari, G., Mostajeran, A., Shebli, M., 2009. Curcuminoid and essential oil components of turmeric at different stages of growth cultivated in Iran. Res. Pharm. Sci. 4, 55–61.

A-25. Awasthi, P., Dixit, S., 2009. Chemical Composition of *Curcuma Longa* Leaves and Rhizome Oil from the Plains of Northern India. J. Young Pharm. 1, 312–316. doi:10.4103/0975-1483.59319

A-26. Ayas, N., Yilmaz, O., 2014. A shrinking core model and empirical kinetic approaches in supercritical CO_2 extraction of safflower seed oil. J. Supercrit. Fluids 94, 81–90. doi:10.1016/j.supflu.2014.06.019

A-27. Azevedo, A.B.A. de, Mazzafera, P., Mohamed, R.S., Vieira De Melo, S.A.B., Kieckbusch, T.G., 2008. Extraction of caffeine, chlorogenic acids and lipids from green coffee beans using supercritical carbon dioxide and co-solvents. Brazilian J. Chem. Eng. 25, 543-552. doi:10.1590/S0104-66322008000300012

B-1. Bagchi, A., 2012. Extraction of Curcumin. J. Environ. Sci. Toxicol. Food Technol. 1, 1–16. doi:10.9790/2402-0130116

B-2. Baldino, L., Della Porta, G., Reverchon, E., 2017. Supercritical CO_2 processing strategies for pyrethrins selective extraction. J. CO_2 Util. 20, 14–19. doi:10.1016/j.jcou.2017.04.012

B-3. Banchero, M., Pellegrino, G., Manna, L., 2013. Supercritical fluid extraction as a potential mitigation strategy for the reduction of acrylamide level in coffee. J. Food Eng. 115, 292–297. doi:10.1016/j.jfoodeng.2012.10.045

B-4. Barbosa, H.M.A., De Melo, M.M.R., Coimbra, M.A., Passos, C.P., Silva, C.M., 2014. Optimization of the supercritical fluid coextraction of oil and diterpenes from spent coffee grounds using experimental design and response surface methodology. J. Supercrit. Fluids 85, 165–172. doi:10.1016/j.supflu.2013.11.011

B-5. Barrado, I., Meseguer, V., Bermudez, M.-D., Martinez-Nicolas, G., 1997. Supercritical carbon dioxide extraction of liquid crystalline azobenzenes. J. Supercrit. Fluids 11, 73–80.

B-6.   Barrales, F.M., Rezende, C.A., Martinez, J., 2015. Supercritical CO_2 extraction of passion fruit (Passiflora edulis sp.) seed oil assisted by ultrasound. J. Supercrit. Fluids 104, 183–192. doi:10.1016/j.supflu.2015.06.006

B-7.   Bartle, K.D., Clifford, A.A., Hawthorne, S.B., Langenfeld, J.J., Miller, D.J., Robinsona, R., 1990. A Model for Dynamic Extraction Using a Supercritical Fluid. J. Supercrit. Fluids 3, 143–149.

B-8.   Beckman, E.J., 2004. Supercritical and near-critical CO_2 in green chemical synthesis and processing. J. Supercrit. Fluids 28, 121–191. doi:10.1016/S0896-8446(03)00029-9

B-9.   Began, G., Goto, M., Kodama, A., Hirose, T., 2000. Response surfaces of total oil yield of turmeric (*Curcuma longa*) in supercritical carbon dioxide. Food Res. Int. 33, 341–345. doi:10.1016/S0963-9969(00)00053-3

B-10.   Belayneh, H.D., Wehling, R.L., Cahoon, E., Ciftci, O.N., 2015. Extraction of omega-3-rich oil from Camelina sativa seed using supercritical carbon dioxide. J. Supercrit. Fluids 104, 153–159. doi:10.1016/j.supflu.2015.06.002

B-11.   Belbaki, A., Louaer, W., Meniai, A.H., 2017. Supercritical CO_2 extraction of oil from Crushed Algerian olives. J. Supercrit. Fluids 130, 165–171. doi:10.1016/j.supflu.2017.08.005

B-12.   Bensebia, O., Barth, D., Bensebia, B., Dahmani, A., 2009. Supercritical CO_2 extraction of rosemary: Effect of extraction parameters and modelling. J. Supercrit. Fluids 49, 161–166. doi:10.1016/j.supflu.2009.01.007

B-13.   Bermejo, D.V., Ibáñez, E., Reglero, G., Fornari, T., 2016. Effect of cosolvents (ethyl lactate, ethyl acetate and ethanol) on the supercritical CO_2 extraction of caffeine from green tea. J. Supercrit. Fluids 107, 507–5012. doi:10.1016/j.supflu.2015.07.008

B-14.   Bhattacharjee, P., Singhal, R.S., Tiwari, S.R., 2007. Supercritical carbon dioxide extraction of cottonseed oil. J. Food Eng. 79, 892–898. doi:10.1016/j.jfoodeng.2006.03.009

B-15.   Bhattacharya, M., Srivastav, P.P., Mishra, H.N., 2014. Optimization of process variables for supercritical fluid extraction of ergothioneine and polyphenols from Pleurotus ostreatus and correlation to free-radical scavenging activity. J. Supercrit. Fluids 95, 51–59. doi:10.1016/j.supflu.2014.07.031

B-16.   Bimakr, M., Rahman, R.A., Ganjloo, A., Taip, F.S., Salleh, L.M., Sarker, M.Z.I., 2012. Optimization of Supercritical Carbon Dioxide Extraction of Bioactive Flavonoid Compounds from Spearmint (Mentha spicata L.) Leaves by Using Response Surface

Methodology. Food Bioprocess Technol. 5, 912–920. doi:10.1007/s11947-010-0504-4

B-17.   Bogdanovic, A., Tadic, V., Stamenic, M., Petrovic, S., Skala, D., 2016. Supercritical carbon dioxide extraction of Trigonella foenum-graecum L. seeds: Process optimization using response surface methodology. J. Supercrit. Fluids 107, 44–50. doi:10.1016/j.supflu.2015.08.003

B-18.   Boutin, O., De Nadaï, A., Perez, A.G., Ferrasse, J.H., Beltran, M., Badens, E., 2011. Experimental and modelling of supercritical oil extraction from rapeseeds and sunflower seeds. Chem. Eng. Res. Des. 89, 2477–2484. doi:10.1016/j.cherd.2011.02.032

B-19.   Bozan, B., Temelli, F., 2003. Extraction of Poppy Seed Oil Using Supercritical CO_2. J. Food Sci. 68, 422–426.

B-20.   Brachet, A., Christen, P., Gauvrit, J.Y., Longeray, R., Lantéri, P., Veuthey, J.L., 2000. Experimental design in supercritical fluid extraction of cocaine from coca leaves. J. Biochem. Biophys. Methods 43, 353–366. doi:10.1016/S0165-022X(00)00062-2

B-21.   Braga, M.E.M., Leal, P.F., Carvalho, J.E., Meireles, M.A. a, 2003. Comparison of yield, composition, and antioxidant activity of turmeric (Curcuma longa L.) extracts obtained using various techniques. J. Agric. Food Chem. 51, 6604–6611. doi:10.1021/jf0345550

B-22.   Braga, M.E.M., Moreschi, S.R.M., Meireles, M.A.A., 2006. Effects of supercritical fluid extraction on *Curcuma longa L.* and *Zingiber officinale R.* starches. Carbohydr. Polym. 63, 340–346. doi:10.1016/j.carbpol.2005.08.055

C-1.   Campos, L.M.A.S., Michielin, E.M.Z., Danielski, L., Ferreira, S.R.S., 2005. Experimental data and modeling the supercritical fluid extraction of marigold (Calendula officinalis) oleoresin. J. Supercrit. Fluids 34, 163–170. doi:10.1016/j.supflu.2004.11.010

C-2.   Casas, L., Mantell, C., Rodríguez, M., Torres, A., Macías, F.A., Martínez de la Ossa, E., 2007. Effect of the addition of cosolvent on the supercritical fluid extraction of bioactive compounds from Helianthus annuus L. J. Supercrit. Fluids 41, 43-49. doi:10.1016/j.supflu.2006.09.001

C-3.   Castro-Vargas, H.I., Rodriguez-Varela, L.I., Ferreira, S.R.S., Parada-Alfonso, F., 2010. Extraction of phenolic fraction from guava seeds (Psidium guajava L.) using supercritical carbon dioxide and co-solvents. J. Supercrit. Fluids 51, 319–324. doi:10.1016/j.supflu.2009.10.012

C-4.   Catchpole, O.J., Grey, J.B., I-, P.B., Hutt, L., Zealand, N., Smallfield, B.M., 1996. Near-Critical Extraction of Sage , Celery , and Coriander Seed. J. Supercrit. Fluids 9, 273–279.

C-5.   Catchpole, O.J., Grey, J.B., Perry, N.B., Burgess, E.J., Redmond, W.A., Porter, N.G., 2003. Extraction of chili, black pepper, and ginger with near-critical CO_2, propane, and dimethyl ether: Analysis of the extracts by quantitative nuclear magnetic resonance. J. Agric. Food Chem. 51, 4853–4860. doi:10.1021/jf0301246

C-6.   Chahal, K.K., Kaur, P., Kataria, D., Kaur, R., 2016. Carotol : A Sesquiterpenoid Isolated from Carrot Seed Oil. ASIAN J. Chem. 28, 1004–1006.

C-7.   Chang, L.H., Jong, T.T., Huang, H.S., Nien, Y.F., Chang, C.M.J., 2006. Supercritical carbon dioxide extraction of turmeric oil from *Curcuma longa Linn* and purification of turmerones. Sep. Purif. Technol. 47, 119–125. doi:10.1016/j.seppur.2005.06.018

C-8.   Chassagnez-mendez, A.L., Machado, N.T., Araújo, M.E., Maia, J.G., Meireles, M.A.A., 2000. Supercritical CO_2 Extraction of Curcumins and Essential Oil from the Rhizomes of Turmeric (Curcuma longa L .). Ind. Eng. Chem. Res. 39, 4729–4733. doi:10.1021/ie000171c

C-9.   Chaudhury, R.R., Rafei, U.M., 2001. Traditional medicine in Asia, Stylus Pub Llc.

C-10.   Cheah, E.L.C., Heng, P.W.S., Chan, L.W., 2010. Optimization of supercritical fluid extraction and pressurized liquid extraction of active principles from Magnolia officinalis using the Taguchi design. Sep. Purif. Technol. 71, 293–301. doi:10.1016/j.seppur.2009.12.009

C-11.   Clifford, a. a., Basile, A., Al-Saidi, S.H.R., 1999. A comparison of the extraction of clove buds with supercritical carbon dioxide and superheated water. Fresenius. J. Anal. Chem. 364, 635–637. doi:10.1007/s002160051400

C-12.   Cocero, M.J., Calvo, L., 1996. Supercritical fluid extraction of sunflower seed oil with CO_2-ethanol mixtures. J. Am. Oil Chem. Soc. 73, 1573–1578. doi:10.1007/BF02523527

C-13.   Cocero, M.J., García, J., 2001. Mathematical model of supercritical extraction applied to oil seed extraction by CO_2 +saturated alcohol — I. Desorption model. J. Supercrit. Fluids 20, 229–243.

C-14.   Comim, S.R.R., Madella, K., Oliveira, J. V., Ferreira, S.R.S., 2010. Supercritical fluid extraction from dried banana peel (Musa spp., genomic group AAB): Extraction yield, mathematical modeling, economical analysis and phase equilibria. J. Supercrit. Fluids 54, 30–37. doi:10.1016/j.supflu.2010.03.010

C-15.   Cornelio-Santiago, H.P., Gonçalves, C.B., de Oliveira, N.A., de Oliveira, A.L., 2017. Supercritical CO_2 extraction of oil from green coffee beans: Solubility, triacylglycerol

composition, thermophysical properties and thermodynamic modelling. J. Supercrit. Fluids 128, 386–394. doi:10.1016/j.supflu.2017.05.030

C-16. Corso, M.P., Fagundes-Klen, M.R., Silva, E.A., Cardozo Filho, L., Santos, J.N., Freitas, L.S., Dariva, C., 2010. Extraction of sesame seed (Sesamun indicum L.) oil using compressed propane and supercritical carbon dioxide. J. Supercrit. Fluids 52, 56–61. doi:10.1016/j.supflu.2009.11.012

C-17. Costa, A.R.M., Freitas, L.A.P., Mendiola, J., Ib Nez, E., 2015. Copaifera langsdorffii supercritical fluid extraction: Chemical and functional characterization by LC/MS and in vitro assays. J. Supercrit. Fluids 100, 86–96. doi:10.1016/j.supflu.2015.02.028

C-18. Couto, R.M., Fernandes, J., Gomes da Silva, M.D.R., Simoes, P.C., 2009. Supercritical fluid extraction of lipids from spent coffee grounds. J. Supercrit. Fluids 51, 159–166.

C-19. Cruz, P.N., Pereira, T.C.S., Guindani, C., Oliveira, D.A., Rossi, M.J., Ferreira, S.R.S., 2017. Antioxidant and antibacterial potential of butia (Butia catarinensis) seed extracts obtained by supercritical fluid extraction. J. Supercrit. Fluids 119, 229–237. doi:10.1016/j.supflu.2016.09.022

C-20. Cu, J., Perineau, F., Delmas, M., Gaset, A., 1989. Comparison of the Chemical Composition of Carrot Seed Essential Oil Extracted by Different Solvents. Flavour Fragr. J. 4, 225–231.

C-21. Cygnarowicz-Provost, M., O'Brien, D.J., Boswell, R.T., Kurantz, M.J., 1995. Supercritical-fluid extraction of fungal lipids: Effect of cosolvent on mass-transfer rates and process design and economics. J. Supercrit. Fluids. doi:10.1016/0896-8446(95)90050-0

C-22. Cygnarowicz-Provost, M., O'Brien, D.J., Maxwell, R.J., Hampson, J.W., 1992. Supercritical-fluid extraction of fungal lipids using mixed solvents: Experiment and modeling. J. Supercrit. Fluids 5, 24–30. doi:10.1016/0896-8446(92)90037-K

D-1. Da Porto, C., Decorti, D., Natolino, A., 2014a. Water and ethanol as co-solvent in supercritical fluid extraction of proanthocyanidins from grape marc: A comparison and a proposal. J. Supercrit. Fluids 87, 1–8. doi:10.1016/j.supflu.2013.12.019

D-2. Da Porto, C., Natolino, A., Decorti, D., 2014b. Extraction of proanthocyanidins from grape marc by supercritical fluid extraction using CO_2 as solvent and ethanol-water mixture as co-solvent. J. Supercrit. Fluids 87, 59–64. doi:10.1016/j.supflu.2013.12.013

D-3. Dalvi, S. V., Mukhopadhyay, M., 2009. A novel process for precipitation of ultra-fine particles using sub-critical CO_2. Powder Technol. 195, 190–195.

doi:10.1016/j.powtec.2009.05.029

D-4.   Danh, L.T., Mammucari, R., Truong, P., Foster, N., 2009. Response surface method applied to supercritical carbon dioxide extraction of *Vetiveria zizanioides* essential oil. Chem. Eng. J. 155, 617–626. doi:10.1016/j.cej.2009.08.016

D-5.   Danh, L.T., Truong, P., Mammucari, R., Foster, N., 2010. Extraction of vetiver essential oil by ethanol-modified supercritical carbon dioxide. Chem. Eng. J. 165, 26–34. doi:10.1016/j.cej.2010.08.048

D-6.   Danlami, J.M., Zaini, M.A.A., Arsad, A., Yunus, M.A.C., 2015. A parametric investigation of castor oil (Ricinus comminis L) extraction using supercritical carbon dioxide via response surface optimization. J. Taiwan Inst. Chem. Eng. 53, 32–39. doi:10.1016/j.jtice.2015.02.033

D-7.   Davarnejad, R., Kassim, K.M., Zainal, A., Sata, S.A., 2008. Supercritical fluid extraction of β-carotene from crude palm oil using CO_2. J. Food Eng. 89, 472–478. doi:10.1016/j.jfoodeng.2008.05.032

D-8.   de Franca, L.F., Reber, G., Angela, M., Meireles, A., Machado, N.T., Brunner, G., 1999. Supercritical extraction of carotenoids and lipids from buriti (Mauritia flexuosa), a fruit from the Amazon region. J. Supercrit. Fluids 14, 247–256.

D-9.   de Melo, M.M.R.., Silvestre, A.J.D., Silva, C.M., 2014. Supercritical fluid extraction of vegetable matrices: Applications, trends and future perspectives of a convincing green technology. J. Supercrit. Fluids 92, 115–176. doi:10.1016/j.supflu.2014.04.007

D-10. Del Valle, J.M., De La Fuente, J.C., M Del Valle, J.E., 2006. Supercritical CO_2 Extraction of Oilseeds: Review of Kinetic and Equilibrium Models. Crit. Rev. Food Sci. Nutr. 46, 131–160. doi:10.1080/10408390500526514

D-11. Della Porta, G., Porcedda, S., Marongiu, B., Reverchon, E., 1999. Isolation of eucalyptus oil by supercritical fluid extraction. Flavour Fragr. J. 14, 214–218. doi:10.1002/(SICI)1099-1026(199907/08)14:4<214::AID-FFJ814>3.0.CO;2-H

D-12. Demirbas, A., 2000. Liquefaction of olive husk by supercritical fluid extraction. Energy Convers. Manag. 41, 1875–1883. doi:10.1016/S0196-8904(00)00029-7

D-13. Derrien, M., Aghabararnejad, M., Gosselin, A., Desjardins, Y., Angers, P., Boumghar, Y., 2018. Optimization of supercritical carbon dioxide extraction of lutein and chlorophyll from spinach by-products using response surface methodology. Lwt 93, 79–87. doi:10.1016/j.lwt.2018.03.016

D-14. Dias, A.L.B., Arroio Sergio, C.S., Santos, P., Barbero, G.F., Rezende, C.A., Martinez, J., 2016. Effect of ultrasound on the supercritical CO_2 extraction of bioactive compounds from dedo de moca pepper (Capsicum baccatum L. var. pendulum). Ultrason. Sonochem. 31, 284–294. doi:10.1016/j.ultsonch.2016.01.013

D-15. Diaz-Reinoso, B., Moure, A., Dominguez, H., Parajo, J.C., 2006. Supercritical CO_2 extraction and purification of compounds with antioxidant activity. J. Agric. Food Chem. 54, 2441–2469. doi:10.1021/jf052858j

D-16. Dobarganes Nodar, M., Molero Gomez, A., Martinez de la Ossa, E., 2002. Characterisation and Process Development of Supercritical Fluid Extraction of Soybean Oil. Food Sci. Technol. Int. 8, 337–342. doi:10.1106/108201302031651

D-17. Doker, O., Salgin, U., Sanal, I., Mehmetoglu, U., Calimli, A., 2004. Modeling of extraction of β-carotene from apricot bagasse using supercritical CO_2 in packed bed extractor. J. Supercrit. Fluids 28, 11–19. doi:10.1016/S0896-8446(03)00006-8

D-18. Döker, O., Salgin, U., Yildiz, N., Aydoğmuş, M., Çalimli, A., 2010. Extraction of sesame seed oil using supercritical CO_2 and mathematical modeling. J. Food Eng. 97, 360–366. doi:10.1016/j.jfoodeng.2009.10.030

D-19. Domingues, R.M.A., De Melo, M.M.R., Neto, C.P., Silvestre, A.J.D., Silva, C.M., 2012. Measurement and modeling of supercritical fluid extraction curves of Eucalyptus globulus bark: Influence of the operating conditions upon yields and extract composition. J. Supercrit. Fluids 72, 176–185. doi:10.1016/j.supflu.2012.08.010

D-20. Domingues, R.M.A., De Melo, M.M.R., Oliveira, E.L.G., Neto, C.P., Silvestre, A.J.D., Silva, C.M., 2013. Optimization of the supercritical fluid extraction of triterpenic acids from Eucalyptus globulus bark using experimental design. J. Supercrit. Fluids 74, 105–114. doi:10.1016/j.supflu.2012.12.005

D-21. Dutta, S., Bhattacharjee, P., 2016. Modeling of supercritical carbon dioxide extraction of piperine from Malabar black pepper. Mater. Today Proc. 3, 3238–3252. doi:10.1016/j.matpr.2016.10.005

D-22. Dutta, S., Bhattacharjee, P., 2015. Enzyme-assisted supercritical carbon dioxide extraction of black pepper oleoresin for enhanced yield of piperine-rich extract. J. Biosci. Bioeng. 120, 17–23. doi:10.1016/j.jbiosc.2014.12.004

D-23. Duval, J., Destandau, E., Pecher, V., Poujol, M., Tranchant, J.-F.O., Lesellier, E., 2016. Selective enrichment in bioactive compound from Kniphofia uvaria by super/subcritical

fluid extraction and centrifugal partition chromatography. J. Chromatogr. A 1447, 26–38. doi:10.1016/j.chroma.2016.04.029

E-1.   Escobedo-Flores, Y., Chavez-Flores, D., Salmeron, I., Molina-Guerrero, C., Perez-Vega, S., 2018. Optimization of supercritical fluid extraction of polyphenols from oats (Avena sativa L.) and their antioxidant activities. J. Cereal Sci. 80, 198–204. doi:10.1016/j.jcs.2018.03.002

F-1.   Falcao, M.A., Scopel, R., Almeida, R.N., do Espirito Santo, A.T., Franceschini, G., Garcez, J.J., Vargas, R.M.F., Cassel, E., 2017. Supercritical fluid extraction of vinblastine from Catharanthus roseus. J. Supercrit. Fluids 129, 9–15. doi:10.1016/j.supflu.2017.03.018

F-2.   Fathordoobady, F., Mirhosseini, H., Selamat, J., Manap, M.Y.A., 2016. Effect of solvent type and ratio on betacyanins and antioxidant activity of extracts from Hylocereus polyrhizus flesh and peel by supercritical fluid extraction and solvent extraction. Food Chem. 202, 70–80. doi:10.1016/j.foodchem.2016.01.121

F-3.   Felfoldi-Gava, A., Szarka, S., Simandi, B., Blazics, B., Simon, B., Kery, A., 2012. Supercritical fluid extraction of Alnus glutinosa (L.) Gaertn. J. Supercrit. Fluids 61, 55–61. doi:10.1016/j.supflu.2011.10.003

F-4.   Fernandez, I., Dachs, J., Bayona, J.M., 1996. Application of experimental design approach to the optimization of supercritical fluid extraction of polychlorinated biphenyls and polycyclic aromatic hydrocarbons. J. Chromatogr. A 719, 77–85.

F-5.   Ferreira, S., Nikolov, Z., Doraiswamy, L., Meireles, A.A., Petenate, A., 1999. Supercritical fluid extraction of black pepper (Piper nigrun L.) essential oil. J. Supercrit. Fluids 14, 235–245.

F-6.   Ferreira, S.L.C., Bruns, R.E., Ferreira, H.S., Matos, G.D., David, J.M., Brandão, G.C., da Silva, E.G.P., Portugal, L.A., dos Reis, P.S., Souza, A.S., dos Santos, W.N.L., 2007. Box-Behnken design: An alternative for the optimization of analytical methods. Anal. Chim. Acta 597, 179–186. doi:10.1016/j.aca.2007.07.011

F-7.   Ferreira, S.R.S., Meireles, M.A. a., 2002. Modeling the supercritical fluid extraction of black pepper (Piper nigrum L.) essential oil. J. Food Eng. 54, 263–269. doi:10.1016/s0260-8774(01)00212-6

F-8.   Fiori, L., 2009. Supercritical extraction of sunflower seed oil: Experimental data and model validation. J. Supercrit. Fluids 50, 218–224. doi:10.1016/j.supflu.2009.06.011

F-9.   Fiori, L., Basso, D., Costa, P., 2009. Supercritical extraction kinetics of seed oil: A new

model bridging the "broken and intact cells" and the "shrinking-core" models. J. Supercrit. Fluids 48, 131–138. doi:10.1016/j.supflu.2008.09.019

F-10. Fujii, K., 2012. Process integration of supercritical carbon dioxide extraction and acid treatment for astaxanthin extraction from a vegetative microalga. Food Bioprod. Process. 90, 762–766. doi:10.1016/j.fbp.2012.01.006

F-11. Fullana, M., Trabelsi, F., Recasens, F., 2000. Use of neural net computing for statistical and kinetic modelling and simulation of supercritical # uid extractors. Chem. Eng. Sci. 55, 79–95.

G-1. Gao, F., Birch, J., 2016. Oxidative stability, thermal decomposition, and oxidation onset prediction of carrot, flax, hemp, and canola seed oils in relation to oil composition and positional distribution of fatty acids. Eur. J. Lipid Sci. Technol. 118, 1042–1052. doi:10.1002/ejlt.201670094

G-2. Gao, F., Yang, S., Birch, J., 2016. Physicochemical characteristics, fatty acid positional distribution and triglyceride composition in oil extracted from carrot seeds using supercritical CO_2. J. Food Compos. Anal. 45, 26–33. doi:10.1016/j.jfca.2015.09.004

G-3. Gao, Y., Liu, X., Xu, H., Zhao, J., Wang, Q., Liu, G., Hao, Q., 2010. Optimization of supercritical carbon dioxide extraction of lutein esters from marigold (Tagetes erecta L.) with vegetable oils as continuous co-solvents. Sep. Purif. Technol. 71, 214–219. doi:10.1016/j.seppur.2009.11.024

G-4. García-Abarrio, S.M., Martin, L., Burillo, J., Porta, G. Della, Mainar, A.M., 2014. Supercritical fluid extraction of volatile oil from Lippia alba (Mill.) cultivated in Aragón (Spain). J. Supercrit. Fluids 94, 206–211. doi:10.1016/j.supflu.2014.07.016

G-5. Garcia-Risco, M.R., Vazquez, E., Sheldon, J., Steinmann, E., Riebesehl, N., Fornari, T., Reglero, G., 2015. Supercritical fluid extraction of heather (Calluna vulgaris) and evaluation of anti-hepatitis C virus activity of the extracts. Virus Res. 198, 9–14. doi:10.1016/j.virusres.2014.12.022

G-6. Garg, S.N., Mengi, N., Patra, N.K., Charles, R., Kumar, S., 2002. Chemical examination of the leaf essential oil of *Curcuma longa L.* from the north Indian plains. Flavour Fragr. J. 17, 103–104. doi:10.1002/ffj.1056

G-7. Gaspar, F., Lu, T., Santos, R., <u>Al-Duri, B.</u>, 2003. Modelling the extraction of essential oils with compressed carbon dioxide. J. Supercrit. Fluids 25, 247–260. doi:10.1016/S0896-8446(02)00149-3

G-8.   Ghafoor, K., Park, J., Choi, Y.H., 2010. Optimization of supercritical fluid extraction of bioactive compounds from grape (Vitis labrusca B.) peel by using response surface methodology. Innov. Food Sci. Emerg. Technol. 11, 485–490. doi:10.1016/j.ifset.2010.01.013

G-9.   Ghasemi, E., Raofie, F., Najafi, N.M., 2011. Application of response surface methodology and central composite design for the optimisation of supercritical fluid extraction of essential oils from Myrtus communis L. leaves. Food Chem. 126, 1449–1453. doi:10.1016/j.foodchem.2010.11.135

G-10.   **Ghoreishi, S.M., Hedayati, A., Mohammadi, S., 2016a. Optimization of periodic static-dynamic supercritical CO_2 extraction of taxifolin from pinus nigra bark with ethanol as entrainer. J. Supercrit. Fluids 113, 53–60. doi:10.1016/j.supflu.2016.03.015**

G-11.   **Ghoreishi, S.M., Hedayati, A., Mousavi, S.O., 2016b. Quercetin extraction from Rosa damascena Mill via supercritical CO_2: Neural network and adaptive neuro fuzzy interface system modeling and response surface optimization. J. Supercrit. Fluids 112, 57–66. doi:10.1016/j.supflu.2016.02.006**

G-12.   **Ghoreishi, S.M., Heidari, E., 2013. Extraction of Epigallocatechin-3-gallate from green tea via supercritical fluid technology: Neural network modeling and response surface optimization. J. Supercrit. Fluids 74, 128–136. doi:10.1016/j.supflu.2012.12.009**

G-13.   **Ghoreishi, S.M., Shahrestani, G.R., Ghaziaskar, H.S., 2009. Experimental and modeling investigation of supercritical extraction of mannitol from Olive leaves. Chem. Eng. Technol. 32, 45–54. doi:10.1002/ceat.200800441**

G-14.   **Ghoreishi, S.M., Shahrestani, R.G., 2009a. Innovative strategies for engineering mannitol production. Trends Food Sci. Technol. 20, 263–270. doi:10.1016/j.tifs.2009.03.006**

G-15.   **Ghoreishi, S.M., Shahrestani, R.G., 2009b. Subcritical water extraction of mannitol from olive leaves. J. Food Eng. 93, 474–481. doi:10.1016/j.jfoodeng.2009.02.015**

G-16.   Gilbert-Lopez, B., Mendiola, J.A., van den Broek, L.A.M., Houweling-Tan, B., Sijtsma, L., Cifuentes, A., Herrero, M., Ibanez, E., 2017. Green compressed fluid technologies for downstream processing of *Scenedesmus obliquus* in a biorefinery approach. Algal Res. 24, 111–121. doi:10.1016/j.algal.2017.03.011

G-17.   Glisic, S.B., Misic, D.R., Stamenic, M.D., Zizovic, I.T., Asanin, R.M., Skala, D.U., 2007.

Supercritical carbon dioxide extraction of carrot fruit essential oil: Chemical composition and antimicrobial activity. Food Chem. 105, 346–352. doi:10.1016/j.foodchem.2006.11.062

G-18. Goleroudbary, M.G., Ghoreishi, S.M., 2016. Response surface optimization of Safranal and Crocin extraction from Crocus sativus L. via supercritical fluid technology. J. Supercrit. Fluids 108, 136–144. doi:10.1016/j.supflu.2015.10.024

G-19. Goodarznia, I., Abdollahi Govar, A., 2009. Superheated Water Extraction of Catechins from Green Tea Leaves: Modeling and Simulation. Trans. C Chem. Chem. Eng. 16, 99–107.

G-20. Goodarznia, I., Eikani, M.H., 1998. Supercritical carbon dioxide extraction of essential oils: Modeling and simulation. Chem. Eng. Sci. 53, 1387–1395. doi:10.1016/S0009-2509(97)90445-0

G-21. Gooding, O.W., 2004. Process optimization using combinatorial design principles: Parallel synthesis and design of experiment methods. Curr. Opin. Chem. Biol. 8, 297–304. doi:10.1016/j.cbpa.2004.04.009

G-22. Gopalan, B., Goto, M., Kodama, A., Hirose, T., 2000. Supercritical carbon dioxide extraction of turmeric (Curcuma longa). J Agric Food Chem 48, 2189–2192. doi:jf9908594 [pii]

G-23. Goto, M., Roy, B.C., Hirose, T., 1996. Shrinking-Core Leaching Model for Supercritical-Fluid Extraction. J. Supercrit. Fluids 9, 128–133.

G-24. Goto, M., Sato, M., Hirose, T., 1993. Extraction of peppermint oil by supercritical carbon dioxide. J. Chem. Eng. Japan 26, 401–407.

G-25. Gracia, I., Rodríguez, J.F., De Lucas, A., Fernandez-Ronco, M.P., García, M.T., 2011. Optimization of supercritical CO_2 process for the concentration of tocopherol, carotenoids and chlorophylls from residual olive husk. J. Supercrit. Fluids 59, 72–77. doi:10.1016/j.supflu.2011.05.019

G-26. Grosso, C., Ferraro, V., Figueiredo, A.C., Barroso, J.G., Coelho, J.A., Palavra, A.M., 2008. Supercritical carbon dioxide extraction of volatile oil from Italian coriander seeds. Food Chem. 111, 197–203. doi:10.1016/j.foodchem.2008.03.031

G-27. Guan, W., Li, S., Yan, R., Tang, S., Quan, C., 2007. Comparison of essential oils of clove buds extracted with supercritical carbon dioxide and other three traditional extraction methods. Food Chem. 101, 1558–1564. doi:10.1016/j.foodchem.2006.04.009

G-28. Guan, Y., Tang, Q., Fu, X., Yu, S., Wu, S., Chen, M., 2014. Preparation of antioxidants from sugarcane molasses. Food Chem. 152, 552–557. doi:10.1016/j.foodchem.2013.12.016

G-29. Guenther, E., 2008. The Essential Oils - Vol 1: History - Origin In Plants - Production - Analysis, Reprint. ed. Read Books Ltd., Redditch, England.

G-30. Gui, M.M., Lee, K.T., Bhatia, S., 2009. Supercritical ethanol technology for the production of biodiesel: Process optimization studies. J. Supercrit. Fluids 49, 286–292. doi:10.1016/j.supflu.2008.12.014

G-31. Guindani, C., Podestá, R., Block, J.M., Rossi, M.J., Mezzomo, N., Ferreira, S.R.S., 2016. Valorization of chia (Salvia hispanica) seed cake by means of supercritical fluid extraction. J. Supercrit. Fluids 112, 67–75. doi:10.1016/j.supflu.2016.02.010

H-1. Haider, M.A., Pakshirajan, K., 2007. Screening and optimization of media constituents for enhancing lipolytic activity by a soil microorganism using statistically designed experiments. Appl. Biochem. Biotechnol. 141, 377–390. doi:10.1007/BF02729074

H-2. Hampson, J.W., Ashby, R.D., 1999. Extraction of lipid-grown bacterial cells by supercritical fluid and organic solvent to obtain pure medium chain-length polyhydroxyalkanoates. J. Am. Oil Chem. Soc. 76, 1371–1374. doi:10.1007/s11746-999-0152-x

H-3. Hatami, T., Meireles, M.A.A., Zahedi, G., 2010. Mathematical modeling and genetic algorithm optimization of clove oil extraction with supercritical carbon dioxide. J. Supercrit. Fluids 51, 331–338. doi:10.1016/j.supflu.2009.10.001

H-4. He, W., Gao, Y., Yuan, F., Bao, Y., Liu, F., Dong, J., 2010. Optimization of Supercritical Carbon Dioxide Extraction of Gardenia Fruit Oil and the Analysis of Functional Components. J. Am. Oil Chem. Soc. 87, 1071–1079. doi:10.1007/s11746-010-1592-z

H-5. Hedayati, A., Ghoreishi, S.M., 2015. Supercritical carbon dioxide extraction of glycyrrhizic acid from licorice plant root using binary entrainer: Experimental optimization via response surface methodology. J. Supercrit. Fluids 100, 209–217. doi:10.1016/j.supflu.2015.03.005

H-6. Hegel, P.E., Camy, S., Destrac, P., Condoret, J.S., 2011. Influence of pretreatments for extraction of lipids from yeast by using supercritical carbon dioxide and ethanol as cosolvent. J. Supercrit. Fluids 58, 68–78. doi:10.1016/j.supflu.2011.04.005

H-7. Herzi, N., Camy, S., Bouajila, J., Destrac, P., Romdhane, M., Condoret, J.-S., 2013. Supercritical CO_2 extraction of Tetraclinis articulata: Chemical composition, antioxidant activity and mathematical modeling. J. Supercrit. Fluids 82, 72–82.

doi:10.1016/j.supflu.2013.06.007

H-8. Honarvar, B., Sajadian, S.A., Khorram, M., Samimi, A., 2013. Mathematical modeling of supercritical fluid extraction of oil from canola and sesame seeds. Brazilian J. Chem. Eng. 30, 159–166. doi:10.1590/S0104-66322013000100018

H-9. Hong, I.K., Rho, S.W., Lee, K.S., Lee, W.H., Yoo, K.P., 1990. Modeling of soybean oil bed extraction with supercritical carbon dioxide. Korean J. Chem. Eng. 7, 40–46. doi:10.1007/BF02697340

H-10. Hong, S., Sowndhararajan, K., Joo, T., Lim, C., Cho, H., Kim, S., Kim, G.Y., Jhoo, J.W., 2015. Ethanol and supercritical fluid extracts of hemp seed (Cannabis sativa L.) increase gene expression of antioxidant enzymes in HepG2 cells. Asian Pacific J. Reprod. 4, 147–152. doi:10.1016/S2305-0500(15)30012-9

H-11. Hong, S.I., Pyun, Y.R., 2001. Membrane damage and enzyme inactivation of Lactobacillus plantarum by high pressure CO_2 treatment. Int. J. Food Microbiol. 63, 19–28. doi:10.1016/S0168-1605(00)00393-7

H-12. Hou, Z., Zheng, Y., Gao, Y., Liu, X., Yuan, F., Liu, G., 2010. Optimization of supercritical carbon dioxide removal of lipid and cholesterol from goat placenta using response surface methodology. Food Bioprod. Process. 88, 298–304. doi:10.1016/j.fbp.2009.12.001

H-13. Huang, W., Li, Z., Niu, H., Li, D., Zhang, J., 2008. Optimization of operating parameters for supercritical carbon dioxide extraction of lycopene by response surface methodology. J. Food Eng. 89, 298–302. doi:10.1016/j.jfoodeng.2008.05.006

H-14. Hurtado-Benavides, A., Dorado, D.A., Sánchez-Camargo, A.D.P., 2016. Study of the fatty acid profile and the aroma composition of oil obtained from roasted Colombian coffee beans by supercritical fluid extraction. J. Supercrit. Fluids 113, 44–52. doi:10.1016/j.supflu.2016.03.008

H-15. Huynh, K.P.H., Maridable, J., Gaspillo, P., Hasika, M., Malaluan, R., Kawasaki, J., 2007. Modeling and Optimization of Supercritical Carbon Dioxide Extraction on Essential Oil from Lemongrass using Response Surface Methodology. J. Res. Sci. Comput. Eng. 4, 1–10.

I-1. Illes, V., Daood, H.G., Perneczki, S., Szokonya, L., Then, M., 2000. Extraction of coriander seed oil by CO2 and propane at super- and subcritical conditions. J. Supercrit. Fluids 17, 177-186. doi:10.1016/S0896-8446(99)00049-2

I-2. Ivanovic, J., Dimitrijevic-Brankovic, S., Misic, D., Ristic, M., <u>Zizovic, I.</u>, 2013. Evaluation and improvement of antioxidant and antibacterial activities of

supercritical extracts from clove buds. J. Funct. Foods 5, 416–423. doi:10.1016/j.jff.2012.11.014

I-3. Izadifar, M., Abdolahi, F., 2006. Comparison between neural network and mathematical modeling of supercritical CO_2 extraction of black pepper essential oil. J. Supercrit. Fluids 38, 37–43. doi:10.1016/j.supflu.2005.11.012

J-1. Jasicka-Misiak, I., Lipok, J., Nowakowska, E.M., Wieczorek, P.P., Mlynarz, P., Kafarski, P., 2004. Antifungal activity of the carrot seed oil and its major sesquiterpene compounds. Zeitschrift fur Naturforsch. - Sect. C J. Biosci. 59, 791–796.

J-2. Jawad, M., Schoop, R., Suter, A., Klein, P., Eccles, R., 2013. Supercritical carbon dioxide extraction of sea buckthorn (Hippophae rhamnoides L.) pomace. Rev. Fitoter. 13, 125–135. doi:10.1002/jsfa

J-3. Jayaprakasha, G.K., Negi, P.S., Anandharamakrishnan, C., Sakariah, K.K., 2001. Chemical composition of turmeric oil - A byproduct from turmeric oleoresin industry and its inhibitory activity against different fungi. Zeitschrift fur Naturforsch. - Sect. C J. Biosci. 56, 40–44. doi:10.1515/znc-2001-1-207

J-4. Jiao, S., Li, D., Zhang, Z., Bhandari, B., Dong Chen, X., Dong, X., Huang, Z., Mao, Z., 2008. Optimization of Supercritical Carbon Dioxide Extraction of Flaxseed Oil Using Response Surface Methodology. Int. J. Food Eng. 4, 1–17. doi:10.2202/1556-3758.1409

J-5. Jokic, S., Nagy, B., Aladi, K., Simándi, B., 2013. Supercritical fluid extraction of soybean oil from the surface of spiked quartz sand - modelling study. Croat. J. Food. Sci. Technol. 5, 70–77.

J-6. Jokic, S., Nagy, B., Zekovic, Z., Vidovic, S., Bilic, M., Velic, D., Simandi, B., 2012. Effects of supercritical CO_2 extraction parameters on soybean oil yield. Food Bioprod. Process. 90, 693-699. doi:10.1016/j.fbp.2012.03.003

K-1. Kagliwal, L.D., Patil, S.C., Pol, A.S., Singhal, R.S., Patravale, V.B., 2011. Separation of bioactives from seabuckthorn seeds by supercritical carbon dioxide extraction methodology through solubility parameter approach. Sep. Purif. Technol. 80, 533–540. doi:10.1016/j.seppur.2011.06.008

K-2. Kane, M., Dean, J.R., Hltchen, S.M., Dowle, C.J., Tranter, R.L., 1993. Experimental design approach for supercritical fluid extraction. Anal. Chotuca Acta Elsevler Sci. Pubhshers B V 271, 83–90.

K-3. Kao, L., Chen, C.R., Chang, C.M.J., 2007. Supercritical CO_2 extraction of turmerones from

turmeric and high-pressure phase equilibrium of CO_2+ turmerones. J. Supercrit. Fluids 43, 276–282. doi:10.1016/j.supflu.2007.06.007

K-4. Kao, T.H., Chien, J.T., Chen, B.H., 2008. Extraction yield of isoflavones from soybean cake as affected by solvent and supercritical carbon dioxide. Food Chem. 107, 1728–1736. doi:10.1016/j.foodchem.2007.10.015

K-5. **Kazan, A., Koyu, H., Turu, I.C., <u>Yesil-Celiktas, O.</u>, 2014. Supercritical fluid extraction of Prunus persica leaves and utilization possibilities as a source of phenolic compounds. J. Supercrit. Fluids 92, 55–59. doi:10.1016/j.supflu.2014.05.006**

K-6. **Keshav, A., <u>Wasewar, K.L.</u>, Chand, S., 2009a. Reactive extraction of propionic acid using tri-n-octylamine, tri-n-butyl phosphate and aliquat 336 in sunflower oil as diluent. J. Chem. Technol. Biotechnol. 84, 484–489. doi:10.1002/jctb.2066**

K-7. **Keshav, A., <u>Wasewar, K.L.</u>, Chand, S., Uslu, H., 2009b. Effect of binary extractants and modifier-diluents systems on equilbria of propionic acid extraction. Fluid Phase Equilib. 275, 21–26. doi:10.1016/j.fluid.2008.09.012**

K-8. Khajeh, M., 2011. Optimization of process variables for essential oil components from Satureja hortensis by supercritical fluid extraction using Box-Behnken experimental design. J. Supercrit. Fluids 55, 944–948. doi:10.1016/j.supflu.2010.10.017

K-9. Khajeh, M., Yamini, Y., Shariati, S., 2010. Comparison of essential oils compositions of Nepeta persica obtained by supercritical carbon dioxide extraction and steam distillation methods. Food Bioprod. Process. 88, 227–232. doi:10.1016/j.fbp.2008.11.003

K-10. Khoddami, A., Man, Y.B.C., Roberts, T.H., 2014. Physico-chemical properties and fatty acid profile of seed oils from pomegranate (Punica granatum L.) extracted by cold pressing. Eur. J. Lipid Sci. Technol. 116, 553–562. doi:10.1002/ejlt.201300416

K-11. King, J.W., Mohamed, A., Taylor, S.L., Mebrahtu, T., Paul, C., 2001. Supercritical fluid extraction of Vernonia galamensis seeds. Ind. Crops Prod. 14, 241–249. doi:10.1016/S0926-6690(01)00089-9

K-12. Kiriamiti, H.K., Rascol, E., Marty, A., Condoret, J.S., 2001. Extraction rates of oil from high oleic sunflower seeds with supercritical carbon dioxide. Chem. Eng. Process. 41,711-718. doi:10.1016/S0255-2701(01)00191-X

K-13. Kitryte, V., Bagdonaite, D., Rimantas Venskutonis, P., 2017. Biorefining of industrial hemp (Cannabis sativa L.) threshing residues into cannabinoid and antioxidant fractions by supercritical carbon dioxide, pressurized liquid and enzyme-assisted extractions. Food

Chem. In press, 1–10. doi:10.1016/j.foodchem.2017.09.080

K-14. Kitzberger, C.S.G., Lomonaco, R.H., Michielin, E.M.Z., Danielski, L., Correia, J., Ferreira, S.R.S., 2009. Supercritical fluid extraction of shiitake oil: Curve modeling and extract composition. J. Food Eng. 90, 35–43. doi:10.1016/j.jfoodeng.2008.05.034

K-15. Koga, Y., Iwai, Y., Hata, Y., Yamamoto, M., Arai, Y., 1996. Influence of cosolvent on solubilities of fatty acids and higher alcohols in supercritical carbon dioxide. Fluid Phase Equilib. 125, 115–128.

K-16. Kong, Y., Fu, Y.J., Zu, Y.G., Liu, W., Wang, W., Hua, X., Yang, M., 2009. Ethanol modified supercritical fluid extraction and antioxidant activity of cajaninstilbene acid and pinostrobin from pigeonpea [Cajanus cajan (L.) Millsp.] leaves. Food Chem. 117, 152–159. doi:10.1016/j.foodchem.2009.03.091

K-17. Konuskan, D.B., Arslan, M., Oksuz, A., 2018. Physicochemical properties of cold pressed sunflower, peanut, rapeseed, mustard and olive oils grown in the Eastern Mediterranean region. Saudi J. Biol. Sci. In press. doi:10.1016/j.sjbs.2018.04.005

K-18. Koubaa, M., Mhemdi, H., Vorobiev, E., 2016. Influence of canola seed dehulling on the oil recovery by cold pressing and supercritical CO_2 extraction. J. Food Eng. 182, 18–25. doi:10.1016/j.jfoodeng.2016.02.021

K-19. Kueh, B.W. Bin, Yusup, S., Osman, N., 2018. Supercritical carbon dioxide extraction of Melaleuca cajuputi leaves for herbicides allelopathy: Optimization and kinetics modelling. J. CO_2 Utilization 24, 220–227. doi:10.1016/j.jcou.2018.01.005

K-20. Kuk, M., Hron, R.J., 1994. Supercritical Carbon Dioxide Extraction of Cottonseed with Co-Solvents. JAOCS, J. Am. Oil Chem. Soc. 71, 1353–1356.

K-21. Kumhom, T., Elkamel, A., Douglas, P.L., Douglas, S., Pongamphai, S., Teppaitoon, W., 2011. Prediction of isoflavone extraction from soybean meal using supercritical carbon dioxide with cosolvents. Chem. Eng. J. 172, 1023–1032. doi:10.1016/j.cej.2011.07.019

K-22. Kumoro, A.C., Hasan, M., 2006. Modelling of supercritical carbon dioxide extraction of Andrographolide from *Andrographis Paniculata* leaves by employing integral desorption concept. Int. J. Eng. Technol. 3, 13–20.

L-1. Lack, E.A., 1985. Kriterien zur Auslegung von Anlagen fiir die Hochdruckextraktion von Naturstoffen. Ph.D. thesis.

L-2. Lancas, F.M., Queiroz, M.E.C., Silva, I.C.E., 1995. Simplex optimization of extraction of soybean oil by supercritical pentane. Chromatographia 40, 421–424.

doi:10.1007/BF02269906

L-3. Lang, Q., Wai, C., 2001. Supercritical fluid extraction in herbal and natural product studies—a practical review. Talanta 53, 771–782.

L-4. Langa, E., Cacho, J., Palavra, A.M.F., Burillo, J., Mainar, A.M., Urieta, J.S., 2009a. The evolution of hyssop oil composition in the supercritical extraction curve. Modelling of the oil extraction process. J. Supercrit. Fluids 49, 37–44. doi:10.1016/j.supflu.2008.11.022

L-5. Langa, E., Porta, G. Della, Palavra, A.M.F., Urieta, J.S., Mainar, A.M., 2009b. Supercritical fluid extraction of Spanish sage essential oil: Optimization of the process parameters and modelling. J. Supercrit. Fluids 49, 174–181. doi:10.1016/j.supflu.2008.12.007

L-6. Laokuldilok, N., Utama-ang, N., Kopermsub, P., Thakeow, P., 2015. Characterization of odor active compounds of fresh and dried turmeric by gas chromatography-mass spectrometry , gas chromatography olfactometry and sensory evaluation. Food Appl. Biosci. J. 3, 216–230.

L-7. Lee, A.K.K., Bulley, N.R., Fattori, M., Meisen, A., 1986. Modelling of supercritical carbon dioxide extraction of canola oilseed in fixed beds. J. Am. Oil Chem. Soc. 63, 921–925. doi:10.1007/BF02540928

L-8. Lee, J.-H., Kim, Y.-G., Park, J.G., Lee, J., 2017. Supercritical fluid extracts of Moringa oleifera and their unsaturated fatty acid components inhibit biofilm formation by Staphylococcus aureus. Food Control 80, 74–82. doi:10.1016/j.foodcont.2017.04.035

L-9. Lemonis, I., Tsimogiannis, D., Louli, V., Voutsas, E., Oreopoulou, V., Magoulas, K., 2013. Extraction of Dittany (Origanum dictamnus) using supercritical CO_2 and liquid solvent. J. Supercrit. Fluids 76, 48–53. doi:10.1016/j.supflu.2013.01.019

L-10. Li, B., Meng, X., Li, Y., Xue, X., 2010. Use of box-behnken design for the optimization of supercritical carbon dioxide extraction of oil from Schisandra Chinensis(Turcz.) Baill, in: Proceedings - 2010 3rd International Conference on Biomedical Engineering and Informatics, BMEI 2010. doi:10.1109/BMEI.2010.5640059

L-11. Li, J., Zhang, X., Liu, Y., 2016. Supercritical carbon dioxide extraction of Ganoderma lucidum spore lipids. LWT - Food Sci. Technol. 70, 16–23. doi:10.1016/j.lwt.2016.02.019

L-12. Li, Q., Zhang, Z., Zhong, C., Liu, Y., Zhou, Q., 2003. Solubility of solid solutes in supercritical carbon dioxide with and without cosolvents. Fluid Phase Equilib. 207, 183–192. doi:10.1016/S0378-3812(03)00022-0

L-13. Liau, B.C., Shen, C.T., Liang, F.P., Hong, S.E., Hsu, S.L., Jong, T.T., Chang, C.M.J., 2010. Supercritical fluids extraction and anti-solvent purification of carotenoids from microalgae and associated bioactivity. J. Supercrit. Fluids 55, 169–175. doi:10.1016/j.supflu.2010.07.002

L-14. Lim, S., Lee, K.T., 2013. Influences of different co-solvents in simultaneous supercritical extraction and transesterification of Jatropha curcas L. seeds for the production of biodiesel. Chem. Eng. J. 221, 436–445. doi:10.1016/j.cej.2013.02.014

L-15. Lin, C.H., Lin, H.W., Wu, J.Y., Houng, J.Y., Wan, H.P., Yang, T.Y., Liang, M.T., 2015. Extraction of lignans from the seed of Schisandra chinensis by supercritical fluid extraction and subsequent separation by supercritical fluid simulated moving bed. J. Supercrit. Fluids 98, 17–24. doi:10.1016/j.supflu.2014.12.025

L-16. Lin, M.C., Tsai, M.J., Wen, K.C., 1999. Supercritical fluid extraction of flavonoids from Scutellariae Radix. J. Chromatogr. A 830, 387–395. doi:10.1016/S0021-9673(98)00906-6

L-17. Lin, Y.-L., Yang, C.-C., Hsu, H.-K., Hsu, S.-L., Chang, C.-M.J., 2006. Response surface methodology to supercritical fluids extraction of artemisinin and the effects on rat hepatic stellate cell in vitro. J. Supercrit. Fluids 39, 48–53. doi:10.1016/j.supflu.2006.02.012

L-18. Liu, B., Shen, B., Guo, F., Chang, Y., 2008. Optimization of supercritical fluid extraction of dl-tetrahydropalmatine from rhizome of Corydalis yanhusuo W.T. Wang with orthogonal array design. Sep. Purif. Technol. 64, 242–246. doi:10.1016/j.seppur.2008.10.003

L-19. Liu, D., Schwimer, J., Liu, Z., Woltering, E.A., Greenway, F.L., 2008. Antiangiogenic Effect of Curcumin in Pure Versus in Extract Forms. Pharm. Biol. 46, 677–682. doi:10.1080/13880200802215826

L-20. Liu, J., Lin, S., Wang, Z., Wang, C., Wang, E., Zhang, Y., Liu, J., 2011. Supercritical fluid extraction of flavonoids from Maydis stigma and its nitrite-scavenging ability. Food Bioprod. Process. 89, 333–339. doi:10.1016/j.fbp.2010.08.004

L-21. Liu, S., Yang, F., Zhang, C., Ji, H., Hong, P., Deng, C., 2009. Optimization of process parameters for supercritical carbon dioxide extraction of Passiflora seed oil by response surface methodology. J. Supercrit. Fluids 48, 9–14. doi:10.1016/j.supflu.2008.09.013

L-22. Liu, W., Fu, Y.J., Zu, Y.G., Tong, M.H., Wu, N., Liu, X.L., Zhang, S., 2009. Supercritical carbon dioxide extraction of seed oil from Opuntia dillenii Haw. and its antioxidant activity. Food Chem. 114, 334–339. doi:10.1016/j.foodchem.2008.09.049

L-23. Louli, V., Folas, G., Voutsas, E., Magoulas, K., 2004. Extraction of parsley seed oil by supercritical CO_2. J. Supercrit. Fluids 30, 163–174. doi:10.1016/j.supflu.2003.07.003

L-24. Lu, T., Gaspar, F., Marriott, R., Mellor, S., Watkinson, C., <u>Al-Duri, B.,</u> Seville, J., Santos, R., 2007. Extraction of borage seed oil by compressed CO_2: Effect of extraction parameters and modelling. J. Supercrit. Fluids 41, 68–73. doi:10.1016/j.supflu.2006.10.002

L-25. Lucas, S., Calvo, M.P., García-Serna, J., Palencia, C., Cocero, M.J., 2007. Two-parameter model for mass transfer processes between solid matrixes and supercritical fluids: Analytical solution. J. Supercrit. Fluids 41, 257–266. doi:10.1016/j.supflu.2006.10.007

L-26. Lummaetee, K., Ku, H.M., Wongrat, W., Elkamel, A., 2017. Optimization of supercritical fluid extraction of isoflavone from soybean meal. Can. J. Chem. Eng. 95, 1141–1149. doi:10.1002/cjce.22786

M-1. Machado, B.A.S., Pereira, C.G., Nunes, S.B., Padilha, F.F., Umsza-Guez, M.A., 2013. Supercritical Fluid Extraction Using CO_2:Main Applications and Future Perspectives. Sep. Sci. Technol. 48, 2741–2760. doi:10.1080/01496395.2013.811422

M-2. Mackela, I., Kraujalis, P., Baranauskien, R., Rimantas Venskutonis, P., 2015. Biorefining of blackcurrant (Ribes nigrum L.) buds into high value aroma and antioxidant fractions by supercritical carbon dioxide and pressurized liquid extraction. J. Supercrit. Fluids 104, 291–300. doi:10.1016/j.supflu.2015.07.007

M-3. Maksimovic, S., Ivanovic, J., Skala, D., 2012. Supercritical extraction of essential oil from Mentha and mathematical modelling- the influence of plant particle size. Procedia Eng. 42, 1767–1777. doi:10.1016/j.proeng.2012.07.571

M-4. Manna, L., Bugnone, C.A., Banchero, M., 2015. Valorization of hazelnut, coffee and grape wastes through supercritical fluid extraction of triglycerides and polyphenols. J. Supercrit. Fluids 104, 204–211. doi:10.1016/j.supflu.2015.06.012

M-5. Maran, J.P., Priya, B., 2015. Supercritical fluid extraction of oil from muskmelon (*Cucumis melo*) seeds. J. Taiwan Inst. Chem. Eng. 47, 71–78. doi:10.1016/j.jtice.2014.10.007

M-6. Mark McHugh, V.K., 1994. Supercritical Fluid Extraction. Butterworth Heinemann, Boston.

M-7. Marr, R., Gamse, T., 2000. Use of supercritical fluids for different processes including new developments—a review. Chem. Eng. Process. Process Intensif. 39, 19–28. doi:10.1016/S0255-2701(99)00070-7

M-8.   Marrone, C., Poletto, M., Reverchon, E., Stassi, A., 1998. Almond oil extraction by supercritical CO_2: experiments and modelling. Chem. Eng. Sci. 53, 3711–3718. doi:10.1016/S0009-2509(98)00150-X

M-9.   Marsili, R., Callahan, D., 1993. Comparison of a liquid solvent extraction technique and supercritical fluid extraction for the determination of alpha- and beta-carotene in vegetables. J. Chromatogr. Sci. 31, 422–428.

M-10.   Marsni, Z. El, Casas, L., Mantell, C., Rodriguez, M., Torres, A., Macias, F.A., Martinez De La Ossa, E.J., 2013. Allelopathic properties of the fractions obtained from sunflower leaves using supercritical carbon dioxide: The effect of co-solvent addition. J. Supercrit. Fluids 82, 221–229. doi:10.1016/j.supflu.2013.07.016

M-11.   Martin, L., Gonzalez-Coloma, A., Diaz, C.E., Mainar, A.M., Urieta, J.S., 2011. Supercritical CO_2 extraction of Persea indica: Effect of extraction parameters, modelling and bioactivity of its extracts. J. Supercrit. Fluids 57, 120–128. doi:10.1016/j.supflu.2011.03.004

M-12.   Martín, L., Mainar, A.M., González-Coloma, A., Burillo, J., Urieta, J.S., 2011. Supercritical fluid extraction of wormwood (Artemisia absinthium L.). J. Supercrit. Fluids 56, 64–71. doi:10.1016/j.supflu.2010.11.017

M-13.   Martinez-Correa, H.A., Bitencourt, R.G., Kayano, A.C.A.V., Magalhães, P.M., Costa, F.T.M., Cabral, F.A., 2017. Integrated extraction process to obtain bioactive extracts of Artemisia annua L. leaves using supercritical CO_2, ethanol and water. Ind. Crops Prod. 95, 535–542. doi:10.1016/j.indcrop.2016.11.007

M-14.   Martinez, J., Rosa, P.T.V., Meireles, M.A.A., 2007. Extraction of Clove and Vetiver Oils with Supercritical Carbon Dioxide: Modeling and Simulation. Open Chem. Eng. Journal,11 1-7. doi:10.2174/187412310701011013

M-15.   Martins, P.F., De Melo, M.M.R., Silva, C.M., 2016. Techno-economic optimization of the subcritical fluid extraction of oil from Moringa oleifera seeds and subsequent production of a purified sterols fraction. J. Supercrit. Fluids 107, 682–689. doi:10.1016/j.supflu.2015.07.031

M-16.   Masek, A., Chrzescijanska, E., Zaborski, M., 2013. Characteristics of curcumin using cyclic voltammetry, UV-vis, fluorescence and thermogravimetric analysis. Electrochim. Acta 107, 441–447. doi:10.1016/j.electacta.2013.06.037

M-17.   McNally, M.E.P., 2006. Supercritical Fluid Chromatography. Compr. Anal. Chem. 47,

561–574. doi:10.1016/S0166-526X(06)47016-1

M-18. Melo, M.M.R. de, Barbosa, H.M.A., Passos, C.P., Silva, C.M., 2014. Supercritical fluid extraction of spent coffee grounds: Measurement of extraction curves, oil characterization and economic analysis. J. Supercrit. Fluids 86 86, 150–159.

M-19. Melo, M.M.R. de, Martins, P.F., Silvestre, A.J.D., Sarmento, P., Silva, C.M., 2016. Measurement and modeling of supercritical fluid extraction curves of Eichhornia crassipes for enhanced stigmasterol production: Mechanistic insights of the process. Sep. Purif. Technol. 163, 189–198. doi:10.1016/j.seppur.2016.02.038

M-20. Mendes, R.L., Reis, A.D., Pereira, A.P., Cardoso, M.T., Palavra, A.F., Coelho, J.P., 2005. Supercritical CO_2 extraction of γ-linolenic acid (GLA) from the cyanobacterium arthrospira (spirulina)maxima: Experiments and modeling. Chem. Eng. J. 105, 147–152. doi:10.1016/j.cej.2004.10.006

M-21. Mhemdi, H., Rodier, E., Kechaou, N., Fages, J., 2011a. A supercritical tuneable process for the selective extraction of fats and essential oil from coriander seeds. J. Food Eng. 105, 609–616. doi:10.1016/j.jfoodeng.2011.03.030

M-22. Mhemdi, H., Rodier, E., Kechaou, N., Fages, J., 2011b. A supercritical tuneable process for the selective extraction of fats and essential oil from coriander seeds. J. Food Eng. 105, 609–616. doi:10.1016/j.jfoodeng.2011.03.030

M-23. Micic, V., Novakovic, D., Lepojevic, Z., Jotanovic, M., Pejovic, B., Dugic, P., Petrovic, Z., 2011. Supercritical fluid extraction with carbon dioxide at different pressures. Contemp. Mater. 2, 84–87. doi:10.5767/anurs.cmat.110201.en.084M

M-24. Mihalcea, L., Turturica, M., Ghinea, I.O., Barbu, V., Ionita, E., Cotarlet, M., Stanciuc, N., 2017. Encapsulation of carotenoids from sea buckthorn extracted by CO_2 supercritical fluids method within whey proteins isolates matrices. Innov. Food Sci. Emerg. Technol. 42, 120–129. doi:10.1016/j.ifset.2017.06.008

M-25. Misic, D., <u>Zizovic, I.</u>, Stamenic, M., Asanin, R., Ristic, M., Petrovic, S.D., Skala, D., 2008. Antimicrobial activity of celery fruit isolates and SFE process modeling. Biochem. Eng. J. 42, 148–152. doi:10.1016/j.bej.2008.06.008

M-26. Mitra, P., Ramaswamy, H.S., Chang, K.S., 2009. Pumpkin (Cucurbita maxima) seed oil extraction using supercritical carbon dioxide and physicochemical properties of the oil. J. Food Eng. doi:10.1016/j.jfoodeng.2009.04.033

M-27. Mohamed, R.S., Mansoori, G.A., 2002. The use of supercritical fluid extraction technology

in food processing. Food Technol. WMRC 3–15.

M-28. Moldao-Martins, M., Palavra, A., Beirao Da Costa, M.L., Bernardo-Gil, M.G., 2000. Supercritical CO_2 extraction of Thymus zygis L. subsp. sylvestris aroma. J. Supercrit. Fluids 18, 25-34. doi:10.1016/S0896-8446(00)00047-4

M-29. Moncada, J., Tamayo, J.A., Cardona, C.A., 2016. Techno-economic and environmental assessment of essential oil extraction from Oregano (*Origanum vulgare*) and Rosemary (*Rosmarinus officinalis*) in Colombia. J. Clean. Prod. 112, 172–181. doi:10.1016/j.jclepro.2015.09.067

M-30. Mongkholkhajornsilp, D., Douglas, S., Douglas, P.L., Elkamel, A., Teppaitoon, W., Pongamphai, S., 2005. Supercritical CO_2 extraction of nimbin from neem seeds - A modelling study. J. Food Eng. 71, 331–340. doi:10.1016/j.jfoodeng.2004.08.007

M-31. Montanari, L., Fantozzi, P., Snyder, J.M., King, J.W., 1999. Selective extraction of phospholipids from soybeans with supercritical carbon dioxide and ethanol. J. Supercrit. Fluids 14, 87–93. doi:10.1016/S0896-8446(98)00110-7

M-32. Montgomery, D., 2004. Design and analysis of experiments, 5th ed. Wiley-Interscience.

M-33. Moura, P.M., Prado, G.H.C., Meireles, M.A.A., Pereira, C.G., 2012. The Journal of Supercritical Fluids Supercritical fluid extraction from guava (Psidium guajava) leaves: Global yield, composition and kinetic data. J. Supercrit. Fluids 62, 116–122. doi:10.1016/j.supflu.2011.11.014

M-34. Mukhopadhyay, M., 2009. Extraction and processing with supercritical fluids. J. Chem. Technol. Biotechnol. 84, 6–12. doi:10.1002/jctb.2072

M-35. Mukhopadhyay, M., 2000. Natural Extracts using Supercritical Carbon Dioxide.

N-1. Nabati, M., Mahkam, M., Heidari, H., 2014. Isolation and characterization of curcumin from powdered rhizomes of turmeric plant marketed in Maragheh city of Iran with soxhlet technique. Iran. Chem. Commun. 2, 236–243.

N-2. Nagy, B., Andi, S., 2008. Effects of particle size distribution, moisture content, and initial oil content on the supercritical fluid extraction of paprika. J. Supercrit. Fluids 46, 293–298. doi:10.1016/j.supflu.2008.04.009

N-3. Naik, S., <u>Goud, V. V.</u>, Rout, P.K., Dalai, A.K., 2010. Supercritical CO2fractionation of bio-oil produced from wheat-hemlock biomass. Bioresour. Technol. 101, 7605–7613. doi:10.1016/j.biortech.2010.04.024

N-4. Nam, K.-S., King, J.W., 1994. Supercritical Fluid Extraction and Enzyme Immunoassay for

Pesticide Detection in Meat Products. J. Agric. Food Chem. 42, 1469–1474.

N-5.   Negi, P.S., Jayaprakasha, G.K., Rao, L.J.M., Sakariah, K.K., 1999. Antibacterial Activity of Turmeric Oil: A Byproduct from Curcumin Manufacture. J. Agric. Food Chem. 47, 4297–4300.

N-6.   Nei, H.Z.N., Fatemi, S., Mehrnia, M.R., Salimi, A., 2008. Mathematical modeling and study of mass transfer parameters in supercritical fluid extraction of fatty acids from Trout powder. Biochem. Eng. J. 40, 72–78. doi:10.1016/j.bej.2007.11.015

N-7.   Nejad-Sadeghi, M., Taji, S., Goodarznia, I., 2015. Optimization of supercritical carbon dioxide extraction of essential oil from Dracocephalum kotschyi Boiss: An endangered medicinal plant in Iran. J. Chromatogr. A 1422, 73–81. doi:10.1016/j.chroma.2015.10.040

N-8.   Nerome, H., Ito, M., Machmudah, S., Wahyudiono, Kanda, H., Goto, M., 2016. Extraction of phytochemicals from saffron by supercritical carbon dioxide with water and methanol as entrainer. J. Supercrit. Fluids 377–383. doi:10.1016/j.supflu.2015.10.007

N-9.   Nguyen, H.N., Gaspillo, P. asa D., Maridable, J.B., Malaluan, R.M., Hinode, H., Salim, C., Huynh, H.K.P., 2011. Extraction of oil from Moringa oleifera kernels using supercritical carbon dioxide with ethanol for pretreatment: Optimization of the extraction process. Chem. Eng. Process. Process Intensif. 50, 1207–1213. doi:10.1016/j.cep.2011.08.006

N-10.   Nie, S.-P., Li, J.-E., Yang, C., Qiu, Z.-H., Xie, M.-Y., 2010. Optimization of Supercritical Fluid Extraction of Essential Oil from Herba Moslae by Response Surface Methodology and Its Chemical Composition Analysis. Food Sci. Technol. Res. 16, 185–190. doi:10.3136/fstr.16.185

N-11.   Nimet, G., da Silva, E.A., Palú, F., Dariva, C., Freitas, L. dos S., Neto, A.M., Filho, L.C., 2011. Extraction of sunflower (Heliantus annuus L.) oil with supercritical CO_2 and subcritical propane: Experimental and modeling. Chem. Eng. J. 168, 262–268. doi:10.1016/j.cej.2010.12.088

N-12.   Nobre, B.P., Mendes, R.L., Queiroz, E.M., Pessoa, F.L.P., Coelho, J.P., Palavra, A.F., 2006. Supercritical carbon dioxide extraction of pigments from bixa orellana seeds (experiments and modeling). Brazilian J. Chem. Eng. 23, 251–258. doi:10.1590/S0104-66322006000200013

N-13.   Notar, M., Leskovsek, H., 1997. Optimisation of supercritical fluid extraction of polynuclear aromatic hydrocarbons from spiked soil and marine sediment standard reference material. Fresenius J Anal Chem 358, 623–629.

N-14. Nyam, K.L., Tan, C.P., Karim, R., Lai, O.M., Long, K., Man, Y.B.C., 2010. Extraction of tocopherol-enriched oils from Kalahari melon and roselle seeds by supercritical fluid extraction (SFE-CO_2). Food Chem. 119,1278-1283. doi:10.1016/j.foodchem.2009.08.007

N-15. Nyam, K.L., Tan, C.P., Lai, O.M., Long, K., Che Man, Y.B., 2010. Optimization of supercritical fluid extraction of phytosterol from roselle seeds with a central composite design model. Food Bioprod. Process. 88, 239–246. doi:10.1016/j.fbp.2009.11.002

N-16. Nyam, K.L., Tan, C.P., Lai, O.M., Long, K., Man, Y.B.C., 2011. Optimization of supercritical CO_2 extraction of phytosterol-enriched oil from Kalahari melon seeds. Food Bioprocess Technol. 4,1432-1441. doi:10.1007/s11947-009-0253-4

O-1. Oliveira, A.L., Silva, S.S., Da Silva, M.A.P., Eberlin, M.N., Cabral, F.A., 2001. Sensory and yield response surface analysis of supercritical CO_2 extracted aromatic oil from roasted coffee. J. Food Sci. Technol. 38, 38–42.

O-2. Oliveira, P.M.A. de, Almeida, R.H. de, Oliveira, N.A. de, Bostyn, S., Gonçalves, C.B., Oliveira, A.L. de, 2014. Enrichment of diterpenes in green coffee oil using supercritical fluid extraction – Characterization and comparison with green coffee oil from pressing. J. Supercrit. Fluids 95, 137–145. doi:10.1016/j.supflu.2014.08.016

O-3. Oliveira, R., Rodrigues, M.F., Bernardo-Gil, M.G., 2002. Characterization and supercritical carbon dioxide extraction of walnut oil. JAOCS, J. Am. Oil Chem. Soc. 79, 225–230. doi:10.1007/s11746-002-0465-y

O-4. Orsavova, J., Misurcova, L., Vavra Ambrozova, J., Vicha, R., Mlcek, J., 2015. Fatty acids composition of vegetable oils and its contribution to dietary energy intake and dependence of cardiovascular mortality on dietary intake of fatty acids. Int. J. Mol. Sci. 16, 12871–12890. doi:10.3390/ijms160612871

O-5. Ortega, A.B., Gracia, A.C., Szekely, E., Skerget, M., Knez, Z., 2017. Supercritical fluid extraction from Saw Palmetto berries at a pressure range between 300 bar and 450 bar. J. Supercrit. Fluids 120, 132–139. doi:10.1016/j.supflu.2016.11.003

O-6. Ospina, M., Castro-Vargas, H.I., Parada-Alfonso, F., 2017. Antioxidant capacity of Colombian seaweeds: 1. Extracts obtained from Gracilaria mammillaris by means of supercritical fluid extraction. J. Supercrit. Fluids 128, 314–322. doi:10.1016/j.supflu.2017.02.023

O-7. Ozcan, M.M., Chalchat, J.C., 2007. Chemical composition of carrot seeds (Daucus carota L .) cultivated in Turkey: characterization of the seed oil and essential oil. Grasas y Aceites

58, 359–365. doi:10.3989/gya.2007.v58.i4.447

O-8.   Ozkal, S.G., 2009. Response Surface Analysis and Modeling of Flaxseed Oil Yield in Supercritical Carbon Dioxide. J Am Oil Chem Soc 86, 1129–1135. doi:10.1007/s11746-009-1448-6

O-9.   Ozkal, S.G., Yener, M.E., Bayindirli, L., 2005a. Response surfaces of apricot kernel oil yield in supercritical carbon dioxide. LWT - Food Sci. Technol. 38, 611–616.

O-10.   Ozkal, S.G., Yener, M.E., Bayındırlı, L., 2005b. Mass transfer modeling of apricot kernel oil extraction with supercritical carbon dioxide. J. Supercrit. Fluids 35, 119–127. doi:10.1016/j.supflu.2004.12.011

P-1.   Papamichail, I., Louli, V., Magoulas, K., 2000. Supercritical fluid extraction of celery seed oil. J. Supercrit. Fluids 18, 213–226. doi:10.1016/S0896-8446(00)00066-8

P-2.   Park, S.Y., Jin, M.L., Kim, Y.H., Kim, Y., Lee, S.J., 2012. Anti-inflammatory effects of aromatic-turmerone through blocking of NF-κB, JNK, and p38 MAPK signaling pathways in amyloid β-stimulated microglia. Int. Immunopharmacol. 14, 13–20. doi:10.1016/j.intimp.2012.06.003

P-3.   Parker, T.D., Adams, D.A., Zhou, K., Harris, M., Yu, L., 2003. Fatty acid composition and oxidative stability of cold-pressed edible seed oils. J. Food Sci. 68, 1240–1243. doi:10.1111/j.1365-2621.2003.tb09632.x

P-4.   Patel, R.N., Bandyopadhyay, S., Ganesh, A., 2011. A simple model for super critical fluid extraction of bio oils from biomass. Energy Convers. Manag. 52, 652–657. doi:10.1016/j.enconman.2010.07.043

P-5.   Patil, A.A., Sachin, B.S., Wakte, P.S., Shinde, D.B., 2014. Optimization of supercritical fluid extraction and HPLC identification of wedelolactone from Wedelia calendulacea by orthogonal array design. J. Adv. Res. doi:10.1016/j.jare.2013.09.002

P-6.   Patil, P.D., Dandamudi, K.P.R., Wang, J., Deng, Q., Deng, S., 2018. Extraction of bio-oils from algae with supercritical carbon dioxide and co-solvents. J. Supercrit. Fluids 135, 60–68. doi:10.1016/j.supflu.2017.12.019

P-7.   Paul, B.K., Munushi, M.M.U., Ahmed, M.N., Saha, G.C., Roy, S.K., 2011. The Fatty Acid Composition and Properties of Oil Extracted from Fresh Rhizomes of Turmeric (*Curcuma longa Linn.*) Cultivars of Bangladesh. BANGLADESH J. Sci. Ind. Res. 46, 127–132.

P-8.   Pavlić, B., Vidović, S., Vladić, J., Radosavljević, R., Zeković, Z., 2015. Isolation of coriander (Coriandrum sativum L.) essential oil by green extractions versus traditional

techniques. J. Supercrit. Fluids 99, 23–28. doi:10.1016/j.supflu.2015.01.029

P-9.   Pavlovic, N., Lendic, K.V., Miskulin, M., Moslavac, T., Jokic, S., 2016. Supercritical CO_2 Extraction of Sea Buckthorn. Food Heal. Dis. Sci. J. Nutr. Diet. 5, 55–61.

P-10. Pawar, H., Karde, M., Mundle, N., Jadhav, P., Mehra, K., 2014. Phytochemical Evaluation and Curcumin Content Determination of Turmeric Rhizomes Collected From Bhandara District of Maharashtra (India). Med. Chem. (Los. Angeles). 4, 588–591. doi:10.4172/2161-0444.1000198

P-11. Pederssetti, M.M., Palú, F., Da Silva, E.A., Rohling, J.H., Cardozo-Filho, L., Dariva, C., 2011. Extraction of canola seed (Brassica napus) oil using compressed propane and supercritical carbon dioxide. J. Food Eng. 102, 189–196. doi:10.1016/j.jfoodeng.2010.08.018

P-12. Peker, H., Srinivasan, M.P., Smith, J.M., McCoy, B.J., 1992. Caffeine extraction rates from coffee beans with supercritical carbon dioxide. AIChE J. 38, 761–770. doi:10.1002/aic.690380513

P-13. Pekhov, A.V.; Goncharenko, G.K., 1968. Ekstrakcija prjanogo rastitelnogo syrja szhizhennymi gazami. Maslozhirovaja promyshlennost 34, 26–29.

P-14. Perakis, C., Louli, V., Magoulas, K., 2005. Supercritical fluid extraction of black pepper oil. J. Food Eng. 71, 386–393. doi:10.1016/j.jfoodeng.2004.10.049

P-15. Pereira, C.G., Meireles, M.A.A., 2010. Supercritical fluid extraction of bioactive compounds: Fundamentals, applications and economic perspectives. Food Bioprocess Technol. 3, 340–372. doi:10.1007/s11947-009-0263-2

P-16. Pereira, C.G., Meireles, M.A.A., 2007. Economic analysis of rosemary, fennel and anise essential oils obtained by supercritical fluid extraction. Flavour Fragr. J. 22, 407–413. doi:10.1002/ffj

P-17. Pereira, P., Cebola, M.J., Oliveira, M.C., Bernardo-Gil, M.G., 2016. Supercritical fluid extraction vs conventional extraction of myrtle leaves and berries: Comparison of antioxidant activity and identification of bioactive compounds. J. Supercrit. Fluids 113, 1–9. doi:10.1016/j.supflu.2015.09.006

P-18. Perrut, M., Clavier, J.Y., Poletto, M., Reverchon, E., 1997. Mathematical Modeling of Sunflower Seed Extraction by supercritical CO_2. Ind. Eng. Chem. Res. 36, 430–435. doi:10.1021/ie960354s

P-19. Phelps, C.L., Smart, N.G., Wai, C.M., 1996. Past, Present, and Possible Future

Applications of Supercritical Fluid Extraction Technology. J. Chem. Educ. 73, 1163–1168. doi:10.1021/ed073p1163

P-20. **Pilavtepe, M., <u>Yesil-Celiktas, O.</u>, 2013. Mathematical modeling and mass transfer considerations in supercritical fluid extraction of Posidonia oceanica residues. J. Supercrit. Fluids 82, 244–250. doi:10.1016/j.supflu.2013.07.020**

P-21. Pimentel, F.A., Cardoso, M. das G., Guimaraes, L.G.L., Queiroz, F., Barbosa, L.C.A., Morais, A.R., Nelson, D.L., Andrade, M.A., Zacaroni, L.M., Pimentel, S.M.N.P., 2013. Extracts from the leaves of Piper piscatorum (Trel. Yunc.) obtained by supercritical extraction of with CO_2, employing ethanol and methanol as co-solvents. Ind. Crops Prod. 43, 490–495. doi:10.1016/j.indcrop.2012.07.067

P-22. Piras, A., Rosa, A., Marongiu, B., Porcedda, S., Falconieri, D., Dessi, M.A., Ozcelik, B., Koca, U., 2013. Chemical composition and in vitro bioactivity of the volatile and fixed oils of Nigella sativa L. extracted by supercritical carbon dioxide. Ind. Crops Prod. 46, 317–323. doi:10.1016/j.indcrop.2013.02.013

P-23. **Pitchaiah, K.C., Lamba, N., Sivaraman, N., <u>Madras, G.</u>, 2018. Solubility of trioctylmethylammonium chloride in supercritical carbon dioxide and the influence of co-solvents on the solubility behavior. J. Supercrit. Fluids 138, 102–114. doi:10.1016/j.supflu.2018.04.002**

P-24. Popuri, A.K., Pagala, B., 2013. Extraction of Curcumin From Turmeric Roots. Int. J. Innov. Res. Stud. 2, 289–299.

P-25. Porto, C. Da, Decorti, D., Natolino, A., 2016. Microwave pretreatment of Moringa oleifera seed: Effect on oil obtained by pilot-scale supercritical carbon dioxide extraction and Soxhlet apparatus. J. Supercrit. Fluids 107, 38–43. doi:10.1016/j.supflu.2015.08.006

P-26. Porto, C. Da, Decorti, D., Tubaro, F., 2012. Fatty acid composition and oxidation stability of hemp (Cannabis sativa L.) seed oil extracted by supercritical carbon dioxide. Ind. Crop. Prod. 36, 401-404. doi:10.1016/j.indcrop.2011.09.015

P-27. Porto, C. Da, Natolino, A., 2017. Supercritical fluid extraction of polyphenols from grape seed (Vitis vinifera): Study on process variables and kinetics. J. Supercrit. Fluids 130, 239–245. doi:10.1016/j.supflu.2017.02.013

P-28. Pourmortazavi, S.M., Baghaee, P., Mirhosseini, M.A., 2004. Extraction of volatile compounds from Juniperus communis L. leaves with supercritical fluid carbon dioxide: Comparison with hydrodistillation. Flavour Fragr. J. 19, 417–420. doi:10.1002/ffj.1327

P-29. Pourmortazavi, S.M., Hajimirsadeghi, S.S., 2007. Supercritical fluid extraction in plant

essential and volatile oil analysis. J. Chromatogr. A 1163, 2–24. doi:10.1016/j.chroma.2007.06.021

P-30. Povilaitis, D., Venskutonis, P.R., 2015. Optimization of supercritical carbon dioxide extraction of rye bran using response surface methodology and evaluation of extract properties. J. Supercrit. Fluids. doi:10.1016/j.supflu.2015.02.012

P-31. Prado, J.M., Prado, G.H.C., Meireles, M.A.A., 2011. Scale-up study of supercritical fluid extraction process for clove and sugarcane residue. J. Supercrit. Fluids 56, 231–237. doi:10.1016/j.supflu.2010.10.036

P-32. Prasad, R., Patsariya, R., <u>Dalvi, S. V.</u>, 2017. Precipitation of curcumin by pressure reduction of CO_2-expanded acetone. Powder Technol. 310, 143–153. doi:10.1016/j.powtec.2016.12.042

P-33. Priyadarsini, K.I., 2014. The Chemistry of Curcumin: From Extraction to Therapeutic Agent. Molecules 19, 20091–20112. doi:10.3390/molecules191220091

P-34. Priyanka, Khanam, S., 2018. Selection of suitable model for different matrices of raw materials used in supercritical fluid extraction process. Sep. Sci. Technol. 53, 71–96. doi:10.1080/01496395.2017.1378233

P-35. Przygoda, K., Zyna Wejnerowska, G., 2015. Extraction of tocopherol-enriched oils from Quinoa seeds by supercritical fluid extraction. Ind. Crop. Prod. 63, 41–47. doi:10.1016/j.indcrop.2014.09.038

P-36. Pyo, D., Yoo, J., Surh, J., 2009. Comparison of supercritical fluid extraction and solvent extraction of isoflavones from soybeans. J. Liq. Chromatogr. Relat. Technol. 32, 923–932. doi:10.1080/10826070902787351

Q-1. Qaderi, M.M., Reid, D.M., Yeung, E.C., 2007. Morphological and physiological responses of canola (Brassica napus) siliquas and seeds to UVB and CO_2 under controlled environment conditions. Environ. Exp. Bot. 60, 428–437. doi:10.1016/j.envexpbot.2006.12.019

R-1. Rai, A., Mohanty, B., Bhargava, R., 2017. Experimental Modeling and Simulation of Supercritical Fluid Extraction of *Moringa oleifera* Seed Oil by Carbon Dioxide. Chem. Eng. Commun. 204, 957–964. doi:10.1080/00986445.2017.1328415

R-2. Rai, A., Mohanty, B., Bhargava, R., 2016a. Supercritical extraction of sunflower oil: A central composite design for extraction variables. Food Chem. 192, 647–659. doi:10.1016/j.foodchem.2015.07.070

R-3.   Rai, A., Mohanty, B., Bhargava, R., 2016b. Fitting of broken and intact cell model to supercritical fluid extraction (SFE) of sunflower oil. Innov. Food Sci. Emerg. Technol. 38, 32–40. doi:10.1016/j.ifset.2016.08.019

R-4.   Rai, A., Mohanty, B., Bhargava, R., 2015. Modeling and response surface analysis of supercritical extraction of watermelon seed oil using carbon dioxide. Sep. Purif. Technol. 141, 354–365. doi:10.1016/j.seppur.2014.12.016

R-5.   Raina, V.K., Srivastava, S.K., Jain, N., Ahmad, A., Syamasundar, K. V., Aggarwal, K.K., 2002. Essential oil composition of *Curcuma longa L. cv. Roma* from the plains of northern India. Flavour Fragr. J. 17, 99–102. doi:10.1002/ffj.1053

R-6.   Raina, V.K., Srivastava, S.K., Syamasundar, K. V, 2005. Rhizome and leaf oil composition of *Curcuma longa* from lower Himalayan region of northern India. J. Essent. Oil Res. 17, 556–559. doi:10.1080/10412905.2005.9698993

R-7.   Rajaei, A., Barzegar, M., Yamini, Y., 2005. Supercritical fluid extraction of tea seed oil and its comparison with solvent extraction. Eur. Food Res. Technol. 220, 401–405. doi:10.1007/s00217-004-1061-8

R-8.   Rao, G.V.R., Srinivas, P., Sastry, S.V.G.K., Mukhopadhyay, M., 1992. Modeling Solute-co-solvent interactions for supercritical-fluid extraction of fragrances. J. Supercrit. Fluids 5, 19–23. doi:10.1016/0896-8446(92)90036-J

R-9.   Reategui, J.L.P., Machado, A.P.D.F., Barbero, G.F., Rezende, C.A., Martinez, J., 2014. Extraction of antioxidant compounds from blackberry (Rubus sp.) bagasse using supercritical CO_2 assisted by ultrasound. J. Supercrit. Fluids 94, 223–233. doi:10.1016/j.supflu.2014.07.019

R-10.   Reis-Vasco, E.M.C., Coelho, J.A.P., Palavra, A.M.F., Marrone, C., Reverchon, E., 2000. Mathematical modelling and simulation of pennyroyal essential oil supercritical extraction. Chem. Eng. Sci. 55, 2917–2922.

R-11.   Reddy, S.N., Madras, G., 2012. Semi empirical models for selectivity of supercritical carbon dioxide for solid mixtures. Sep. Purif. Technol. 89, 181–188. doi:10.1016/j.seppur.2012.01.029

R-12.   Revathy, S., Elumalai, S., Benny, M., Antony, B., 2011. Isolation , Purification and Identification of Curcuminoids from Turmeric (*Curcuma longa L* .) by Column Chromatography. J. Exp. Sci. 2, 21–25.

R-13.   Reverchon, E., 1997. Supercritical fluid extraction and fractionation of essential oils and

related products. J. Supercrit. Fluids 10, 1–37.

R-14. Reverchon, E., 1996. Mathematical Modeling of Supercritical Extraction of Sage Oil. Bioeng. Food Nat. Prod. 42, 1765–1771. doi:10.1002/aic.690420627

R-15. Reverchon, E., Daghero, J., Marrone, C., Mattea, M., Poletto, M., 1999. Supercritical fractional extraction of fennel seed oil and essential oil: Experiments and Mathematical Modeling. Ind. Eng. Chem. Res. 38, 3069–3075. doi:10.1021/ie990015+

R-16. Reverchon, E., De Marco, I., 2006. Supercritical fluid extraction and fractionation of natural matter. J. Supercrit. Fluids 146–166. doi:10.1016/j.supflu.2006.03.020

R-17. Reverchon, E., Della Porta, G., Gorgoglione, D., 1995. Supercritical CO_2 fractionation of jasmine concrete. J. Supercrit. Fluids 8, 60–65. doi:10.1016/0896-8446(95)90051-9

R-18. Reverchon, E., Donsl, G., Osseo, L.S., 1993a. Modeling of Supercritical Fluid Extraction from Herbaceous Matrices. Ind. Eng. Chem. Res 32, 2721–2726.

R-19. Reverchon, E., Kaziunas, A., Marrone, C., 2000. Supercritical CO_2 extraction of hiprose seed oil: Experiments and mathematical modelling. Chem. Eng. Sci. 55, 2195–2201. doi:10.1016/S0009-2509(99)00519-9

R-20. Reverchon, E., Marrone, C., 1997. Supercritical extraction of clove bud essential oil: Isolation and mathematical modeling. Chem. Eng. Sci. 52, 3421–3428. doi:10.1016/S0009-2509(97)00172-3

R-21. Reverchon, E., Poletto, M., 1996. Mathematical Modelling of Supercritical CO_2 Fractionation of Flower Concretes. Chem. Eng. Sci. 51, 3741–3753.

R-22. Reverchon, E., Sesti Osseo, L., Gorgoglione, D., 1994. Supercritical CO_2 extraction of basil oil: Characterization of products and process modeling. J. Supercrit. Fluids 7, 185–190. doi:10.1016/0896-8446(94)90024-8

R-23. Reyes, F.A., Mendiola, J.A., Suárez-Alvarez, S., Ibañez, E., Del Valle, J.M., 2016. Adsorbent-assisted supercritical CO_2 extraction of carotenoids from Neochloris oleoabundans paste. J. Supercrit. Fluids 112, 7–13. doi:10.1016/j.supflu.2016.02.005

R-24. Rivero, E., Costa, F.M., Watanabe, E.O., Hori, C.E., 2015. Study of soybean oil extraction with supercritical CO_2: effect of temperature on the yield and fatty acids composition. Congr. Bras. Eng. Quim. em Iniciac. Cient. 1.

R-25. Rodrigues, L.M., Alcázar-Alay, S.C., Petenate, A.J., Meireles, M.A.A., 2014. Bixin extraction from defatted annatto seeds. Comptes Rendus Chim. 17, 268–283. doi:10.1016/j.crci.2013.10.010

R-26. Rodrigues, V.H., de Melo, M.M.R., Portugal, I., Silva, C.M., 2018. Supercritical fluid extraction of Eucalyptus globulus leaves. Experimental and modelling studies of the influence of operating conditions and biomass pretreatment upon yields and kinetics. Sep. Purif. Technol. 191, 207–213. doi:10.1016/j.seppur.2017.09.026

R-27. Rodriguez-Perez, C., Mendiola, J.A., Quirantes-Pine, R., Ibanez, E., Segura-Carretero, A., 2016. Green downstream processing using supercritical carbon dioxide, CO_2-expanded ethanol and pressurized hot water extractions for recovering bioactive compounds from Moringa oleifera leaves. J. Supercrit. Fluids 116, 90–100. doi:10.1016/j.supflu.2016.05.009

R-28. Rodriguez-Solana, R., Salgado, J.M., Dominguez, J.M., Cortes-Dieguez, S., 2014. Estragole quantity optimization from fennel seeds by supercritical fluid extraction (carbon dioxide-methanol) using a Box-Behnken design. Characterization of fennel extracts. Ind. Crops Prod. 60, 186–192. doi:10.1016/j.indcrop.2014.05.027

R-29. Rohman, A., 2012. Analysis of curcuminoids in food and pharmaceutical products. Int. Food Res. J. 19, 19–27.

R-30. Romo-Hualde, A., Yetano-Cunchillos, A.I., González-Ferrero, C., Sáiz-Abajo, M.J., González-Navarro, C.J., 2012. Supercritical fluid extraction and microencapsulation of bioactive compounds from red pepper (Capsicum annum L.) by-products. Food Chem. 133, 1045–1049. doi:10.1016/j.foodchem.2012.01.062

R-31. Rónyai, E., Simándi, B., Tömösközi, S., Deák, A., Vigh, L., Weinbrenner, Z., 1998. Supercritical fluid extraction of corn germ with carbon dioxide-ethyl alcohol mixture. J. Supercrit. Fluids 14, 75–81. doi:10.1016/S0896-8446(98)00096-5

R-32. Rosa, P.T. V, Meireles, M.A.A., 2005. Rapid estimation of the manufacturing cost of extracts obtained by supercritical fluid extraction. J. Food Eng. 67, 235–240. doi:10.1016/j.jfoodeng.2004.05.064

R-33. Rostagno, M.A., Araújo, J.M.A., Sandi, D., 2002. Supercritical fluid extraction of isoflavones from soybean flour. Food Chem. 78, 111–117. doi:10.1016/S0308-8146(02)00106-1

R-34. Rovetto, L.J., Aieta, N. V., 2017. Supercritical carbon dioxide extraction of cannabinoids from Cannabis sativa L. J. Supercrit. Fluids 129, 16–27. doi:10.1016/j.supflu.2017.03.014

R-1. Rout, P.K., <u>Naik, S.N.</u>, Rao, Y.R., 2008. Subcritical CO_2 extraction of floral fragrance from Quisqualis indica. J. Supercrit. Fluids 45, 200–205. doi:10.1016/j.supflu.2008.02.011

R-35.   **Rout, P.K., <u>Naik, S.N.</u>, Rao, Y.R., Jadeja, G., Maheshwari, R.C., 2007. Extraction and composition of volatiles from Zanthoxylum rhesta: Comparison of subcritical CO$_2$ and traditional processes. J. Supercrit. Fluids 42, 334–341. doi:10.1016/j.supflu.2007.01.001**

R-36.   Roy, B.C., Goto, M., Hirose, T., 1996. Extraction of Ginger Oil with Supercritical Carbon Dioxide: Experiments and Modeling. Ind. Eng. Chem. Res 35, 607–612. doi:10.1021/ie950357p

R-37.   Roy, B.C., Goto, M., Hirose, T., Navaro, O., Hortacsu, O., 1994. Extraction rate of oil from tamato seed with supercriticle carbondi oxide. J. Chem. Eng. Japan 27, 768–772.

R-38.   Roy, B.C., Goto, M., Kodama, A., Hirose, T., 1996. Supercritical CO2 Extraction of Essential Oils and Cuticular Waxes from Peppermint Leaves. J. Chem. Technol. Biotechnol. 67, 21–26. doi:10.1002/(SICI)1097-4660(199609)67:1<21::AID-JCTB522>3.0.CO;2-0

R-39.   Rozzi, N.L., Phippen, W., Simon, J.E., Singh, R.K., 2002. Supercritical fluid extraction of essential oil components from lemon-scented botanicals. LWT - Food Sci. Technol. 35, 319–324. doi:10.1006/fstl.2001.0873

R-40.   Ruan, X., Cui, W. xia, Yang, L., Li, Z. hui, Liu, B., Wang, Q., 2017. Extraction of total alkaloids, peimine and peiminine from the flower of Fritillaria thunbergii Miq using supercritical carbon dioxide. J. CO$_2$ Util. 18, 283–293. doi:10.1016/j.jcou.2017.01.024

R-41.   Ruetsch, L., Daghero, J., Mattea, M., 2003. Supercritical extraction of solid matrices. Model formulation and experiments. Lat. Am. Appl. Res. 33, 103–107.

R-42.   Ruttarattanamongkol, K., Siebenhandl-Ehn, S., Schreiner, M., Petrasch, A.M., 2014. Pilot-scale supercritical carbon dioxide extraction, physico-chemical properties and profile characterization of Moringa oleifera seed oil in comparison with conventional extraction methods. Ind. Crops Prod. 58, 68–77. doi:10.1016/j.indcrop.2014.03.020

S-1.   Safaralie, A., Fatemi, S., Salimi, A., 2010. Experimental design on supercritical extraction of essential oil from valerian roots and study of optimal conditions. Food Bioprod. Process. 88, 312–318. doi:10.1016/j.fbp.2009.02.002

S-2.   Sahu, R., Saxena, J., 2014. Isolation of Flavonoid derivative from *Curcuma Longa*. World J. Pharm. Res. 3, 740–745.

S-3.   Saikaew, C., Kajorncheappunngam, S., 2008. An Application of Design of Experiments and Response Surface Methodology to Optimize Proanthocyanidins Yield Extracted from

Grape Seeds, in: Technology and Innovation for Sustainable Development Conference. pp. 725–733.

S-4.   Salea, R., Veriansyah, B., Tjandrawinata, R.R., 2017. Optimization and scale-up process for supercritical fluids extraction of ginger oil from Zingiber officinale var. Amarum. J. Supercrit. Fluids 120, 285–294. doi:10.1016/j.supflu.2016.05.035

S-5.   Salgin, U., 2007. Extraction of jojoba seed oil using supercritical CO_2+ethanol mixture in green and high-tech separation process. J. Supercrit. Fluids 39, 330–337. doi:10.1016/j.supflu.2006.03.013

S-6.   Salgin, U., Calimli, A., Zuhtu Uysal, B., 2004. Supercritical Fluid Extraction of Jojoba Oil. Jaocs 81, 293–296. doi:10.1007/s11746-004-0898-3

S-7.   Salgin, U., Doker, O., Calimli, A., 2006. Extraction of sunflower oil with supercritical CO_2: Experiments and modeling. J. Supercrit. Fluid 38, 326–331.

S-8.   Salgin, U., Salgin, S., 2013. Effect of main process parameters on extraction of pine kernel lipid using supercritical green solvents: Solubility models and lipid profiles. J. Supercrit. Fluids 73, 18–27. doi:10.1016/j.supflu.2012.11.002

S-9.   Salimi, A., Fatemi, S., Nei Nei, H.Z., Safaralie, A., 2008. Mathematical modeling of supercritical extraction of valerenic acid from Valeriana officinalis L. Chem. Eng. Technol. 31, 1470–1480. doi:10.1002/ceat.200800228

S-10.   Sanal, I.S., Bayraktar, E., Mehmetoglu, U., Calimli, A., 2005. Determination of optimum conditions for SC-(CO_2 + ethanol) extraction of β-carotene from apricot pomace using response surface methodology. J. Supercrit. Fluids 34, 331–338. doi:10.1016/j.supflu.2004.08.005

S-11.   Sánchez-Vicente, Y., Cabã, A., Renuncio, J.A.R., Pando, C., 2009. Supercritical fluid extraction of peach (Prunus persica) seed oil using carbon dioxide and ethanol. J. Supercrit. Fluids 49, 167–173. doi:10.1016/j.supflu.2009.01.001

S-12.   Santos, W.J. Dos, Silva, E.A., Taranto, O.P., 2013. Supercritical Fluid Extraction from Mango (Mangifera indica L.) Leaves: Experiments and Modeling. Chem. Eng. Trans. 32, 2005–2010.

S-13.   Santos, E.R.M., Oliveira, H.N.M., Oliveira, E.J., Azevedo, S.H.G., Jesus, A.A., Medeiros, A.M., Dariva, C., Sousa, E.M.B.D., 2017. Supercritical fluid extraction of Rumex Acetosa L. roots: Yield, composition, kinetics, bioactive evaluation and comparison with conventional techniques. J. Supercrit. Fluids 122, 1–9. doi:10.1016/j.supflu.2016.11.019

S-14. Santos, P., Aguiar, A.C., Barbero, G.F., Rezende, C.A., Martínez, J., 2015. Supercritical carbon dioxide extraction of capsaicinoids from malagueta pepper (Capsicum frutescens L.) assisted by ultrasound. Ultrason. Sonochem. 22, 78–88. doi:10.1016/j.ultsonch.2014.05.001

S-15. Santos, S.A.O., Villaverde, J.J., Silva, C.M., Neto, C.P., Silvestre, A.J.D., 2012. Supercritical fluid extraction of phenolic compounds from Eucalyptus globulus Labill bark. J. Supercrit. Fluids 71, 71–79. doi:10.1016/j.supflu.2012.07.004

S-16. Saravana, P.S., Getachew, A.T., Cho, Y.J., Choi, J.H., Park, Y.B., Woo, H.C., Chun, B.S., 2017. Influence of co-solvents on fucoxanthin and phlorotannin recovery from brown seaweed using supercritical CO_2. J. Supercrit. Fluids 120, 295–303. doi:10.1016/j.supflu.2016.05.037

S-17. Sato, T., Fukuda, F., Nihei, K. ichi, Itoh, N., 2017. Effect of temperature and pressure on the extraction of strawberry receptacles with a mixture of supercritical carbon dioxide and entrainers. J. Supercrit. Fluids 130, 23–29. doi:10.1016/j.supflu.2017.07.011

S-18. Schaeffer, S.T., Zalkow, L.H., Teja, A.S., 1989. Extraction of monocrotaline from Crotalaria spectabilis using supercritical carbon dioxide and carbon dioxide-Ethanol mixtures. Biotechnol. Bioeng. 34, 1357–1365. doi:10.1002/bit.260341103

S-19. Scopel, R., Neto, R.G., Falcão, M.A., Cassel, E., Vargas, R.M.F., 2013. Supercritical CO_2 extraction of Schinus molle L with co- solvents: Mathematical modeling and antimicrobial applications. Brazilian Arch. Biol. Technol. 56, 1–6. doi:10.1590/S1516-89132013000300020

S-20. Sen, A., De Melo, M.M.R., Silvestre, A.J.D., Pereira, H., Silva, C.M., 2015. Prospective pathway for a green and enhanced friedelin production through supercritical fluid extraction of Quercus cerris cork. J. Supercrit. Fluids 97, 247–255. doi:10.1016/j.supflu.2014.12.008

S-21. Shao, Q., Deng, Y., Liu, H., Zhang, A., Huang, Y., Xu, G., Li, M., 2014. Essential oils extraction from Anoectochilus roxburghii using supercritical carbon dioxide and their antioxidant activity. Ind. Crops Prod. 60, 104–112. doi:10.1016/j.indcrop.2014.06.009

S-22. Sharif, K.M., Rahman, M.M., Azmir, J., Mohamed, A., Jahurul, M.H.A., Sahena, F., Zaidul, I.S.M., 2014. Experimental design of supercritical fluid extraction - A review. J. Food Eng. 124, 105–116. doi:10.1016/j.jfoodeng.2013.10.003

S-23. Sharif, K.M., Rahman, M.M., Azmir, J., Shamsudin, S.H., Uddin, M.S., Fahim, T.K., Zaidul, I.S.M., 2015. Ethanol modified supercritical carbon dioxide extraction of

antioxidant rich extract from Pereskia bleo. J. Ind. Eng. Chem. 21, 1314–1322. doi:10.1016/j.jiec.2014.05.047

S-24. Sheibani, A., Ghaziaskar, H.S., 2008. Pressurized fluid extraction of pistachio oil using a modified supercritical fluid extractor and factorial design for optimization. LWT - Food Sci. Technol. 41, 1472–1477. doi:10.1016/j.lwt.2007.09.002

S-25. Shen, C.T., Hsu, S.L., Chang, C.M.J., 2008. Co-solvent-modified supercritical carbon dioxide extractions of cholesterol and free amino acids from soft-shell turtle fish egg. Sep. Purif. Technol. 60, 215–222. doi:10.1016/j.seppur.2007.08.014

S-26. Shi, J., Yi, C., Xue, S.J., Jiang, Y., Ma, Y., Li, D., 2009. Effects of modifiers on the profile of lycopene extracted from tomato skins by supercritical CO_2. J. Food Eng. 93, 431–436. doi:10.1016/j.jfoodeng.2009.02.008

S-27. Shilpi, A., Shivhare, U.S., Basu, S., 2013. Supercritical CO_2 Extraction of Compounds with Antioxidant Activity from Fruits and Vegetables Waste -A Review. Focus. Mod. Food Ind. 2, 43–62.

S-28. Shortle, E., Kerry, J., Furey, A., Gilroy, D., 2013. Optimisation of process variables for antioxidant components from Crataegus monogyna by supercritical fluid extraction (CO_2) using Box-Behnken experimental design. J. Supercrit. Fluids 81, 112–118. doi:10.1016/j.supflu.2013.05.007

S-29. Sieniawska, E., Swiątek, L., Rajtar, B., Koziol, E., Polz-Dacewicz, M., Skalicka-Wozniak, K., 2016. Carrot seed essential oil—Source of carotol and cytotoxicity study. Ind. Crops Prod. 92, 109–115. doi:10.1016/j.indcrop.2016.08.001

S-30. Singh, G., Kapoor, I.P.S., Singh, P., de Heluani, C.S., de Lampasona, M.P., Catalan, C.A.N., 2010. Comparative study of chemical composition and antioxidant activity of fresh and dry rhizomes of turmeric (*Curcuma longa Linn.*). Food Chem. Toxicol. 48, 1026–1031. doi:10.1016/j.fct.2010.01.015

S-31. Singh, R.P., Jain, D.A., 2011. Evaluation of antimicrobial activity of volatile oil and total curcuminoids extracted from turmeric. Int. J. ChemTech Res. 3, 1172–1178.

S-32. Skerget, M., Knez, Z., 2001. Modelling high pressure extraction processes. Comput. Chem. Eng. 25, 879–886. doi:10.1016/S0098-1354(01)00662-7

S-33. Sodeifian, G., Ardestani, N.S., Sajadian, S.A., Moghadamian, K., 2018. Properties of Portulaca oleracea seed oil via supercritical fluid extraction: Experimental and optimization. J. Supercrit. Fluids 135, 34–44. doi:10.1016/j.supflu.2017.12.026

S-34. Sodeifian, G., Azizi, J., Ghoreishi, S.M., 2014. Response surface optimization of Smyrnium cordifolium Boiss (SCB) oil extraction via supercritical carbon dioxide. J. Supercrit. Fluids 95, 1–7. doi:10.1016/j.supflu.2014.07.023

S-35. Sodeifian, G., Ghorbandoost, S., Sajadian, S.A., Ardestani, N.S., 2016a. Extraction of oil from Pistacia khinjuk using supercritical carbon dioxide: Experimental and modeling. J. Supercrit. Fluids 110, 265–274. doi:10.1016/j.supflu.2015.12.004

S-36. Sodeifian, G., Sajadian, S.A., Saadati Ardestani, N., 2017a. Experimental optimization and mathematical modeling of the supercritical fluid extraction of essential oil from Eryngium billardieri: Application of simulated annealing (SA) algorithm. J. Supercrit. Fluids 127, 146–157. doi:10.1016/j.supflu.2017.04.007

S-37. Sodeifian, G., Sajadian, S.A., Saadati Ardestani, N., 2017b. Supercritical fluid extraction of omega-3 from Dracocephalum kotschyi seed oil: Process optimization and oil properties. J. Supercrit. Fluids 119, 139–149. doi:10.1016/j.supflu.2016.08.019

S-38. Sodeifian, G., Sajadian, S.A., Saadati Ardestani, N., 2016b. Extraction of Dracocephalum kotschyi Boiss using supercritical carbon dioxide: Experimental and optimization. J. Supercrit. Fluids 107, 137–144. doi:10.1016/j.supflu.2015.09.005

S-39. Sokmen, M., Demir, E., Alomar, S.Y., 2018. Optimization of sequential supercritical fluid extraction (SFE) of caffeine and catechins from green tea. J. Supercrit. Fluids 133, 171–176. doi:10.1016/j.supflu.2017.09.027

S-40. Solana, M., Boschiero, I., Dall'Acqua, S., Bertucco, A., 2015. A comparison between supercritical fluid and pressurized liquid extraction methods for obtaining phenolic compounds from Asparagus officinalis L. J. Supercrit. Fluids 100, 201–208. doi:10.1016/j.supflu.2015.02.014

S-41. Solana, M., Boschiero, I., Dall'Acqua, S., Bertucco, A., 2014. Extraction of bioactive enriched fractions from Eruca sativa leaves by supercritical CO_2 technology using different co-solvents. J. Supercrit. Fluids. doi:10.1016/j.supflu.2014.08.022

S-42. Sovova, H., 2005. Mathematical model for supercritical fluid extraction of natural products and extraction curve evaluation. J. Supercrit. Fluids 33, 35–52. doi:10.1016/j.supflu.2004.03.005

S-43. Sovova, H., 1994. Rate of the vegetable oil extraction with supercritical CO_2-I. Modelling of extraction curves. Chem. Eng. Sci. 49, 40–414.

S-44. Sovova, H., Jez, J., Bartlova, M., Stastova, J., 1995. Supercritical carbon dioxide extraction

of black pepper. J. Supercrit. Fluids 8, 295–301. doi:10.1016/0896-8446(95)90004-7

S-45. Sovova, H., Kucera, J., Jez, J., 1994a. Rate of the vegetable oil extraction with supercritical CO_2 - II. Modeling of extraction curves. Chem. Eng. Sci. 49, 415–420.

S-46. Span, R., Wagner, W., 1996. A New Equation of State for Carbon Dioxide Covering the Fluid Region from the Triple - Point Temperature to 1100 K at Pressures up to 800 MPa. J. Phys. Chern. Ref. Data 25, 1509–1596. doi:10.1063/1.555991

S-47. Srivastava, G., Paul, A.K., <u>Goud, V. V.,</u> 2018. Optimization of non-catalytic transesterification of microalgae oil to biodiesel under supercritical methanol condition. Energy Convers. Manag. 156, 269–278. doi:10.1016/j.enconman.2017.10.093

S-48. Stahl, E., Schuetz, E., Mangold, H.K., 1980. Extraction of seed oils with liquid and supercritical carbon dioxide. J. Agric. Food Chem. 28, 1153–1157. doi:10.1021/jf60232a023

S-49. Stamenić, M., Zizovic, I., 2013. The mathematics of modelling the supercritical fluid extraction of essential oils from glandular trichomes. Comput. Chem. Eng. 48, 89–95. doi:10.1016/j.compchemeng.2012.08.006

S-50. Stastova, J., Jez, J., Bartlova, M., Sovova, H., 1996. Rate of the Vegetable oil Extraction with Supercritical CO_2-III. Extraction from Sea Buckthorn. Chem. Eng. Sci. 51, 4347–4352.

S-51. Sun, M., Temelli, F., 2006. Supercritical carbon dioxide extraction of carotenoids from carrot using canola oil as a continuous co-solvent. J. Supercrit. Fluids 37, 397–408. doi:10.1016/j.supflu.2006.01.008

S-52. Survase, V.S., Laddha, K. s., Kale, R.V., Hashmi, S.I., Lokhande, S.M., 2011. Extraction and isolation of turmerone from turmeric. Electron. J. Environ. Agric. food Chem. 10, 2173–2179.

T-1. Taguchi, M., Hobo, T., Maeda, T., 1991. Evaluation and Application of a Supercritical Fluid Extraction System using Capillary Supercritical Fluid Chromatography. J. High Resolut. Chromatogr. 14, 140–143.

T-2. Taham, T., Silva, D.O., Barrozo, M.A.S., 2016. Improvement of bixin extraction from annatto seeds using a screen-topped spouted bed. Sep. Purif. Technol. 158, 313–321. doi:10.1016/j.seppur.2015.12.037

T-3. Taher, H., Al-Zuhair, S., Al-Marzouqi, A.H., Haik, Y., Farid, M., Tariq, S., 2014. Supercritical carbon dioxide extraction of microalgae lipid: Process optimization and

laboratory scale-up. J. Supercrit. Fluids 86, 57–66. doi:10.1016/j.supflu.2013.11.020

T-4.   Talansier, E., Braga, M.E.M., Rosa, P.T. V, Paolucci-Jeanjean, D., Meireles, M.A.A., 2008. Supercritical fluid extraction of vetiver roots: A study of SFE kinetics. J. Supercrit. Fluids 47, 200–208. doi:10.1016/j.supflu.2008.07.018

T-5.   Taleb, A., 1885. Supercritical Fluids.

T-6.   Tan, T.-J., Jinap, S., Kusnadi, A.E., Hamid, N.S.A., 2008. Extraction of cocoa butter by supercritical carbon dioxide optimization of operating conditions and effect of particle size. J. Food Lipids 15, 263–276.

T-7.   Taylor, S.L., King, J.W., List, G.R., 1993. Determination of Oil Content in Oilseeds by Analytical Supercritical Fluid Extraction 4, 437–439.

T-8.   Taylor, S.L., King, J.W., Montanari, L., Fantozzi, P., Blanco, M.A., 2000. Enrichment and fractionation of phospholipid concentrates by supercritical fluid extraction and chromatography. Ital. J. Food Sci. 12, 65–76.

T-9.   Tello, J., Viguera, M., Calvo, L., 2011. Extraction of caffeine from Robusta coffee (Coffea canephora var. Robusta) husks using supercritical carbon dioxide. J. Supercrit. Fluids 59, 53-60. doi:10.1016/j.supflu.2011.07.018

T-10.   Tian, Y., He, X., Liu, S., Dong, J., 2017. Comparative analysis of lipid profile and in vitro cytotoxic activity of fermented and unfermented soybean extracted by supercritical CO_2 extraction. J. Funct. Foods 34, 369–378. doi:10.1016/j.jff.2017.05.006

T-11.   Todd, R., Baroutian, S., 2017. A techno-economic comparison of subcritical water, supercritical CO_2 and organic solvent extraction of bioactives from grape marc. J. Clean. Prod. 158, 349–358. doi:10.1016/j.jclepro.2017.05.043

T-12.   Tomasko, D.L., Li, H., Liu, D., Han, X., Wingert, M.J., Lee, L.J., Koelling, K.W., 2003. A Review of CO_2 Applications in the Processing of Polymers. Ind. Eng. Chem. Res. 42, 6431–6456. doi:10.1021/ie030199z

T-13.   Tong, P., Imagawa, T., 1995. Optimization of supercritical fluid extraction for polychlorinated biphenyls from sediments. Anal. Chim. Acta 310, 93–100. doi:10.1016/0003-2670(95)00104-8

T-14.   Tonthubthimthong, P., Douglas, P.L., Douglas, S., Luewisutthichat, W., Teppaitoon, W., Pengsopa, L.E., 2004. Extraction of nimbin from neem seeds using supercritical CO_2 and a supercritical CO_2-methanol mixture. J. Supercrit. Fluids 30, 287-301. doi:10.1016/j.supflu.2003.07.007

T-15. Trung, L., Chi, H., City, M., Ward, T.P., Chi, H., City, M., 2014. Optimization of supercritical CO_2 extraction of oleoresin from black pepper (Piper nigrum L .) and antioxidant capacity of the oleoresin. Int. Food Res. J. 21, 1489–1493.

T-16. Tsai, S.-Y., Huang, S.-J., Chyau, C.-C., Tsai, C.-H., Weng, C.-C., Mau, J.-L., 2011. Composition and antioxidant properties of essential oils from Curcuma rhizome. Asian J.Arts Sci. 2, 57–66.

T-17. Turner, W.L., Knowles, V.L., Plaxton, W.C., 2005. Cytosolic pyruvate kinase: Subunit composition, activity, and amount in developing castor and soybean seeds, and biochemical characterization of the purified castor seed enzyme. Planta 222, 1051–1062. doi:10.1007/s00425-005-0044-8

T-18. Turton, R., Bailie, R.C., Whiting, W.B., Shaeiwitz, J.A., 1998. Analysis, Synthesis, and Design of Chemical Process. PTR, Upper Saddle River: Prentice Hall.

V-1. Valadez-Carmona, L., Ortiz-Moreno, A., Ceballos-Reyes, G., Mendiola, J.A., Ibanez, E., 2018. Valorization of cacao pod husk through supercritical fluid extraction of phenolic compounds. J. Supercrit. Fluids 131, 99–105. doi:10.1016/j.supflu.2017.09.011

V-2. Valle, J.M. del, Uquiche, E.L., 2002. Particle size effects on supercritical CO_2 extraction of oil-containing seeds. J. Am. Oil Chem. Soc. 79, 1261–1266. doi:10.1007/s11746-002-0637-9

V-3. Vardanega, R., Dalmolin, I.A., Nogueira, G.C., Hatami, T., Meireles, M.A.A., 2017. Phase behaviour and mathematical modelling for the system annatto seed oil in compressed carbon dioxide + ethanol as co-solvent. J. Supercrit. Fluids 130, 56–62. doi:10.1016/j.supflu.2017.07.038

V-4. Vargas, R.M.F., Cassel, E., Gomes, G.M.F., Longhi, L.G.S., Atti-Serafini, L., Atti-Santos, A.C., 2006. Supercritical extraction of carqueja essential oil: Experiments and modeling. Brazilian J. Chem. Eng. 23, 1–9. doi:10.1590/S0104-66322006000300011

V-5. Vedaraman, N., Srinivasakannan, C., Brunner, G., Rao, P.G., 2008. Kinetics of Cholesterol Extraction Using Supercritical Carbon Dioxide with Cosolvents. Ind. Eng. Chem. Res 47, 6727–6733. doi:10.1021/ie070703q

V-6. Veggi, P.C., Cavalcanti, R.N., Meireles, M.A.A., 2011. Modifier effects on Supercritical Fluid Extraction (SFE) of some Brazilian plants: Antioxidant activity and Economical evaluation. Procedia Food Sci. 1, 1717–1724. doi:10.1016/j.profoo.2011.09.253

V-7. Vegh, K., Alberti, Á., Riethmüller, E., Toth, A., Beni, S., Kery, Á., 2014. Supercritical

fluid extraction and convergence chromatographic determination of parthenolide in Tanacetum parthenium L.: Experimental design, modeling and optimization. J. Supercrit. Fluids 95, 84–91. doi:10.1016/j.supflu.2014.07.029

V-8.   Villanueva-Bermejo, D., Zahran, F., García-Risco, M.R., Reglero, G., Fornari, T., 2017. Supercritical fluid extraction of Bulgarian Achillea millefolium. J. Supercrit. Fluids 119, 283–288. doi:10.1016/j.supflu.2016.10.005

W-1.   Wang, L., Wang, X., Wang, P., Xiao, Y., Liu, Q., 2016. Optimization of supercritical carbon dioxide extraction, physicochemical and cytotoxicity properties of Gynostemma pentaphyllum seed oil: A potential source of conjugated linolenic acids. Sep. Purif. Technol. 159, 147–156. doi:10.1016/j.seppur.2016.01.007

W-2.   Wang, L., Yang, B., Du, X., Yi, C., 2008. Optimisation of supercritical fluid extraction of flavonoids from Pueraria lobata. Food Chem. 108, 737–741. doi:10.1016/j.foodchem.2007.11.031

W-3.   Wang, W., Yang, H.J., Hu, J., Guo, C.Y., 2009. Extraction of metal ions with non-fluorous bipyridine derivatives as chelating ligands in supercritical carbon dioxide. J. Supercrit. Fluids 51, 181–187. doi:10.1016/j.supflu.2009.07.010

W-4.   Wang, Y., Gao, Y., Ding, H., Liu, S., Han, X., Gui, J., Liu, D., 2017. Subcritical ethanol extraction of flavonoids from Moringa oleifera leaf and evaluation of antioxidant activity. Food Chem. 218, 152–158. doi:10.1016/j.foodchem.2016.09.058

W-5.   Wei, M.C., Xiao, J., Yang, Y.C., 2016. Extraction of α-humulene-enriched oil from clove using ultrasound-assisted supercritical carbon dioxide extraction and studies of its fictitious solubility. Food Chem. 210, 172–181. doi:10.1016/j.foodchem.2016.04.076

W-6.   Wen, D., Jiang, H., Zhang, K., 2009. Supercritical fluids technology for clean biofuel production. Prog. Nat. Sci. 19, 273–284. doi:10.1016/j.pnsc.2008.09.001

W-7.   Westerman, D., Santos, R.C.D., Bosley, J.A., Rogers, J.S., Al-Duri, B., 2006. Extraction of Amaranth seed oil by supercritical carbon dioxide. J. Supercrit. Fluids 37, 38–52. doi:10.1016/j.supflu.2005.06.012

W-8.   Wheeler, J.R., McNally, M.E., 1989. Supercritical fluid extraction and chromatography of representative agricultural products with capillary and microbore columns. J. Chromatogr. Sci. 27, 534–539. doi:10.1093/chromsci/27.9.534

W-9.   Wilson, R.E., Keith, P.C., Haylett, R.E., 1936. Liquid propane: Use in Dewaxing, Deasphalting, and Refining Heavy Oils. Ind. Eng. Chem. 28, 1065–1078.

doi:10.1021/ie50321a022

X-1. Xavier, V.B., Vargas, R.M.F., Cassel, E., Lucas, A.M., Santos, M.A., Mondin, C.A., Santarem, E.R., Astarita, L. V., Sartor, T., 2011. Mathematical modeling for extraction of essential oil from Baccharis spp. by steam distillation. Ind. Crops Prod. 33, 599–604. doi:10.1016/j.indcrop.2010.12.019

X-2. Xiao, J.B., Chen, J.W., Xu, M., 2007. Supercritical fluid CO_2 extraction of essential oil from Marchantia convoluta: Global yields and extract chemical composition. Electron. J. Biotechnol. 10, 141–148. doi:10.2225/vol10-issue5-fulltext-3

X-3. Xu, L., Zhan, X., Zeng, Z., Chen, R., Li, H., Xie, T., Wang, S., 2011. Recent advances on supercritical fluid extraction of essential oils. African J. Pharm. Pharmacol. Pharmacol. 5, 1196–1211. doi:10.5897/AJPP11.228

Y-1. Yang, C.C., Lee, M.R., Hsu, S.L., Chang, C.M.J., 2007. Supercritical fluids extraction of capillarisin from Artemisia capillaris and its inhibition of in vitro growth of hepatoma cells. J. Supercrit. Fluids 42, 96–103. doi:10.1016/j.supflu.2006.12.022

Y-2. Yang, S.X.. b, Shi, W.., Zeng, J.., 2004. Modelling the supercritical fluid extraction of lycopene from tomato paste waste using neuro-fuzzy approaches. Lect. Notes Comput. Sci. (including Subser. Lect. Notes Artif. Intell. Lect. Notes Bioinformatics) 3174, 880–885.

Y-3. Yang, Y.C., Wei, M.C., Hong, S.J., 2014. Ultrasound-assisted extraction and quantitation of oils from Syzygium aromaticum flower bud (clove) with supercritical carbon dioxide. J. Chromatogr. A 1323, 18–27. doi:10.1016/j.chroma.2013.10.098

Y-4. Yepez, B., Espinosa, M., López, S., Bolaos, G., 2002. Producing antioxidant fractions from herbaceous matrices by supercritical fluid extraction. Fluid Phase Equilib. 194, 879–884. doi:10.1016/S0378-3812(01)00707-5

Y-5. Yilmaz, E.E., Özvural, E.B., Vural, H., 2011. Extraction and identification of proanthocyanidins from grape seed (Vitis Vinifera) using supercritical carbon dioxide. J. Supercrit. Fluids 55, 924–928. doi:10.1016/j.supflu.2010.10.046

Y-6. Yin, J., Wang, A., Wei, W., Liu, Y., Shi, W., 2005. Analysis of the operation conditions for supercritical fluid extraction of seed oil. Sep. Purif. Technol. 43, 163–167. doi:10.1016/j.seppur.2004.10.016

Y-7. Yothipitak, W., Thana, P., Goto, M., Shotipruk, A., 2008. Experiments and Statistical Analysis of Supercritical Carbon Dioxide Extraction. Chiang Mai J. Sci 35, 109–115.

Z-1. Zaghdoudi, K., Framboisier, X., Frochot, C., Vanderesse, R., Barth, D., Kalthoum-Cherif,

J., Blanchard, F., Guiavarch, Y., 2016. Response surface methodology applied to Supercritical Fluid Extraction (SFE) of carotenoids from Persimmon (Diospyros kaki L.). Food Chem. 208, 209–216. doi:10.1016/j.foodchem.2016.03.104

Z-2.   Zahedi, G., Elkamel, A., Lohi, A., Hatami, T., 2010. Optimization of supercritical extraction of nimbin from neem seeds in presence of methanol as co-solvent. J. Supercrit. Fluids 55, 142–148. doi:10.1016/j.supflu.2010.08.006

Z-3.   Zarena, A.S., Manohar, B., Udaya Sankar, K., 2010. Optimization of Supercritical Carbon Dioxide Extraction of Xanthones from Mangosteen Pericarp by Response Surface Methodology. Food Bioprocess Technol. 5, 1181–1188. doi:10.1007/s11947-010-0404-7

Z-4.   Zekovic, Z., Bera, O., Durovic, S., Pavlic, B., 2017. Supercritical fluid extraction of coriander seeds: Kinetics modelling and ANN optimization. J. Supercrit. Fluids 125, 88–95. doi:10.1016/j.supflu.2017.02.006

Z-5.   Zekovic, Z., Busic, A., Komes, D., Vladic, J., Adamovic, D., Pavlic, B., 2015. Coriander seeds processing: Sequential extraction of non-polar and polar fractions using supercritical carbon dioxide extraction and ultrasound-assisted extraction. Food Bioprod. Process. 95, 218–227. doi:10.1016/j.fbp.2015.05.012

Z-6.   Zekovic, Z., Pavlic, B., Cvetanovic, A., Durovic, S., 2016. Supercritical fluid extraction of coriander seeds: Process optimization, chemical profile and antioxidant activity of lipid extracts. Ind. Crops Prod. 94, 353–362. doi:10.1016/j.indcrop.2016.09.008

Z-7.   Zhang, S., Zu, Y.G., Fu, Y.J., Luo, M., Li, W.L., Efferth, T., 2010. Supercritical carbon dioxide extraction of seed oil from yellow horn (Xanthoceras sorbifolia Bunge.) and its anti-oxidant activity. Bioresour. Technol. 101, 2537–2544. doi:10.1016/j.biortech.2009.11.082

Z-8.   Zhao, S., Zhang, D., 2014. An experimental investigation into the solubility of Moringa oleifera oil in supercritical carbon dioxide. J. Food Eng. 138, 1–10. doi:10.1016/j.jfoodeng.2014.03.031

Z-9.   Zhao, S., Zhang, D., 2013a. Supercritical fluid extraction and characterisation of Moringa oleifera leaves oil. Sep. Purif. Technol. 118, 497–502. doi:10.1016/j.seppur.2013.07.046

Z-10.   Zhao, S., Zhang, D., 2013b. A parametric study of supercritical carbon dioxide extraction of oil from Moringa oleifera seeds using a response surface methodology. Sep. Purif. Technol. 113, 9–17. doi:10.1016/j.seppur.2013.03.041

Z-11.   Zheng, L., Shi, L.K., Zhao, C.W., Jin, Q.Z., Wang, X.G., 2017. Fatty acid, phytochemical,

oxidative stability and in vitro antioxidant property of sea buckthorn (Hippophaë rhamnoides L.) oils extracted by supercritical and subcritical technologies. LWT - Food Sci. Technol. 86, 507–513. doi:10.1016/j.lwt.2017.08.042

Z-12.   Zhiyi, L., Xuewu, L., Shuhua, C., Xiaodong, Z., Yuanjing, X., Yong, W., Feng, X., 2006. An experimental and simulating study of supercritical CO_2 extraction for pepper oil. Chem. Eng. Process. Process Intensif. 45, 264–267. doi:10.1016/j.cep.2005.08.005

Z-13.   Zhou, D., Qi, L., Qiao, B.Q., Xu, Q.Q., Yin, J.Z., 2017. Continuous production of biodiesel from soybean flakes by extraction coupling with transesterification under supercritical conditions: Original research article. J. Supercrit. Fluids 120, 395–402. doi:10.1016/j.supflu.2016.05.051

Z-14.   Zhou, M., Trubey, R.K., Keil, Z.O., Sparks, D.L., 1997. Study of the Effects of Environmental Variables and Supercritical Fluid Extraction Parameters on the Extractability of Pesticide Residues from Soils Using a Multivariate Optimization Scheme. Environ. Sci. Technol. 31, 1934–1939. doi:10.1021/es960709z

Z-15.   Zhou, R., Li, S., 2009. Supercritical carbon dioxide and co-solvent extractions of estradiol and progesterone from antler velvet. J. Food Compos. Anal. 22, 72–78. doi:10.1016/j.jfca.2008.07.008

Z-16.   Zizovic, I., Ivanovic, J., Misic, D., Stamenic, M., Djordjevic, S., Kukic-Markovic, J., Petrovic, S.D., 2012. SFE as a superior technique for isolation of extracts with strong antibacterial activities from lichen Usnea barbata L. J. Supercrit. Fluids 72, 7–14. doi:10.1016/j.supflu.2012.07.018

Z-17.   Zizovic, I., Stamenic, M., Ivanovic, J., Orlovic, A., Ristic, M., Djordjevic, S., Petrovic, S.D., Skala, D., 2007a. Supercritical carbon dioxide extraction of sesquiterpenes from valerian root. J. Supercrit. Fluids 43, 249–258. doi:10.1016/j.supflu.2007.05.007

Z-18.   Zizovic, I., Stamenic, M., Orlovic, A., Skala, D., 2007b. Supercritical carbon dioxide extraction of essential oils from plants with secretory ducts: Mathematical modelling on the micro-scale. J. Supercrit. Fluids 39, 338–346. doi:10.1016/j.supflu.2006.03.009

Z-19.   Zizovic, I., Stamenic, M., Orlovic, A., Skala, D., 2005. Supercritical carbon dioxide essential oil extraction of Lamiaceae family species: Mathematical modelling on the micro-scale and process optimization. Chem. Eng. Sci. 60, 6747–6756. doi:10.1016/j.ces.2005.03.068

Z-20.   Zkal, S.G., Yener, M.E., Bayındırlı, L., 2005. Response surfaces of apricot kernel oil yield

in supercritical carbon dioxide. LWT 38, 611–616. doi:10.1016/j.lwt.2004.08.003

Z-21. Zordi, N. De, Cortesi, A., Kikic, I., Moneghini, M., Solinas, D., Innocenti, G., Portolan, A., Baratto, G., Acqua, S.D., 2014. The supercritical carbon dioxide extraction of polyphenols from Propolis: A central composite design approach. J. Supercrit. Fluids 95, 491–498. doi:10.1016/j.supflu.2014.10.006

Z-22. Zuo, Y.B., Zeng, A.W., Yuan, X.G., Yu, K.T., 2008. Extraction of soybean isoflavones from soybean meal with aqueous methanol modified supercritical carbon dioxide. J. Food Eng. 89, 384–389. doi:10.1016/j.jfoodeng.2008.05.004

ABBREVIATIONS OF DIFFERENT RAW MATERIALS

S. No.	Solute	Code	S. No.	Solute	Code
1	Coriander seed	COR	130	Jasmine flowers	JF
2	Apricot pomace	APR	131	Tomato seed	TOS
3	Sesame seed	SES	132	Beef liver	BeL
4	Moringa oleifera	MO	133	Ground beef	GBe
5	Sunflower	SF	134	Lard	Lrd
6	Vetiver roots	VET	135	Sediment	SDMT
7	Green tea	GT	136	Spilanthes americana	SA
8	Olive husk	OH	137	Evening primrose	EP
9	Polychlorinated biphenyls	PCB	138	Plasticized PVC	PPVC
10	Spent coffee grounds	SCG	139	Animal tissue	AT
11	Eucalyptus globulus bark	EG	140	A-naphthol-impregnated	α-naph
12	Sugarcane molasses.	SG	141	Citrus peel oil	CPO
13	Monoraphidium sp. (GK12)	GK12	142	Wheat germ	WG
14	Soybean flakes	SBF	143	Cedarwood chips	CWC
15	Defatted soybean flakes	DSBF	144	Thyme	TYM
16	Seabuckthorn	SBT	145	White pine needles	WPN
17	Rosemary leaves	Rose	146	Plane tree leaf	PTL
18	Andrographis paniculata	AP	147	Poppy seed	POS
19	Opuntia dillenii Haw.	OD	148	Medlar seeds	MS
20	Lavandin essential oil	LDO	149	Chamomile flower heads	CFH
21	Orange peel	OP	150	Apium graveolens l.	AGL
22	Persea indica L.	PIL	151	Annatto seed	ANS
23	German beech wood	GBW	152	Loquat seed	LOS
24	Clove bud	CB	153	Physic nut	PYN
25	Eremanthus erythropappus	EE	154	Nepeta persica	NP
26	Banana peel	BP	155	Olive oil	OO
27	Psidium guajava L.	PGL	156	Herba moslae	HM
28	Celery seeds	Cel	157	Schisandra chinensis baill	SCB
29	Corn germ	CG	158	Caper seed	CpS
30	Curry flower	CF	159	Roselle seed	RoS
31	Sage leaves	SL	160	Rye bran	RB
32	Fig leaf gourd	FLG	161	Hylocereus polyrhizus	HyP
33	Scutellaria baicalensis	SB	162	Watermelon seed	WM
34	Vernonia galamensis	VG	163	Phaseolus vulgaris L.	PVL
35	Nannochloropsis oculata	NO	164	Kniphofia uvaria	KU

36	Fungal mycelia	FM	165	Chia seed (Salvia hispanica)	ChS
37	Biphenyl-soil	B-S	166	Guava seeds	Gus
38	Cashew nut shell	CNS	167	Jatropha curcas l.	JCL
39	Jojoba seed	JOJ	168	Jordanian oil shale	JOS
40	Grape seed	GS	169	Fenugreek(Trigonella foenum-graecum L.)	FG
41	Canola seed	Rap	170	Black eyed pea	BEP
42	Schizochytrium	SCM	171	Peanut (Arachis hypogaea)	Pea
43	Spirulina	SPL	172	Muskmelon (Cucumis melo)	MM
44	Rape seed	Rape	173	Camelina seed	CMS
45	Soyabeen	SB	174	Coffee	CFE
46	Cow brain	COB	175	Hemp seed	HMP
47	Black pepper	BLP	176	Amaranth seed	AMS
48	Saccharomyces cerevisiae	SC	177	Butia seed	BTS
49	Dunaliella salina	DC	178	Cacao pod husk	CPH
50	Posidonia oceanica	PO	179	Oats	OTS
51	Trout fish powder	TFP	180	Portulaca oleracea	POA
52	Tuberose	Trose	181	Peppermint oil	PMO
53	Basil leaves	BL	182	Corydalis yanhusuo	CY
54	Marjoram leaves	ML	183	Glycyrrhiza glabra	GG
55	Cocoa liquor	COL	184	Heteropterys aphrodisiaca	HA
56	Caraway seeds	CAS	185	Rumex acetosa	RA
57	Hiprose seed	HS	186	Rose flower	RoseF
58	Parsley seed	PS	187	Hawthorn flower	HF
59	Marigold flowers	MGF	188	Dittany (O. Dictamnus)	Ditt
60	Fennel seeds	FS	189	Calluna vulgaris	CV
61	Nutmeg seed	NUS	190	Rosa damascena Mill	RDM
62	Baccharis trimera	BT	191	Fritillaria thunbergii Miq	FTM
63	Borage seed	BS	192	Rosemary leaves	RoseL
64	Hazelnut	HN	193	Oregano bracts	OB
65	Walnut	WN	194	Myrtus communis L.	MCL
66	Pumpkin seed	PPS	195	Hawthorn leaf	HL
67	Calendula	CAL	196	Pereskia bleo	PB
68	Paprika	PAP	197	Broccoli leaves	BrL
69	Shiitake	SHI	198	Sunflower leaves	SFL
70	Safflower seed	SFF	199	Pyrostegia venusta Leaves	PV
71	Spanish sage	SS	200	Inga edulis Leaves	IE
72	Hyssopus officinalis L.	HOL	201	Prunus persica	PP
73	Yellow horn	YH	202	Piper piscatorum	PiP
74	Ilex paraguariensis St. Hil.	IPSH	203	Eruca sativa	ES

75	Mango leaves	MAL	204	Eichhornia crassipes	EC
76	Basil leaves	BL	205	Portuguese myrtle	PM
77	Almond seeds	AS	206	Pigeonpea leaves	PPL
78	Hop of Magnum cultivar	MC	207	Wormwood	WW
79	Sesame seed	SES	208	Baccharis dracunculifolia	BD
80	Turmeric rhizomes	TR	209	Uvaia Leaves	UL
81	B-naphthol	β-naph	210	Eucalyptus globulus leaves	EGL
82	Crotalaria spectabifis	CrS	211	Melaleuca cajuputi leaves	MCJ
83	Peppermint leaves	PL	212	Catharanthus roseus	CR
84	1,2-dichlorobenzene	1,2-DCB	213	Achillea millefolium	ACM
85	1,2,4-trichlorobenzene	1,2,4-TCB	214	Stevia leaf	STL
86	Pennyroyal leaves	PEL	215	Spinach	SPH
87	Lavender flowers	LF	216	Arthrospira maxima	AM
88	Egg yolk powder	EYP	217	Saffron (Crocus sativus L.)	SaFF
89	Silybum marianum	SM	218	Maydis stigma	MaS
90	Ginger	Gin	219	Feverfew	FeF
91	Rosehip seed	RS	220	G. Lucidum	GL
92	Neem seed	NS	221	Neochloris oleoabundans	NeO
93	Bixa orellana	BO	222	Anoectochilus roxburghii	AR
94	Chamomile flower	CMF	223	Antler velvet	AV
95	Valeriana officinalisl.	VOL	224	Turtle fish egg powder	TFEP
96	Olive leaves	OL	225	Nannochloropsis oculata	NNS
97	Schinus molle L.leaves	SML	226	Pleurotus ostreatus	PLS
98	Filamentous fungi	FF	227	Red seaweeds	RSW
99	Cottonseed	CTS	228	Brown seaweed	BSW
100	Tomato skins	TS	229	Scenedesmus obliquus	SO
101	Peach seed	PES	230	Satureja hortensis	SH
102	Anise	Ani	231	Smyrnium cordifolium	SmC
103	Black cumin seed	BCS	232	Alnus glutinosa (L.) Gaertn	AGG
104	Phenol	Phn	233	Lippia alba (Mill.)	LA
105	Mentha piperita	MP	234	Asparagus officinalis L.	AOL
106	Lemongrass	LG	235	Wedelia calendulacea	WC
107	Pueraria lobata	PLB	236	Quercus cerris	QC
108	Beef	Beef	237	Hypericum caprifoliatum	HC
109	Coca leaves	CL	238	Copaifera langsdorffii	CLa
110	Castor seed	CTR	239	Dracocephalum kotschyi Boiss	DKB
111	Apricot kernel	AK	240	Red pepper	RP
112	Tea seed	TES	241	Artemisia capillaris	AC

113	Amaranth cruentus	AMC	242	Eryngium billardieri	EB
114	Haematococcus pluvialis	HP	243	Grape peel	GrP
115	Amomum krevanh Pierre.	AKP	244	Carrot	CRT
116	Pistachio nut	PN	245	Pine kernel	PK
117	Marchantia convoluta	MCC	246	Hawthorn berry	HB
118	Tomato pomace	TP	247	Persimmon fruits	PF
119	Flax seed	FXS	248	Blackcurrant	BC
120	Crude palm oil	CPO	249	Propolis	Pro
121	Passion fruit seed	PFS	250	Blackberry	BB
122	Gardenia jasminoides Ells	GJE	251	Malagueta pepper fruit	MPF
123	Mangosteen fruit pericarp	MFP	252	Pistacia khinjuk stocks fruit	PKS
124	Goat placenta	GP	253	Strawberry	STW
125	Magnolia officinalis	MLO	254	Pequi	Peq
126	Milk fat	MF	255	Saw palmetto	SP
127	Fish oil	FO	256	Buriti	Bur
128	Link sausage	LS	257	Herbaceous	Her
129	White fir sapwood	WFS			

Use of COMSOL multyphysics 5.3 to solve the mathematical models
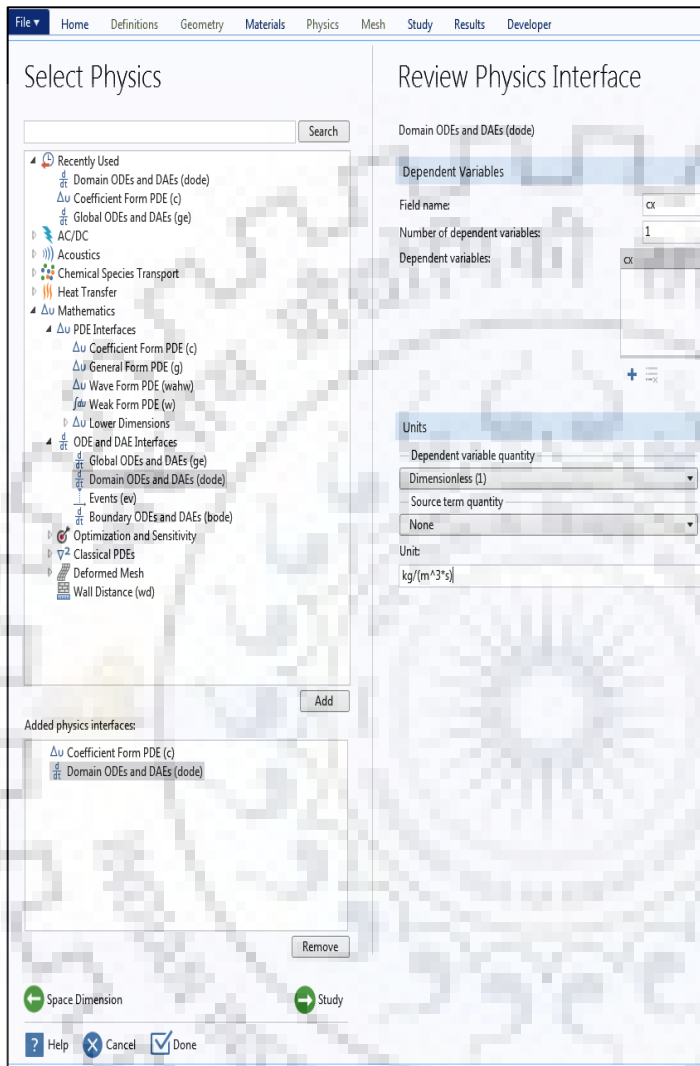
Fig. B.1: Physics setting window.
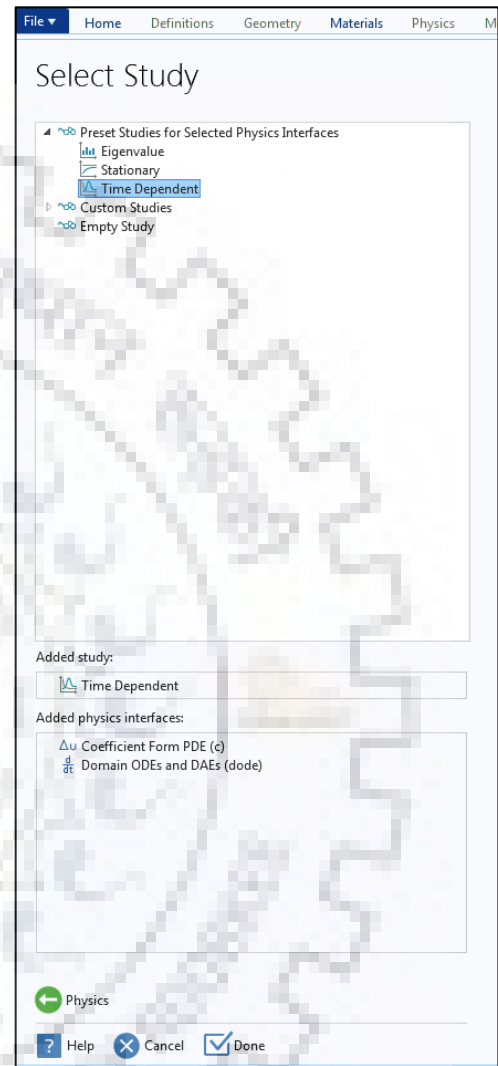
Fig. B.2: Type of study window.
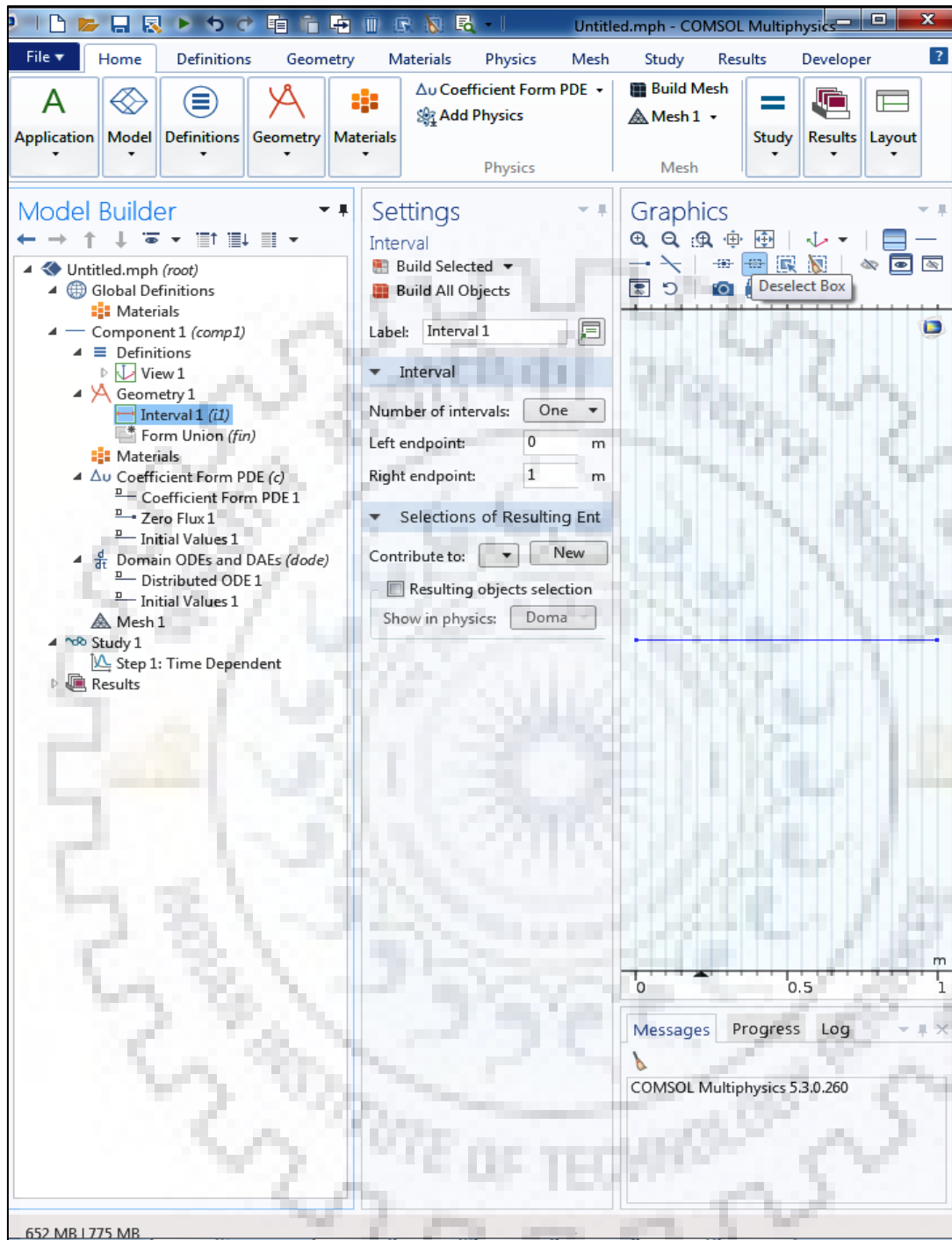
Fig. B.3: Geometry setting window.
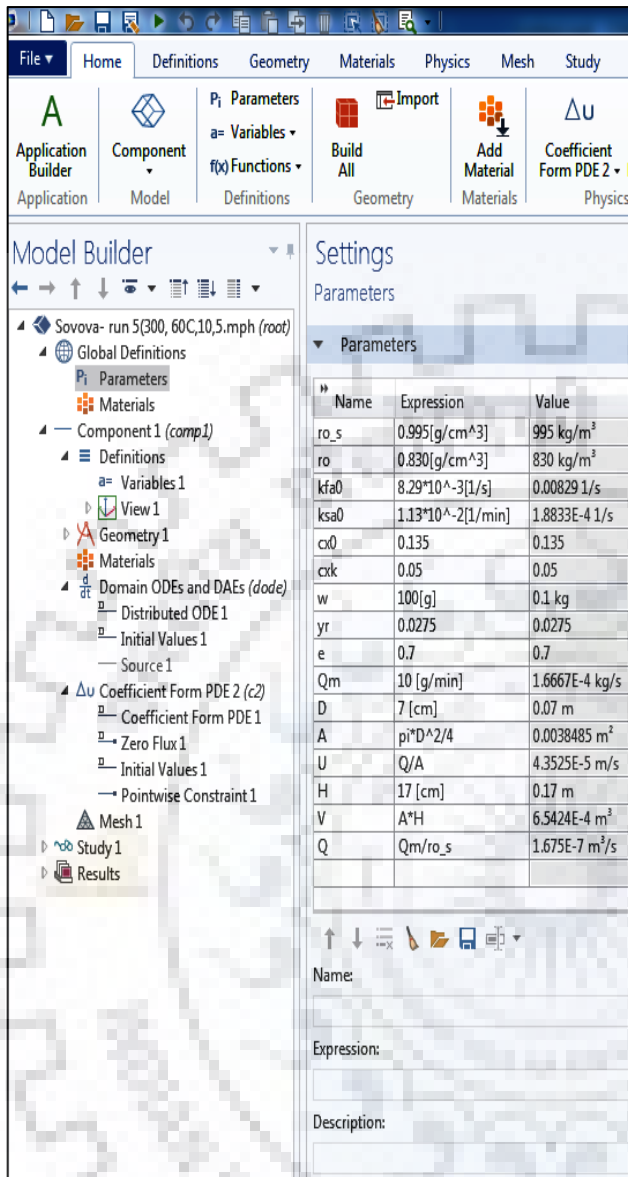
Fig. B.4: Parameters setting window.
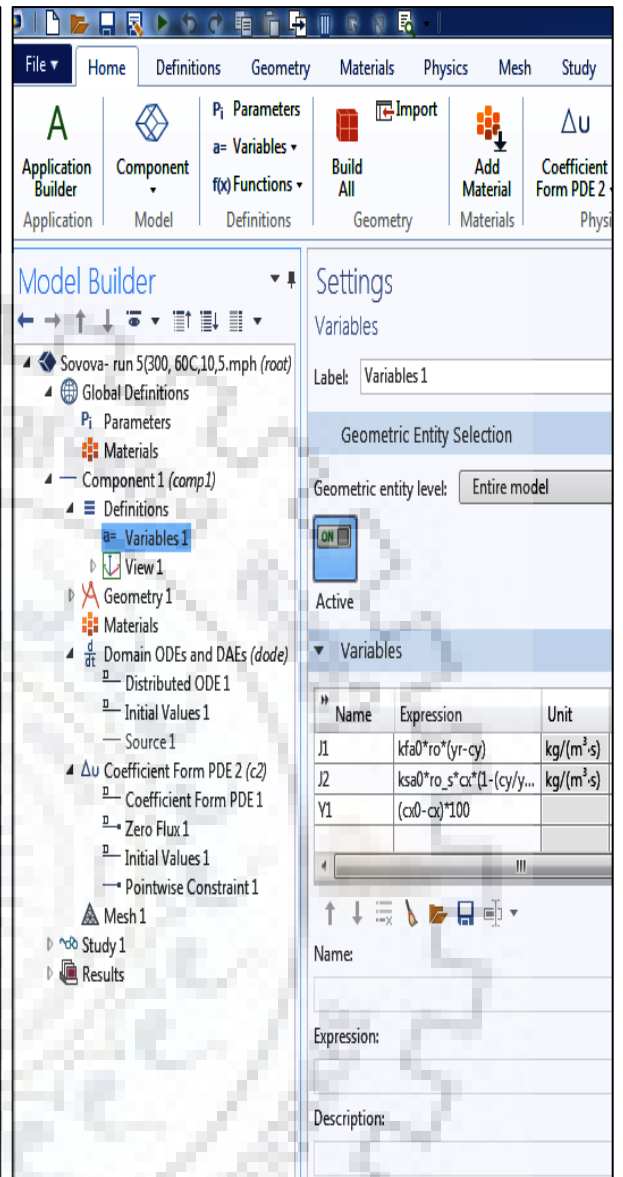
Fig. B.5: Variables setting window.
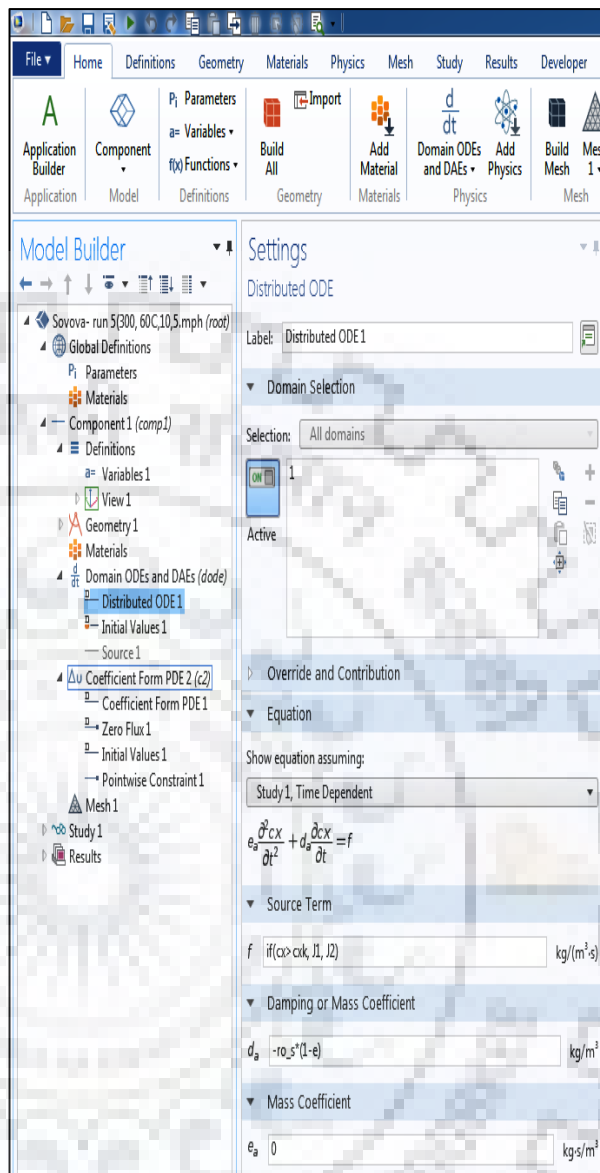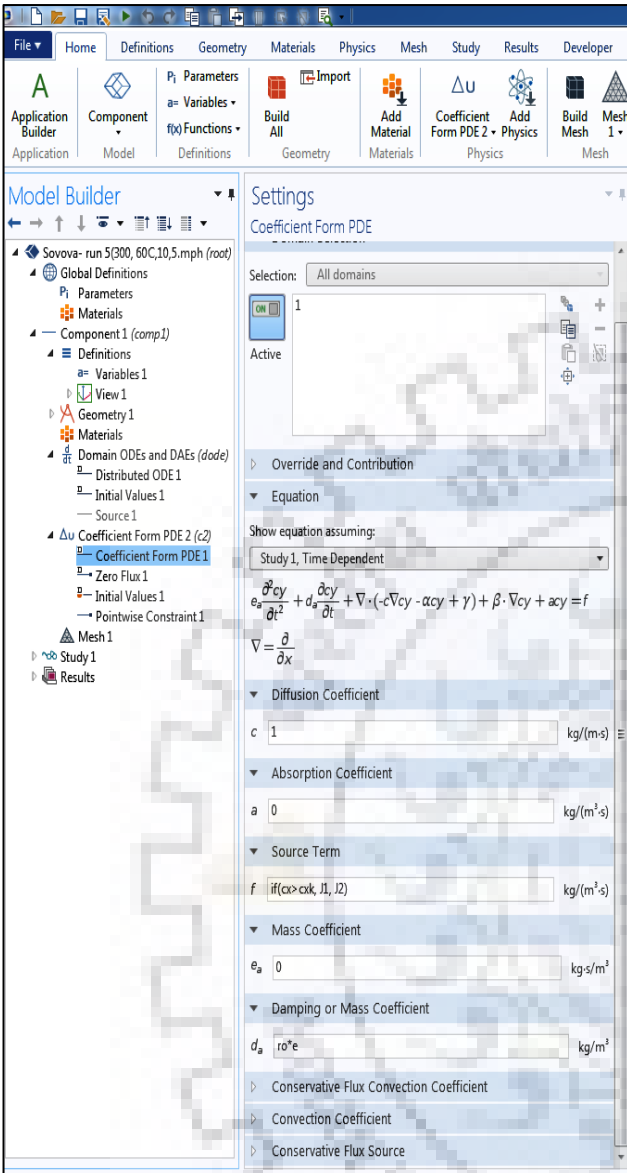
Fig. B.6: Coefficient form PDE setting window.

Fig. B.7: Distributed ODE 1 setting window.
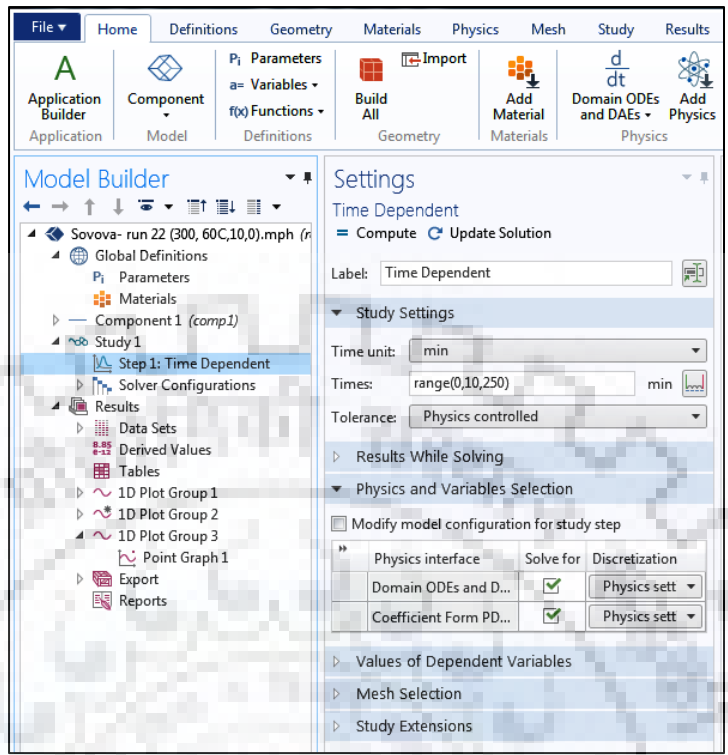
Fig. B.8: Time dependent Study setting window.
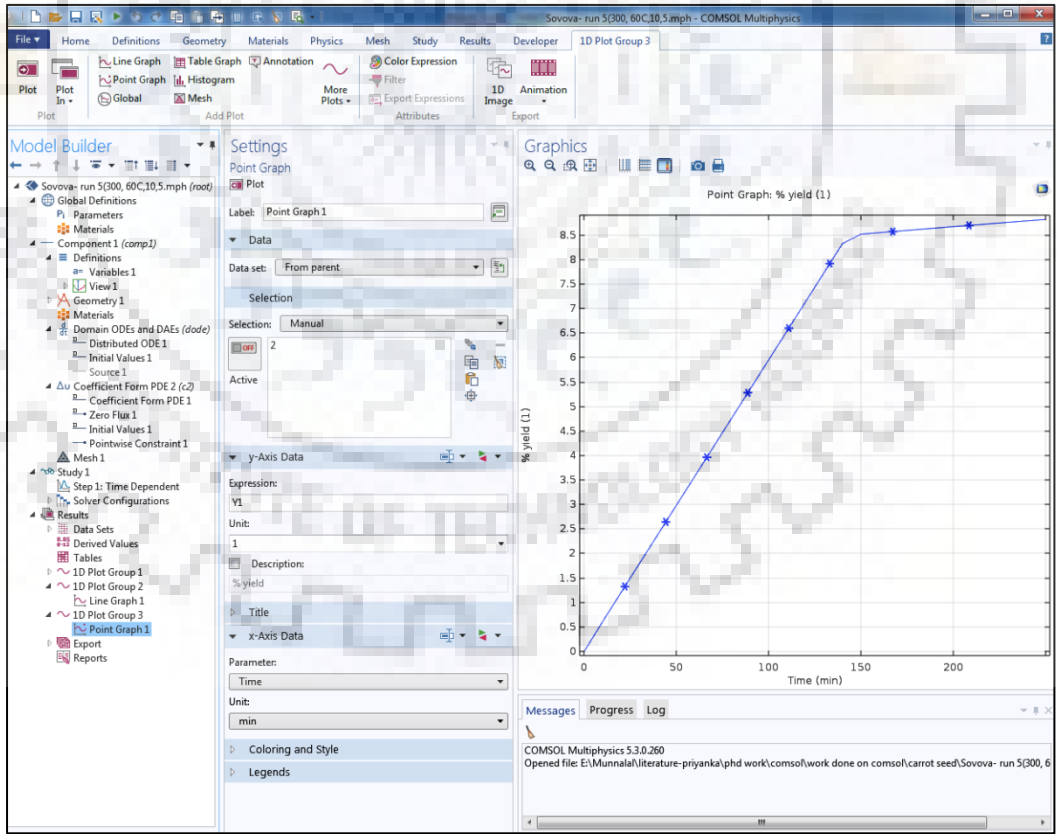
Fig. B.9: Results setting window of model.

Gas chromatogram of Turmeric root essential oil (Run 1 to 50, Soxhlet extraction)
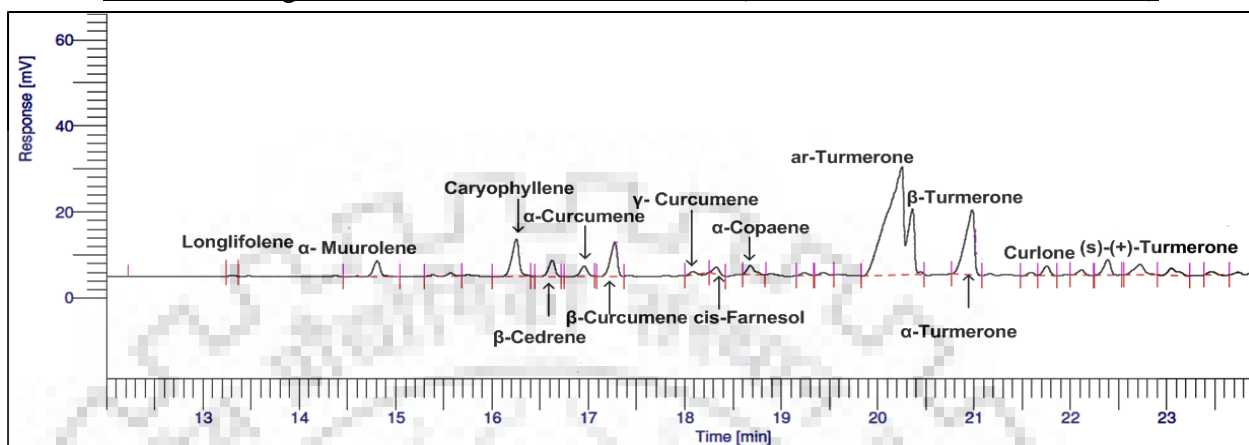
Fig. C.1: Gas chromatogram of Turmeric root essential oil, Run No. 01.
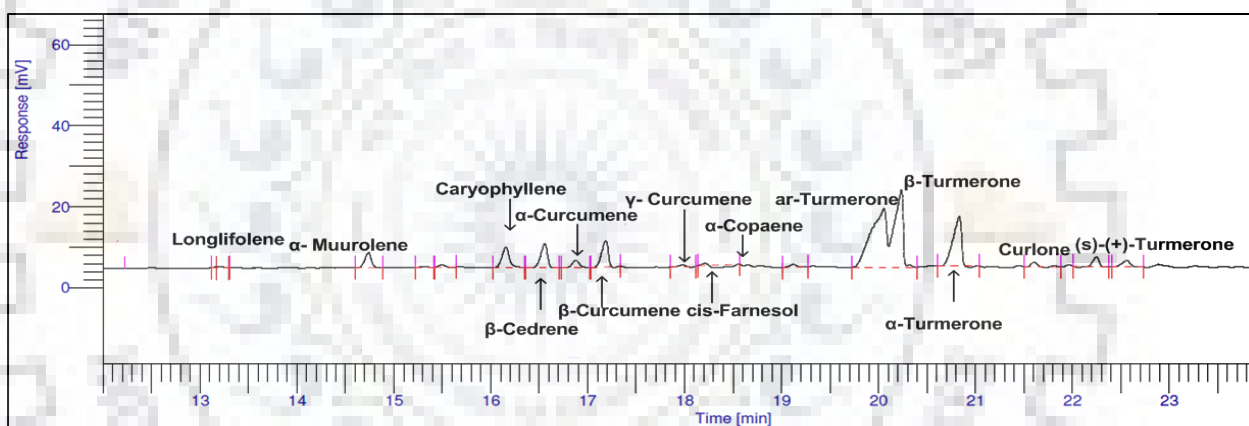

Fig. C.2: Gas chromatogram of Turmeric root essential oil, Run No. 02.
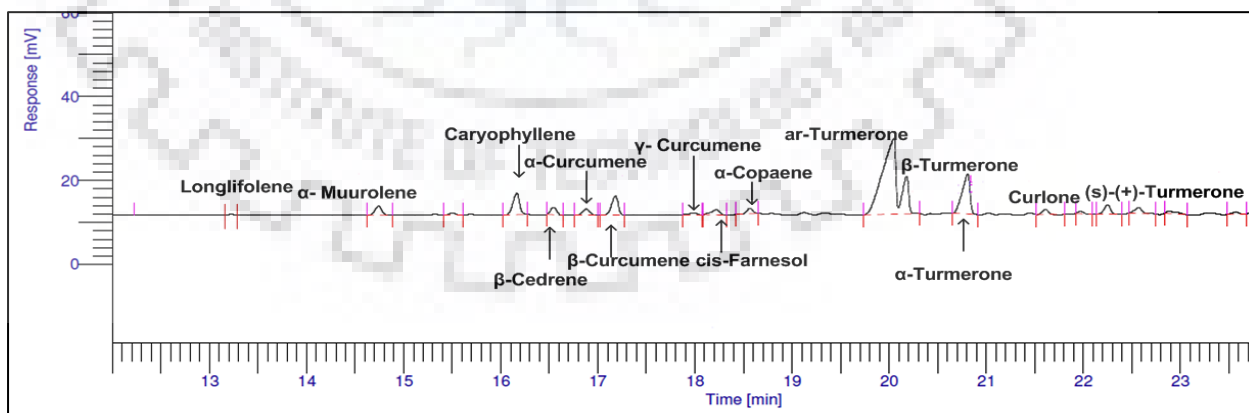
Fig. C.3: Gas chromatogram of Turmeric root essential oil, Run No. 03.
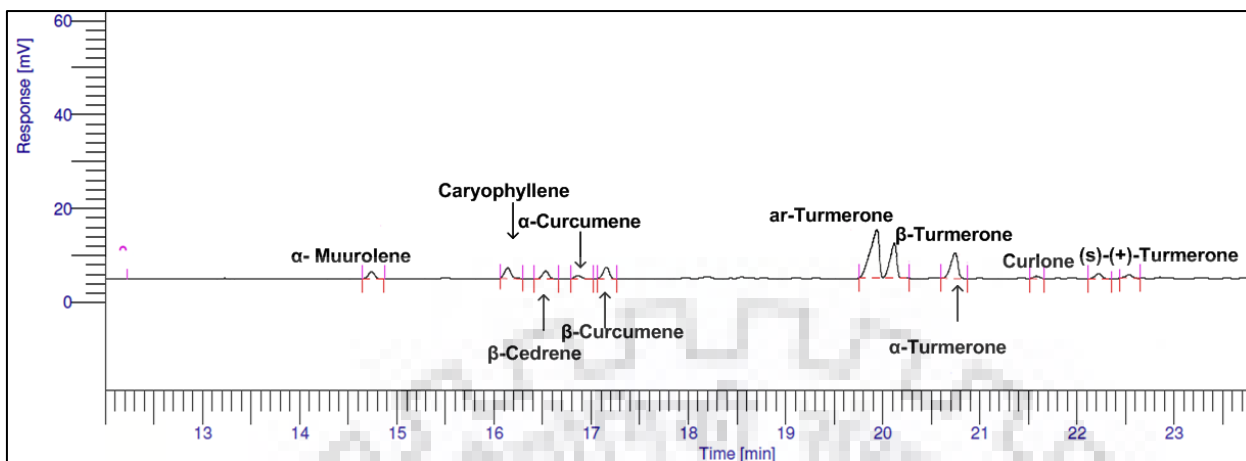
Fig. C.4: Gas chromatogram of Turmeric root essential oil, Run No. 04.
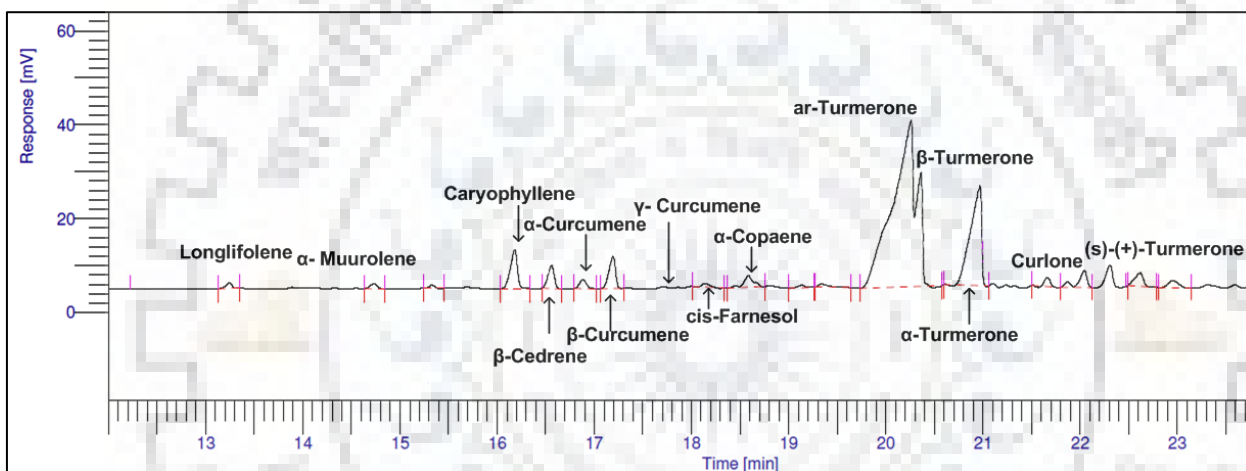
Fig. C.5: Gas chromatogram of Turmeric root essential oil, Run No. 05.
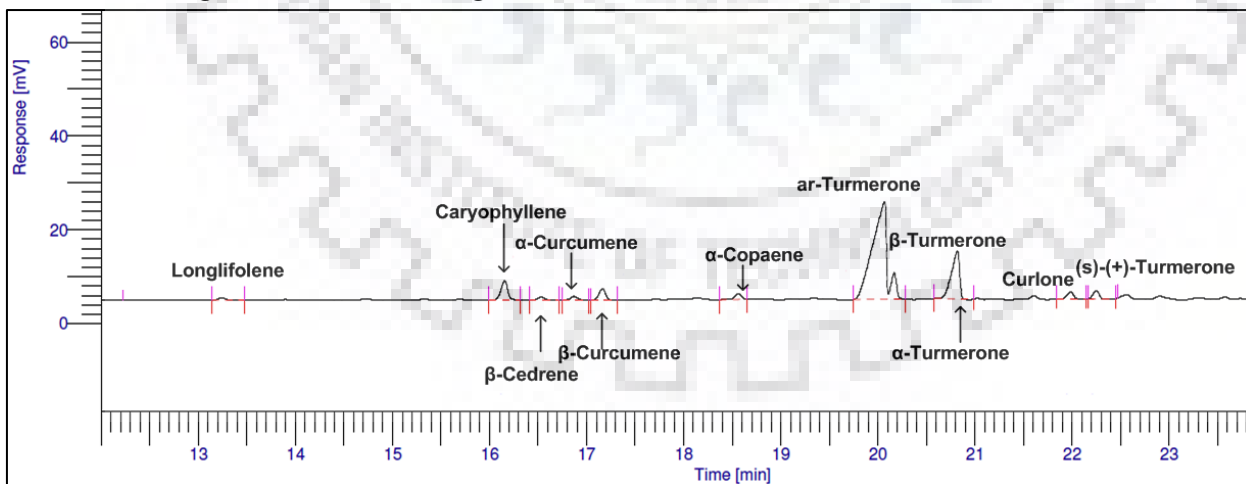
Fig. C.6: Gas chromatogram of Turmeric root essential oil, Run No. 06.
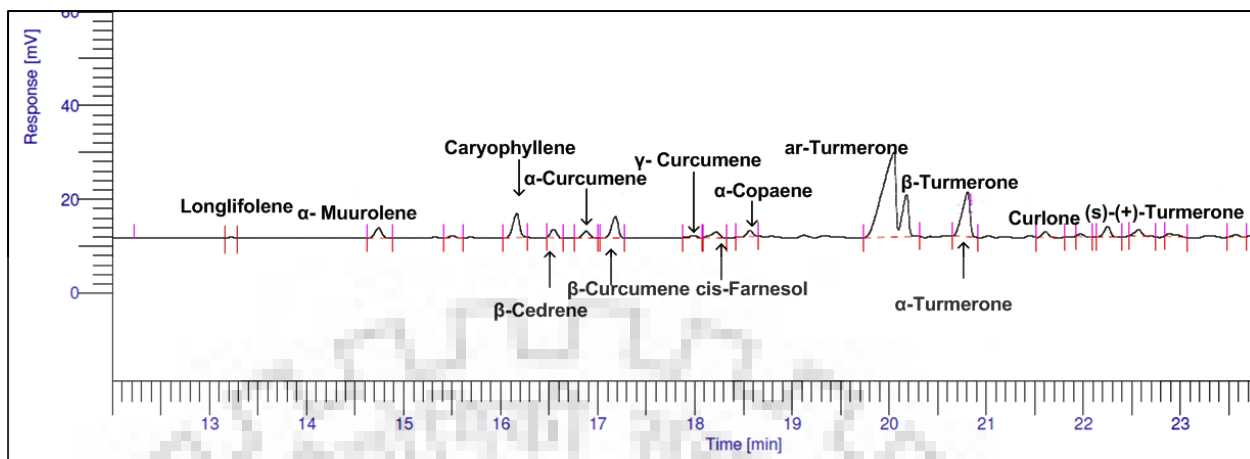
Fig. C.7: Gas chromatogram of Turmeric root essential oil, Run No. 07.
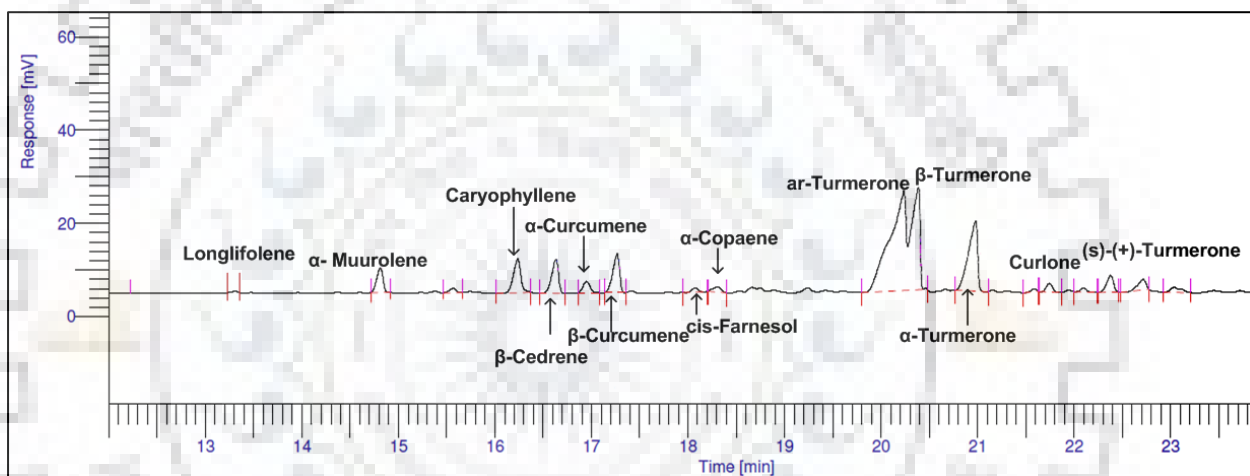
Fig. C.8: Gas chromatogram of Turmeric root essential oil, Run No. 08.
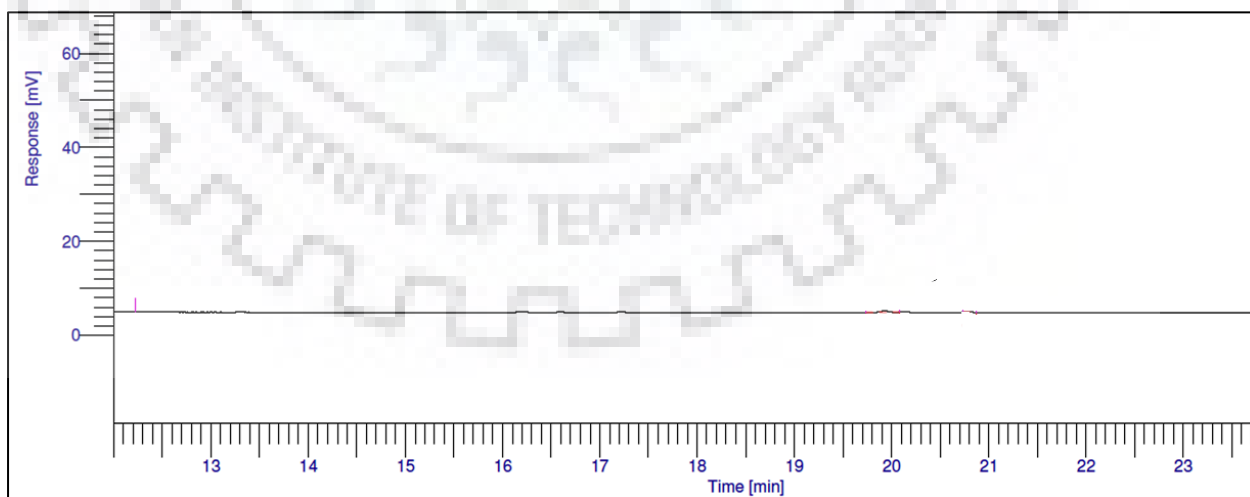
Fig. C.9: Gas chromatogram of Turmeric root essential oil, Run No. 09.
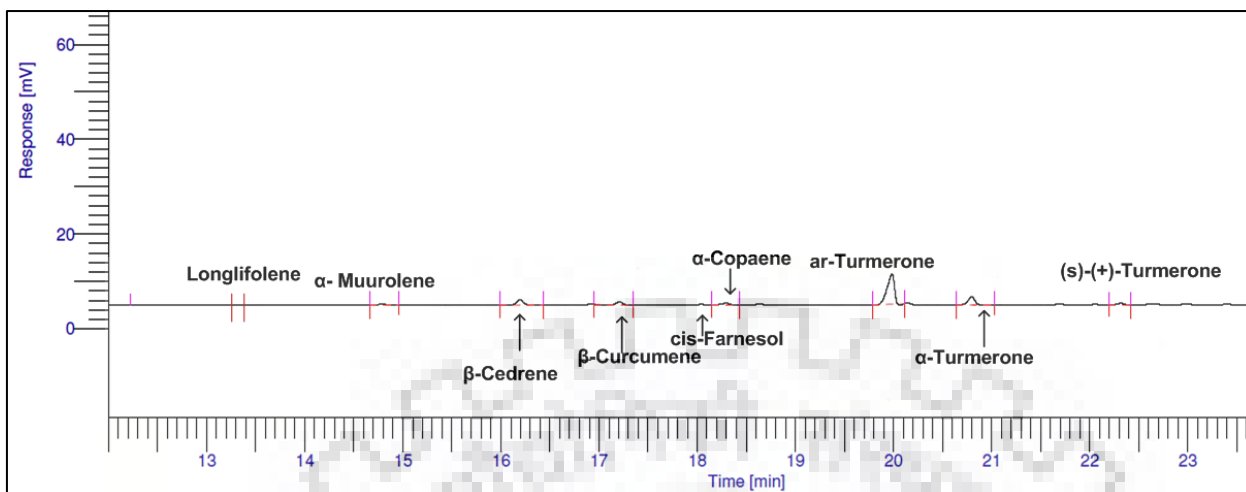
Fig. C.10: Gas chromatogram of Turmeric root essential oil, Run No. 10.
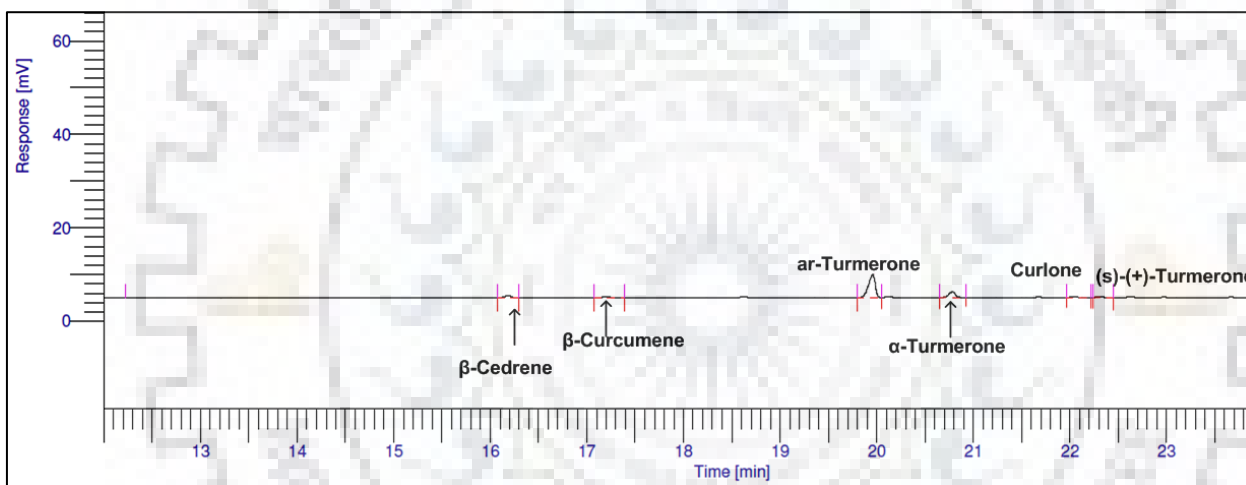
Fig. C.11: Gas chromatogram of Turmeric root essential oil, Run No. 11.
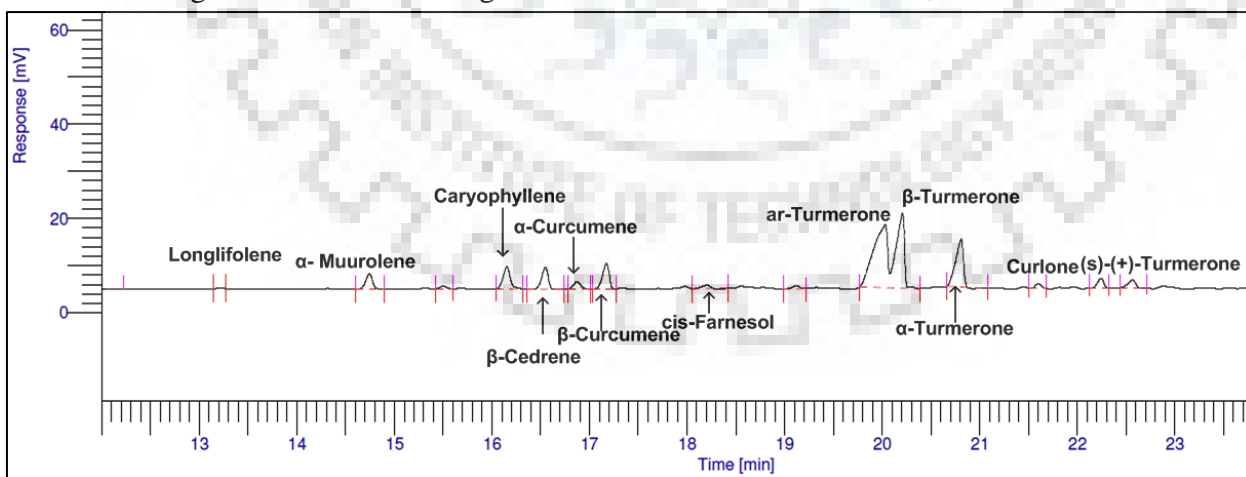
Fig. C.12: Gas chromatogram of Turmeric root essential oil, Run No. 12.
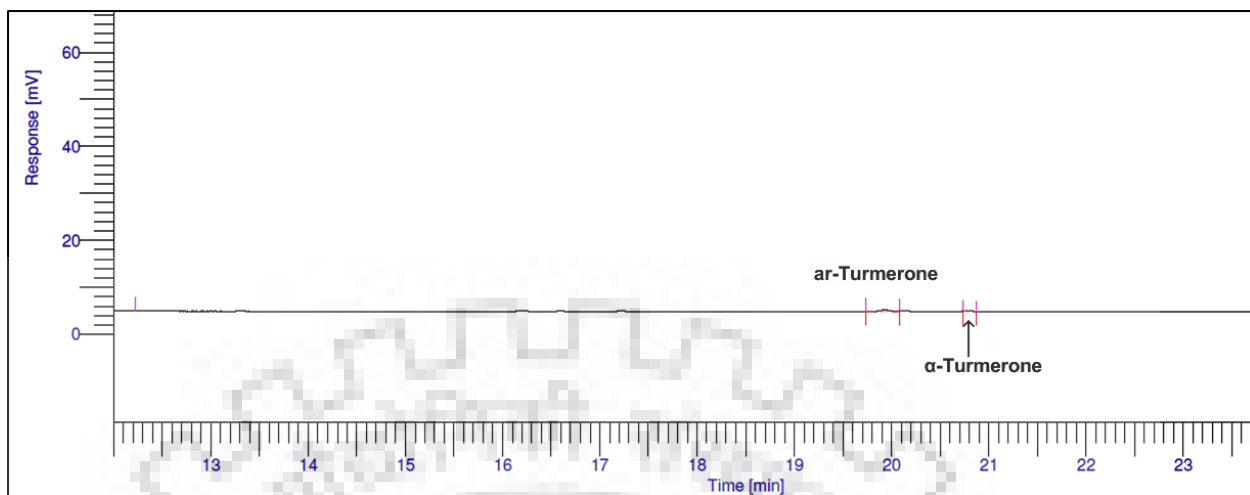
Fig. C.13: Gas chromatogram of Turmeric root essential oil, Run No. 13.
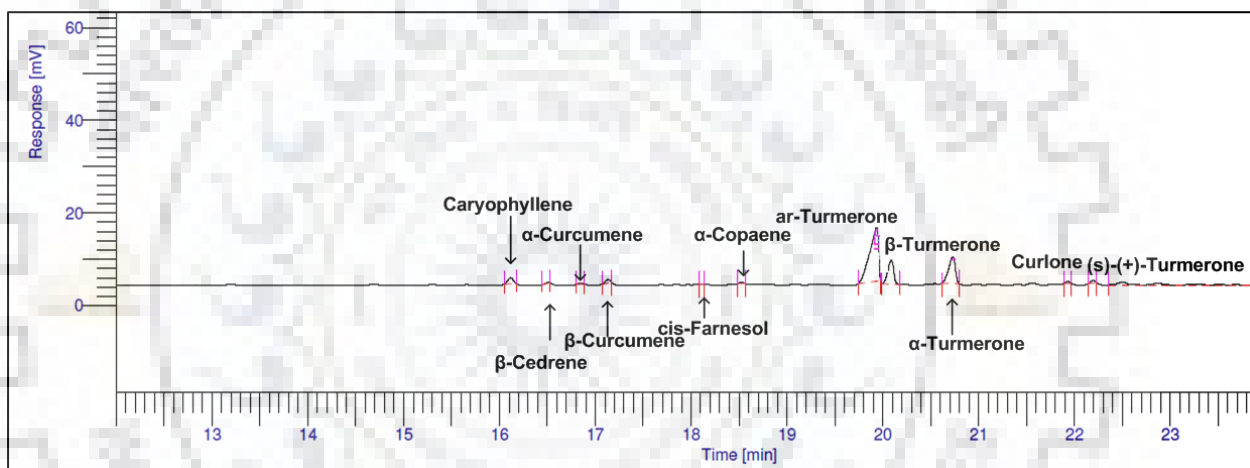
Fig. C.14: Gas chromatogram of Turmeric root essential oil, Run No. 14.
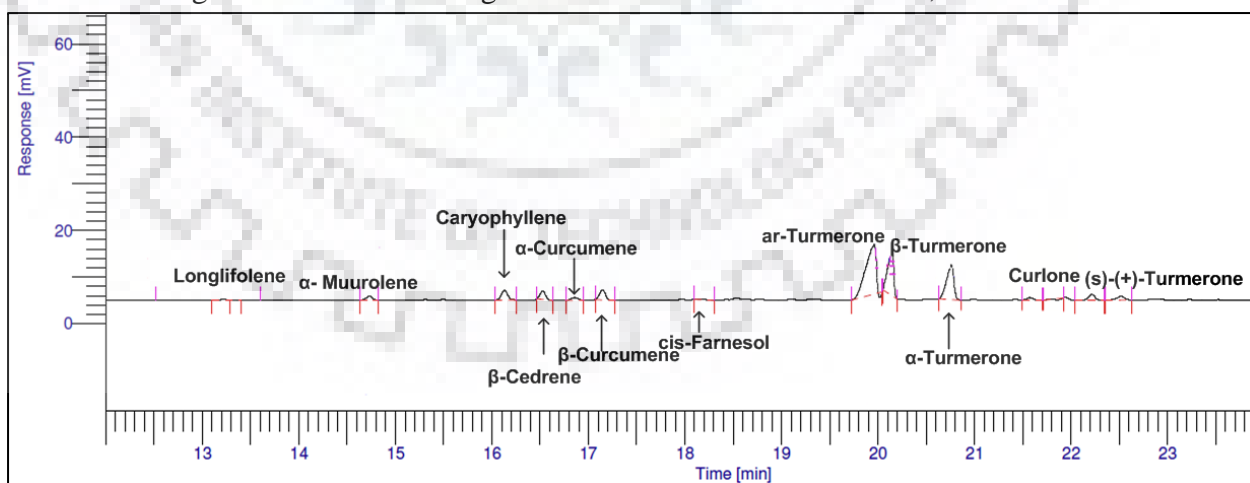
Fig. C.15: Gas chromatogram of Turmeric root essential oil, Run No. 15.
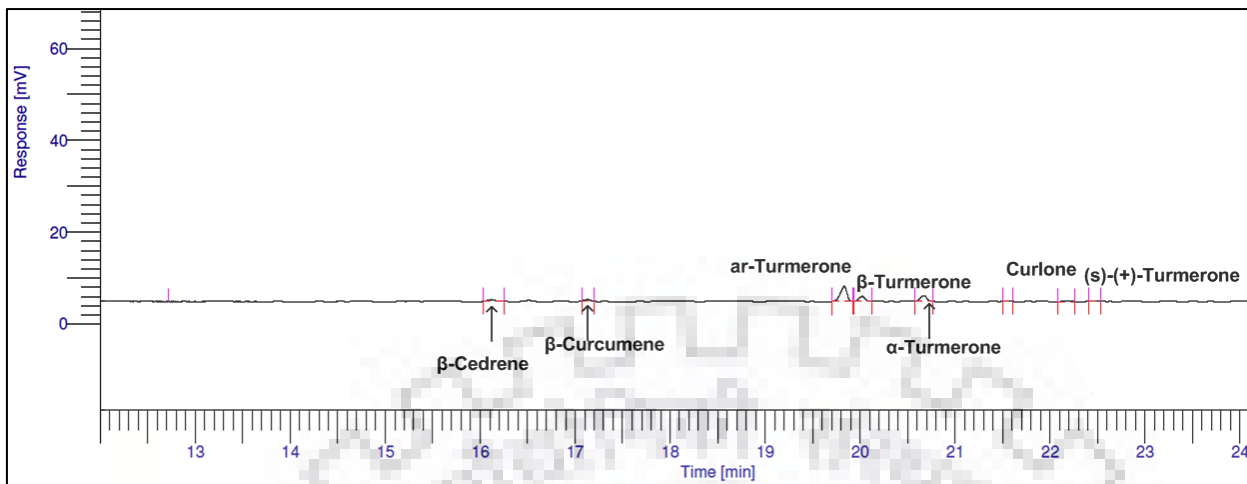
Fig. C.16: Gas chromatogram of Turmeric root essential oil, Run No. 16.
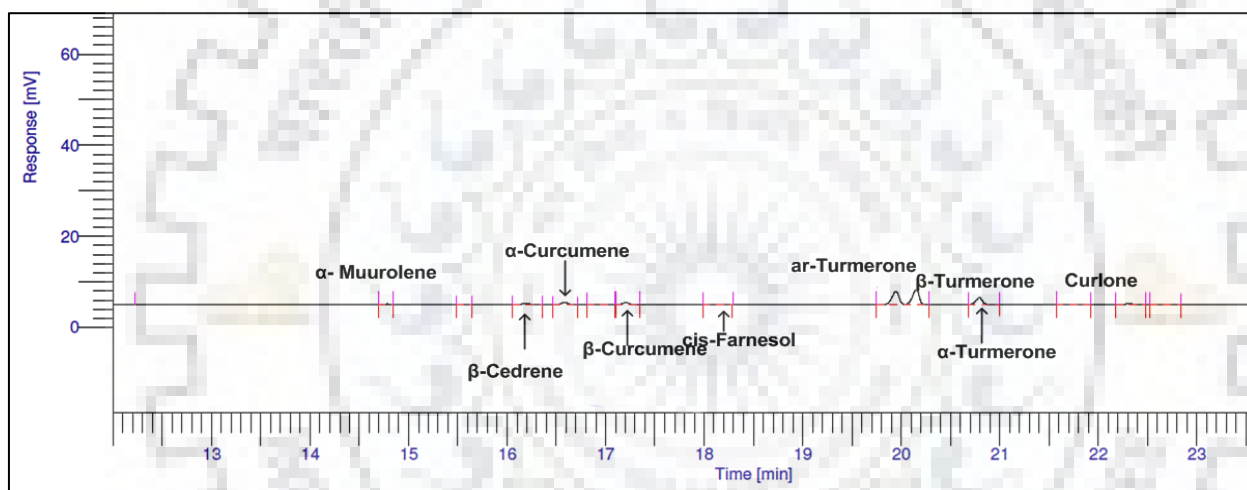

Fig. C.17: Gas chromatogram of Turmeric root essential oil, Run No. 17.
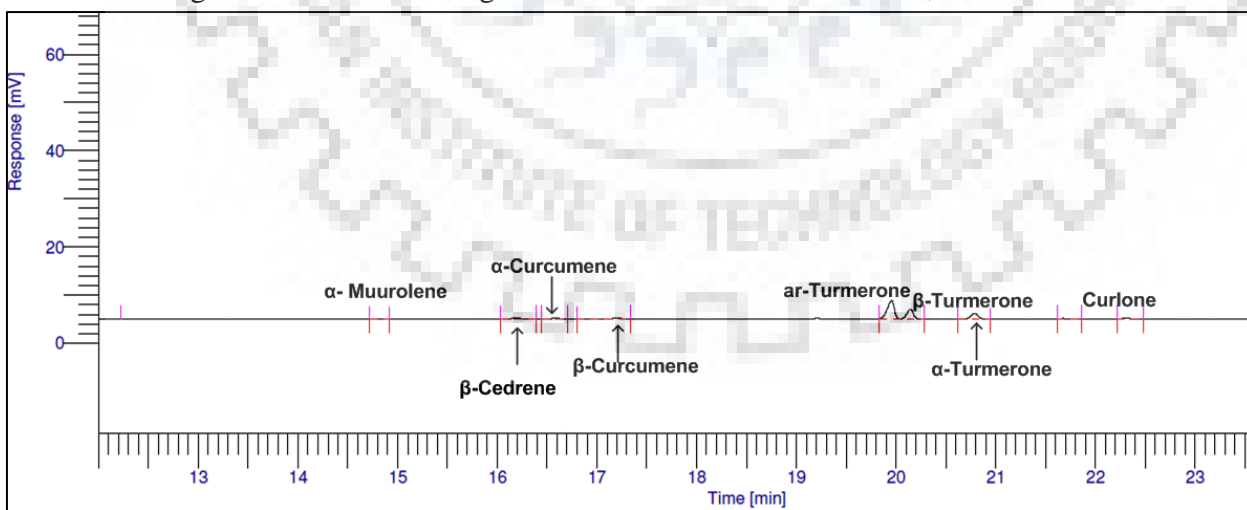

Fig. C.18: Gas chromatogram of Turmeric root essential oil, Run No. 18.
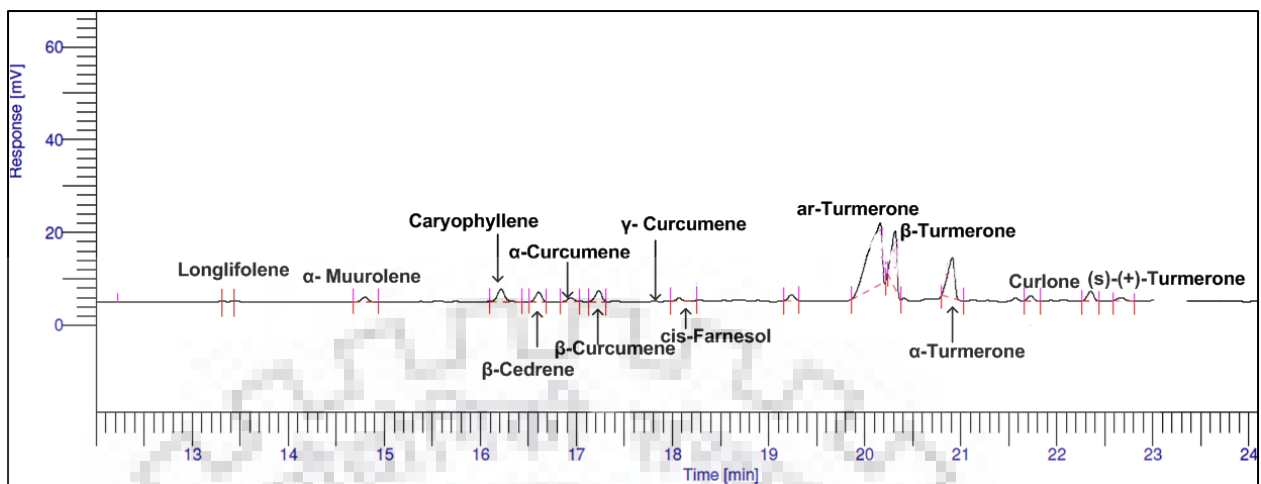
Fig. C.19: Gas chromatogram of Turmeric root essential oil, Run No. 19.
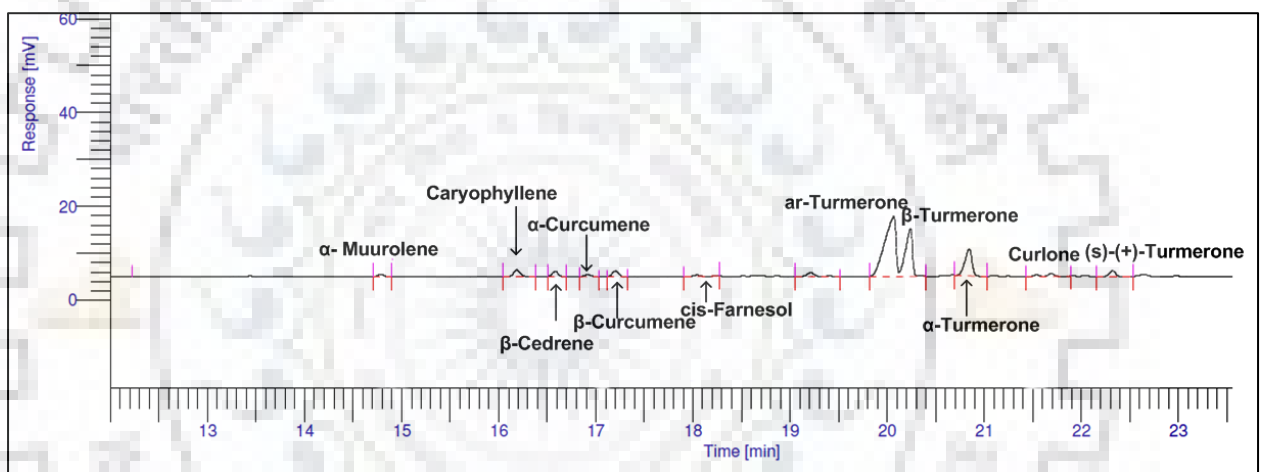
Fig. C.20: Gas chromatogram of Turmeric root essential oil, Run No. 20.
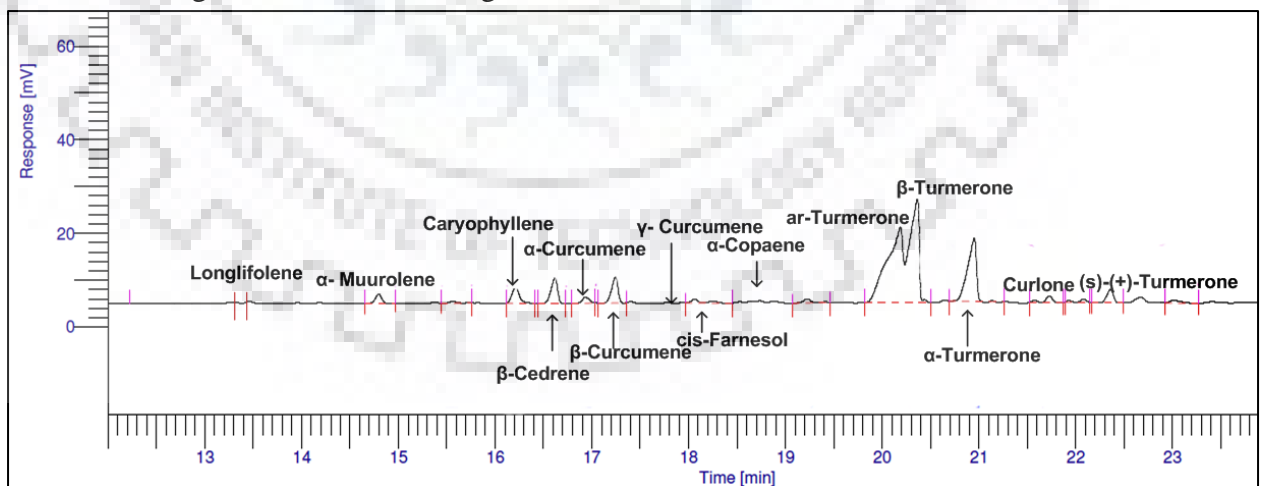
Fig. C.21: Gas chromatogram of Turmeric root essential oil, Run No. 21.
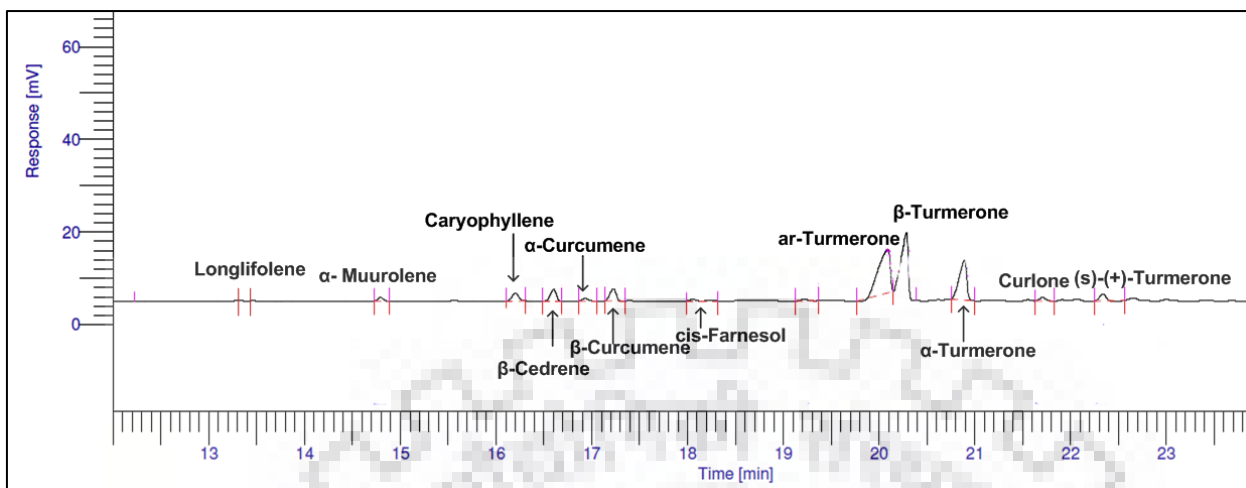
Fig. C.22: Gas chromatogram of Turmeric root essential oil, Run No. 22.
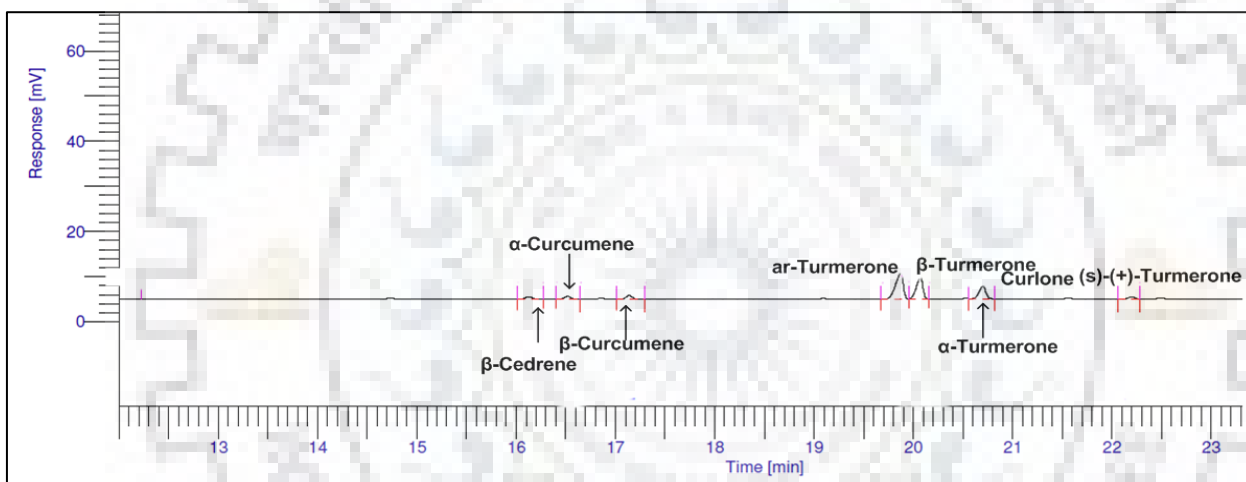
Fig. C.23: Gas chromatogram of Turmeric root essential oil, Run No. 23.
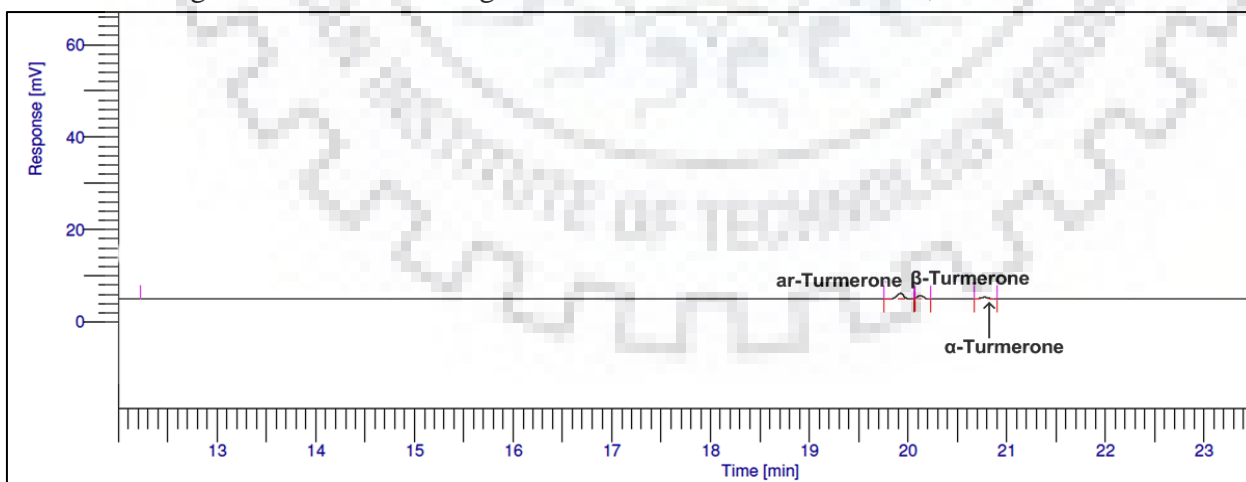
Fig. C.24: Gas chromatogram of Turmeric root essential oil, Run No. 24.
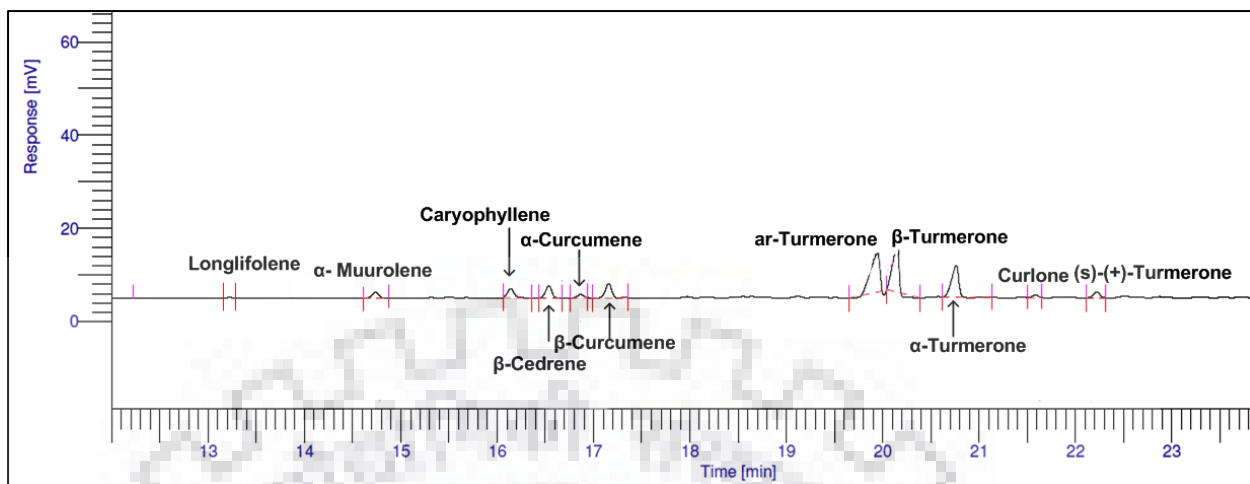
Fig. C.25: Gas chromatogram of Turmeric root essential oil, Run No. 25.
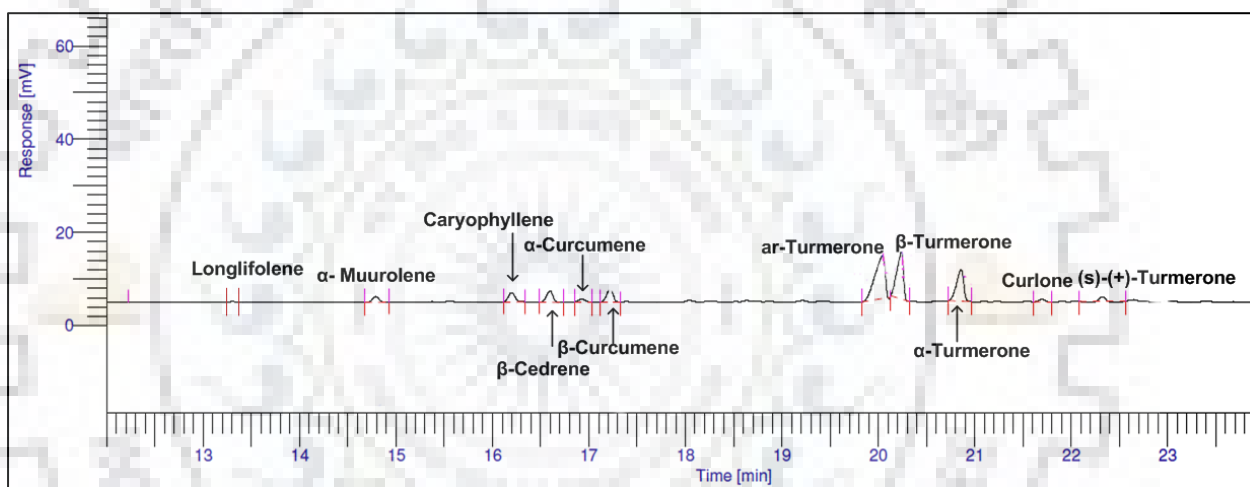
Fig. C.26: Gas chromatogram of Turmeric root essential oil, Run No. 26.
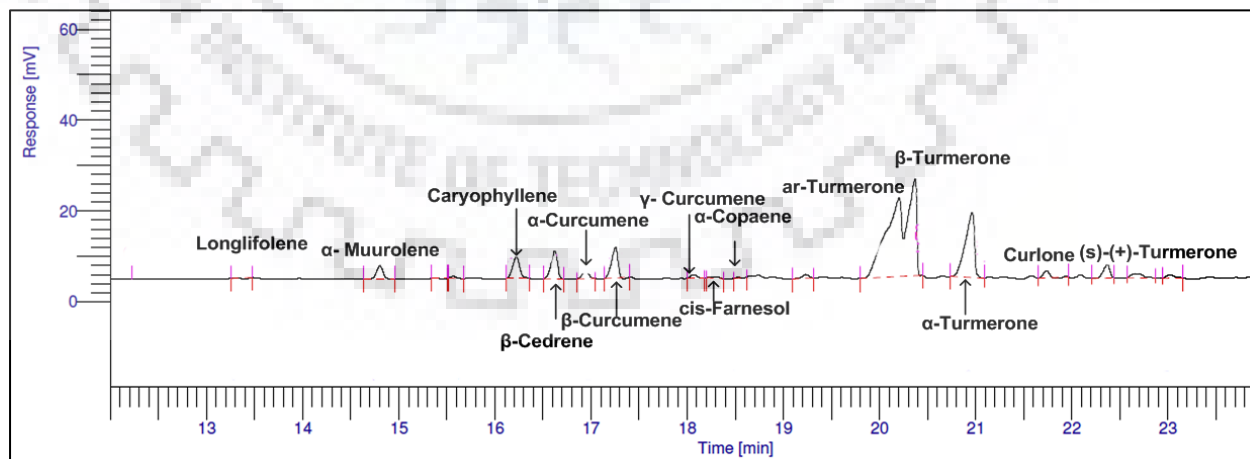
Fig. C.27: Gas chromatogram of Turmeric root essential oil, Run No. 27.
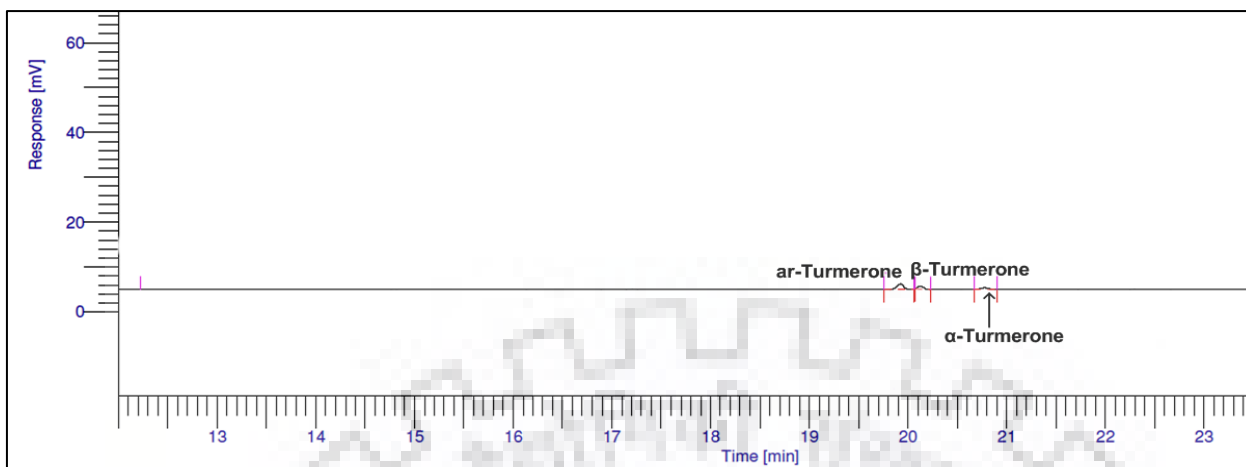
Fig. C.28: Gas chromatogram of Turmeric root essential oil, Run No. 28.
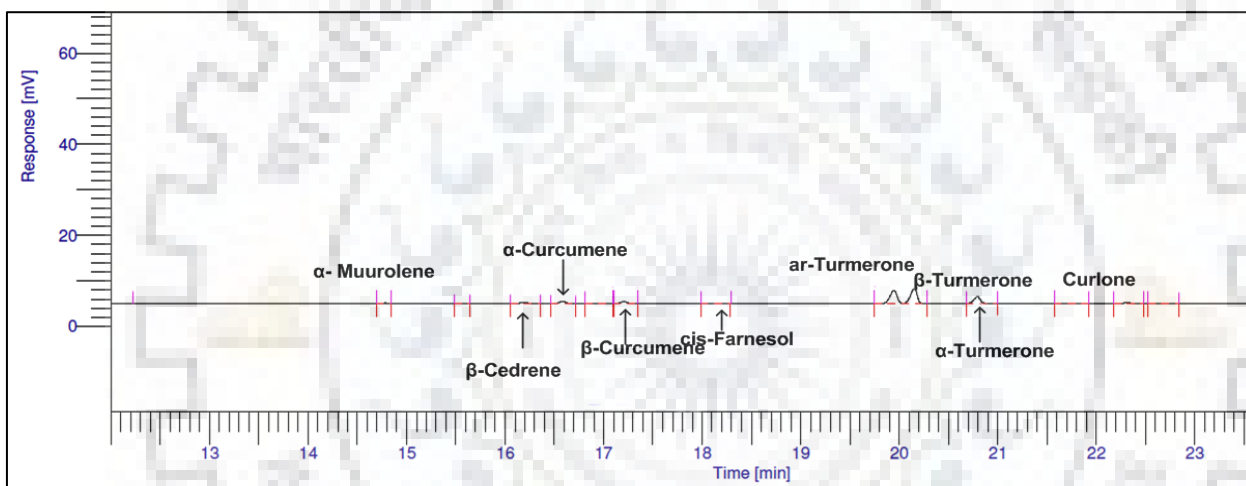
Fig. C.29: Gas chromatogram of Turmeric root essential oil, Run No. 29.
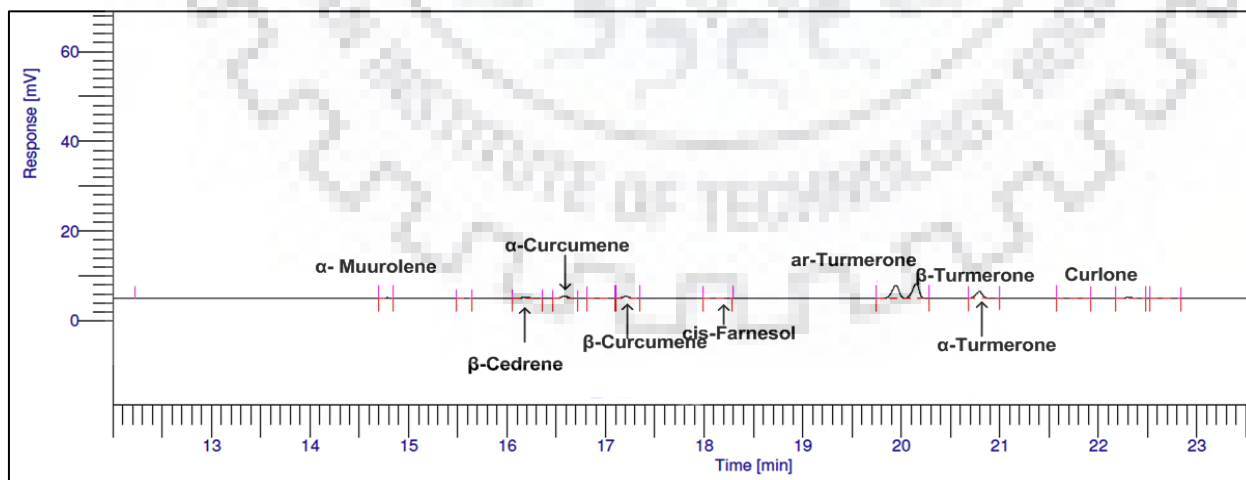
Fig. C.30: Gas chromatogram of Turmeric root essential oil, Run No. 30.
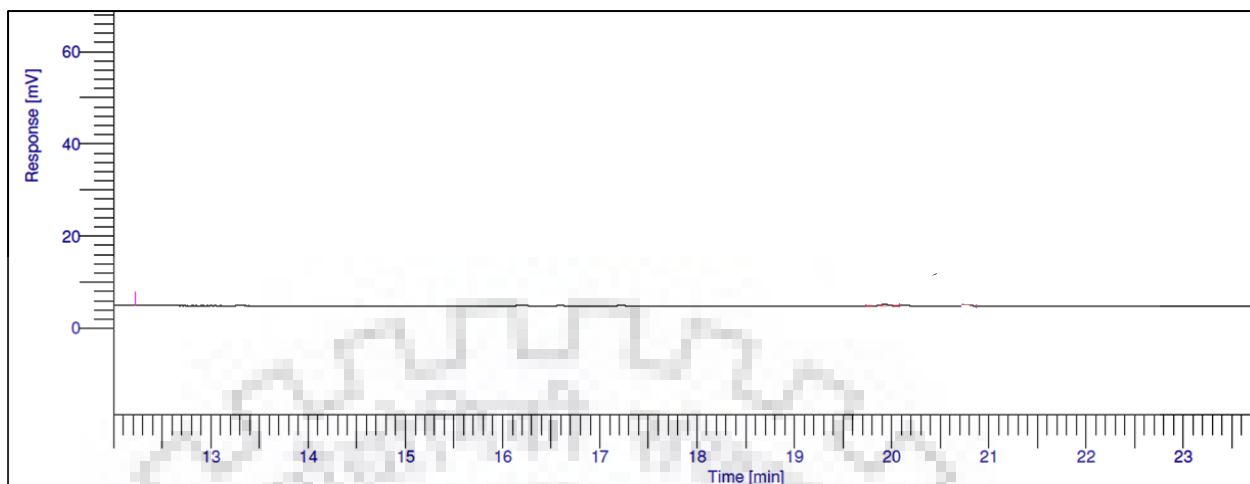
Fig. C.31: Gas chromatogram of Turmeric root essential oil, Run No. 31.
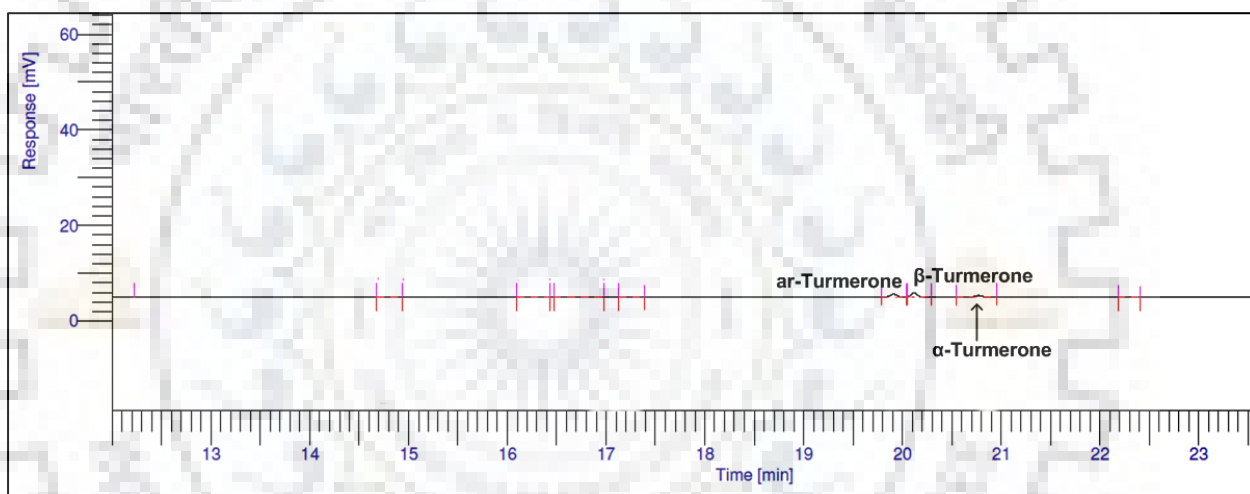
Fig. C.32: Gas chromatogram of Turmeric root essential oil, Run No. 32.
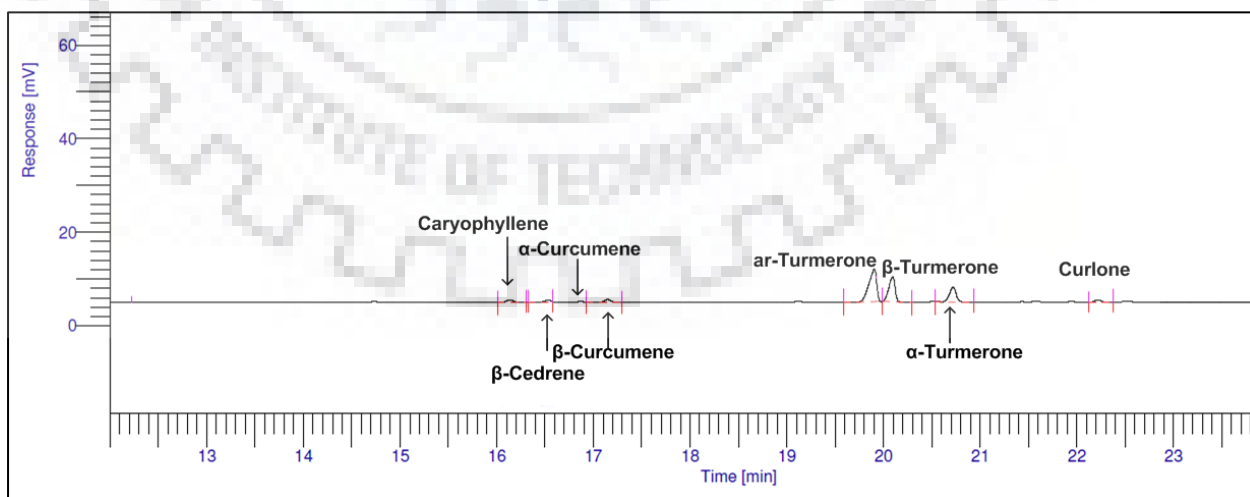
Fig. C.33: Gas chromatogram of Turmeric root essential oil, Run No. 33.
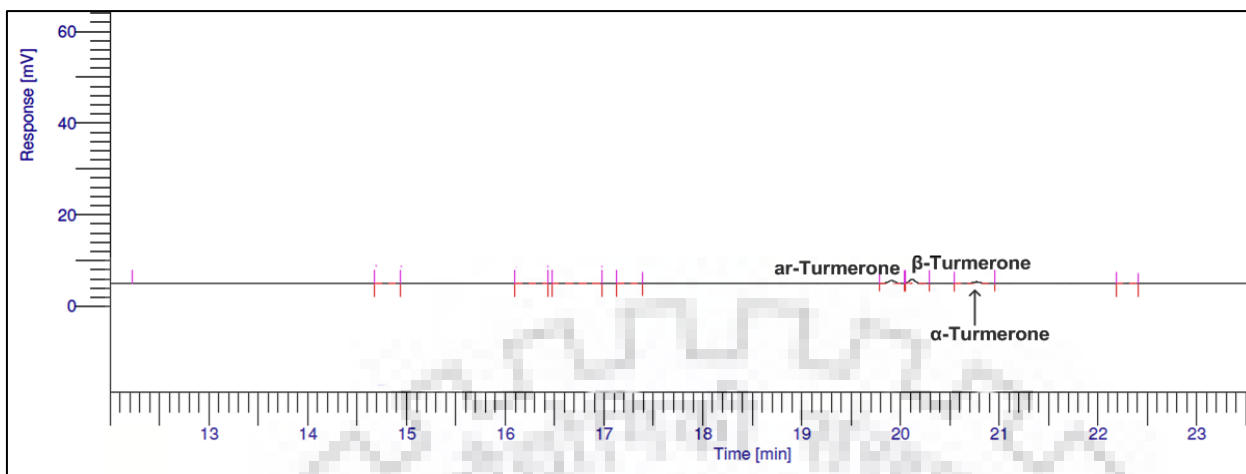
Fig. C.34: Gas chromatogram of Turmeric root essential oil, Run No. 34.
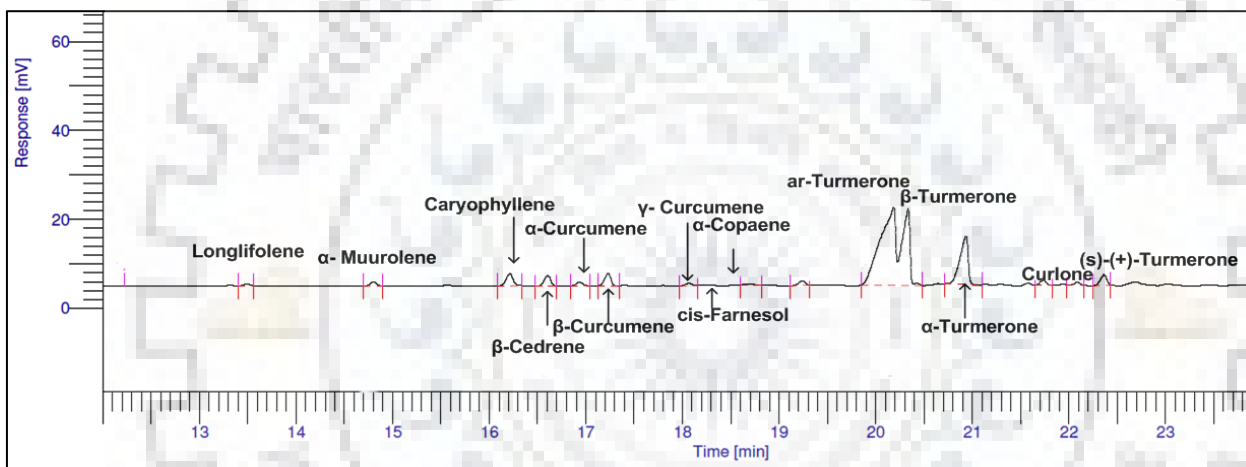
Fig. C.35: Gas chromatogram of Turmeric root essential oil, Run No. 35.
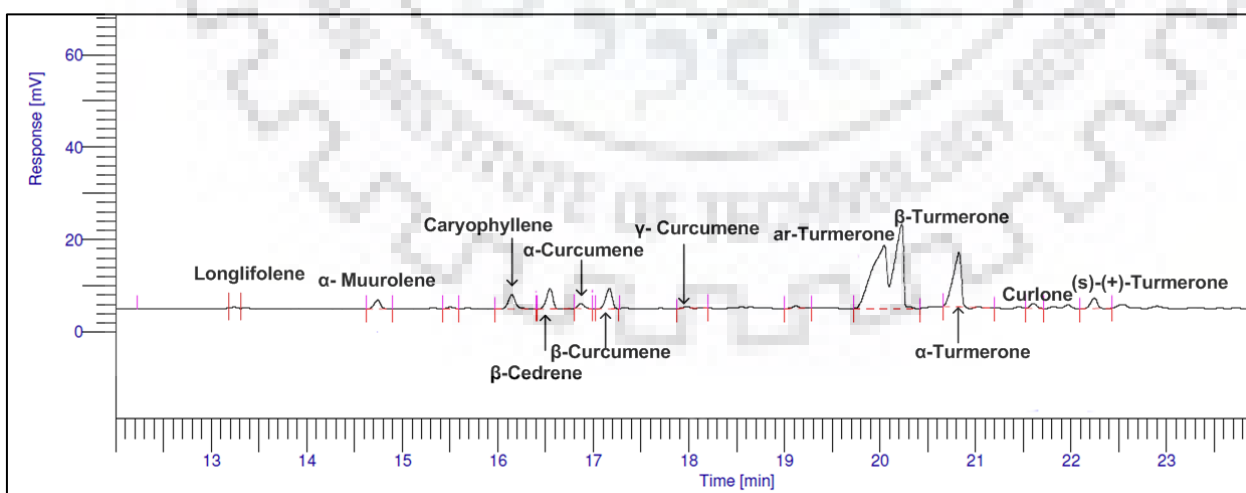
Fig. C.36: Gas chromatogram of Turmeric root essential oil, Run No. 36.
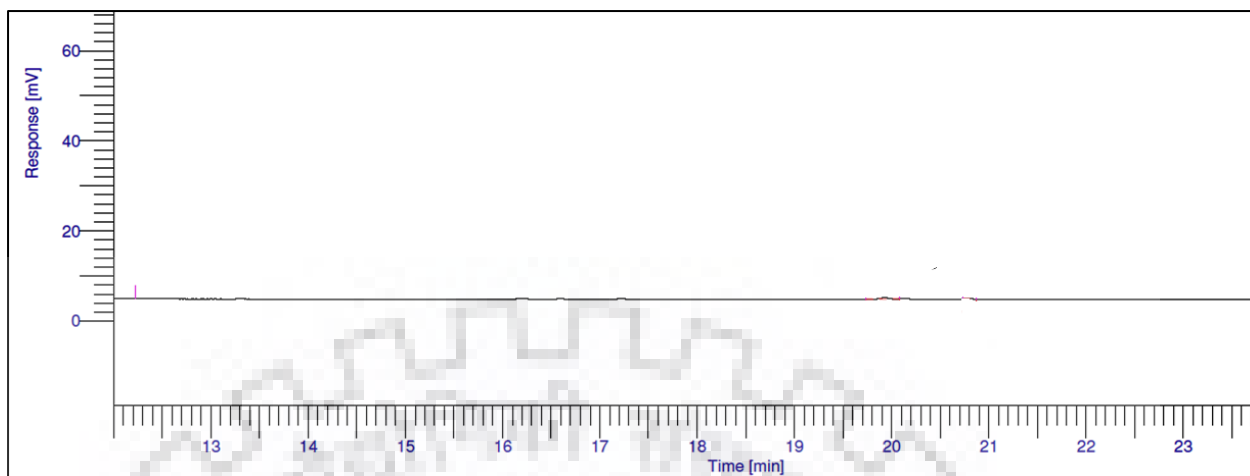
Fig. C.37: Gas chromatogram of Turmeric root essential oil, Run No. 37.
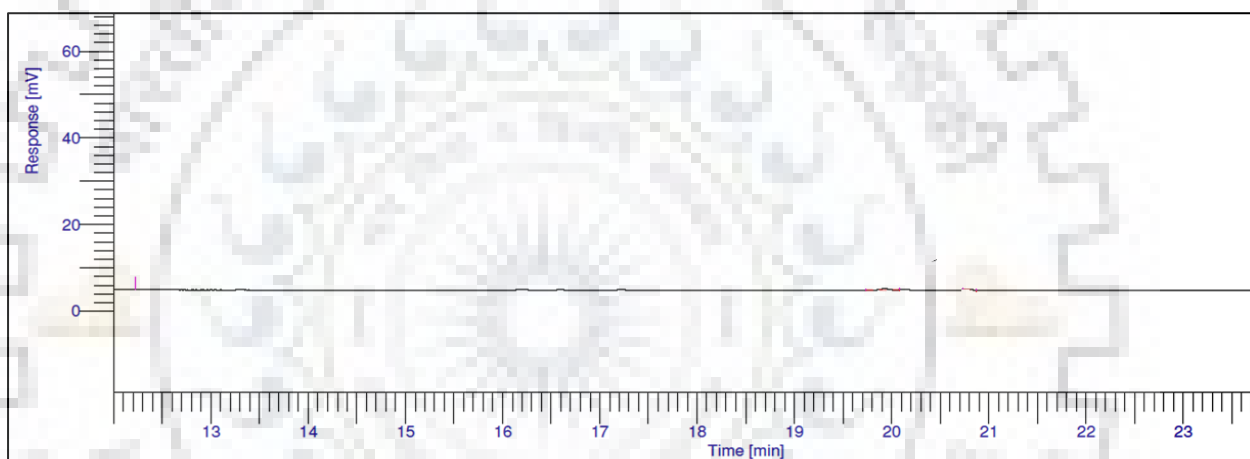
Fig. C.38: Gas chromatogram of Turmeric root essential oil, Run No. 38.
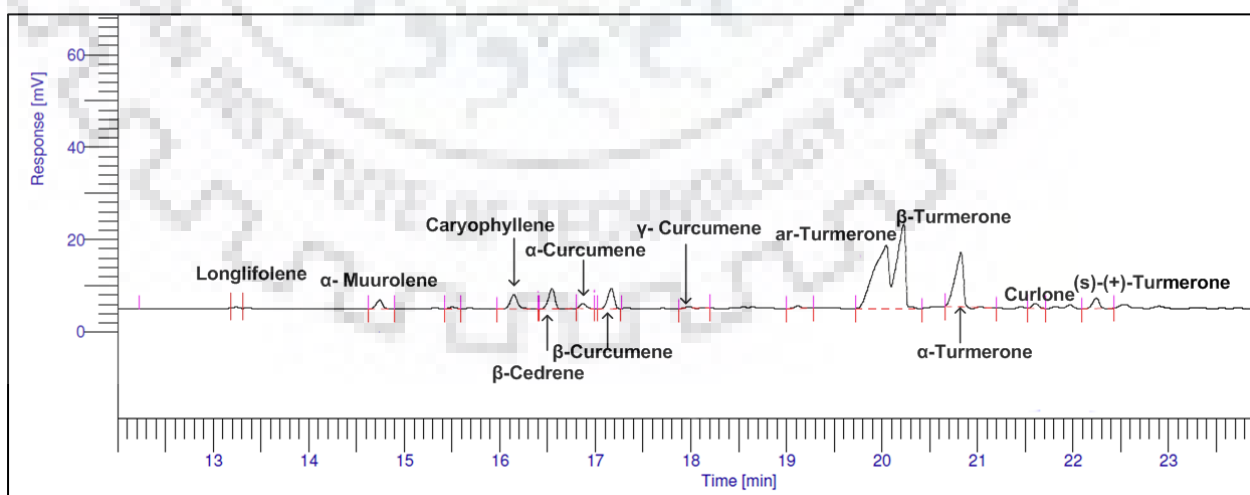
Fig. C.39: Gas chromatogram of Turmeric root essential oil, Run No. 39.
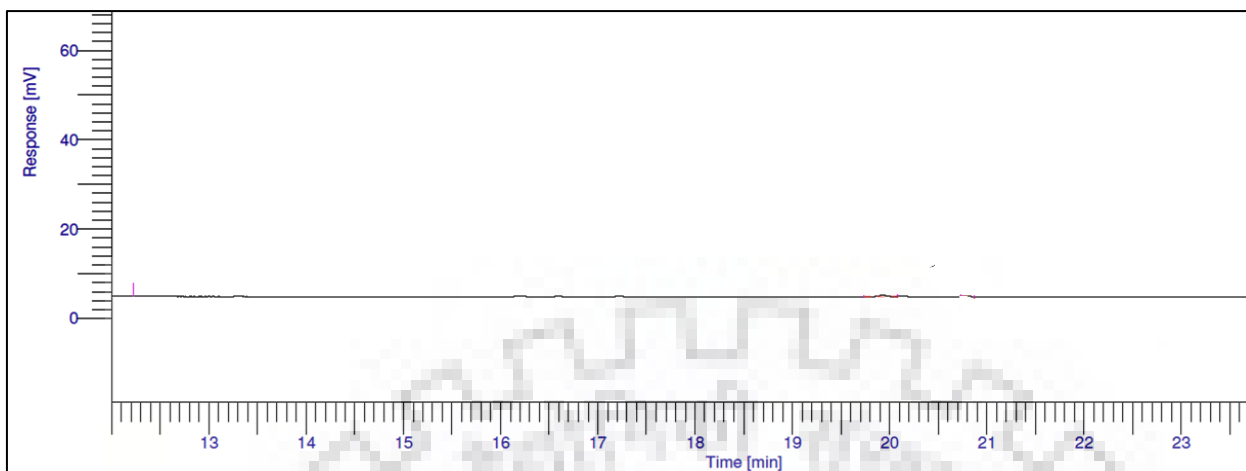
Fig. C.40: Gas chromatogram of Turmeric root essential oil, Run No. 40.
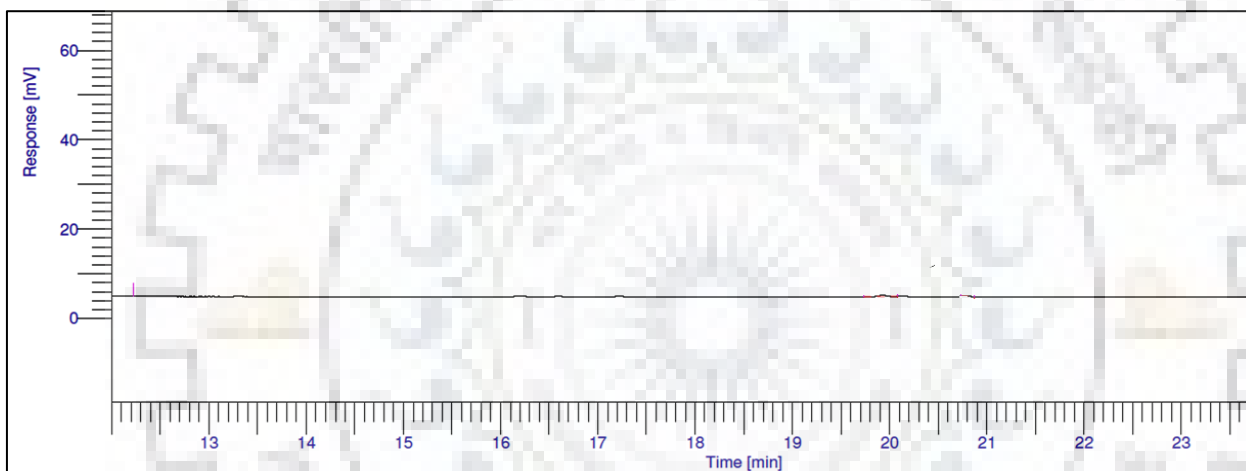
Fig. C.41: Gas chromatogram of Turmeric root essential oil, Run No. 41.
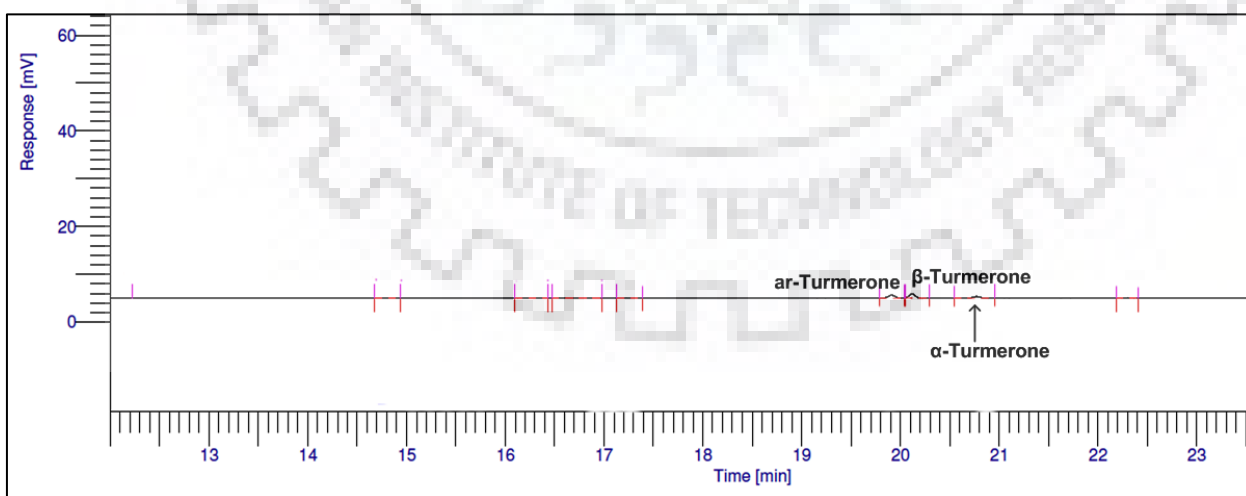
Fig. C.42: Gas chromatogram of Turmeric root essential oil, Run No. 42.

C-14
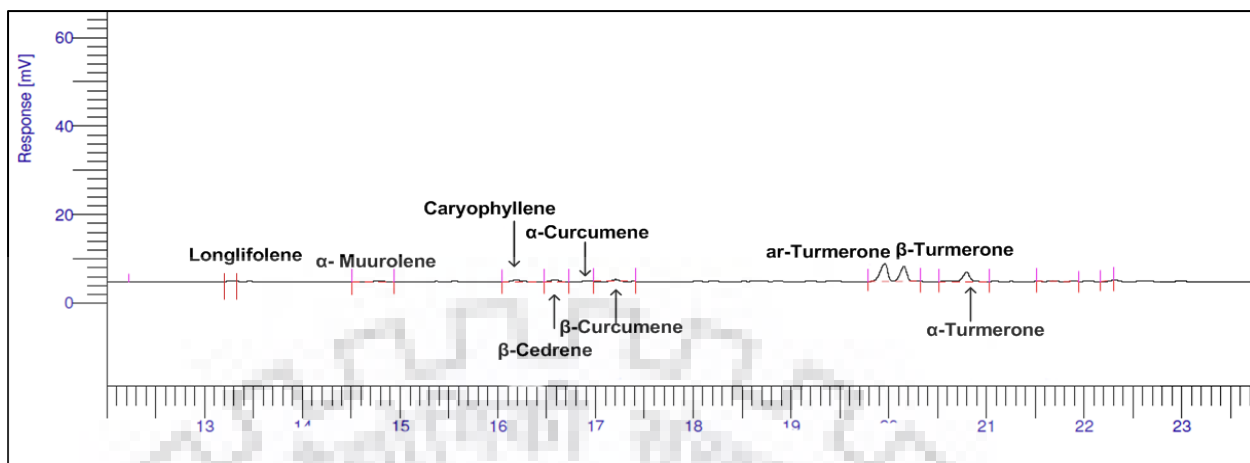
Fig. C.43: Gas chromatogram of Turmeric root essential oil, Run No. 43.
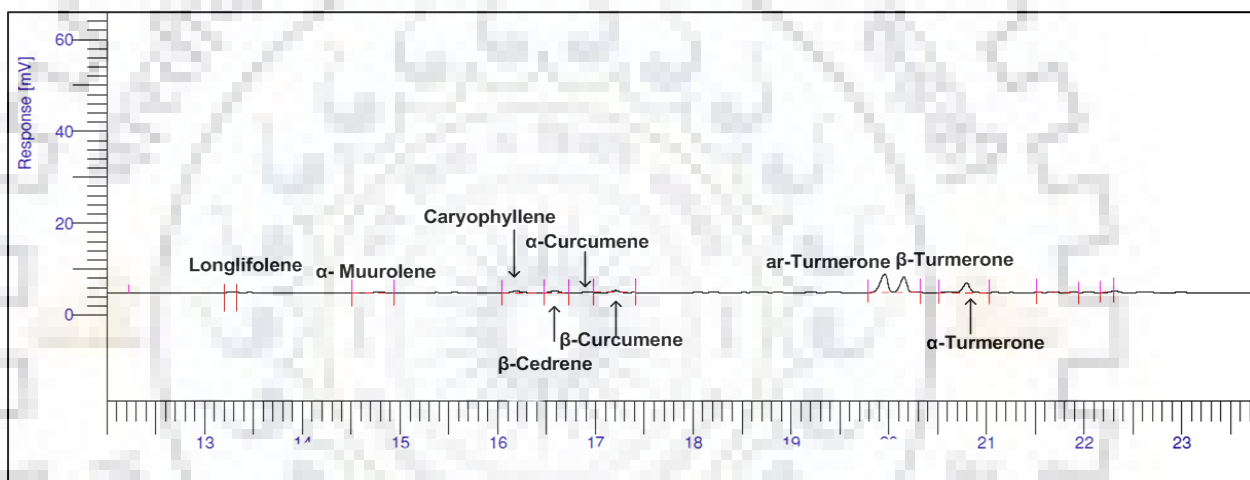
Fig. C.44: Gas chromatogram of Turmeric root essential oil, Run No. 44.
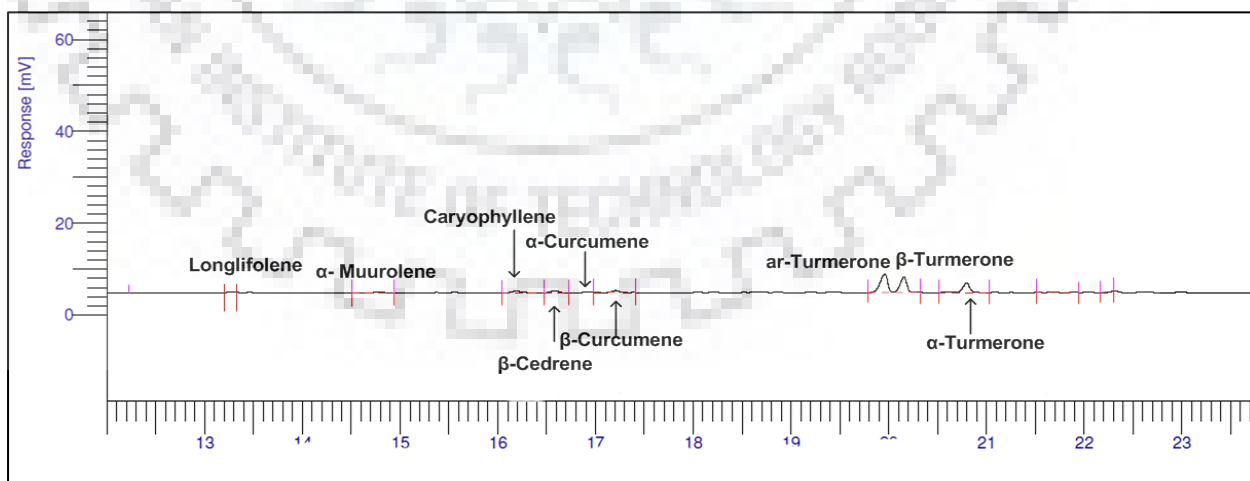
Fig. C.45: Gas chromatogram of Turmeric root essential oil, Run No. 45.
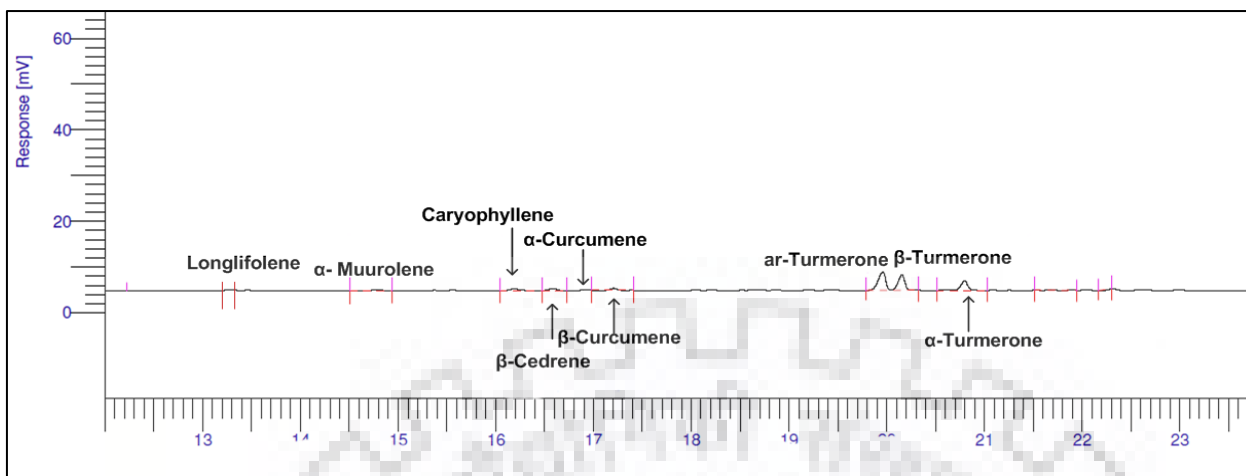
Fig. C.46: Gas chromatogram of Turmeric root essential oil, Run No. 46.
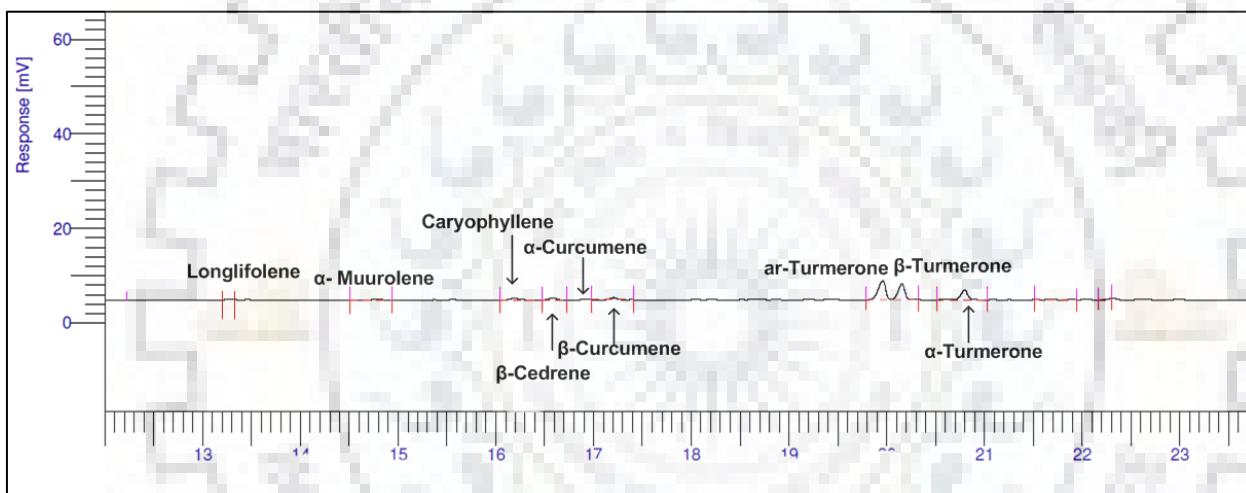
Fig. C.47: Gas chromatogram of Turmeric root essential oil, Run No. 47.
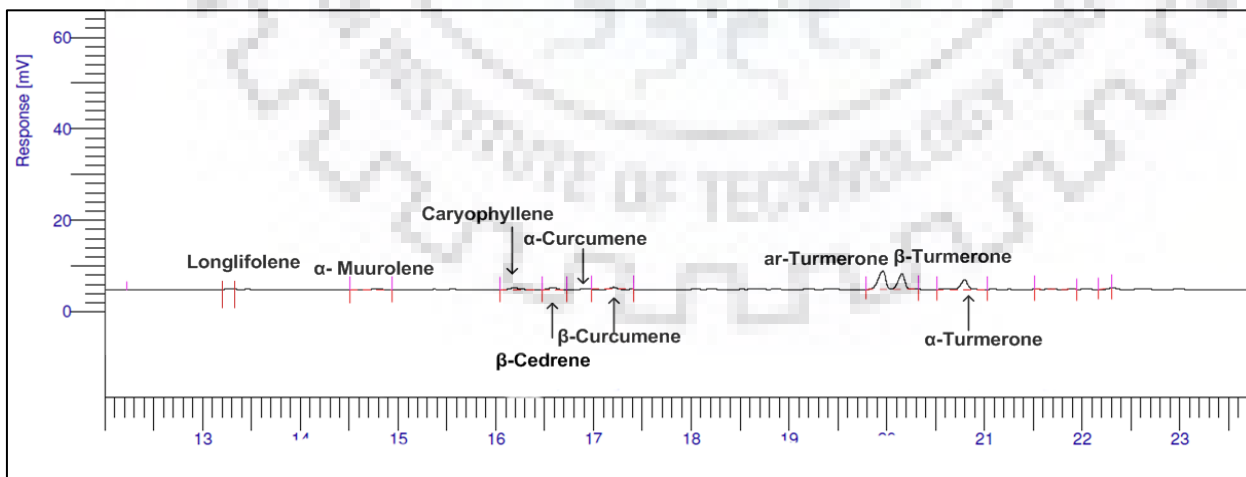
Fig. C.48: Gas chromatogram of Turmeric root essential oil, Run No. 48.
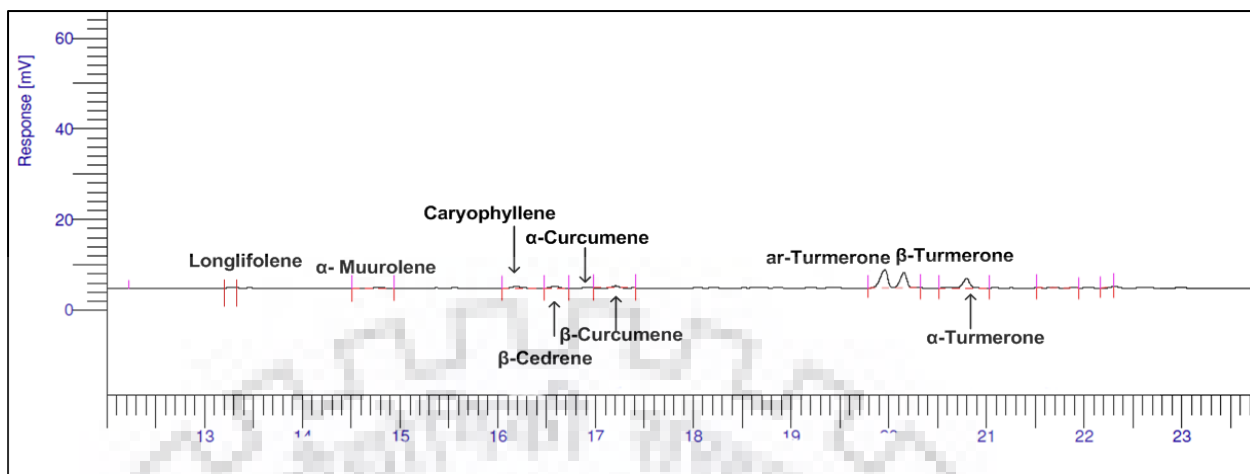
Fig. C.49: Gas chromatogram of Turmeric root essential oil, Run No. 49.
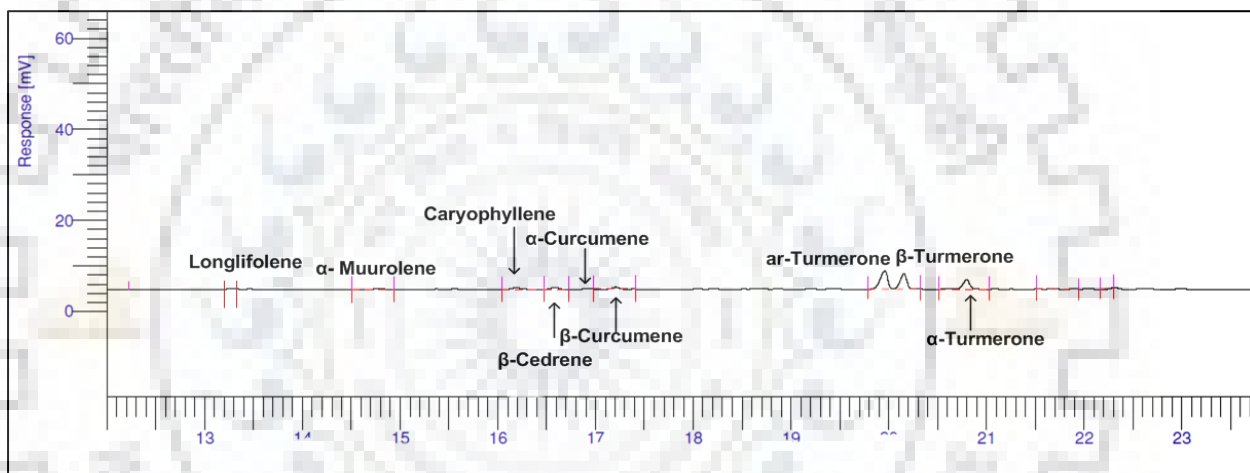
Fig. C.50: Gas chromatogram of Turmeric root essential oil, Run No. 50.
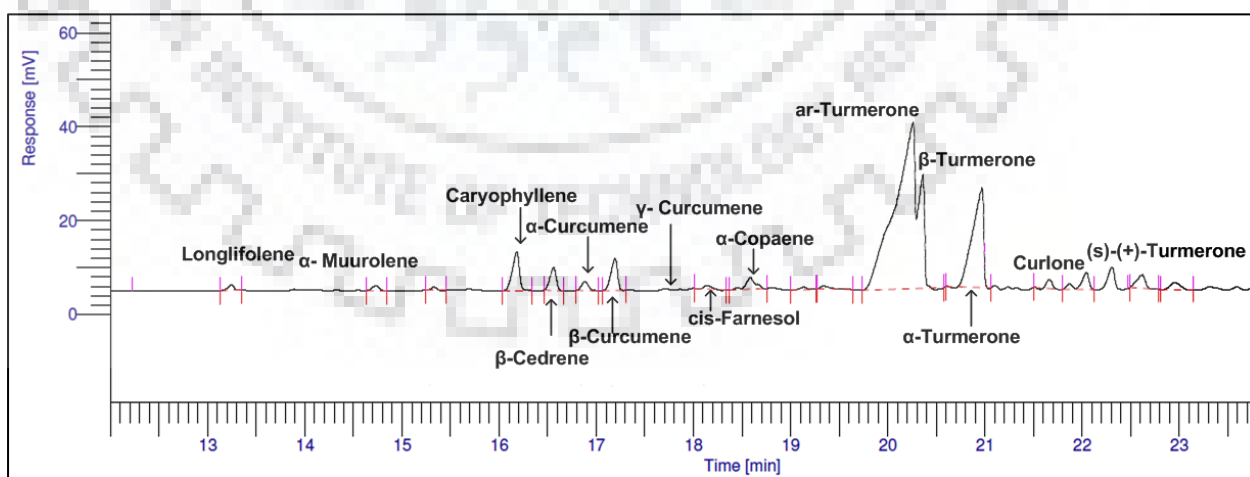
Fig. C.51: Gas chromatogram of Turmeric root essential oil, Soxhlet extraction.

C-17
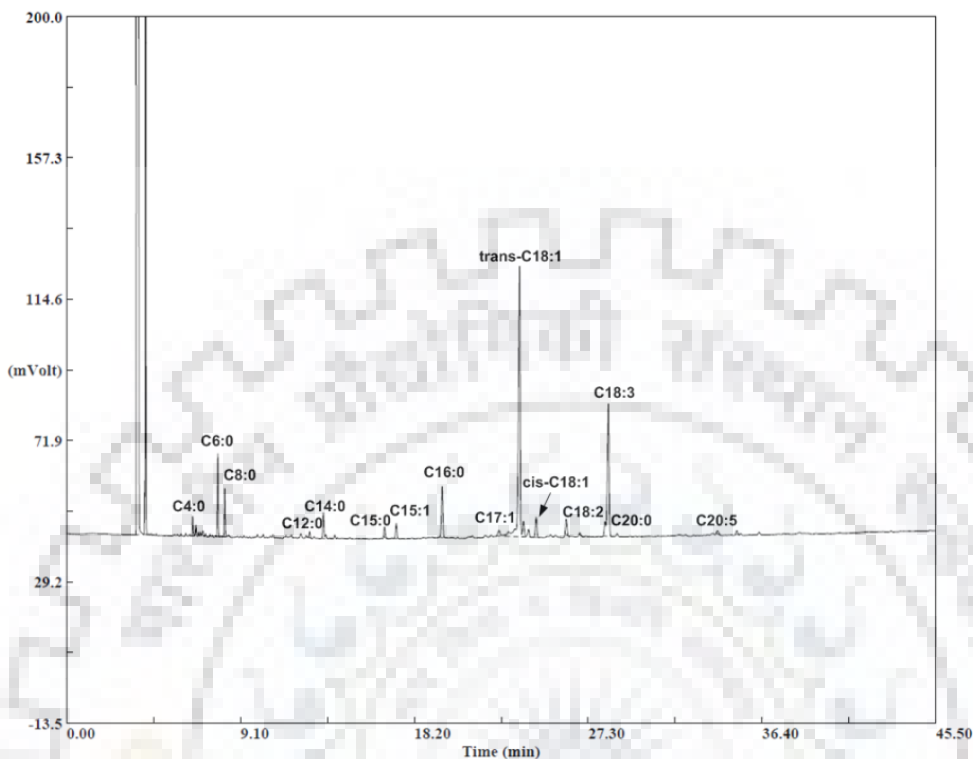
Fig. C.52: Gas chromatogram of Turmeric root fatty acid content, Run No. 01.
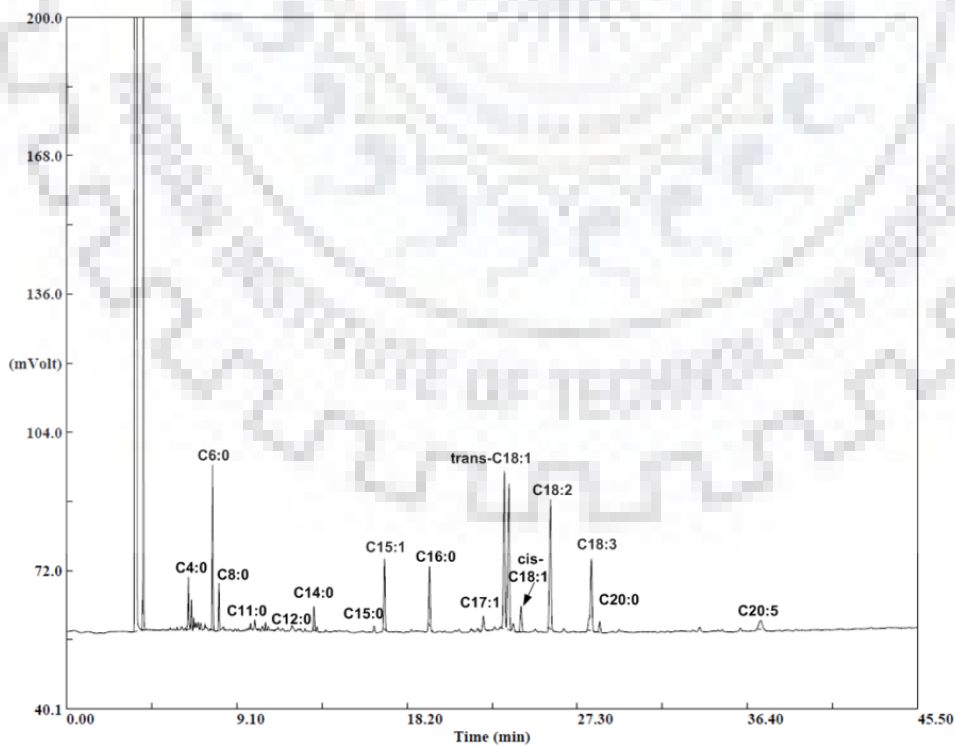
Fig. C.53: Gas chromatogram of Turmeric root fatty acid content, Run No. 02.
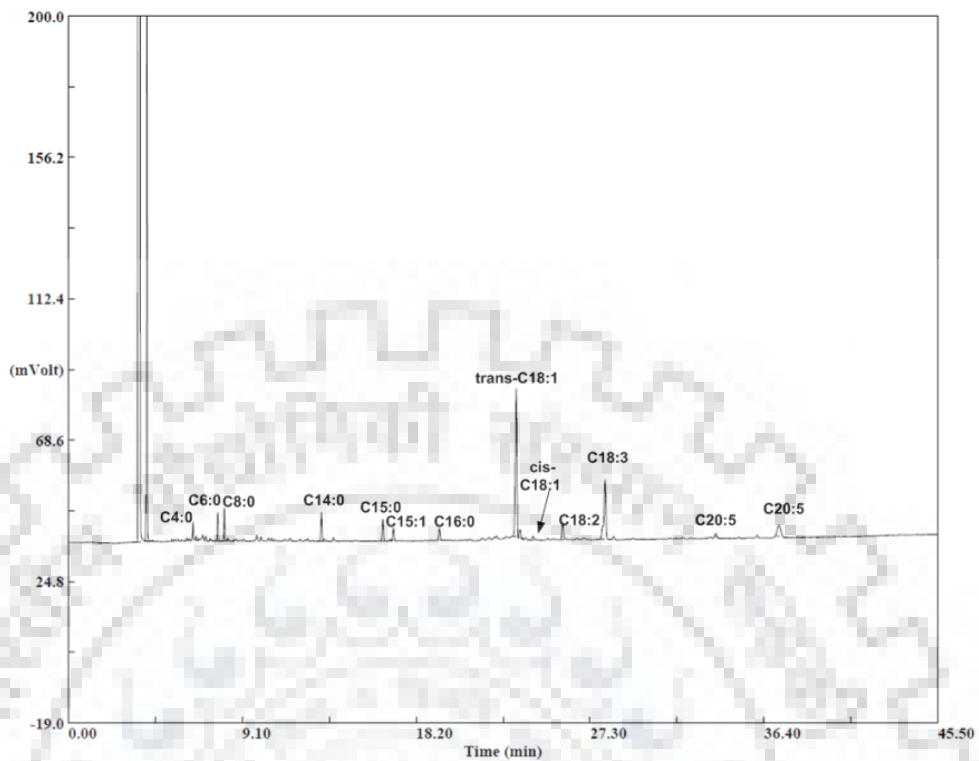
Fig. C.54: Gas chromatogram of Turmeric root fatty acid content, Run No. 03.
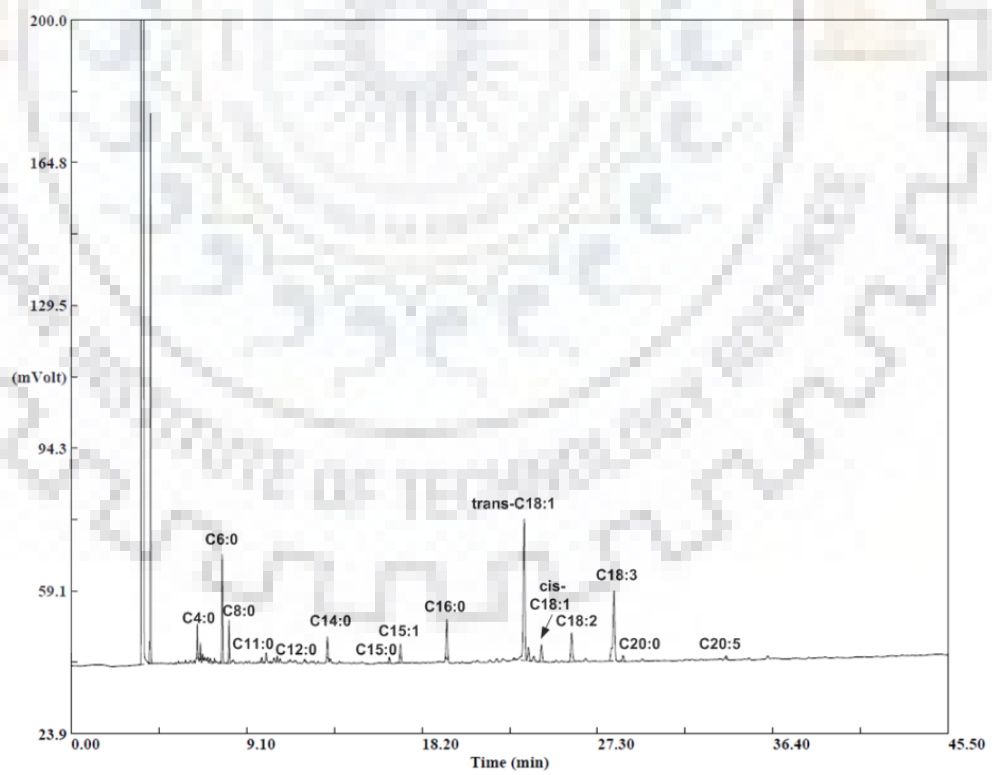
Fig. C.55: Gas chromatogram of Turmeric root fatty acid content, Run No. 04.

C-19
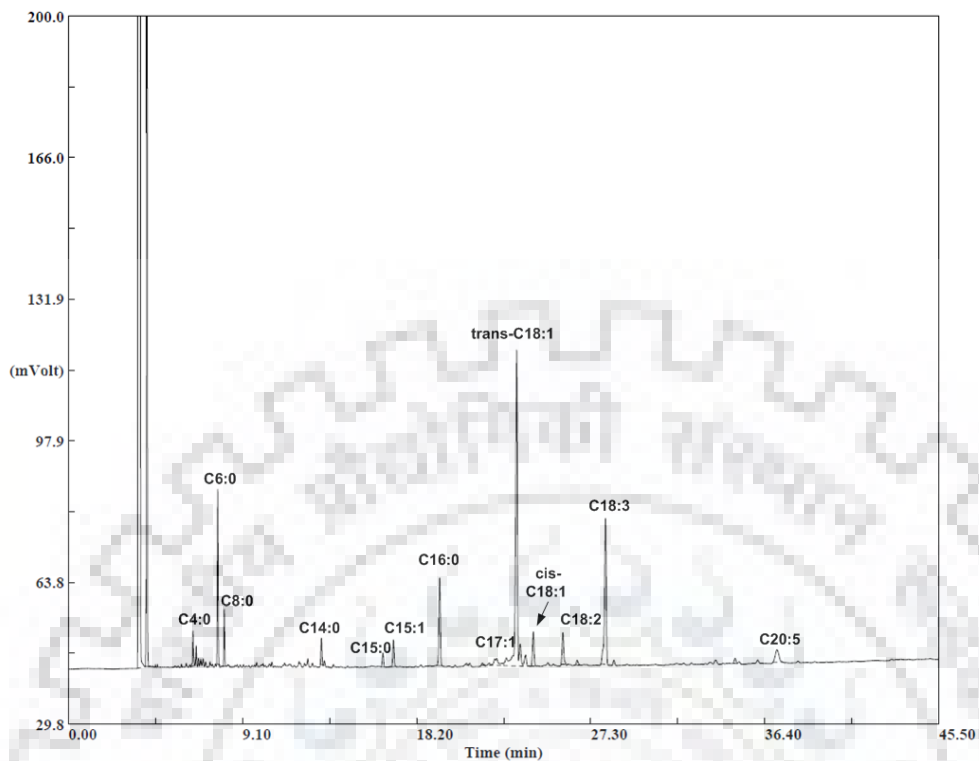
Fig. C.56: Gas chromatogram of Turmeric root fatty acid content, Run No. 05.
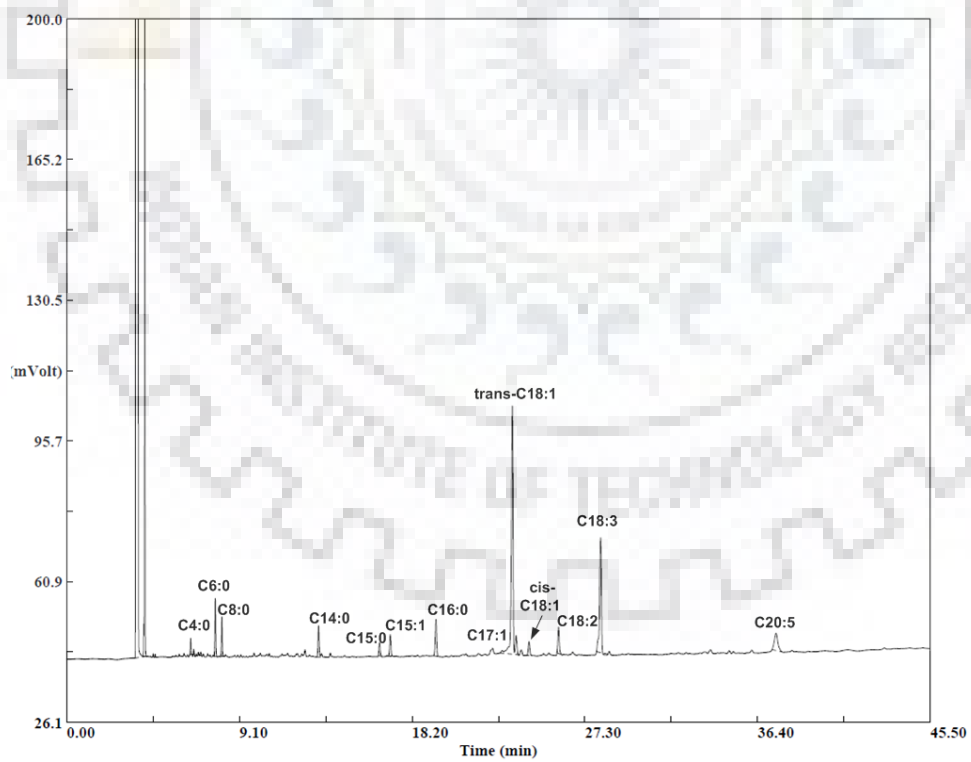
Fig. C.57: Gas chromatogram of Turmeric root fatty acid content, Run No. 06.
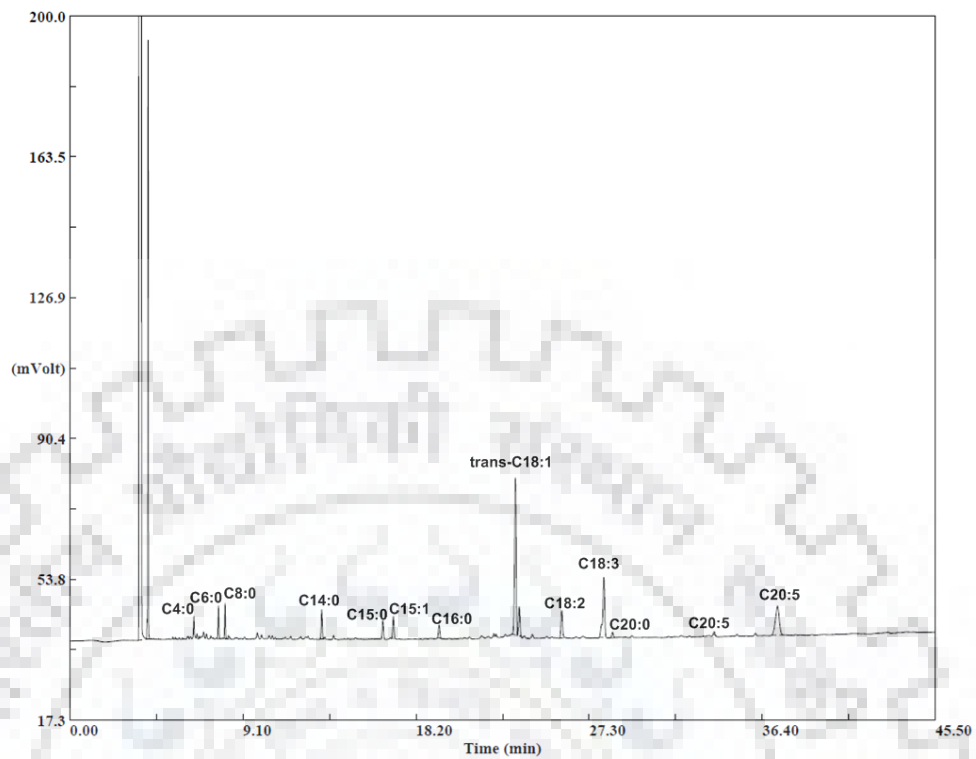
Fig. C.58: Gas chromatogram of Turmeric root fatty acid content, Run No. 07.
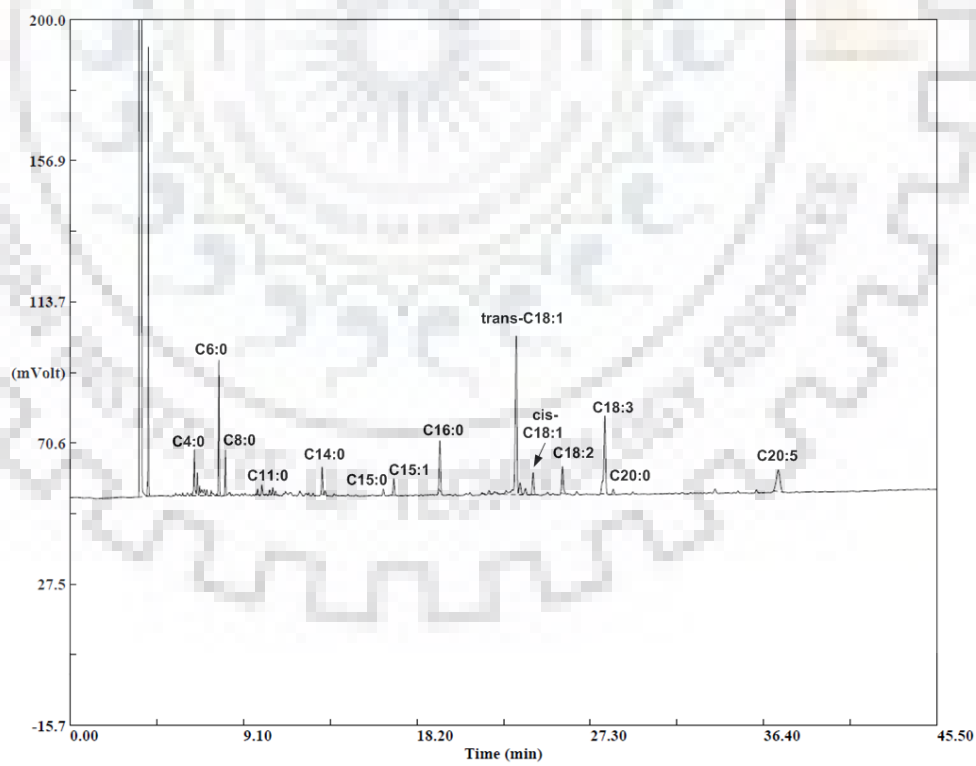
Fig. C.59: Gas chromatogram of Turmeric root fatty acid content, Run No. 08.

C-21
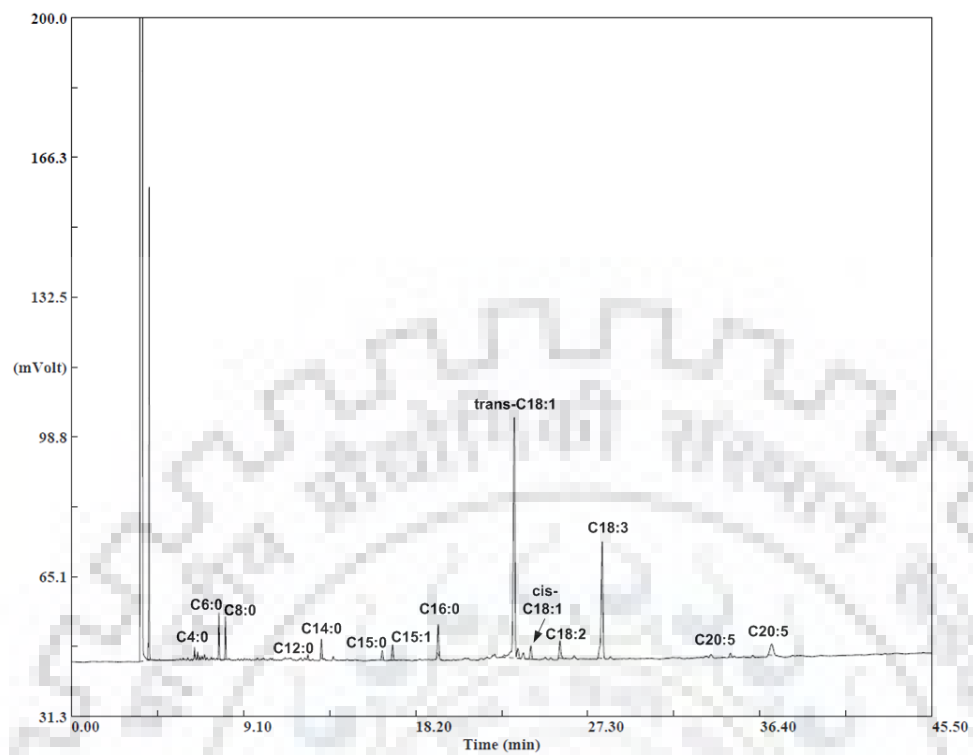
Fig. C.60: Gas chromatogram of Turmeric root fatty acid content, Run No. 09.
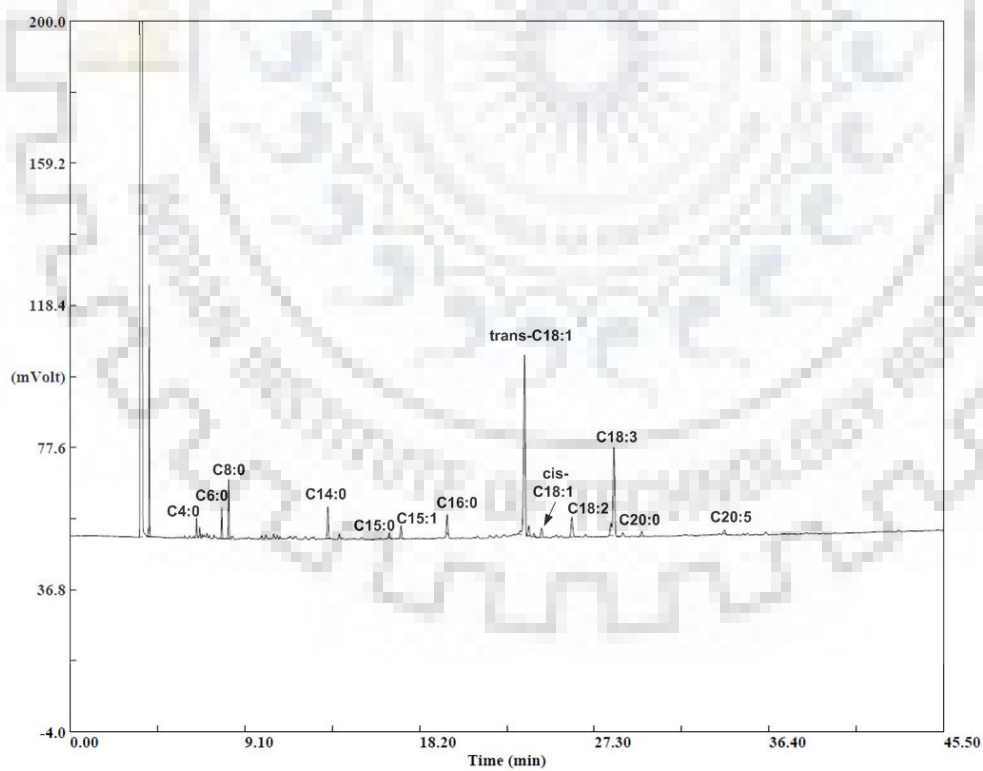
Fig. C.61: Gas chromatogram of Turmeric root fatty acid content, Run No. 10.
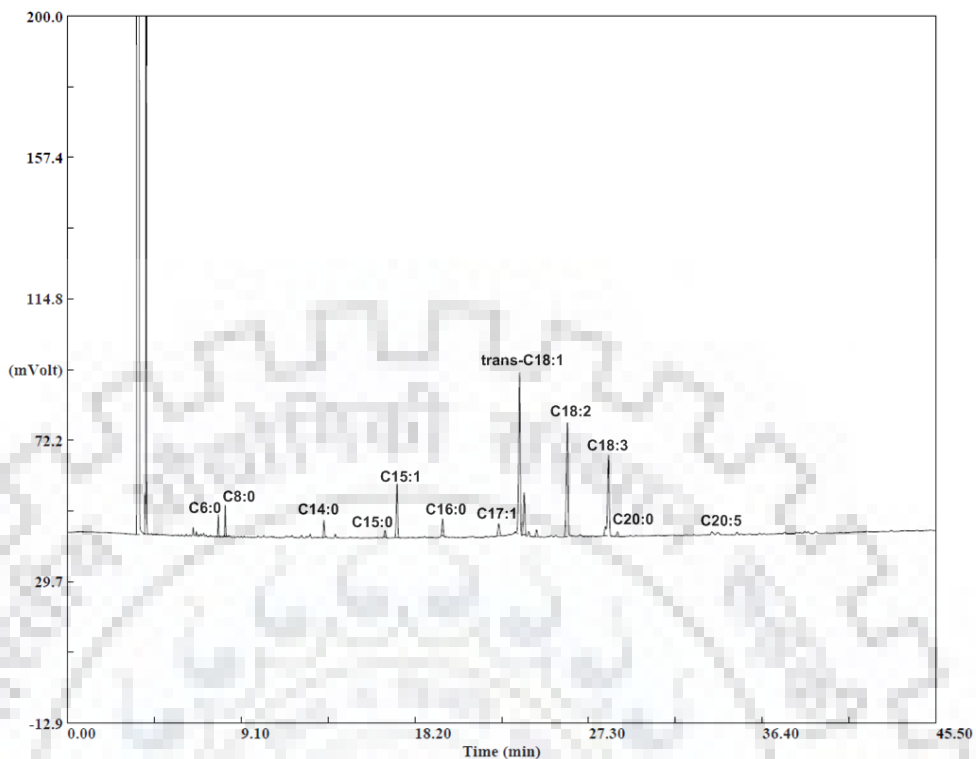
Fig. C.62: Gas chromatogram of Turmeric root fatty acid content, Run No. 11.
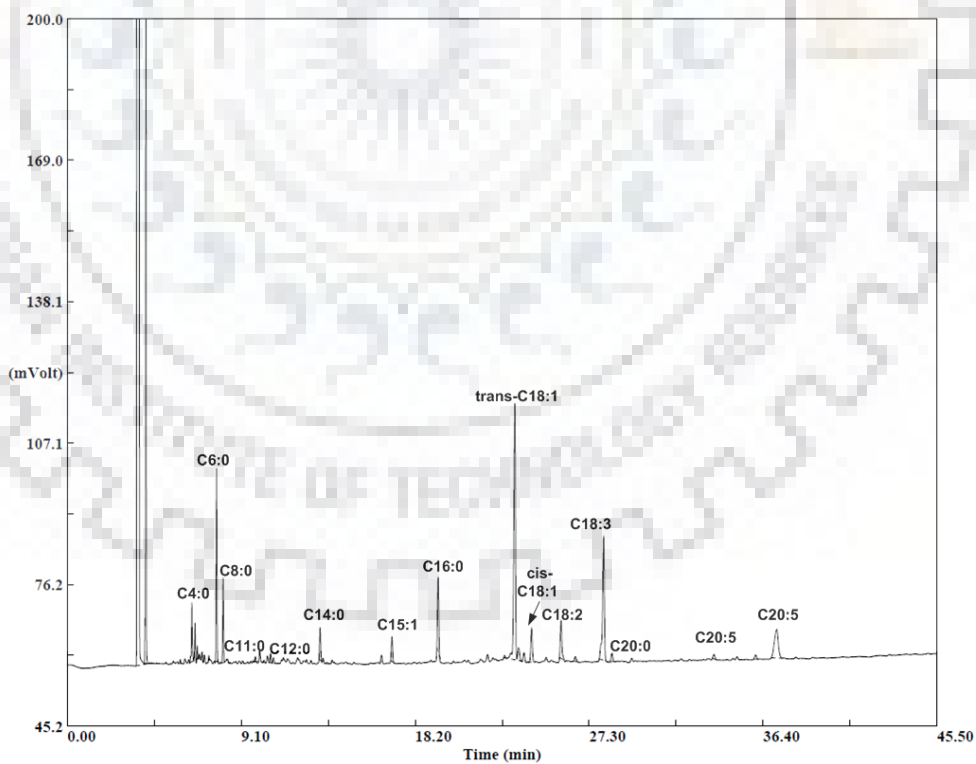
Fig. C.63: Gas chromatogram of Turmeric root fatty acid content, Run No. 12.

C-23
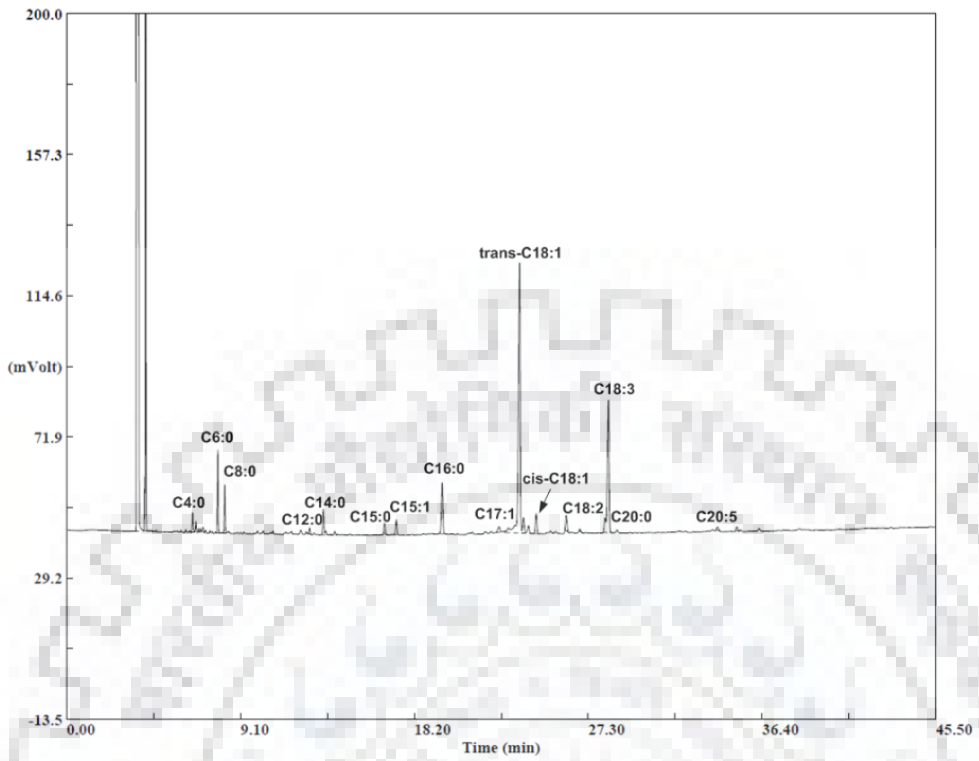
Fig. C.64: Gas chromatogram of Turmeric root fatty acid content, Run No. 13.
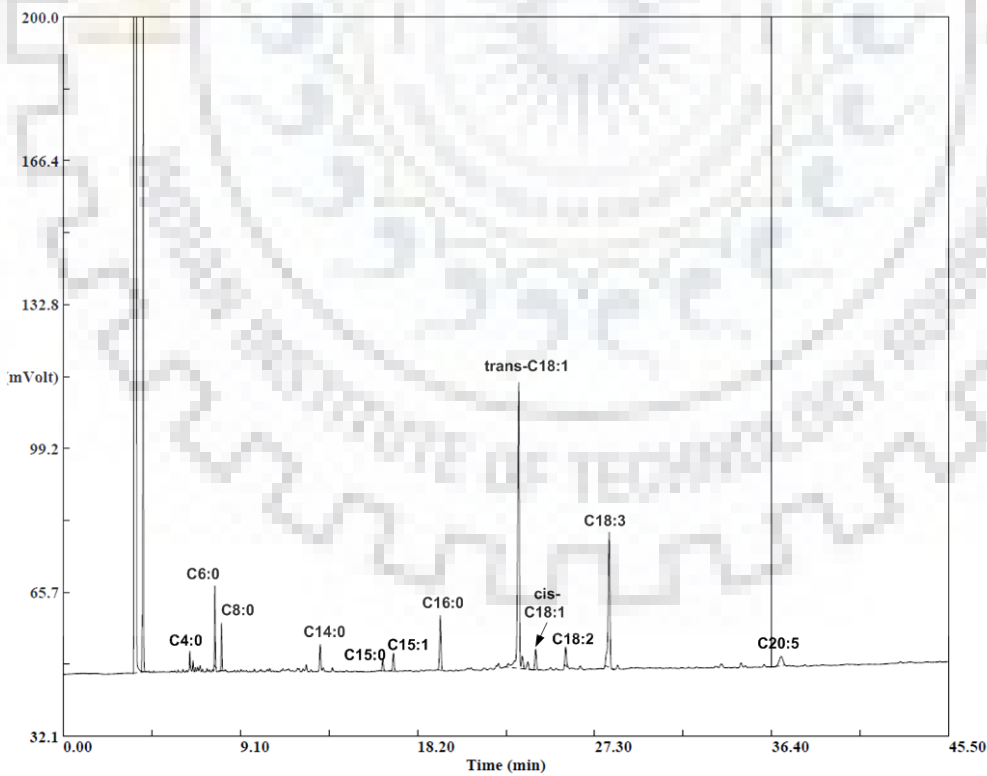
Fig. C.65: Gas chromatogram of Turmeric root fatty acid content, Run No. 14.

C-24
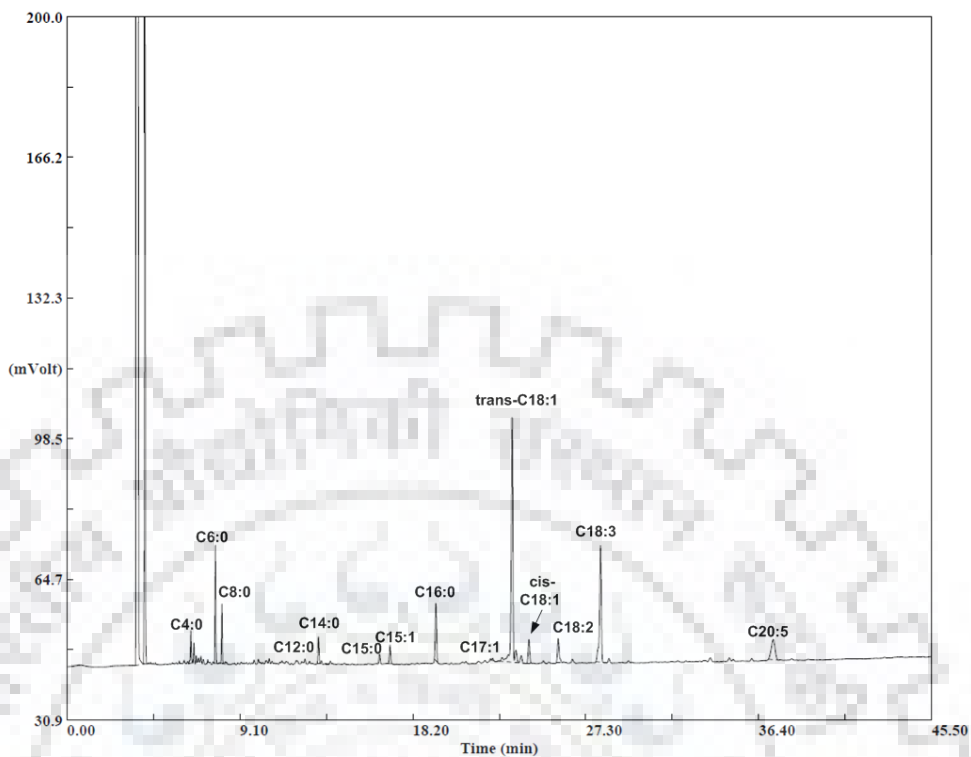
Fig. C.66: Gas chromatogram of Turmeric root fatty acid content, Run No. 15.
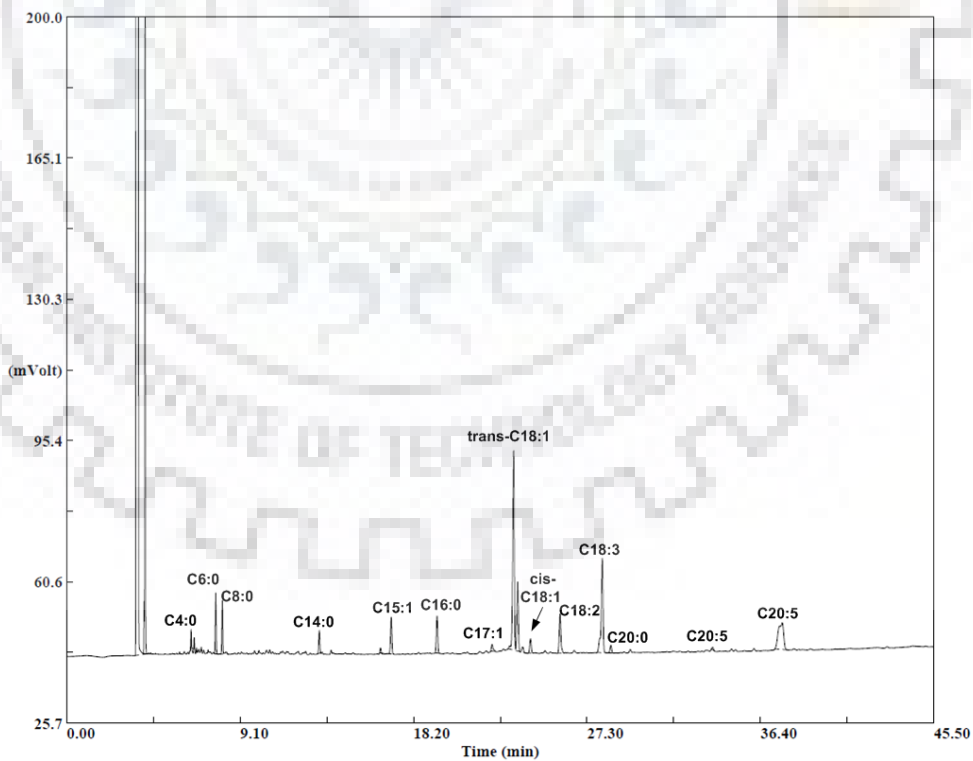
Fig. C.67: Gas chromatogram of Turmeric root fatty acid content, Run No. 16.

C-25
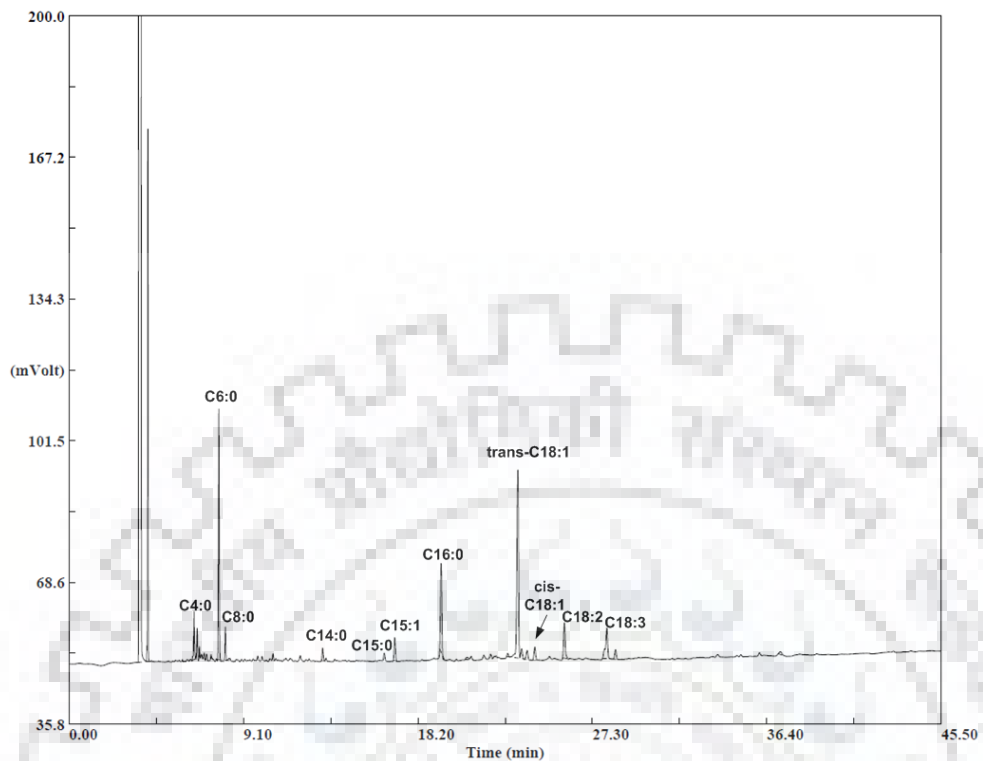
Fig. C.68: Gas chromatogram of Turmeric root fatty acid content, Run No. 17.
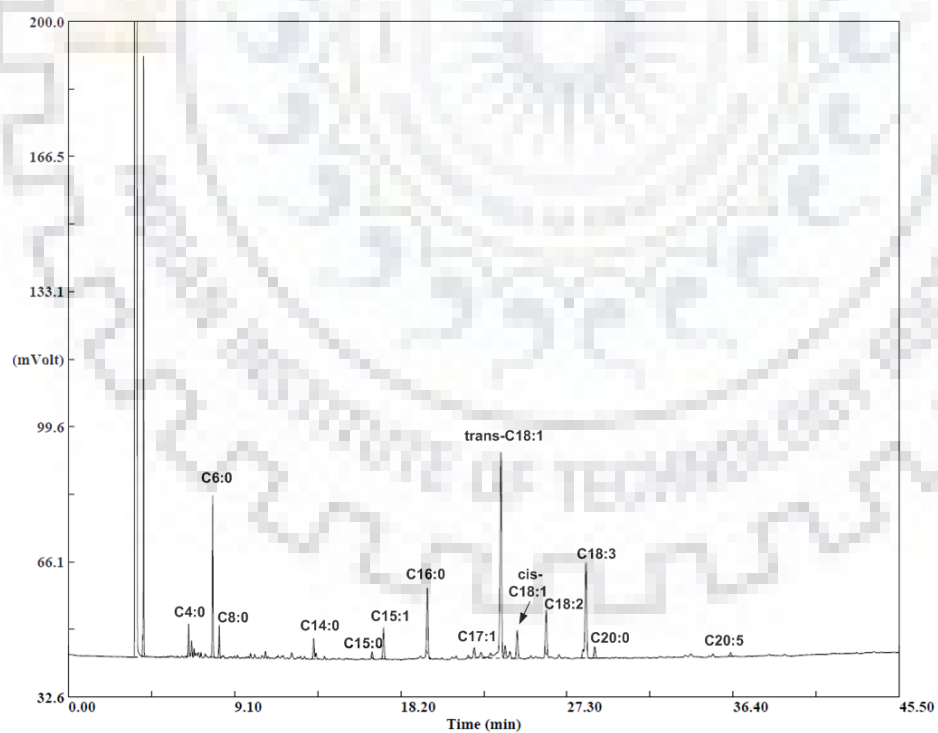
Fig. C.69: Gas chromatogram of Turmeric root fatty acid content, Run No. 18.
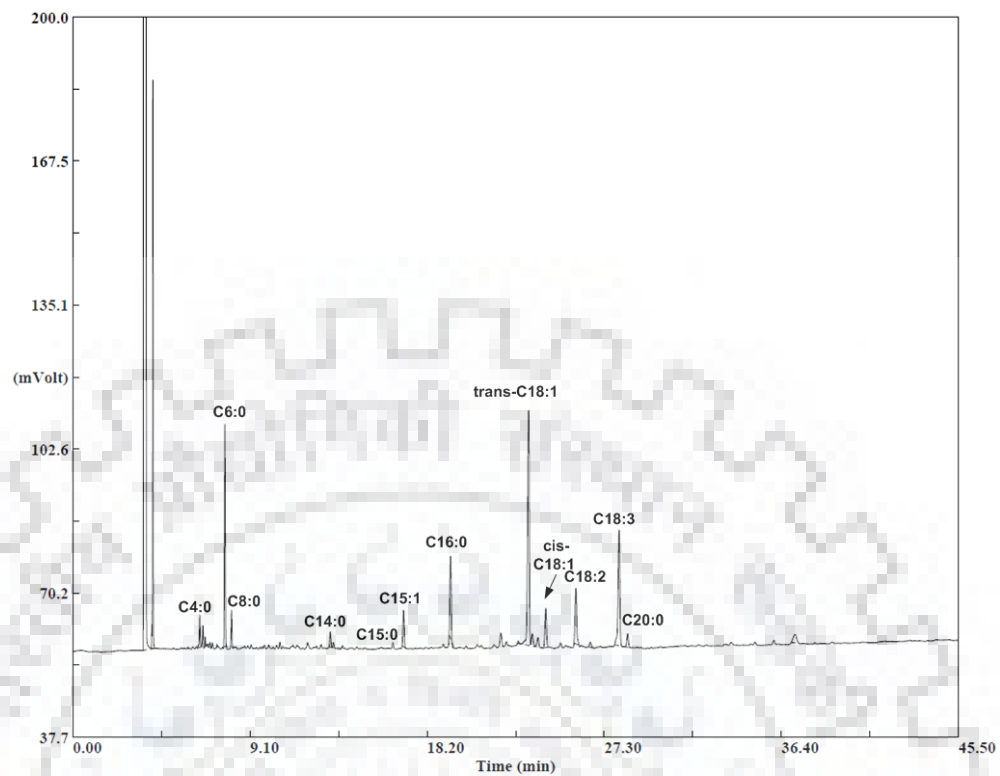
Fig. C.70: Gas chromatogram of Turmeric root fatty acid content, Run No. 19.
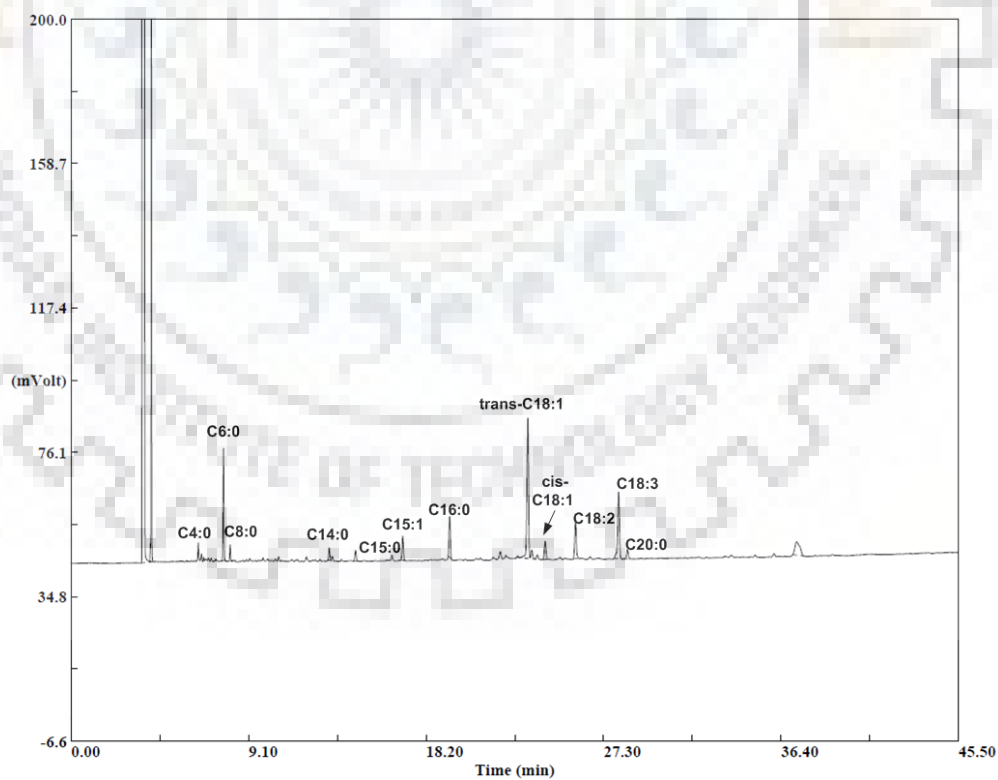
Fig. C.71: Gas chromatogram of Turmeric root fatty acid content, Run No. 20.
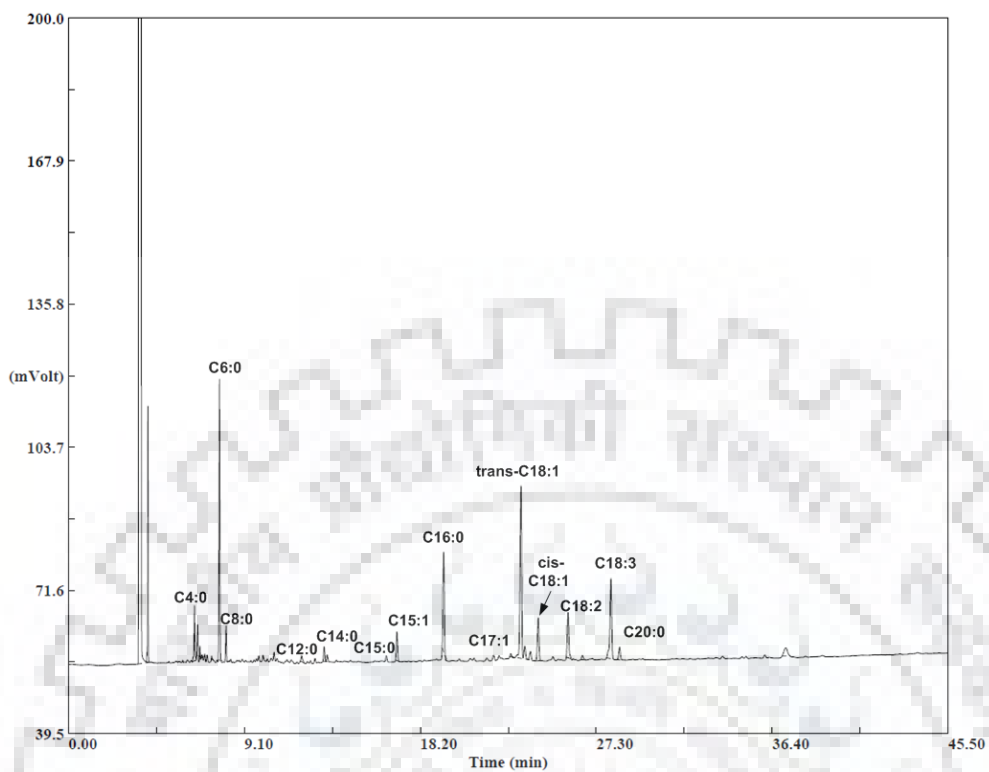
Fig. C.72: Gas chromatogram of Turmeric root fatty acid content, Run No. 21.
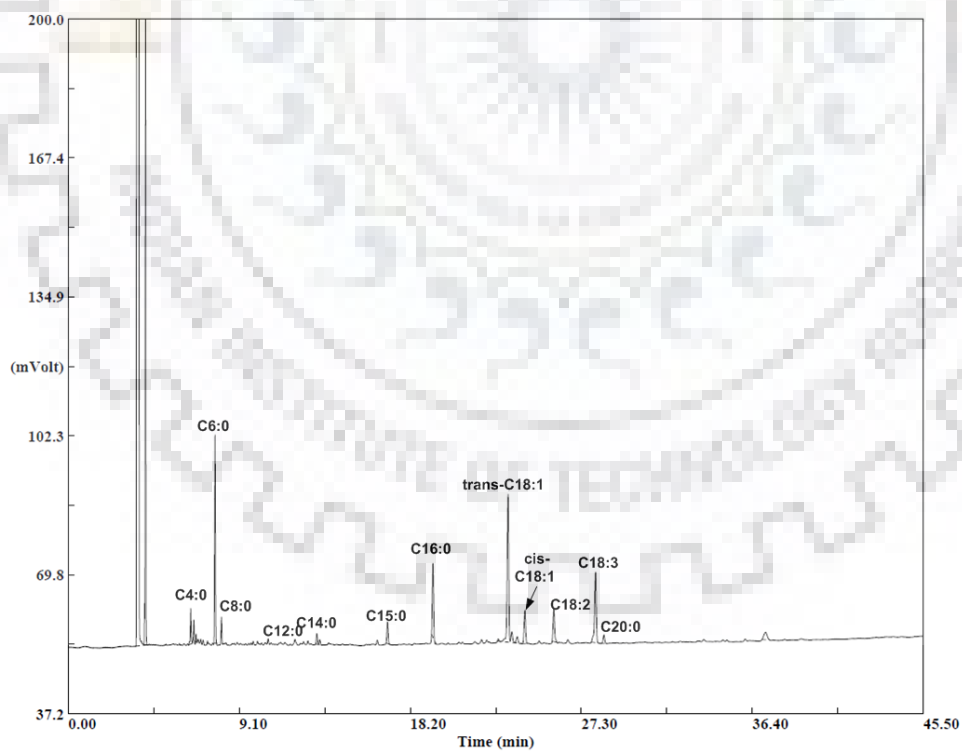
Fig. C.73: Gas chromatogram of Turmeric root fatty acid content, Run No. 22.
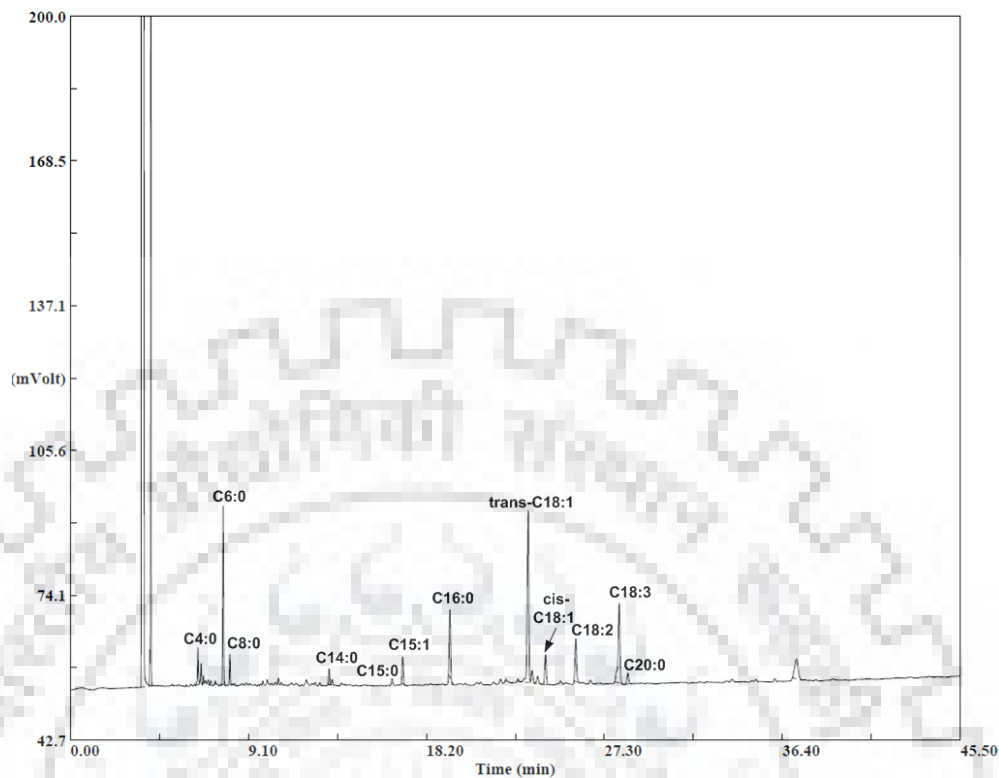
Fig. C.74: Gas chromatogram of Turmeric root fatty acid content, Run No. 23.
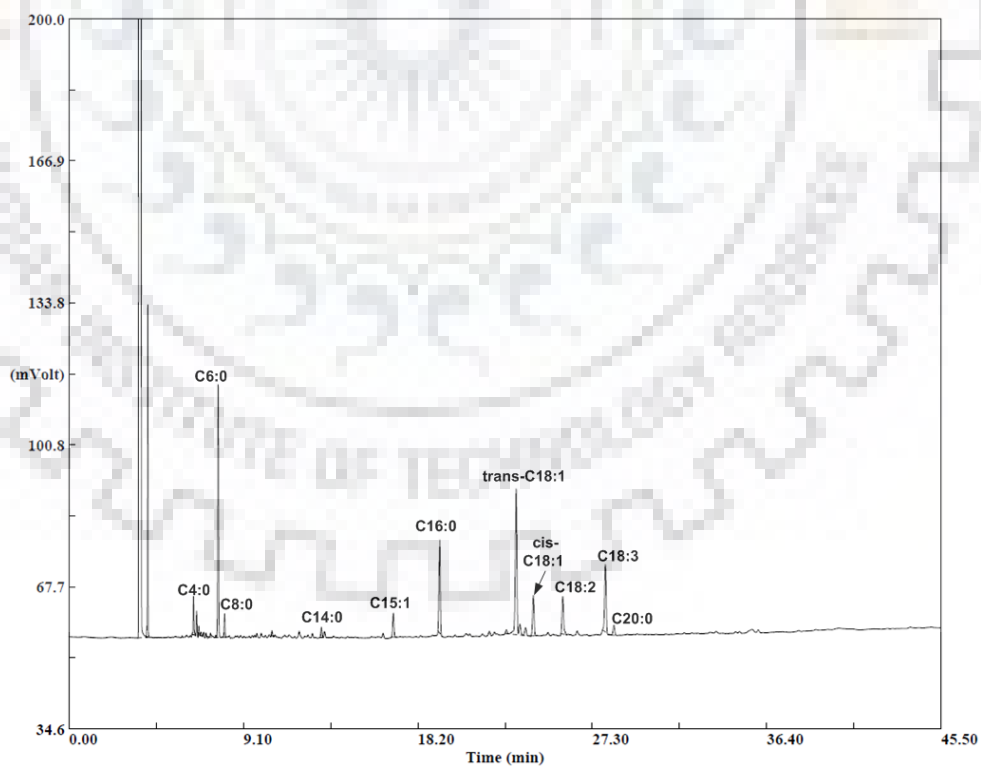

Fig. C.75: Gas chromatogram of Turmeric root fatty acid content, Run No. 24.
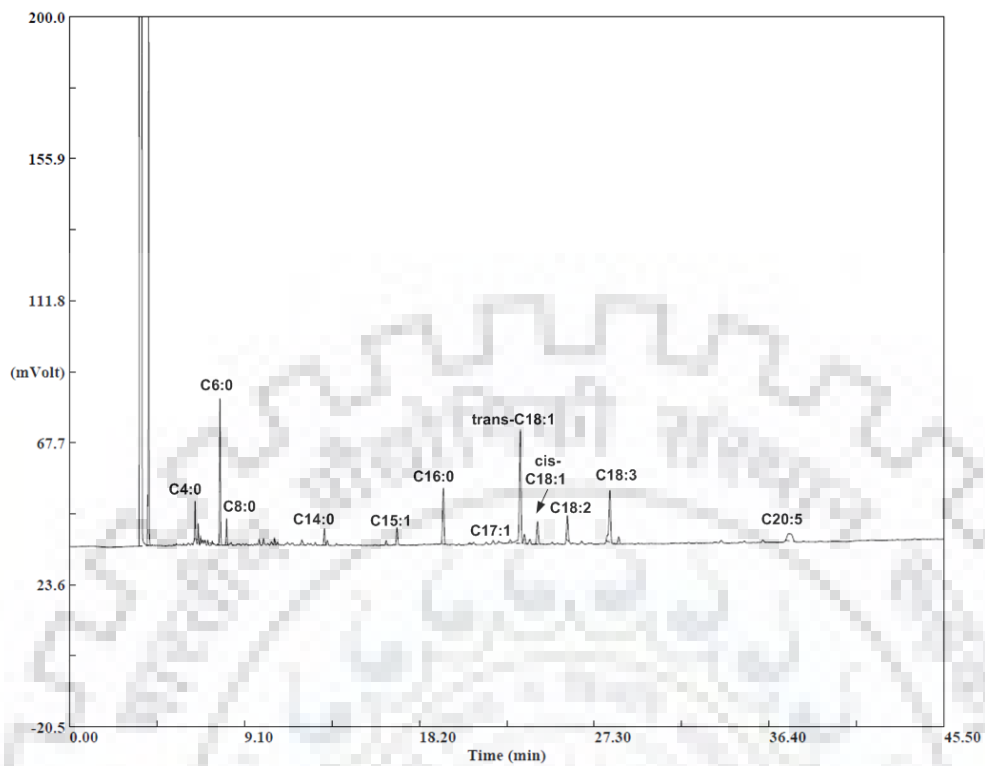
Fig. C.76: Gas chromatogram of Turmeric root fatty acid content, Run No. 25.
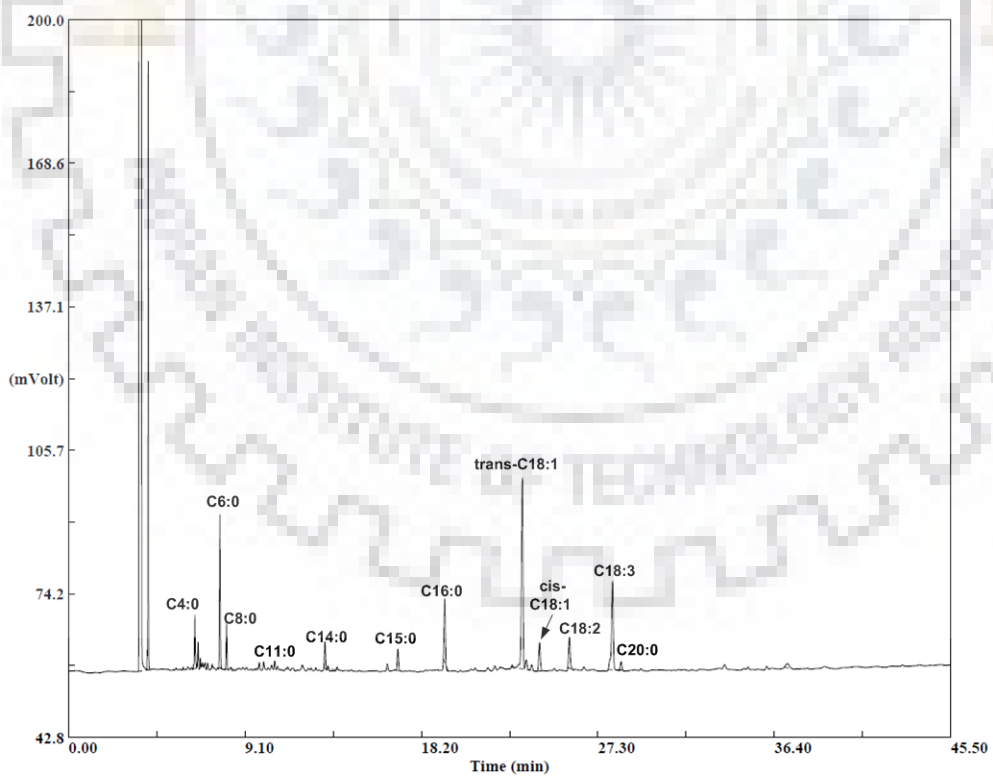
Fig. C.77: Gas chromatogram of Turmeric root fatty acid content, Run No. 26.
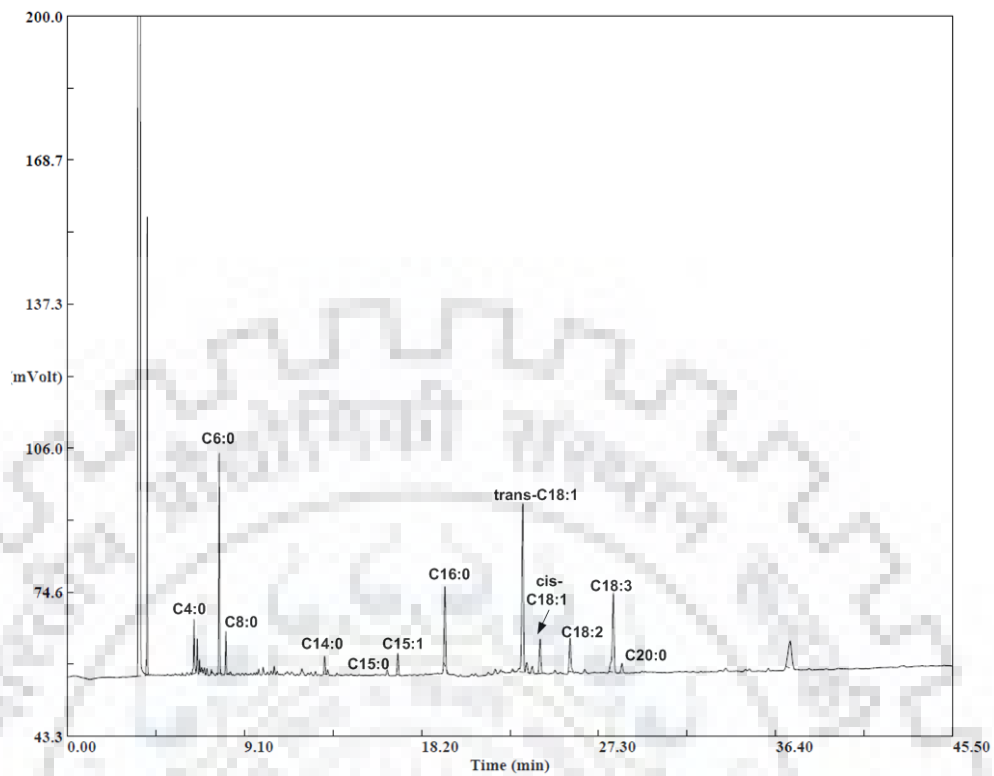
Fig. C.78: Gas chromatogram of Turmeric root fatty acid content, Run No. 27.
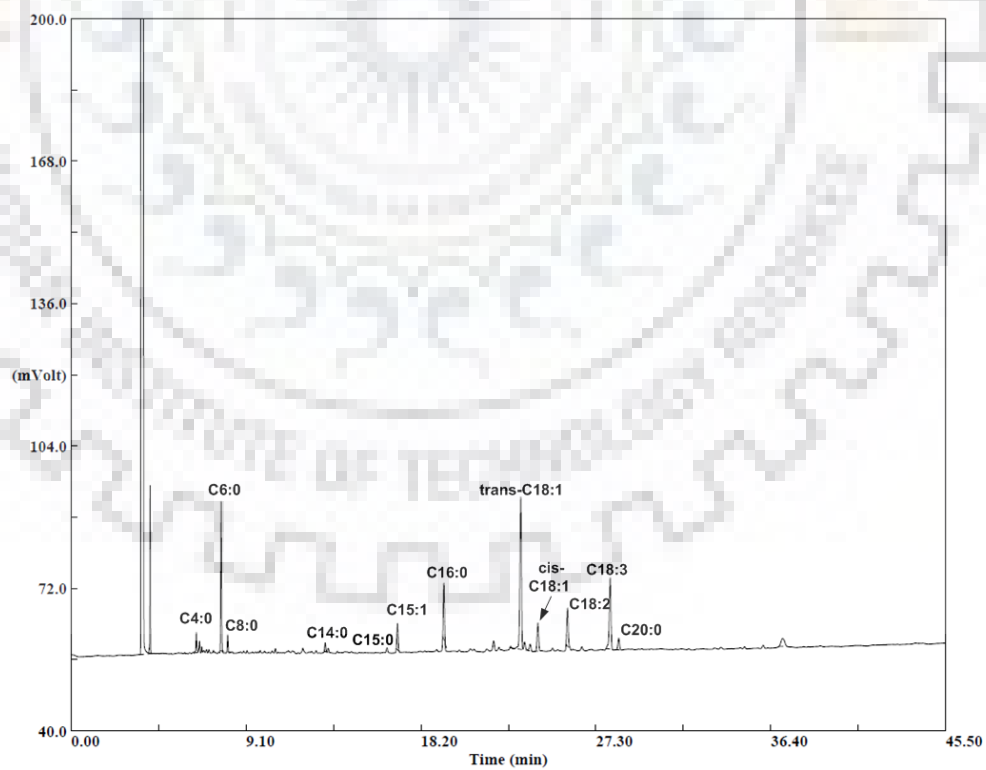
Fig. C.79: Gas chromatogram of Turmeric root fatty acid content, Run No. 28.

C-31
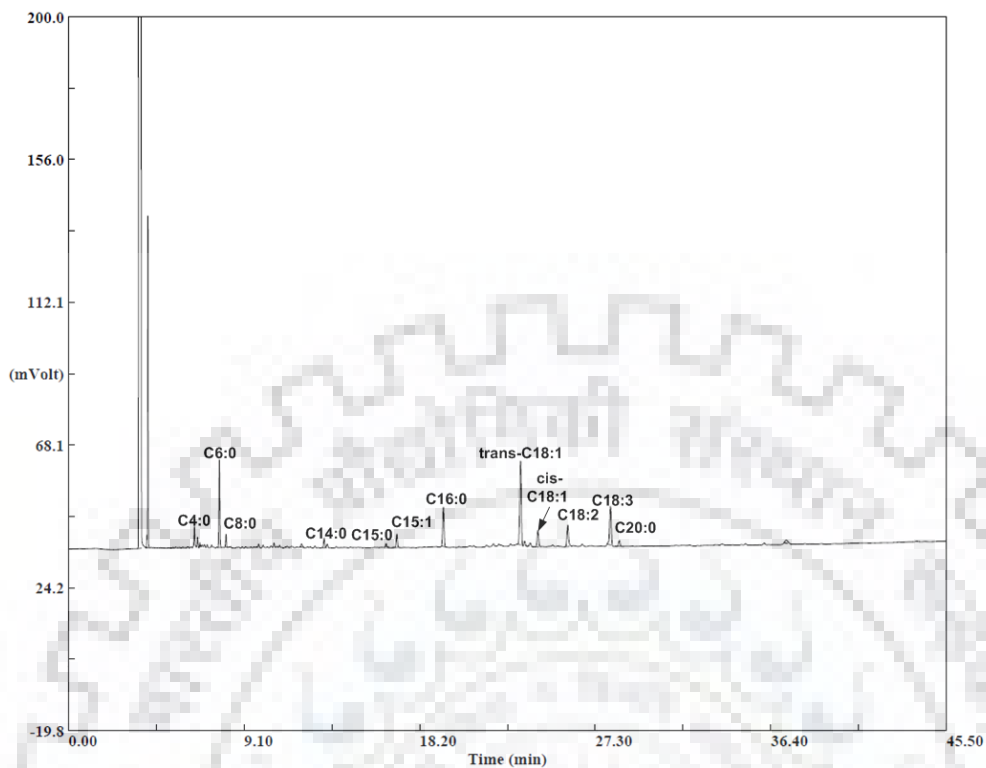
Fig. C.80: Gas chromatogram of Turmeric root fatty acid content, Run No. 29.
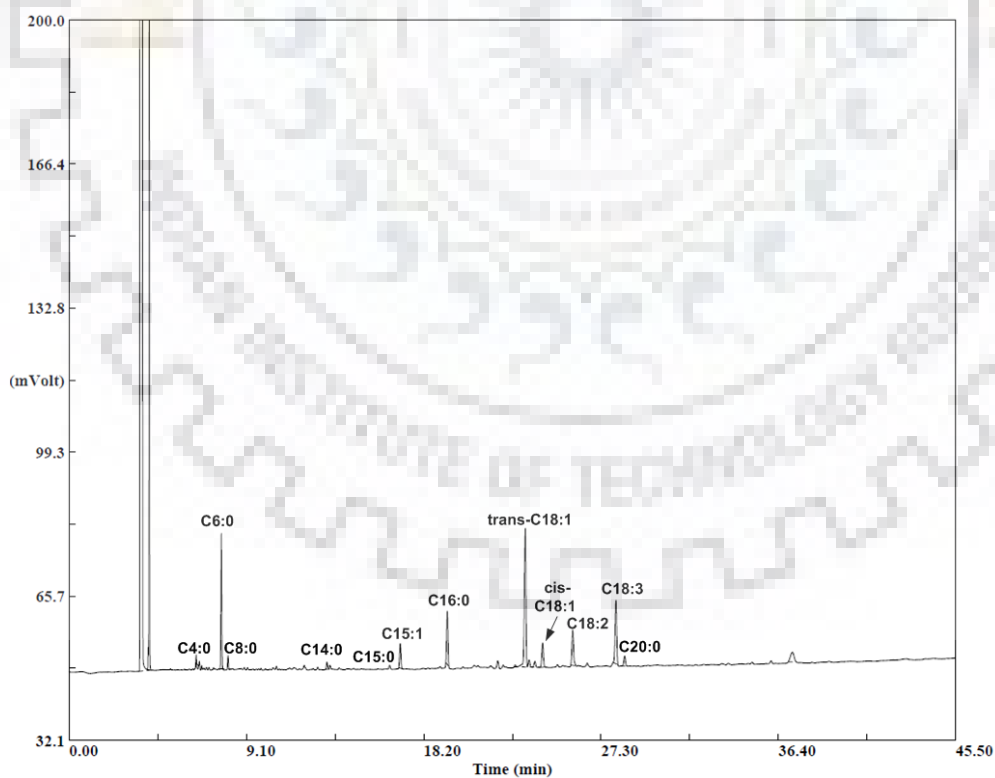

Fig. C.81: Gas chromatogram of Turmeric root fatty acid content, Run No. 30.
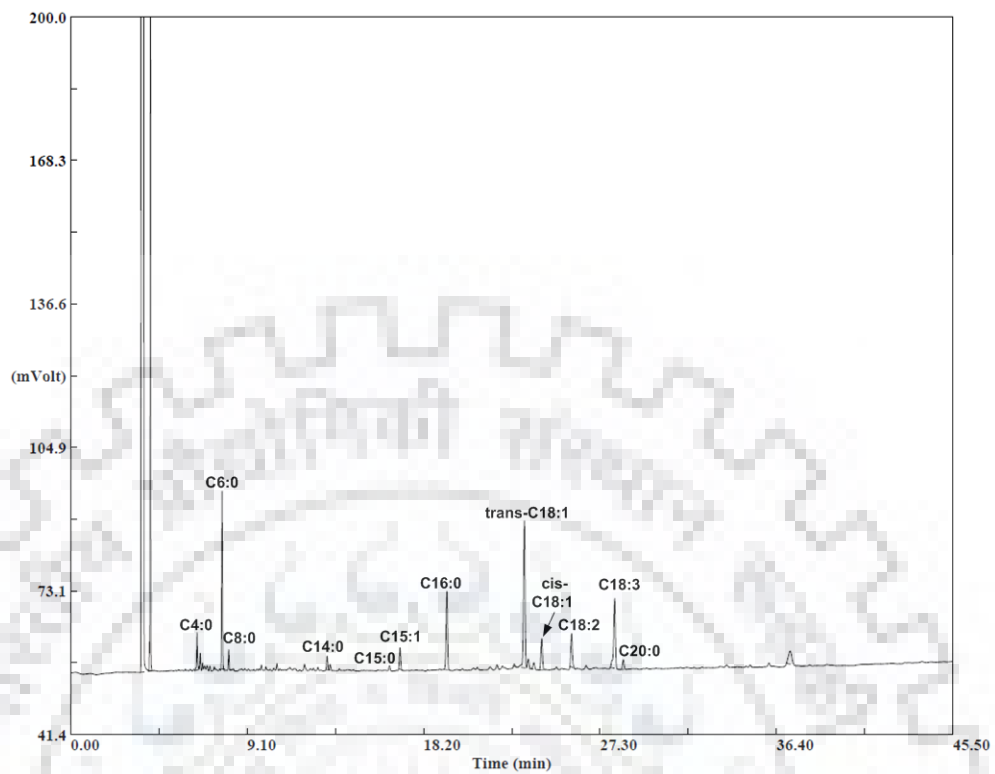
Fig. C.82: Gas chromatogram of Turmeric root fatty acid content, Run No. 31.
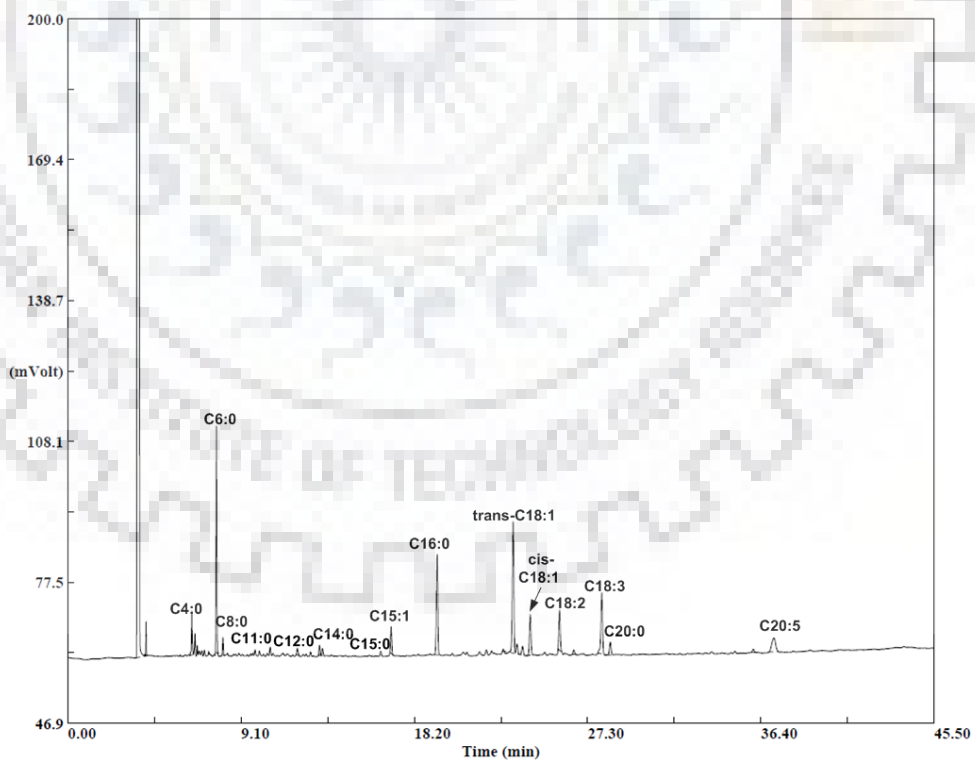
Fig. C.83: Gas chromatogram of Turmeric root fatty acid content, Run No. 32.

C-33
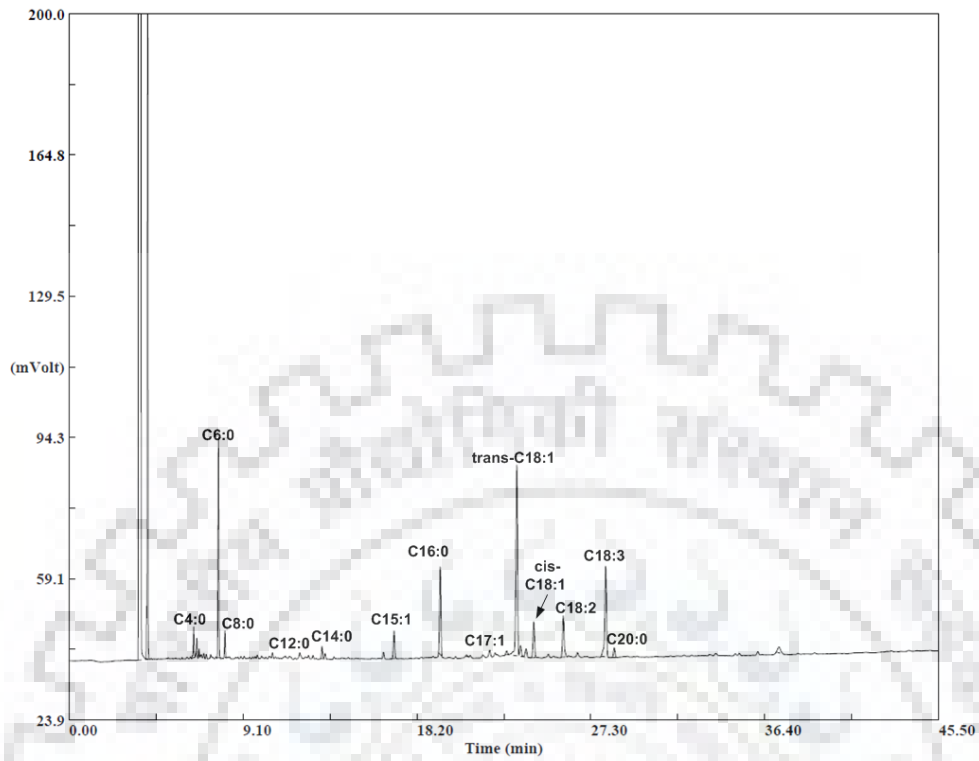
Fig. C.84: Gas chromatogram of Turmeric root fatty acid content, Run No. 33.
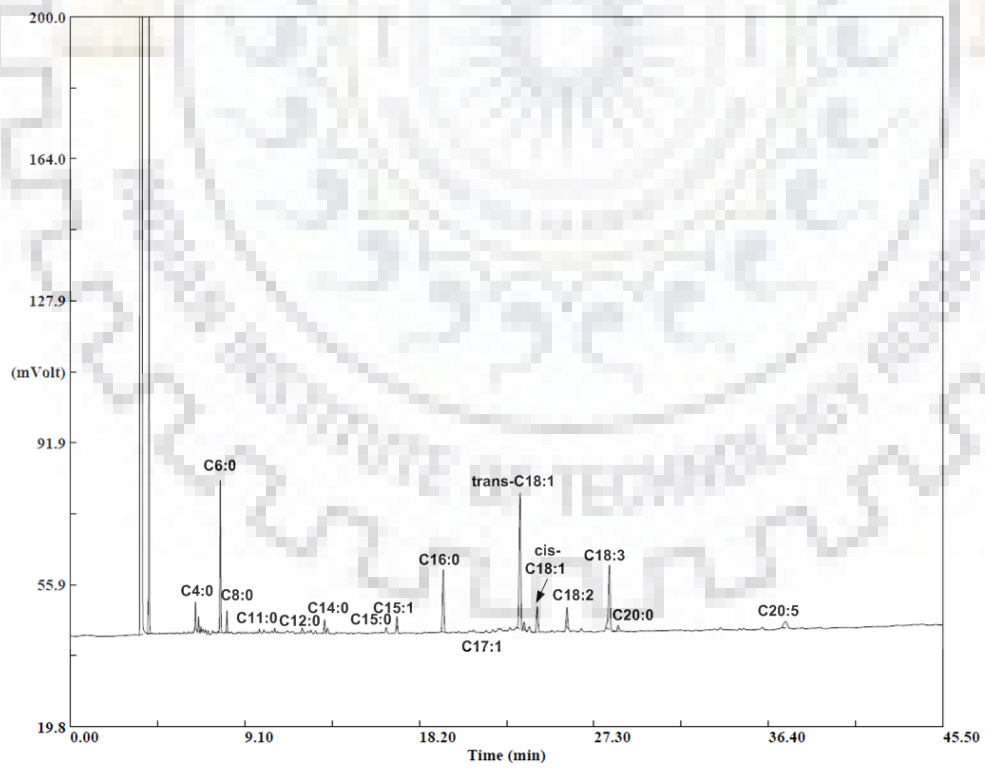
Fig. C.85: Gas chromatogram of Turmeric root fatty acid content, Run No. 34.

C-34
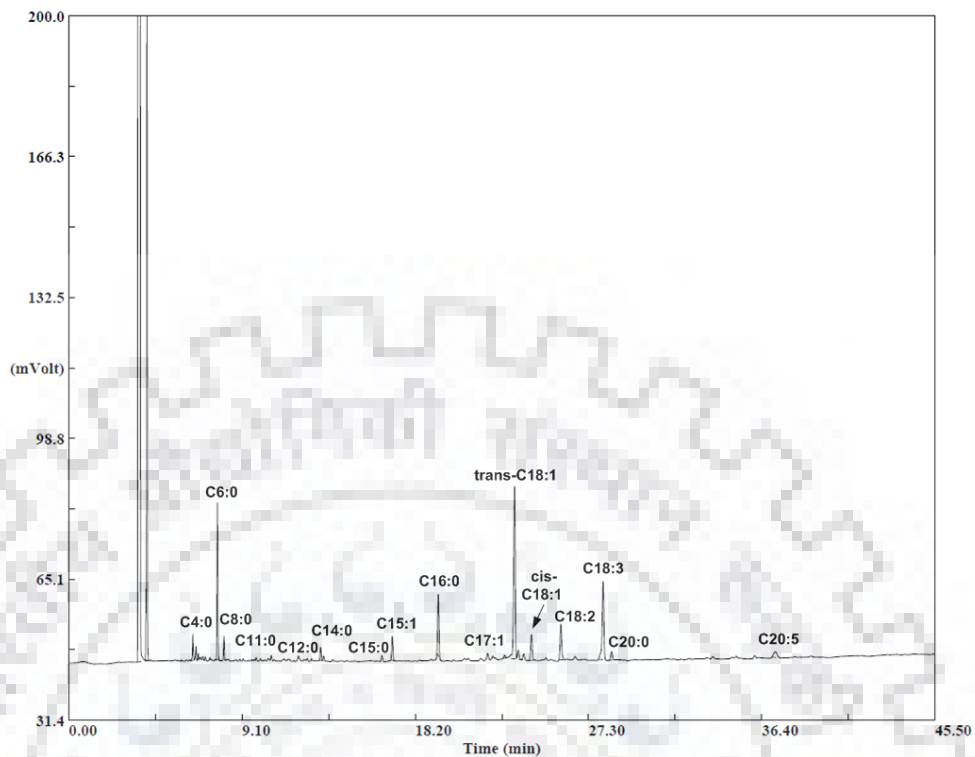
Fig. C.86: Gas chromatogram of Turmeric root fatty acid content, Run No. 35.
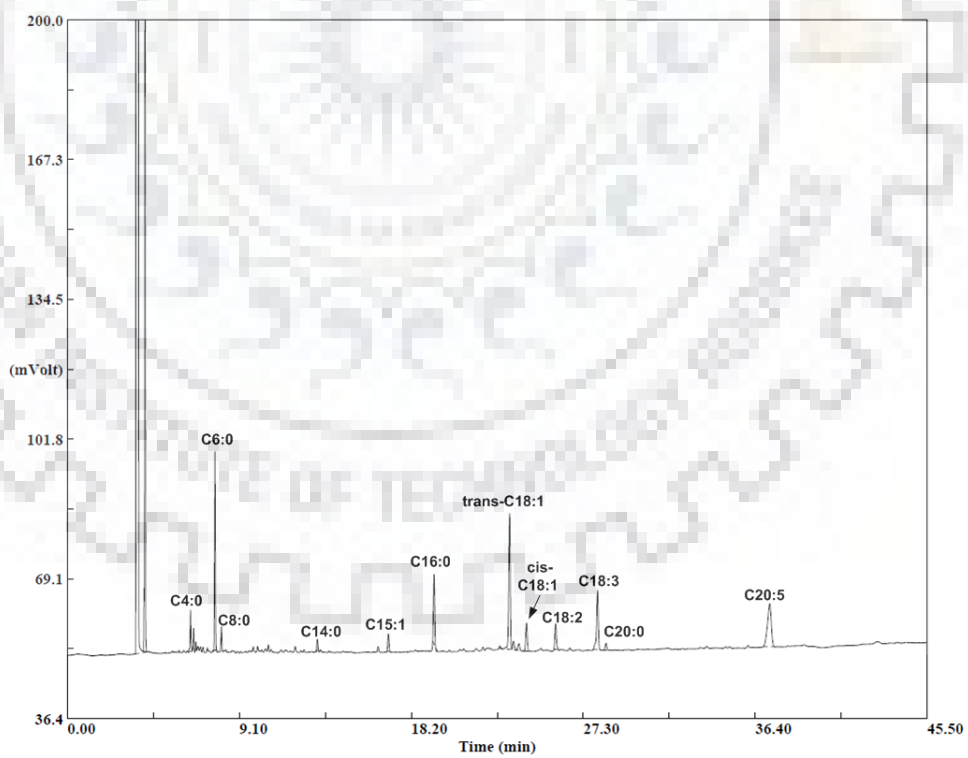
Fig. C.87: Gas chromatogram of Turmeric root fatty acid content, Run No. 36.
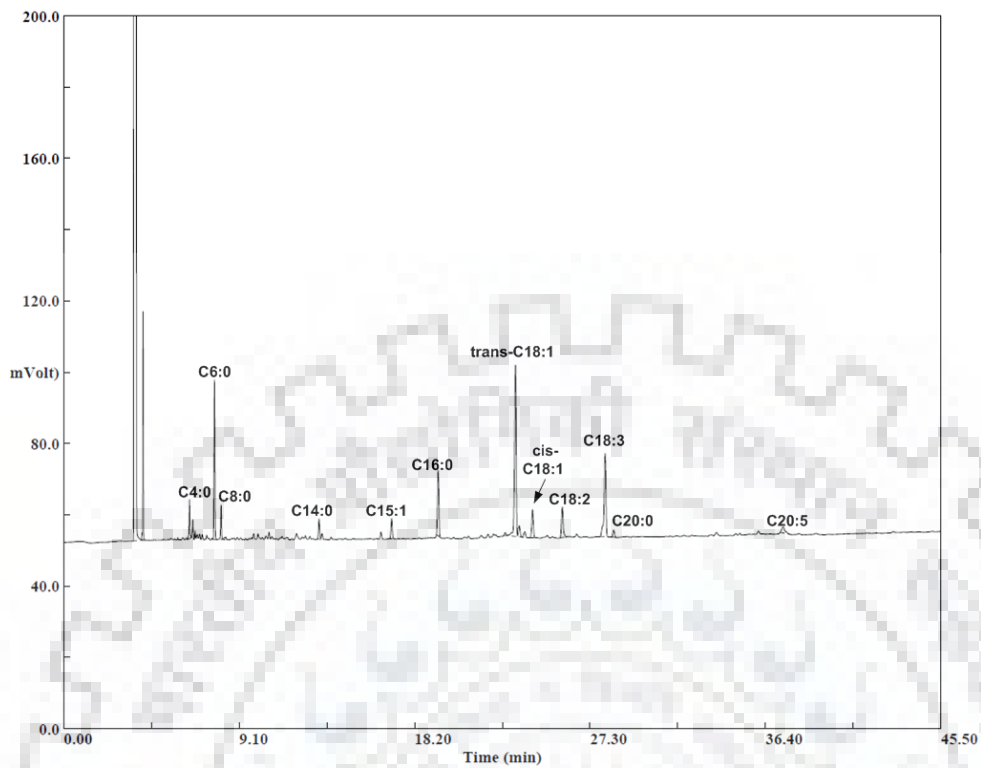
Fig. C.88: Gas chromatogram of Turmeric root fatty acid content, Run No. 37.
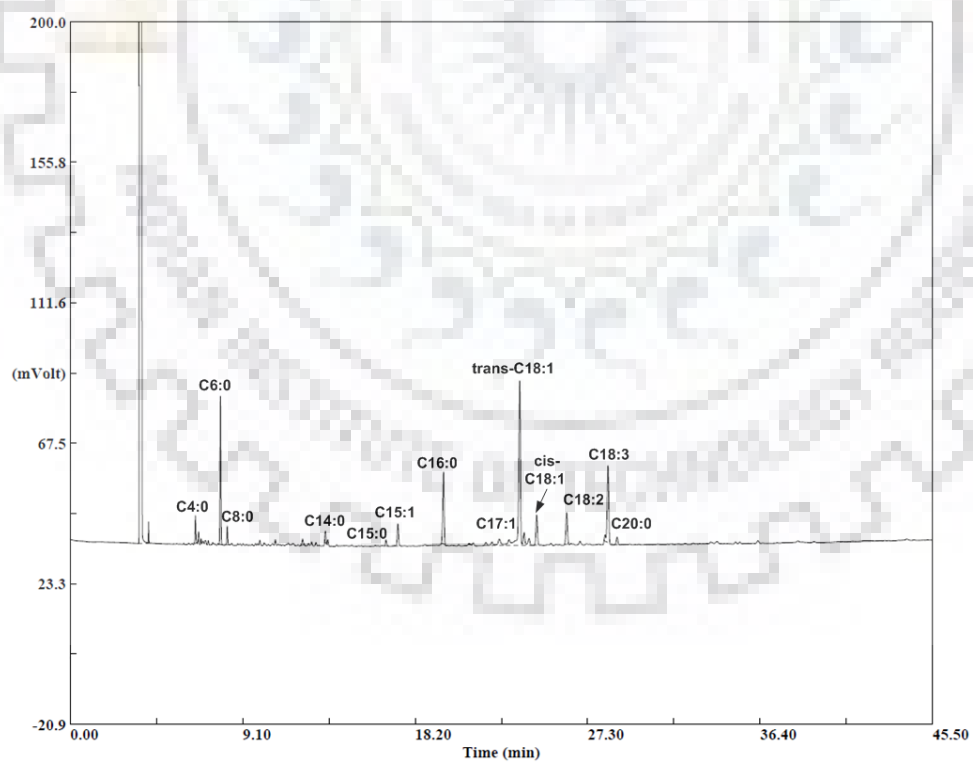

Fig. C.89: Gas chromatogram of Turmeric root fatty acid content, Run No. 38.
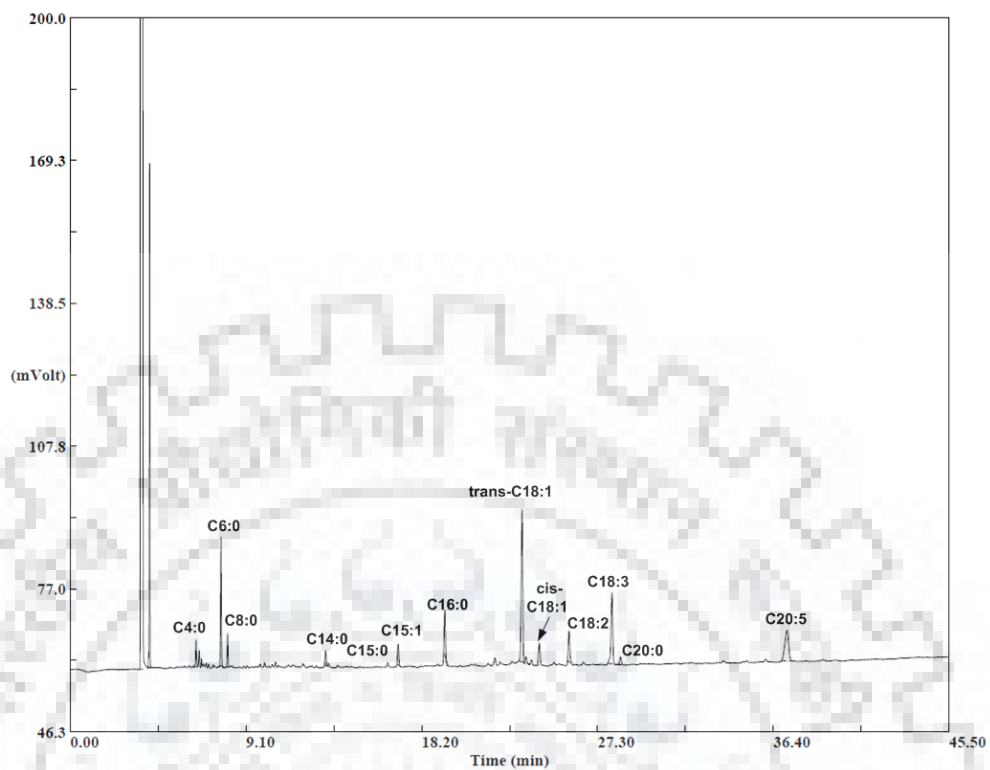
Fig. C.90: Gas chromatogram of Turmeric root fatty acid content, Run No. 39.
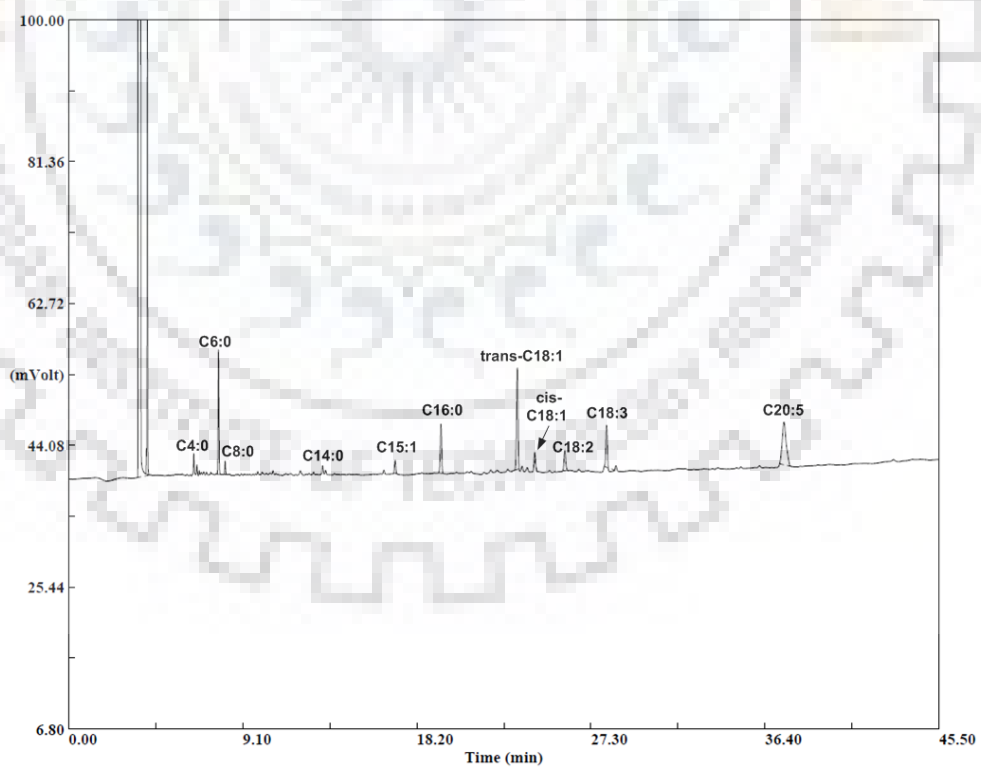
Fig. C.91: Gas chromatogram of Turmeric root fatty acid content, Run No. 40.

C-37
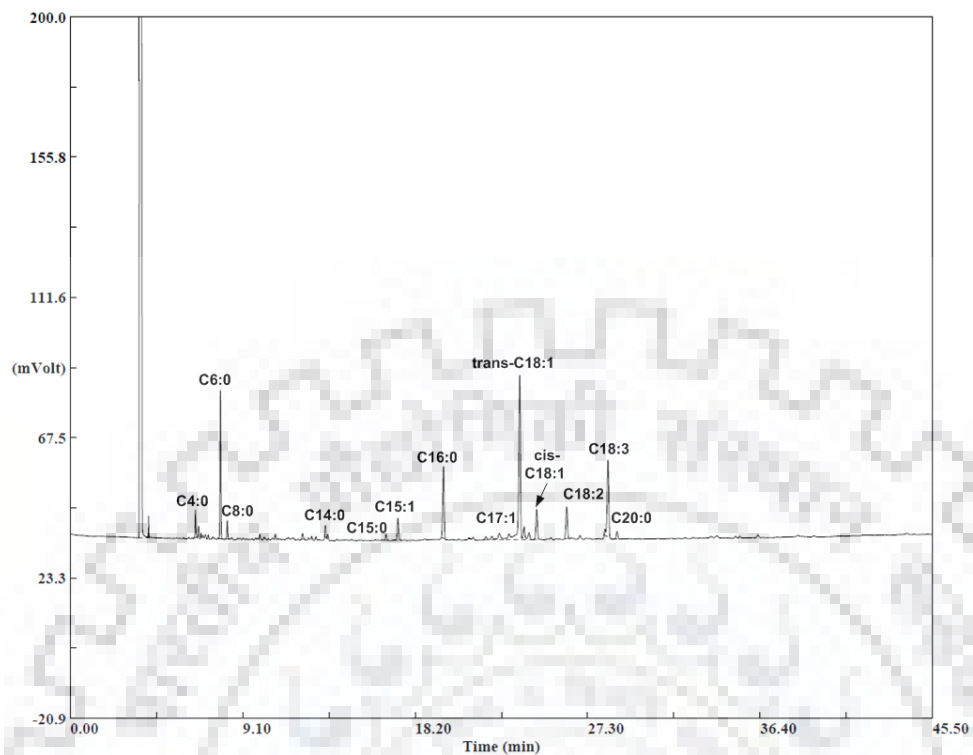
Fig. C.92: Gas chromatogram of Turmeric root fatty acid content, Run No. 41.
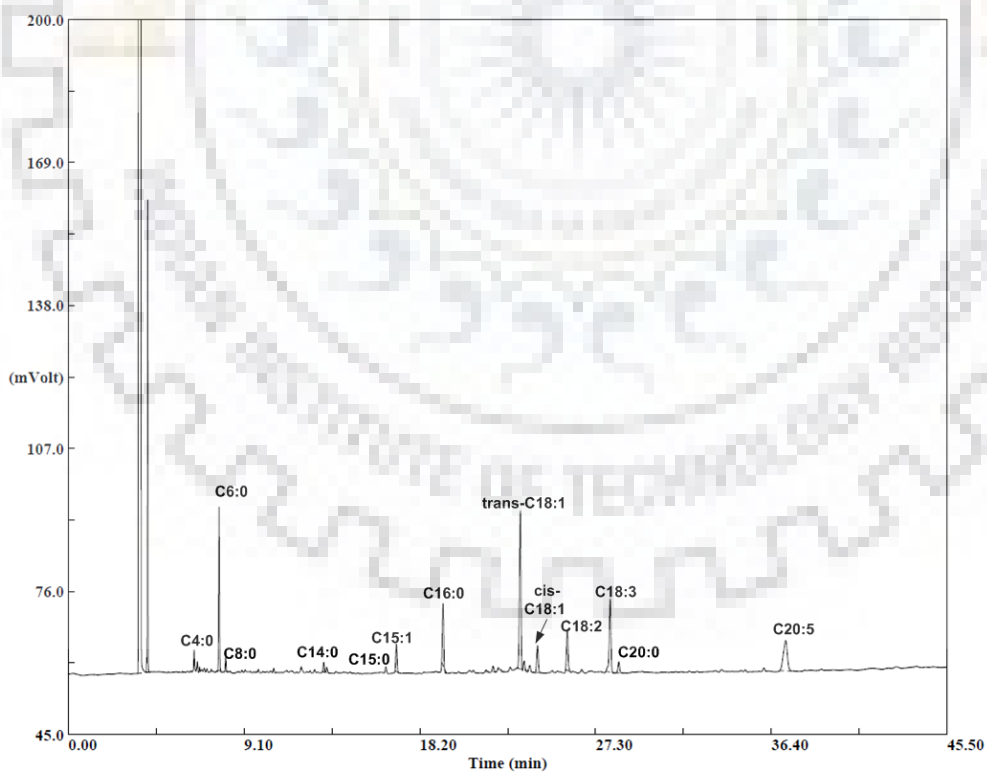
Fig. C.93: Gas chromatogram of Turmeric root fatty acid content, Run No. 42.

C-38
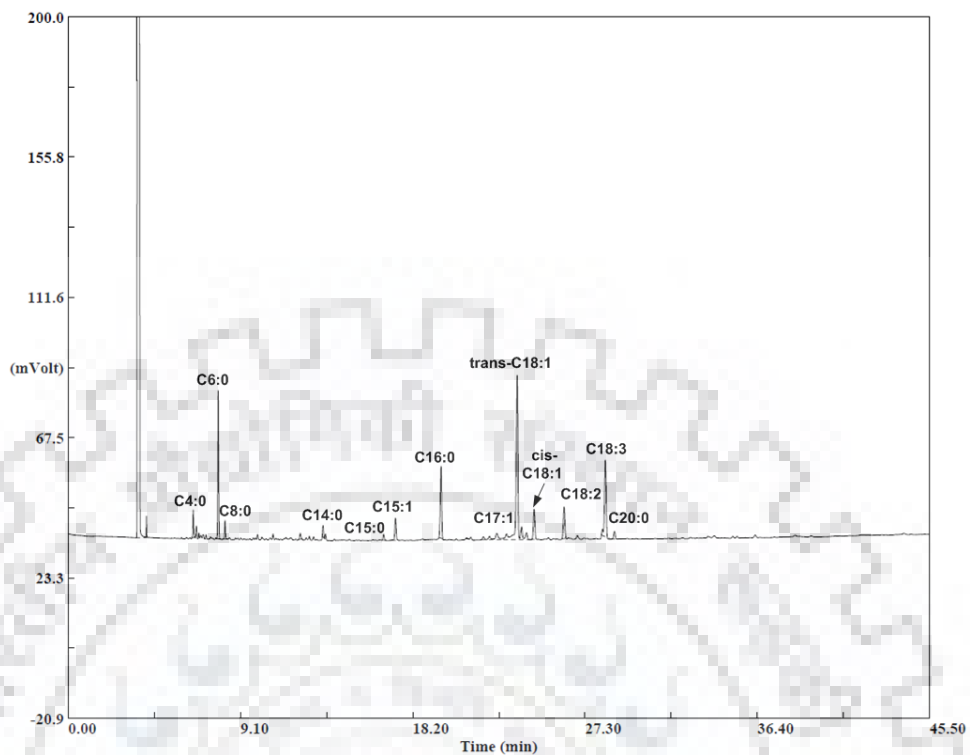
Fig. C.94: Gas chromatogram of Turmeric root fatty acid content, Run No. 43.
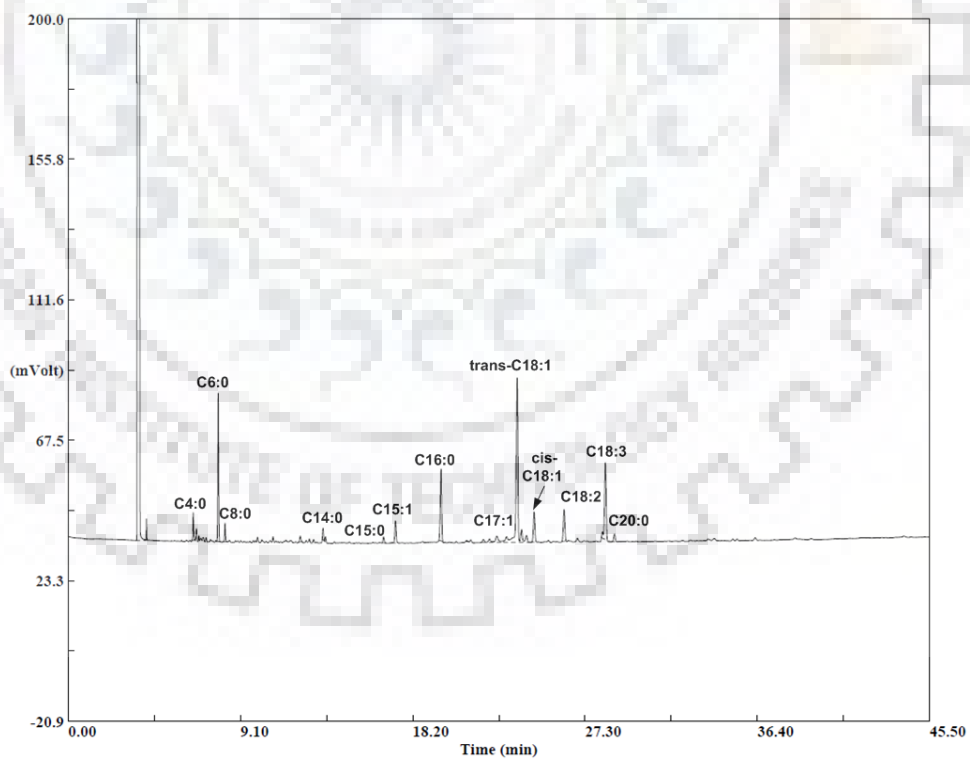
Fig. C.95: Gas chromatogram of Turmeric root fatty acid content, Run No. 44.
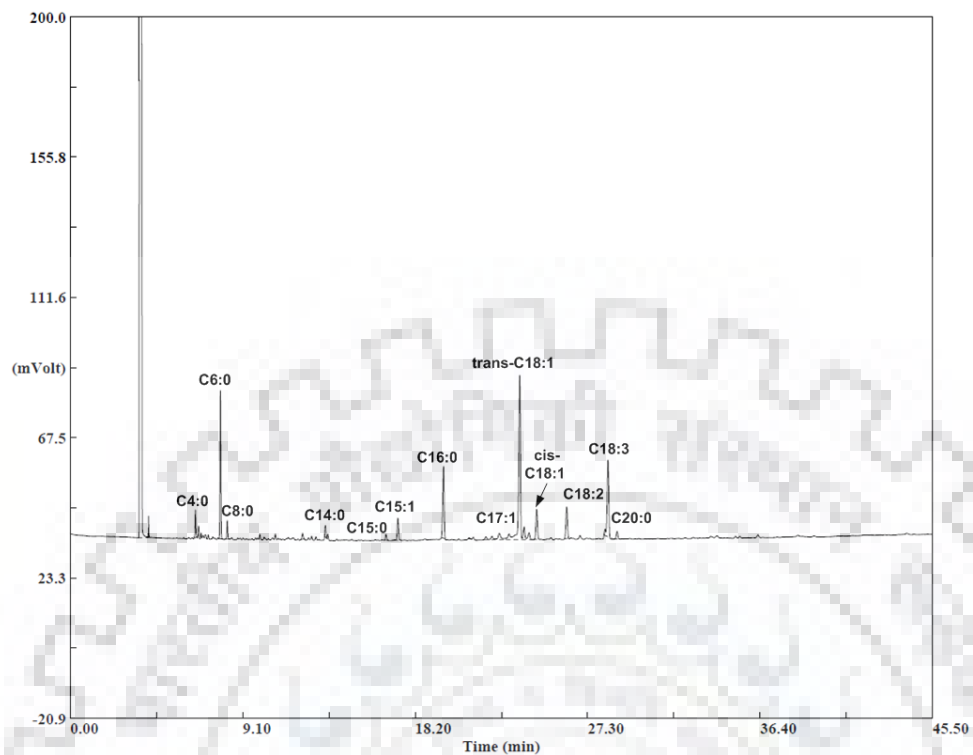
Fig. C.96: Gas chromatogram of Turmeric root fatty acid content, Run No. 45.
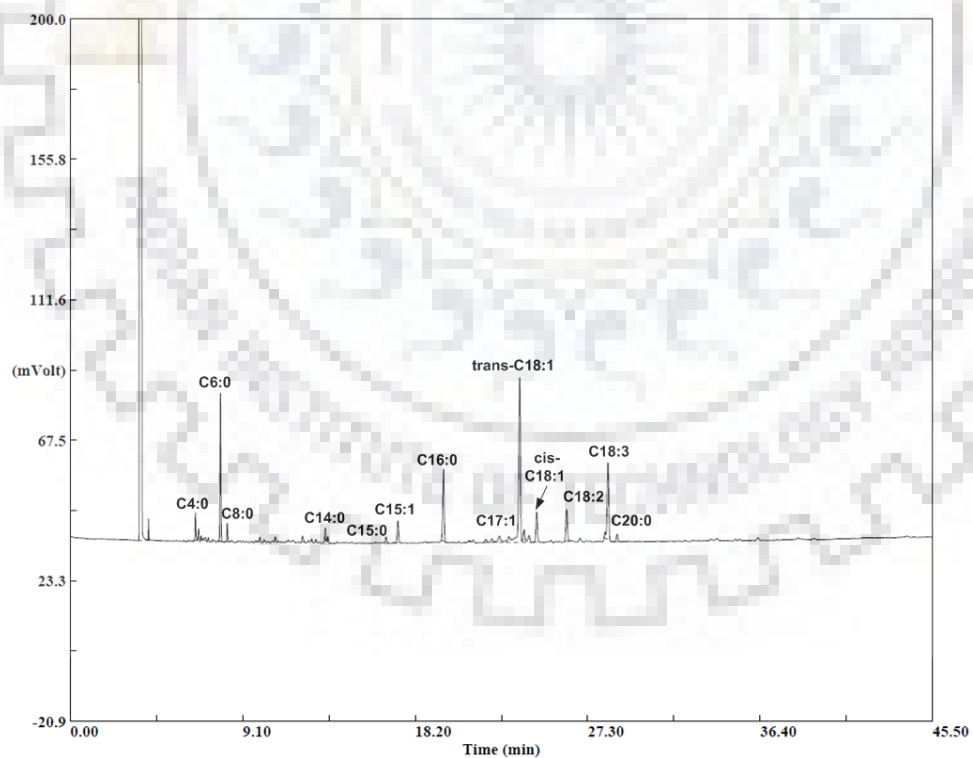
Fig. C.97: Gas chromatogram of Turmeric root fatty acid content, Run No. 46.
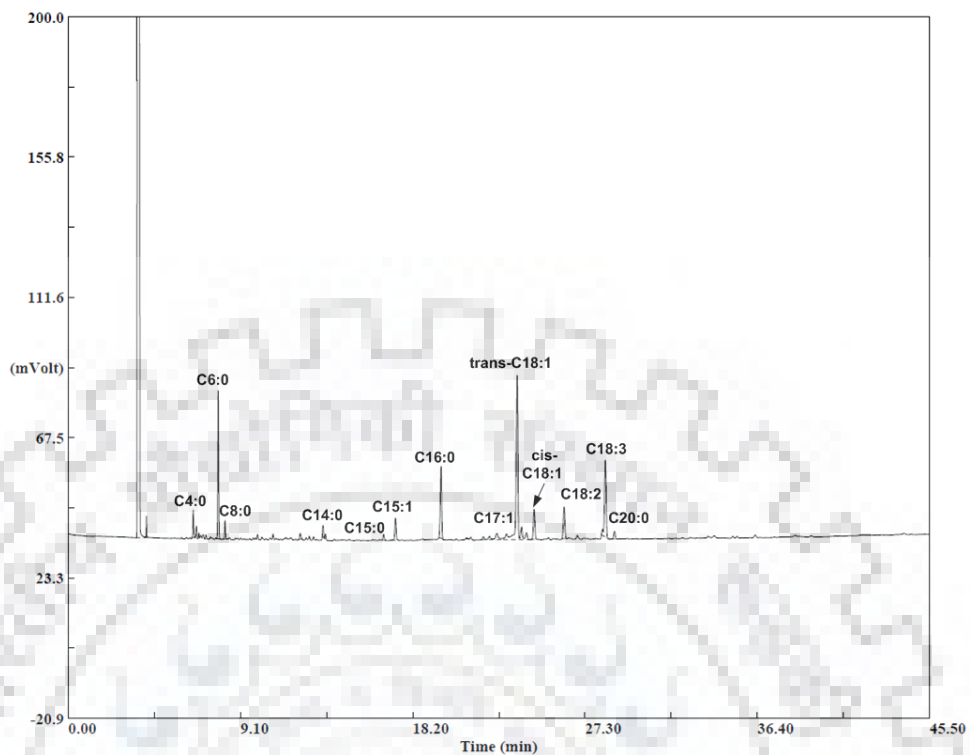
Fig. C.98: Gas chromatogram of Turmeric root fatty acid content, Run No. 47.
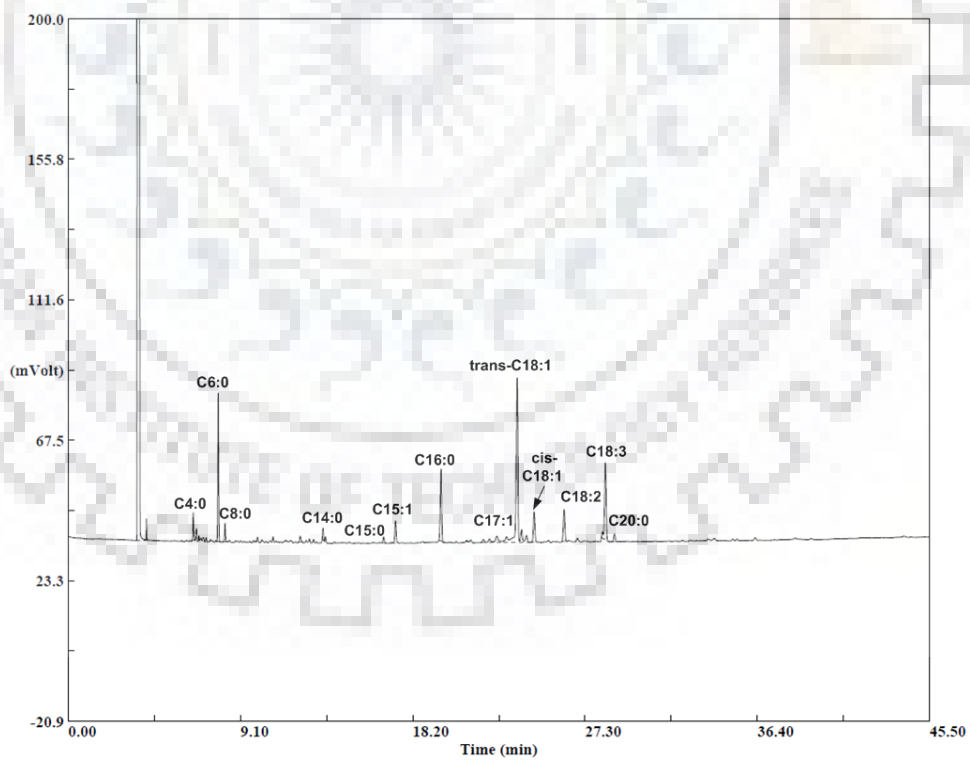
Fig. C.99: Gas chromatogram of Turmeric root fatty acid content, Run No. 48.
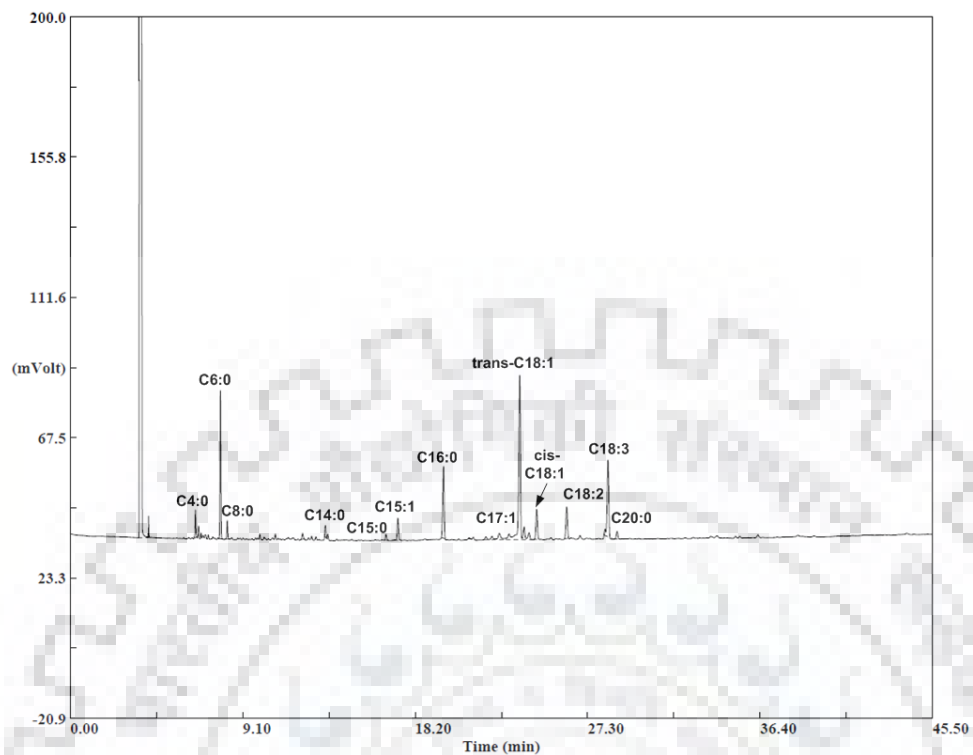
Fig. C.100: Gas chromatogram of Turmeric root fatty acid content, Run No. 49.
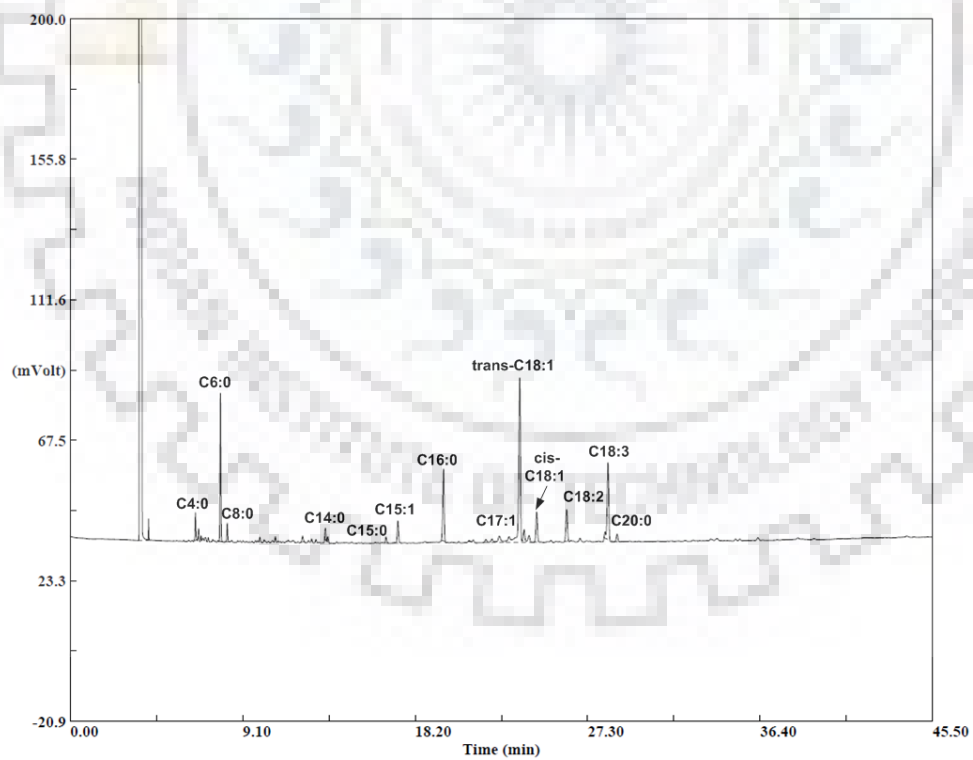
Fig. C.101: Gas chromatogram of Turmeric root fatty acid content, Run No. 50.
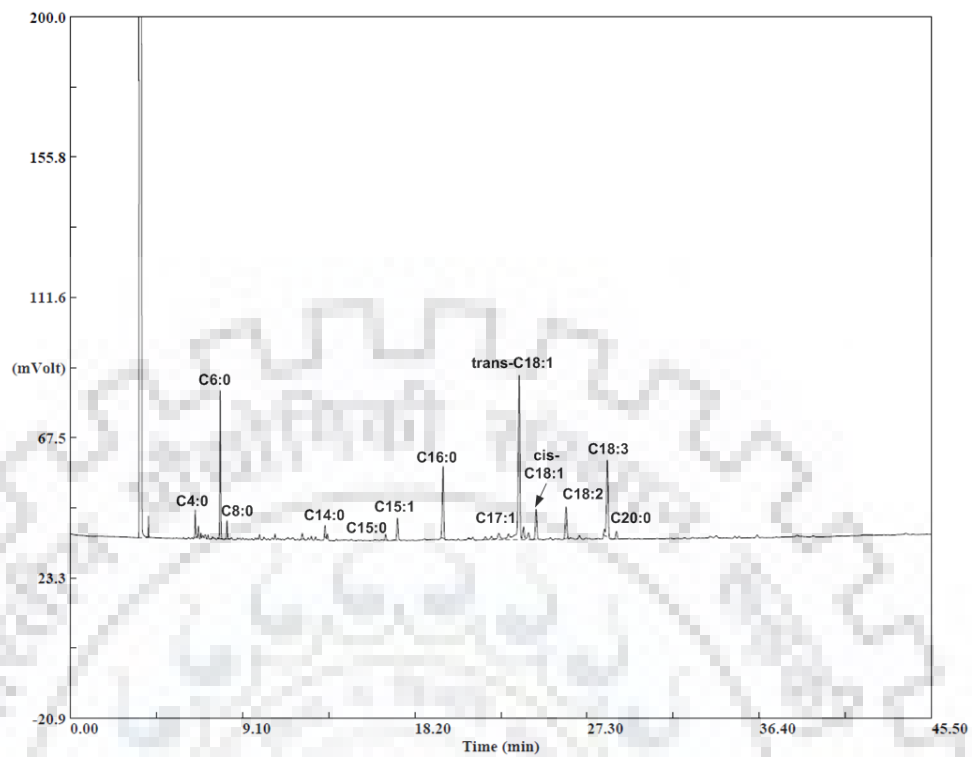
Fig. C.102: Gas chromatogram of Turmeric root fatty acid content, Soxhlet extraction.

Gas chromatogram of Carrot seed essential oil (Run 1 to 30, Soxhlet extraction)
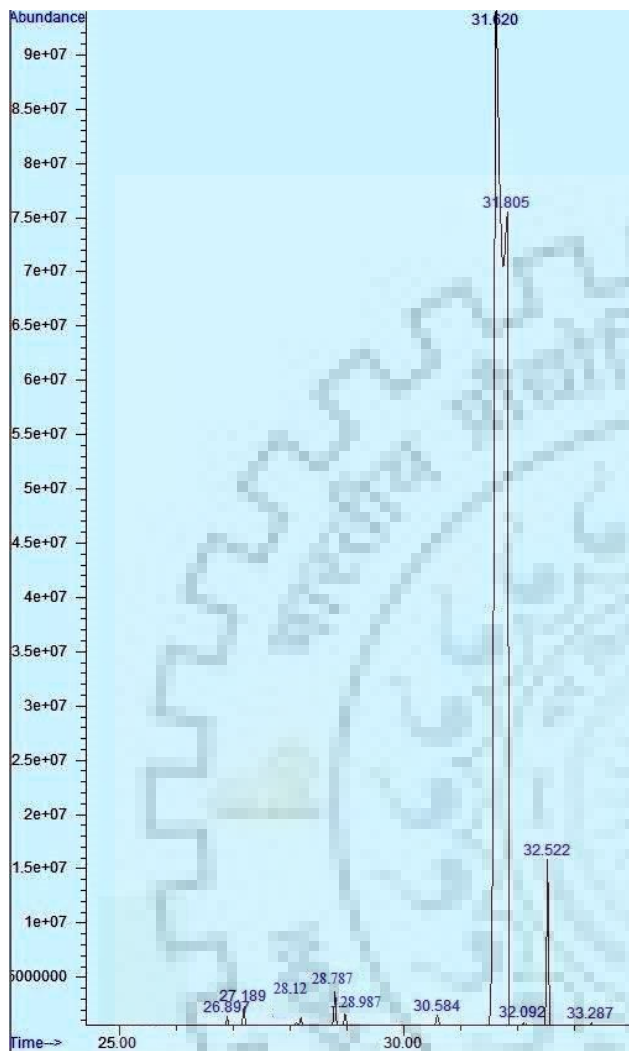
Fig. C.103: Gas chromatogram of Carrot seed essential oil, Run No. 01.
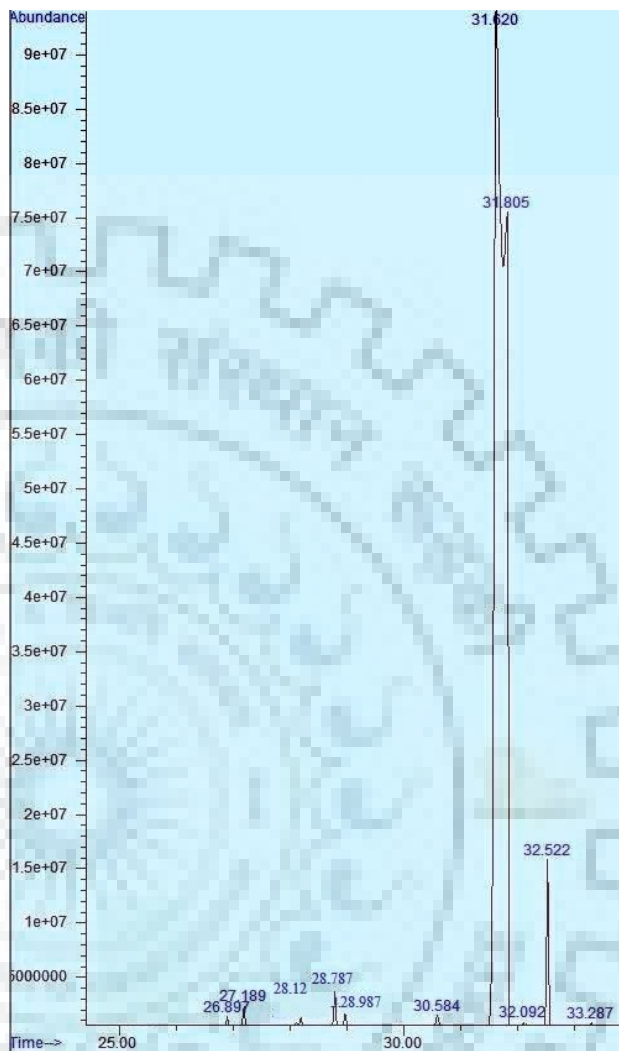
Fig. C.104: Gas chromatogram of Carrot seed essential oil, Run No. 02.
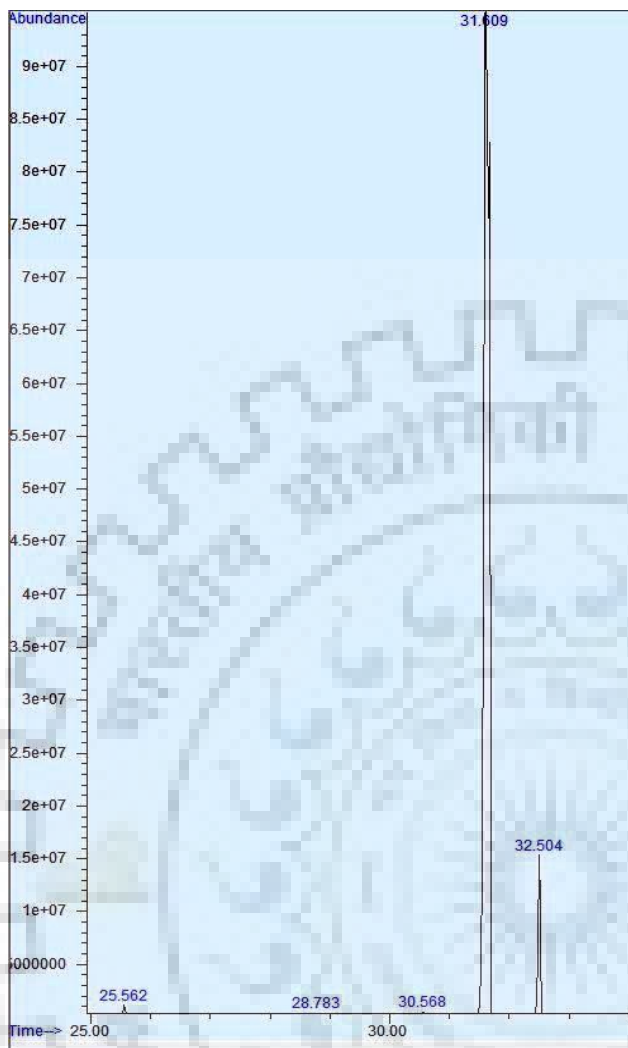
Fig. C.105: Gas chromatogram of Carrot seed essential oil, Run No. 03.
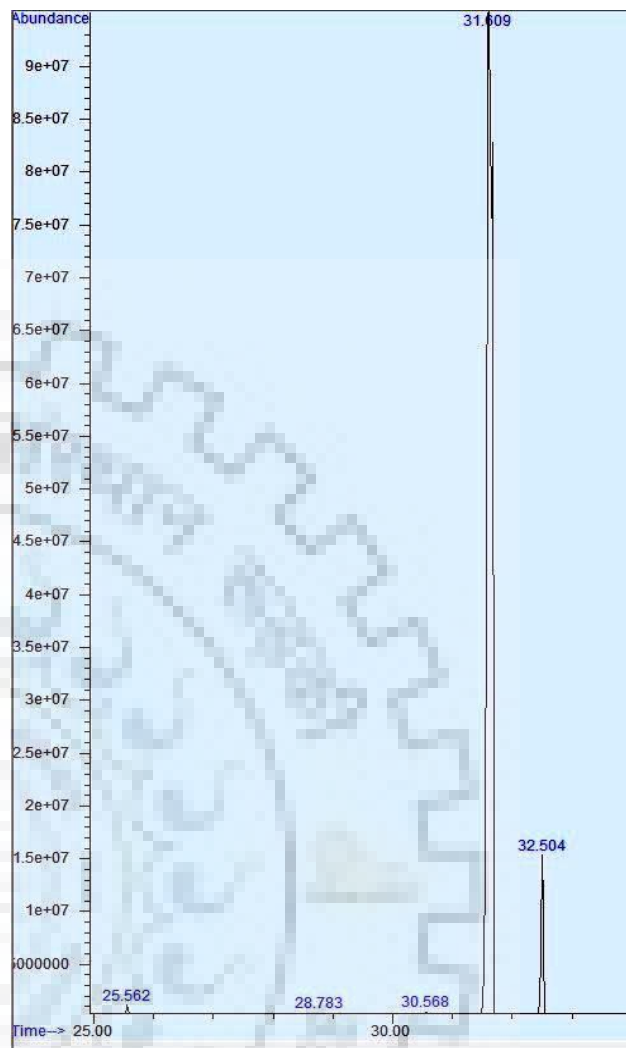
Fig. C.106: Gas chromatogram of Carrot seed essential oil, Run No. 04.
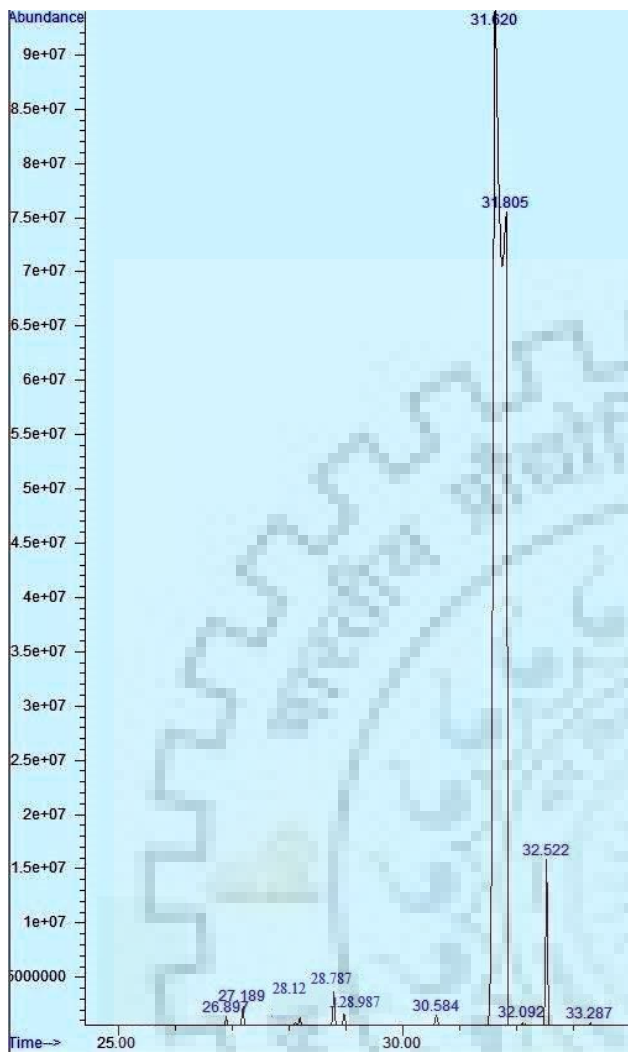
Fig. C.107: Gas chromatogram of Carrot seed essential oil, Run No. 05.
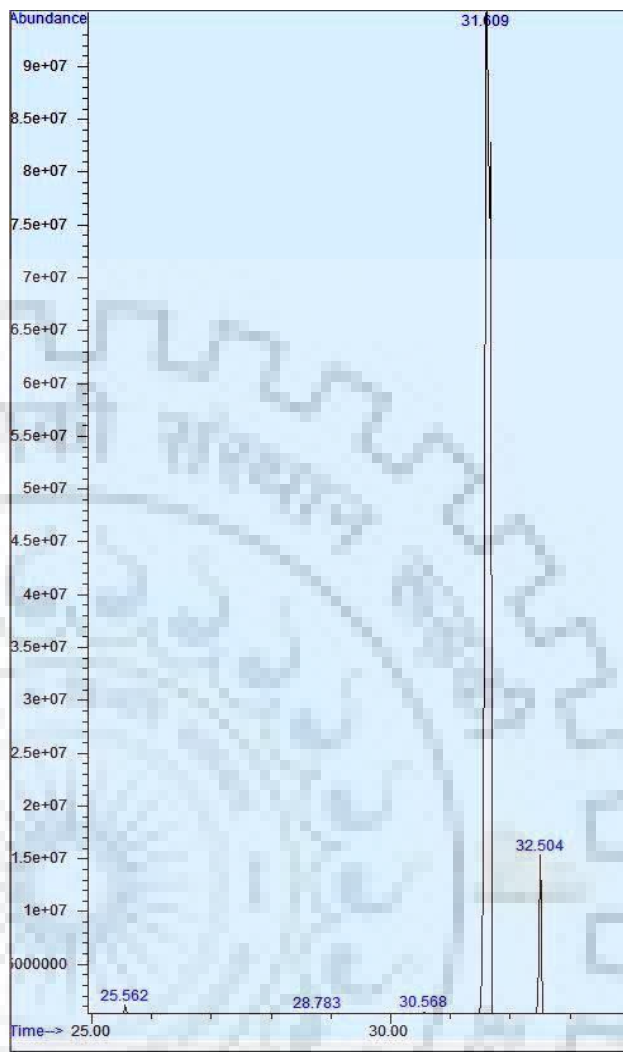
Fig. C.108: Gas chromatogram of Carrot seed essential oil, Run No. 06.
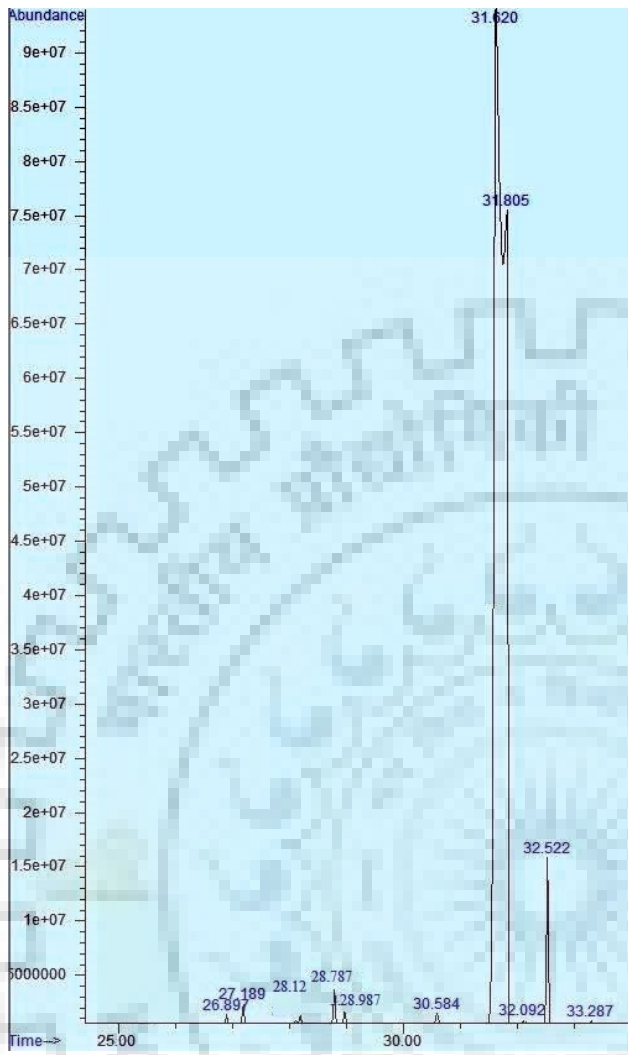
Fig. C.109: Gas chromatogram of Carrot seed
essential oil, Run No. 07.
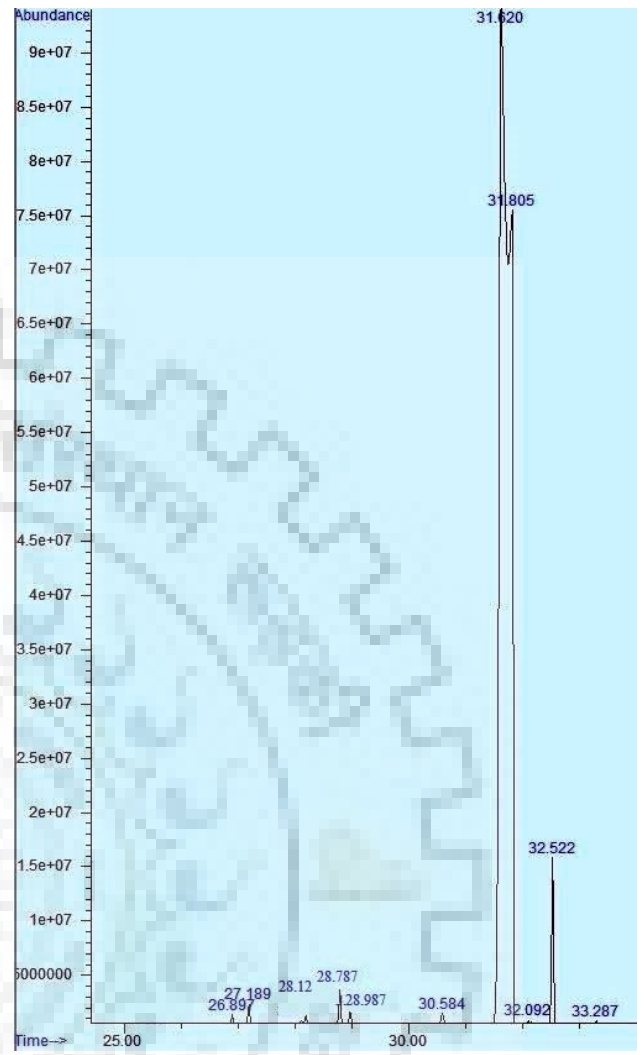
Fig. C.110: Gas chromatogram of Carrot seed
essential oil, Run No. 08.
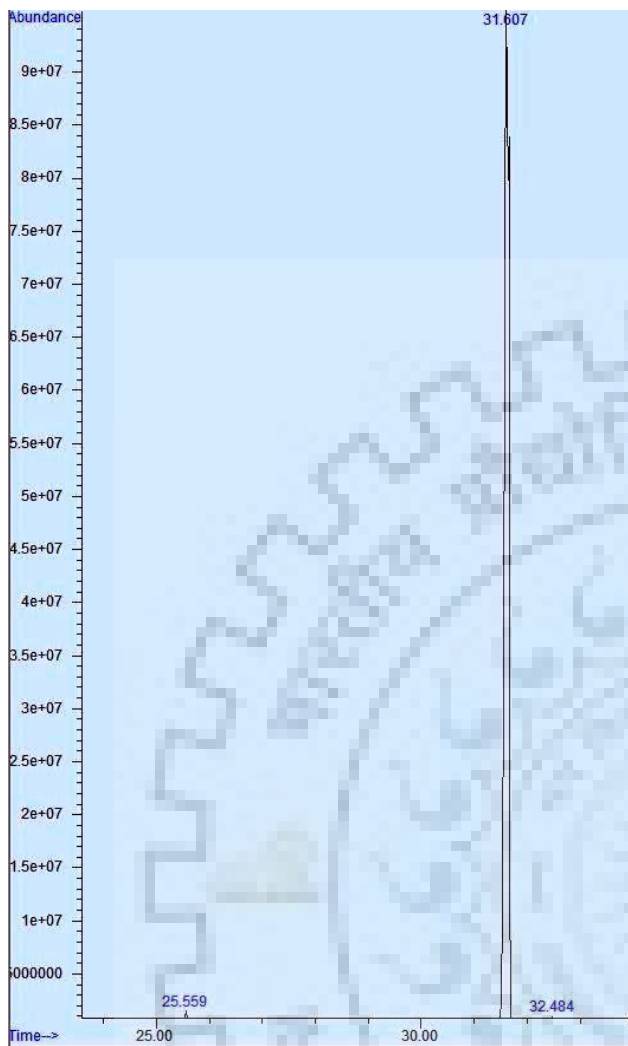
Fig. C.111: Gas chromatogram of Carrot seed essential oil, Run No. 09.
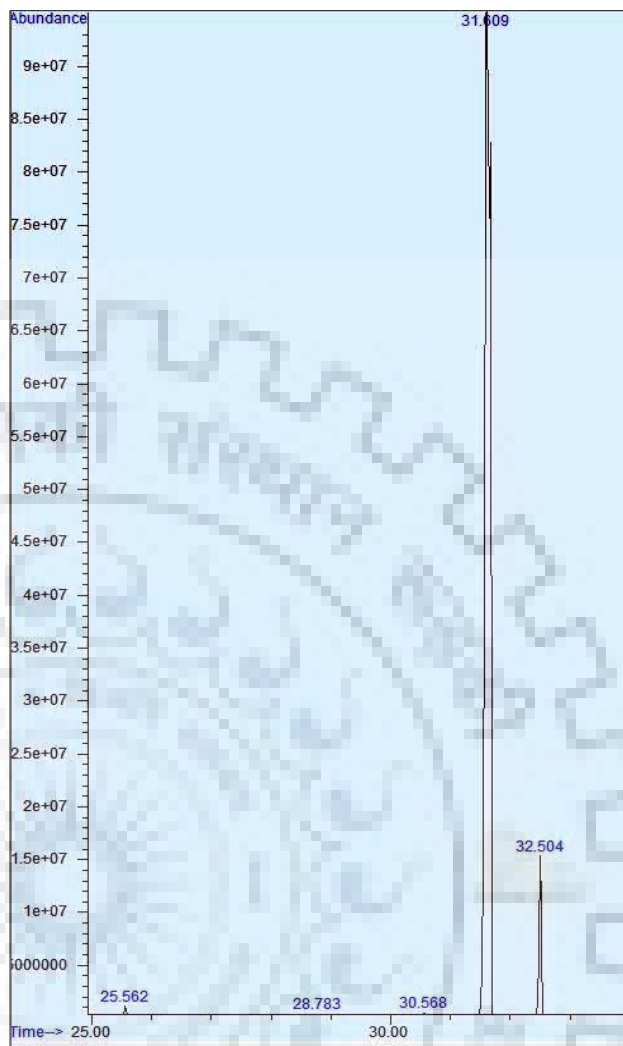
Fig. C.112: Gas chromatogram of Carrot seed essential oil, Run No. 10.
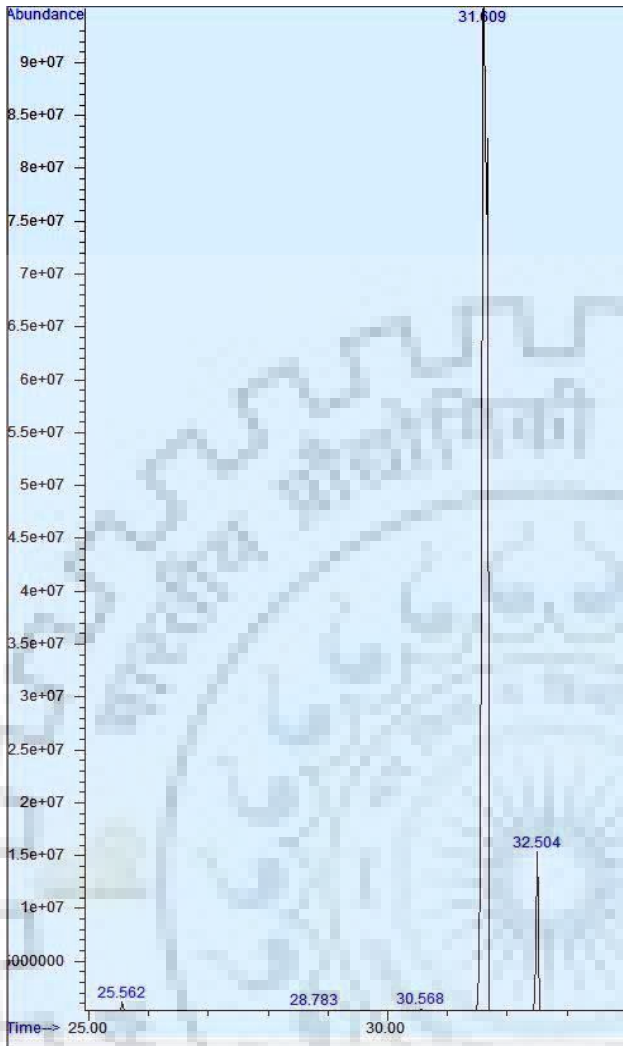
Fig. C.113: Gas chromatogram of Carrot seed essential oil, Run No. 11.
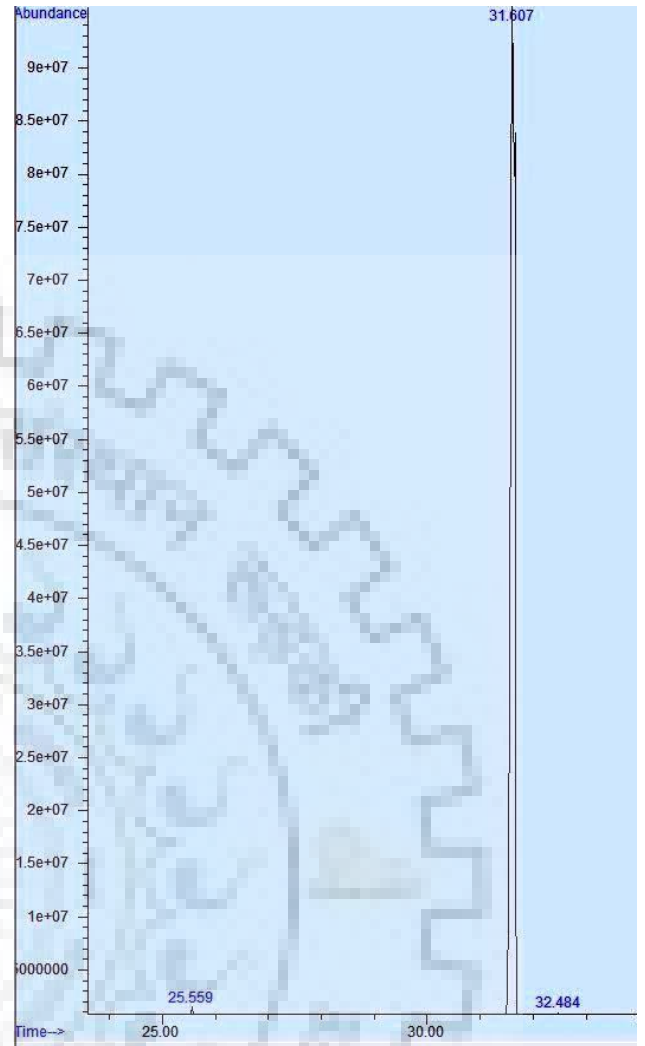
Fig. C.114: Gas chromatogram of Carrot seed essential oil, Run No. 12.
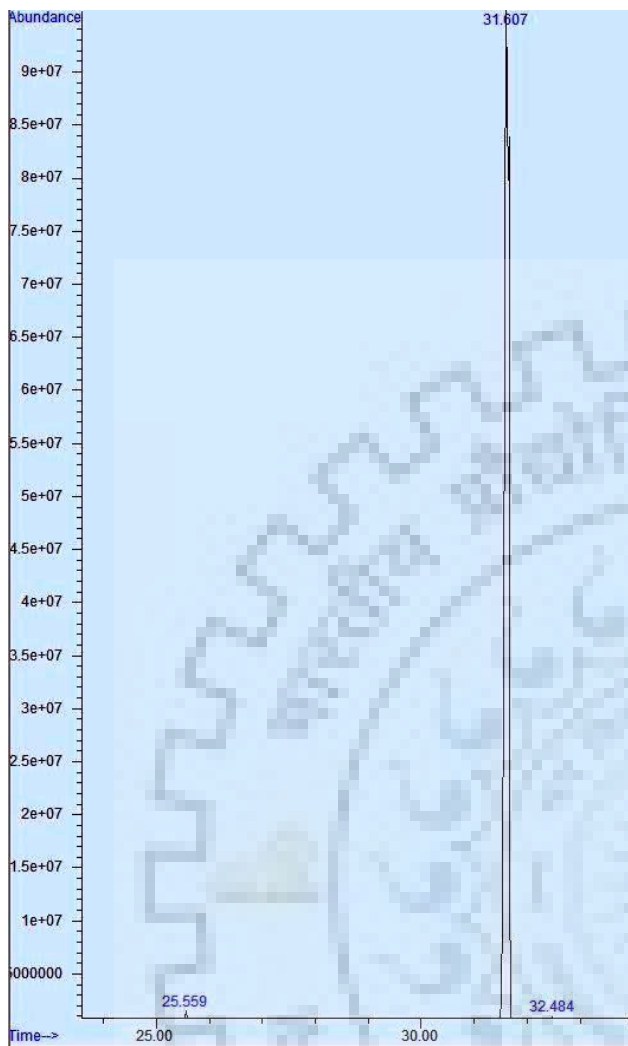
Fig. C.115: Gas chromatogram of Carrot seed essential oil, Run No. 13.
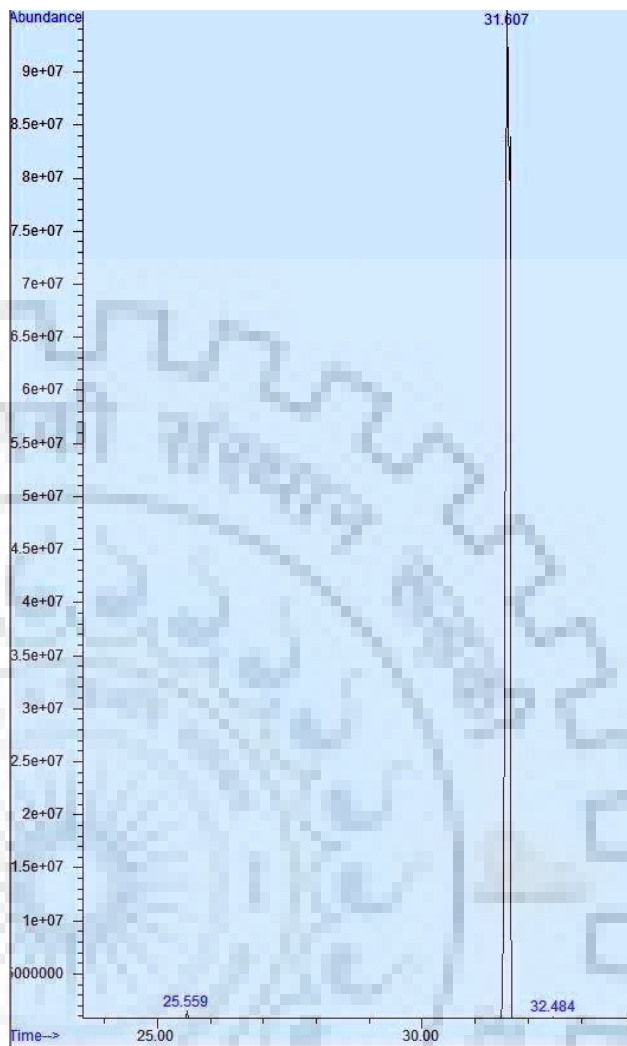
Fig. C.116: Gas chromatogram of Carrot seed essential oil, Run No. 14.
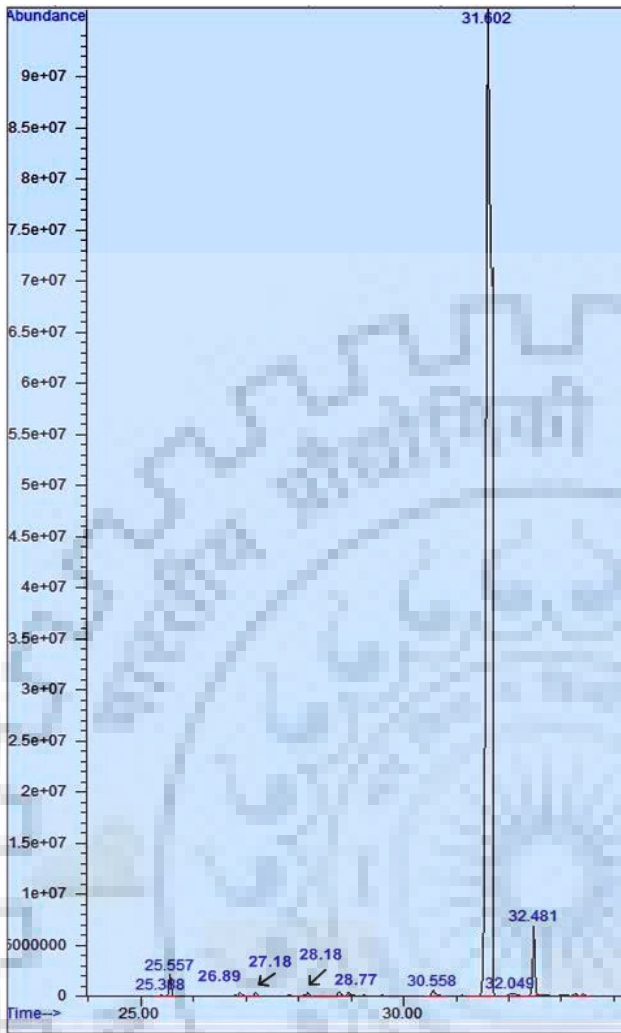
Fig. C.117: Gas chromatogram of Carrot seed essential oil, Run No. 15.
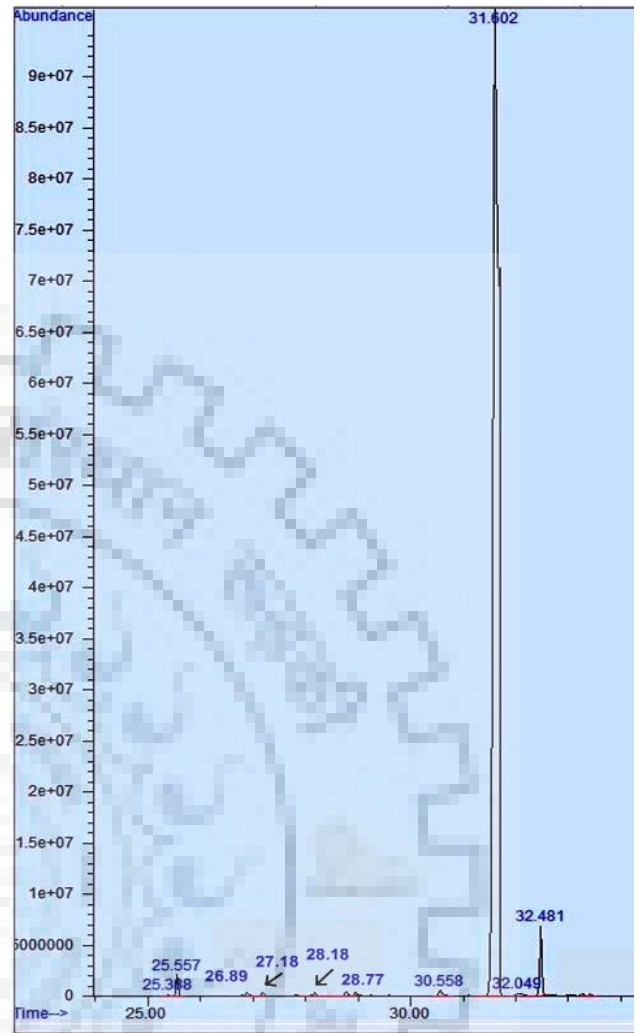
Fig. C.118: Gas chromatogram of Carrot seed essential oil, Run No. 16.
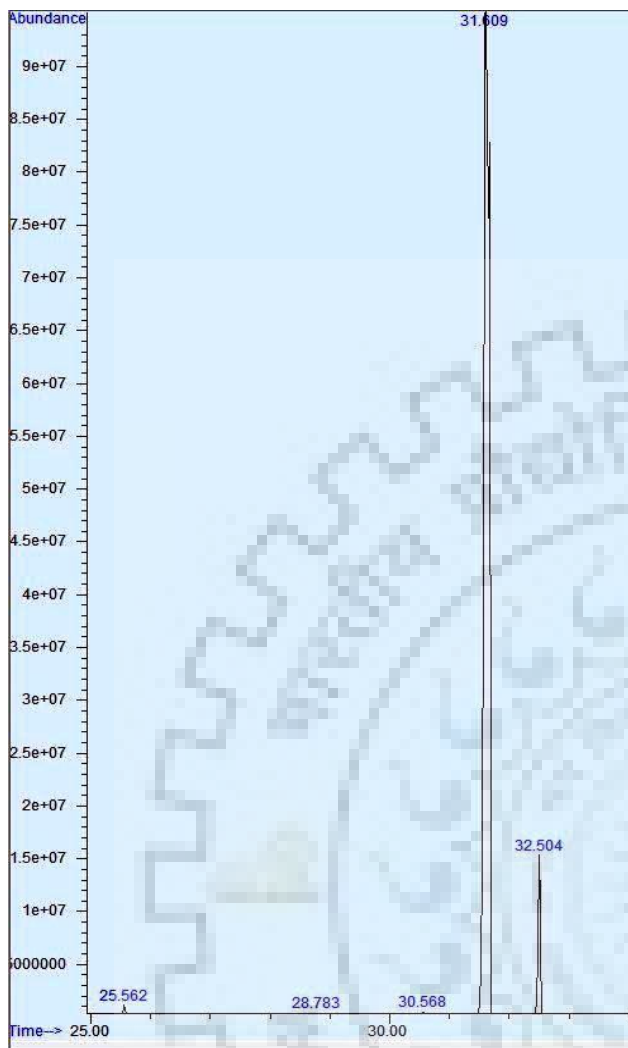
Fig. C.119: Gas chromatogram of Carrot seed essential oil, Run No. 17.
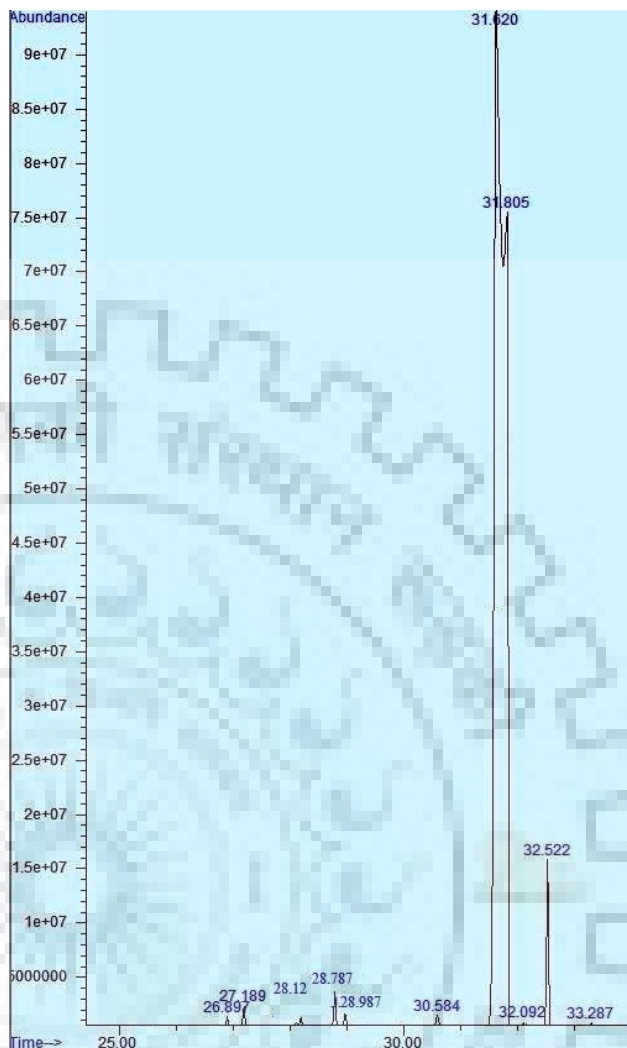
Fig. C.120: Gas chromatogram of Carrot seed essential oil, Run No. 18.
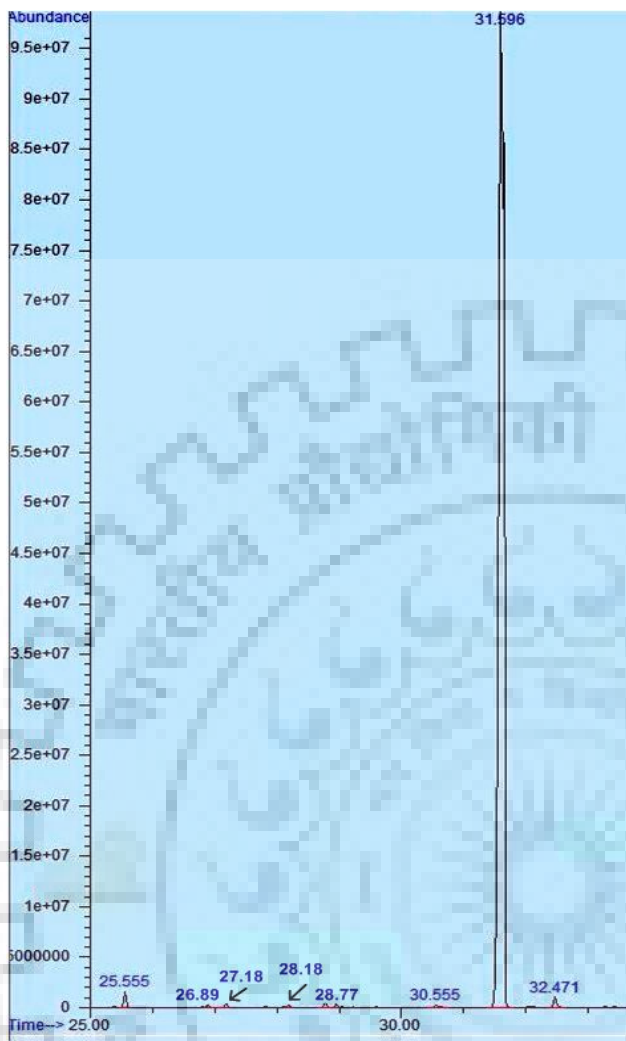
Fig. C.121: Gas chromatogram of Carrot seed essential oil, Run No. 19.
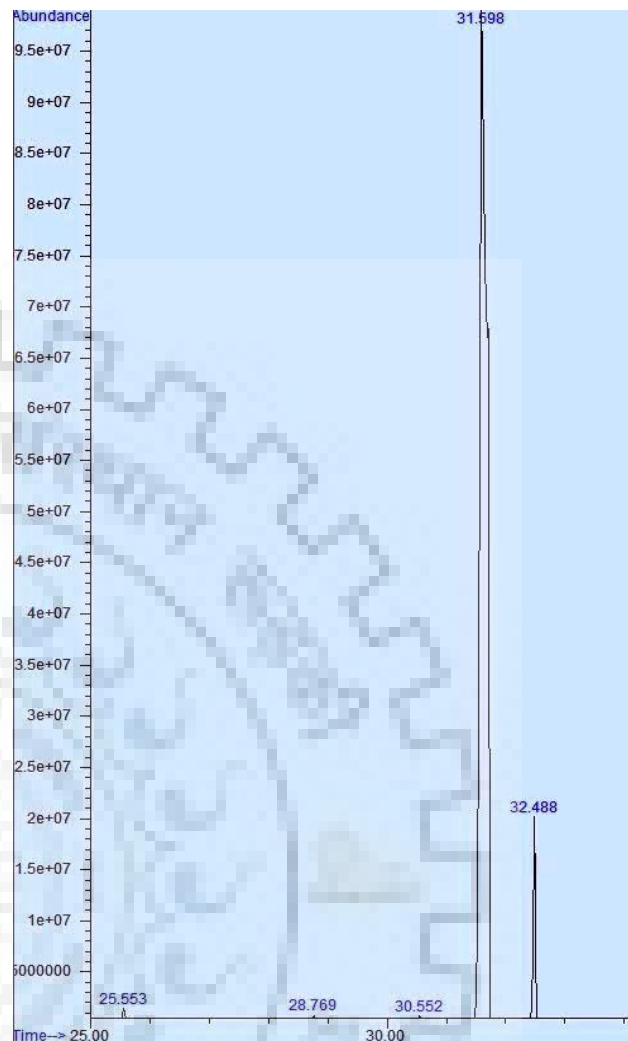
Fig. C.122: Gas chromatogram of Carrot seed essential oil, Run No. 20.
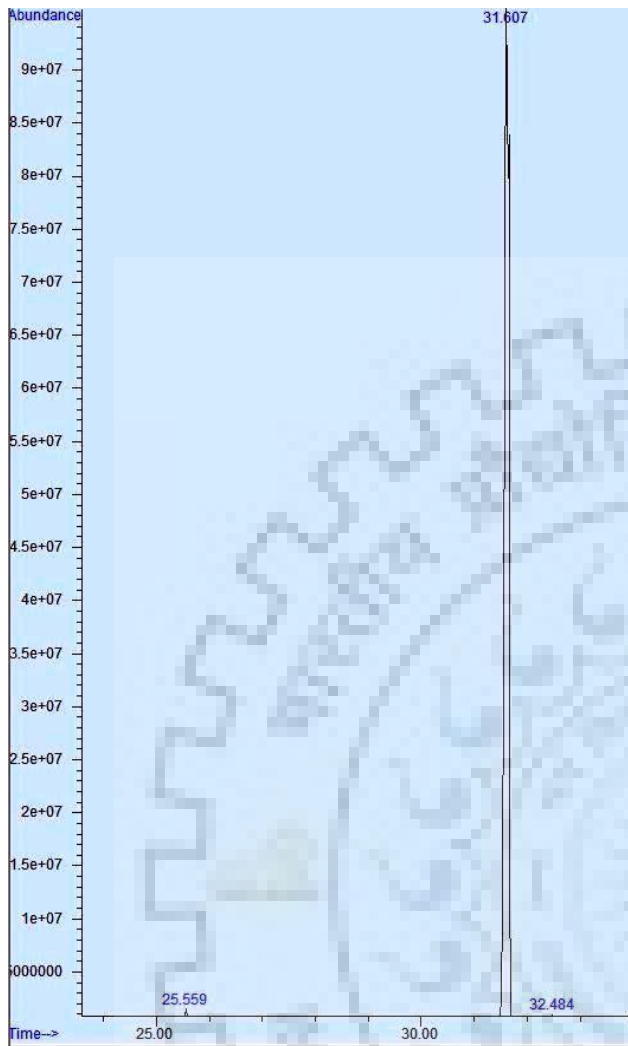
Fig. C.123: Gas chromatogram of Carrot seed essential oil, Run No. 21.
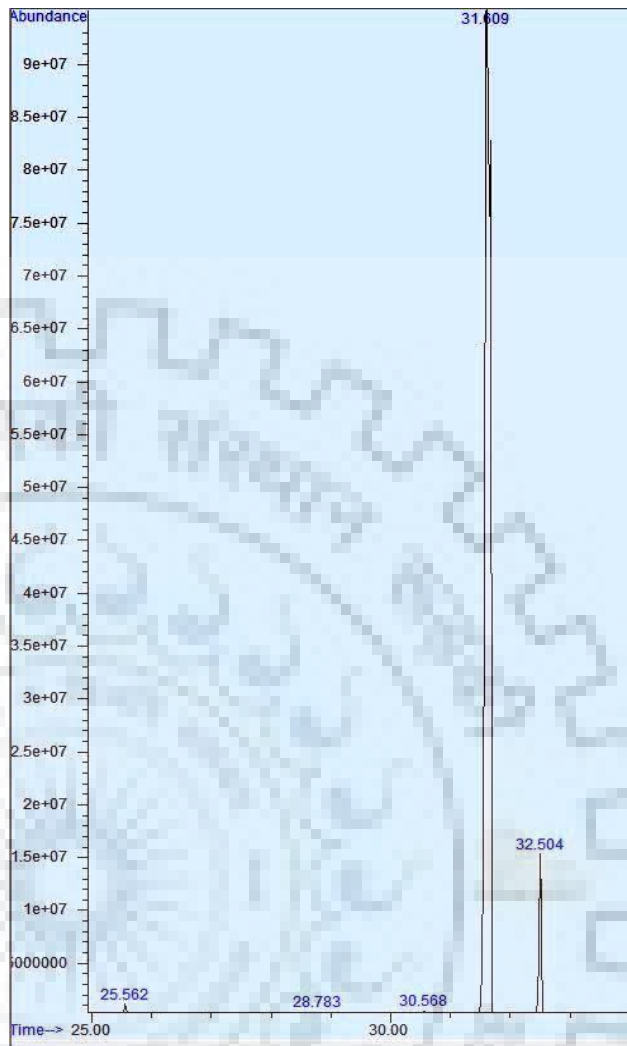
Fig. C.124: Gas chromatogram of Carrot seed essential oil, Run No. 22.
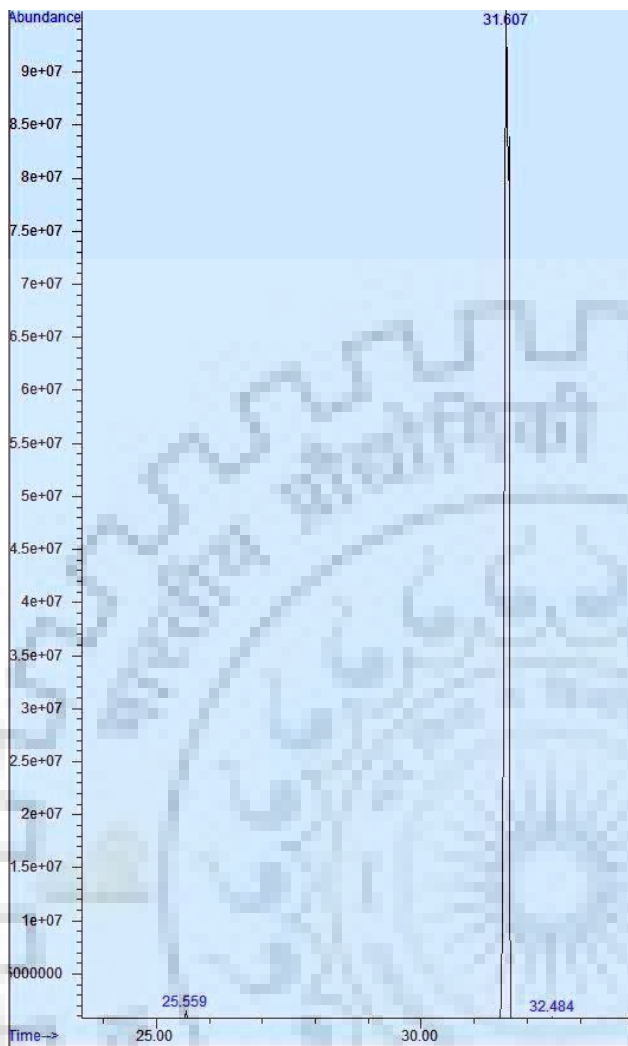
Fig. C.125: Gas chromatogram of Carrot seed essential oil, Run No. 23.
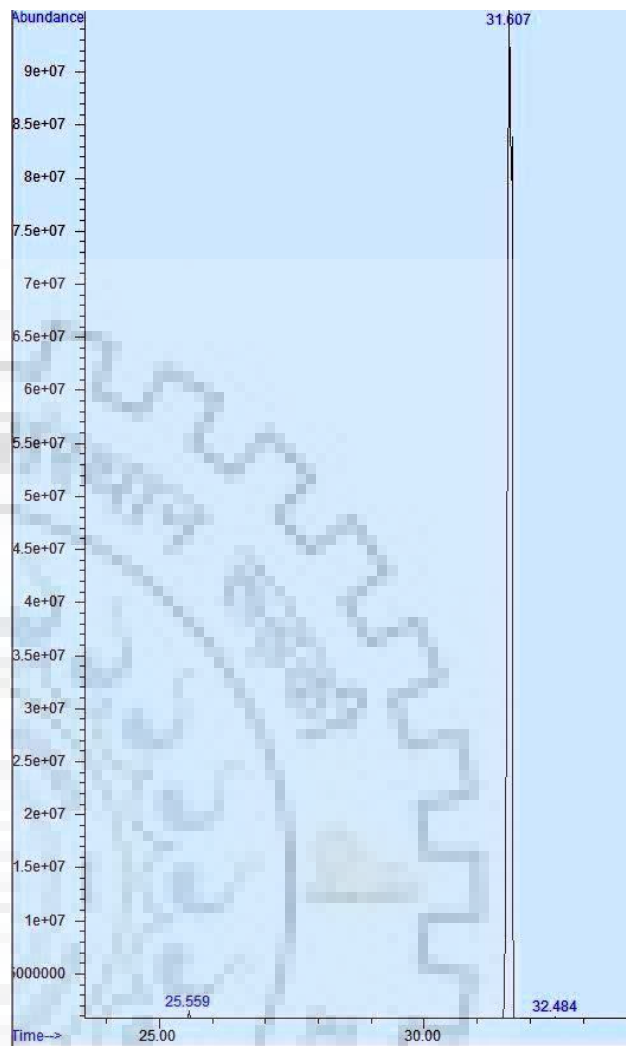
Fig. C.126: Gas chromatogram of Carrot seed essential oil, Run No. 24.
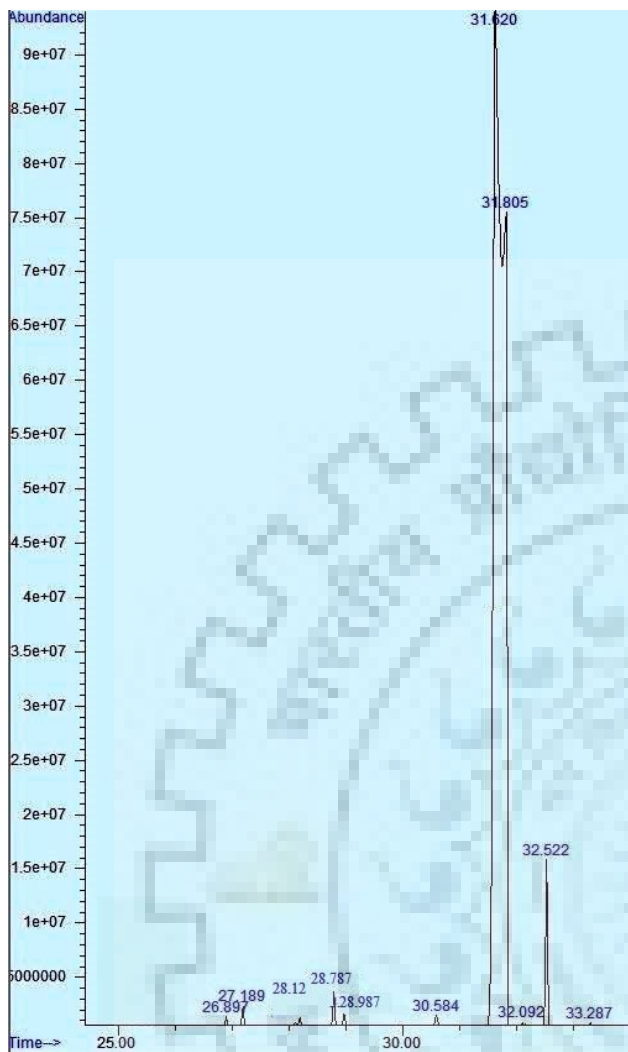
Fig. C.127: Gas chromatogram of Carrot seed essential oil, Run No. 25.
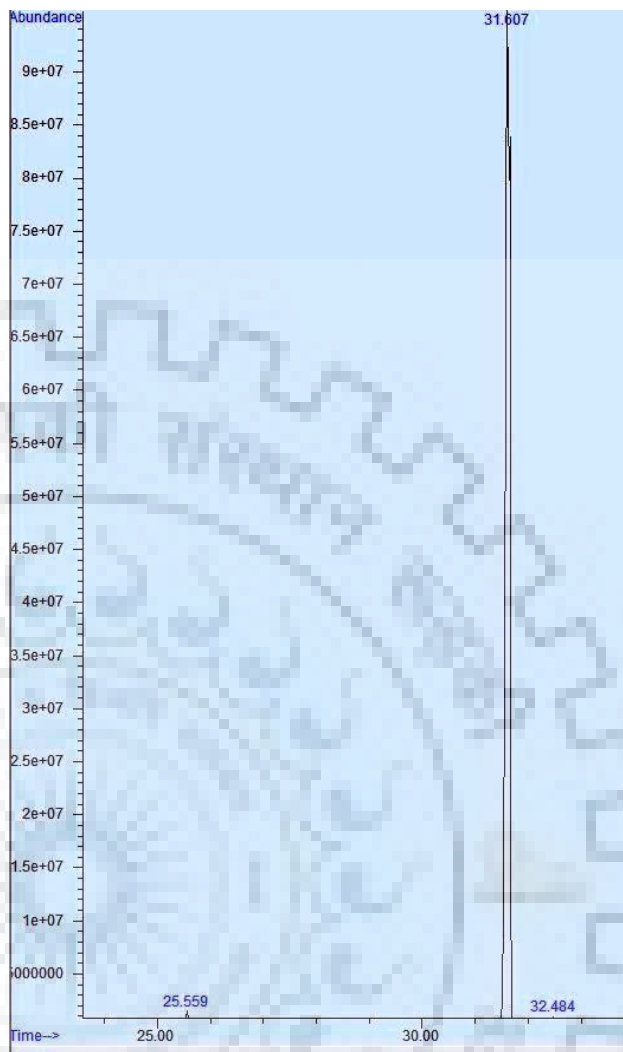
Fig. C.128: Gas chromatogram of Carrot seed essential oil, Run No. 26.
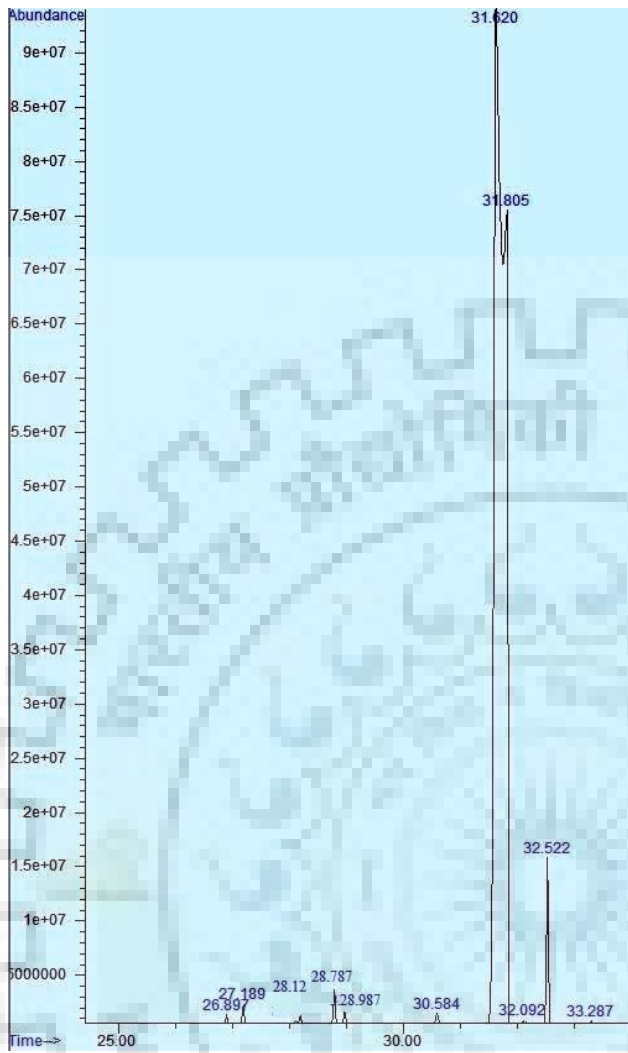
Fig. C.129: Gas chromatogram of Carrot seed essential oil, Run No. 27.
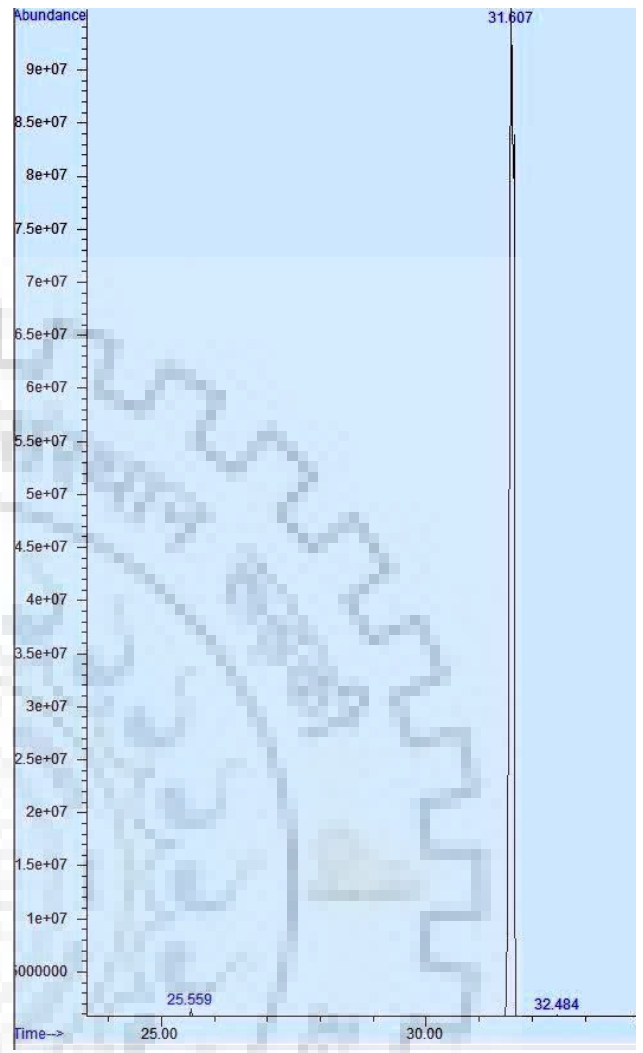
Fig. C.130: Gas chromatogram of Carrot seed essential oil, Run No. 28.
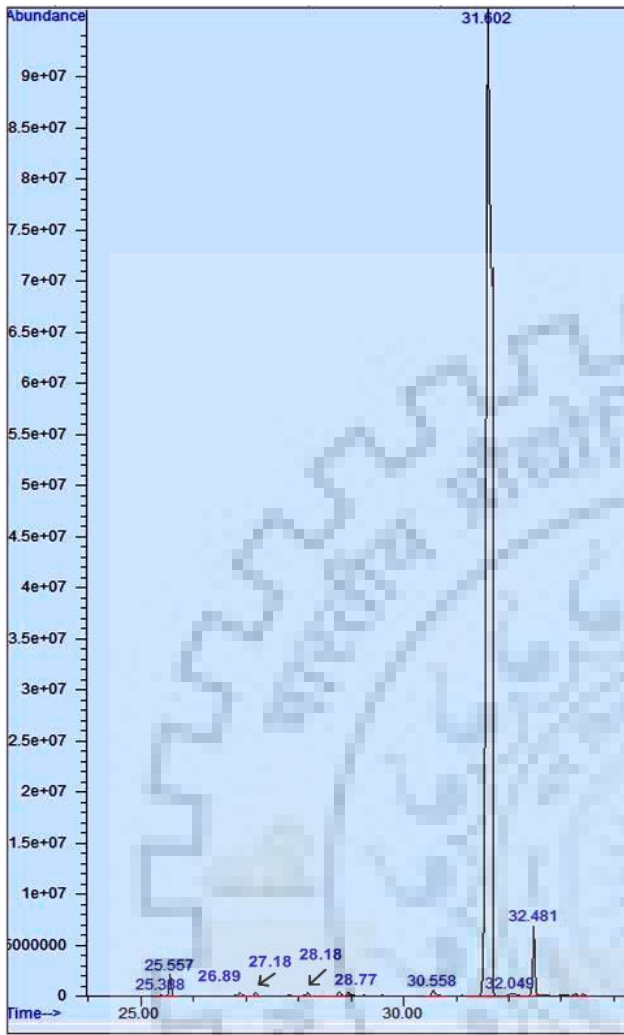
Fig. C.131: Gas chromatogram of Carrot seed essential oil, Run No. 29.
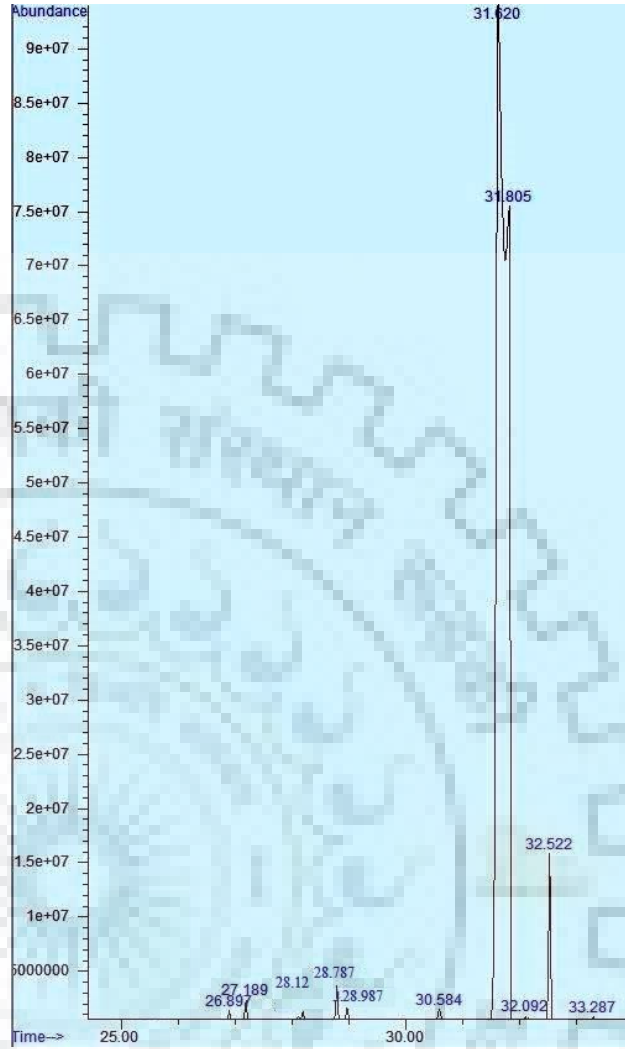
Fig. C.132: Gas chromatogram of Carrot seed essential oil, Run No. 30.
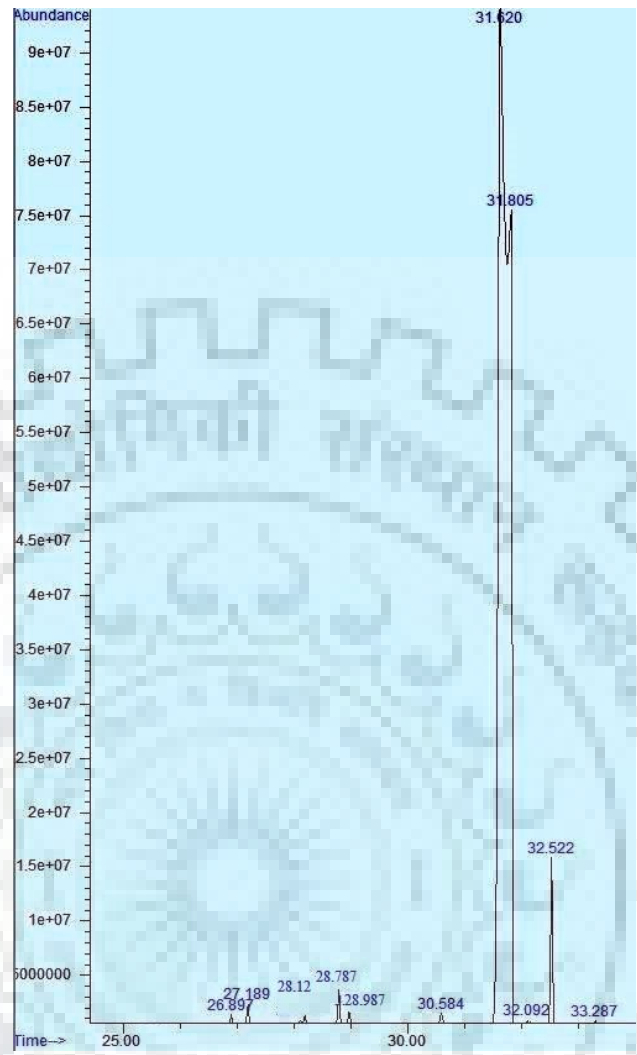
Fig. C.133: Gas chromatogram of Carrot seed essential oil, Soxhlet extraction

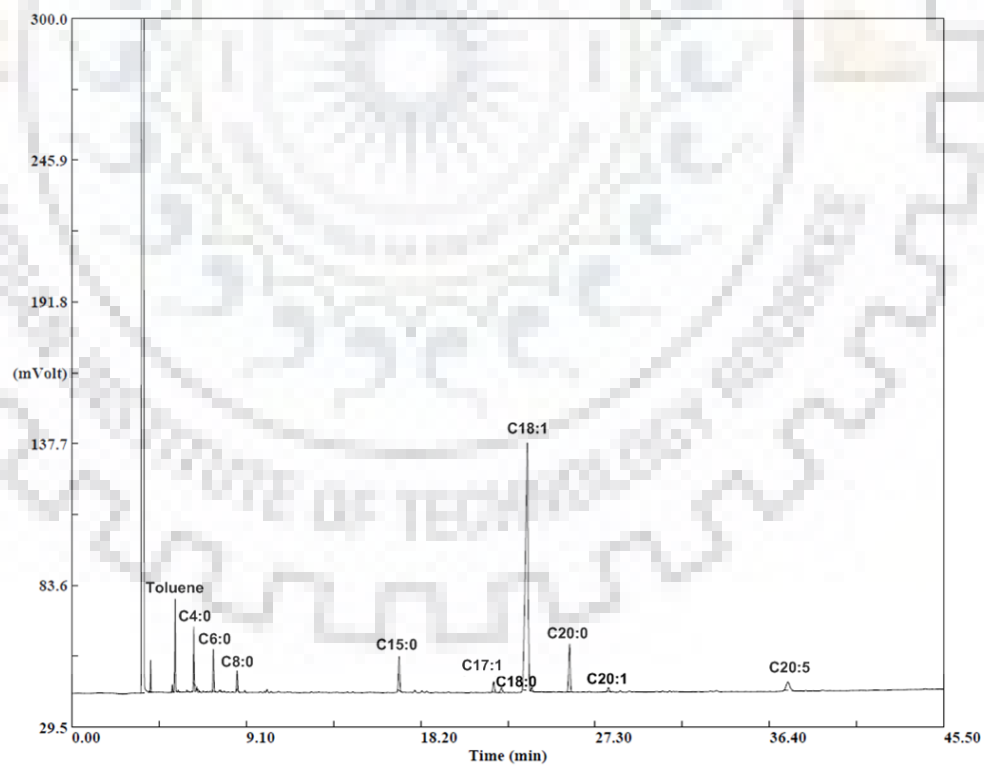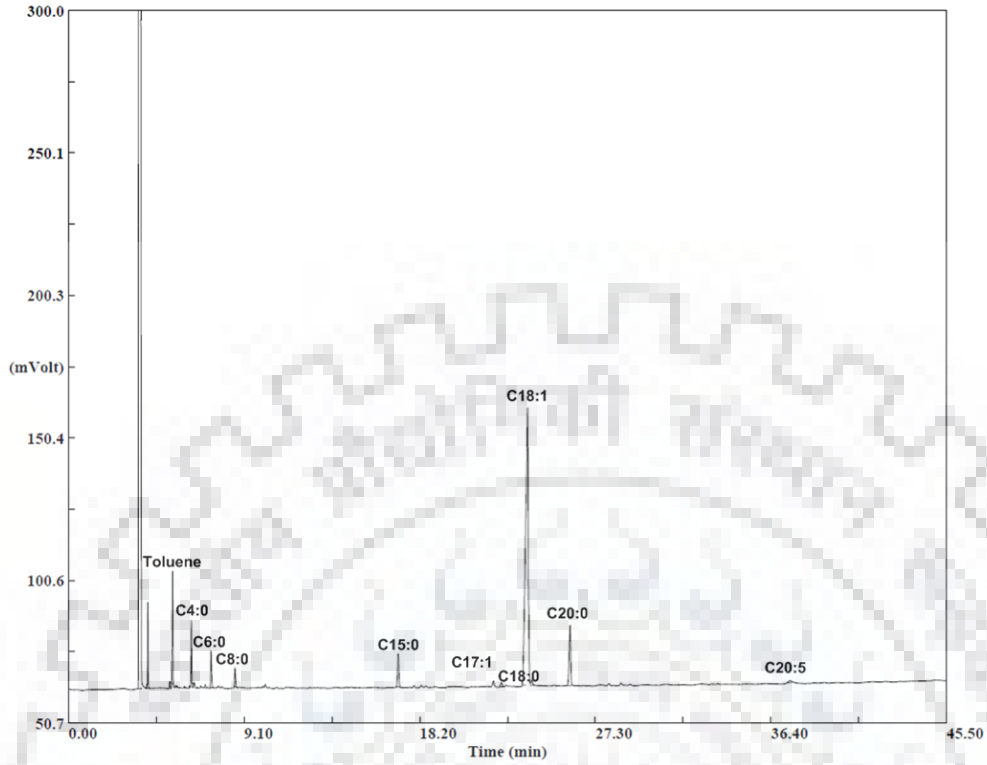Gas chromatogram of Carrot seed fatty acid content (Run 1 to 30, Soxhlet extraction)
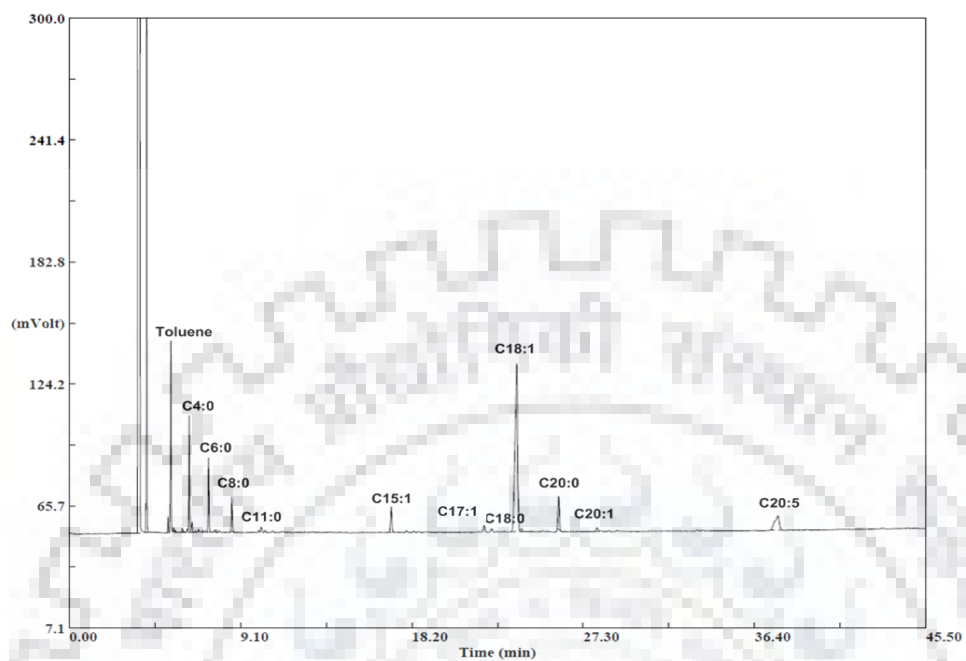
Fig. C.134: Gas chromatogram of Carrot seed fatty acid content, Run No. 01.
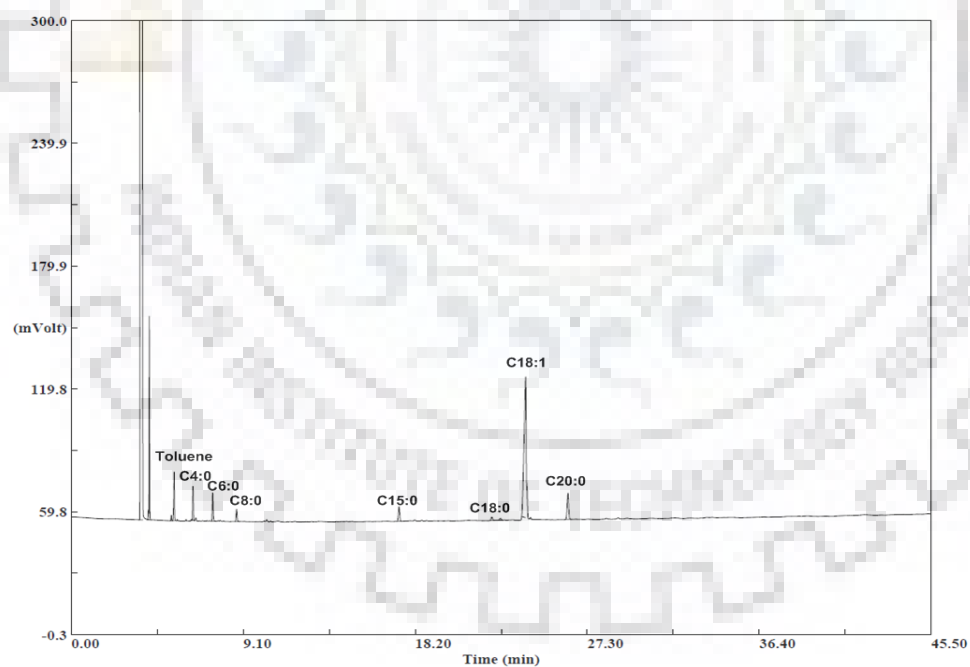
Fig. C.135: Gas chromatogram of Carrot seed fatty acid content, Run No. 02.
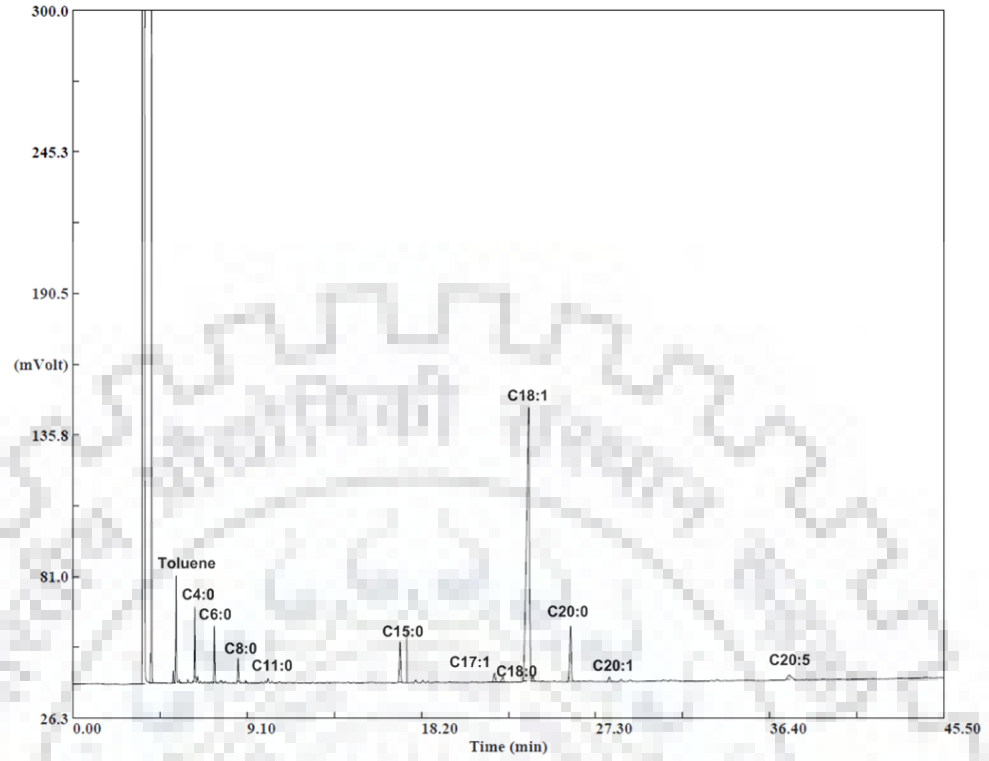
Fig. C.136: Gas chromatogram of Carrot seed fatty acid content, Run No. 03.
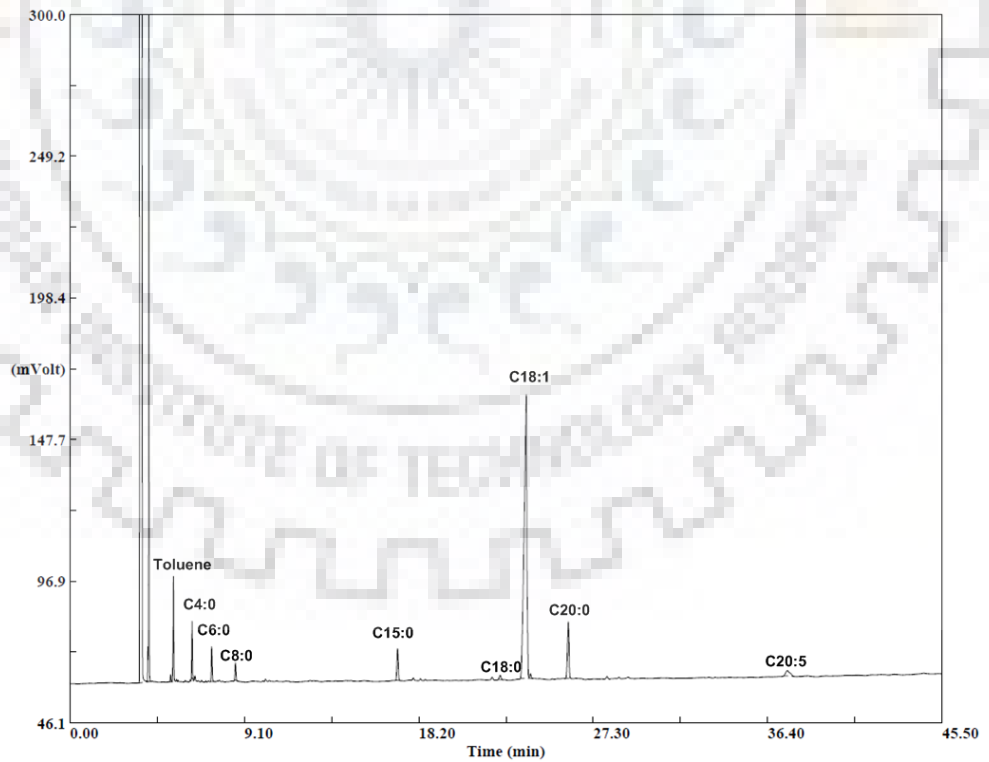
Fig. C.137: Gas chromatogram of Carrot seed fatty acid content, Run No. 04.
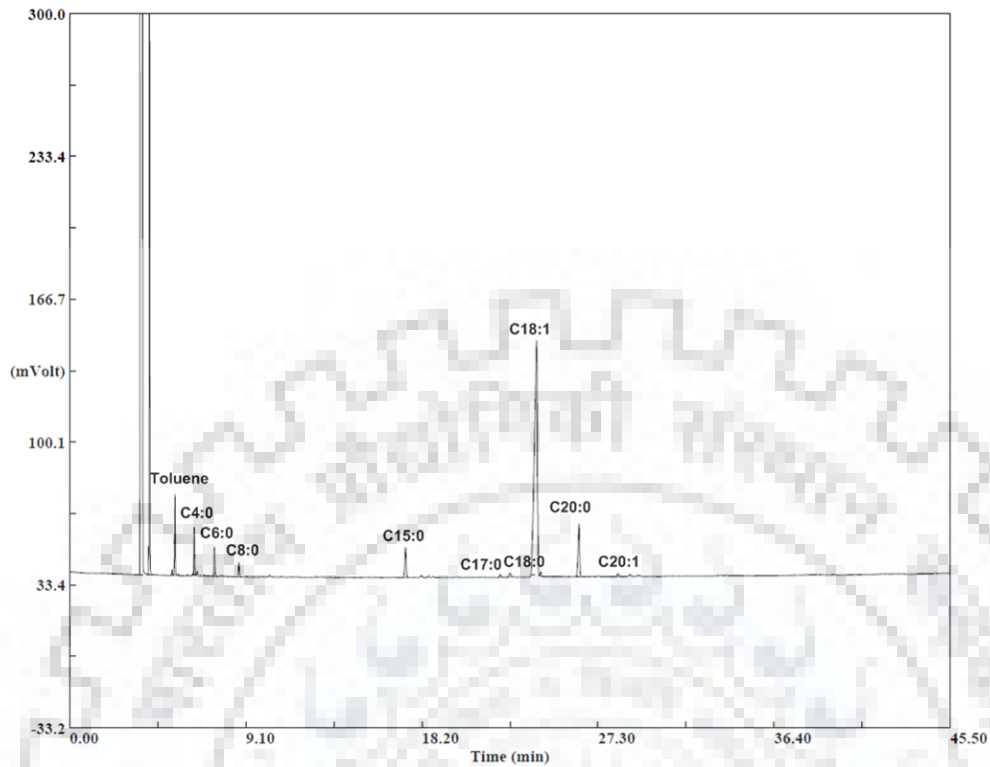
Fig. C.138: Gas chromatogram of Carrot seed fatty acid content, Run No. 05.
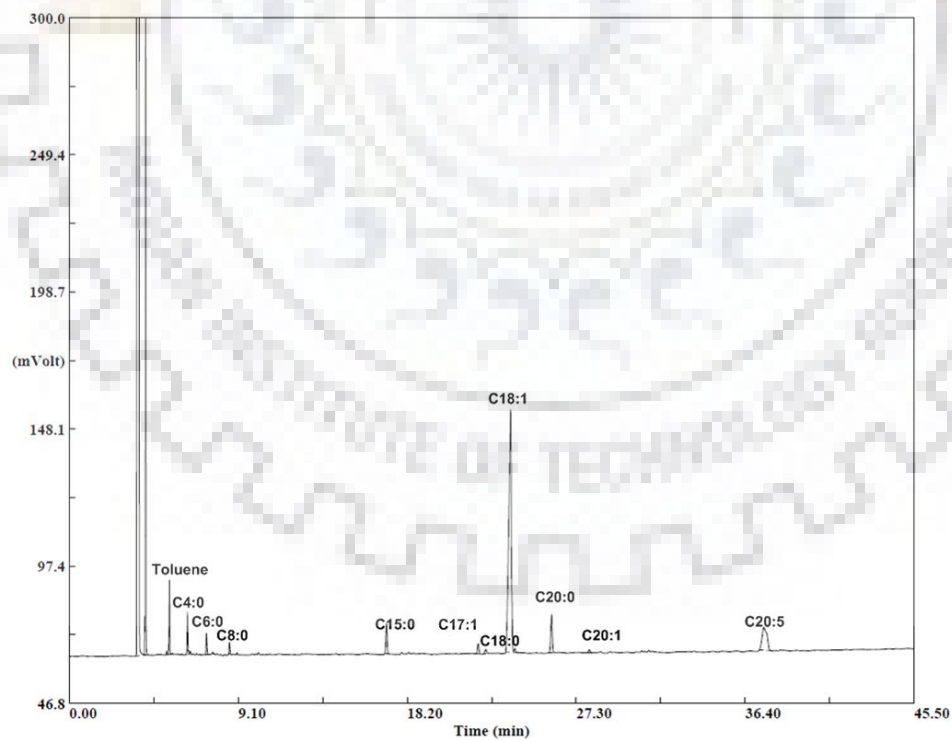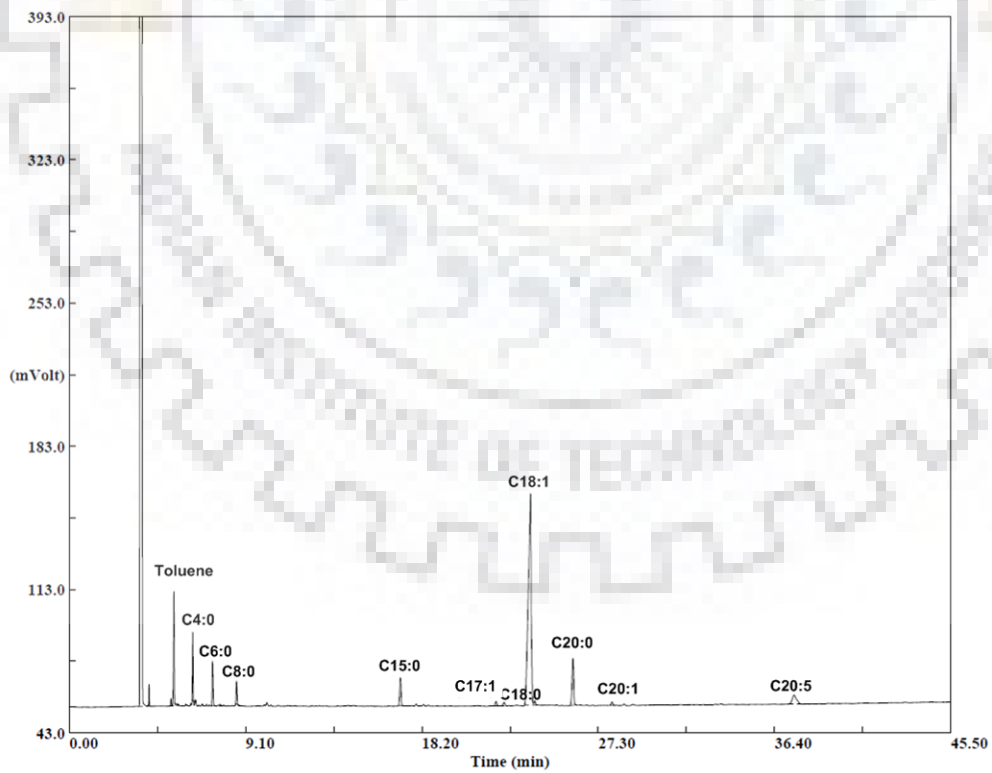

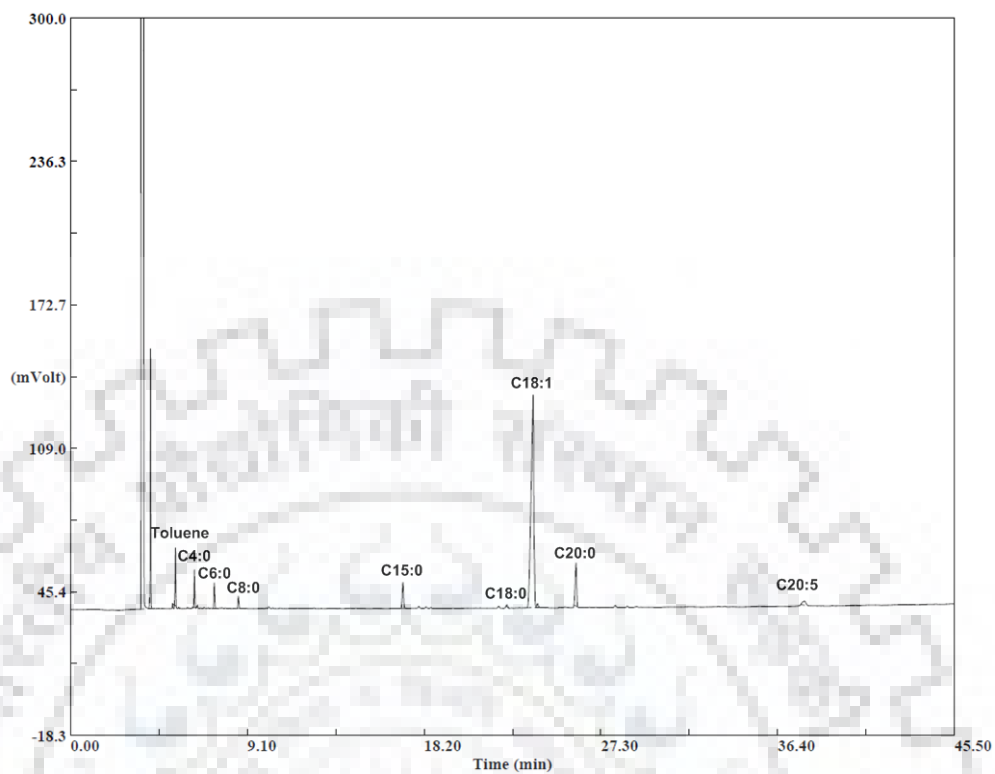Fig. C.139: Gas chromatogram of Carrot seed fatty acid content, Run No. 06.

C-62
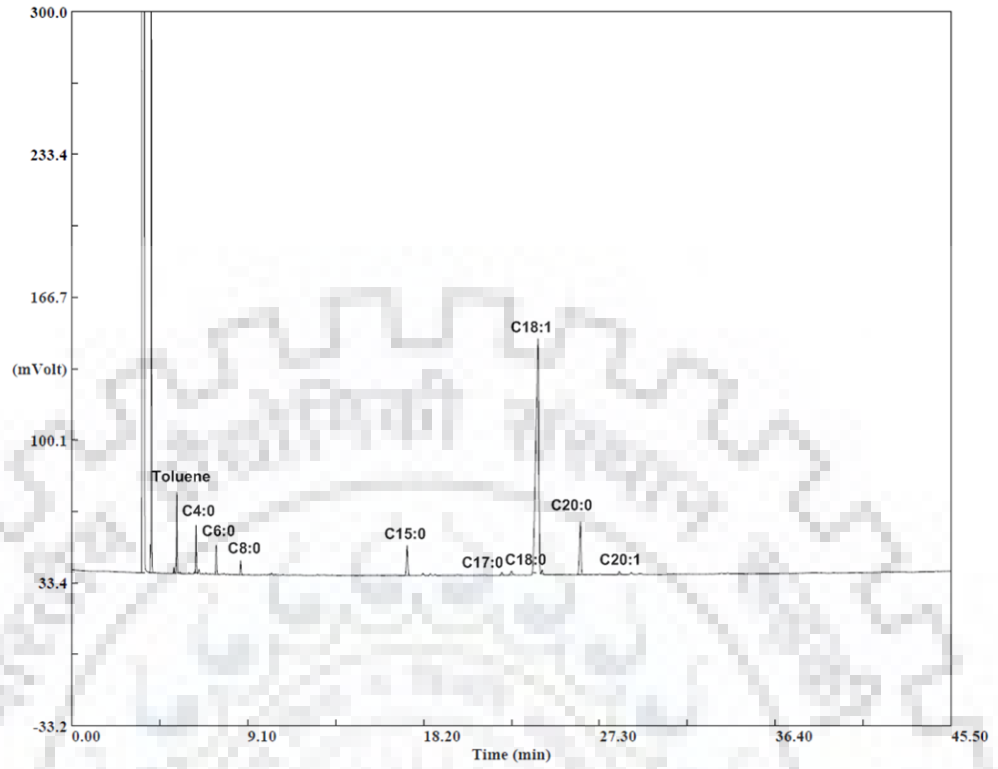
Fig. C.140: Gas chromatogram of Carrot seed fatty acid content, Run No. 07.
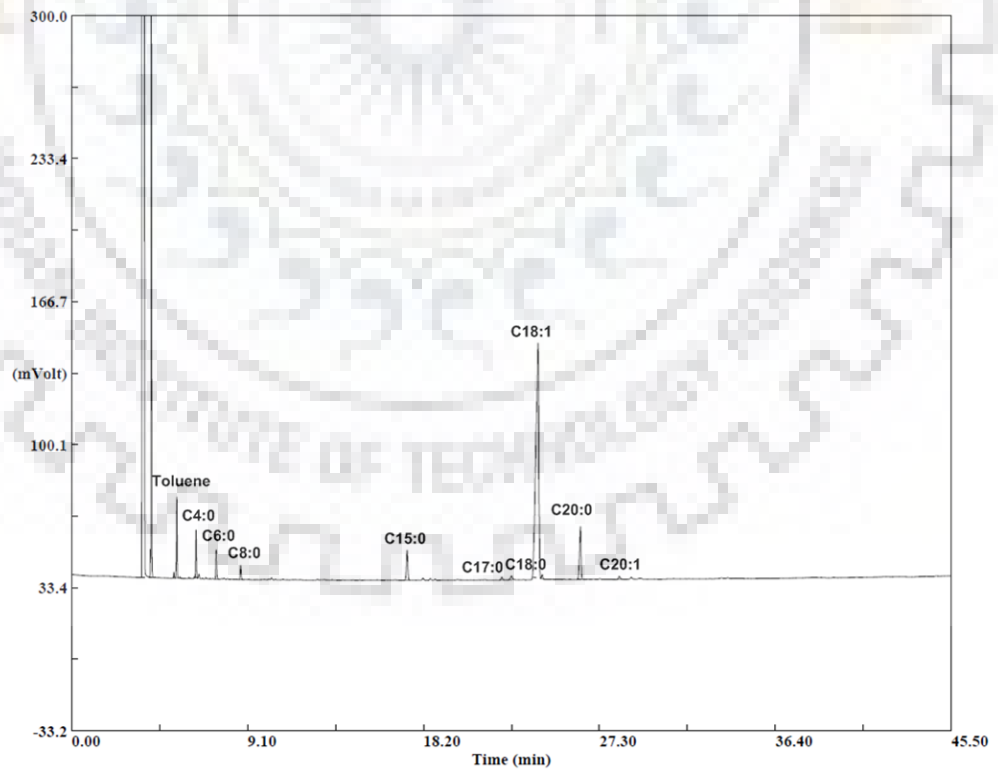
Fig. C.141: Gas chromatogram of Carrot seed fatty acid content, Run No. 08.
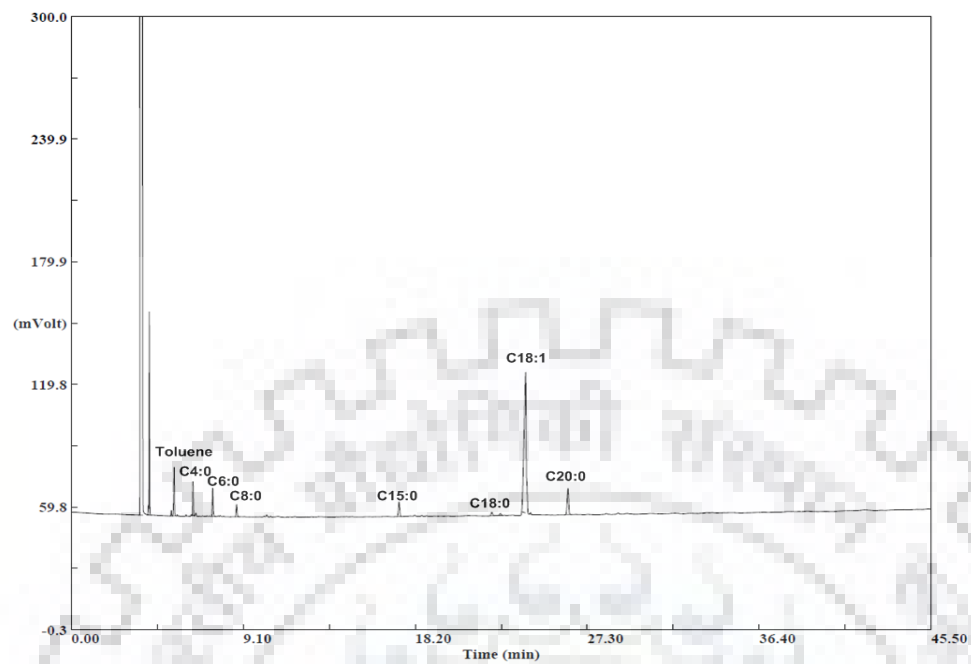
Fig. C.142: Gas chromatogram of Carrot seed fatty acid content, Run No. 09.
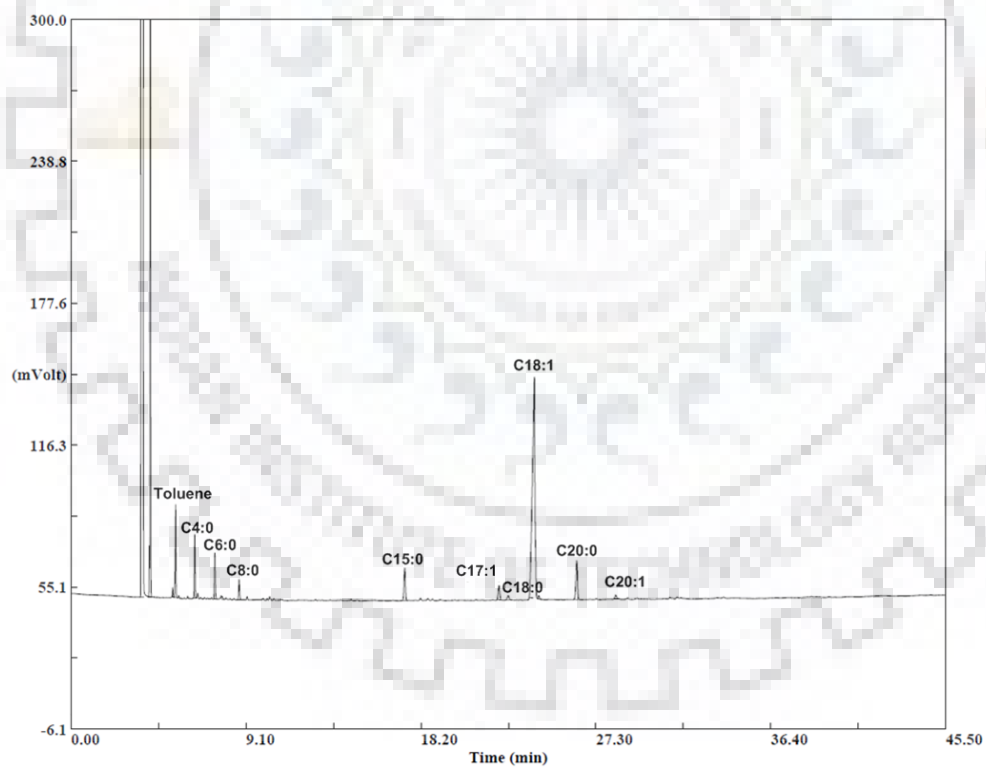
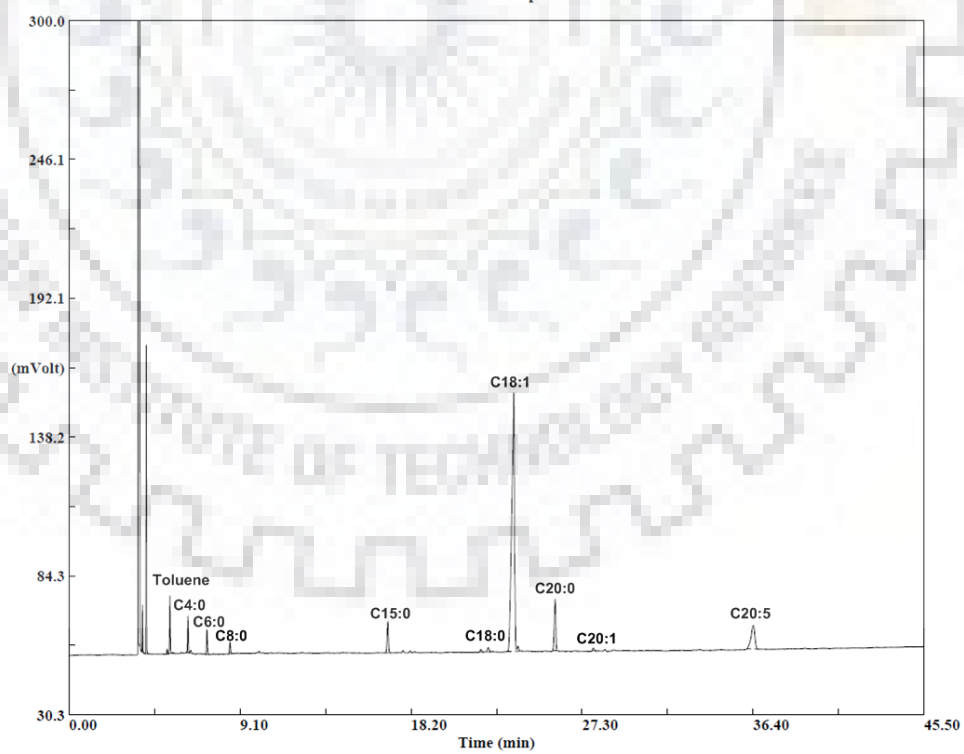Fig. C.143: Gas chromatogram of Carrot seed fatty acid content, Run No. 10.
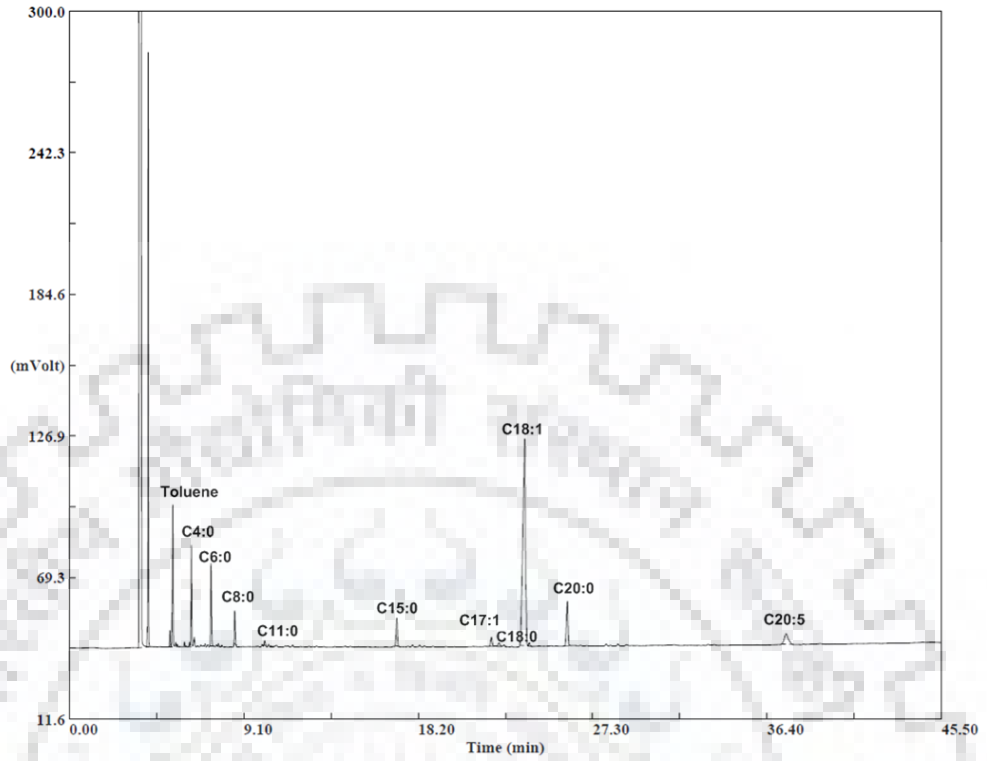
Fig. C.144: Gas chromatogram of Carrot seed fatty acid content, Run No. 11.
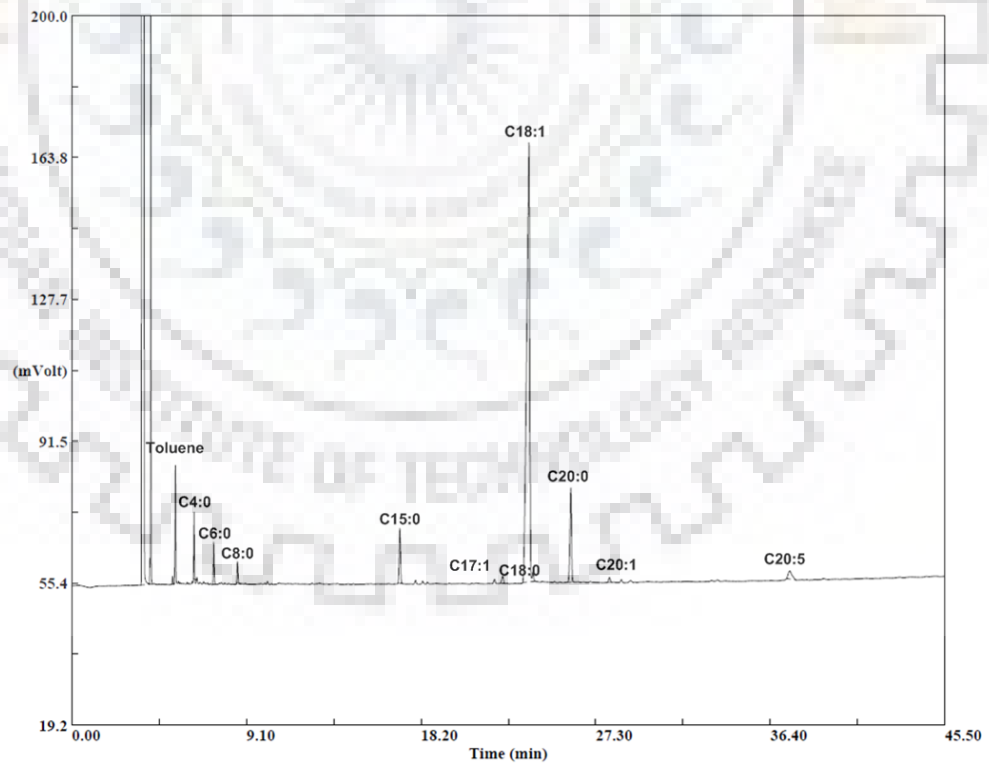
Fig. C.145: Gas chromatogram of Carrot seed fatty acid content, Run No. 12.
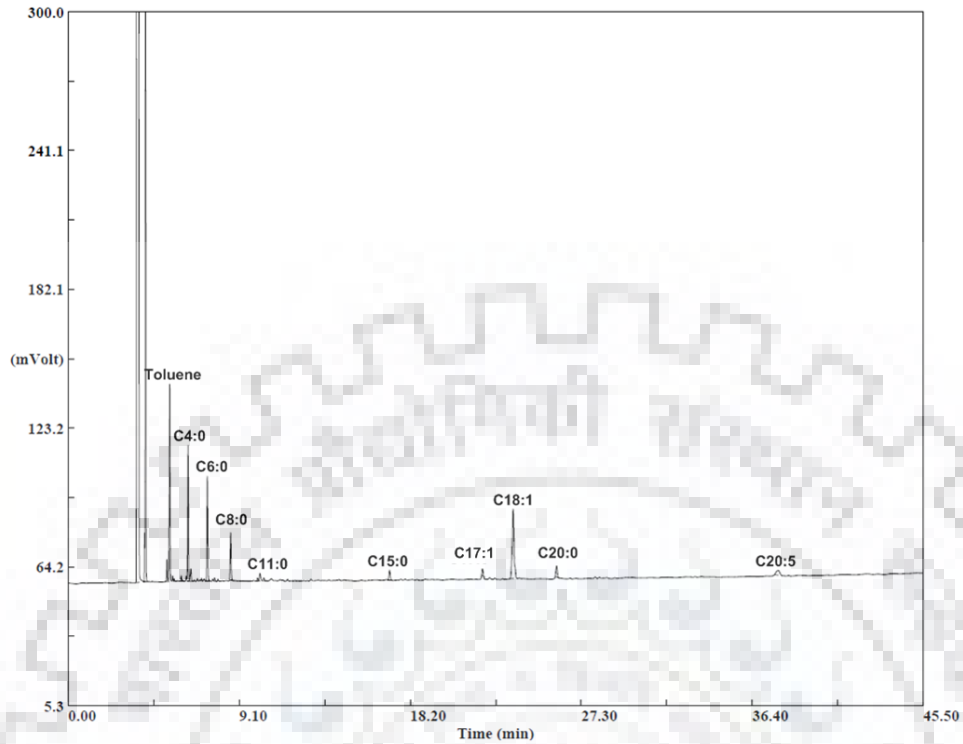
Fig. C.146: Gas chromatogram of Carrot seed fatty acid content, Run No. 13.
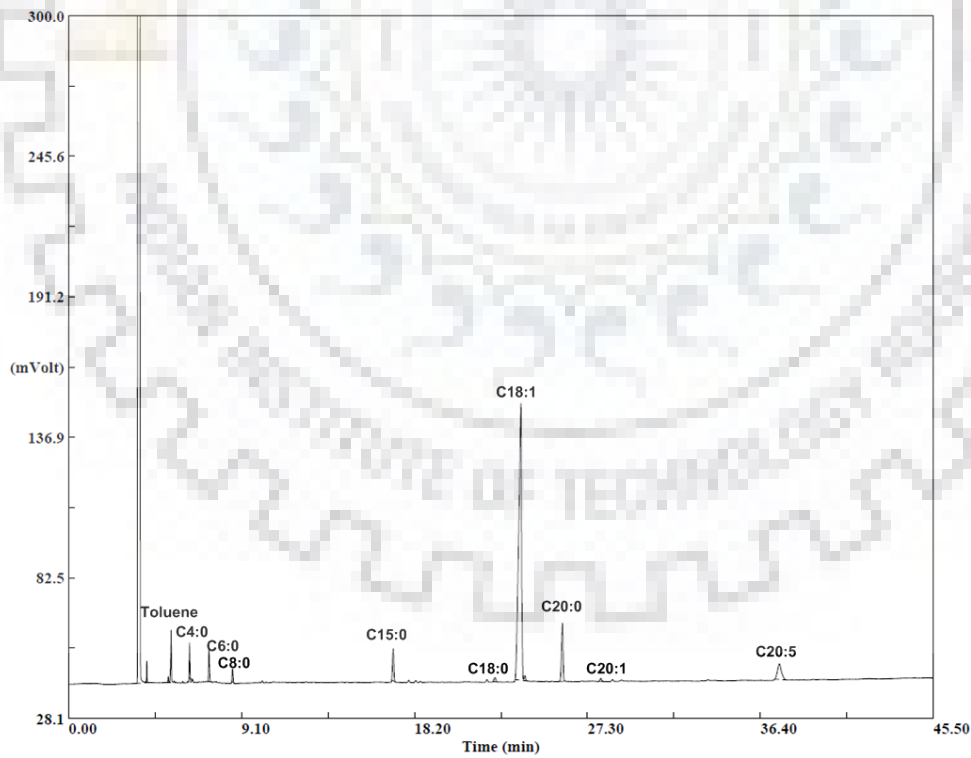
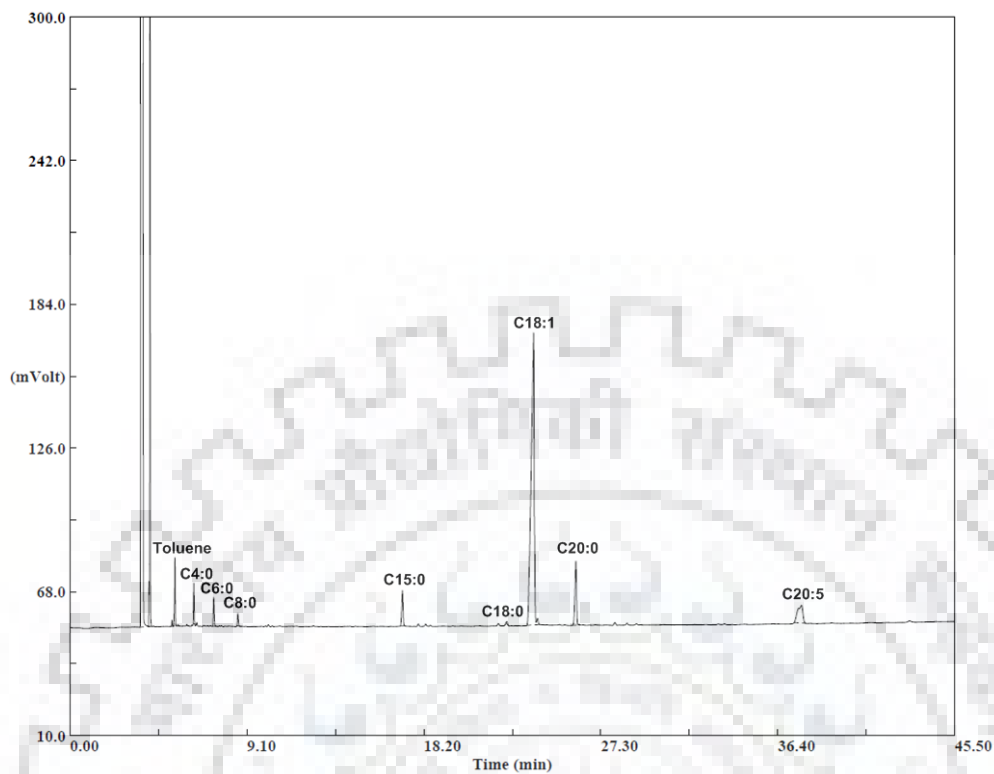Fig. C.147: Gas chromatogram of Carrot seed fatty acid content, Run No. 14.
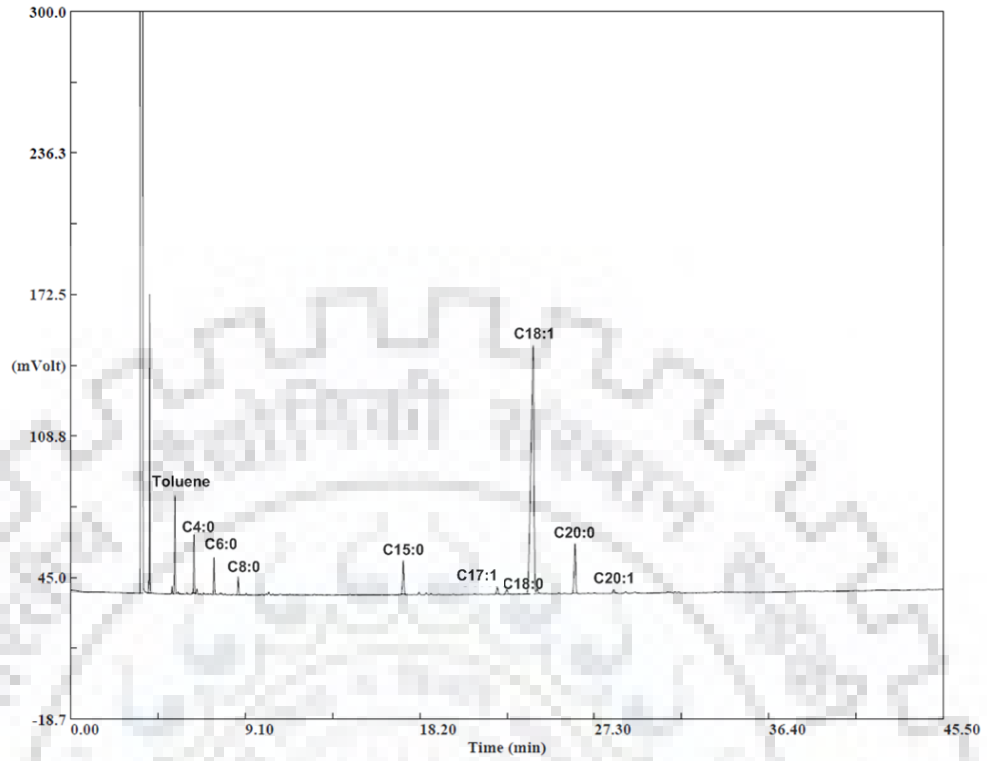
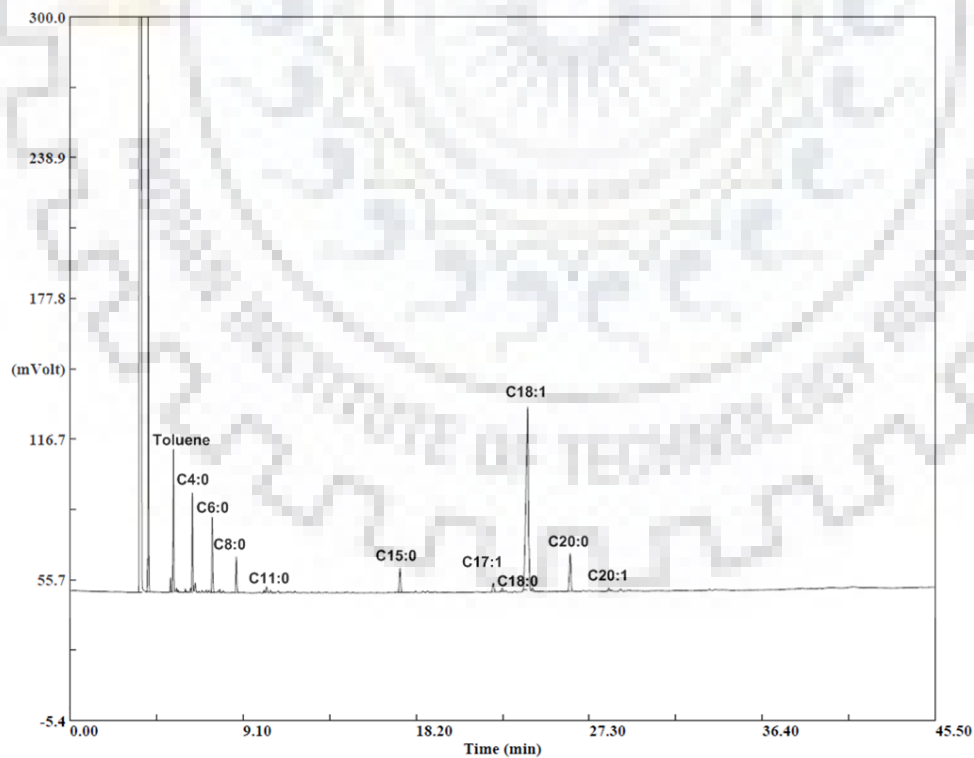Fig. C.148: Gas chromatogram of Carrot seed fatty acid content, Run No. 15.
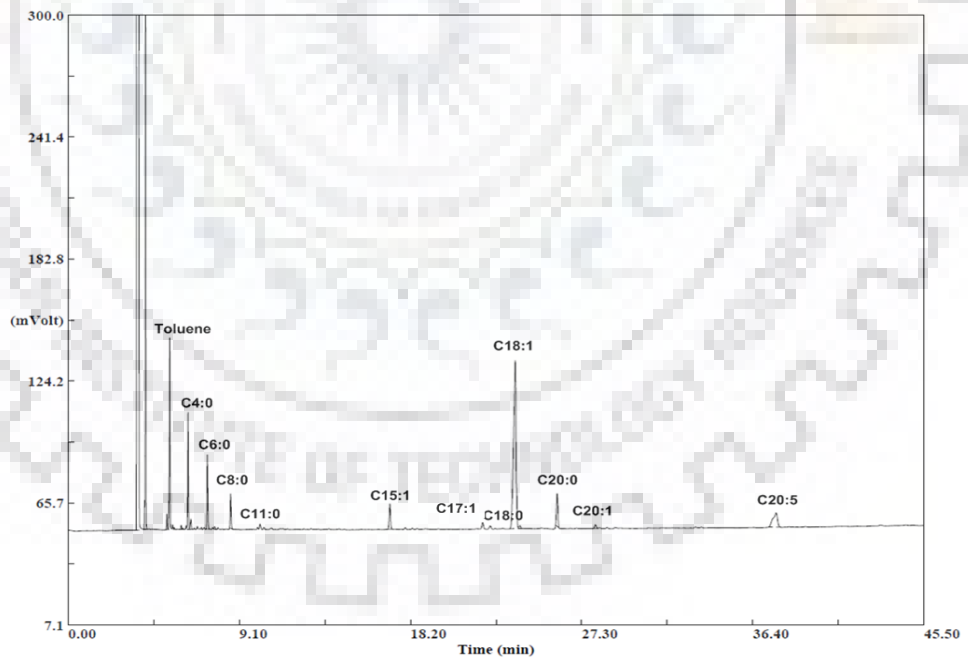
Fig. C.149: Gas chromatogram of Carrot seed fatty acid content, Run No. 16.
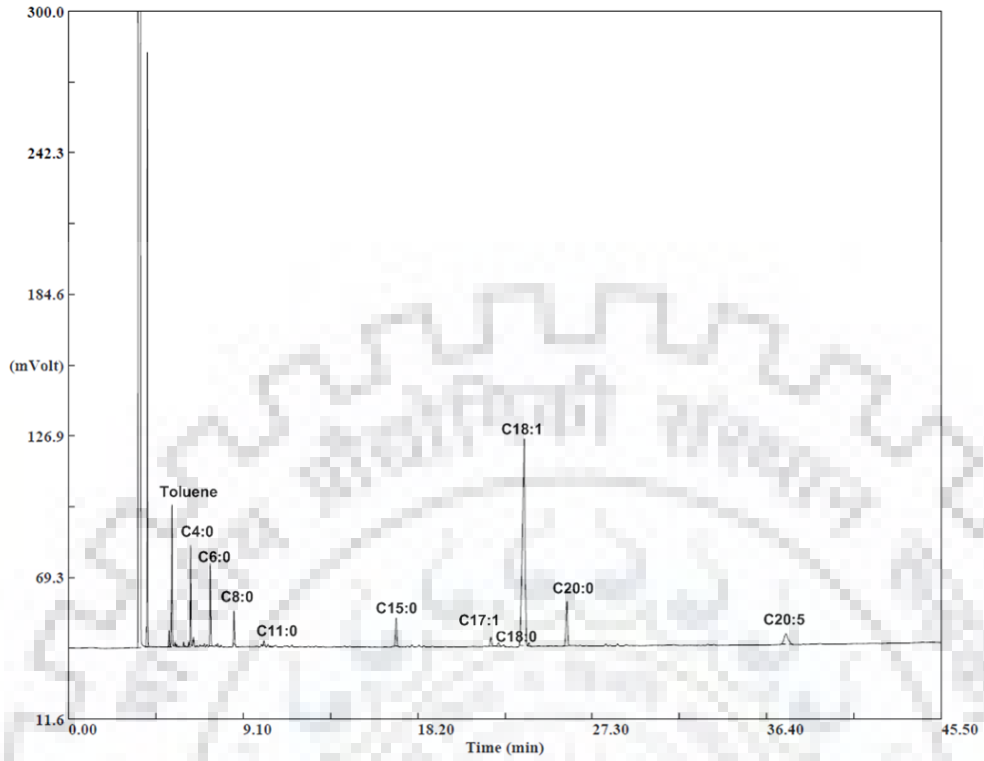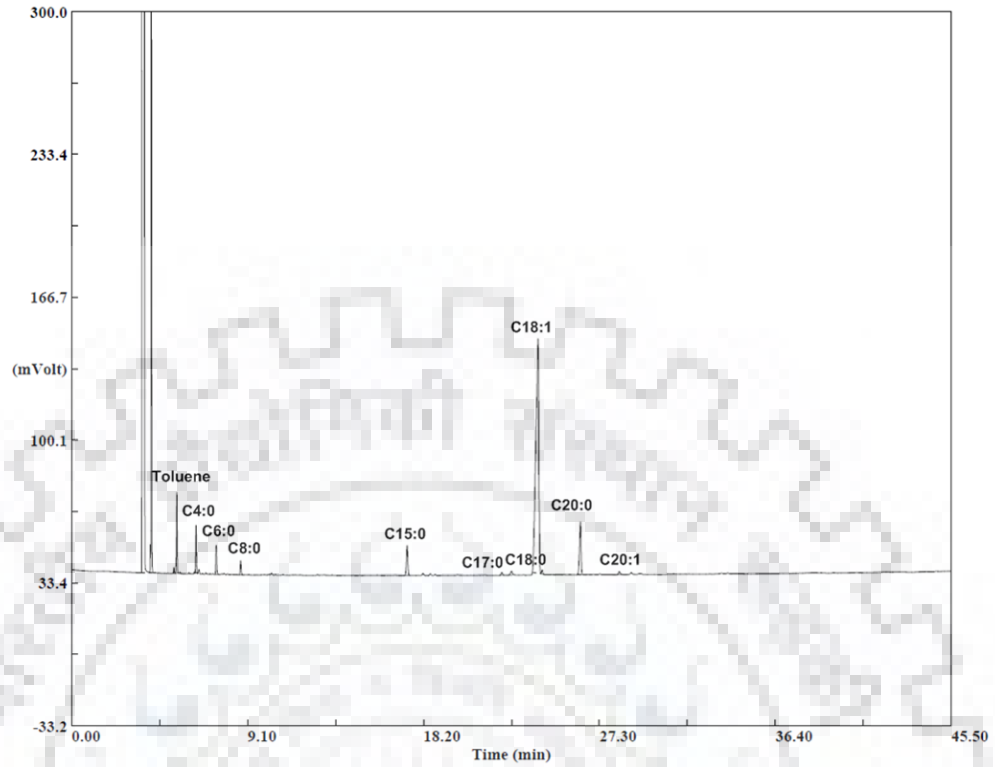
Fig. C.150: Gas chromatogram of Carrot seed fatty acid content, Run No. 17.
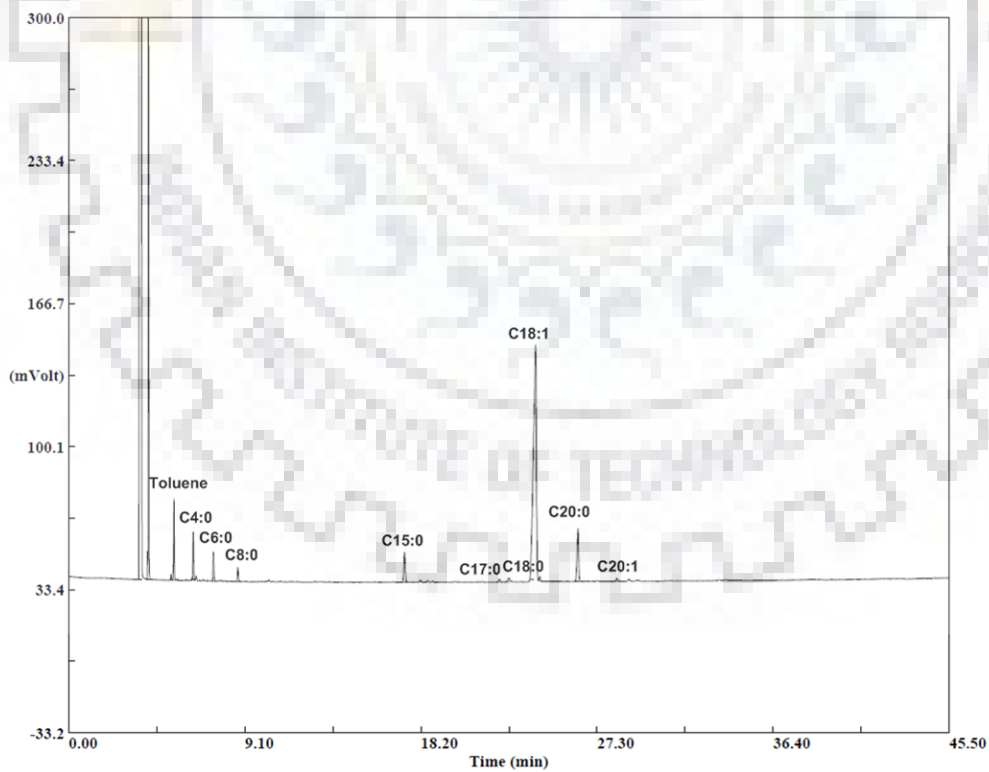
Fig. C.151: Gas chromatogram of Carrot seed fatty acid content, Run No. 18.

C-68
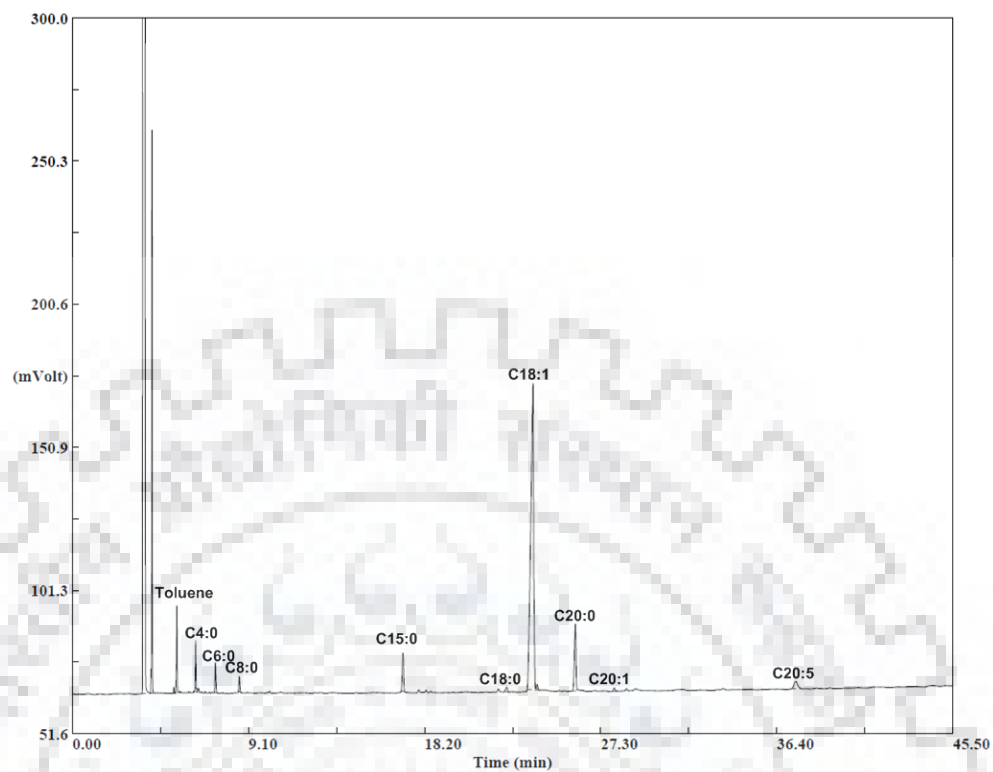
Fig. C.152: Gas chromatogram of Carrot seed fatty acid content, Run No. 19.

Fig. C.153: Gas chromatogram of Carrot seed fatty acid content, Run No. 20.

Fig. C.154: Gas chromatogram of Carrot seed fatty acid content, Run No. 21

Fig. C.155: Gas chromatogram of Carrot seed fatty acid content, Run No. 22.

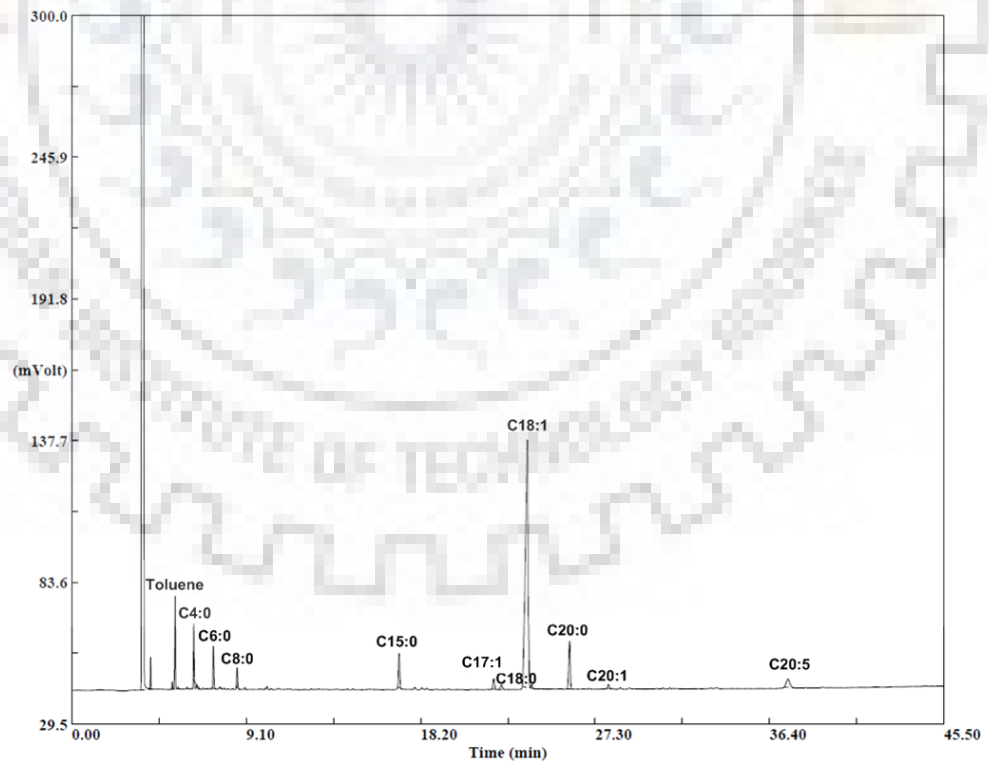Fig. C.156: Gas chromatogram of Carrot seed fatty acid content, Run No. 23.

Fig. C.157: Gas chromatogram of Carrot seed fatty acid content, Run No. 24.

Fig. C.158: Gas chromatogram of Carrot seed fatty acid content, Run No. 25.

Fig. C.159: Gas chromatogram of Carrot seed fatty acid content, Run No. 26.

C-72

Fig. C.160: Gas chromatogram of Carrot seed fatty acid content, Run No. 27.

Fig. C.161: Gas chromatogram of Carrot seed fatty acid content, Run No. 28.
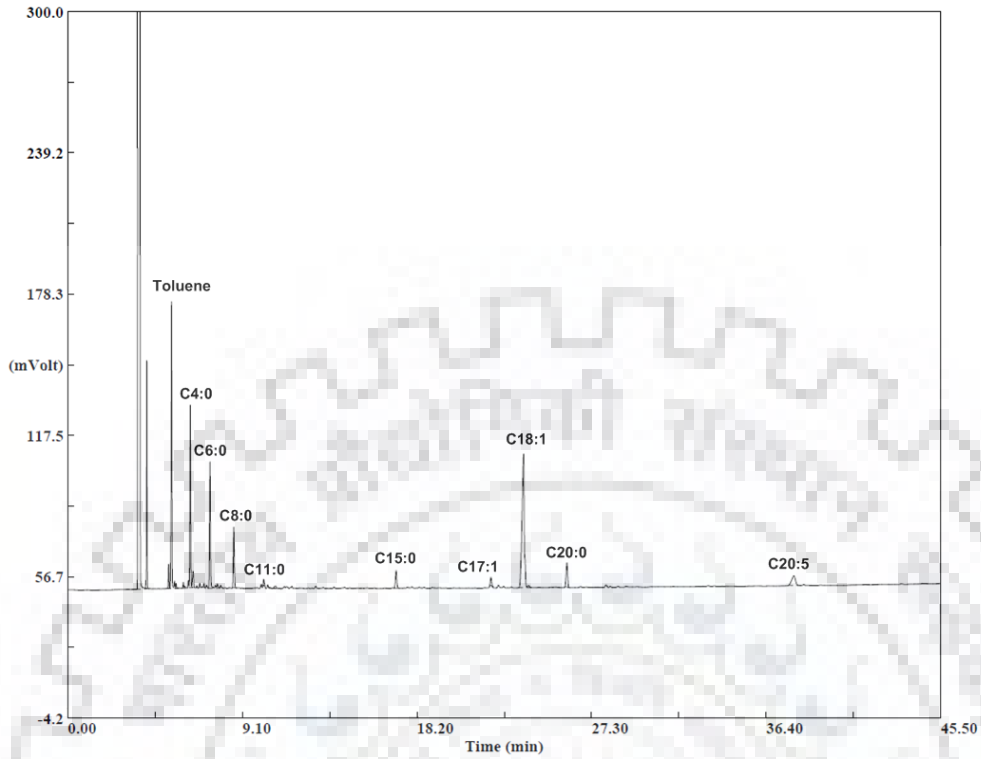
Fig. C.162: Gas chromatogram of Carrot seed fatty acid content, Run No. 29.
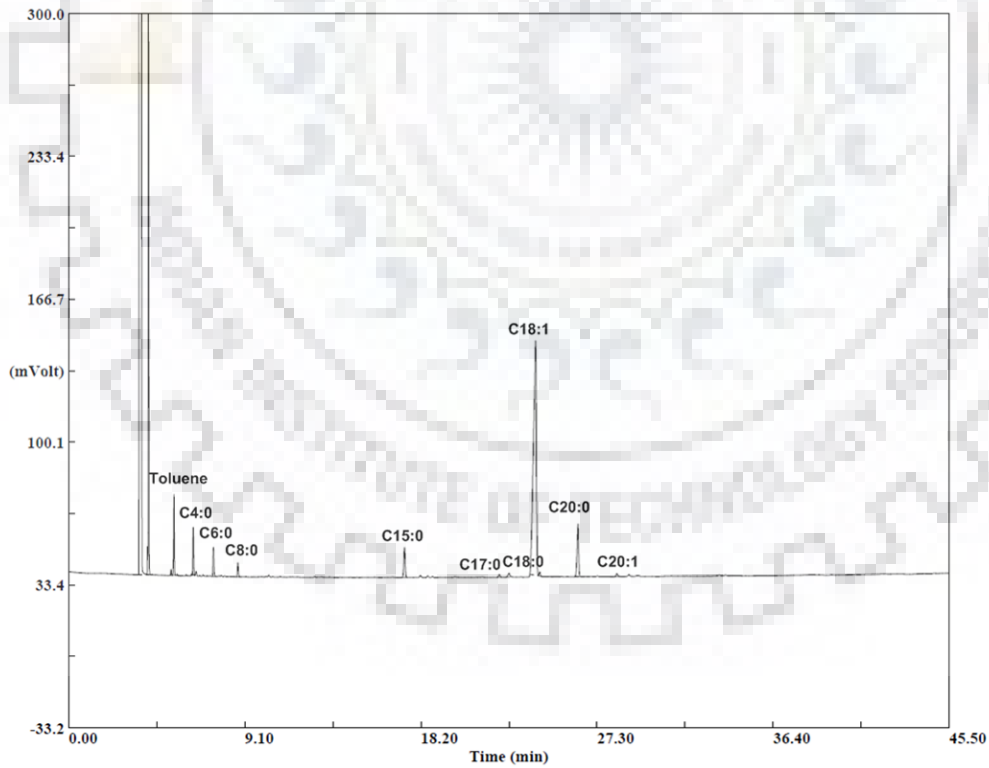

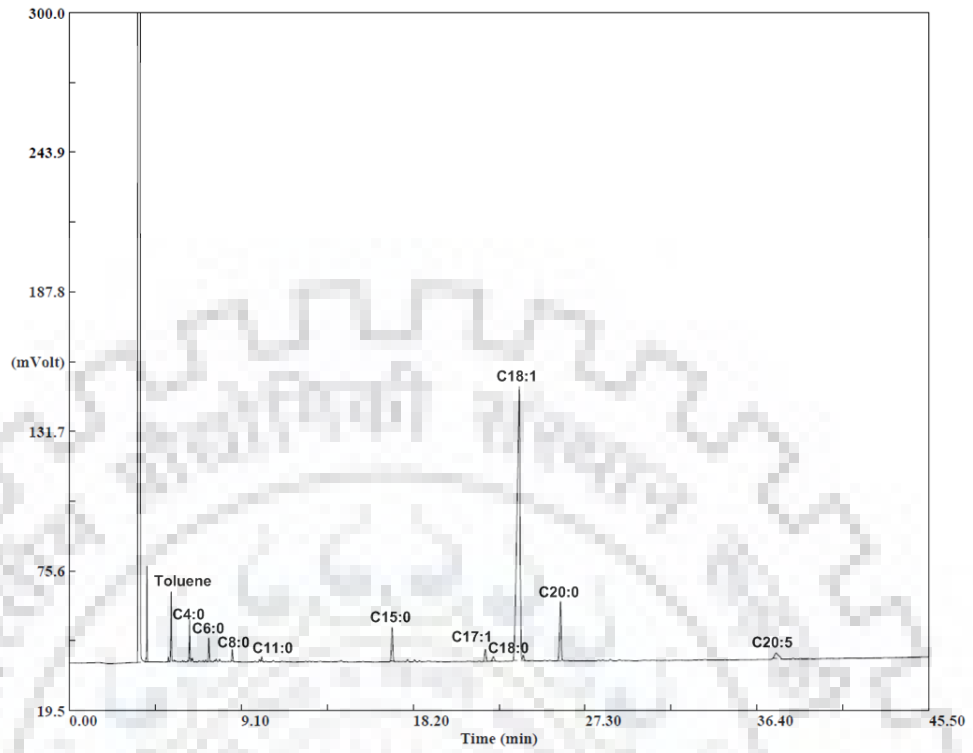Fig. C.163: Gas chromatogram of Carrot seed fatty acid content, Run No. 30.

Fig. C.164: Gas chromatogram of Carrot seed fatty acid content, Soxhlet extraction.

LIST OF PUBLICATIONS

Published in International Journal

1. **Priyanka.** and Khanam, S., "Selection of suitable model for different matrices of raw materials used in supercritical fluid extraction process", *Separation Science and Technology*, *1*,53,71-96, 2017.

2. **Priyanka.** and Khanam, S., "Influence of operating parameters on Supercritical fluid extraction of essential oil from Turmeric root", *Journal of cleaner production*, 188, 816-824, 2018.

3. **Priyanka**, V. Subbaramaiah, V.C. Srivastava, I.D. Mall, "Catalytic oxidation of nitrobenzene by copper loaded activated carbon", Separation and Purification Technology, 125, 284-290, 2014.

4. **Priyanka**, V.C. Srivastava, "Photocatalytic Oxidation of Dye Bearing Wastewater by Iron Doped Zinc Oxide", Industrial & Engineering Chemistry Research ,50,52, 17790−17799 , 2013.

International/National Conference

1. **Priyanka**. and Khanam, S., "Supercritical Fluid Extraction of Natural Products: A Review", International Conference "EEECOS 2014" IJEDR, ISSN: 2321-9939.

2. **Priyanka**. and S. Khanam, "Simulation of Supercritical Fluid Extraction Process", International Conference of COMSOL Multiphysics held in Pune on 28-29 October 2015.

Communicated to International Journal/ under preparation

1. **Priyanka**. and Khanam, S., "Supercritical CO_2 extraction of carrot seed oil: Screening, optimization, and economic analysis", *Journal of CO_2 Utilization* (**Required reviews completed**).

2. **Priyanka**. and Khanam, S., "Selection of suitable model for the supercritical fluid extraction of carrot seed oil: A parametric study", Chemical engineering science (**Communicated**).

3. **Priyanka**. and Khanam, S., "Extraction of Turmeric oil using supercritical CO_2 and mathematical modeling" (**Manuscript under progress**).